*—Plenary Paper—*

# Alpine and Polar Periglacial Processes: The Current State of Knowledge

Ole Humlum
*University of Oslo, Institute of Geosciences, Box 1047 Blindern, 0316 Oslo, Norway*
*and*
*UNIS, Box 156, NO-9171 Longyearbyen, Svalbard, Norway*

## Abstract

Recently the traditional view on the geomorphological evolution of periglacial landscapes has been questioned. The geomorphological processes considered most important for landscapes in periglacial regions, in general, are not unique for periglacial environments. On the other hand, there is a suite of geomorphological processes which may be seen as characteristic for periglacial environments. Based on what the author considers characteristic periglacial phenomena and landforms, this paper attempts to identify what might be conceived as the main characteristic periglacial processes. Seasonal or perennial freezing and conspicuous landforms such as extensive talus sheets, polygonal networks, and large-scale patterned ground, dominate descriptions of periglacial regions. Phenomena controlling bedrock disintegration, rockfall, thermal contraction cracking, and sorting of sediments are therefore all seen as the means to identify characteristic periglacial processes. Each of these periglacial processes is shortly described, and the present state of knowledge, or the lack of such, is outlined.

**Keywords:** climate; geomorphology; modeling; monitoring; periglacial; permafrost.

## Introduction

Periglacial regions at high latitude or high altitude experience rapid changes in the ground thermal regime in response to daily and annual as well as long-term climatic variations. Changes in the ground thermal regime and the associated growth or decay of permafrost may destabilize rock slopes or mobilize sediment slopes, possibly leading to major geomorphic changes, accompanied by natural hazards (e.g., Harris et al. 2001, Haeberli and Burn 2002). One practical priority issue of periglacial geomorphology should therefore by to improve understanding of the climatic controls on geomorphic processes, to predict potential hazards. The ultimate scientific aim of periglacial geomorphology, however, remains the formulation of models for cold-climate landscape evolution (French and Thorn 2006).

By tradition, alpine and polar periglacial landscapes are regarded as characterized by efficient frost-driven geomorphological processes. The importance of frost shattering and related processes was equally emphasized. Hence, the geomorphology of periglacial areas was long regarded as controlled primarily by processes driven by freeze–thaw mechanisms.

Originally, the term periglacial was used to describe the climatic and geomorphic conditions of areas peripheral to Pleistocene ice sheets and glaciers. Modern usage refers, however, to a wider range of cold climatic conditions regardless of their proximity to a glacier, either in space or time. In addition, many, but not all, periglacial environments possess permafrost; but they appear all to be dominated by frost action processes (Dylik 1964, French 1976, Washburn 1979, French 2007). In line with this view, the English version of the Multi-Language Glossary of Permafrost and Related Ground-Ice Terms compiled by the IPA's Terminology Working Group (Everdingen 1998), defines the term periglacial as the conditions, processes and landforms associated with cold, nonglacial environments.

*Periglacial landscapes*

The origin of periglacial landscapes as traditionally defined is recently becoming a theme for renewed debate. The relationship of landscapes to climate is a topic which has simultaneously been regarded as a focus for research in geomorphology and an approach which has fruitlessly occupied the time of geomorphologists over the past several decades. The former view has characterized research by many French and German geomorphologists, whereas the latter has prevailed among Anglo-American researchers. There is little doubt that major differences in climate have a profound effect on landscape development. Disagreement comes with the finer distinctions between degrees of climatic differences evident in past attempts to identify morphoclimatic zones. For instance, if we examine a range of landscapes in periglacial environments, landscape diversity is often more apparent than uniformity. A further problem is the diversity of conditions under which apparently similar landforms can develop. Perhaps the most intractable problem in periglacial geomorphology is the logical temptation of explicit linking of a particular landform with a specific set of climatic conditions. The observation of periglacial phenomena such as, e.g. ice-wedge casts, in climatic environments in which they could not have developed obviously raises the question of climatic change in landform interpretation.

Any modern periglacial landscape should be considered as consisting of a number of landforms currently adjusting according to present climate, and a number of relict features, produced under past climatic conditions. Whether a climatic change is of geomorphic significance depends on its magnitude and duration, and on the properties of the landform considered. The larger or more resistant a

landform, the longer, in general, it takes to adjust to a change in climate. In addition, the broad features of landscapes in periglacial environments are also highly influenced by lithological differences.

The validity of the traditionally view on the evolution of a typical periglacial landscape has therefore been questioned in recent times: The importance of geomorphological processes like chemical weathering, rainfall-induced slope processes and river action are emphasized, even though they are not unique for periglacial environments, but occur also in many other climatic settings. For example, Rapp (1960) in his classical study on weathering in northern Sweden demonstrated that solution was more important than mechanical processes. Later Thorn (1992) suggested that frost action may have been overestimated in relation to explaining the geomorphology of periglacial regions. Weathering and transport processes not related to frost may often modify the landforms resulting from frost action, or even preside over landform evolution in many periglacial environments. The action of wind and running water may be two important examples of such ubiquitous processes not limited to cold regions. This development in 2003 lead André to ask the pertinent question: Do periglacial landscapes evolve under periglacial conditions? The significance of this question was emphasized by French and Thorn (2006). On this background we might even begin to wonder what is understood by periglacial processes.

*Periglacial processes*

The André (2003) paper was published in a special issue of the journal Geomorphology, presenting a selection of papers originally presented at the general session ''Glacial and Periglacial Geomorphology'' of the Fifth International Conference on Geomorphology held in Tokyo, Japan, in August 2001 (Matsuoka et al. 2003). A study of these papers provide some assistance in identifying what is understood as periglacial processes at the beginning of the 21st century. Broadly the papers could be categorized into four themes: effects of diurnal frost, mountain permafrost, paleo-periglaciation and nonfrost processes in periglacial environments.

This suggests that many periglacial geomorphologists still have their research focus on frost-related processes. Low temperatures as a driving mechanism apparently remain a valid criterion for defining periglacial processes, even though the evolution of landscapes in periglacial environments may be controlled by other azonal processes. Also the steady interest in fossil periglacial features as indicators of past cold environments, points toward this conclusion. The validity of paleoclimatic indicators depends on precise description of, among other things, the climatic control on processes responsible for the landform or sedimentary structure studied. Otherwise, the periglacial feature observed would clearly be of little use as indicator for past cold environments.

So, at the beginning of the 21st century periglacial geomorphologists apparently are defining key periglacial processes as those related to seasonal or perennial frost, a point of view supported by French and Thorn (2006). At the same time, it is recognized that landscapes in periglacial regions are not always dominated by such periglacial processes, but quite often by more omnipresent processes such as wind and running water. On this background it might be considered if the future use of the term periglacial should be limited to describe processes and environments, rather than landscapes?

Having identified the modern implication of periglacial processes, we may proceed towards identifying a number of especially important or characteristic processes. To achieve this goal, we must first consider what is generally seen as characteristic landforms in periglacial environments. Due to space limitations, this will clearly not represent a comprehensive analysis, but will focus on a few landforms and phenomena, by the present author seen as characteristic for landscapes in periglacial environments.

*Characteristic periglacial landforms and processes*

The perhaps most obvious and impressive landforms in periglacial environments are those associated with steep slopes. In many mountain areas, glacial over-steepening, combined with weathering has led to rock slope instability and the production of large volumes of debris. Outside Holocene permafrost environments, a fundamental distinction is often recognized in valleys partly filled by glacier ice during Stadials of the last ice age. Within the former glacier limits, volumes of talus are limited relative to those at the foot of slopes outside the limits. By implication, the greater volumes of debris reflect the more severe periglacial conditions that prevailed during the Stadial and perhaps also during the deglaciation. Indeed, the impressive size of talus accumulations in periglacial highlands environments has led many researchers to conclude that rockfall is particularly pronounced under cold-climate conditions, due to release of debris from cliffs by frost wedging.

Low-relief periglacial areas are characterized by extensive polygonal networks, patterned ground and different types of frost mounds. All these phenomena are related to temperature induced volume changes of bedrock, sediments, ice, or mixtures of thereof. A highly diversified terminology is attached to the description of the surface expression of such phenomena. For example polygonal networks may appear in the literature under the headings of tundra polygons, frost-fissure polygons, ice-wedge polygons, and sand-wedge polygons, just to mention a few.

These observations suggest that frost-related non-glacial processes leading to rock disintegration, rockfall, rupturing by thermal contraction, and the deformation and sorting of thawed soil may be among what might be seen as characteristic periglacial processes. This assumption will provide the basis for the discussion below.

## Characteristic Periglacial Phenomena

*Rock disintegration*

Evidence suggests that frost action is not the only weathering process leading to rock decay in periglacial

environments. Cold-climate weathering is caused by the broader concept of cryogenic weathering, a collective term for a combination of little known physical and chemical processes which cause the in situ breakdown of rock under cold-climate conditions. Pressure release, salt weathering, chemical weathering, biological activity or thermal shocks may all play a role. In fact, chemical weathering (Roberts, 1968, Dixon et al., 2002) and biological processes (André, 2002) are more and more often considered as important actors in cold environments.

Field data on rock temperature and moisture content is essential for improved understanding of rock weathering in periglacial environments and for setting up realistic laboratory experiments. Unfortunately, such data are scarce in literature. In recent years, however, this situation is beginning to change through the publication of such data (e.g., Hall 1997, Hall 2006, Hall et al. 2002, Prick 2003).

This new accessibility of high-quality field data has provided the background for conducting realistic laboratory experiments, investigating the importance of ice segregation for low temperature bedrock breakdown under permafrost conditions (Murton et al. 2001). This experiment demonstrated that ice segregation, frost heave and brecciation in artificial permafrost formed in moist chalk are fundamentally similar to the processes associated with the growth of natural permafrost formed in frost-susceptible sediment. Similarities between the experimentally formed brecciation and naturally brecciated bedrock in areas of contemporary and former permafrost suggest that ice segregation during perennial and seasonal freezing is an important weathering process of frostsusceptible bedrock. By implication, the coarse, angular debris produced by ice segregation in bedrock during cold Quaternary periods was suggested being the sediment source for many of the coarse periglacial slope deposits. It is also very likely that bedrock fracture by ice segregation is significant for rockwall stability in regions of mountain permafrost, and for landform development in such areas in general. On this background Büdel's (1977) original 'Eisrinde' hypothesis absolutely deserves renewed research interest.

*Rockfalls*

The term rockfall describes the fall of relatively small (< 10 $m^3$) fragments of rock debris that are released from bedrock cliffs. By tradition, rockfall in periglacial environments has been widely attributed to frost wedging, the widening of cracks and joints by ice during freezing and detachment of debris from cliffs during thaw. Frost wedging is, however, only one of several processes operating on cliff faces (André 2003). Rockfall may also be triggered by stress-release, progressive failure along joints, or build-up of hydrostatic pressure within a rock mass. Indeed, some researchers view the role of freeze-thaw in rockfall as trivial in comparison with intrinsic controls such as stress release, weathering and build-up of joint-water pressures.

The timing of rockfalls remains the main reason for seeing frost wedging as the foremost cause of rockfall in cold environments. Rapp (1960) noted that rockfall at high latitudes is most frequent in spring and autumn, when cliffs was assumed to experience a maximum frequency of freeze-thaw cycles. Rockfall inventories in the Arctic and the Alps (e.g. Luckman, 1976, Coutard and Francou 1989) suggest maximum activity during the spring thaw. In Japan, Matsuoka and Sakai (1999) observed peak rockfall rate 5-15 days after meltout of the cliff face, when seasonal thaw reached an estimated depth of 1 m. Other rockfall inventories, however, emphasize diurnal variations, rather than seasonal trends. This is observed at alpine cliffs with frequent diurnal freeze-thaw cycles penetrating to depths of 50 cm (Coutard and Francou 1988). Rockfalls may also coincide with summer rainstorms, implying that build-up of joint-water pressures is also instrumental in releasing debris. Conversely, Matsuoka and Sakai (1999) in Japan found that intensive rockfall activity is rarely associated with either diurnal freeze-thaw cycles or precipitation events. So it is actually difficult to confirm the hypothesis regarding frost wedging as the main trigger of rockfall in periglacial environments.

*Wind action*

Due to the general lack of trees, many periglacial regions experience high wind speeds (Seppälä 2004), leading to the formation of different types of deflation surfaces. The vegetation, soil and fine material debris is removed to leave an armoured surface where large clasts are embedded within a matrix of finer sediment. Grains of sand and fine gravel can often be observed in motion during strong winds, blasting vegetation and rock surfaces. Sand dunes or sand sheets may occur downwind of such areas (Ballantyne and Harris 1994, Humlum and Christiansen 1998), but often much of the debris seems not to accumulate as dunes or sheets. Some may become temporarily resident in the snow pack, to thaw out in spring. Some probably finds its way into lakes and rivers on valleys floors. Some may be transported into the sea suspended in the air.

Another characteristic feature related to wind action in periglacial environments is wind-facetted blocks or wind polished bedrock surfaces (Christiansen and Svensson 1998). The wind-eroded surfaces are identified from their smooth and polished surfaces, together with facets and grooves (Christensen 2004). Blowing snow at low temperatures has apparently been the abrading agent for several examples of periglacial bedrock windpolish (Fristrup 1953).

*Snowblow*

Snowblow by wind is important in most periglacial environments, partly because of the typical absence of high vegetation providing lee at the ground surface, partly because many periglacial regions are found at high latitudes or high altitudes, where wind speed may be high.

The process of snow drifting is important in low-relief periglacial terrain, where the resulting distribution of snow controls heat exchange between atmosphere and the ground surface during the winter, for example on palsas (Seppälä 2004). The thermal importance of the snow cover for perma-

frost is well demonstrated by the efforts put into determining the n-factor, describing the thermal insulation provided by the snow cover (Smith and Riseborough 2002). In high-relief areas, snow accumulation on steep slopes contributes to the release of avalanches, especially on slopes downwind of extensive mountain plateaus (Humlum et al. 2007).

At low temperatures, the hardness of snow crystals increases, and wind transported snow may act as an efficient abrasive agent in relation to boulders and bedrock (Fristrup 1953). In addition, wind induced accumulations of snow are important as sources of water during the summer, as precipitation generally is low in periglacial environments.

Bagnold (1941) provided much of the groundwork for current steady-state models of sand drift (e.g. Sørensen 1991). The same physical basis has been applied to existing numerical models of snowdrift, such as SnowTran-3D (Liston and Sturm 1998) and the snowdrift index in SNOWPACK (Lehning et al. 2000, 2002a, 2002b). Snow drift prediction models using weather station data have also been developed for meteorological services (e.g., Li and Pomeroy 1997a, 1997b). These models, however, tend to consider snow drift as a probabilistic event and relate conditions to a measurement height, rather than to surface conditions.

*Snow avalanches*

Snow avalanches represent a periglacial transport process especially important during winter and spring. Although many shallow or midwinter avalanches contain only snow, deeper and late winter avalanches frequently incorporate and transport varying volumes of rock debris. As avalanches tend to follow gulleys, this debris accumulates on valley floors at the mouths of these gulleys in the form of avalanche boulder lobes (Rapp 1960), protalus ramparts (Ballantyne and Harris 1994), or rock glaciers (Humlum et al. 2006).

The meteorological control of snow avalanches represents a research theme in its own right, highly developed especially in Switzerland, Austria, USA and Norway. Several factors affect the likelihood of an avalanche, including weather, temperature, slope steepness, slope aspect, wind direction, terrain, vegetation, and the general snowpack conditions. Different combinations of these factors can create low, moderate or extreme avalanche conditions. Despite the existence of large databases with observations on avalanches, avalanche safety rules still are based mainly on empirical rules of thumb, rather that on strict meteorological-geotechnical analysis.

Another way of investigating the climatic control on avalanches is through analysis of avalanche deposits accumulated during the Holocene (e.g., Blikra and Selvik 1998). Such analyses, however, important as they are, only indicate that avalanches become more frequent during cold periods with frequent snow precipitation, but do not provide the means of detailed insights into meteorological controls on avalanche release. Indeed, some attempts at analysis simply assumes that the presence of what is interpreted as avalanche-derived debris indicate past periods with cold and snowy conditions.

*Thermal contraction of frozen ground*

Periglacial thermal contraction phenomena such as ice-wedge casts are widespread in periglacial environments. Fossil features in the form of ice-wedge casts are often used to estimate palaeotemperatures, specifically the maximum values of the mean annual air temperature or the mean air temperature of the coldest month (e.g., Washburn 1979, Vandenberghe et al. 1998). The now common use of ice-wedge casts as palaeotemperature indicators arose from an influential study by Péwé (1966a, 1966b) of ice-wedges in Alaska. As later pointed out by Murton and Kolstrup (2003), however, the validity of such attempts at reconstructions still remains uncertain because of limited knowledge of the frequency of thermal contraction cracking under contemporary permafrost environments. In addition, the perhaps complex controls other than meteorological on cracking are still incompletely understood. In fact, snow thickness appears to represent a decisive factor on ice-wedge cracking near the Western Arctic coast of Canada (Mackay 1993). Also the role of surface vegetation still needs to be quantified (Murton and Kolstrup 2003).

Progress in knowledge on thermal contraction cracking requires detailed field observations, supplemented by laboratory and numerical experiments, using real-world meteorological data on climate, landforms and sediments. A numerical modeling experiment on ice-wedge formation was recently presented by Plug and Werner (2001). This attempt at modeling ice-wedge growth turned out to be premature, because of lack of insight in real world conditions (Burn 2004).

Examples of how to expand knowledge on thermal contraction cracking of frozen sediments is given by careful field studies such as, e.g., Mackay (1993) and Christiansen (2005), in great detail describing meteorological and snow conditions related to thermal cracking of frozen ground.

*Sediment sorting*

Sorting of near-surface sediments in periglacial areas is responsible for the distinct, and often symmetrical geometric shapes known under the general heading patterned ground. The details of the sorting process and the origin of patterned ground has remained elusive for ages, despite much research effort.

Patterned ground is perhaps the most striking feature of the periglacial landscape, and can be found in a variety of forms: Polygons, circles, nets, steps, and stripes. The individual surface forms may range in size from a few centimeters to several meters in diameter. Typically, the type of patterned ground in a given area is related to the amount of larger stones present in local soils and the frequency of freeze-thaw cycles.

Polygons, circles and nets normally occur on level or gently sloping surfaces, while steps and stripes are found on steeper gradients. Both sorted and non-sorted varieties are recognized. The sorted varieties are typically outlined by coarse, stony material, and so are termed “stone circles,” “stone polygons,” “stone nets,” “stone steps,” and “stone stripes.”

The origin of patterned ground involves a complex interaction of several geomorphological processes, including differential frost heaving and mass movement. Recurrent freezing and thawing of water is usually believed to be critical for the development of patterned ground. In permafrost regions and non-permafrost regions affected by seasonal frost, repeated freezing and thawing of soil water transports larger stones toward the surface as smaller soils flow and settle underneath larger stones. At the surface, areas that are rich in larger stones contain less water than highly porous areas of finer grained sediments. These water saturated areas of finer sediments have greater ability to expand and contract as freezing and thawing occur, leading to lateral forces which ultimately pile larger stones into clusters and stripes. Through time, repeated freeze-thaw cycles form the common polygons, circles, and stripes of patterned ground.

There is still much debate as to the detailed mechanisms involved in freeze-thaw sorting, but it is widely agreed that the large scale patterned ground reflects the former existence of permafrost (Ballantyne 1996). Recurrent freezing and thawing of ground is also considered important for other periglacial phenomena such as solifluction and ploughing blocks.

*The way ahead for periglacial geomorphology*

Periglacial geomorphology is very special. It usually requires some mastery of geology, meteorology and geophysics to plan and carry out efficient investigations of complex geomorphological problems in periglacial environments. On the other hand, especially Quaternary geologists can in a very real sense be seen as applied periglacial (and glacial) geomorphologists. This relation emerges because periglacial (and glacial) geomorphologists combine the historical perspective so dear to geologists with an accentuated awareness and interest of contemporary geomorphological processes. In my opinion, it is exactly this study of geomorphological processes in periglacial environments which provides periglacial geomorphology with integrity, and upon which periglacial geomorphology relies for future scientific credibility.

Geomorphological processes clearly unique to periglacial environments relate to seasonal or perennial freezing, including the growth of segregated ice and associated frost heaving. Many of these processes operate in the near-surface layer subject to seasonal freezing and thaw; the active layer in permafrost regions. Ground seasonally frozen experience a range of special conditions associated with pore-water expulsion and thaw consolidation (French and Thorn 2006). On sediment slopes, this may promote rapid mass failures. On bedrock slopes, disintegration of exposed rock by mechanical frost weathering and several still poorly understood physical and biochemical processes may lead to rock falls. In addition to such characteristic periglacial processes the enhanced effect of wind in periglacial regions clearly deserves further study (Seppälä 2004).

Any study contributing to increased knowledge on geomorphological processes in periglacial environments are by definition important, no matter the specific theme chosen. From a strategic point of view, however, it appears that improved understanding of especially processes related to seasonal or perennial freezing should be seen as having tactical research priority within future periglacial research. Rock weathering in periglacial environments may be considered the mother of many types of sediments, and therefore a key factor for a range of other processes and landforms. Rock weathering in periglacial environments definitely deserves a concerted research effort, along with research on thermal contraction cracking and sediment sorting. These three phenomena together typify landscapes in most periglacial environments.

What is needed within periglacial geomorphology is a detailed monitoring scheme of meteorological parameters and geomorphological processes. Clearly, the use of dataloggers and other automatic equipment will have an important role in this development (Matsuoka 2006).

In this context, the organization in 2004 of a new Working Group (WG) on 'Periglacial Landforms, Processes and Climate' under the International Permafrost Association (IPA) may prove helpful. This WG is aiming at making a database for temporal and spatial variability of periglacial processes with special attention to meteorological controls and the impact of climatic change. To achieve this goal, the WG attempts to establish a global network for monitoring periglacial processes (Matsuoka and Humlum 2005, Matsuoka 2006), highlighting geomorphological processes associated with ground thermal regimes, inside and outside permafrost regions.

The recommended parameters to be measured depend primarily on the purpose of the study and the spatial scale. A cold-climate drainage basin is subjected to a variety of geomorphic processes, including glacial, periglacial, fluvioglacial, nival, gravitational and eolian processes. One research approach may focus on the mechanism of a specific process like rock fall, solifluction or ice-wedge growth, whereas other may aim at evaluating the sediment budget for the whole catchment. Whatever the approach chosen, the search for knowledge on past and present processes influencing landform evolution in periglacial regions is becoming increasingly influenced by more and more refined monitoring protocols, relying upon automatic and sophisticated equipment.

To the present author the common denominator for future periglacial research appears to be a coordinated research scheme embracing mapping, monitoring, experiments, and modeling, with focus on geomorphological processes relating to seasonal or perennial freezing.

## Acknowledgments

Most of this paper was written during my sabbatical at University of St. Andrew (Scotland), where space facilities were kindly provided by Professor Colin Ballantyne. Both Professor Hugh French and Professor Norikazu Matsuoka have shared their thoughts on periglacial geomorphology

with me during stays at UNIS (Svalbard), and in this way they have influenced the present paper. The responsibility for the actual content, and for any errors and omissions, however, remains fully with me. To everyone, I extend my warmest thanks.

## References

André M.-F. 2002. Rates of postglacial rock weathering on glacially scoured outcrops (Abisko-Riksgränsen area, 68°N). *Geografiska Annaler* 84A, 3-4: 139-150.

André, M.-F. 2003. Do periglacial landscapes evolve under periglacial conditions? *Geomorphology* 52: 149-164.

Büdel, J. 1977. *Klima-Geomorphologie*. Berlin and Stuttgart: Gebrüder Borntraeger, 304 pp.

Bagnold, R.A. 1941. *The Physics of Blown Sand and Desert Dunes*. London: Chapman and Hall, 265 pp.

Ballantyne, C.K. 1996. Formation of miniature sorted patterns by shallow ground freezing: A field experiment. *Permafrost and Periglacial Processes* 7: 409-424.

Ballantyne, C.K. & Harris, C. 1994. *The Periglaciation of Great Britain*. Cambridge: Cambridge University Press, 330 pp.

Blikra, L.H. & Selvik, S.F. 1998. Climatic signals recorded in snow avalanche-dominated colluvium in western Norway: depositional facies successions and pollen records. *The Holocene* 8: 631-658.

Burn, C.R. 2004. A Field Perspective on Modelling 'Single-ridge' Ice-wedge Polygons. *Permafrost and Periglacial Processes* 15: 59-65.

Christiansen, H.H. 2004. Windpolished boulders and bedrock in the Scottish Highlands: evidence and implications of Late Devensian wind activity. *Boreas* 33: 82-94.

Christiansen, H.H. 2005. Thermal Regime of Ice-wedge Cracking in Adventdalen, Svalbard. *Permafrost and Periglacial Processes* 16: 87-98.

Christiansen, H.H. & Svensson, H. 1998. Windpolished boulders as indicators of a late Weichselian wind regime in Denmark in relation to neighbouring areas. *Permafrost and Periglacial Processes* 9: 1-21.

Coutard, J.P. & Francou, B. 1989. Rock Temperature-Measurements in 2 Alpine Environments: Implications for Frost Shattering. *Arctic and Alpine Research* 21: 399-416.

Dixon J.C., Thorn, C.E., Darmody, R.G. & Campbell, S.W. 2002. Post-glacial rock weathering processes on a rocke moutonnée in the Riksgränsen area (68°N), northern Norway. *Norsk Geografisk Tidskrift* 56: 257-264.

Dylik, J. 1964. Eléments essentials de la notion de 'périglaciaire'. *Biuletyn Peryglacjalny* 14 : 111-132.

Everdingen, R.v. 1998. *Glossary of Permafrost and Related Ground-Ice Terms*. Compiled by the IPA's Terminology Working Group and edited by Robert van Everdingen. Dr. Everdingen made some minor updates and corrections to the Glossary in 2002.

French, H.M. 1976. *The Periglacial Environment*. London: Longman, 308 pp.

French, H.M. 2007. *The Periglacial Environment.* Chichester: John Wiley & Sons, Ltd., 458 pp.

French, H.M. & Thorn, C.E. 2006. The changing nature of periglacial geomorphology. *Géomorphologie: relief, processus, environment* 3: 165-174.

Fristrup, B. 1953. Wind erosion within the Arctic deserts. *Geografisk Tidsskrift* 52: 51-56.

Hall, K. 1997. Rock temperatures and implications for cold regions weathering. 1: New data from Viking Valley, Alexander Island (Antarctica). *Permafrost and Periglacial Processes* 8: 69-90.

Hall, K. 2006. Perceptions of rock weathering in cold regions: a discussion on space and time attributes of scale. *Géomorphologie: relief, processus, environment* 3: 187-196.

Hall, K., Thorn, C.E., Matsuoka, N. & Prick, A. 2002. Weathering in cold regions: some thoughts and perspectives. *Progress in Physical Geography* 26: 577-604.

Haeberli, W. & Burn, C.R., 2002. Natural hazards in forests: glacier and permafrost effects as related to climate change. In: Sidle, R.C. (Ed.), Environmental Changes and Geomorphic Hazards in Forests. CABI Publishing, Oxfordshire: pp. 167-202.

Harris, C., Davies, M.C.R. & Etzelmüller, B. 2001. The assessment of potential geotechnical hazards associated with mountain permafrost in a warming global climate. Permafrost and Periglacial Processes 12: 145-156.

Humlum, O. & Christiansen, H.H. 1998. Mountain climate and periglacial phenomena in the Faeroe Islands. *Permafrost and Periglacial Processes* 9: 189-211.

Humlum, O., Christiansen, H.H. & Juliussen, H. 2007. Avalanche-Derived Rock Glaciers in Svalbard. *Permafrost and Periglacial Processes* 18: 75-88.

Lehning, M., Doorschot, J. & Bartelt, P. 2000. A snowdrift index based on SNOWPACK model calculations. *Annals of Glaciology* 31: 382-386.

Lehning, M., Bartelt, P., Brown, B., Fierz, C. & Satyawali, P. 2002a. A physical SNOWPACK model for the Swiss avalanche warning. Part II. Snow microstructure. *Cold Reg. Sci. Technol.* 35: 147-167.

Lehning, M., Bartelt, P., Brown, B. & Fierz, C. 2002b. A physical SNOWPACK model for the Swiss avalanche warning. Part III. Meteorological forcing, thin layer formation and evaluation. *Cold Reg. Sci. Technol.* 35: 169-184.

Li, L. & Pomeroy, J.W. 1997a. Estimates of threshold wind speeds for snow transport using meteorological data. *Journal of Applied Meteorology* 36: 205-213.

Li, L. & Pomeroy, J.W. 1997b. Probability of occurrence of blowing snow. *Journal of Geophysical Research* 102(D18): 21,955-21,964.

Liston, G.E. & Sturm, M. 1998. A snow-transport model for complex terrain. *Journal of Glaciology* 44: 498-516.

Luckman, B. H. 1976. Rockfalls and Rockfall Inventory Data: Some Observations from Surprise-Valley, Jasper-

National-Park, Canada. *Earth Surface Processes and Landforms* 1: 287-298.

Mackay, J.R. 1993. Air temperature, snow cover, creep of frozen ground, and the time of ice-wedge cracking, western Arctic coast. *Canadian Journal of Earth Sciences* 30: 1720–29.

Matsuoka, N. 2006. Monitoring periglacial processes: Towards construction of a global network. *Geomorphology* 80: 20–31.

Matsuoka, N. & Sakai, H. 1999. Rockfall activity from an alpine cliff during thawing periods. *Geomorphology* 28: 309-328.

Matsuoka, N., Iwata, S. & Haeberli, W. 2003. Periglacial geomorphology at the beginning of the 21st century: introduction. *Geomorphology* 52: 1-3.

Matsuoka, N. & Humlum, O. 2003. Monitoring Periglacial Processes: New Methodology and Technology. *Permafrost and Periglacial Processes* 14: 299-303.

Murton, J. B., Coutard, Ł J.-P., Lautridou, J.-P., Ozouf, J.-C., Robinson, D.A. & Williams, R.B.G. 2001. Physical Modelling of Bedrock Brecciation by Ice Segregation in Permafrost. *Permafrost and Periglacial Processes* 12: 255-266.

Murton, J.B. & Kolstrup, E. 2003. Ice-wedge casts as indicators of palaeotemperatures: precise proxy or wishful thinking? Progress in Physical Geography 27(2): 155-170.

Péwé, T.L. 1966a. *Ice wedges in Alaska: classification, distribution and climatic significance.* In: Proceedings, First International Conference on Permafrost. 11–15 November 1963. National Academy of Science: National Research Council of Canada, Publication 1287: 76–81.

Péwé, T.L. 1966b. Palaeoclimatic significance of fossil ice wedges. *Biuletyn Peryglacjalny* 15: 65-73.

Plug L.J. & Werner B.T. 2002. Nonlinear dynamics of icewedge networks and resulting sensitivity to severe cooling events. *Nature* 417: 929–933.

Prick, A. 2003. Frost weathering and rock fall in an arctic environment, Longyearbyen, Svalbard. In: Phillips, M., Springman, S.M., Arenson, L.U., eds., *Permafrost, Proceedings of the Eight International Conference on Permafrost*, 21-25 July, Zürich, Switzerland. Balkema, Lisse, vol.2: 907-159.

Rapp, A. 1960. Recent development of mountain slopes in Kärkevagge and surroundings, Northern Sweden. *Geografiska Annaler* 42: 71-200.

Roberts, D. 1968. Occurrences of weathering pits from Sørøy, Northern Norway. *Geografiska Annaler* 50A: 60-63.

Smith, M.W. & Riseborough, D.W. 2002. Climate and the Limits of Permafrost: A Zonal Analysis. *Permafrost and Periglacial Research* 13: 1-15.

Seppälä, M. 2004. *Wind as a geomorphic agent in cold climates*. Cambridge: Cambridge University Press, 358 pp.

Sørensen, M. 1991. An analytical model of wind-blown sand transport. *Acta Mech.*,1 (Suppl.): 67-81.

Thorn, C.E. 1992. Periglacial geomorphology: What? Where? When? In: Dixon, J.C. & Abrahams, A.D. (eds.). *Periglacial Geomorphology*. Chichester: John Wiley & Sons, 3-31.

Vandenberghe, J., Coope, R. & Kasse, K. 1998. Quantitative reconstructions of palaeoclimates during the last interglacial-glacial in western and central Europe: an introduction. *Journal of Quaternary Science* 13: 361-66.

Washburn, A.L. 1979. *Geocryology: A Survey of Periglacial Processes and Environments*. London: Edward Arnold, 406 pp.

# Interseasonal Connection of Hydrothermal Components in a Permafrost Region in Eastern Siberia

Yoshihiro Iijima
*Institute of Observational Research for Global Change, Japan Agency for Marine-Earth Science and Technology*
Hoteak Park
*Data Integration and Analysis Group, Japan Agency for Marine-Earth Science and Technology*
Takeshi Yamazaki
*Department of Geophysics, Graduate School of Science, Tohoku University*
Hironori Yabuki
*Institute of Observational Research for Global Change, Japan Agency for Marine-Earth Science and Technology*
Trofim C. Maximov
*Institute for Biological Problems of Cryolithozone, RB RAS*
Tetsuo Ohata
*Institute of Observational Research for Global Change, Japan Agency for Marine-Earth Science and Technology*

## Abstract

The present study aims to examine the interseasonal impacts of water cycle components on subsequent hydrothermal processes in permafrost, focusing on rainfall, snow amounts, and snow start and disappearance timings in the Lena River basin over recent decades. According to climatological analysis, there is a significant correspondence between the interannual variation in snow depth and soil temperature. In addition, both snow cover start and disappearance dates have negative correlations with soil temperature and moisture. These relationships indicate that a wetter climate with earlier snow season tends to produce an earlier start of subsequent growing season, which has been observed in the central Lena River basin in recent years. Based on a one-dimensional land surface model, earlier snow cover start and disappearance dates are correlated with significant increases in evapotranspiration from the boreal forest due to an earlier soil thawing and earlier plant growth and increased supply of soil moisture for plant uptake.

**Keywords:** active layer; eastern Siberia; evapotranspiration; rainfall in previous year; snow start and disappearance.

## Introduction

The Eurasian continent has been a major topic of studies on land-surface-atmosphere interaction and the corresponding impact on not only the adjacent regional climate, such as Asia monsoon (Liu and Yanai 2002) and Arctic climate (Saito et al. 2001, Gong et al. 2007), but global climate change (Bonan et al. 1992, Yasunari et al. 1991). Especially, the variation in water cycle components in cold regions, containing rainfall, snow cover, soil moisture and frozen ground rich with ice, is a distinctive feature of the continental climate systems and has a delayed and durable influence on the overlying atmosphere through the land-surface fluxes of heat and moisture.

In eastern Siberia, which contains vast areas of permafrost, snow melt water directly contributes to the runoff of large rivers (Peterson et al. 2002, Ye et al. 2004) and evapotranspiration via soil moisture and photosynthesis in boreal forest following snow disappearance (Ohta et al. 2001, Sugimoto et al. 2003). These marked variations in water circulation play important roles in climatic feedback by modifying atmospheric anomalies. Thus, the preceding rain and snow conditions are very important for understanding variations in both the basin- and continental-scale water cycle and the climate system of neighboring regions. For instance, several statistical analyses have demonstrated that the timing of snow disappearance and increasing surface temperature in eastern Siberia is one of the possible candidates for long memory of an atmospheric anomaly from winter arctic oscillation and subsequent summer atmospheric circulation over the East Asia (Ogi et al. 2003, Arai & Kimoto 2005). However, few studies have investigated interactions between snow, permafrost, and climate or interannual variations in permafrost related hydrothermal conditions and water and energy cycle processes during the warm season that are possible effects of land memory in eastern Siberia.

The present study, therefore, aims to examine interseasonal impacts of water cycle components on subsequent land-surface processes, mainly focusing on the relationship between permafrost conditions and hydro-climatic components, such as rainfall in pre-winter, snow depth, snow starting timing in early winter and disappearance timing in spring at Yakutsk area in the central Lena River basin, based on observational meteorological data for recent decades. Our analysis is then extended to reveal the durable relationship and processes between these hydrothermal components influenced on the permafrost conditions and interannual variations in surface energy balance, using detailed land-surface energy balance model simulation.

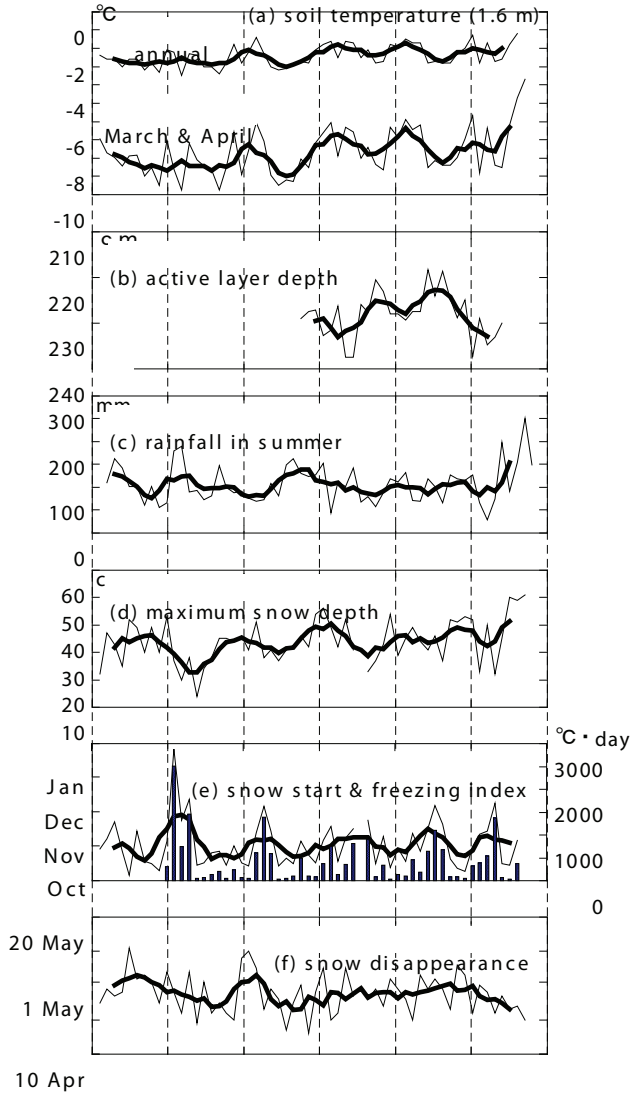


Figure 1. Long-term variations in hydrothermal components; (a) mean annual and minimum (average in March and April) soil temperature at 1.6 m depth at Pokrovsk, (b) active layer depth at Pokrovsk, (c) rainfall amount from July to September at Yakutsk, (d) maximum snow depth at Yakutsk, (e) snow start date with more than 10 cm snow depth (line) and freezing index until the date (bar), and (f) snow disappearance date at Yakutsk from 1950 to 2007. Bold lines denote 5–year running mean.

## Data and Methods

We used the routine observational data at Yakutsk (62.01°N, 129.43°E) and Pokrovsk (61.48°N, 129.15°E) from a dataset of the Baseline Meteorological Data in Siberia Version 4 (BMDS; Suzuki et al. 2006). The dataset contains daily values of air temperature (°C), precipitation (mm), snow depth (cm) and soil temperature from 40 to 320 cm depth (°C) over a 19-year period (1986–2004). We used soil temperature data at only Pokrovsk since the data at Yakutsk shows strong influences of anthropogenic disturbances. After 2004, daily data was added from a dataset of the NCDC Global Summary of Day up to September 2007. Past data from 1950 to 1985 are added utilizing the Global

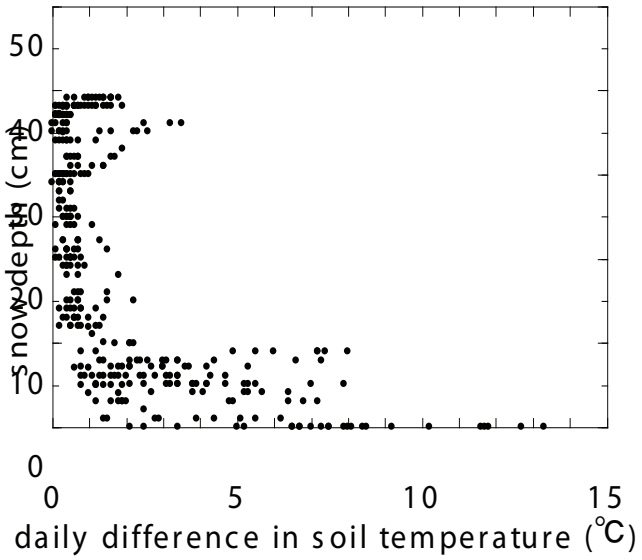


Figure 2. Relationship between daily difference in soil temperature at surface at larch forest site and daily snow depth at Yakutsk from October to December during four winters (2003–2006).

Summary of Day for daily air temperature, the Global Synoptic Climatology Network of the former USSR (NCDC D9290C) dataset for daily precipitation, the Historical Soviet Daily Snow Depth (HSDSD) dataset for daily snow depth, and Roshydromet station data for monthly soil temperature. Based on the snow depth data, the first date of 0 cm of snow depth in each spring was defined as "snow disappearance date" and the first date of more than 10 cm of snow depth in early winter with lasting snow cover throughout the winter was defined as "snow start date" since this quantity of snow accumulation acts as an effective layer of thermal insulation.

The intensive hydrometeorological observation at larch forest at Spasskaya-pad, Yakutsk, Russia has been ongoing since 1998 by GAME-Siberia project and it continues up to the present. We used several components of the dataset from 1998 to 2007 for the present study. That is, soil temperature in the active layer (0, 0.1, 0.2, 0.4, 0.8, and 1.2 m depth) and volumetric soil moisture content (0.1, 0.2, 0.4, 0.6, and 0.8 m depth).

Before 1998, there is no information on water and energy balance conditions at the larch forest site. Thus, we used estimated surface energy flux calculated by a one-dimensional land surface model (Yamazaki et al. 2004). The model includes three submodels; vegetation, snow cover, and soil. The model divided the canopy into two layers and then represented the fluxes above and within the canopy. The model was applied to the larch forest site at Yakutsk. Daily forcing meteorological quantities of each grid were reconstructed based on the BMDS dataset from 1986 to 2000. Using the daily forcing data, the model simulated hourly water and energy fluxes above and within the forest. The more detailed settings for estimating energy and water flux using the model are documented in Yamazaki et al.

(2007). Yamazaki et al. (2007) demonstrated that the model could reasonably estimate diurnal and seasonal variations in surface energy fluxes at the larch forest.

## Results and Discussions

*Interannual variations in hydrothermal components*

Figure 1 shows interannual variations in hydrothermal components in relation to permafrost conditions at Yakutsk and Pokrovsk sites from 1950 to 2007. Rainfall and snow amounts and variations show hardly any differences between Yakutsk and Pokrovsk.

Soil temperature variation at 1.6m depth indicates decadal fluctuations (Fig. 1a); that is, high temperature peak in 1971, 1981, 1991, and 2000 and low peak in 1966, 1974, 1988, 1994 and 2004. Soil temperatures in March and April at Pokrovsk show annual minimum value contributing to the amplification of the interannual variation in mean annual temperature. The active layer depth calculated by daily soil temperature data at Pokrovsk from 1977 to 2004 (Fig. 1b) has significant positive correlation with mean annual soil temperature ($R = 0.65$, $p < 0.001$). Deeper thawing occurred in early 1980s and early 2000s, corresponding with the warmer soil temperature.

Interannual variation in soil temperature has significant relationship with snow accumulation and its timing rather than rainfall amount in pre-winter (Fig. 1c). Maximum snow depths at Yakutsk (Fig. 1d) range between 15 cm and 50 cm. Basically, years with slow snow depths tend to show a decrease in annual minimum soil temperature ($R = 0.58$, $p < 0.001$). The significant relationship between soil temperature and snow depth indicates that variations in the timing and duration of the seasonal snow cover result in the ground thermal regime during winter (Frauenfeld et al. 2004, Zhang 2005). Snow start date with more than 10 cm of snow depth (Fig. 1e) fluctuates between early October and late January at Yakutsk. As shown in Fig. 2, a decrease in soil temperature is effectively enhanced by the longer duration of shallower snow depth with less than 10 cm during early winter (October to December) at Yakutsk. In fact, a large freezing index until the date with 10 cm of snow depth had significant impacts on the decrease in soil temperature. Namely, years with late timing of snow accumulation have longer and greater freezing intensity so that the soil temperature decreases significantly. It suggests that the thin snow cover has an effective cooling effect on the ground thermal regime when the air temperature is below 0°C until sufficient snow accumulation occurs. Also, soil temperatures tend to sustain cooling anomalies for several years after the large decrease in soil temperatures such as from 1973 to 1976, from 1985 to 1988, from 1994 to 1998, and from 2001 to 2004. During these periods, rainfall in pre-winter as well as snow depth was below average in most of the years. The result implies that durable cooling anomalies likely occurred under dry soil condition.

The snow disappearance date (Fig. 1f) shows relatively short interannual variation between mid-April to early May. There is no significant relationship with maximum snow depth ($R = 0.20$, ns). According to Iijima et al. (2007) and Gong et al. (2007), the snow disappearance mainly depends on the atmospheric warming. The snow disappearance dateclosely relate with the date of soil thawing from surface to 80 cm depth at Pokrovsk, although no significant relationship with active layer depth which appears in September. It appears that the snow disappearance timing affects the soil thawing near the surface and also the soil moisture melting which directly affect evapotranspiration from vegetated surface.

Table 1. Correlation matrix of rainfall, snow timings, soil moisture and soil temperature during 1998 to 2006 at the larch forest site, Spasskaya-pad, Yakutsk.

| | Rain autumn | Snow start | Snow disap | Soil moisture | Soil temp |
|---|---|---|---|---|---|
| Rain autumn | 1.00 | | | | |
| Snow start | −0.18 | 1.00 | | | |
| Snow disap | −0.03 | 0.62 | 1.00 | | |
| Soil moisture | 0.87* | −0.80* | −0.35 | 1.00 | |
| Soil temp | 0.38 | −0.57 | −0.53 | 0.75* | 1.00 |

(*: $p < 0.05$)

Rain autumn – rainfall amount in pre-winter (July–September); Snow start – snow start date in previous year; Snow disp. – snow disappearance date; Soil moisture – volumetric soil moisture at 0–40cm depth in July and August; Soil temp. – soil temperature at 120 cm depth in July and August.

Figure 3 shows interannual variations in soil temperature and soil moisture at the larch forest site in Spasskaya-pad near Yakutsk during 1998 through 2007 and variations in snow depth and snow start and disappearance date at Yakutsk. It is found that both soil temperature during wintertime (which indicates intensity of freezing) and soil moisture content at the beginning of warm season show simultaneous interannual variations. That is, there are warmer and wetter years in 2000, 2005, and 2006, while colder and drier years in 1998, 2003, and 2004. Table 1 demonstrates a correlation matrix between rainfall in pre-winter (from July to September), snow start date in previous winter, snow disappearance date, soil temperature and moisture in summer. As described above, it appears that there is a significant correspondence in interannual variation between soil temperature and soil moisture. It implies that thermal condition in active layer is strongly connected with hydro-climatic variations. In addition, rainfall in pre-winter has strong correlation with soil moisture in next summer. It appears that rainfall remains in the active layer through winter and possibly acts as climatic memory of soil moisture. Moreover, both snow start and disappearance timings have negative correlations with soil temperature and moisture. It might be suggested that snow start timing determines intensity of freezing in active layer during early winter, and wet condition during winter also affects soil freezing.

As shown in long-term variation in soil temperature at Pokrovsk, interannual warming and cooling trends are found at the larch forest site. These trends in successive years are basically due to the similar snow and rainfall conditions. These continuous hydro-climatic conditions may maintain

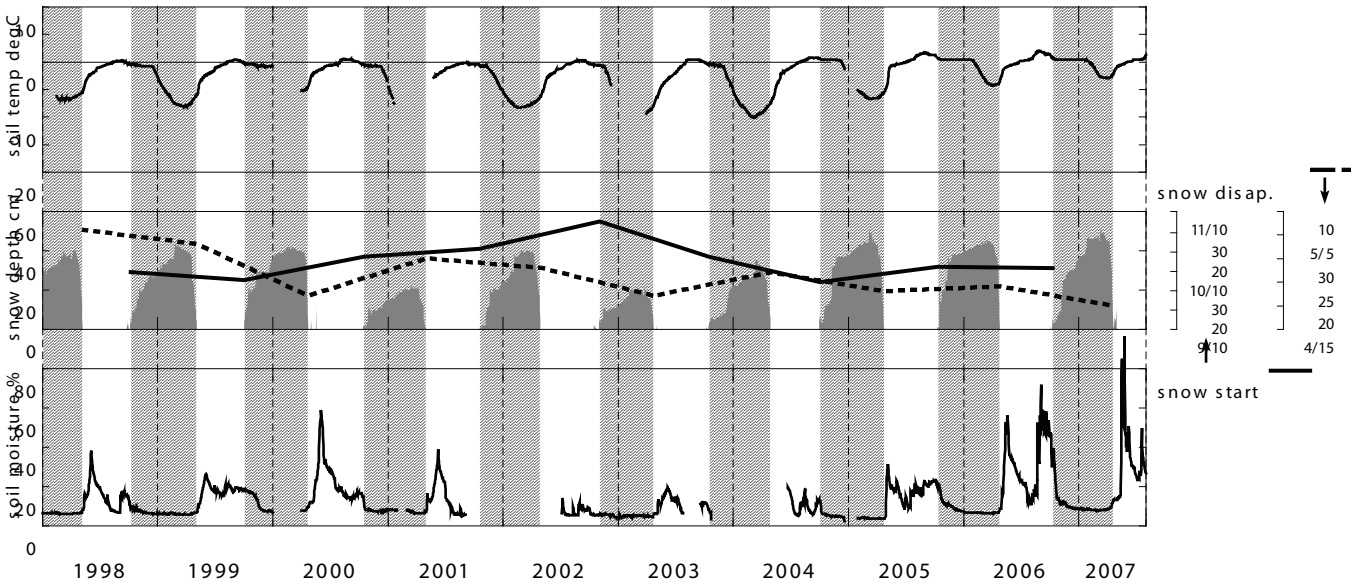


Figure 3. Nine-year (1998–2007) variation in (a) soil temperature, (b) snow depth, and (c) soil moisture. Soil temperature (120 cm depth) and soil moisture (10 cm depth) were observed at larch forest site in Spasskaya-pad, Yakutsk. Snow depth was observed at Yakutsk. Bold and dotted lines denote snow start date and snow disappearance date, respectively. Dark area denotes snow cover period in each winter.

the trend of previous soil temperature anomalies through reemergence in deeper soil layer through soil moisture anomalies (Schaefer et al. 2007).

*Snow timing and evapotranspiration in spring*

Estimated monthly average of latent heat flux above the larch forest canopy from 1986 to 2000 and its standard deviation are shown in Figure 4. Annual maximum appears in June or July due to the maximum activity of evapotranspiration from the forest. Interannual variation in latent heat flux is less variable in comparison with variation in precipitation. This tendency was recently confirmed by eight-year (from 1998 to 2006) variation in energy flux above the larch forest canopy at the same station based on micro-meteorological observation (Ohta et al. 2006). Though there is a small variation in latent heat flux, the maximum variation appears in May with the largest standard deviation (±6 $Wm^{-2}$).

Figure 5 shows the relationship between estimated latent heat flux in May normalized by net radiation above the larch forest canopy by the model and both snow starting date in previous winter and snow disappearance date from 1986 to 2000. It appears that both timings have significant negative correlations (snow start date: $R$ = -0.76, $p < 0.01$, snow disappearance date: $R$ = -0.59, $P < 0.05$). The relationship with snow disappearance date directly corresponds to the beginning of transpiration since the timing of soil warming after snow disappearance determines foliating of plants at forest floor and trees and also determines timing of soil thawing for supplying plant available soil moisture, which parameterized in the model (Yamazaki et al. 2007). On the other hand, the significant relationship with snow start date in previous winter suggests that the warmer (cooler) anomaly of soil temperature during winter remains until

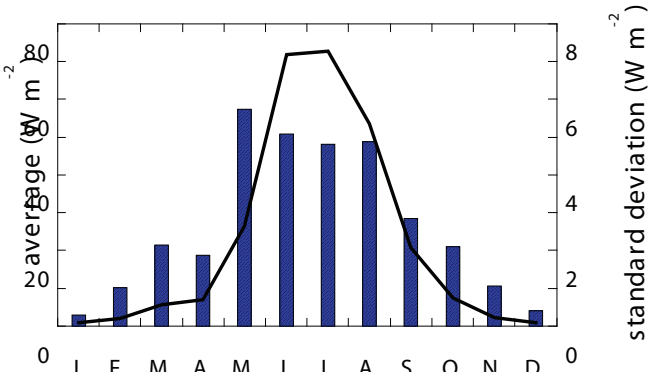


Figure 4. Monthly average and standard deviation of latent heat flux above the canopy at larch forest from 1986 to 2000 simulated by one-dimensional land surface model.

snow disappearance and also cause the earlier (later) timing of soil thawing. Thus, the relationship implies that soil temperature modulated by snow timing strongly influence the evapotranspiration processes in the early growing season.

Figure 6 exhibits the difference of hydrothermal conditions (mainly years with either high or low latent heat fluxes in May) from the difference between the average of the four high years (low years) and the average of the four prior years (same). These values were averaged using each four years (high years: 1990, 1992, 1994, and 2000; low years: 1987, 1989, 1995, and 1998) and the preceding four years in each case. The difference in latent heat flux in May between high and low years exceeds 10 W $m^{-2}$ (Fig. 6a). Snow depth difference is apparent during snow disappearance timing (Fig. 6b). Namely, earlier melting appears in high years. Inversely, snow start timing in early winter shows earlier snow accumulation in high years. In addition, deeper snow depth appears during the winter two years ago. During the previous

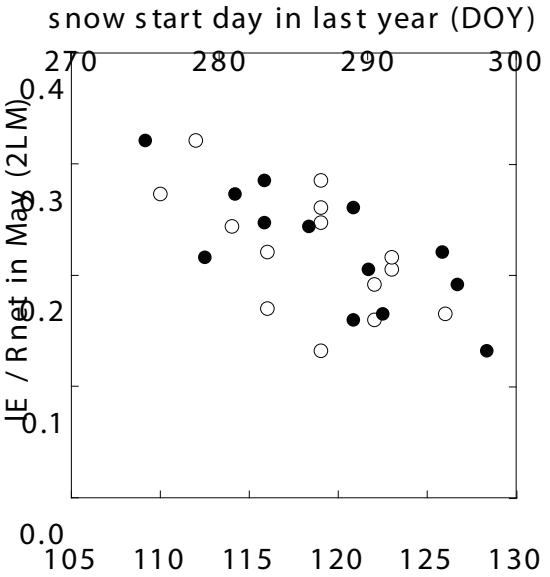


Figure 5. Relationship between snow timings and estimated mean monthly evapotranspiration ratio (latent heat/net radiation). Open and solid circles denote snow start date and snow disappearance date, respectively.

warm season, rainfall in the high years is larger than in low years (Fig. 6c). Due to the large difference in snow depth in the winter two years ago and earlier snow accumulation in previous winter, soil temperature shows large difference during the successive two winters (Fig. 6d). It should be noted that the warmer temperature continuously lasts throughout two years in deeper layer. These durable warming tends to enhance earlier thawing of frozen layer (Fig. 6e). Thus, it might be earlier start of evapotranspiration due to earlier soil moisture supply. Ohta et al. (2006) exhibited that there was a remarkable positive relationship between surface soil moisture and annual amounts of evapotranspiration. They also implied that the effects of snowfall from previous cold seasons and the permafrost conditions affect soil moisture into subsequent growing season and are important to the interannual variations in evapotranspiration.

## Conclusions

The present study investigates climatological features of hydrothermal components in the Yakutsk region and its relationship with evapotranspiration during subsequent warming season. The results of the present study are summarized as follows:

1. Long-term variation in soil temperature at Pokrovsk indicates decadal fluctuations and has significant relationship with snow accumulation and its timing. The drier climate with later snow accumulation may produce an anomaly of lower soil temperature and thus shallower active layer.

2. There is a significant correspondence in interannual variation between soil temperature and soil moisture at the larch forest site. In addition, both snow start and disappearance dates have negative correlations with them.

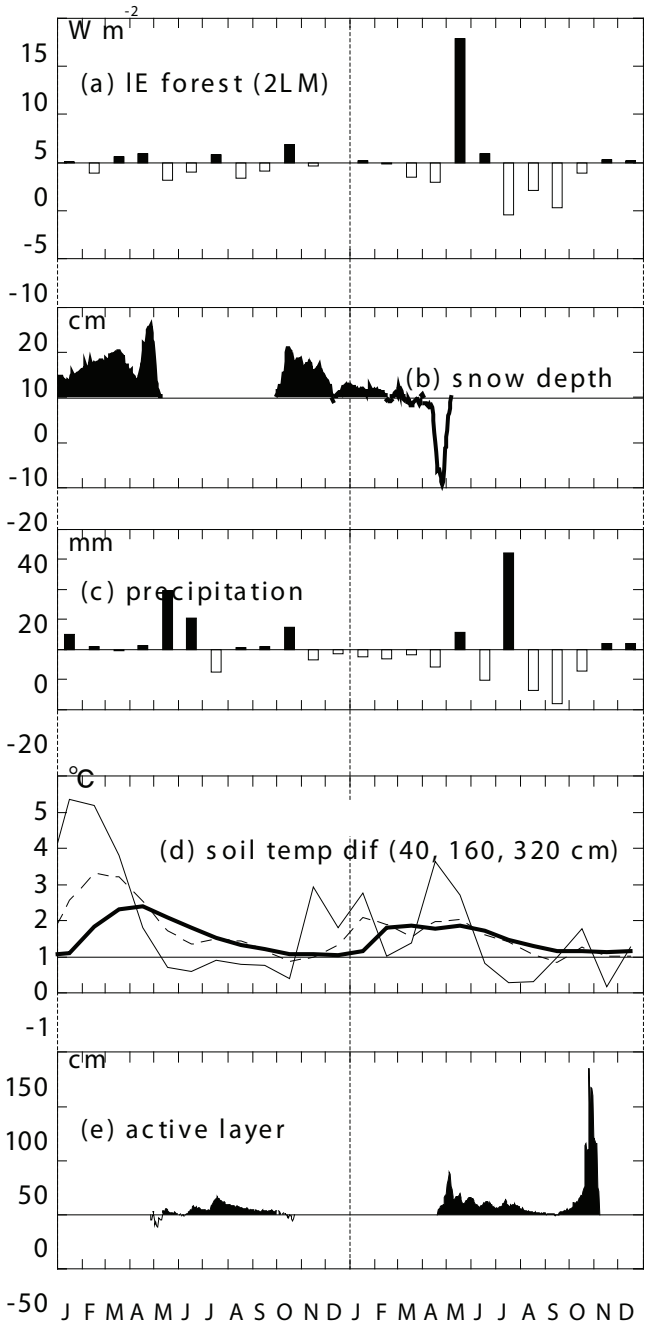


Figure 6. Differences of hydrothermal conditions for the average of the four highest years and the average of the previous for years for high evapotranspiration in May (left panel) and the same for low evapotranspiration in May (right panel); (a) latent heat flux from forest canopy by one-dimensional land surface model, (b) daily snow depth at Yakutsk, (c) monthly rainfall at Yakutsk, (d) monthly soil temperature at 40 cm (thin line), 160 cm (broken line), and 320 cm (bold line) depths at Pokrovsk, and (e) daily thawing depth at Pokrovsk.

3. Both snow start in previous winter and snow disappearance have significant negative correlation with latent heat flux from the boreal forest in May simulated by a one-dimensional land surface model associated with the start of subsequent plant growing season.

## Acknowledgments

We extend our appreciation to Prof. B. Ivanov of the Institute for Biological Problems of Cryolithozone for allowing us the opportunity to investigate in Siberia. This work was financially supported by Institute of Observational Research for Global Change, Japan Agency of Marine-Earth Science and Technology.

## References

Arai, M. & Kimoto, M. 2005. Relationship between springtime surface temperature and early summer blocking activity over Siberia. *Journal of Meteorological Society of Japan* 83: 261-267.

Bonan, G. B., Pollard, D. & Thompson S. L. 1992. Effects of boreal forest vegetation on global climate. *Nature* 359 (6397): 716-718.

Frauenfeld, O.W., Zhang, T. & Barry R.G. 2004. Inter-decadal changes in seasonal freeze and thaw depths in Russia, *Journal of Geophysical Research* 109: D05101, doi:10.1029/2003JD004245.

Gong, G., Cohen, J., Entekhabi, D. & Ge, Y. 2007. Hemispheric-scale climate response to Northern Eurasia land surface characteristics and snow anomalies. *Global and Planetary Changes* 56: 359-370.

Iijima, Y., Masuda, K. & Ohata, T. 2007. Snow disappearance in Eastern Siberia and its relationship to atmospheric influences. *International Journal of Climatology* 27: 169-177.

Liu, X, & Yanai, M. 2002. Influence of Eurasian spring snow cover on Asian summer rainfall. *International Journal of Climatology* 22: 1075-1089. doi:10.1002/joc.784.

Ogi, M., Tachibana, Y. & Yamazaki, K. 2003. Impact of the wintertime North Atlantic Oscillation (NAO) on the summertime atmospheric circulation. *Geophysical Research Letter* 30(13): 1704. doi:10.1029/2003GL017280.

Ohta, T., Hiyama, T., Tanaka, H., Kuwada, T., Maximov, T. C., Ohata, T. & Fukushima, Y. 2001. Seasonal variation in the energy and water exchanges above and below a larch forest in eastern Siberia. *Hydrological Processes* 15: 1459-1476.

Ohta, T., Kuwada, T., Dolman, H., Moors, E., Maximov, T. C., Kononov, A.V. & Yabuki, H. 2006. Interannual variation in water and energy exchanges at a larch forest in Spasskaya Pad, eastern Siberia. *International Workshop on $H_2O$ and $CO^2$ Exchange I Siberia:* 67-70.

Peterson, B.J., Holmes, R.M., McClelland, J.W., Vorosmarty, C.J., Lammers, R.B., Shiklomanov, A.I., Shiklomanov, I.A. & Rahmstorf, S. 2002. Increasing river discharge to the Arctic Ocean. *Science* 298: 2171-2173.

Saito, K., Cohen, J. & Entekhabi, D. 2001. Evolution of atmospheric response to early-season Eurasian snow cover anomalies. *Monthly Weather Review* 129(11): 2746-2760.

Schaefer, K.M., Zhang, T., Tans, P.P. & Stockli R. 2007. Temperature anomaly reemergence in seasonally frozen soils. *Journal of Geophysical Research* 112: D20102, doi:10.1029/2007JD008630.

Sugimoto A., Naito, D., Yanagisawa, N., Ichiyanagi, K., Kurita, N., Kubota, J., Kotake, T., Ohata, T., Maximov, T.C. & Fedorov, A.N. 2003. Characteristics of soil moisture in permafrost observed in East Siberian taiga with stable isotopes of water. *Hydrological Processes* 17: 1073-1092.

Suzuki, R., Razuvaev, V.N., Bulygina, O.N. & Ohata, T. 2006. *Baseline Meteorological Data in Siberia Version 4*. Institute of Observational Research for Global Change, Japan Agency for Marine-Earth Science and Technology, Yokosuka, Japan.

Yamazaki, T., Yabuki, H., Ishii, Y., Ohta, T. & Ohata, T. 2004. Water and energy exchanges at forest and a grassland in Eastern Siberia evaluated using a one-dimensional land surface model. *Journal of Hydrometeorology* 79: 1107-1118.

Yamazaki, T., Ohta T., Suzuki R. & Ohata T. 2007. Flux variation in a Siberian taiga forest near Yakutsk estimated by a one-dimensional model with routine data, 1986–2000. *Hydrological Processes* 21: 2009-2015, doi:10.1002/hyp.6708.

Yasunari, T., Kitoh, A. & Tokioka, T. 1991. Local and remote responses to excessive snow mass over Eurasia appearing in the northern spring and summer climate – a study with the MRI GCM. *Journal of the Meteorological Society of Japan* 69: 473-487.

Ye, H., Yang, D., Zhang, T., Zhang, X., Ladochy, S. & Ellison M. 2004. The impact of climatic conditions on seasonal river discharges in Siberia. *Journal of Hydrometeorology* 5: 286-29

Zhang, T. 2005. Influence of the seasonal snow cover on the ground thermal regime: An overview. *Reviews of Geophysics* 43: RG4002, doi:10.1029/2004RG000157.

# Topographical Controls on the Distribution and Size of Rock Glaciers in the Central Brooks Range, Alaska

Atsushi Ikeda
*Graduate School of Life and Environmental Sciences, University of Tsukuba*
Kenji Yoshikawa
*Water and Environmental Research Center, University of Alaska Fairbanks*

## Abstract

Distribution, morphology, internal structure and thermal conditions of rock glaciers were studied in the central Brooks Range, Alaska, an area characterized by continuous permafrost. A positive size correlation was found between the active talus-derived rock glaciers and the source rock walls. The source rock walls of the inactive rock glaciers were limited to a relatively small size. These topographical relationships indicate that direct debris supply from the rock walls at least partly controls the size and activity of these rock glaciers. On six talus-derived rock glaciers, low mean annual ground surface temperatures (-3°C to -7°C) were monitored, and similar low ice content was indicated by DC resistivity measurements. The results approve the interpretation of the topographical analysis based on the assumption that a number of rock glaciers have similar creep property and composition. In contrast, rock glaciers interacting with glacial processes enlarged below the relatively small rock walls.

**Keywords:** Brooks Range; continuous permafrost; DC resistivity; GIS; rock glacier; rock wall.

## Introduction

Distribution, size, and structure of rock glaciers probably reflect the complex input of debris, ground water, and snow which is controlled by local climate and geology. Rock glaciers have been often classified into active and inactive types to discuss the climatic and geological factors that control their long-term movement (e.g., Wahrhaftig & Cox 1959, Calkin et al. 1987, Ikeda & Matsuoka 2002). Active rock glaciers are moving downslope by internal ice deformation. Inactive rock glaciers are stagnant but still contain ice. Barsch (1992) suggested two kinds of inactivity: climatic and dynamic. The melting of ice in a rock glacier accounts for climatic inactivity. Dynamic inactivity results from reducing shear stress within the perennially frozen layer in a rock glacier, which is caused either by a temporal decrease in debris supply or by a downslope decrease in slope gradient. In continuous permafrost areas, where climatic inactivation rarely occurs, the inactivation of rock glaciers has been attributed to the dynamic concept (e.g., Calkin et al. 1987, Solid & Sørbel 1992).

Although size relationships between rock glaciers and their debris source (i.e., rock walls) have indicated quantitative rates of debris production and transportation in mountainous periglacial environments (e.g., Barsch 1977, Barsch & Jakob 1998, Humlum 2000), debris supply has been rarely explored to discuss the size and activity of rock glaciers (cf. Frauenfelder et al. 2003). A topographical analysis by Frauenfelder et al. (2003) indicated that the size of rock glaciers appears to reflect the temperature conditions rather than the size of the debris source. In addition, variable ice content in rock glaciers should be tested further to discuss this matter (Humlum 2000).

In this study the distribution and size of rock glaciers near Atigun Pass in the central Brooks Range, Alaska, were re-examined using recent technologies (see also Calkin et al. 1987, for the previous achievement), because the area characterized by simple geology and ubiquitous permafrost appeared suitable for testing 'dynamic' controls from topographical analysis. In addition, temperature conditions and internal structure were studied to assist in the

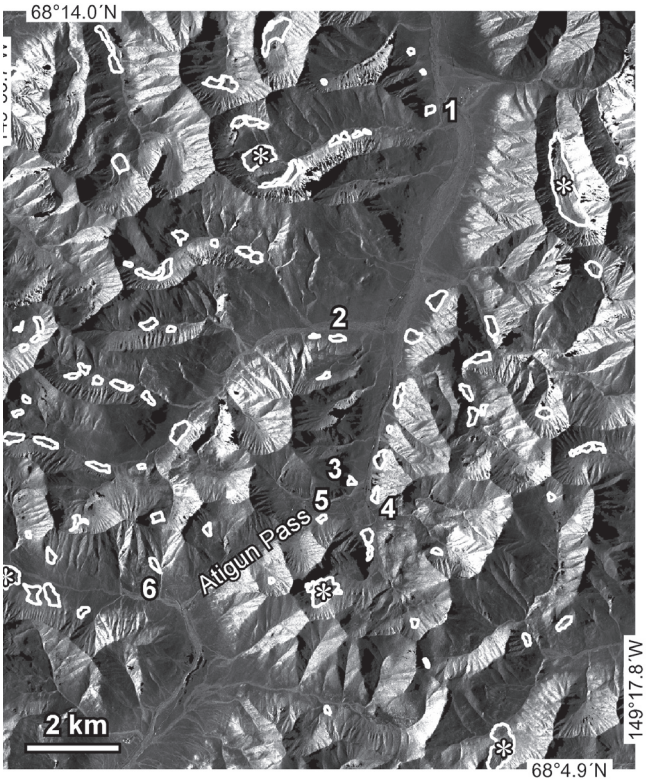


Figure 1. Distribution of rock glaciers (outlined in white) in the Atigun Pass area. An asterisk indicates a rock glacier overflowing from a cirque. The numbered rock glaciers underwent geophysical measurements.

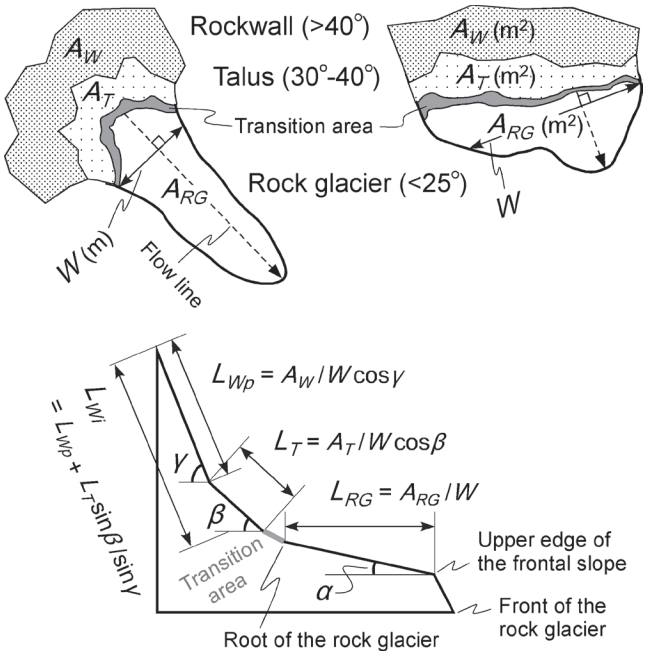


Figure 2. Definition of morphological parameters discussed in the text. Upper figures are plan views and lower figure is a cross section.

interpretation of the topographical analysis.

Atigun Pass lies on the continental divide between the Yukon Basin and Arctic basins (Fig. 1). Permafrost continuously underlies the study area having low mean annual air temperature (MAAT < -7°C) and low precipitation (400–700 mm $a^{-1}$). Cirque glaciers only remain on the north-facing slopes below the highest peaks ,which reach 2000 m above sea level (a.s.l.), whereas the area was mostly covered with glaciers until the Late Glacial (Hamilton & Porter 1975, Ellis & Calkin 1979). The area consists of sandstone or conglomerate, interbedding shale. The methods of this study are mapping on a digital elevation model (DEM), temperature monitoring on the ground surface and one- and two-dimensional (1D and 2D) geoelectrical resistivity measurements.

## Distribution and Morphology

*Mapping and measurement of terrain parameters*

Using GIS software (ArcGIS ver. 9.2, ESRI Inc., USA), the distribution of rock glaciers was traced on 10 m grid DEM. Topographical parameters assumed to represent climatic and mechanical conditions of rock glaciers (altitude, length, slope angle, area, etc.) were measured for 99 rock glaciers which were clearly identified in 1/63,000 aerial photographs in a selected 13.8 km × 16.5 km area (Fig. 1). The areas of a source rock wall and a talus slope were unambiguously defined by the slope angle: a slope steeper than 40° as a rock wall and a slope between 30° and 40° as a talus slope. A relatively short slope 25°–30° below a talus slope indicated sedimentation by debris flows and avalanches; transportation by permafrost creep can also be responsible for such slope relaxation. Thus, the uppermost point of a slope gentler than 25° was defined as the root of a rock glacier. Besides the 99 rock glaciers, two rock glaciers developed from conspicuous terminal moraines in the selected area. Both of them were excluded from the measurements because they had no direct connection with the cirque walls.

The measured parameters for a rock glacier were: along the central flow line, the altitudes at the upper and lower ends (i.e., root and front), altitude of the upper edge of the frontal slope, horizontal length and aspect of the front (Fig. 2). Horizontal width ($W$) at the root and horizontal area ($A_{RG}$) were also measured. The average slope angle of the upper surface ($\alpha$) was calculated from the horizontal length and the altitudes at the root and edge, and the average length ($L_{RG}$) from $W$ and $A_{RG}$. The measured parameters for a source slope were the horizontal areas of the source rock wall ($A_W$) and the underlying talus slope ($A_T$), and the average angles of the talus slope ($\beta$) and the rock wall ($\gamma$). The present size of a source rock wall was represented by the average length of a source rock wall ($L_{Wp}$), which is $A_W$ normalized by $W$ (see Fig. 2). In addition, the average length of an initial source rock wall after the deglaciation ($L_{Wi}$) was roughly estimated from the average length of the underlying talus slope ($L_T$), which probably buried the lower part of the initial rock wall (see Fig. 2 for the calculation of $L_{Wi}$). Additional data on altitudes and aspect were obtained from 61 rock glaciers around the selected area.

The activity status of rock glaciers (i.e., active or inactive) must be determined by repeated geodetic surveys in the strict sense (Roer & Nyenhuis 2007). In many studies, however, the activity status has been presumed from visual features (e.g., Wahrhaftig & Cox 1959, Calkin et al. 1987, Ikeda & Matsuoka 2002). In this study, rock glaciers having a frontal slope steeper than 35° were classified into the active type and those having a frontal slope gentler than 35° into the inactive type. According to Ikeda & Matsuoka (2002), this classification mostly guarantees the inactive type, although the rock glaciers classified into the active type inevitably include some inactive rock glaciers (see also Roer & Nyenhuis 2007). If a frontal slope mostly steeper than 35° showed partly subsided form (i.e., having a much gentler and thinner part) and a rounded upper edge, the rock glacier was tentatively classified into the active/inactive type. In addition, two rock glaciers were also classified into the active/inactive type, because of the significant disagreement between the steep frontal slopes (c. 10 m high) on the aerial photographs and the gentle angles calculated from the DEM.

*Distribution*

The rock glaciers in the selected area were classified into 44 active, 40 inactive, and 15 active/inactive rock glaciers. The fronts of the rock glaciers were distributed in all aspects over elevations between 970 m a.s.l. and 1730 m a.s.l. (Fig. 3). The roots of the rock glaciers had a distribution pattern similar to the fronts, ranging between 1015 m a.s.l. and 1835 m a.s.l. The source rock walls mostly faced the same direction as the rock glaciers, whereas the sources of large rock glaciers often faced several directions. The upper limit of the distribution was 100–200 m lower than the major mountain ridges, and on the north-facing slopes it corresponded to

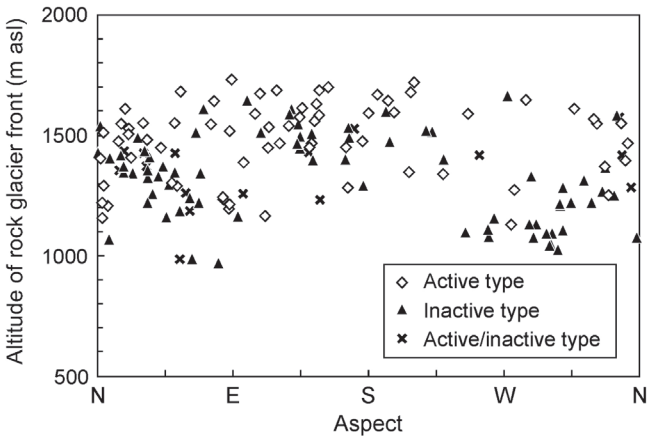


Figure 3. Distribution of the fronts of rock glaciers in the Atigun Pass area.

the present glacial equilibrium line. The lower limit of the distribution corresponded to the piedmont line. The active rock glaciers were distributed at relatively higher altitudes than the inactive rock glaciers, whereas the distributions were largely overlapping except for the west-facing slopes.

*Sizes of rock glacier and source rock wall*

The topographical parameters were analyzed in terms of the following concepts. The deformation of a rock glacier can be represented by the density, acceleration by gravity, thickness, sine of slope angle, and a creep parameter depending on temperature and structure, using a pseudoplastic flow law for glacier ice (e.g., Wagner 1992). In addition, the long-term (i.e., more than several hundred years) deformation has been assumed to result in a certain length of the rock glacier balancing with debris supply (Olyphant 1983, 1987, Haeberli et al. 1999).

In this study, the $L_{RG}$ values were compared with the $L_W$ (i.e., $L_{Wi}$ or $L_{Wp}$) values. This was because the size of the rock walls was preliminarily assumed to mainly control the rate of debris supply (determining the thickness of the rock glacier under the balancing condition), although the rate reflected various conditions of the rock wall, such as size, strength, temperature variation, and water content. The assumption was made because parameters other than size were too difficult to evaluate on a large number of rock walls.

The active rock glaciers showed a linear relationship between $L_W$ and $L_{RG}$, if large rock glaciers overflowing from a cirque were excluded (Fig. 4). In contrast, such a relationship was lacking for inactive rock glaciers. Even larger inactive rock glaciers ($L_{RG}$ > 200 m) had small $L_W$ values. This pattern was more distinct in the $L_{Wp}$–$L_{RG}$ diagram than that of $L_{Wi}$–$L_{RG}$, because the ratios of $L_{Wi}$ to $L_{Wp}$ were, on average, 2:1 for the active type and 3:1 for the inactive type. This indicated the thickening of the talus slopes above the inactive rock glaciers.

The three longest rock glaciers ($L_{RG}$ = 950, 1140 m and 1680 m), all of which overflowed from a cirque, are not within Figure 4a. The longest one was active and had a huge source ($L_{Wi}$ = 2840 m and $L_{Wp}$ = 1940 m); the others were inactive or active/inactive and had relatively small sources (e.g., $L_{Wi}$ = 800 m and 1160 m). Such rock glaciers probably

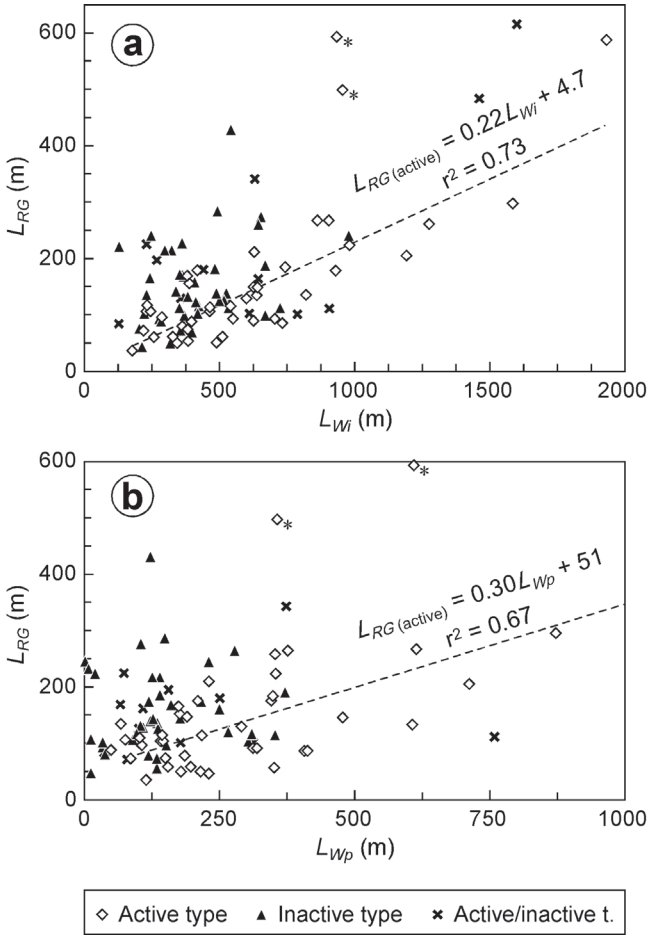


Figure 4. Relationship between average lengths of source rock walls ($L_W$) and rock glaciers ($L_{RG}$). Lengths of (a) initial rock walls ($L_{Wi}$) and (b) present rock walls ($L_{Wp}$) are examined. See Figure 2 for definition of parameters. *Data of rock glaciers overflowing from a cirque.

included significant amounts of debris that had once deposited as moraines. In addition, glacial ice was often observed at the roots of such large rock glaciers in the active status, which originated from altitudes close to the glacial equilibrium line (Calkin et al. 1987).

The upper surface of the rock glaciers sloped from 2° to 25°. The ranges of $\alpha$ were almost equal between the active type (12° ± 4°) and inactive type (13° ± 4°). The $\alpha$ values of the rock glaciers longer than 400 m also ranged from 8° to 15°. Thus, slope angle appeared to be a minor factor for inactivation and outgrowing.

## Temperature and Internal Structure

*Ground surface temperature*

Ground surface temperatures were monitored on six rock glaciers (A1–6) using miniature data loggers, Thermo Recorder TR-51A (T & D, Japan) (see Fig. 1 for the location). On five rock glaciers (A1–4, A6), a data logger was placed at the surface that was 30–40 m distant from the upper edge of the frontal slope in mid May 2005. A data logger was also placed near the talus foot on A5 rock glacier in late August

Table 1. Mean annual ground surface temperature (MAGST) and DC resistivity stratigraphy of rock glaciers. ρ = calculated resistivity, D = depth of the layer base and AB/2 = half length of the sounding profile (roughly equal to the maximum depth of the sounding). Frontal altitude and aspect for each rock glacier are also displayed.

| Site | Altitude | Aspect | MAGST | DC resistivity stratigraphy | | | | | |
|---|---|---|---|---|---|---|---|---|---|
| | | | | First layer | | Second layer | | Third layer | AB/2 |
| | (m a.s.l.) | (degree) | (°C) | ρ (kΩm) | D (m) | ρ (kΩm) | D (m) | ρ (kΩm) | (m) |
| A1 | 970 | 80 | −5.1 ± 0.4 | 8.4–1.6 | 3.0 | 25 | 19 | 0.22 | 50 |
| A2 | 1065 | 5 | −3.3 ± 0.4 | 0.3 | 0.7 | 52 | 35 | 20 | 100 |
| A3 | 1165 | 110 | −3.6 ± 0.2 | 1.3 | 2.7 | 38 | | | 64 |
| A4 | 1155 | 265 | −6.6 ± 0.3 | 0.8 | 1.6 | 19 | | | 80 |
| A5 | 1345 | 15 | −4.8 ± 0.3 | 1.1 | 2.8 | 41 | | | 50 |
| A6 | 1230 | 145 | −3.9 ± 0.3 | 0.8 | 2.2 | 24 | 16 | 13 | 64 |

2005. These loggers recorded surface temperatures under a 2–4 cm thick clast at one-hour intervals with a resolution of 0.1°C until the beginning of July 2007. Then, the mean annual ground surface temperature (MAGST) values were determined.

The lack of daily variations in the ground surface temperatures indicated that snow covered the lower part of the rock glaciers from late September to mid May, whereas snow remained near the north-facing talus foot at 1350 m a.s.l. until mid June. The variations in the observed winter temperatures were largely different between the sites. The difference in the temperatures, however, hardly correlated with the elevation of the sites (see Table 1 for the altitudes), which implied irregular distribution of snow cover. As a result, MAGST on the rock glaciers ranged from −3°C to −7°C without correlation with the elevation (Table 1).

*DC resistivity*

On the six rock glaciers (A1–6), 1D DC resistivity measurements were performed in late July 2005 with the SYSCAL R1 resistivity meter (Iris Instruments, France). All of the rock glaciers were talus-derived and had no contact with glaciers during the Holocene (Ellis & Calkin 1979). The setting of the electrodes followed the Schlumberger array. Modeled resistivity curves fitting with measured values were calculated with WinSev6 software (W_GeoSoft, Switzerland). To compare resistivity stratigraphies, the settings of the inversion analysis were fixed as described in Ikeda (2006). In addition, 2D DC resistivity distributions at a shallow depth (<10 m deep) were estimated by a tomographical method for three rock glaciers (A3–5). The electrode configuration followed the Wenner array. The measurements were carried out with a lightweight resistivity meter, Handy-ARM (OYO, Japan), in early July 2007. Then, we computed the 2D distributions of modeled DC resistivities with RES2DINV software (Geotomo Software, Malaysia), employing the same settings of the inversion analysis as those in Ikeda & Matsuoka (2006).

The 2D resistivity distributions showed low resistivities (1–16 kΩm) within the uppermost layer (<2 m deep), probably corresponding to the active layer. The resistivities near the surface in the 1D profiles, which largely depend on the surface material at the center of the survey profiles, were close to 0.3 kΩm on A2, 1 kΩm on A3–6 and 8 kΩm on A1 (Table 1). Vegetated thin soil on the surface resulted in such low surface resistivities for rock glaciers, because the shale part of the source rock walls produced relatively fine and weathering-susceptible clasts on the rock glaciers. The main components of the debris, however, appeared to be boulders. In fact, the average intermediate-axis diameter of 25 clasts that were measured at intervals of 0.5 or 1 m along a line on a less vegetated part ranged from 25–45 cm for A3–5 rock glaciers (cf. pebbly rock glaciers composed of much smaller debris in Ikeda & Matsuoka 2006).

The resistivities of the layers below 2–3 m deep (i.e., permafrost) were 20–50 kΩm in the 1D profiles (Table 1), whereas those in the 2D distributions increased from 4–16 kΩm at 3 m depth to 30–250 kΩm at 10 m depth. In the case of A4, the exponentially increasing resistivities toward the bottom of the tomogram indicated resistivities higher than 250 kΩm for the permafrost below the measurement limit. The 1D sounding profiles of A3–5 were too short to detect the third layer.

## Discussion and Perspectives

*Topographical controls through debris supply*

Topography of the mountain range roughly restricts the distribution of the rock glaciers. Besides the main divide and piedmont line of the mountain range (i.e., the uppermost and lowermost limits of the distribution), for example, the straight mountain slopes that lack enough concavity to lay rock glaciers strongly restricted the number of westbound rock glaciers above 1300 m a.s.l. (see Fig. 3). In the selected area, the area of the rock walls decreased from 8.8 km$^2$ on the north-facing slope (0°–45°, 315°–360°) to 3.7 km$^2$ on the south-facing slope (135°–225°), which may result in fewer rock glaciers on the south-facing slopes through less debris production from the rock walls (see Fig. 3).

The positive correlation between $L_{RG}$ and $L_W$ for the (talus-derived) active rock glaciers (Fig. 4) implies that the amounts of debris supply from the source rock walls control the size of these rock glaciers. This result is contrasted with that of a similar study in the Alps where such a relationship is unclear (cf. Frauenfelder et al. 2003). The correlation in this study partly

accounts for the bedrock geology that is much more uniform than the case in the Alps. In fact, such a correlation was found in the Alps for a small number of rock glaciers under a limited geological condition (Ikeda & Matsuoka 2006).

In Figure 4, the $L_{RG}$ values of the extremely long rock glaciers (overflowing from a cirque) are out of the linear trends for the active talus-derived rock glaciers. The lengths that appear not to balance with the relatively small rock walls are primarily attributed to former glacial deposits, which were probably incorporated into these rock glaciers. In addition, if these rock glaciers include glacial ice, the resulting high ice content also contributes to the large size in spite of low debris content. According to the field observation by Calkin et al. (1987), such interaction with glaciers probably occurred on large tongue-shaped rock glaciers in this area.

About two thirds of the data on the inactive rock glaciers (mostly shorter than 200 m) is plotted within the band of the talus-derived active type in the LW–LRG diagrams (Fig. 4). Thus, the difference in the classified activity is difficult to interpret from the size of the source rock walls alone. The LW values of the inactive rock glaciers, however, concentrate in relatively smaller values, which indicates the low potential of the debris supply. The talus thickening above the inactive rock glaciers, which was presumed from the difference in Figures 4a and 4b, is partly because the debris down-transportation by permafrost creep was terminated at the talus foots. This burial of the rock walls with the talus materials decreases the potential of the debris supply from the rock walls. The resulting small input of debris probably prevents the underlying rock glaciers from advancing further, although the initial cause of the inactivation remains unsolved.

As well as the data on the largest rock glaciers that were probably affected by glacial processes, the data on the large inactive and active/inactive rock glaciers (> 150 to 200 m in $L_{RG}$) in Figure 4 appear not to balance with the size of the source rock walls. This may indicate that the former rate of rock wall erosion per area was higher, or the present source slopes became smaller than the former slopes. Both processes can be responsible for the inactivation of the rock glaciers through decrease in debris supply, although we should exhibit additional data to discuss this matter, avoiding a vicious circle.

*Significance of topographical controls in the Brooks Range*

The inactivation and restriction of the lower distribution boundary found in Figure 3 cannot reasonably be attributed to the degradation and absence of permafrost in a study area that is classified continuous permafrost, although such phenomena mainly depend on the permafrost distribution and its temporal change in mid-latitude high mountains such as the Alps (e.g., Frauenfelder et al. 2001, Ikeda & Matsuoka 2002).

Additionally, Frauenfelder et al. (2003) found correlation between the length and velocity of active rock glaciers. The latter depended on the MAAT, which was estimated from the locality and altitude for each site, rather than the source area and slope angle. This is mainly because frozen ground softens significantly as the permafrost temperature increases in warm permafrost environments (MAAT > -4°C). In contrast, the dependence of velocity on temperature was insignificant in cold environments (MAAT < -7°C) such as the Brooks Range (Kääb et al. 2007). The MAGST, much lower in the Brooks Range than in the Alps (Fig. 5), also indicates that the creeping depth (mostly within a few tenth meters in depth) of the studied rock glaciers is much lower than the melting point in contrast to the case in the Alps (cf. Arenson et al. 2002). Thus, the difference in a creep parameter between the rock glaciers in the study area is assumed to be much smaller than that in the Alps. This means that in the Brooks Range the effect of debris supply on the size of rock glaciers can be tested using the $L_W$–$L_{RG}$ diagrams without one major source of noise.

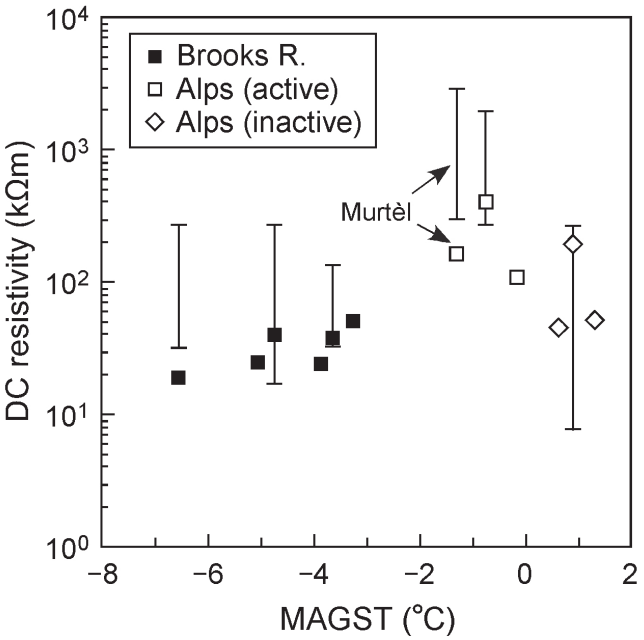


Figure 5. Relationship between MAGST and DC resistivity at 5–9 m depth in the Brooks Range and Swiss Alps. Resistivities from a one-dimensional method are indicated by symbols and ranges of resistivities from a two-dimensional (2D) method by bars. The data in the Alps are from Ikeda (2006) and Ikeda & Matsuoka (2006), except for the 2D data of the Murtèl site from Hauck (2001).

To examine the ice content of the studied talus-derived rock glaciers, the relationship between MAGST and DC resistivity of permafrost (5–9 m deep) of the rock glaciers is displayed with the data of typical talus-derived rock glaciers in the Alps in Figure 5. The DC resistivities from the 1D measurement in the Brooks Range (10–50 kΩm) are lower and less scattered than those in the Alps (50–400 kΩm). The absolute values of the resistivities derived from the 2D measurements are also within the smaller ranges in the study area than in the Alps. These results imply that the ice content in the studied rock glaciers is relatively small for rock glaciers, and the variation in ice content between different rock glaciers is also smaller than that in the Alps (see Haeberli & Vonder Mühll 1996, Hauck & Vonder Mühll 2003, Ikeda 2006, for the interpretation of DC resistivity). Thus, we can interpret the $L_W$–$L_{RG}$ diagrams assuming that the size of the talus-derived rock glaciers in the study area is roughly proportional to the debris volume in the rock glaciers.

This study shows that the central Brooks Range is a suitable area to investigate topographical controls on rock glaciers. More detailed study will address the long-term rates of rock wall erosion and the advance of talus-derived rock glaciers, and will possibly evaluate the dynamic inactivation and interaction with glacial processes of the rock glaciers quantitatively.

## Acknowledgments

This study was financially supported by the Grant-in-Aid for Research Fellow of the Japan Society for the Promotion of Science from the Ministry of Education, Science and Culture, Japan, and the Inoue Fund for Field Science from the Japanese Society of Snow and Ice. We acknowledge K. Koui, A. Mittermeier, and A. Kikuchi for field assistance; S. Berezovskaya, M. and M. Kawauchi, and S. Sawaguchi for logistical help; R. Busey, P. Prokein, L. Hinzman, D. Kane, Y. Hayakawa, N. Matsuoka, and K. Moriwaki for academic support.

## References

Arenson, L., Hoelzle, M. & Springman, S. 2002. Borehole deformation measurements and internal structures of some rock glaciers in Switzerland. *Permafrost and Periglacial Processes* 13: 117-135.

Barsch, D. 1977. Nature and importance of mass-wasting by rock glaciers in alpine permafrost environments. *Earth Surface Processes* 2: 231-245.

Barsch, D. 1992. Permafrost creep and rockglaciers. *Permafrost and Periglacial Processes* 3: 175-188.

Barsch, D. & Jakob, M. 1998. Mass transport by active rock glaciers in the Khumbu Himalaya. *Geomorphology* 26: 215-222.

Calkin, P.E., Haworth, L.A. & Ellis, J.M. 1987. Rock glaciers of central Brooks Range, Alaska, U.S.A. In: J.R. Giardino, J.F. Shroder, Jr. & J.D. Vitek (eds.), *Rock Glaciers*. London: Allen and Unwin, 65-82.

Ellis, J.M. & Calkin, P.E. 1979. Nature and distribution of glaciers, neoglacial moraines, and rock glaciers, east-central Brooks Range, Alaska. *Arctic and Alpine Research* 11: 403-420.

Frauenfelder, R., Haeberli, W., Hoelzle, M. & Maisch, M. 2001. Using relict rockglaciers in GIS-based modelling to reconstruct Younger Dryas permafrost distribution patterns in the Err-Julier area, Swiss Alps. *Norsk Geografisk Tidsskrift* 55: 195-202.

Frauenfelder, R., Haeberli, W. & Hoelzle, M. 2003. Rockglacier occurrence and related terrain parameters in a study area of the Eastern Swiss Alps. *Proceedings of the Eighth International Conference on Permafrost*, *Zurich*, *Switzerland*, *July 21–25*, *2003*: 253-258.

Haeberli, W. & Vonder Mühll, D. 1996. On the characteristics and possible origins of ice in rock glacier permafrost. *Zeitschrift für Geomorphologie N. F. Suppl.-Bd.* 104: 43-57.

Haeberli, W., Kääb, A., Wagner, S., Vonder Mühll, D., Geissler, P., Haas, J.N., Glatzel-Mattheier, H. & Wagenbach, D. 1999. Pollen analysis and $^{14}C$ age of moss remains in a permafrost core recovered from the active rock glacier Murtèl-Corvatsch, Swiss Alps: geomorphological and glaciological implications. *Journal of Glaciology* 45(149): 1-8.

Hamilton, T.D. & Porter, S.C. 1975. Itkillik Glaciation in the Brooks Range, northern Alaska. *Quaternary Research* 5: 471-497.

Hauck, C. 2001. Geophysical methods for detecting permafrost in high mountains. *Mitteilungen der Versuchsanstalt für Wasserbau, Hydrologie und Glaziologie*, *ETH Zürich* 171: 204 pp.

Hauck, C. & Vonder Mühll, D. 2003. Inversion and interpretation of two-dimensional geoelectrical measurements for detecting permafrost in mountainous regions. *Permafrost and Periglacial Processes* 14: 305-318.

Humlum, O. 2000. The geomorphic significance of rock glaciers: estimates of rock glacier debris volumes and headwall recession rates in West Greenland. *Geomorphology* 35: 41-67.

Ikeda, A. 2006. Combination of conventional geophysical methods for sounding the composition of rock glaciers in the Swiss Alps. *Permafrost and Periglacial Processes* 17: 35-48.

Ikeda, A. & Matsuoka, N. 2002. Degradation of talus-derived rock glaciers in the Upper Engadin, Swiss Alps. *Permafrost and Periglacial Processes* 13: 145-161.

Ikeda, A. & Matsuoka, N. 2006. Pebbly versus bouldery rock glaciers: Morphology, structure and processes. *Geomorphology* 73: 279-296.

Kääb, A., Frauenfelder, R. & Roer, I. 2007. On the response of rockglacier creep to surface temperature increase. *Global and Planetary Change* 56: 172-187.

Olyphant, G.A. 1983. Computer simulation of rock-glacier development under viscous and pseudoplastic flow. *Geological Society of America Bulletin* 94: 499-505.

Olyphant, G.A. 1987. Rock glacier response to abrupt changes in talus production. In: J.R. Giardino, J.F. Shroder, Jr. & J.D. Vitek (eds.), *Rock Glaciers*. London: Allen and Unwin, 55-64.

Roer, I. & Nyenhuis, M. 2007. Rockglacier activity studies on a regional scale: comparison of geomorphological mapping and photogrammetric monitoring. *Earth Surface Processes and Landforms* 32: 1747-1758.

Solid, J.L. & Sørbel, L. 1992 . Rock glaciers in Svalbard and Norway. *Permafrost and Periglacial Processes* 3: 215-220.

Wagner, S. 1992. Creep of Alpine permafrost, investigated on the Murtel Rock Glacier. *Permafrost and Periglacial Processes* 3: 157-162.

Wahrhaftig, C. & Cox, A. 1959. Rock glaciers in the Alaska Range. *Bulletin of the Geological Society of America* 70: 383-436.

# Geophysical Investigation of Saline Permafrost at Ilulissat, Greenland

Thomas Ingeman-Nielsen
*Arctic Technology Centre, Department of Civil Engineering, Technical University of Denmark, DK-2800 Kgs. Lyngby, Denmark*

Niels Foged
*Arctic Technology Centre, Department of Civil Engineering, Technical University of Denmark, DK-2800 Kgs. Lyngby, Denmark*

Rune Butzbach
*ASIAQ, Greenland Survey, DK-3900 Nuuk, Greenland*

Anders Stuhr Jørgensen
*Arctic Technology Centre, Department of Civil Engineering, Technical University of Denmark, DK-2800 Kgs. Lyngby, Denmark*

## Abstract

The technical properties and general state of permafrost in Greenland is not well documented. A new coordinated investigation has been initiated for ground temperature measurements and permafrost mapping in Greenlandic towns in sporadic, discontinuous, and continuous permafrost zones. We present investigation results from one of the sites, located at Ilulissat in an area of discontinuous saline permafrost. We have established ground temperature measurement stations and conducted a shallow geoelectrical study. Our results show that the sediments in the study area mainly consist of frost susceptible silty clays. The area has permafrost with a maximum active layer thickness between 0.9 m and 1 m. In spite of low permafrost temperatures, a considerable part of the pore water is unfrozen due to high residual salt concentrations. Consequently, the unfrozen water content dominates the geotechnical properties, and the sediments have a limited heat capacity available should the temperature conditions change.

**Keywords:** ice content; resistivity survey; saline permafrost; temperature measurements.

## Introduction

The variability in the thermal state of permafrost in Greenland is presently not very well mapped. A series of well-organized ground temperature stations were operated in a number of West Greenlandic towns from the late 1960s to the early 1980s; however only part of these datasets have ever been published, and no large coordinated investigations have been conducted since. With the NSF ARC-0612533 project, "Recent and future permafrost variability, retreat and degradation in Greenland and Alaska: An integrated approach," a new coordinated investigation has been initiated for ground temperature measurements in Greenlandic towns in sporadic, discontinuous, and continuous permafrost zones. The project conducted in cooperation between Asiaq Greenland Survey, the Danish Meteorological Institute (DMI), University of Alaska Fairbanks (UAF), and Technical University of Denmark (DTU).

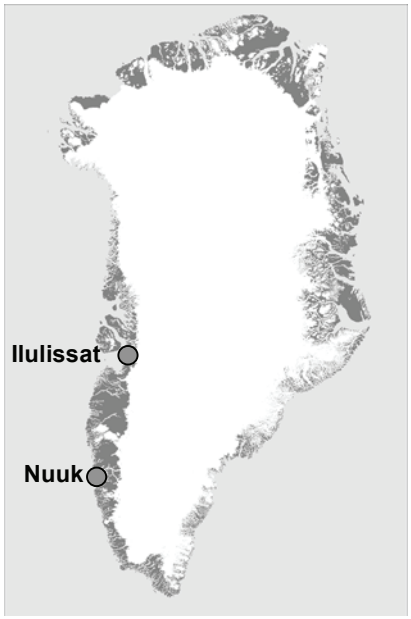


Figure 1. Map of Greenland with the location of the field site (Ilulissat) indicated.

This paper concerns one of the locations studied in this project, a field site located close to the airport in the town of Ilulissat, West Greenland (Fig. 1). Here we present the first results from fieldwork conducted in the summer 2007, which included shallow drilling, installation of ground temperature sensors (thermistors), and a shallow geoelectrical survey. Furthermore, we compare these results with investigations conducted from 1978 to 1980 in connection with the construction of the airport.

## Site Description

Ilulissat is situated in the inner part of the Disko Bay at approximately 69.2°N and 51.1°W. The climate is arctic with a Mean Annual Air Temperature (MAAT) around -3.3°C (average from 1997 to 2006) with an increasing trend. The long-term variation in MAAT is shown in Figure 2. In the most recent classification by Christiansen & Humlum (2000), Ilulissat is located in the discontinuous permafrost zone.

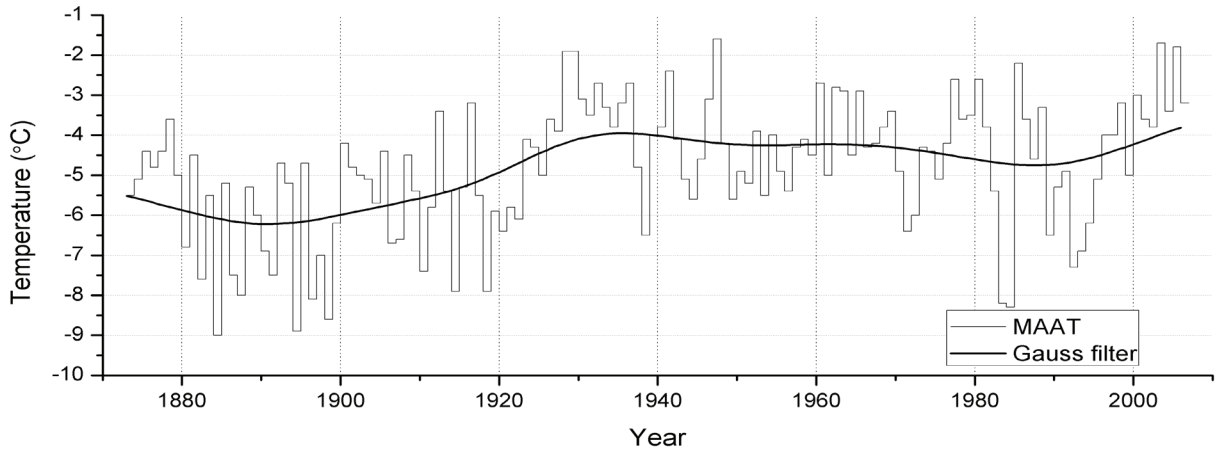


Figure 2. Mean Annual Air Temperature (MAAT) at Ilulissat from 1873 to 2006, as well as a Gauss filter with a filter width of 9 years (Cappelen 2007). These temperatures are measured at a DMI climate station (04216+04221) located in town, not at the airport field site.


Figure 3. Aerial photo of field site with selected boreholes and survey lines included.

The bedrock in the area consists of Nagsugtoquidian gneisses with amphibolitic bands. It is affected by a series of fault and fracture systems, most importantly a northwest-southeast situated system. The entire area was ice covered during the last glaciation (Weichsel-Wisconsin), and the area was not deglaciated until approximately 9600 years BP (Bennicke & Björck 2002). A series of marine silt and clay rich sediments were later deposited at relatively high sea levels of <50 m. Interaction between eustatic changes and isostatic uplift raised the area above sea level about 5000 years ago (Rasch 2000), exposing the sediments to percolation of precipitation and possibly groundwater flow. This has resulted in depletion of salts in the upper part of the soil profile.

Permafrost was formed relatively early and the sediments have thereby been exposed to the consolidation and fracturing phenomena caused by ice lens formation in fine-grained sediments (Foged 1979).

## Previous Investigations

In the period from 1978 to 1980, a series of investigations were undertaken in relation to the construction of the present airport facility. These investigations included drilling of a number of boreholes. Some of these boreholes were equipped with PT100 temperature sensors, which were manually logged at irregular intervals during the survey period. Furthermore samples from the boreholes were analyzed with respect to water content, pore water chemistry, freezing point depression, and consolidation parameters. A geoelectrical study was also conducted, including a number of electrical soundings at the borehole locations. Some of these results were previously published in Foged & Bæk-Madsen (1980), but many have never been published except in internal reports. In this paper, we present data from borehole 78020 as reference data for the new study.

## Methodology and Instrumentation

In 2005, ASIAQ installed a ground temperature station (ET545, Fig. 3) next to their climate station at the airport site (climate station operational since 1993 and measures air temperature, humidity, and precipitation). This ground temperature station has PT100 temperature probes at the ground surface as well as depths of 0.25 m, 0.5 m, 1 m, 2 m, 3 m, and 4 m.

In 2007 we installed ground temperature sensors at locations GT1 and GT2 as well as at borehole locations 78020 and 78060 in order to establish information on the spatial variability in the area. All locations are equipped with Tinytag dataloggers with thermistors at 25 cm and 1.6 m depth. The new borehole at 78020, which is 4 m deep, is also equipped with Hobo U12 loggers with thermistors at the surface, 0.25 m, 0.5 m, 0.75 m, 1 m, 2 m, 3 m, and 4 m depths.

Our geophysical survey consisted of three Continuous Vertical Electrical Sounding (CVES) profiles conducted with Wenner and Wenner-Schlumberger configurations using an ABEM SAS4000 terrameter with the Lund Imaging system. This system consists of 61 electrodes on four cables with unit spacing on the two central cables and double spacing on the two outer cables. We used a unit electrode spacing of 5 m on profiles L1 and T1, and 1.5 m spacing on L2. We

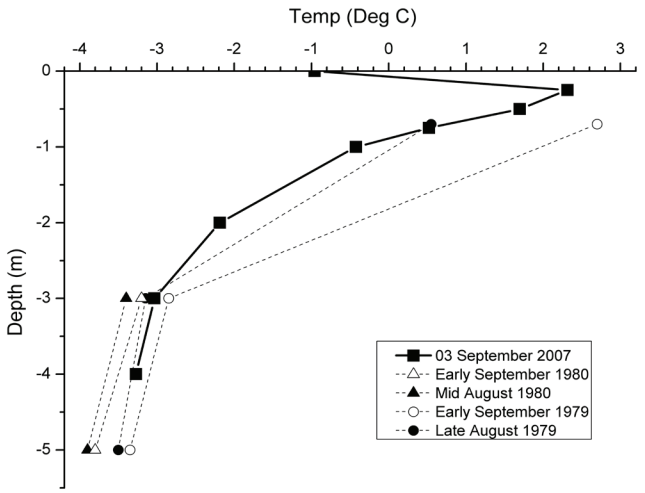


Figure 4. Ground temperature measurements from 1979–1980 (dashed lines) and 2007 (solid line).

have also made Vertical Electrical Soundings (VES) of the Schlumberger type at borehole locations 78018, 78020, and 78060, as well as at the intersection of L2 and T1, using the ABEM SAS4000 terrameter in standard setup. The CVES profiles have been inverted using Res2Dinv from Geotomo Software, and VES soundings using SELMA (Christensen & Auken 1992).

## Results

Our continuous measurements of ground temperatures show that the present day maximum Active Layer Thickness (ALT) at the airport field site occurs in the beginning of September. At station ET545 the ALT was 1.0 m in 2006 and estimated to be 0.9 m in 2005 (the estimate is based on late August temperatures at surface and 1 m depth, as the sensors at 25 cm and 50 cm were not yet installed). Figure 4 shows a plot of the temperature measurements from the new installation at the old borehole 78020 location from September 3, 2007. This dataset indicates an ALT of 0.9 m in 2007. The same figure shows a plot of the temperature measurements from late August and early September of 1979 and 1980. In 1979 the ALT is estimated to have been between 1.0 m and 1.2 m. The estimate is based on temperatures at 0.7 m, 3 m, and 5 m depth. In 1980, the upper temperature probe had ceased functioning. The temperatures from the deeper probes were slightly lower than those observed in 2007, indicating a smaller ALT. We conclude that the ALT today is the same or slightly shallower than that observed in 1979 and 1980.

Olesen (2003) established and operated a ground temperature station (OBO) in Ilulissat from 1968 to 1982. It was equipped with 21 PT100 sensors at depths down to 15 m. In the upper 2 m, sensors were spaced at 0.25 m intervals. The sensors in the upper 1 m were only operational from 1969 to 1972. During this period, the average ALT was 1.1 m. This OBO site is located in town, some 3 km from the airport site. The airport site is slightly warmer than the DMI town station (0.4°C average 1997–2006). This shows that there may be significant local variations in air temperature.

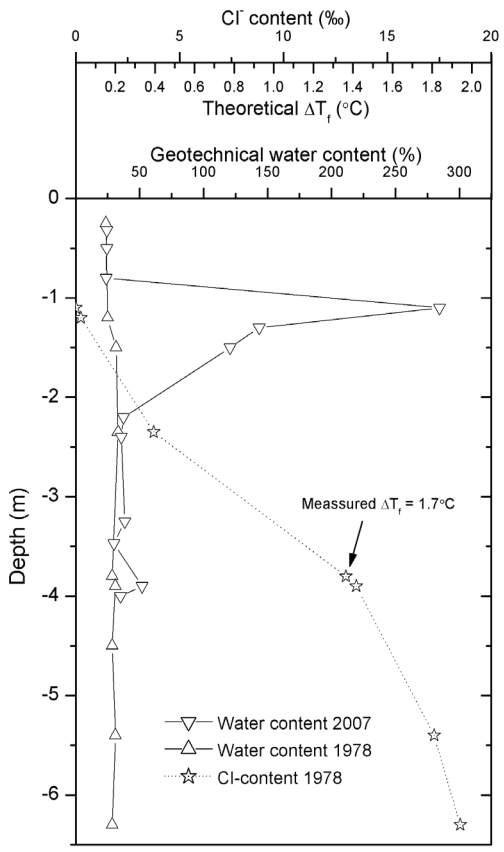


Figure 5. Water contents and Chloride ($Cl^-$) concentration from borehole location 78020, based on analysis from 1978 and 2007. The figure also shows the theoretical freezing point depression ($\Delta T_f$) based on a pure NaCl solution of the same chloride concentration. Actual measured values of ΔTf are somewhat larger than the theoretical value.

The present ALT is apparently smaller than that observed in early 1970s at the OBO site. However, the difference may be related to a difference in air temperature . The old OBO station no longer exists, and the original location is crossed by a paved road. However, in order to obtain comparative measurements we have installed a new station as close as possible to the old OBO station.

Borehole 78020 was drilled July 26 1978, and is typical for the area. It showed a 6.9 m thick sequence of marine silty to very silty clay deposits, over gneiss bedrock. At the time of drilling, the active layer was 0.4 m thick, and the permafrost was very ice rich down to a dept of 4 m. Figure 5 shows the original water contents measured on samples collected from the borehole, as well as water contents from samples collected at the new drilling in 2007. Typical water contents lie between 23% and 35% and correlates well between the two datasets. However, from 1 m to 2 m depth, the new measurements show much larger water content when compared to the original measurements made in 1978. This is not necessarily due to temporal changes, but more to the fact that during the drilling in 1978, there was no focus on the importance of establishing the actual ice content. The collection of samples was organized to minimize the volume

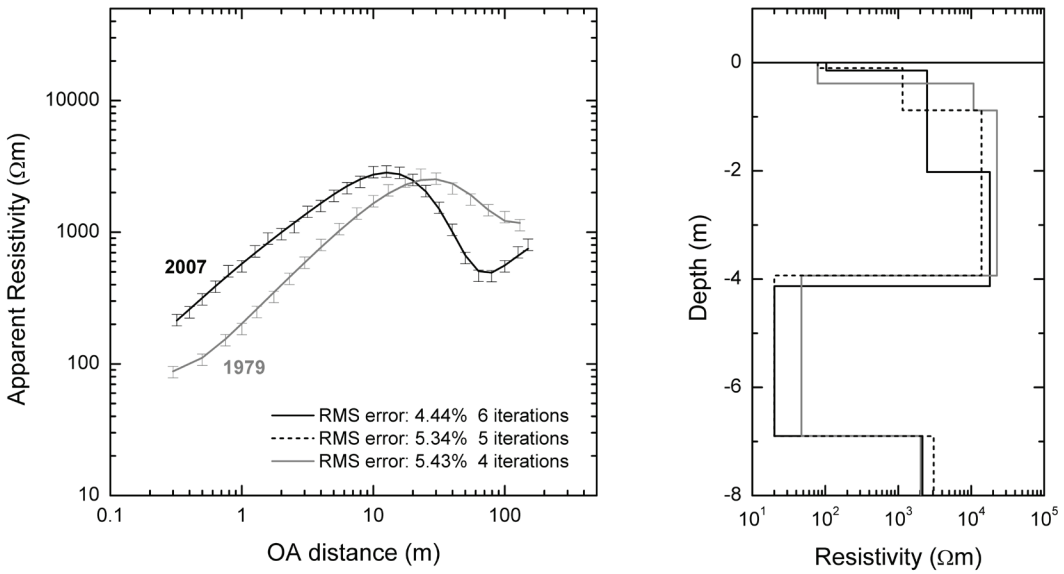


Figure 6. Inversion results from vertical electrical soundings at borehole location 78020, measurements from 1979 (grey lines) and 2007 (black lines). Five layer resistivity models are necessary in order to fit the datasets properly. However, the models are very poorly defined, and for the 2007 dataset two different models fitting the data equally well are indicated (black solid and dashed lines).

of ice lenses in the samples; however, the notes did record the occurrence of an ice rich zone.

Below the 4 m depth, ice was no longer observed in the samples, although temperatures are known to be subzero. The cause is the residual salt content in the marine clay deposits. Figure 5 also shows the variation of the pore water chloride content with depth in the borehole. It is seen to increase drastically from 3.75‰ at a depth of 2.35 m to 18.5‰, almost seawater concentration, at a depth of 6.3 m. These chloride concentrations have been used to calculate the theoretical freezing point depressions ($\Delta T_f$) based on a pure NaCl solution of the same chloride concentration (see separate scale in Fig. 5), using the formula (adapted from Atkins 1994):

$$\Delta T_f = K \cdot c \cdot (1 + \alpha) \quad ,$$

where $K$ is the cryoscopic factor (1.86 K·kg·mol$^{-1}$ for water), $c$ is the chloride concentration in mol/L, and α is the dissociation factor (assumed unity). The observed maximum concentration corresponds to a theoretical freezing point depression of 1.94°C. The actual measured values are somewhat lower however, due to a combination of other salts in the pore water solution, the electrochemical properties of the clay particles, and capillary tension in the pores.

The result of the freezing point depression below approximately 4 m depth is that the sediments are unfrozen as observed during drilling in 1978 and that unfrozen water content dominates the technical properties.

One of the effects of the unfrozen state is that the resistivity of the clay deposits is very low. This is observable on the Vertical Electrical Soundings (VES) collected at borehole 78020 location in 2007 and 1979 (Fig. 6). The two VES were collected June 6, 2007 and August 3, 1979. The different active layer thicknesses account for most of the difference observed in the apparent resistivity curves. The inverted resistivity models are also shown in Figure 6, and consist of five layers. Layer 1 is the unfrozen active layer, layers 2 and 3 are frozen sediments of varying but high resistivity, layer 4 is the technically unfrozen layer with low resistivity, and layer 5 is the bedrock. The models are highly undetermined when inverted with no constraints. The inversion of the 1979 data (solid grey line in Fig. 6) was strongly constrained at the depth of the bedrock interface, and loosely constrained within the depth of the active layer and the zone of frozen sediment. The 2007 dataset (solid black line) was first inverted with constraints on the depth to bedrock as well as the bedrock resistivity. In both datasets the apparent resistivity data could only be properly fitted, when the frozen zone was split into a shallow part with lower resistivity (layer 2), and a deeper part with higher resistivity (layer 3). Although poorly determined the depth to layer 3 corresponds well with the ALT in the 1979 data inversion, approximately 0.9 m, so that layer 2 corresponds to the frozen part of the active layer. For the 2007 data, the depth to layer 3 is much greater, and thus a similar interpretation is not possible. However, by constraining thicknesses of the layers, as well as the unfrozen active layer and bedrock resistivities, to fit the values obtained in the inversion of the 1979 data, it was possible to fit the 2007 dataset equally well (black dashed line, indistinguishable in apparent resistivity plot, see Fig. 6). Therefore, the VES results support the hypothesis that no significant changes have occurred in the permafrost conditions of the area over the period of study.

The inverted T1 CVES profile shown in Figure 7 (Fig. 3 shows the location of profile T1) shows the resistivity structure of the area. The upper part of the profile is highly resistive, with resistivities of more than 20 kΩm. Below is a conductive layer with resistivities between 50 Ωm and 600 Ωm. The lower part of the profile corresponds to bedrock at medium to high resistivity. Bedrock is outcropping immediately to the

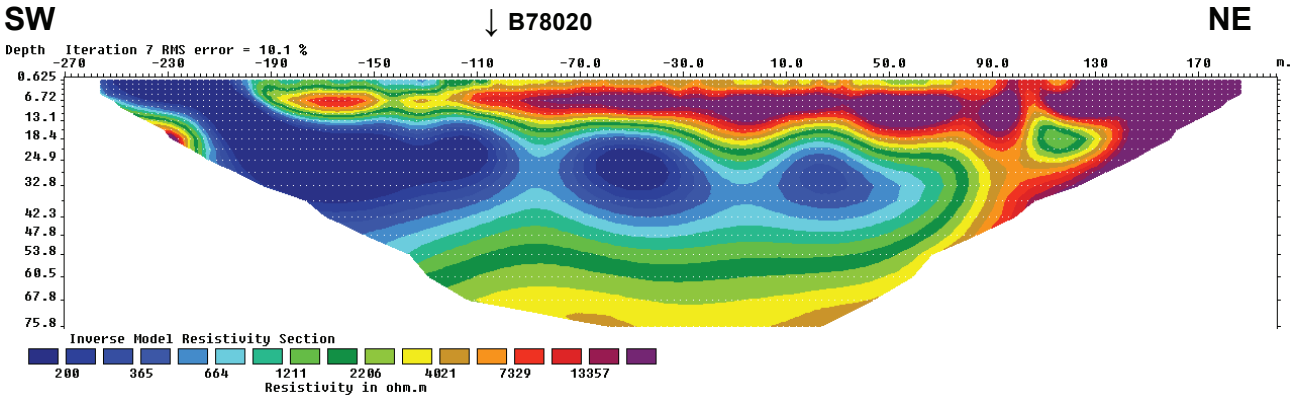


Figure 7. CVES profile (profile T1 in Fig. 3) with an electrode spacing of 5m using ABEM SAS4000 and LUND Imaging System. The profile clearly shows a low resistive layer corresponding to the technically unfrozen layer observed in soundings and boreholes. However the interpreted depths are invalid, due to macro anisotropy caused by ice lenses, and related equivalency problems.

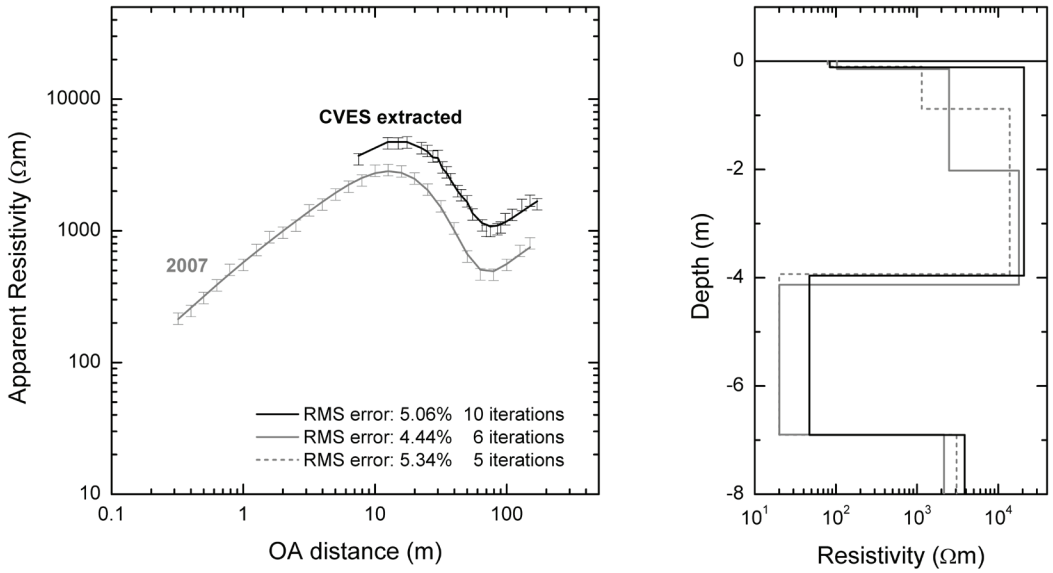


Figure 8. A dataset has been extracted from the CVES profile and inverted as a 1D sounding using a general array inversion scheme. The data could be fitted with essentially the same model as the normal Schlumberger sounding. Only a four layer model was used in this case, as the data density in the top of the profile is not large enough to support an extra layer. The reason for the offset between the Schlumberger sounding curve and the extracted data is the larger potential electrode distance used in the Wenner-Schlumberger configuration in the CVES profile.

southwest and northeast of the profile.

The general resistivity structure of the profile corresponds well with the collected VES. Nevertheless, the depths observed in the inverted resistivity model are much larger than the actual values. The bedrock interface for example is located at a depth of more than 35 m. No efforts to constrain the model resulted in a reasonable fit to the dataset. Similar problems have been observed previously in ice-rich permafrost areas in Greenland (Ingeman-Nielsen 2005, 2006), and are probably caused by pseudo anisotropy due to the presence of massive ice lenses. High ice content in the form of near horizontal ice lenses in the upper 2 meters of the permafrost gives rise to equivalency problems when the measurement system is geometrically large compared to the individual layers. In fact, a thin layered sequence with large resistivity contrasts is electrically equivalent to and indistinguishable from a thicker and isotropic sequence.

Combined with the normal equivalency problem of sandwiching a thin conductive layer between two thicker and resistive layers, this geoelectrical setting proves very difficult to resolve, as indicated by the wrong depths in the CVES inversion and the highly undetermined parameters in the VES inversions.

In order to substantiate this interpretation, we have extracted a subset from the CVES dataset, consisting of all measurements with a center point at the B78020 location plus or minus 10 m, and inverted this dataset using a 1D general array inversion scheme. As presented in Figure 8, it was possible to fit this dataset using essentially the same model as for the 2007 VES. In this case we used a four layer model, as the data density in the upper part of the profile is not large enough to support the extra layer. The only constraints on the inversion were a strong fix on the depth to

the bedrock and very loose constraints on the resistivities of the conductive layer and the bedrock. All other parameters we left unconstrained.

This shows that it is indeed possible to construct a geoelectrical model that fits all the collected datasets. Furthermore it indicates that in this type of setting, a 1D laterally constrained inversion scheme could be superior to the more generally applied 2D blocky inversion scheme.

## Conclusions

In order to determine permafrost properties in Ilulissat, we have established a number of ground temperature measurement stations and conducted a shallow geoelectrical study. Our results show that the sediments in the study area mainly consist of very frost susceptible, silty clays of marine origin. The area has permafrost with a maximum active layer thickness (ALT) between 0.9 m and 1 m. The ALT today is similar to that observed in 1979 and 1980, although ALT may have been smaller in the cold period during the early 1990s. Permafrost temperatures as low as -3°C to -4°C have been registered, but still a considerable part of the pore water is unfrozen at depths below 4 m, due to high residual salt concentrations and clay surface electrochemical properties. As a result, the unfrozen water content dominates the geotechnical properties. The unfrozen layer was observed directly while drilling in 1978 and in 2007 with vertical electrical soundings and CVES profiles as a low resistive layer. Consequently, these sediments have only a limited heat capacity available should the temperature conditions change.

## Acknowledgments

This research was funded by the Polar Earth Science Program, Office of Polar Programs, National Science Foundation (ARC-0612533).

## References

Atkins, P.W. 1994. *Physical Chemistry* (6th ed.). Oxford University Press, 1031 pp.

Bennike, O. & Björck, S. 2002. Chronology of the last recession of the Greenland Ice Sheet. *Journal of Quaternary Science* 17(3): 211-219.

Cappelen, J. 2007. *DMI Annual Climate Data Collection 1873-2006, Denmark, The Faroe Islands and Greenland.* Danish Meteorological Institute. Technical Report 07-05. www.dmi.dk/dmi/tr07-05.

Christensen, N.B. & Auken, E. 1992. SELMA - Simultaneous Electromagnetic Layered Modelling and Analysis. Proceedings of Interdisciplinary Inversion Workshop 1 Aarhus 1992, Methodology and Applications within Geophysics, Astronomy, and geodesy. *Geoskrifter*: 49-56.

Christiansen H.H. & Humlum, O. 2000. Permafrost. In: B.H. Jakobsen, J. Böcher, N. Nielsen, R. Guttesen, O. Humlum & E. Jensen (eds.), *Topografisk Atlas Grønland*. Copenhagen: C.A. Reitzets Forlag, 32-35.

Foged, N. 1979. *Engineering Geological Investigations of Quaternary Marine Clay Deposits on West Greenland.* Ph.D. Thesis (in Danish). The Institute for Applied Geology. Technical University of Denmark.

Foged, N. & Bæk-Madsen. 1980. Jakobshavn Airport thermal stability in marine deposits. *Second International Symposium on Ground Freezing, Trondheim, June 24–26.* Norwegian Institute of Technology.

Ingeman-Nielsen, T. 2005. *Geophysical Techniques Applied to Permafrost Investigations in Greenland.* Ph.D. Thesis. Department of Civil Engineering, Technical University of Denmark, 177 pp.

Ingeman-Nielsen, T. 2006. Mapping ice-bonded permafrost with electrical methods in Sisimiut, *West Greenland EAGE Near Surface 2006, Extended Abstracts*, 4 pp.

Olesen, O.B. 2003. *Shallow Borehole Temperatures, Ilulissat, Greenland. Copenhagen, Denmark: Greenlandic Geological Survey (GEUS).* Distributed by National Snow and Ice Data Center/World Data Center for Glaciology. Digital Media.

Rasch, M. 2000. Holocene Relative Sea Level Changes in Disko Bugt, West Greenland. *Journal of Coastal Research* 16(2): 306-315.

# Climate Change and Arctic Infrastructure

Arne Instanes
*Instanes Svalbard AS, N-9171 Longyearbyen, Norway*
Oleg Anisimov
*State Hydrological Institute, St. Petersburg, Russia*

## Abstract

Several authors report that impacts of climate change on infrastructure in the Arctic are already evident. Damage to infrastructure and engineering structures in permafrost regions are often linked to observed increase in air temperature over the last 10 to 20 years. However, these reports do not show in detail how the change in air temperature may affect the active layer thickness and permafrost temperature at specific sites and for specific structures in the Arctic. This paper presents the results of a study of the impact of climate change on Arctic infrastructure based on historical meteorological records. The temperature data are used together with a numerical model to evaluate the possible warming of permafrost at depth, and theoretical impacts on pile foundation capacity at specific sites in the Arctic. Results from permafrost model forced by several GCM-based climatic projections are used to construct the predictive map indicating threats to infrastructure due to potential weakening of the frozen ground.

**Keywords:** climate change; engineering; foundations; geotechnical; permafrost; warming.

## Introduction

For several decades, air temperatures in the Arctic have warmed at approximately twice the global rate (McBean et al. 2005). Zonal-mean temperature north of 60°N has increased up to 2°C since the late 1960s. Contemporary warming in the Arctic is strongest (~ 1°C/decade) in winter and spring, and smallest in autumn. Such changes lead to warming, thawing, and degradation of permafrost. Observational data are limited, and are not available throughout the entire Arctic. Borehole measurements indicate that permafrost temperatures have increased markedly during the last 50 years, (Romanovsky et al. 2002), with rapid warming in Alaska (Hinzman et al. 2005), Canada (Beilman et al. 2001), Europe (Harris et al. 2003), and Siberia (Pavlov & Moskalenko 2002).

In the context of the future climate change one of the key concerns associated with the thawing of permafrost is the detrimental impact on the infrastructure built upon it. Several authors report that such impacts are already evident (Khrustalev 2001, Romanovsky & Osterkamp 2001, Zernova 2003, Gribchatov 2004, Vasilieva 2004). Instanes et al. (2005) and Instanes (2003) conclude that human interaction and engineering construction very often lead to extensive thawing of both continuous and discontinuous permafrost even if climatic conditions remain unchanged. The intergovernmental panel on climate change (Anisimov & Vaughan 2007) also points out that the effect of heated buildings on underlying ice-rich permafrost has been known for a very long time, and may be mistaken for an impact of climate change.

In this paper we used historical air temperature records from three different cities to investigate the change in pile foundation bearing capacity during the last 100 years. We upscaled the results of this historical analysis and constructed the map of potential threats to infrastructure using the hazard index that takes into account regionality of projected climatic and permafrost changes.

## Pile Design

*Design ground temperature*

The strength and deformation characteristics of frozen soils are temperature dependent. It is, therefore, necessary to determine the thickness of the active layer (maximum thaw depth) and the maximum ground temperature along the embedded pile length (Andersland & Ladanyi 2004). These two parameters are incorporated into the site-specific design of foundations in permafrost regions. Conventional engineering design is based on the analysis of historical variations of climatic and permafrost data and accounts for the frequency of extreme events, such as abnormally high temperatures resulting in deeper seasonal thawing of permafrost. Each foundation is designed with construction-specific safety factors that depend on the probability of such extremes.

*Adfreeze bonds*

The adfreeze bond strength between the pile surface and surrounding frozen permafrost soil is temperature and time dependent. For a specific pile foundation design, this parameter should be determined from geotechnical field and laboratory investigations. For the purpose of this study, a simplified relationship is used, as shown in Figure 1.

Data in Figure 1 may be used to evaluate the effect of changing climatic conditions on the bearing capacity of piles and thus to predict the potentially detrimental impacts of warming and thawing permafrost on the structures built upon it.

## Air Temperature Records

The climatic data used in the present analysis were mean monthly air temperatures from three different locations in the Arctic: (1) Fairbanks, Alaska (N64°15′, W147°37′);

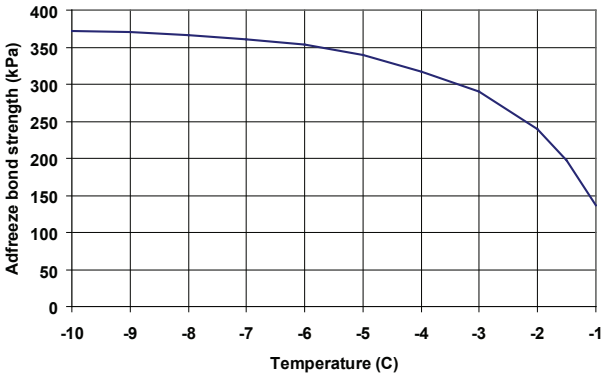


Figure 1. Adfreeze bond strength used in the analysis.

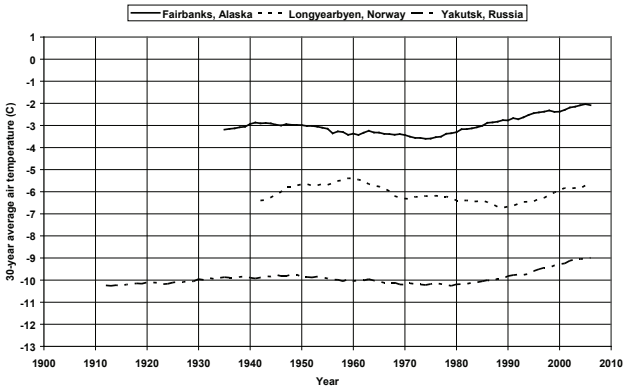


Figure 2. Mean annual air temperatures for Fairbanks, Alaska; Longyearbyen, Norway; and Yakutsk, Russia, smoothed with 30-years running filter.

(2) Longyearbyen, Norway (N78°25′, E15°47′); and (3) Yakutsk, Russia (N62°02′, E129°45′). The sites were chosen based on:

- station time series approximately 100 years or more,
- location near population concentrations and major infrastructure,
- locations representing different climatic and environmental conditions in the Arctic.

All three stations show some indication of increased air temperatures during the last 20 to 30 years. Yakutsk has the longest time series starting in 1829, while the time series for Fairbanks and Longyearbyen start in 1904 and 1912, respectively.

Figure 2 shows mean annual air temperatures for Yakutsk, Longyearbyen, and Fairbanks, smoothed with 30-years running filter. In the last three to four decades temperatures increased by almost 2ºC in Yakutsk, and by 1ºC in Fairbanks (see Fig. 2).

In Longyearbyen there was the decrease of the annual mean air temperature from the maximum of –5.2ºC in 1960 to the minimum of –6.8ºC in 1990 followed by rapid increase by ca. 1ºC since then. Based on Figure 2, the temperatures in the 1960s were still higher than now. However, Longyearbyen had a mean annual air temperature in 2006 that was the warmest on record (-1.6ºC).

Mean monthly air temperatures were used in the thermal model to calculate the changes in the ground temperature at different depth and to evaluate the effect on the bearing capacity of piles.

## Permafrost Models and Results

Two permafrost models of different complexity were used in this study. The first is the TEMP/W, version 7.03 (Geo-Slope 2007) software that can model the thermal changes in the ground due to changing temperature or heat flux boundary conditions. This simple model is often used in practical engineering applications and gives good results at point locations given that the model is validated by observational data. More sophisticated model that was used for constructing predictive hazard map for Russian permafrost region is detailed in the next section. The TEMP/W model accounts for the effects of the temperature dependent thermal conductivity, volumetric latent heat of fusion, and soil unfrozen water content. In this study we used a simplified homogenous soil profile consisting of silty sand with the following parameters:

- dry density ($\gamma_d$): 16.7 kN/m$^3$ ($\rho_d$=1700 kg/m$^3$),
- water content (w): 20%,
- degree of saturation ($S_r$): 100%
- porosity (n): 37.1%,
- volumetric heat capacity frozen ($c_{vu}$): 2300 kJ/(m$^3$K),
- volumetric heat capacity unfrozen ($c_{vu}$): 3150 kJ/(m$^3$K).

Thermal conductivity and heat capacity was adjusted to changing ground temperature and unfrozen water content using simplified empirical relationships.

The soil profile was modeled using isoparametric 8-nodes quadrilateral finite elements. Mean monthly air temperatures were applied to the surface boundary of the finite element mesh. The initial ground temperature at the start of the analyses (1904 for Fairbanks, 1912 for Longyearbyen, and 1900 for Yakutsk) was set approximately equal to the mean annual air temperature in Figure 2.

It should be noted that n-factors of 1.0 was used in the analysis presented in this paper. Andersland & Ladanyi (2004) suggest that n-factors between 1.2 and 2.0 would be appropriate for sand and gravel surfaces during thawing.

The ultimate goal of the calculations was to evaluate the probability for the ground temperature to exceed the threshold beyond which the pile becomes unstable and is incapable of bearing the load of construction above it. Figure 3 presents the maximum ground temperatures along the embedded pile length for selected years in Fairbanks, Longyearbyen, and Yakutsk, respectively. Maximum ground temperatures for each decade are presented in Tables 1, 2, and 3. It can be observed from the figures and tables that all three locations have the highest ground temperatures after year 2000.

Computed and measured ground temperatures are in good agreement in Longyearbyen. For Fairbanks and Yakutsk the computed values seem to be lower than observed ground temperatures. This is probably due to the effect of the n-factor used in the analysis (see above). The thermal model

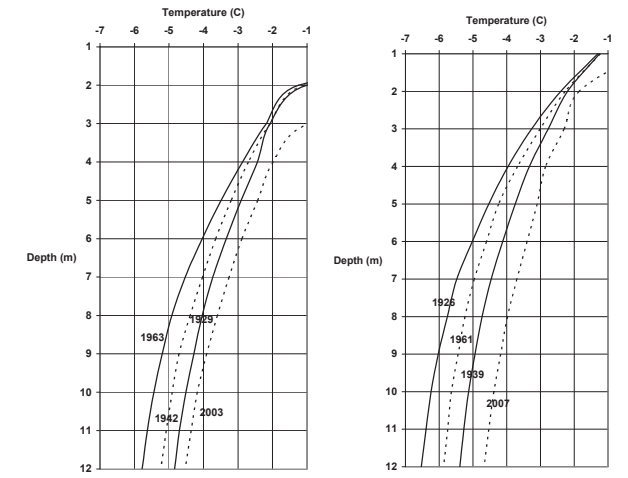


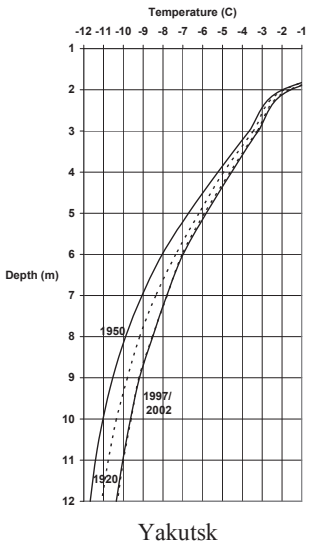


Figure 3. Maximum ground temperature along the embedded pile length, Fairbanks 1929, 1942, 1963, and 2003 (a); Longyearbyen 1926, 1939, 1961, and 2007 (b);and Yakutsk 1920, 1950, and 1997/2002 (c).

should, therefore, be tuned with actual ground temperature observations. However, the main purpose of the study was to look at the relative effect of variations in air temperature over the last 100 years for an idealized soil profile, and the results show that this goal has been achieved.

## Pile Capacity

Based on the maximum ground temperatures presented in Tables 1, 2, and 3 and the adfreeze bond strength presented in Figure 1, theoretical pile capacities for a 200 mm diameter pile for the three locations are presented in Figure 4. As follows from the figure, for Fairbanks the theoretical pile capacity has been reduced by 6.5% from the maximum capacity of 627 kN in 1963 to 587 kN in 2003. In Longyearbyen the pile capacity has been reduced by 12.5% from the maximum capacity of 717 kN in 1977 (and 1926) to 636 kN in 2007.

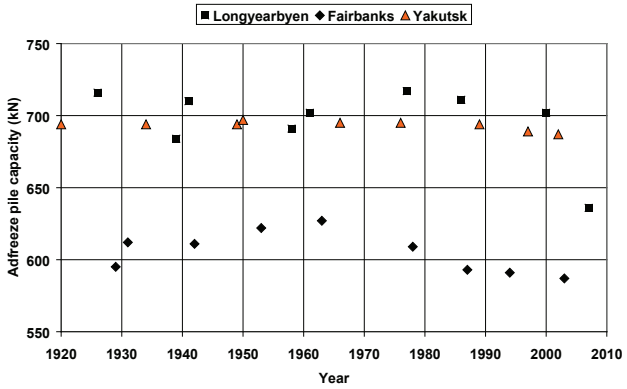


Figure 4. Theoretical adfreeze pile capacity for a 200 mm pile.

In Yakutsk, the theoretical pile capacity has remained almost unchanged, with only slight reduction by 1.5% in the period 1950–2002. This is because ground temperatures in Yakutsk are low (<-6ºC below 5 meters depth, see Table 3), while the adfreeze bond strength does not change much for temperatures below -5 to -6ºC (see Fig. 1). Pile capacities in Longyearbyen are higher than in Yakutsk because the active layer thickness here is much smaller due to the relatively cold summers in Spitsbergen compared to central Yakutia. It implies that the embedded length of the pile that has a temperature below -1ºC (also called the effective pile length) is bigger in Longyearbyen (approximately 11 m) than in Fairbanks and Yakutsk (approximately 10 m).

## Hazard Map

Nelson et al. (2001) suggested the hazard index for predictive large-scale mapping of potential risks to infrastructure due to warming and thawing of permafrost. The more recent study by Anisimov & Lavrov (2004) uses modified hazard index, $I_G$, that is given by the following equation:

$$I_G = \Delta Z_{al} V_{ice} K_s \quad (1)$$

Here $\Delta Z_{al}$ is the projected change in the depth of seasonal thawing, expressed in relative units with respect to modern norm; $V_{ice}$ is the volumetric ground ice content, and $K_s$ is the coefficient that characterizes soil salinity.

Changes in the depth of seasonal thawing have been calculated using an equilibrium permafrost model forced by several climatic scenarios. The baseline algorithm developed by V. Kudryavtcev (1974) was modified to account for the presence of the organic layer and for the effects of the changing thermal conductivity of the snow cover. The mathematical formalism has been detailed in several preceding publications (i.e., Anisimov et al. 2007; Sazonova & Romanovsky 2003). All calculations were made in the nodes of 0.5° lat/long grid spanning the northern Eurasian permafrost region.

The model was forced by the contemporary and projected for the future climatic data. We used gridded monthly norms

Table 1. Maximum ground temperature along the embedded pile length for each decade, Fairbanks, Alaska.

| Depth (m) | 1929 (ºC) | 1931 (ºC) | 1942 (ºC) | 1953 (ºC) | 1963 (ºC) | 1978 (ºC) | 1987 (ºC) | 1994 (ºC) | 2003 (ºC) |
|---|---|---|---|---|---|---|---|---|---|
| 1 | +5.99 | +5.54 | +5.41 | +5.31 | +5.42 | +6.30 | +6.69 | +6.39 | +7.66 |
| 2 | -1.00 | -1.36 | -1.09 | -1.25 | -1.24 | -1.11 | -0.92 | -0.71 | -0.89 |
| 3 | -2.07 | -2.19 | -2.07 | -2.15 | -2.18 | -2.02 | -1.96 | -1.93 | -1.98 |
| 4 | -2.44 | -2.71 | -2.70 | -2.75 | -2.87 | -2.63 | -2.48 | -2.48 | -2.43 |
| 5 | -2.91 | -3.18 | -3.20 | -3.34 | -3.49 | -3.20 | -2.97 | -2.96 | -2.89 |
| 6 | -3.34 | -3.63 | -3.65 | -3.88 | -4.04 | -3.63 | -3.42 | -3.37 | -3.26 |
| 7 | -3.73 | -4.02 | -4.03 | -4.37 | -4.53 | -4.04 | -3.73 | -3.76 | -3.60 |
| 8 | -4.04 | -4.36 | -4.39 | -4.80 | -4.92 | -4.42 | -4.05 | -4.08 | -3.91 |
| 9 | -4.28 | -4.57 | -4.71 | -5.04 | -5.20 | -4.74 | -4.33 | -4.32 | -4.18 |
| 10 | -4.51 | -4.74 | -4.91 | -5.30 | -5.44 | -4.95 | -4.58 | -4.55 | -4.36 |
| 11 | -4.70 | -4.92 | -5.08 | -5.52 | -5.63 | -5.16 | -4.70 | -4.72 | -4.53 |
| 12 | -4.84 | -5.01 | -5.24 | -5.67 | -5.78 | -5.33 | -4.81 | -4.84 | -4.68 |

Table 2. Maximum ground temperature along the embedded pile length for each decade, Longyearbyen, Norway.

| Depth (m) | 1926 (ºC) | 1939 (ºC) | 1941 (ºC) | 1958 (ºC) | 1961 (ºC) | 1977 (ºC) | 1986 (ºC) | 2000 (ºC) | 2007 (ºC) |
|---|---|---|---|---|---|---|---|---|---|
| 1 | -1.30 | -1.25 | -1.50 | -1.30 | -1.23 | -1.43 | -1.36 | -1.08 | -0.08 |
| 2 | -2.40 | -2.20 | -2.49 | -2.18 | -2.27 | -2.38 | -2.34 | -2.30 | -1.86 |
| 3 | -3.26 | -2.77 | -3.28 | -2.84 | -3.01 | -3.20 | -3.14 | -2.98 | -2.30 |
| 4 | -3.96 | -3.33 | -3.88 | -3.38 | -3.68 | -3.91 | -3.80 | -3.63 | -2.85 |
| 5 | -4.53 | -3.75 | -4.32 | -3.85 | -4.24 | -4.55 | -4.37 | -4.23 | -3.10 |
| 6 | -5.02 | -4.12 | -4.76 | -4.30 | -4.60 | -5.13 | -4.83 | -4.64 | -3.40 |
| 7 | -5.48 | -4.46 | -5.09 | -4.71 | -4.96 | -5.48 | -5.25 | -5.03 | -3.70 |
| 8 | -5.76 | -4.73 | -5.29 | -5.00 | -5.24 | -5.82 | -5.56 | -5.34 | -3.98 |
| 9 | -6.03 | -4.94 | -5.49 | -5.23 | -5.44 | -6.05 | -5.81 | -5.60 | -4.18 |
| 10 | -6.24 | -5.13 | -5.59 | -5.45 | -5.64 | -6.25 | -6.00 | -5.81 | -4.38 |
| 11 | -6.39 | -5.27 | -5.68 | -5.60 | -5.75 | -6.40 | -6.15 | -5.98 | -4.53 |
| 12 | -6.53 | -5.39 | -5.74 | -5.74 | -5.87 | -6.52 | -6.28 | -6.11 | -4.67 |

Table 3. Maximum ground temperature along the embedded pile length for each decade, Yakutsk, Russia.

| Depth (m) | 1920 (ºC) | 1934 (ºC) | 1949 (ºC) | 1950 (ºC) | 1966 (ºC) | 1976 (ºC) | 1989 (ºC) | 1997 (ºC) | 2002 (ºC) |
|---|---|---|---|---|---|---|---|---|---|
| 1 | +4.89 | +5.16 | +5.36 | +5.22 | +4.80 | +6.02 | +5.15 | +5.94 | +5.95 |
| 2 | -1.89 | -1.88 | -1.84 | -1.97 | -1.92 | -1.93 | -1.87 | -1.65 | -1.56 |
| 3 | -3.45 | -3.43 | -3.46 | -3.65 | -3.51 | -3.48 | -3.51 | -3.25 | -3.19 |
| 4 | -4.95 | -4.93 | -5.02 | -5.23 | -5.04 | -5.00 | -4.94 | -4.62 | -4.54 |
| 5 | -6.19 | -6.33 | -6.38 | -6.72 | -6.47 | -6.42 | -6.29 | -5.91 | -5.82 |
| 6 | -7.36 | -7.60 | -7.50 | -8.04 | -7.75 | -7.69 | -7.50 | -7.04 | -6.99 |
| 7 | -8.37 | -8.50 | -8.50 | -9.06 | -8.57 | -8.67 | -8.37 | -7.80 | -7.81 |
| 8 | -9.18 | -9.26 | -9.38 | -9.89 | -9.38 | -9.38 | -9.10 | -8.54 | -8.52 |
| 9 | -9.80 | -9.98 | -10.10 | -10.54 | -10.12 | -10.08 | -9.80 | -9.22 | -9.19 |
| 10 | -10.35 | -10.47 | -10.58 | -11.03 | -10.58 | -10.59 | -10.27 | -9.61 | -9.64 |
| 11 | -10.76 | -10.88 | -11.00 | -11.41 | -11.02 | -10.98 | -10.68 | -10.00 | -10.03 |
| 12 | -11.10 | -11.23 | -11.33 | -11.67 | -11.35 | -11.33 | -11.02 | -10.30 | -10.36 |

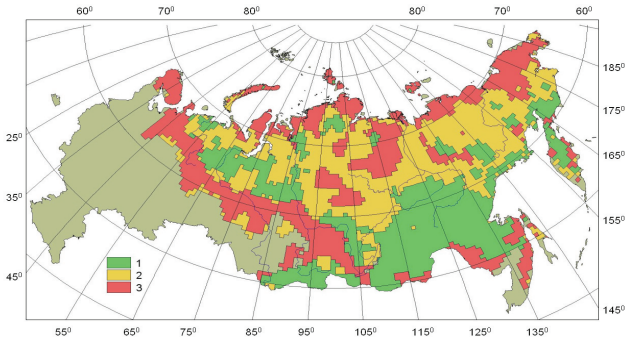


Figure 5. Predictive map of potential threats to infrastructure for 2050. Red, yellow, and green colors designate regions with high, moderate, and low susceptibility of buildings and engineered structures to the ongoing climatic and permafrost changes.

of air temperature and precipitation with 0.5° lat/long resolution as baseline data characterizing modern climate (New et al. 1999). Set of five scenarios of climate change for the 11-year long time periods centered on 2030, 2050, and 2080 has been constructed by superimposing predicted by CGCM2, CSM_1.4, ECHAM4/OPYC3, GFDL-R30_c and HadCM3 GCMs changes of climatic parameters on baseline data. These GCMs were selected as a result of the survey made in the course of the ACIA (Arctic Climate Impact Assessment) because they account for many key processes in the Arctic and provide reasonable fit to the observed climatic trends (Symon 2005). All climate models were forced by the B2 emission scenario. The climatic scenarios are fully documented in the ACIA report (2005) and are available on the web sites of the data distribution center of the Intergovernmental Panel on Climate Change (IPCC; http://ipcc-ddc.cru.uea.ac.uk/ and http://igloo.atmos.uiuc.edu/IPCC/).

Soil thermal properties were calculated using parameterizations that take into account soil type, soil moisture and ground ice content. We calculated winter-average snow depth at each node using monthly precipitation data. The density, thermal conductivity, and heat capacity of snow were prescribed at 300 kg $m^{-3}$, 0.23 W $m^{-1}$ $K^{-1}$ and 2090 J $kg^{-1}$ $K^{-1}$, respectively. Vegetation types with prescribed thermal properties and soil type were obtained from the digital global ecosystems database (1992). The model was validated by the data from Circumpolar Active Layer Monitoring program (Brown et al. 2000) and used to calculate permafrost parameters under modern and projected for the future climatic conditions. Results of such calculations differ in detail depending on climatic scenario. Predictive map of hazard index in Figure 7 was constructed using the "median" climatic projection of GFDL model for 2050.

## Summary and Conclusions

Historical air temperature records indicate warming during the last few decades in three selected locations representing different climatic and environmental conditions in Spitsbergen, in central Yakutia, and in Alaska. The results from this study suggest that piled foundations have not suffered sufficient loss in bearing capacity to become unstable due to the observed increase in air temperatures. However, the loss in capacity of piles in Longyearbyen from 702 kN to 636 kN in the period 2000–2007 is the early warning of the potentially detrimental impacts of changing climate.

One of the apparent features of the climate change impacts in permafrost regions is strong regionality. Susceptibility of permafrost to climatic changes and associated risks to infrastructure depend on the combinations of local soil, topographic, hydrological, vegetation, and snow conditions. In this paper the large-scale pattern of the future impacts was studied using the hazard index. Although such index provides highly generalized information about the potential impacts on the infrastructure, it may serve as effective tool for resource and land use planning, environmental risk management, and civil engineering in permafrost regions.

Areas of greatest hazard potential in Figure 5 include the Arctic coastline and parts of Siberia in which substantial development has occurred in recent decades. Particular concerns are associated with Yamal peninsula that falls into the highest risk zone, because of the ongoing expansion of the oil and gas extracting and transportation industry into this region. Although temperatures here are relatively low, frozen ground is already very unstable, largely because of its high salinity, and thus even small warming may cause extensive thawing of permafrost and ground settlement with serious impacts on the inrastructure.

## Acknowledgments

Anisimov's research of the contemporary climatic changes in Russia and predictive modeling of the impacts of thawing permafrost on infrastructure is supported by the Russian Foundation for Basic Research, grants # 07-05-00209 and 07-05-13527.

## References

Andersland, O.B. & Ladanyi, B. 2004. *Frozen ground engineering*. 2nd edition. New Jersey, USA: John Wiley & Sons, Inc. Published in cooperation with ASCE press, 363 pp.

Anisimov, O.A. & Lavrov, C.A. 2004. Global warming and permafrost degradation: risk assessment for the infrastructure of the oil and gas industry. *Technologies of oil and gas industry* (3): 78-83 (in Russian).

Anisimov, O.A. & Vaughan, D.G. 2007. Polar Regions. In: *Climate Change 2007: Climate change impacts, adaptation, and vulnerability. Contribution of Working group II to the Fourth Assessment Report of the Intergovernmental Panel on Climate Change*.

Anisimov, O.A., Lobanov, V.A., Reneva, S.A., Shiklomanov, N.I. & Zhang, T. 2007. *Uncertainties* in gridded air temperature fields and their effect on predictive active layer modeling**.** *Journal of Geophysical Research* 112 (F02S14), doi:10.1029/2006JF000593/

Beilman, D.W., Vitt, D.H. & Halsey, L.A. 2001: Localized permafrost peatlands in Western Canada: Definition, distributions, and degradation. *Arct. Antarct. Alp. Res.* 33(1): 7077.

Brown, J., Hinkel, K.M., Nelson, F.E. 2000. The Circumpolar Active Layer Monitoring (CALM) program: research designs and initial results. *Polar Geography* 24(3): 165-258.

Geo-Slope. 2007. Thermal modeling with TEMP/W 2007. An engineering methodology. Calgary, Canada: GEO-SLOPE International Ltd., 240 pp.

Global ecosystems database version 1.0 on CD-ROM. 1992. Series USDOC/NOAA National Geophysical Data Center, Boulder.

Harris, C., Vonder Mühll, D., Isaksen, K., Haeberli, W., Sollid, J.L., King, L., Holmlund, P., Dramis, F., Guglielmin, M. & Palacios, D. 2003: Warming permafrost in European mountains. *Global and Planetary Change* 39: 215-225.

Hinzman, L.D., Bettez, N.D., Bolton, W. Chapin III, R.F.S., Dyurgerov, M.B. Fastie, C.L., Griffith, B., Hollister, R., Hope, D.A., Huntington, H., Jensen, A.M., Jia, G.J., Jorgenson, T., Kane, D.L., Klein, D.R., Kofinas, G., Lynch, A.H., Lloyd, A.H., McGuire, A.D., Nelson, F.E., Nolan, M., Oechel, W.C., Osterkamp, T.E., Racine, C.H., Romanovsky, V.E., Stone, R.S., Stow, D.A., Sturm, M., Tweedie, C.E., Vourlitis, G.L., Walker, M.D., Walker, D.A., Webber, P.J., Welker, J., *Winker*, K.S. & Yoshikawa, K. 2005. Evidence and implications of recent climate change in northern Alaska and other arctic regions. *Climatic Change* 72: 251-298.

Instanes, A., Anisimov, O., Brigham, L., Goering, D., Ladanyi, B., Larsen, J.O. & Khrustalev, L.N. 2005. Chapter 16: Infrastructure: Buildings, Support Systems, and Industrial Facilities. In: *Arctic Climate Impact Assessment, ACIA*. Cambridge: Cambridge University Press, 907-944.

Intergovernmental panel on Climate Change (IPCC). 2007. *IPCC Working Group II Climate Change Impacts, Adaptation and Vulnerability Fourth Assessment Report, Chapter 15 Polar Regions (Arctic and Antarctic)*. www.ipcc.ch.

Khrustalev, L.N. 2001. Problems of permafrost engineering as related to global climate warming. In: R. Paepe & V. Melnikov (eds.), *Permafrost Response on Economic Development, Environmental Security and Natural Resources*. Dordrecht, the Netherlands: Kluwer Academic Publishers, 407-423.

Kudryavtsev, V.A., Garagulya, L.S., Kondrat'yeva, K.A. & Melamed, V.G. 1974. *Fundamentals of Frost Forecasting in Geological Engineering Investigations* Nauka, Moscow. (in Russian). English translation appears as U.S. Army Cold Regions Research and Engineering Laboratory Draft Translation 606 (1977).

Nelson, F.E., Anisimov, O.A. & Shiklomanov, N.I. 2001. Subsidence risk from thawing permafrost. *Nature* 410: 889-890.

New, M., Hulme, M. & Jones, P. 1999. Representing twentieth-century space-time climate variability. Part I: Development of a 1961–90 mean monthly terrestrial climatology. *Journal of Climate* 12(3): 829-856.

McBean, G., Alekseev, G., Chen, D., Førland, E., Fyfe, J., Groisman, P.Y, King, R., Melling, H., Vose, R. &.Whitfield, P.H. 2005: Chapter 2: Arctic Climate–Past and Present. *Arctic Climate Impacts Assessment (ACIA)*. C. Symon, L. Arris, B. Heal (eds.), Cambridge, UK:Cambridge University Press, 21-60.

Romanovsky, V.E. and Osterkamp, T.E. 2001. Permafrost: Changes and impacts. In: R. Paepe and V. Melnikov (eds.), *Permafrost Response on Economic Development, Environmental Security and Natural Resources*. Dordrecht, the Netherlands: Kluwer Academic Publishers, 297-315.

Pavlov, A.V. & Moskalenko, N.G. 2002: The thermal regime of soils in the north of Western Siberia. *Permafrost Periglacial Process* 13(1): 43-51.

Romanovsky, V.E., M. Burgess, S. Smith, Yoshikawa, K. & Brown, J. 2002: Permafrost temperature records: Indicators of climate change. *EOS, Transactions, American Geophysical Union* 83: 589-594.

Sazonova, T.S. & Romanovsky, V.E. 2003. A model for regional-scale estimation of temporal and spatial variability of active-layer thickness and mean annual ground temperatures. *Permafrost and Periglacial Processes* 14(2): 125-140.

Symon, C. (ed.). 2005. *Impacts of a Warming Arctic: Arctic Climate Impacts Assessment.* Cambridge: Cambridge University Press, 1042 pp.

Vasilieva, I. 2004: *Climate, thawing permafrost, and buildings in the Northern lands*. *Expert* - 9 *Siberia.* Yakutsk, pp. 2nd October 2004.

Zernova, L. 2003. *Has the frost cancelled the predicted global warming? The City*. St. Petersburg, Russia, 14-15.

# Foundation Design Using a Heat Pump Cooling System

Bjarne Instanes
*Instanes Svalbard AS, N-9171 Longyearbyen, Norway*
Arne Instanes
*Instanes Svalbard AS, N-9171 Longyearbyen, Norway*

## Abstract

On several locations in Svalbard, Norway, it is advantageous to design buildings with on-grade foundations over ice-rich permafrost soils. These types of foundations require insulation material underneath the concrete floor slab and a cooling system underneath the insulation to prevent thawing of the underlying ice-rich permafrost. This type of foundation design may also be beneficial to mitigate the effect of possible future climate warming on the structure. The heat pump cooling system presented in this paper is designed to decrease the temperature of the permafrost foundations soils to a design value. The heat extracted from the ground is used for heating of the building above. The foundation system has been installed at several locations in Longyearbyen and Sveagruva in Svalbard over the last 20 years. From our point of view the foundation design presents an attractive alternative to pile foundations both from an economical and a technical point of view. The paper describes in detail the foundation design using heat pumps, including case studies and cost comparison with conventional pile foundations of the frozen ground.

**Keywords:** engineering; foundations; geotechnical; permafrost; warming.

## Introduction

Foundation design in Svalbard was traditionally based on pile foundations or shallow foundations. These foundation techniques require a ventilated air space of 0.5–1.0 m between the insulated floor and the ground surface. Pipelines for water supply and sewage were insulated and heated and attached outside under the insulated floor of the building. In this manner the heat flow from the building was restricted from entering the ice-rich permafrost soils.

The new technique described in this paper has several advantages compared to conventional piles or shallow foundations.

## Climatic Conditions in Svalbard

The Svalbard archipelago is situated 74°N–81°N and 10°E–35°E. The land area is approximately 62,000 km$^2$ (Fig. 1). Svalbard has an exceptionally mild climate compared to North America and Russia at the same latitude, mainly due to the warming effect of the Gulf Stream and low pressures transporting heat northwards. Longyearbyen is located at 78°N, 11°E on Spitsbergen in the Svalbard Archipelago. Longyearbyen is the main settlement in Svalbard and has today approximately 2000 citizens. The main activities are coal mining, education, research and tourism.

Figure 2 shows the mean annual air temperature at the Longyearbyen/Svalbard Airport during the period 1912–2006. Monitoring of air temperature at the Svalbard airport commenced in 1975. Data earlier than 1975 is from air temperature monitoring in Longyearbyen. Figures 3 and 4 present the air freezing index and thawing index for Longyearbyen. It can be observed from the figures that there is a trend of increasing mean annual air temperatures during the last 20 to 30 years. In the same period the air freezing index is decreasing (indicating warmer winters) and the air thawing index is increasing (indicating warmer summers). However, Figures 2, 3, and 4 also show that the area has previously experienced warm periods, especially 1920 to the 1940s and 1950s.

It can also be observed from the figures that 2006 and 2007 have been extremely warm years, and this advocates a foundation design that can mitigate the effects of possible climate warming.

## Conventional Foundation Design in Svalbard

Foundation design in Svalbard was traditionally based on pile foundations or shallow foundations. These foundation

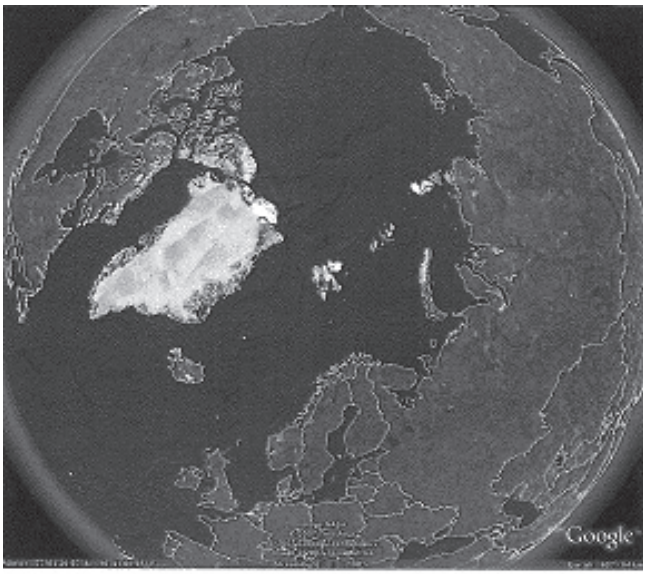


Figure 1. Location of the Svalbard archipelago (map from Google Earth, earth.google.com).

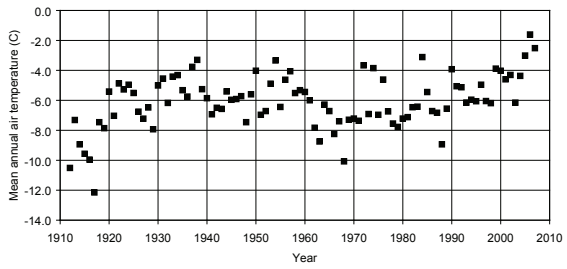


Figure 2. Mean annual air temperatures, Longyearbyen 1912–2007.

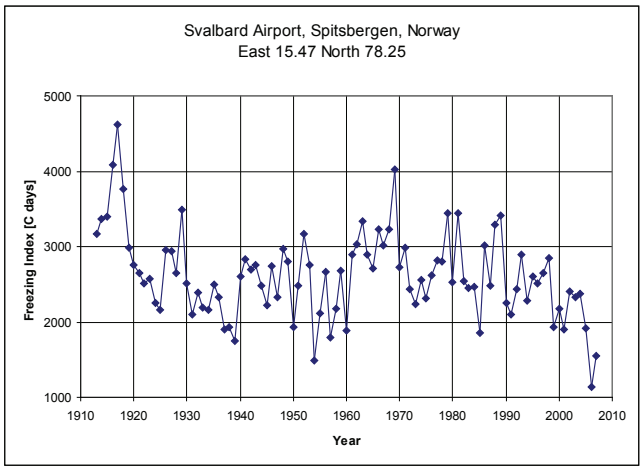


Figure 3. Air freezing index, Longyearbyen 1912–2006.

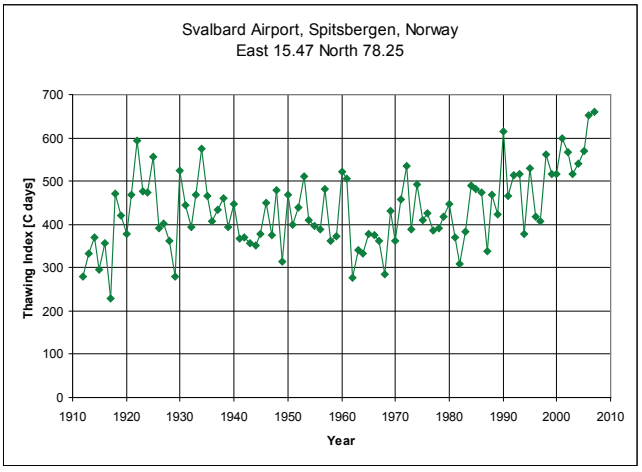


Figure 4. Air thawing index, Longyearbyen 1912–2007

techniques require a ventilated air space of 0.5–1.0 m between the insulated floor and the ground surface. Pipelines for water supply and sewage were insulated and heated and attached to under the insulated floor of the building. In this manner the heat flow from the building was restricted from entering the ice-rich permafrost soils.

In the 1980s the main author, in collaboration with a contractor and the local mining company, developed new equipment for predrilling boreholes for pile installation. The new drill rig was capable of drilling 300 mm diameter holes to a depth of 12 m beneath the surface. This meant that installation and grouting of prefabricated concrete, steel, or wooden piles became the preferred foundation technique in Svalbard.

However, this meant as mentioned above, that the building had to be elevated above the ground which is, in our opinion, not ideal from an esthetical, practical, or economical point of view.

## Heat Pump Cooling System

Based on experience from the development of a district heating system utilizing heat pumps in Bergen Harbour, Norway, the idea of using heat pumps in permafrost areas was born. A heat pump will lower the ground temperature, and the heat extracted from the ground can be used in the heating of the interior of the building. In 1986 the first building using the new technique was constructed in Sveagruva, Svalbard (N77°53′, E16°41′) (Instanes 1988). The storage building had an area of 900 m$^2$. Because of the high foundation loads, pile foundations were not a good solution for this project. The building was therefore placed directly on the ground using heat pumps to artificially lower the ground temperature (Fig. 5).

The following procedure was used for clearing the site and installing the heat pump system (Fig. 6):

- The site was drained and leveled in order to lead surface water away from the building.
- A mimimum 0.5 m thick layer of sand, gravel fill was placed on the natural terrain and compacted.
- Forty mm PVC cooling pipes were placed on the sand, gravel layer in a 100 mm thick reinforced concrete slab.
- The cooling fluid circulated in the pipes is a mixture of glycol and water.
- Two hundred mm thick Styrofoam insulation was placed on top of the concrete slab.
- A plastic film was placed on top of the insulation in order to stop vapour diffusion.
- A 700 mm layer of fine sand was placed between the insulation and the floor of the building (gravel size can also be used in this layer). The thickness of this layer is governed by the necessary slope of drainage pipes.
- The concrete slab on top of the sand layer was reinforced and had a thickness of 150 mm. It was designed for large mobile loads from cranes and vehicles inside the building.

In addition to the first use in Sveagruva described above, the foundation system has been installed for three buildings in Longyearbyen: *Næringsbygget* (1989 and 1992), *Svalbardbutikken* (1990) and more recently in the ISS-building (20052006)(Fig. 7).

The technique is especially useful when the foundation loads are high and in areas with difficult foundation soils such as marine, saline, ice-rich, silts and clays, frequently found in Longyearbyen and Sveagruva (Instanes & Instanes 1998).

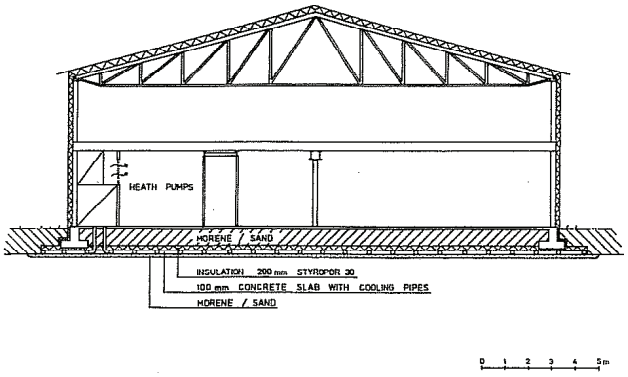


Figure 5. Cross-section of the storage building in Sveagruva.

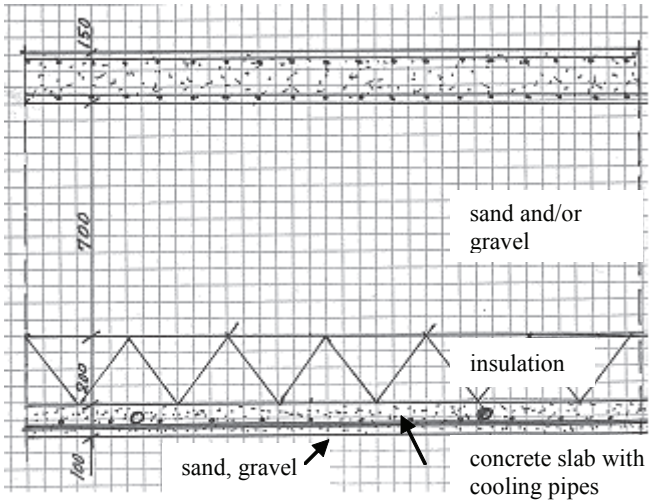


Figure 6. Detail of the foundation system.

## ISS-Building, Longyearbyen

The ISS-building is a laundry that was constructed in 2004–2005. The site lies close to the Advetfjord and is thermally affected by the sea. The foundation soils consist of saline (3%–4%), ice-rich, silty clay. The permafrost temperature at 10 m depth is approximately -3°C to -4°C. The design criterion for the foundations was maximum settlement of 5 cm in 20 years. The foundation principle for this building is similar to what has been described in the previous section.

Figure 8 shows the layout of the cooling pipes for the ISS-building.

The total area covered by the cooling pipes is 600 m$^2$ (15 m x 40 m) and the total length of the pipes was 760 m. The maximum horizontal distance between parallel pipes was 0.75 m. Two parallel systems were installed, one primary main system and one secondary backup system

Pile foundations were considered for this building, but due to the difficult soil conditions, relatively warm permafrost, and the warm interior of the building (up to +40°C), it was not considered a technically safe solution during possible climate warming. The heat pump cooling system was therefore selected.

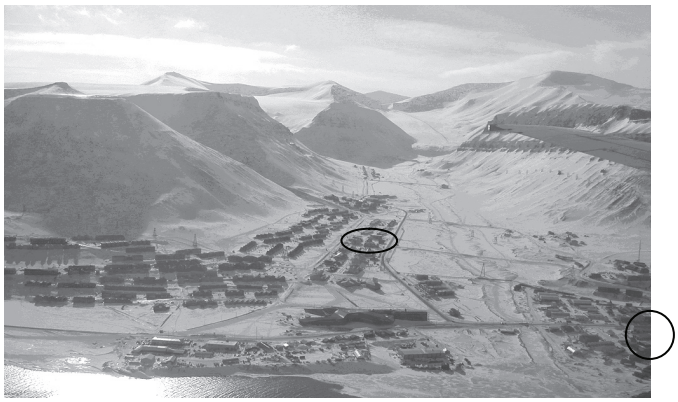

Figure 7. Overview of Longyearbyen. *Næringsbygget* and *Svalbardbutikken* are located in the center of the photo, ISS-building in the lower right corner.

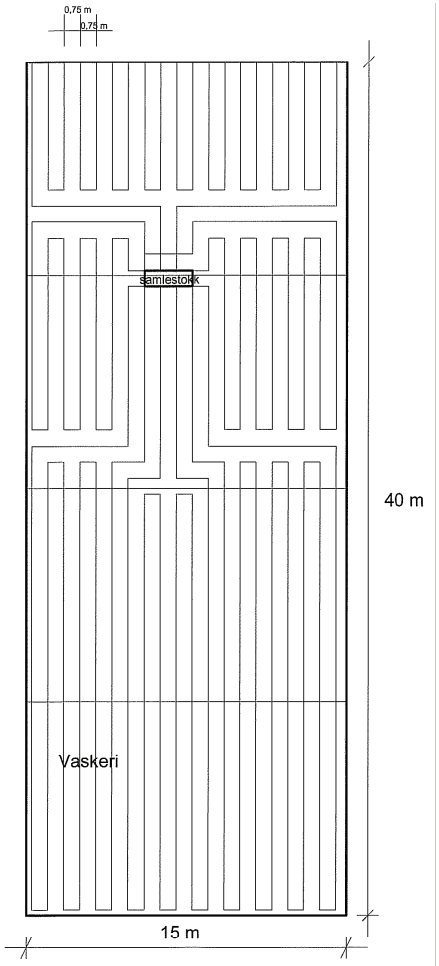


Figure 8. Layout of the cooling pipes at the ISS-buildings.

## Thermal Considerations and Costs

The thermal design of the foundation system was based on the principle that the subsurface soils were to be cooled down to -5°C. To estimate the time needed to cool down the surface layers after construction, the thermal model TEMP/W, version 7.03 (Geo-Slope 2007) was used. TEMP/W is a finite element software that can model the thermal changes in the

ground due to changing temperature or heat flux boundary conditions. It also accounts for the effects of the temperature dependent thermal conductivity, volumetric latent heat of fusion, and soil unfrozen water content.

Based on the thermal calculations and present climate warming, it was decided to let the cooling system run continuously with an internal fluid temperature varying between -5°C and -10°C.

The additional cost associated with the heat pump cooling system compared to conventional pile foundations was estimated to NOK1000 per $m^2$ (approximately USD180 per $m^2$).

## Advantages Using a Heat Pump Cooling System

A foundation system in permafrost regions using a heat pump system is advantageous due to a number of reasons:

- The foundation design can be used in marginal zones with discontinuous permafrost or saline soils.
- The energy consumption is limited. The heat loss through the floor is regained by the heat pumps.
- The building can be constructed with the floor directly on the ground and the air space between the floor and the ground is avoided.
- The heat loss from the building because of wind blowing under the building is eliminated.
- The water supply and sewage pipes can be buried in the sand/gravel layer, making the access to the building and the entrance to the building easier.
- It becomes possible to have a warm "ground floor" in the building.
- Heating using hot water pipes can be installed in the floor; additional insulation may then be needed beneath the floor surface.
- For large buildings such as storage buildings and industrial facilities, it becomes costly to have floor structure spanning between piles or pillars. Using an embankment fill, the loads can be transferred directly to the embankment.
- Possible climate change and permafrost temperature increase can be mitigated.

## References

Instanes, A. & Instanes, D. 1999. Pile design in saline permafrost at Longyearbyen. *Proceedings of the 10th International Conference on Cold Regions Engineering, Lincoln, NH, USA, August 16-19, 1999*: 222-231.

Instanes, B. 1988. Foundation design on permafrost with heat pumps. *Proceedings of the Fifth International Conference on Permafrost, Trondheim, Norway, August 2-5, 1988*: Volume 3: 73-74.

Geo-Slope. 2007. *Thermal Modelling with TEMP/W 2007. An Engineering Methodology.* Calgary, Canada: GEO-SLOPE International Ltd. 240 pages.

# Five-Year Ground Surface Temperature Measurements in Finnmark, Northern Norway

Ketil Isaksen, Herman Farbrot
*Norwegian Meteorological Institute, Oslo, Norway*
Lars Harald Blikra
*International Centre for Geohazards, Oslo, Norway*
Bernt Johansen
*Northern Research Institute Tromsø, Tromsø, Norway*
Johan Ludvig Sollid, Trond Eiken
*Department of Geosciences, University of Oslo, Oslo, Norway*

## Abstract

In 2002 a new permafrost monitoring program was initiated in Finnmark, northern Norway. A series of miniature temperature dataloggers were installed for continuous monitoring of ground surface and air temperatures. Results suggest that permafrost is widespread in Finnmark. However, the great areas of birch and pine forest in Finnmark appear to correspond to areas without permafrost, due to the forest acting as a snow fence and causing snow to accumulate. Above the timberline, snow depth seems to be the most critical factor for the formation of permafrost.

**Keywords:** mean ground surface temperatures; Northern Norway; permafrost distribution.

## Introduction

Permafrost is widespread in the higher mountains of Norway. Extensive studies in southern Norway show that the lower regional altitudinal limit of mountain permafrost is strongly correlated to the mean annual air temperature (MAAT) and decreases eastwards with increasing continentally (e.g., Etzelmüller et al. 2003). However, there are, to date, few quantitative studies of the distribution of permafrost in northern Norway.

In 2002, a new permafrost monitoring program was initiated in Finnmark, which is the northernmost county of mainland Norway (Fig. 1). A series of miniature temperature dataloggers (MTDs) were installed for monitoring ground surface and air temperatures. Continuous ground surface monitoring was performed at five main sites in a transect starting at Varangerhalvøya in the extreme northeast of Norway, continuing southwest to the interior of Finnmarksvidda, and then northeastwards to the Gaissane.

The main aim of this study is to determine mean ground surface temperatures (MGST) at representative sites in Finnmark in order to provide an initial indication of the presence or absence of permafrost. The results are related to climate data, mainly air temperature and snow cover. In addition, a land-cover classification of the whole county is made that gives a first qualitative picture of the relationship between climate, vegetation and permafrost distribution in Finnmark. A review of the literature of permafrost occurrence in northern Scandinavia is presented, together with new results from 5 years of temperature monitoring.

## Literature Review

*Permafrost in northern Scandinavia*

Until the 1980s, permafrost research in Northern Scandinavia was mainly concentrated on palsas, and a number of studies (cf. references in Åhman 1977) were undertaken following the pioneer work of Fries and Bergström (1910).

However, in the beginning of the 20th Century, field observations and theoretical considerations by Reusch (1901) suggested that permafrost was present in the mountains of Scandinavia. In the following decades few reports on permafrost occurrence in northern Scandinavia were published. A review of Scandinavian permafrost investigations up to 1950s is provided by Ekman (1957). During the drilling of a well at 1220 m a.s.l. in northern Sweden, permafrost was encountered at 70 m depth in bedrock (Ekman 1957). Frozen ground was also encountered during construction work in northern Finland and Sweden (e.g., Ekman 1957, Åhman 1977), but it is often difficult to decide whether these findings are perennially or only seasonally frozen ground (King & Seppälä 1988).

Since the beginning of the 1960s, research on permafrost outside the palsa mires has increased, with most reports on geomorphological indicators (Jeckel 1988).

In the 1980s, studies using geophysical methods encountered extensive permafrost at 50–100 m depth in bedrock in mountain areas of northern Sweden (e.g., King 1982) and Finland (King & Seppälä 1987). On a mountain in northern Sweden, Jeckel (1988) reported a mean ground temperature (MGT) at 2.3 m depth to be -0.8°C at 880 m a.s.l. In a 100 m deep borehole at Tarfalaryggen (1550 m a.s.l.) in northern Sweden, it has subsequently been shown that MGT is approximately -3 ºC and permafrost thickness is estimated to exceed 300 m (Isaksen et al. 2001). In northern Finland, Bottom Temperature of Snow (BTS) measurements suggested a lower limit of permafrost at 600-650 m a.s.l. on north-facing slopes (Jeckel 1988). In Finnmark, quantitative studies on permafrost distribution are limited and are

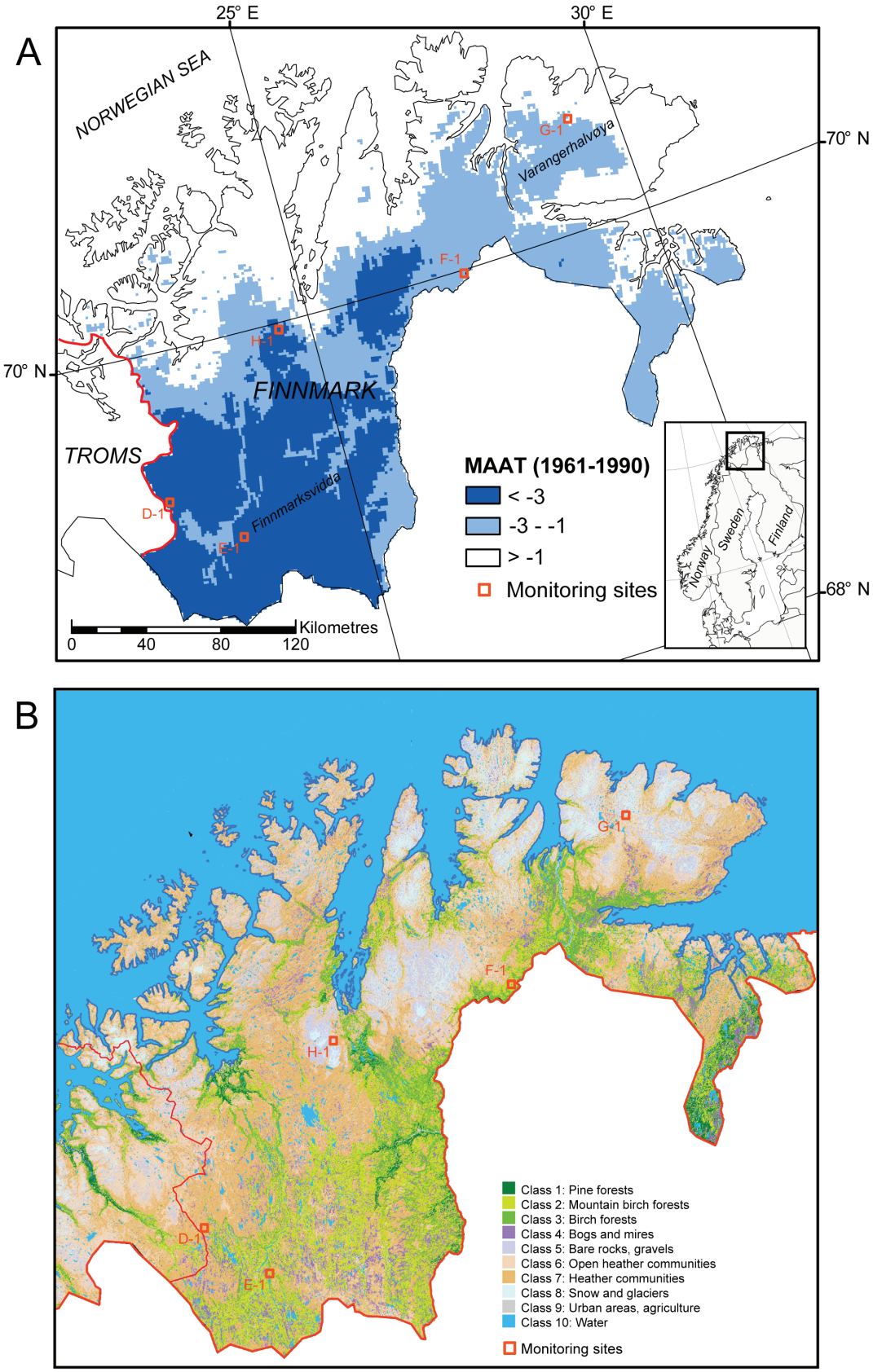


Figure 1. A) Location map showing the monitoring locations and three classes of the mean annual air temperature (MAAT, 1961-1990) in Finnmark (based on Tveito et al. 2000). (D-1) Biedjovággi; (E-1) Ávži; (F-1) Eliasvárri; (G-1) Basečearru; (H-1) Gaissane. The dark blue shows areas where MAAT is below -3°C, light blue shows areas where MAAT is between −3°C and −1°C and white is MAAT above -1°C. B) Classified land-cover map of Finnmark county based on Landsat TM/ETM+ satellite images (see text for details).

mostly restricted to palsa mires (e.g., Sollid & Sørbel 1998, Hofgaard 2007). In some settlements, however, permafrost degradation has caused problems during construction work (e.g., Lien 1991).

## Study Sites

Three of the sites (D, G, and H), were chosen to optimize comparability and to ensure that the thermal properties were not excessively complex (Fig. 1). These were located at exposed locations, in the main ridge-crest or plateau areas, where snow accumulation is low. The last two sites are located in open (F) and dense (E) mountain birch forest.

The inner part of Finnmark (Finnmarksvidda, site E) is a plain having strong continentally and has the lowest MAAT when reduced to sea level in Norway. Typically, in this area, MAAT is -2.5°C to -4°C, with mean summer temperatures of 8°C to 10°C and mean winter temperatures of -15°C to -20°C. In winter, mean maximum snow depth is 25–75 cm. Towards the N (Site H) and NW (Site D), continentality decreases, with more mountains and more complex climate settings. Towards the NE, at Varangerhalvøya (Site G), mountain plateaus dominate, and the area is in the Arctic climate zone.

## Methods

*Land-cover classification*

In this study, a land-cover map of Finnmark county (Fig. 1B) is developed (in 200 x 200 m resolution), reflecting degrees of density in the vegetation cover. The land-cover map is a subsection of the vegetation map produced for the entire country of Norway. In this map, a total number of 45 Landsat TM/ETM+ images were processed during six operational stages: (1) spectral classification, (2) spectral similarity analysis, (3) generation of classified image mosaics, (4) ancillary data analysis, (5) contextual correction, and (6) standardization of the final map products (Johansen & Karlsen 2005). Analysis performed on the spectral-only data is often denoted as the pre-classification stage of the process, whereas the post-classification process involves analysis and subsequent contextual corrections of the pre-classified image using ancillary data. In the final standardization part of the process, the defined classification units are related and described according to classification schemes well-established in the Norwegian botanical literature (Fremstad 1997). From the overall vegetation map of Norway, different thematic maps can be extracted.

*Continuous temperature measurements*

Nine (out of 20 in total) UTL-1 (Geotest, Switzerland) MTDs were used to determine the mean ground surface temperatures (MGST). They were buried at the surface (c. 0.05 m depth) and installed in Autumn 2002 and 2003. In addition, one logger was used to monitor the air temperature at G-1. At the other sites, air temperatures were obtained by interpolation from nearby weather stations (Table 1). The thermistors in the MTDs are of the type TMC-1T, with accuracy better than the 0.27°C given by

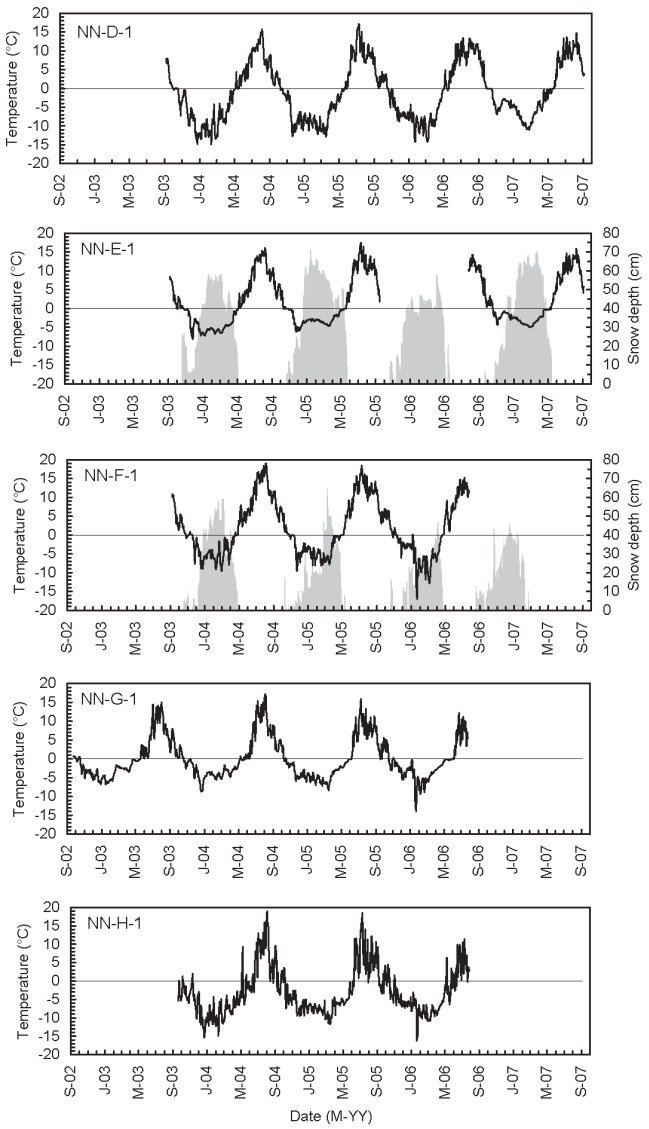


Figure 2. Daily ground surface temperatures obtained at the 5 main locations in Finnmark during 2002–2007. For E-1 and F-1, observed snow depth (grey bars) from nearby official stations are shown.

the manufacturer (Hoelzle et al. 1999). The MTDs were programmed to record the ground surface temperature every 6 hours (2 hours in Gaissane). In addition, the MTDs gave important information concerning damping of short-term air temperature fluctuations through the snow (reflecting the development and thickness of snow cover), the time when melting occurred at the bottom of the snowpack, and when snow disappeared.

Climate data from official weather stations were used to normalize the data sets in respect to the normal standard period 1961–1990, in order to establish the long-term MGST. The method is described by Ødegård et al. (2008). From the MTDs, monthly mean of ground surface temperatures were calculated and analyzed with the best nearby correlated air temperature from an official meteorological station having long-time series (e.g., 30-year period or more). A high correlation suggests low influence of snow and latent heat effects, which give a strong coupling between the air

Table 1. Key temperatures observed at monitoring sites. MGST = Mean ground surface temperature for observation period, maximum and minimum of 12-months running mean of MGST during observation period. MAT = Mean air temperature observed (Obs) and interpolated from nearest station (Int). MAT-anomaly: Air temperature deviation for observation period from nearest station. Air temperature at G-1 is for the period Sep03–Jun06. For interpolation of air temperature at G: 2,3,4, a gradient 0.53°C/100 m was used from G-1 (Laaksonen 1976). For the other interpolated values, the same gradient was used from nearest official weather station. H-1 and H-2 were from Farbrot et al. (2008). Type = Land type class (cf. Fig. 1B).

| Site | Type | Alt. m a.s.l. | Period observed | MGST Obs. | MGST max Obs. | MGST min Obs. | MAT Obs. | MAT Int. | MAT-anomaly | MAGST Normal | MAAT Normal |
|---|---|---|---|---|---|---|---|---|---|---|---|
| D-1 | 6 | 739 | Oct 03-Aug 07 | -1.1 | -0.1 | -1.7 | - | -3.4 | 1.5 | -2.2 | -4.9 |
| E-1 | 3 | 355 | Oct 03-Aug 07 | 1.6 | 2.0 | 1.0 | -1.2 | - | 1.5 | 1.2 | -2.6 |
| F-1 | 2 | 130 | Oct 03-Jun 06 | 2.2 | 2.5 | 1.9 | - | 0.6 | 1.9 | 0.8 | -1.3 |
| G-1 | 5 | 502 | Oct 02-Jun 06 | 0.3 | 0.7 | -0.2 | -1.2 | - | 1.4 | -1.0 | -2.9 |
| G-2 | 5 | 480 | Oct 02-Jun 06 | 1.0 | 1.2 | 0.5 | -1.1 | - | 1.4 | -0.4 | -2.8 |
| G-3 | 5,6 | 415 | Oct 02-Jun 06 | 1.3 | 2.1 | 0.5 | -0.8 | - | 1.4 | -0.3 | -2.4 |
| G-4 | 6 | 355 | Oct 02-Jun 06 | 1.7 | 2.2 | 1.2 | -0.5 | - | 1.4 | 0.1 | -2.1 |
| H-1 | 5 | 1034 | Oct 03-Jun 06 | -2.4 | -2.1 | -2.8 | - | -2.9 | 1.6 | -3.6 | -4.5 |
| H-2 | 5 | 618 | Oct 03-Jun 06 | -0.9 | -0.6 | -1.2 | - | -0.9 | 1.6 | -2.2 | -2.5 |

and ground surface temperatures. Monthly air temperature anomalies (in respect to the 1961–1990 average) can then be used to correct the monthly observed ground surface temperature during the observation period (see Table 1).

## Results

*Vegetation types in Finnmark*

The land cover map of Finnmark portrays the density of the vegetation cover at different levels. The coniferous pine forests are mainly located to the southern, continental parts of the county, constituting the largest areas along the main rivers in the area. In addition, the Pasvik area, south of Varangerhalvøya, is characterized by well-developed pine forests. The mountain birch forest, occupying large areas on Finnmarksvidda, is characterized by an open forest layer with heather and lichen species dominating the ground layer. The more dense and fertile birch forests are located mainly in the coastal regions. The differentiation in the mountain belt generally reflects the low-, the mid-, and the high-alpine belt of the region. Heather communities, with a closed vegetation cover, characterize the low-alpine belt. In the mid-alpine belt, the vegetation cover is more scattered due to harsher climate conditions. The high-alpine belt has bare rocks, boulder fields, and gravel ridges. Few vascular species are adapted to the climate conditions found here. This belt is characterized by mosses and lichen species.

*Mean ground surface temperature (MGST)*

Mean ground temperatures from 3–5 years of continuous monitoring (Fig. 2 and Table 1) show that:

a) the highest MGST were found in the forested areas (G-1 and E-1);
b) the lowest MGST were observed at the two highest sites (H-1) Gaissane and (D-1) Biedjovággi were bare rock and boulder fields dominate;
c) 12-month running means of MGST show large variation within the observation period at all sites. The difference between the highest and lowest 12-month MGST are between 0.6°C and 1.6°C; and
d) the mean air temperature (MAT) is generally 1–2.5°C lower than MGST. The largest difference is found at the two forested sites (2.8°C), while at the most exposed locations (H) the difference is only 0–0.4°C.

Correlation between ground surface temperature and air temperatures at G-1 is shown in Fig. 3. The results indicate a strong correlation. In general, the site is exposed to strong winds, leading to only a thin snow cover in late winter, probably not more than 0.3–0.5 m.

Data from official weather stations close to the monitoring sites show that the MAT during the observation period was 1.4–1.9°C above the 1961–1990 normal. By normalizing the observed MGT-values (Ødegård et al. 2008), data suggest that mean annual ground surface temperature (MAGST) is below 0°C at six sites. Only the two sites located in forest (E and F) and the lowermost site at Varangerhalvøya (G-4) have positive MAGST.

## Discussion

In Norway, the Nordic mountain birch limit is close to the 8°C tetratherm (mean air temperature for June–September) (Wielgolaski 2005). However, the tetratherm limits decrease in relatively continental areas with high day temperatures during summer. This means that continental sites generally have a higher forest limit than more maritime sites even though the MAAT is equal (Meier et al. 2005, Wielgolaski 2005). Forest (mainly birch) is present in the interior of Finnmark where MAAT is far below 0°C (Fig. 1). The timberline is located at about 500 m a.s.l. on Finnmarksvidda (Meier et al. 2005).

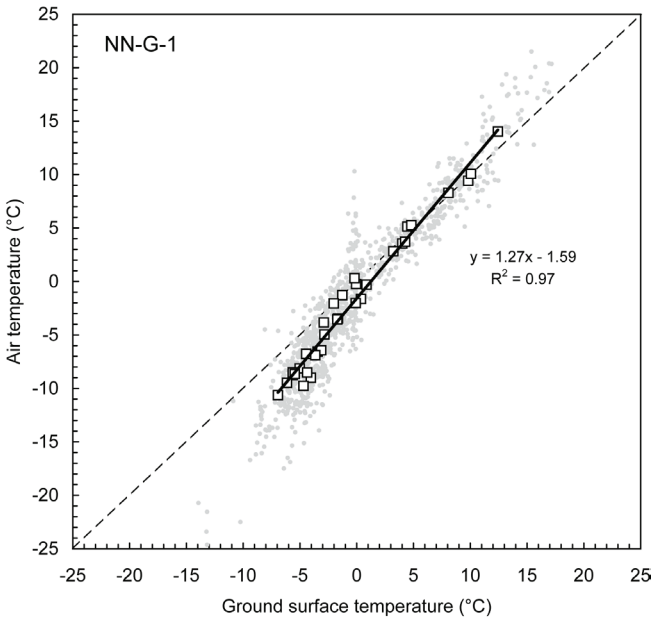


Figure 3. Mean daily (grey small dots) and monthly (open squares) ground surface temperature versus mean daily and monthly air temperature (2 m) during the period of record at G-1 Basečearru (Varangerhalvøya). Linear least squares regression coefficients and coefficient of determination ($R^2$) for the monthly values are shown.

Two sites, E-1 and F-1, are significantly warmer than the other study sites. The reason is the influence of the forest, which collects snow and therefore has a quite different energy-balance compared to wind-swept locations. Although cooler in summer due to radiation interception and higher evaporation (e.g., Rouse 1984), the near-surface ground temperatures in the forest are considerably warmer in winter than the other locations (Table 1). Hence, the forest in Finnmark largely prevents permafrost formation, making the forest line altitude very important in defining the permafrost limits. Although Scandinavian treelines are expected to advance in response to climate warming, there are indications of recessive treelines in northern Norway in contrast to southern Norway (Dalen & Hofgaard 2005). Above timberline, snow depth appears to be the most critical factor for the formation of permafrost (cf. King & Seppälä 1988). Results from Farbrot et al. (2008) and this study (Table 1) suggest that MGST above timberline in Finnmark can differ by 1–2°C due to variations in snow thickness. This is somewhat lower than values reported from southern Norway (e.g., Hauck et al. 2004, Ødegård et al. 2008).

King (1984) suggests that mountain permafrost in Scandinavia may be divided into continuous, discontinuous and sporadic. Their lower limits correspond to MAAT of -6°C and -1.5°C and sporadic permafrost may occur even in areas with positive MAATs. The transition between these belts is gradual. The temperature values for the lower limits are valid for the central Scandinavian mountain areas with moderately continental climate. The climate of Finnmark shows strong continentality, with generally thin snow cover. The results obtained from the MTDs and Farbrot et al. (2008) suggest that the proposed limits suggested by King (1984) can be adjusted in this region by lowering the limit of discontinuous permafrost to a MAAT of -1°C (Fig. 1). In areas colder than -3°C, permafrost seems to be widespread above timberline.

## Conclusions

Miniature temperature dataloggers recording ground surface temperatures have been shown to provide data suitable for mapping the spatial variation in mean annual ground surface temperatures in Finnmark, and thus the possible presence or absence of permafrost at the sites. Results suggest that:

- Permafrost is widespread in Finnmark. The lower limit of discontinuous permafrost outside the palsa mires corresponds to mean annual air temperatures (MAAT) of approximately -1°C,
- Permafrost is probably present in the interior part of Varangerhalvøya. This is probably the northernmost permafrost area in north-western Europe (outside Russia) and can be regarded as polar permafrost
- Birch and pine forest in Finnmark appears to correspond with areas without permafrost. Trees cause snow to accumulate and insulate against strong ground cooling. Below the timberline and beside the palsa mires, formation of permafrost is possible at local exposed sites where snow does not accumulate, or cleared areas (in villages, on roads etc),
- Snow depth seems to be the most critical factor for the formation of permafrost above the timberline. However, variations in mean annual ground surface temperatures due to variations in snow depth seem to be lower in Finnmark (cf. Table 1) than in southern Norway, probably due to generally lower precipitation. Permafrost is apparently widespread in Finnmark in areas above timberline having MAAT lower than -3°C,
- Air temperatures for the previous 3–5 years have been 1.5–2.0°C warmer than the 1961–1990 average. In Finnmark permafrost is "warm" as it is only a few degrees below 0°C, which makes it very vulnerable to warming (cf. Isaksen et al. 2007), and
- The present monitoring program in Finnmark is being continued and will be included within the Norwegian funded IPY-project *Permafrost Observatory Project: A Contribution to the Thermal State of Permafrost in Norway and Svalbard*, (Christiansen et al. 2007). The relation between MGST and snow and vegetation should be further investigated, and similar measurements should be made at other sites to see if these findings can be generalized to larger areas.

## Acknowledgments

This study is part of a Norwegian network project, *Permafrost og ustabile fjellsider,* supported by the Geological Survey of Norway, Norwegian Meteorological Institute and the University of Oslo. In addition, part of the study was financed by the Norwegian Research Council (project no.

157837/V30). C. Harris smoothed the English, and two anonymous reviewers gave important improvements to the manuscript. The contributions of all persons and institutions mentioned are gratefully acknowledged by the authors.

## References

Åhman, R. 1977. Palsar i NordNorge. Meddelanden från Lunds universitets Geografiska institution avhandlingar LXXVIII.

Christiansen H et al. 2007. Permafrost Observatory Project: A Contribution to the Thermal State of Permafrost in Norway and Svalbard, TSP NORWAY. *Eos Trans. AGU* 88(52), Fall Meet. Suppl., Abstract C21A-005.

Dalen, L. & Hofgaard, A. 2005. Differential Regional Treeline Dynamics in the Scandes Mountains. *Arctic, Antarctic and Alpine Research* 37: 284-296.

Ekman, S. 1957. Die Gewässer des Abisko-Gebietes und ihre Bedingungen. Kungl. Sv. Vetenskapsakademiens Handlingar 6:6 (Stockholm).

Etzelmüller, B., Berthling, I. & Sollid, J.L. 2003. Aspects and Concepts on the Geomorphological Significance of Holocene Permafrost in Southern Norway. *Geomorphology* 52: 87-104.

Farbrot, H., Isaksen K & Etzelmüller B. 2008. Present and Past Distribution of Mountain Permafrost in Gaissane Mountains, Northern Norway. *Proceedings of the Ninth International Conference on Permafrost, Fairbanks, Alaska, June 29-July 3, 2008* (this proceedings).

Fremstad, E. 1997. Vegetasjonstyper i Norge. *NINA Temahefte* 12: 1-279.

Fries, T. & Bergström, E. 1910. Några iakttagelser öfver palsar och deres förekomst i nordligaste Sverige. – Stockholm, Geol. Fören. Förh. 32: 195-205.

Hauck, C., Isaksen, K., Vonder Mühll, D. & Sollid, J.L. 2004. Geophysical surveys designed to delineate the altitudinal limit of mountain permafrost; an example from Jotunheimen, Norway. *Permafrost and Periglacial Processes* 15: 191-205.

Hoelzle, M., Wegmann, M. & Krummenacher, B. 1999. Miniature temperature dataloggers for mapping and monitoring of permafrost in high mountain areas: First experience from the Swiss Alps. *Permafrost and Periglacial Processes* 10, 113-124.

Hofgaard, A. 2007. Monitoring of palsa peatlands. Initial investigation in Goahteluoppal, West-Finnmark 2006. *NINA Report* 257, 33 pp.

Isaksen, K., Holmlund, P., Sollid, J.L. & Harris, C. 2001. Three deep alpine-permafrost boreholes in Svalbard and Scandinavia. *Permafrost and Periglacial Processes* 12: 13-25.

Isaksen, K., Sollid, J.L., Holmlund, P. & Harris, C. 2007. Recent warming of mountain permafrost in Svalbard and Scandinavia. *Journal of Geophysical Research* 112: doi:10.1029/2006JF000522.

Jeckel, P.P. 1988. Permafrost and its altitudinal zonation in N. Lapland. In: Senneset, K. (ed.), *Permafrost Fifth International Conference,* 170-175.

Johansen, B. & Karlsen S.R. 2005. Monitoring vegetation changes on Finnmarksvidda, Northern Norway, using Landsat MSS and Landsat TM/ETM+ satellite images. *Phytocoenologia* 35: 969-984.

King, L. 1982. Qualitative and quantitative Erfassung von Permafrost in Tarfala (Schwedisch-Lappland) und Jotunheimen (Norwegen) mit Hilfe geoelektrischer Sondierungen. *Zeitschrift für Geomorphologie, N. F.*, Suppl.-Bd. 43: 139-160.

King, L., 1984. Permafrost in Skandinavien. Untersuchungsergebnisse aus Lappland, Jotunheimen und Dovre/Rondane. *Heidelberger Geographische Arbeiten* 76: 174.

King, L. & Seppälä, M. 1987. Permafrost thickness and distribution in Finnish Lapland; results of geoelectric soundings. *Polarforschung* 57: 127-147.

King, L. & Seppälä, M. 1988. Permafrost sites in Finnish Lapland and their environment occurrences. *Permafrost, ICOP IV*, Trondheim, 1988, Vol 1.

Laaksonen, K. 1976. The dependence of mean air temperatures upon latitude and altitude in Fennoscandia (1921-50). *Ann. Academ. Scient. Fennicae A III* 119, 19 pp.

Lien, R. 1991. Investigation on permafrost in Kautokeino (in Norwegian). *Statens Vegvesen*, 91/3114-01.

Meier, K.-D., Thannheiser, D., Wehberg, J. & Eisenmann V. 2005. Soils and nutrients in northern birch forests: A case study from Finnmarksvidda, northern Norway. In: Wielgolaski, F.E. (ed*.), Plant ecology, herbivory, and human impact in Nordic mountain birch forests*. Berlin: Springer-verlag. P. 19-34.

Ødegård, R.S., Isaksen, K., Eiken, T. & Sollid, J.L. 2008. MAGST in Mountain Permafrost, Dovrefjell, Southern Norway, 2001-2006. *Proceedings of the Ninth International Conference on Permafrost, Fairbanks, Alaska, June 29-July 3, 2008* (this proceedings).

Reusch, H. 1901. Some contributions towards an understanding of the manner in which the valleys and mountains of Norway were formed (in Norwegian). In *NGU Yearbook 1900*. Norwegian Geological Survey, Kristiania, 124-263.

Rouse, W.R. 1984. Microclimate of Arctic tree line. 2: Soil microclimate of tundra and forest. *Water Resources Research* 20: 67-73.

Sollid, J.L. & Sørbel, L. 1998. Palsa bogs as a climate indicator—examples from Dovrefjell, southern Norway. *Ambio* 27: 287-291.

Tveito, O.E., Førland E.J., Heino, R., Hanssen-Bauer, I., Alexandersson, H., Dahlström, B., Drebs, A., Kern-Hansen, C., Jónsson, T., Vaarby-Laursen, E. & Westman, Y. 2000. Nordic Temperature Maps. *DNMI Klima 9/00 KLIMA*. 54pp.

Wielgolaski, F.E. 2005. History and environment of the Nordic mountain birch. In: Wielgolaski, F.E. (ed.), *Plant ecology, herbivory, and human impact in Nordic mountain birch forests*. Berlin: Springer-verlag. P. 3-18.

# Comparable Energy Balance Measurements on the Permafrost and Immediately Adjacent Permafrost-Free Slopes at the Southern Boundary of Eurasian Permafrost, Mongolia

Mamoru Ishikawa
*Institute of Observational Research for Global Change, JAMSTEC, Japan*
*Faculty of Environmental Earth Science, Hokkaido University, Japan*
Yoshihiro Iijima
*Institute of Observational Research for Global Change, JAMSTEC, Japan*
Yinsheng Zhang
*Institute of Observational Research for Global Change, JAMSTEC, Japan*
Tsutomu Kadota
*Marine Work Japan, Japan*
Hironori Yabuki
*Institute of Observational Research for Global Change, JAMSTEC, Japan*
Tetsuo Ohata
*Institute of Observational Research for Global Change, JAMSTEC, Japan*
Battogtokh Dorjgotov
*Institute of Geography, Mongolian Academy of Science, Mongolia*
N. Sharkhuu
*Institute of Geoecology, Mongolian Academy of Science, Mongolia*

## Abstract

Mongolian *Larch* forests are situated at the southern boundary of the Eurasian Taiga that vulnerably coexists with the permafrost. This paper describes hydro-meteorological situations at the permafrost underlying forested areas and also in the immediately adjacent permafrost-free pasture slopes, and evaluates the vulnerable and reciprocal features of permafrost and forest. Records spanning nearly two years showed considerably reduced net radiation onto the ground surface, lower air and soil temperatures, and wetter soils at the forest site. The analysis showed small imbalances of energy balance components between atmospheric and active layer heat fluxes estimated independently, if the effects of organic matter and porosity are considered for the soil thermal parameters. This indicates the importance of considering thermal properties of the forest soil in the preservation of permafrost when the forest shading, which greatly reduces incoming solar radiation, is well known.

**Keywords:** active layer; energy budget; forest; pasture; southern boundary of Eurasian permafrost.

## Introduction

In northern Mongolia, the distribution of permafrost is mosaic-like, yielding ecological contrast even over small geographic areas. *Larch* forests dominate on the north-facing permafrost slopes, while pastures dominate the south-facing slopes. Ongoing degradation of permafrost due to recent climatic warming (Sharkhuu 2003) is expected to lead to reduced forested area and to influence the regional hydro-ecological system.

Since 2002, the Institute of Observational Research for Global Change, of the Japan Agency of the Marine-Earth Science and Technology (JAMSTEC) has continuously made hydro-meteorological observations at sites in northern Mongolia, with the aim of understanding the water cycle on the basin-scale and predicting future changes. The distribution and vulnerability of permafrost are the major focuses of this project, because changes in these parameters would significantly alter river runoff regimes and soil wetness, resulting in the degradation of ecosystem services of this region. This paper describes hydro-meteorological situations at the permafrost underlying forested areas and also in the immediately adjacent permafrost-free pasture slopes, and evaluates the vulnerable and reciprocal features of permafrost and forest.

## Regional Settings and Observations

The observation sites used in this study are located on the northern forested (NF site) and southern pasture (SP site) slopes east of Ulaanbaatar (Fig. 1a). The nearest meteorological station, approximately 2 km away from these sites, had a mean annual air temperature of -3.5°C from 1992 to 2000. Mean annual total precipitation at Ulaanbaatar, where most of the precipitation occurs from June to August, was only 300 mm.

Analyzing cores obtained by drilling investigation, Ishikawa et al. (2005) found ice-rich permafrost and nearly

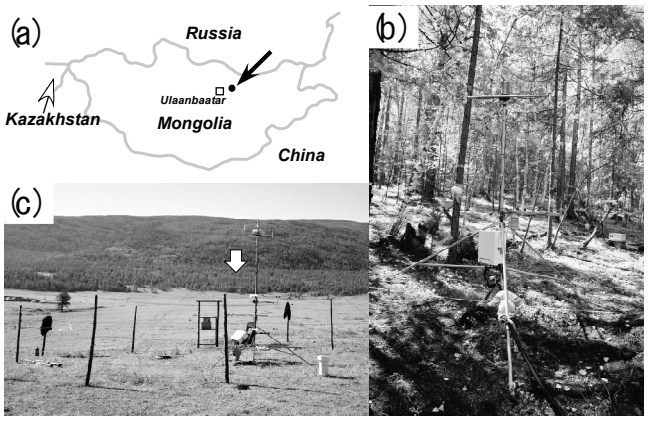


Figure 1. (a) Location of the observational site. Views of the setting of AWS (automatic weather monitoring system) on the (b) NF site and (c) SP site. The arrow in (c) indicates the location of the NF site.

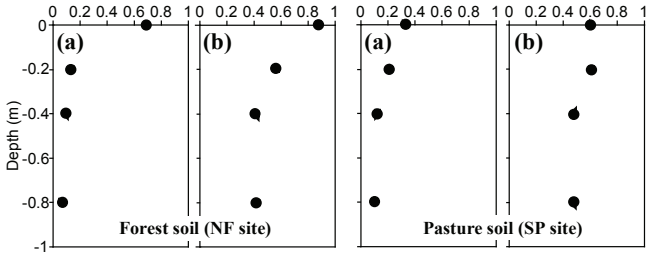


Figure 2. Soil properties at the NF and SP slope sites, based on laboratory analyses. (a) Organic ratio of soil particles ($m^3/m^3$), (b) porosity ($m^3/m^3$).

saturated active layer with a thickness of 2.4 m beneath the NF site, while cores showed the SP site to be permafrost-free, highly unsaturated, seasonally frozen ground beneath this site.

In summer 2003, an automatic weather monitoring system (AWS) with a capacity to measure four radiation components, air temperature, relative humidity, wind speed at two heights and surface soil heat flux, soil temperatures at depths of 0, 0.2, 0.4, 0.8, 1.2, 2.4, and 3.2 m, and moistures at 0, 0.2, 0.4, 0.8, and 1.2 m was installed at both sites (Figs. 1b, 1c). Soils at both sites comprised mainly sand cobbles covered with an organic-rich layer of several centimeters. We sampled undisturbed upper-layer soils and analyzed porosity, density, and organic contents in the laboratory (Fig. 2).

## Analysis

Neglecting heat supplied by rainfall, the surface energy balance equation during the snow-free period is

$$Q_n = Q_h + Q_e + Q_g \tag{1}$$

where $Q_n$ is net radiation calculated simply by adding the four radiation components; sensible heat flux, $Q_h$, latent heat flux, $Q_e$, and the ground heat flux from heat pile, $Q_g$. The turbulent fluxes $Q_h$ and $Q_e$ were estimated by the Bowen ratio method. The Bowen ratio, $B$, is expressed after approximating fluxes using gradients in the following manner:

$$B = Q_h / Q_e = C_a \Delta T / (L^{lv} \Delta q), \tag{2}$$

where $C_a$ is the specific heat of air, $L^{lv}$ is the latent heat for vaporization, and $\Delta T$ and $\Delta q$ are the vertical gradients of air temperature and specific humidity, respectively. Combining equations (1) and (2), the latent heat flux is

$$Q_e = \rho_w (Q_n - Q_g)/(1 + B), \tag{3}$$

where $\rho_w$ is the density of water. $Q_n$ was estimated from measurements of the four radiation components. We used surface soil heat flux sensor data as $Q_g$, relative humidity and air temperatures taken at two (for NF site) and three (SP site) heights, removing spurious data from original 10-minute-interval datasets as indicated by Ohmura (1982).

The conductive (sensible) soil heat flux was calculated using Fourier's law of heat transport,

$$j_h^i = -k_h^i \frac{\partial T}{\partial z} \tag{4}$$

where $k_h$ is bulk thermal conductivity, $T$ is temperature, and $z$ is depth for the $i$-th soil layer from the surface downward. The non-conductive heat component, $r_h$, is expressed in terms of heat production in $W/m^3$, and is estimated by considering the one-dimensional energy conservation as formulated by:

$$r_h^i = \frac{\partial}{\partial t}[c_h^i T] + \frac{\partial}{\partial z} j_h^i \ , \tag{5}$$

where $c_h$ is bulk heat capacity and $t$ is time. Total thermal energy stored in the soil layer, $Q_{g\text{-}c}$, is the summation of conductive and non-conductive heats of each layer as

$$Q_{g-C} = \sum_i (j_h^i + r_h^i d^i), \tag{6}$$

where $d^i$ is thickness of the $i$-th layer. The mid-depth of the $i$-th layer was set to be at the $i$-th depth measurement from the surface. Neglecting energy flux in the deepest soil layer, we calculated energy flux components in the upper three layers, having thicknesses of 0.3, 0.3 and 0.4 m from the surface. The finite element formulation used to solve equation (6) is described in Ishikawa et al. (2006).

Calculation of $Q_{g\text{-}C}$ requires data on the bulk thermal conductivity ($k_h$) and bulk heat capacity ($c_h$) of each soil layer. The spatio-temporal variations of the above variables are known to be largely dependent on the ratio between soil particle, water, and ice. Two models with different numbers of parameters were evaluated. The first model used conventional parameterization, which does not include the effects of thermal parameters of air occupying porosity and organic matter (Farouki 1981):

$$k_h^i = k_m^{1-n} k_s^{\theta_s} k_w^{\theta_w}, \tag{7}$$

$$c_h^i = (1-n)\rho_m c_m + \theta_s \rho_s c_s + \theta_w \rho_w c_w \tag{8}$$

In a second model, we modified equations (7) and (8) in order to consider mineral, water, ice, organic contents, and thermal parameters of air as,

$$k_h^{i'} = k_a^{n-\theta_s-\theta_w} k_o^{\theta_o} k_m^{1-n-\theta_o} k_s^{\theta_s} k_w^{\theta_w}, \quad (9)$$

$$c_h^{i'} = (1-n-\theta_o)\rho_m c_m + \theta_s \rho_s c_s + \theta_w \rho_w c_w + \theta_o \rho_o c_o, \quad (10)$$

where $\theta$ is volumetric fraction, $n$ is porosity, $\rho$ is density, $k$ is thermal conductivity, $c$ is specific heat (for subscripts, as follows: $m$, mineral; $o$, organic matter; $s$, ice; $w$, water). The $\rho$, $c$, and $k$ for the mineral, organic matter, ice, and water components of soil modeled in equations (7) ~ (10) were set as $\{\rho_m, \rho_s, \rho_w, \rho_o\} = \{1.55, 0.92, 1.0, 1.3\} \times 10^3$ kg/m$^3$, $\{c_m, c_s, c_w, c_o\} = \{0.733, 2.11, 4.22, 1.93\} \times 10^3$ J/kg/K, and $\{k_m, k_s, k_w, k_o\} = \{0.54, 2.2, 0.57, 0.026\}$ W/m/K. We used laboratory soil analysis data for the volumetric fraction of organic matter and porosity (Fig. 2).

## Results

Due to forest shading, the summer net radiation at the NF site was greatly reduced, corresponding to 26% of that at the SP site (Figs. 3, 4). This was more pronounced in the winter period. We found nearly zero downward shortwave radiation due to further reductions by topographic relief at this site. Mean $T_a$ during the first December, January, and February was -19.4°C at the NF site and -18.1°C at the SP site.

The forest canopy intercepted rainfalls on the forest floor; the NF site received 87.5% and 97.4% of rainfall of that of the SP site during the summers 2003 and 2004, respectively. The interception loss of snow was not obvious; rather, snow depth (SD) at the SP site remained less than for the forest, possibly due to redistribution by wind.

Permafrost condition was found to occur at below 280

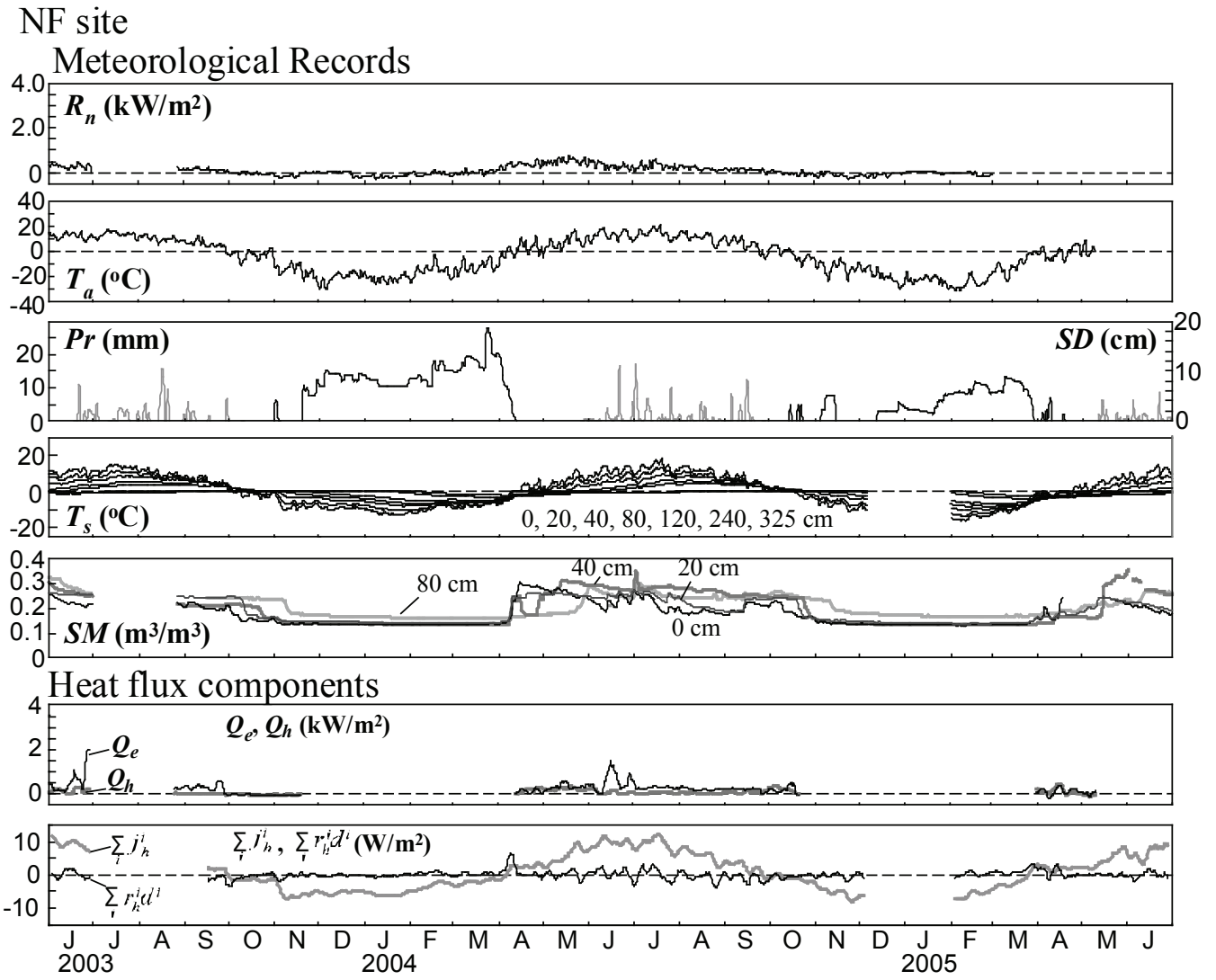


Figure 3. Data and estimated heat flux components at the NF site. See Figure 1b for a picture of the site. Data are missing for some periods due to instrument failure. $R_n$: net radiation, $T_a$: air temperature, $P_r$: rainfall, $SD$: snow depth, $T_s$: soil temperatures, $SM$: soil moistures. For soil moisture, we showed only the upper four depths that were used for calculating soil heat flux components. $Q_e$: atmospheric latent heat flux, $Q_h$: atmospheric sensible heat flux, $\Sigma j_h^i$: total soil conductive heat flux, $\Sigma r_h^i d^i$: non-conductive heat fluxes transferred into the upper three soil layers (0.3, 0.3 and 0.4m in thickness, respectively, extending down from the surface). Five-day running mean values are plotted for each of the heat flux components. For $Q_e$ and $Q_h$, only results obtained during snow-free period are shown. Calculations of $\Sigma j_h^i$ and $\Sigma r_h^i d$ by equations (9) and (10) are plotted.

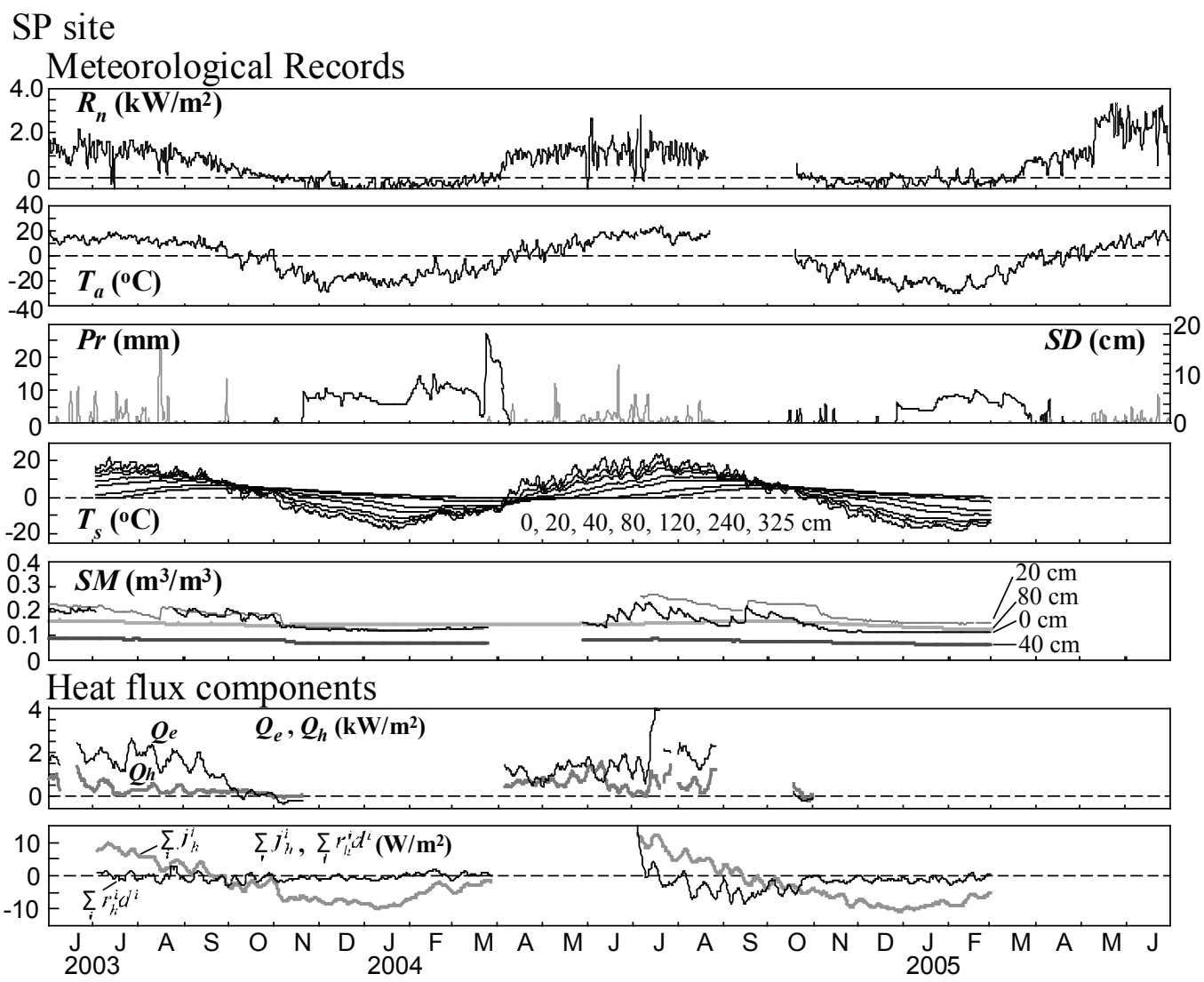


Figure 4. Data records and estimated heat flux components at the southern pasture slope (SP) sites. See Figure 1c for the environments. Same caption as Figure 3.

cm at the NF site, where soil moisture becomes greater for the deeper soils. This is probably due to the impermeability of the underlying permafrost. Contrastingly with the permafrost-free SP site, wet soils were restricted near the surface soil layers. At this site, the regions with significant short-term fluctuation in soil moisture contents are restricted to the shallowest depths (0 and 20 cm), even during the rainy season. Greater net radiation would modulate immediate evaporative soil water loss, as indicated in the greater sensible heat flux at the SP site.

The wet soils at the NF site are probably maintained by lesser atmospheric latent heat (Figs. 3, 4). The ratio of summer evaporation at the FP and SP sites was 0.22; this estimation was approximated with eventual lysimetric measurements. $Q_e$ remained at levels similar to $Q_h$ until the end of May when water for evaporation was mostly derived from snowmelt infiltration and seasonal thawing of the active layer.

Thereafter, $Q_h$ decreased, possibly due to reduced downward shortwave radiation due to the growing forest canopy. Concurrent $Q_e$, on the other hand, remained higher than $Q_h$, largely due to water supply from rainfall. The seasonal development of atmospheric heat flux components mentioned here was generally similar to that at the SP site, which experienced greater evaporation from snowmelts, with higher moisture in the seasonal soil thaw and rainfalls.

The origin of soil latent heat is very complicated (e.g., Kane et al. 2001). Consumption of soil latent heat, $r_h < 0$, possibly arises from evaporation and thawing processes, whereas release, $r_h > 0$, arises from condensation and freezing. Furthermore, $r_h$ reflects the heat transfer accompanied by liquid (water, vapor) movements. Identification and quantification of these processes are required for further comparisons between the energy equivalent of water phase changes and changes in soil moisture contents (e.g., Roth & Boike, 2001).

In our study, more negative $r_h$ for JAS 2004 at the SP site than that at the NF site indicates a larger evaporative water loss at the SP site, as suggested by atmospheric heat fluxes (Figs. 3, 4). At the NF site, the most obvious latent heat releases occurred during the snow disappearance period of April 2004, when the temperature over the active layer

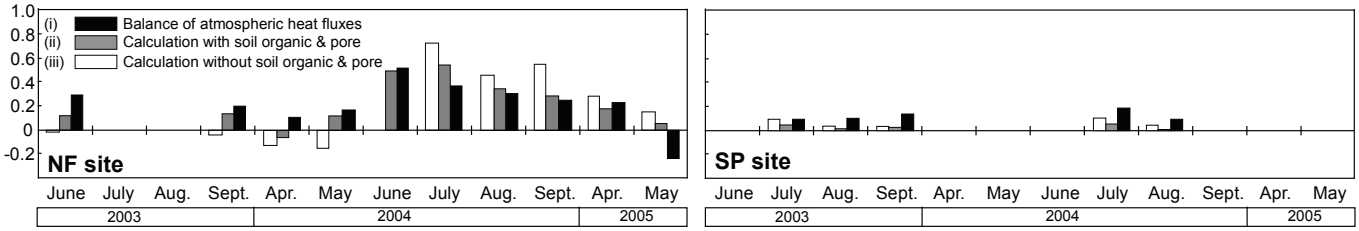


Figure 5. Total soil heat flux transferred into the soil layers ($Q_{g\text{-}c}$ up to depth of 1.0m) as expressed in decimal fractions to the net radiation for the northern forested (NF) and southern pasture (SP) sites during the snow-free period (June to September).

increased due to considerable subfreezing to nearly the thawing point in a short period. Similarly, the active layer was warmed in the second snow disappearance period, but this warming was less obvious. Both warming events were probably triggered by pipe-like snowmelt infiltration, which is controlled by snow cover thickness and thus by soil moisture of the near surface soil layer (Beven & Germann 1982, Ishikawa et al. 2006).

## Discussion

Figure 5 demonstrates the relative importance of the heat flux components transferred into the upper three soil layers (up to depth of 1.0 m), comparing three calculations: (i) from the balance of atmospheric heat balance components, (ii) without soil organic matter and pores occupied by air (using equations 7 and 8), and (iii) with these parameters (equations 9 and 10). For the NF site, the ratio of soil energy storage to net radiation throughout the period was 22.0%. This value agreed well with that from calculation (iii) (22.1%), but differed with that from calculation (iii) (26.5%). These values approximate the observations at other permafrost sites (e.g., Rouse 1984, Boike et al. 1998, Iwahana et al. 2005, Ishikawa et al. 2006).

For the SP site, the ratio of soil energy storage to net radiation was considerably smaller than that at the NF site, indicating soil heat storage to be a minor contributor. The average value through the period from calculations (i), (ii) and (iii) was 11.5, 5.7 and 2.9%, respectively. We postulate that larger energy difference encountered by calculations (i) and (iii) at the NF site reflect unrealistic parameterization of the soil thermal properties (i.e., thermal conductivity and heat capacity). On the other hand, the difference was not obvious at the SP site where the conventional soil parameterizations without organic and pore effects are probably still accurate.

These findings indicate that energy interaction at the forest site greatly depends on the surface organic-rich layers that prevent the active layer from undergoing further warming during the summer period. Furthermore, this shows the importance of thermal properties of forest soils for preservation and development of the permafrost underlying this slope with well-known forest shading that greatly reduces incoming solar radiation to the ground surface. The pore- and organic-rich forest soil would be fed by fallen leaves and branches from *Larch* trees during autumn. Degrading such soils would accelerate permafrost degradation, even though the forests still shade the ground surface.

## Acknowledgments

Local residents and members of the Institute of Hydrology and Meteorology near the observational sites kindly assisted with year-round maintenance of the meteorological instruments. This work was financially supported by the Institute of Observational Research for Global Change, Japan Agency of Marine-Earth Science and Technology.

## References

Beven, K. & Germann, P. 1982. Macropore and water flow in soils. *Water Resources Research* 18: 1311-1325.

Boike, J., Roth, K. & Overduin, PP. 1998. Thermal and hydrologic dynamics of the active layer at a continuous permafrost site (Taymyr Peninsula, Siberia). *Water Resources Research* 34: 355-363.

Farouki, O.T. 1981. *Thermal Properties of Soils*. CRREL Monograph No. 81-1, 136 pp.

Ishikawa, M., Zhang, Y., Kadota, T. & Ohata, T. 2006. Hydrothermal regimes of the dry active layer. *Water Resources Research* 42: W04401, doi:10.1029/2005ER004200.

Ishikawa, M., Sharkhuu, N., Zhang, Y., Kadota, T. & Ohata, T. 2005. Ground thermal and moisture conditions at the southern boundary of discontinuous permafrost, Mongolia. *Permafrost and Periglacial Processes* 15: 1-8.

Iwahana, G., Machimura, T., Kobayashi, Y., Fedrov, A.N., Konstantinov, P.Y. & Fukuda, M. 2005. Influence of the forest-cutting on the thermal and hydrological regimes of the active layer near Yakutsk, eastern Siberia. *Journal Geophysical Research* 110: G02004, doi:10.1029/2005JG000039.

Kane, D., Hinkel, K.M., Goering, D.L., Hinzman L.D. & Outcalt, S.I. 2001. Non-conductive heat transfer associated with frozen soils. *Global Planetary Change* 29: 275-292.

Ohmura, A. 1982. Objective criteria for rejecting data for Bowen ratio flux calculations. *Journal of Applied Meteorology* 21: 595–598.

Roth, K. & Bioke, J. 2001. Quantifying thermal dynamics of a permafrost site near Ny-Ålesund, Svalbard. *Water Resources Research* 37: 2901-2914.

Rouse, W.R. 1984. Microclimate at arctic tree line: 2, Soil microclimate of tundra and forest. *Water Resource Research* 20: 67-73.

Sharkhuu, N. 2003. Recent changes in the permafrost of Mongolia, *Proceedings of the Eighth International Conference on Permafrost:* 1029-1034.

# Developing a Digital Hydrogeological Map of Central Yakutia (The Lena-Aldan Watershed)

L.D. Ivanova
*Melnikov Permafrost Institute, SB RAS, Yakutsk, Russia*
N.M. Nikitina
*Melnikov Permafrost Institute, SB RAS, Yakutsk, Russia*

## Abstract

A digital hydrogeological map of Central Yakutia is being developed in *ArcView* GIS at scale of 1:1,000,000. This project was initiated in 2005 by the Groundwater Laboratory of Permafrost Institute. To implement the project, a *Microsoft Access* database was created containing information obtained from hydrogeological drill holes and on talik water and subpermafrost water in central Yakutia. The digital map model contains the following main themes: *Hydrogeological Zoning*, *Local Talik Aquifers of the Permeable Zone*, *Subpermafrost Aquifers of the Poorly Permeable Zone*, *Local Talik Aquifers Talik-to-Area Rate, Drill Holes, Possible Use of Groundwater for Drinking Purposes, Water in Intrapermafrost and Open Taliks* and others.

**Keywords:** aquitard; groundwater; permafrost; subpermafrost; talik; zoning.

## Introduction

The Lena-Aldan watershed is situated in the southeastern part of the Yakutian artesian basin, a first-order hydrogeological unit (Tolstikhin 1970). The average thickness of permafrost is 300–400 m, and maximal is 600–800 m. This area contains suprapermafrost and intrapermafrost water in the permeable zone and subpermafrost waters in the poorly permeable zone. Suprapermafrost water of lake and river taliks occurs virtually under all lakes and rivers that are common to abundant in the Lena-Aldan watershed. They yield little water, generally of poor quality. Under the largest lakes and rivers of Lena and Amga, open taliks occur that are hydraulically connected with subpermafrost water. Taliks beneath the Lena River present a stable water supply resource and the water is used for drinking. Intrapermafrost water is found in the fourth fluvial terrace of the Lena River in sand deposits along the surface of the contact with carbonate bedrock. It has good quality and is used for drinking. Subpermafrost water of the Lena-Aldan watershed is sterile, because the permafrost protects it from human contamination. Nevertheless, quality and quantity of water depend on complex litho-tectonic, cryohydrogeologic and hydrodynamic factors. In some cases, subpermafrost water can contain high concentrations of natural occurring chemical elements, which limits its use for drinking.

Classification and analysis of voluminous and diverse data is required in support of groundwater quality management and both municipal and industrial water supply use in Central Yakutia. This task is accomplished by developing a digital groundwater map. The digital hydrogeological map of Central Yakutia, at a scale of 1:1,000,000, is visualized in ArcView GIS for users, and is accessible for editing and updating. Compilation and modeling of geological, hydrogeological and geocryological information have been made by standard methods (Vasiliev et al. 1999, Torgovkin & Fedorov 1999) using the Microsoft Access program and the ArcInfo and ArcView GIS technologies. This map is the first digital groundwater map being developed for a permafrost region.

## Methods of Thematic Mapping

During the first phase of the project, a talik and subpermafrost water database was created in *Microsoft Access* compatible with *ArcView* GIS mapping software. The database contains information for more than 200 drill holes. The holes are scattered unevenly over the map area. Most of them are concentrated in major river valleys and lake basins, while the fewest are near watershed divides. The database consists of electronic tables which contain the drill hole identification number and geographic coordinates, hydrogeological unit, lithostratigraphic column, permafrost characteristics, aquifer parameters, and groundwater hydrochemistry.

The next stage was to digitize the Central Yakutia sheet of the Geological Map of Yakutia, 1:500,000 scale (Grinenko et al. 2000) and adjust it to a mapping scale of 1:1,000,000 with generalization of stratigraphic units. The digitized geological contours were used as a raster background for vectorization of thematic layers with consideration of permafrost conditions. Then, statistical processing of data, and analysis and interpretation of general geographical information (descriptive, qualitative and quantitative characteristics, and identification of parameters) were made. This allowed us to integrate the informational resources to the geospatial model and compile the hydrogeological stratification schemes to develop a digital model of the hydrogeological map.

To construct thematic layers of the map, paper maps were first drawn using common mapping methods. Where only sparse data were available, correlation and extrapolation techniques were used (Zarutskaya & Krasilnikova 1988). Then, the layers were scanned and digitized. Numerous and diverse thematic data are referenced in a common spatial

coordinate system in the Gauss-Kruger projection (129 central meridian).

## Content of the Digital Map

The digital map consists of two components. The Basic component includes several layers: frame, grid, inhabited places, roads and hydrographic features. The Thematic Maps component will have the following layers: *Geological Map, Hydrogeological Zoning, Local Talik Aquifers of the Permeable Zone, Subpermafrost Aquifers of the Poorly Permeable Zone, Local Talik Aquifers Talik-to-Area Rate, Chemistry of Local Talik Aquifers of the Permeable Zone, Chemistry of Subpermafrost Aquifers of the Poorly Permeable Zone, Water in Intrapermafrost and Open Taliks, Drill Holes, Permafrost Thickness Isolines, Possible Use of Local Talik Aquifers of the Permeable Zone*, *Possible Use of Subpermafrost Aquifers of the Poorly Permeable Zone*.

*Hydrogeological Zoning* layer; the limits of hydrogeological structures of second order correspond to the *Hydrogeological Zoning Map of Russian Federation* scaled 1:2,500,000. In the Lena-Aldan and Lena-Vilyui artesian basins of second order, third and fourth orders of hydrogeological structural units have been identified (Fig. 1 and Table 1), based on our earlier studies (Shepelev et al. 1984, Ivanova & Nikitina 2000).

*Local Talik Aquifers of the Permeable Zone* layer; aquifers in Cenozoic, Mesozoic, and Paleozoic rocks are mapped in accordance with litho-stratigraphic principle. The aquifer's color in the map corresponds to the stratigraphic subunit color. In case if aquifer is presented by two stratigraphic subunits, two colors are used (Fig. 2)

*Subpermafrost Aquifers of the Poorly Permeable Zone* layer: maps the first subpermafrost aquifer. The map demonstrates subpermafrost groundwater units in Mesozoic, Paleozoic and Proterozoic formations and the aquitard of Archean metamorphic rock. The color of the aquifer or aquifer unit corresponds to the stratigraphic subunit color.

*Local Talik Aquifers' Talik-to-Area Rate* layer: the cross-hatching shows the talik-to-area rate value, which is calculated as a percentage ratio of total talik area in a given geomorphological unit to its area, and ranges between 0.5 and 4.0%.

*Chemistry of Local Talik Aquifers of the Permeable Zone* and *Chemistry of Subpermafrost Aquifers of the Poorly Permeable Zone* layers: background speckle shows the combination of dissolved solids concentration (TDS)

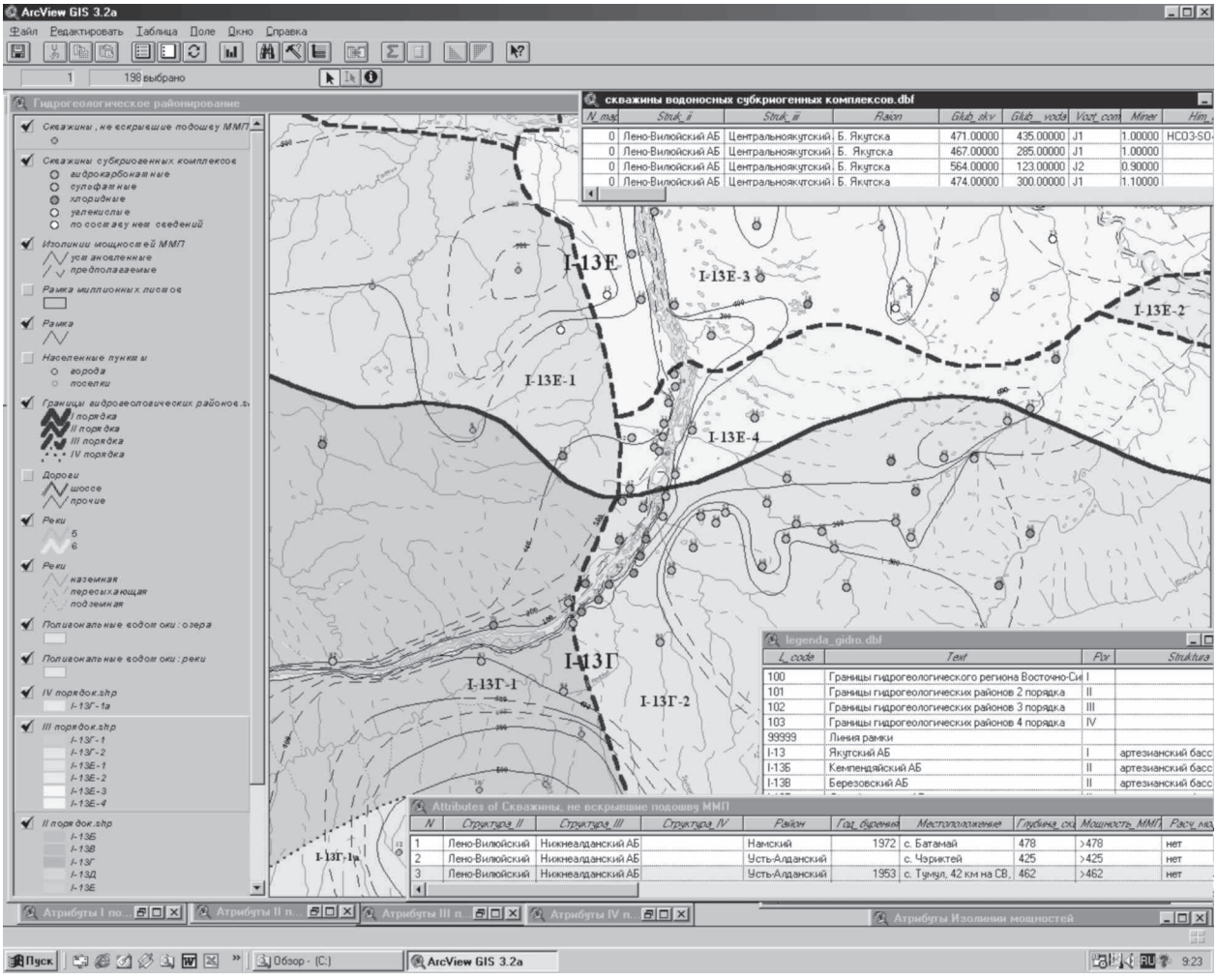


Figure 1. A fragment of *Hydrogeological Zoning* thematic layer combined with *Permafrost Thickness Isolines.*

Table 1. Third- and fourth-order hydrogeological units.

| Hydrogeological Unit | | Strati-graphic age | Thickness of frozen aquitard, m | Groundwater flow type | Groundwater quality |
|---|---|---|---|---|---|
| Lena-Vilyui artesian basin I-13E (I order) | Vilyui artesian basin I-13E-1 (III order) | K | 400-600 | Tabular-pore and tabular in terrigenous sediments and poorly lithified rocks | Fresh |
| | Pre-Verkhoyansk artesian basin I-13E-2 (III order) | $K_1$-$J_1$ | 350-450 | Tabular and tabular-fissured in terrigenous poorly lithified and fissured rocks | Fresh |
| | Lower Aldan artesian basin I-13E-3 (III order) | N-K | 350-500 | Tabular-pore in terrigenous sediments | Fresh |
| | Central Yakutian artesian basin I-13E-4 (III order) | J, T, Є, A | 200-500 | Fissure and fissure-vein in terrigeneous in fissured rocks and fissure and fissure-karst in terrigenous-carbonate rocks | Fresh and slightly saline |
| Lena-Aldan artesian basin I-13Г (I order) | Middle Lena aretesian basin I-13Г-1 (III order) | J, $Є_{1-2}$ | 310-490 | Fissure-tabular and fissure in terrigeneous fissured rocks and fissure-karst in karsted and saline rocks | Fresh and slightly saline |
| | Buotama-Amga cryogeological basin I-13Г-1a (IV order) | A | 600-880 | Lithologic aquitard of metamorphic rocks | – |
| | Lena-Amga artesian basin I-13Г-2 (III order) | J, $Є_{1-2}$ | 200-500 | Fissure-tabular, fissure and fissure-karst in terrigeneous fissured and karsted carbonate rocks | Fresh and slightly saline |

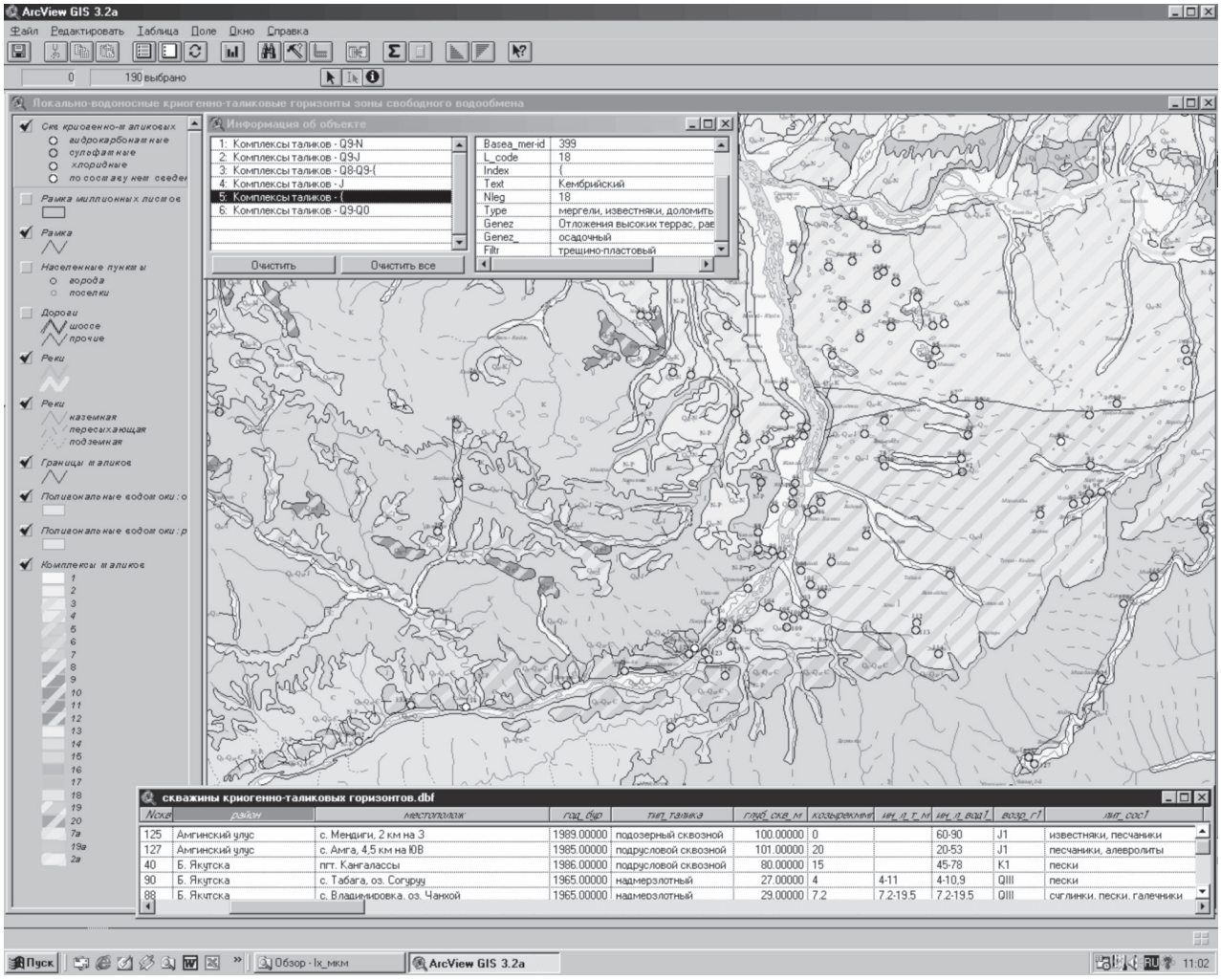


Figure 2. A fragment of *Local Talik Aquifers of the Permeable Zone* thematic layer combined with *Drill Holes* theme.

and anionic composition of underground water in the following gradation (g/dm$^3$): nearly pure freshwater (up to 0.5), freshwater (0.5–1.0), slightly saline water (1.0–3.0), moderately saline water (3.0–10.0), and very saline water (10.0–50.0).

*Water in Intrapermafrost and Open Taliks* layer: not-to-scale symbols show intrapermafrost, river and lake open taliks, springs, icings and glades. In *Drill Holes* layer, different symbols show (a) borings through closed talik, open talik and subpermafrost aquifers; and (b) holes that failed to reach the base of permafrost.

*Permafrost Depth Isolines* layer: shows the depth to the base of permafrost at 100 m intervals. Isolines were constructed based on analysis of measurement data and the well-known method of geographic interpolation.

*Possible Use of Local Talik Aquifers of the Permeable Zone* and *Possible Use of Subpermafrost Aquifers of the Poorly Permeable Zone* layers: delineate the areas where groundwater quality meets drinking water standards.

Each layer contains an attribute table, which is formed automatically and contains a standard data set. These tables are linked to thematic data in the Microsoft Access database. It is possible to connect attribute tables between the layers, to join the layers, and to add table and raster drawing images to the layer layout.

## Conclusions

The digital hydrogeological map will become a more effective tool for accomplishing hydrogeological tasks brought about by groundwater exploration and use in permafrost regions. The map will allow users to change scales without quality loss, abandon the overwhelming integrated maps in favor of interrelated thematic layers in versions that meet their specific purposes, and easily access the data via attribute tables. Information can be stored and added in electronic format and is accessible for analysis and modeling. The digital hydrogeological map will be useful for those involved in water supply, monitoring, conservation, and contamination abatement.

## References

Grinenko, V.S. 2000. *The Geological Map of Yakutia*. Saint-Petersburg: VSEGEI.

Ivanova, L.D. & Nikitina, N.M. 2000. More precise permafrost hydrogeological zonation of the southern portion of the Yakutian artesian basin. *Kriosfera Zemli* IV(2): 52-56.

Kurennoy, V.V., Golitsyn, M.S., Tikhonenkov, Y.E., Shakhnova, R.K., Shpak, A.A. & Leonenko, L.V. 2001. *Construction of Hydrogeological Maps Using Computer Technologies*. Moscow: Russian Ministry of Natural Resources, 196 pp.

Shepelev, V.V., Tolstikhin, O.N., Piguzova, V.M., Nikitina, N.M., Nekrasov, I.A., Lomovtseva, N.S. & Ivanova, L.D. 1984. *Groundwater in the Permafrost Regions of East Siberia*. Novosibirsk: Nauka, 192 pp.

Tolstikhin, O.N. 1970. Hydrogeological Zoning. In: A.I. Efimov & I.K. Zaitsev (ed.), *Hydrogeology of the USSR. Vol. XX: Yakut ASSR*. Moscow: Nedra, 91-99.

Torgovkin, Y.I. & Fedorov, A.N. 1999. An application of GIS-technologies in permafrost-landscape studies (exemplified by Spasskaya Pad study area, Central Yakutia). *INTERCARTO-5. GIS for sustainable development of territories (June. 1999). Papers of the International Conference, part 4. GIS in Regional Research/ - Yakutsk, Yakutsk Universitiy Press*: 68-77.

Zarutskaya, I.P. & Krasilnikova, N.V. 1988. *Mapping of Natural Conditions and Resources*. Moscow: Nedra, 299 pp.

# Sensitivity of Permafrost Landscapes to Anthropogenic Impacts in the Northern Verkhoyansk Area, Subarctic Yakutia

Rozaliya N. Ivanova
*Melnikov Permafrost Institute SB RAS*

## Abstract

Three sensitivity levels to human impacts such as deforestation and agricultural practices have been distinguished for permafrost landscapes in the northern Verkhoyansk area situated within the Northern Taiga subzone. Sensitivity of permafrost landscapes is estimated based on cryoindicators such as volumetric ice content, active layer thickness, depth to wedge ice, and thaw subsidence. An essential criterion of permafrost landscape sensitivity is the ground ice: its form, depth, amount, and pattern of distribution in the ground. Sensitivity of landscapes in the northern Verkhoyansk area is the integral characteristic of its geoecological condition.

**Keywords:** anthropogenic impacts; cryoindicators; geoecological condition; permafrost landscape; sensitivity.

## Introduction

The northern Verkhoyansk is a vast northern area that has received little study in terms of permafrost ecology. It is the world's coldest region "called the "cold pole of Eurasia." It has the whole variety of landscapes, ranging from lowland bogs to high mountains, both natural and anthropogenic.

To understand the microclimatic and thermal conditions, as well as the ecological state of natural and anthropogenic permafrost landscapes in the central part of the Yana River valley, monitoring observations on four sites were conducted by the Permafrost Institute during the period of 1989 to 1992. The study area was located in the vicinity of Batagai, at 67°31′N latitude, 134°41′E longitude, 130 m elevation a.s.l. (Ivanova 2003).

Permafrost landscape is defined as a homogeneous natural complex which functions under the influence of cryogenesis, with unique combinations of permafrost characteristics (Fedorov 1991). Permafrost landscape sensitivity is referred to as the degree of its reaction to anthropogenic impacts (Grave 1980).

The geoecological state of permafrost landscapes is deteriorated by disruption of the ground surface, as well as by formation of numerous polygonal structures, thermokarst depressions, cracking of the ground and heaving of peat soils due to anthropogenic factors (frequent fires, damage to the surface vegetation and soil by off-road movement of vehicles, agricultural practices, etc.).

Forest clearing and surface cover disturbances cause strong changes in ice-rich soils. Among the effects are three- to four-fold increase in seasonal thaw depth, melting of wedge ice and development of thaw depressions up to 0.8 m in depth.

## Results and Discussion

Three sensitivity levels have been distinguished for permafrost landscapes in the northern Verkhoyansk area situated within the Northern Taiga subzone, based on permafrost landscapes classifications according to terrain sensitivity to anthropogenic impacts and environmental changes (Grave & Melnikov 1989, Fedorov 1991, 1996, Zotova & Tumel 1996, Gavriliev et al. 2001) (Table 1).

The low sensitivity landscapes have low volumetric ice contents (less than 20%). Ice wedges occur below 2.0 m from the ground surface. The thickness of the active layer is 1.0 m or more. The development of adverse cryogenic processes is not expected.

The landscapes of moderate sensitivity have volumetric ice contents of 20% to 40%. The active layer is less than 1.0 m in thickness, surface subsidence is 0.2 to 0.5 m and the top of ice wedges occurs below 1.0 m depth.

The highly sensitive landscapes are characterized by volumetric ice contents of over 40%. Adverse soil and cryogenic processes are present, such as thermokarst depressions 0.5 to 0.8 m in depth, soil disruption and erosion. Ice wedges occur within 1.0 m from the ground surface. The active layer thickness does not exceed 0.5 m.

Moderate sensitive landscapes prevail in the Kumakh site with natural, undisturbed conditions (12 km southwest of Batagai, situated in the intermontane saddle in the Yansk Upland). The site is covered by very wet and swamp meadows and bogs with such growth as *Carex*, *Eriophorum* and *Calamagrostis*. Highly sensitive landscapes occupy some part of the site and include meadows and grass-moss bogs (Fig. 1, Table 2).

Table 1. Cryoindicators for sensitivity estimation of Northern Verkhoyansk permafrost landscapes (the Northern Taiga subzone).

| Condition of permafrost landscapes | Volumetric ice content, % | Thickness of active layer, m | Depth to wedge ice, m | Surface subsidence, m |
|---|---|---|---|---|
| Low sensitive | <20 | >1.0 | >2.0 | <0.2 |
| Moderate sensitive | 20-40 | 0.5-1.0 | 1.0-2.0 | 0.2-0.5 |
| Highly sensitive | >40 | <0.5 | <1.0 | >0.5 |

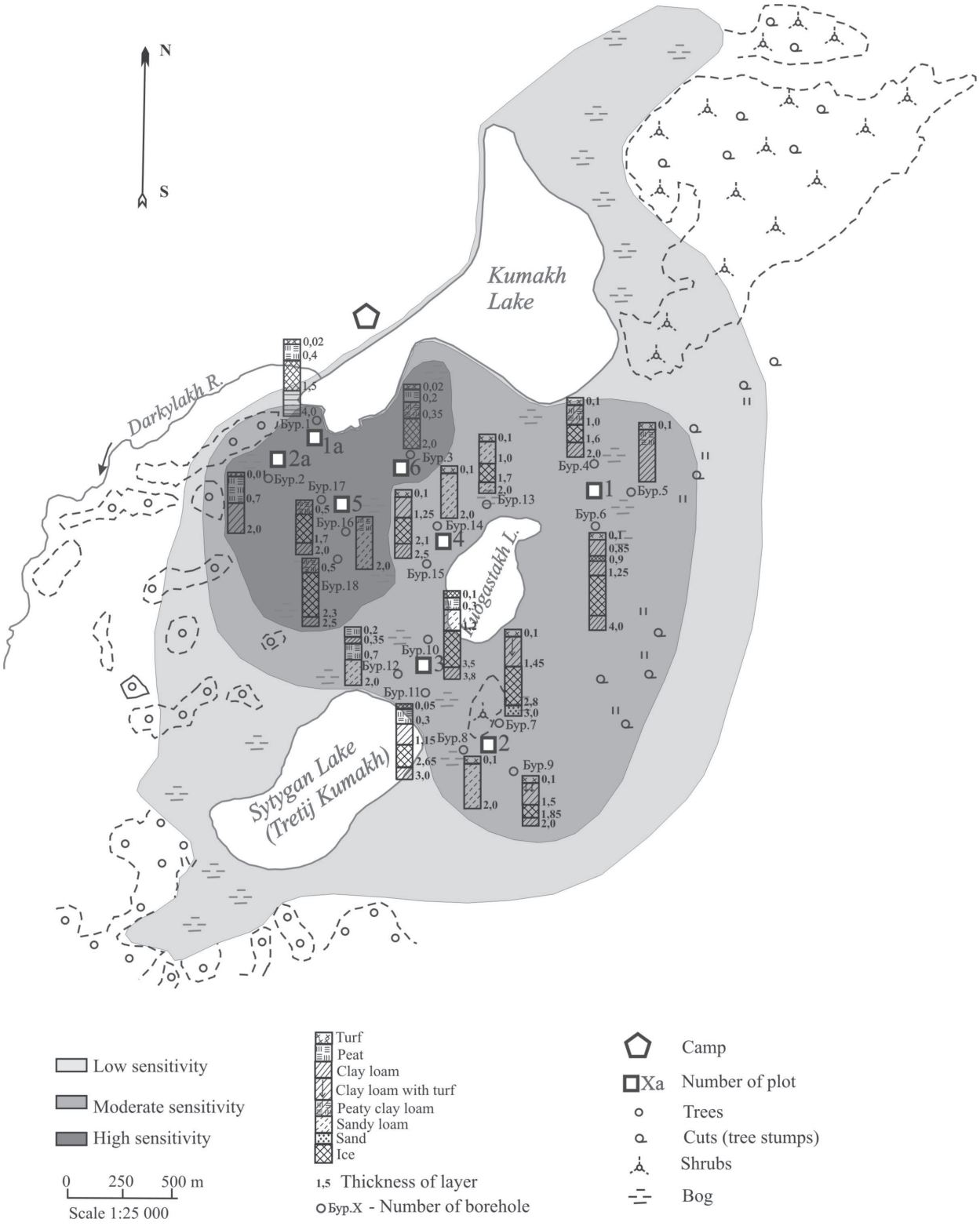


Figure 1. A sensitivity map of meadow landscapes at Kumakh site.

Table 2. Estimation of permafrost landscape sensitivity in Kumakh site.

| Plot | Landscape | Volumetric ice content, % | Thickness of active layer, m | Depth to wedge ice, m | Surface subsidence, m | Condition of permafrost landscapes |
|---|---|---|---|---|---|---|
| 1 | *Carex-Calamagrostis* very wet meadow | >40 | 0.55 | 0.85-1.0 | 0.45 | Moderate sensitive |
| 2 | *Calamagrostis-Carex* meadow | 30 | 0.65 | 1.45-1.5 | 0.35 | |
| 3 | Waterlogged bog with grass vegetation | >40 | 0.6 | 1.15-1.2 | 0.3 | |
| 4 | *Carex-Eriophorum* swamp meadow | >40 | 1.15 | 1.0-1.25 | 0.5 | |
| 5 | Grass-moss bog with low-centered polygons | 50-80 | 0.56 | 0.5 | 0.5-0.6 | Highly sensitive |
| 6 | *Carex-Calamagrostis* swamp meadow | >40 | 0.55 | 0.35 | 0.5-0.7 | |
| 1a | *Carex-Calamagrostis* meadow | 20-40 | 0.45 | 0.4 | 0.4-0.6 | |
| 2a | *Calamagrostis-Carex* flood meadow | 20-40 | 0.46 | 2.5 | 0.3-0.6 | |

The lack of agricultural lands in the Yana River valley causes the clearing of north-taiga forests. We observed agricultural landscapes in the Batymakh and Yuttyakh sites, which are situated on the first terrace of the Yana River. Forest clearing and soil cover disturbance result in intense changes in the soils with high ice content. In the Batymakh site the top 5-10 cm of humus soil was partially removed together with tree roots. Thus the permafrost soils lost 30%-50% of humus reserves that considerably reduced the soil fertility. Ground cover disturbance caused a 3-4 times increase of seasonal thaw depth, from 0.3 to 0.9-1.2 m. Ice content of frozen sandy loams in the site varies from 40% to 60% by volume. The central part of the site is underlain by ice wedges. Here thaw depressions developed up to 0.5 m in depth and 5 m in width. Thus, we can conclude that the top of ice wedges thawed. According to geocryological conditions and sensitivity to anthropogenic impacts, the landscapes in this site are also subdivided to low sensitive, moderate sensitive and highly sensitive categories (Ivanova 2005).

Landscape sensitivity in northern Verkhoyansk area is the integral characteristic of its geoecological condition. The estimation of the sensitivity of permafrost landscape is based mainly on thaw subsidence which directly depends on volumetric ice content of the active layer.

Subsidence is caused by activization of cryogenic phenomena and processes, such as frost cracking in the active layer (width of cracks varies from 0.5 to 6 cm and its depth often penetrates the top of perennially frozen ground); fissured polygons (depth of fissures extends up to 0.5 m); small polygons (depth of cracks extends up to 0.6 m); ice segregation (especially the formation of wedge ice in the top part of permafrost); low-centered polygons and subsidence troughs; block polygons (normally from tens of centimeters to 4-6 m; and occasionally 8-12 m in diameter).

## Conclusion

Present-day climatic variations and anthropogenic impacts (tree removal, surface disturbance, ploughing, etc.) add to the effect of cryogenesis on the adverse processes that disturb and modify the landscapes, as well as on the reduction of ecological and economic values of the landscapes in northern Verkhoyansk.

Terrain zoning according to permafrost landscape sensitivity is essential for geoecological monitoring at a local level. It can provide useful contributions to cryoecological databases, as well as help develop environmental protection standards for subarctic regions.

## References

Fedorov, A.N. 1991. *Permafrost Landscapes in Yakutia: Location Technique and Mapping Issues*. Yakutsk: SB RAS Permafrost Institute Press: 140.

Fedorov, A.N. 1996. Impact of Present Bioclimatic Changes on Permafrost Landscapes Development. In: V.T. Balobaev, *Climatic Impact on Permafrost Landscapes in Central Yakutia*. Yakutsk: SB RAS Permafrost Institute Press, 86-106.

Gavriliev, P.P., Ugarov, I.S. & Efremov, P.V. 2001. *Permafrost and Ecological Characteristics of Agricultural Lands in Central Yakutia*. Yakutsk: SB RAS Permafrost Institute Press, 196.

Grave, N.A. 1980. Place and concept of geocryological researches of environment control and conservation issues in permafrost area. *Terrain Sensitivity to Anthropological Impact in Permafrost Area.* Yakutsk, 6-12.

Grave, N.A. & Melnikov, P.I. 1989. *Criteria and Predictions of Permafrost Landscapes Sensitivity. Factors and Techniques of Geosystems Sensitivity.* Moscow: Academy of Science Press: 163-171.

Ivanova, R.N. 2003. Seasonal thawing of soils in the Yana River valley, northern Yakutia. *Proceedings of the Eighth International Conference on Permafrost, Zurich, Switzerland, 21-25 July 2003, Vol. 1*: 479-482.

Ivanova, R.N. 2005. Sensitivity of permafrost terrain to clearing of North-Taiga forests in the Yana Valley, Northern Yakutia. *Programme and Abstracts of 2nd European Conference on Permafrost (EUCOP II), Potsdam, German, 12-16 July 2005*: 182-183.

Zotova, L.I. & Tumel, N.V. 1996. Permafrost ecological evaluation of landscapes condition affected by anthropogenic impacts. *Proceedings of the First Conference of Geocryologists in Russia,* Moscow: Moscow State University Press, Vol.2: 374-383.

# Micrometeorological Measurements on Mountain Permafrost in the Daisetsu Mountains, Hokkaido, Japan

Go Iwahana
*Graduate School of Engineering, Hokkaido University, Sapporo, Japan*
Yuki Sawada
*Institute of Low Temperature Science, Hokkaido University, Sapporo, Japan*
Mamoru Ishikawa
*Graduate School of Environmental Science, Hokkaido University, Sapporo, Japan*
Fumitaka Katamura
*Kyoto Prefectural University, Kyoto, Japan*
Toshio Sone
*Institute of Low Temperature Science, Hokkaido University, Sapporo, Japan*
Tetsuo Sueyoshi
*Institute of Low Temperature Science, Hokkaido University, Sapporo, Japan*
Koichiro Harada
*Miyagi University, Sendai, Japan*

## Abstract

We commenced micrometeorological measurements in the Daisetsu Mountains, Hokkaido, Japan, including the monitoring of thermal and hydrological conditions in the ground down to 5 m depth, in July 2005. The temperature conditions at the site were as cold as those within a continuous permafrost zone. Persistent, driving westerly winds prevent snow from accumulating on the mountain permafrost site. The depth of the permafrost base was deeper than 5 m. Relative humidity was high, with large amounts of summertime precipitation (~ 700–1000 mm). It is likely that the soil water condition in the active layer is kept high or nearly saturated during the thawing season due to frequent rainfall and the existence of permafrost. The observed and future long-term data are expected to be used to model the ground thermal and hydrological processes and thereby lead to a better understanding of the relation between permafrost and vegetation ecology.

**Keywords:** active layer; Japan; micrometeorology; mountain permafrost.

## Introduction

The occurrence of perennially frozen ground in Japan has been studied by numerous researchers, as summarized by Ishikawa et al. (2003), who categorized the distribution of mountain permafrost in Japan into three groups in terms of geographic location. Mountaintop permafrost occurs in certain summit areas where the mean annual temperature is sufficiently low to allow the occurrence of permafrost. Such areas commonly have little snow cover because of strong winds. Mountainside permafrost occurs mainly on slopes or depressions such as deglaciated cirques in the Japanese Alps (e.g., Fukui 2003). Extra-zonal permafrost occurs upon certain block slopes at low altitudes, where the mean annual air temperature is considerably above 0°C (e.g., Sawada et al. 2003). The mountain permafrost in the Daisetsu Mountains of Hokkaido, Japan is categorized as mountaintop permafrost and is considered to be highly sensitive to global warming because air temperature has a direct control on the ground thermal regime of mountaintop permafrost (Ishikawa et al. 2003), and because the site is located near the southern limit of permafrost occurrence in the Northern Hemisphere (Fig. 1).

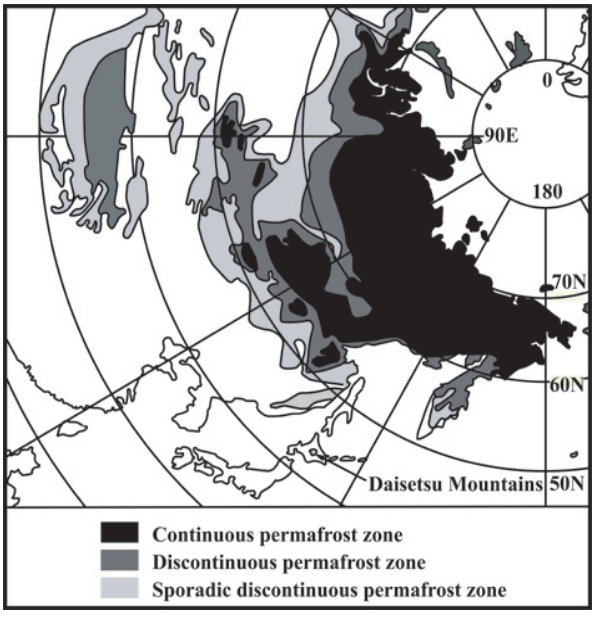


Figure 1. Location of the Daisetsu Mountains. Modified from Harris (1986).

Mountain permafrost within the Daisetsu Mountains is

distributed in a complex manner over a large area at altitudes above approximately 1700 m above sea level (a.s.l.). The occurrence of permafrost in this area has been examined by borehole and geophysical testing, as well as the BTS (bottom temperature of snow cover) measurements (e.g., Fukuda & Kinosita 1974, Sone et al. 1988, Ishikawa & Hirakawa 2000). Numerous periglacial features, including patterned ground (e.g., Koaze 1965, Sone & Takahashi 1986, Fukuda & Sone 1992) and palsa bog (e.g., Takahashi & Sone 1988, Sone 2002) have been studied in the Daisetsu Mountains, suggesting the extensive occurrence of perennially frozen ground; however, long-term variations in permafrost temperature have yet to be reported, and the extent of permafrost remains unclear.

Global climate change could alter the physical factors that control the surface energy and water balance, such as air temperature, precipitation, vegetation, radiation, and wind conditions. Such changes could in turn affect the thermal and hydrological regime of the active layer and underlying permafrost. Koizumi & Shinsho (1983) reported a correlation between vegetation distribution and level of ground water table, which is determined by the depth of the permafrost table, in the mountaintop permafrost area of the Daisetsu Mountains. Kudo (1990) noted the importance of soil temperature as a control of vegetation distribution in the southern part of these mountains.

We initiated micrometeorological measurements with the aim of understanding the physical processes controlling the surface energy and water balance in the mountaintop permafrost area of the Daisetsu Mountains. Similar micrometeorological studies have been conducted in many cold regions (Eugster et al. 2000), although the summit areas of mountains have rarely been targeted. The observed data will be used to model the ground thermal and hydrological processes and thereby lead to a better understanding of the relation between permafrost occurrence and vegetation ecology. The data provide fundamental information for process-based modeling of mountain permafrost distribution. Basic meteorological measurements and geophysical surveys of mountain permafrost have been performed in this range over the past 30 years; however, the available information remains insufficient in terms of discussing environmental controls on the occurrence and temporal variation of mountain permafrost.

This paper describes micrometeorological characteristics, including the current thermal and hydrological status of the active layer and upper permafrost, of a site at which a 4 m tower equipped with micrometeorological instruments was installed at a representative point in the area of mountain permafrost in July 2005.

## Study Site

The Daisetsu Mountains (43°N, 142°E) are located in central Hokkaido, northern Japan (Fig. 1). The current morphology of the mountains formed during early to middle Quaternary volcanic activity that saw the eruption of andesite lavas. The lava flows formed plateaus at 1700 to 2000 m a.s.l. during early to middle Quaternary, followed by the formation of various volcanic cones. The highest peak in the area is Mt. Asahi (2290 m a.s.l.); the timberline occurs at about 1600 m a.s.l.

An automatic micrometeorological observation system is installed about 400 m northeast of the peak of Mt. Goshiki (Fig. 2) at 2015 m a.s.l. The plateau atop of Mt. Goshiki is relatively flat and is one of the most suitable places in the area for micrometeorological measurements, with a 300–

Figure 2. Summertime view of the study site looking toward the west. The peak in the background is Mt. Hakuun.

Table 1. Description of employed instruments.

| Elements | Model | Manufacture | Height or depth (m) | Logging interval | Scan interval |
|---|---|---|---|---|---|
| Air temperature & Relative humidity | HD9009TR-5 | Delta OHM | 1.5 | 30 min. | 10 s. |
| 4-elements radiation | CNR-1 | Kipp & Zonen | 1 | | |
| Ground heat flux | | Huske | 0.01 | | |
| Rainfall | 52203 | R. M. Young | 1 | | |
| Wind direction | 05103-47 | R. M. Young | 4 | | |
| Wind speed | 03101Y-5 | R. M. Young | 4 | | |
| Soil temperature | thermistor probes | Isizuka denshi | 16 depths | | |
| Soil water content | EnviroSMART | Sentek | 6 depths | 6 h. | 6 h. |

400 m fetch in the direction of the prevailing wind. About half of the plateau is covered by patchy vegetation colonies (Fig. 2) of *Diapensia Lapponica* var. *oboata*, *Loiseleuria procumbens, Oxytropis japonica* Maxim. var. *sericea* Koidz, lichens, etc. The heights of the colonies are 20–50 mm. Areas of bare ground reveal volcanic pebble conglomerate (clasts of ~5–20 mm in diameter).

## Methods

The data used in this paper were obtained between 2 July 2005 and 14 October 2006. Data losses of several hours were linearly interpolated. Long-term data loss due to instrumental malfunction occurred over periods ranging from several days to months.

Four-component radiation (shortwave incoming radiation Si, shortwave outgoing radiation So, longwave incoming radiation Li, and longwave outgoing radiation Lo) was measured, and net radiation Rn was calculated as Rn = Si + Li – So – Lo. Ground heat flux at the soil surface was measured using a heat flux plate installed at a depth of 10 mm. Surface albedo α was calculated every 30 minutes as α = So/Si, taking the minimum values from 10:00 to 14:30 (during which time α values were almost constant) to obtain a daily representative midday value. Those values which were thought to be influenced by the accumulation of snow on the upper sensor were removed from the dataset. Air temperature and relative humidity were measured using Pt100 sensors and a capacitance probe, respectively. Rainfall was measured using a tipping bucket rain gauge with a resolution of 0.1 mm. Wind speed and direction were measured using a propeller-type anemometer. These instruments were installed upon a 4 m tripod.

Soil temperature was measured using thermistor probes (104ET; Ishizuka Denshi, Japan) calibrated in an ice-water bath with a precision of 0.02°C and an overall accuracy of less than ± 0.09°C in the temperature range between –20 and 30°C. Measurements were taken at depths of 0.01, 0.05, 0.10, 0.20, 0.30, 0.50, 0.70, 0.90, 1.10, 1.30, 1.50, 1.70, 1.90, 3.00, 4.00, and 5.00 m. Volumetric soil water content was estimated using FDR (Frequency Domain Reflectometry) sensors at depths of 0.10, 0.20, 0.30, 0.40, 0.60, 0.80, 1.00, and 1.20 m.

The model numbers, manufacturer details, heights of measurements, and recording intervals for all meteorological instruments used in this study are summarized in Table 1. Data were recorded using a data logger (CR10X; Campbell Scientific Inc., USA) with a multiplexer (AM16/32; Campbell Scientific Inc., USA). Soil moisture data were measured every 6 hours and recorded; other parameters were measured every 10 seconds, with 30-minute averages being recorded.

## Results and Discussion

*Air temperature and humidity*

Air temperature and relative humidity were measured from July 2005 to October 2006. Figure 3 (upper) shows the seasonal monthly mean, maximum, and minimum air temperature. The mean annual air temperature from October 2005 to September 2006 was -4.6°C. The maximum values of 18.5°C and 17.8°C were observed in August 2005 and August 2006, respectively; the highest daily minimum values of 3.6°C and 6.2°C were observed in the same months, and the minimum air temperature of -27.4°C was recorded in January 2006. The degree of daily variation in air temperature was small in mid-summer and large in winter. For the period from October 2005 to October 2006, the freezing and thawing indexes were 2727 and 1050 degree days, respectively.

Relative humidity was very high. Figure 3 (lower) shows seasonal changes in monthly mean, maximum, and minimum relative humidity. The maximum daily values of relative humidity were 100% on every day of the observation period, meaning that the atmosphere close to the ground was at the dew point especially at night. Daily variations in relative humidity were relatively minor (less than 15%) from mid-November to mid-February, but large (up to 95%) during other periods. The relative humidity fell below 20% only during the daytime on fine days during the snow-free period. Values fluctuated close to the saturation point after every rainfall event.

Largely continuous monitoring of air temperature was undertaken at Hakuun hut (2000 m a.s.l.; ~2 km south of the study site) from 1985 to 1993 (Sone et al. 1988, Tachibana et al. 1991, Nakayama & Sone 1992, Sone & Nakayama 1992, Sone 1994). The mean annual air temperatures in 1985, 1987, and 1988 were -3.8°C, -4.9°C, and -5.2°C, respectively. According to the diagram of Harris (1981), if snow barely covers the ground surface in winter, our study area is characterized as a continuous or discontinuous permafrost zone (Sone 1992). Our temperature measurements also support his conclusion.

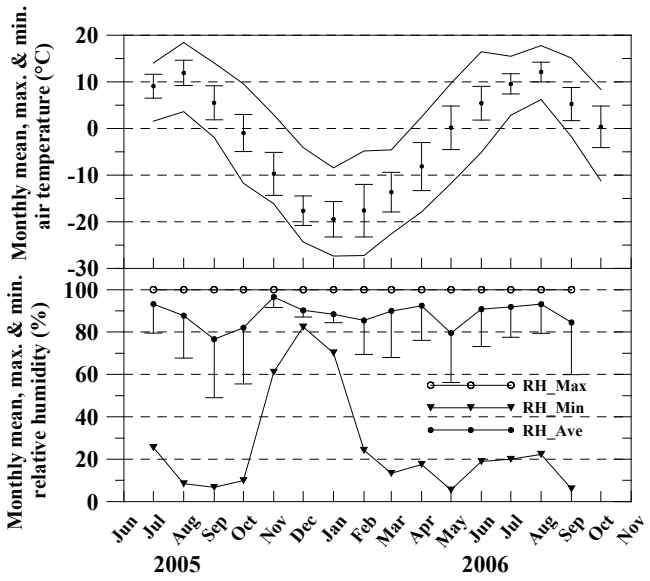


Figure 3. Seasonal changes in monthly mean, maximum, and minimum air temperature (upper) and relative humidity RH (lower). Error bars indicate standard deviations.

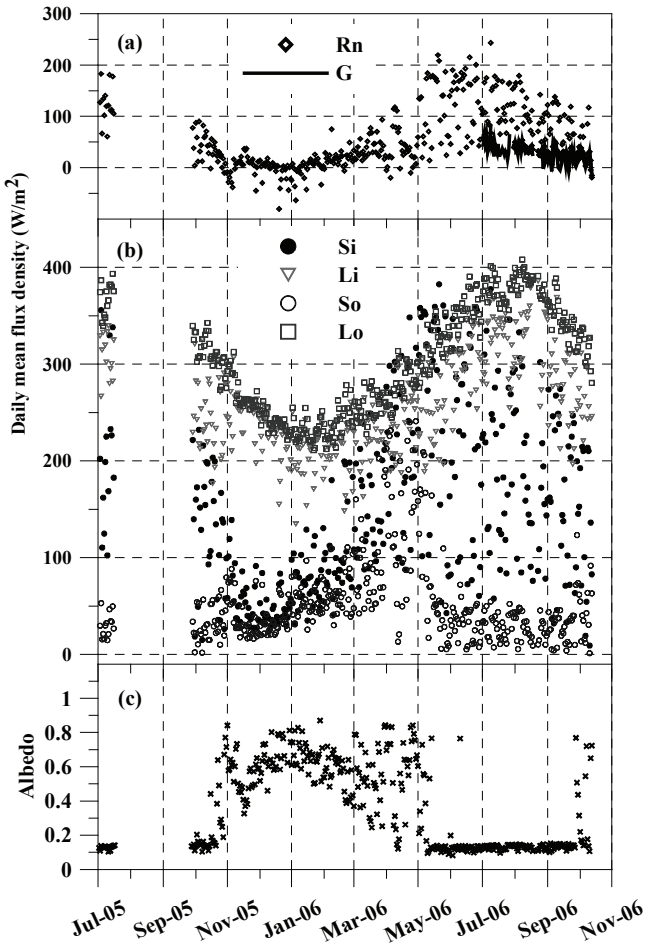


Figure 4. (a) Seasonal changes in daily mean net radiation Rn and daily mean ground heat flux G. (b) Seasonal changes in daily mean values of radiation components (shortwave incoming radiation Si, shortwave outgoing radiation So, longwave incoming radiation Li, and longwave outgoing radiation Lo). (c) Seasonal changes in daily representative albedo (calculated over the period 10:00–14:30).

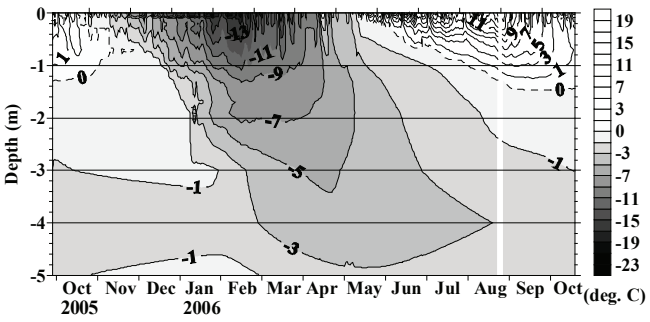


Figure 5. Seasonal variations in the soil temperature profile to a depth of 5 m at the study site from October 2005 to October 2006. Solid isotherms are drawn with increments of 2°C; the dashed line indicates the 0°C isotherm.

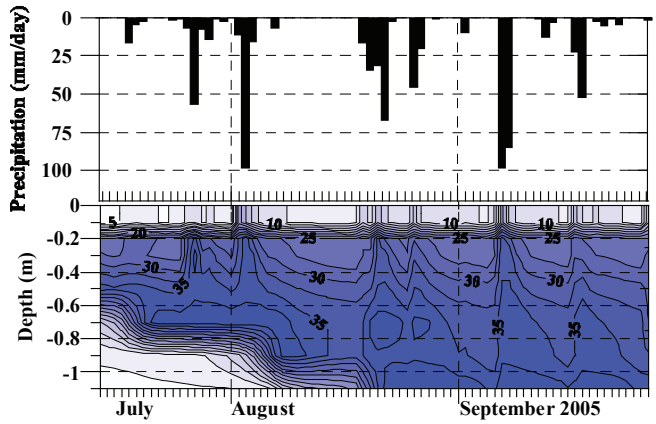


Figure 6. Seasonal changes in daily precipitation (upper) and profile of the volumetric soil water content in the liquid phase (lower; values are given in %).

*Radiation environment and ground heat flux*

Daily mean Rn values were close to or below 0 W/m$^2$ in winter and above 200 W/m$^2$ in early summer (Fig. 4a). These values were strongly dependent on the weather, fluctuating between 50 and 220 W/m$^2$ during summer. Measurements of ground heat flux were initiated in July 2006. The daily mean value was around 50 W/m$^2$ during July 2006, decreasing gradually to 0 W/m$^2$ during the middle of October 2006 (Fig. 4a). The large fluctuations in daily net radiation values were accompanied by similar fluctuations (of 20%–50%) in the ratio of ground heat flux G to Rn (G/Rn). The obtained range in the ratio G/Rn is similar to that reported in some tundra regions, and much higher than that in boreal forests (Eugster et al. 2000).

On fine days from May to July 2006, the maximum values of 30-minute mean Si were about 1100 W/m$^2$, and Rn was calculated to be about 750 W/m$^2$ (data not shown). The daily maximum Si and Rn decreased, respectively, to about 200 and 100 W/m$^2$ on days of bad weather. Si values near the upper envelope were measured on fine days. The recording of Si values lower than those on fine days indicates a large number of days with cloudy or stormy weather (Fig. 4b).

Albedo values were relatively stable (0.08–0.15) in summer but showed large variations in winter related to snow coverage (Fig. 4c).

*Wind direction and speed*

Wind data are limited to the period between July and November 2005 because of sensor malfunction during other periods. Two predominant wind directions were recorded: strong westerly winds and relatively weak south-westerly winds. About 30% of the westerly wind velocities (30-minute averages) were in the range of 10–20 m/s, 40% in the range of 5–10 m/s. The equivalent percentages for the south-westerly wind were about 10 and 40%, respectively. The winds during other periods were of lower velocities. Persistent, strong westerly to south-westerly winds were also reported by Sone (unpubl.), who described strong winds from October to April. It has been observed that most of the summit plateaus in the Daisetsu Mountains have little snow cover because of persistent westerly driving winds (Takahashi & Sato 1994).

*Ground temperature and water conditions*

The ground began to freeze from the surface at the

beginning of October 2005 and from the permafrost upward in the middle of the same month (Fig. 5). The entire active layer fell below 0°C in November, reaching -9°C in February. Thawing of the frozen ground commenced in the middle of May 2006. The thaw front developed at an almost constant average rate of 12.2 mm/day until the end of August. A freezeback from the deeper layer was also observed, induced by prolonged cold weather at the end of June.

The active layer thickness was 1.28 m and 1.46 m in 2005 and 2006, respectively, and the depth of the permafrost base was greater than 5 m. The permafrost temperature at a depth of 4 m fluctuated between -1.70°C and -4.84°C during the observation period.

Large amounts of summertime precipitation were recorded at the study site. The 4-month cumulative rainfall amounts from June to September were 813 mm in 2005 and 693 mm in 2006. Sone (unpubl.) measured 4-month rainfall amounts of 929 mm in 1995 and 976 mm in 1996 at a point located about 1 km west of our study site. Soil water content was close to saturated throughout 2005, and variations in soil water showed a strong correlation with rainfall events (Fig. 6). The values of soil moisture presented in this paper were calculated using default calibration curves for sandy soil; however, *in situ* calibration is required for a more accurate discussion of the absolute amount of soil moisture in the active layer.

Although we did not obtain data on evapotranspiration and runoff ET + R at the study site (with regard to discussing the water budget), we roughly estimated ET + R by differentiation of the water balance equation P = dS + ET +R. P and dS are precipitation and change in the amount of soil water storage in a certain period, respectively. The value of dS in the active layer from 15 July to 27 September 2005 was determined from the measured profiles of soil water content (40 mm). The values of P and ET + R in the same period were 770 and 810 mm, respectively. A relatively minor change in soil water storage was observed; almost all of the precipitation water that fell during this period was likely to have been lost to evapotranspiration or discharged laterally. Rapid changes in soil moisture within the deeper active layer indicate the high permeability of the soil (Fig. 6). It is likely that the soil water condition in the active layer at the site was kept high or near-saturated during the thawing season because of frequent rainfall and the existence of permafrost. However, rapid changes in soil moisture throughout the active layer probably reflect the high permeability of the volcanic soil. A degree of lateral runoff may also have occurred, strongly influencing the hydrological regime of the active layer.

*Changes in surface conditions*

Albedo depends on surface conditions such as snow coverage, soil moisture at the surface, and vegetation phenology. Snowfall began in October 2005 and continued until May of the following year (Fig. 4c). Two snowfall events probably even occurred during June of 2006. Considering that the albedo of fresh snow is 0.75–0.95 (Campbell & Norman 1998), the fact that the measured values were often below 0.7 indicates only partial snow coverage on most days in winter. The large variations in daily mean albedo during winter indicate repeated cycles of snow cover followed by the snow being blown away or sublimated. The observed variations in minimum wintertime albedo values indicate that snow coverage on the ground was highest from the end of December to the beginning of January; most of the accumulated snow had disappeared by the end of February. However, the December–February snow coverage must be confirmed by an alternative method, as the albedo of old snow can be 0.4–0.7 (Campbell & Norman 1998). The summertime albedo showed minor fluctuations (0.08–0.15) relative to those in winter. The summertime day-to-day variations in albedo reflect the moisture conditions of the surface soil: moist soil is darker, with a lower albedo. The albedo values during the snow-free period showed a gradual increase (by about 0.02 on average), together with day-to-day variations. The seasonal change in albedo can likely be attributed to the phenology of surface vegetation. It should be noted that albedo values also depend on the zenith angle and cloud cover (Goodin & Isard 1989); these factors must be considered in further discussions.

*Surface temperature*

Ground surface temperature was obtained using a directly installed thermistor sensor (Tsurf) at a depth of 10 mm and the Lo values from the radiometer (Trad). Trad is calculated using the Stefan–Boltzmann equation with an emissivity of 0.98. The maximum Tsurf was 33.1°C, recorded in June 2006; the maximum daily range in Tsurf (35.3°C) was observed on the same day. The daily range in Tsurf during mid-summer is about twice that in Ta, and monthly averaged Tsurf is 1.1°C –6.0°C higher than Ta. Trad values agreed well with Ta values for the snow-covered period. Trad in summer showed similarly large daily variations to those for Tsurf, but maximum values of Trad showed an increasing trend during mid-summer. Large differences between Ta and ground surface temperature were found in both winter and summer.

## Perspectives

State-of-the-art automatic micrometeorological instruments are able to precisely monitor physical conditions in severe mountaintop areas, where measurements are rarely conducted. We commenced micrometeorological measurements, including the monitoring of thermal and hydrological conditions in the ground down to 5 m depth, with the intention of characterizing the features of the surface energy and hydrological balance at a mountaintop permafrost site in Japan. The information will be used to simulate future changes in the environment.

The newly obtained data support the conclusions proposed in previous studies of wind, rainfall, and air temperature undertaken by other Japanese scientists in areas of mountain permafrost. In addition, we recorded the year-round thermal regime of the active layer and the upper layer of permafrost. We also present, for the first time, continuous and simultaneous measurements of the profile of volumetric

water content in the active layer, surface radiation, and air moisture condition at a Japanese mountaintop site. These data will be a base of future long-term monitoring of mountain permafrost and its environment. Additional measurements are required to determine the characteristics of surface energy and hydrological balance at the site.

## Acknowledgments

This work was initially funded by the Leadership Fund of the Institute of Low Temperature Science, Hokkaido University, in 2004. Financial support was thereafter provided by a Sasakawa Scientific Research Grant from the Japan Science Society (in 2005) and the Northern Advancement Center for Science & Technology and Asahi Breweries Foundation (in 2006).

## References

Campbell, G.S. & Norman, J.M. 1998. *An Introduction to Environmental Biophysics*. New York: Springer-Verlag, 286 pp.

Eugster, W., Rouse, W.R., Sr, R.A.P., Mcfadden, J.P., Baldocchi, D.D., Kittel, T.G.F., III, F.S.C., Listion, G.E., Vidale, P.L., Vaganov, E. & Chambers, S. 2000. Land-atmosphere energy exchange in Arctic tundra and boreal forest: available data and feedbacks to climate. *Global Change Biology* 6(S1): 84-115.

Fukuda, M. & Kinoshita, S. 1974. Permafrost at Mt. Taisetsu, Hokkaido and its climatic environment. *The Quaternary Research (in Japanese with English abstract)* 12(4): 192-202.

Fukuda, M. & Sone, T. 1992. Some characteristics of alpine permafrost, Mt-Daisetsu, Central Hokkaido, Northern Japan. *Geografiska Annaler Series A-Physical Geography* 74(2-3): 159-167.

Fukui, K. 2003. Investigating mountain permafrost distribution by ground temperature measurements in the Tateyama Mountains, the northern Japanese Alps, central Japan. *Zeitschrift Fur Geomorphologie*, 47: 179-193.

Goodin, D.G. & Isard, S.A. 1989. Magnitude and Sources of Variation in Albedo within an Alpine Tundra. *Theoretical and Applied Climatology* 40(1-2): 61-66.

Harris, S.A. 1981. Distribution of active glaciers and rock glaciers compared to the distribution of permafrost landforms, based on freezing and thawing indices. *Can. J. Earth Sci.* 18: 376-381.

Harris, S.A. 1986. *The Permafrost Environment*. Ottawa: Barnes & Noble Books, 276 pp.

Ishikawa, M., Fukui, K., Aoyama, M., Ikeda, A., Sawada, Y. & Matsuoka, N. 2003. Mountain permafrost in Japan: distribution, landforms and thermal regimes. *Zeitschrift Fur Geomorphologie* 47: 99-116.

Ishikawa, M. & Hirakawa, K. 2000. Mountain permafrost distribution based on BTS measurements and DC resistivity soundings in the Daisetsu Mountains, Hokkaido, Japan. *Permafrost and Periglacial Processes* 11(2): 109-123.

Koaze, T. 1965. The patterned grounds on the Daisetsu volcanic group, Central Hokkaido. *Geographical Review of Japan (in Japanese with English abstract)* 38(3): 179-199.

Koizumi, T. & Shinsho, H. 1983. Plant communities on permafrost areas in the alpine zone of the Daisetsu Mountains, Central Hokkaido, Japan. *Jap. J. Ecol. (in Japanese with English abstract)* 33: 357-363.

Kudo, G. & Kodama, Y. 1990. Annual transition of soil temperature in the Taisetsu Mountains. *Low Temperature Science, Ser. A. Data Report (in Japanese)* 49: 15-32.

Nakayama, T. & Sone, T. 1992. Characteristics of air temperature variation. *Low Temperature Science, Ser. A (in Japanese with English abstract)* 51: 173-181.

Sawada, Y., Ishikawa, M. & Ono, Y. 2003. Thermal regime of sporadic permafrost in a block slope on Mt. Nishi-Nupukaushinupuri, Hokkaido Island, Northern Japan. *Geomorphology* 52(1-2): 121-130.

Sone, T. 1992. Permafrost environment of the Daisetsu mountains, Hokkaido, Japan. *Permafrost and Periglacial Processes* 3: 235-240.

Sone, T. 1994. Air temperature data at Hakuun Hut in the Daisetsu Mountains, Central Hokkaido in 1990-1993. *Low Temperature Science, Ser. A (in Japanese with English abstract)* 53: 33-50.

Sone, T. 2002. Internal structure of a palsa in the bog to the south of Mt. Hiragatake, the Daisetsu Mountains, Hokkaido, Japan. *Journal of Geography (in Japanese with English abstract)* 111(4): 546-554.

Sone, T. & Nakayama, T. 1992. Air temperature data at Hakuun Hut in the Daisetsu Mountains, Central Hokkaido, 1987-1989. *Low Temperature Science, Ser. A (in Japanese with English abstract)* 51: 31-48.

Sone, T. & Takahashi, N. 1986. Winter field observations of the frost-fissure polygons on Hokkai-Daira Plataeu, Daisetsu volcanic massif, Hokkaido. *Geographical Review of Japan, Ser. A (in Japanese with English abstract)* 59(11): 654-663.

Sone, T., Takahashi, N. & Fukuda, M. 1988. Alpine permafrost occurrence at Mt. Taisetsu, Central Hokkaido, Northern Japan. In: *Permafrost, Proceedings of Fifth International Conference on Permafrost*, *Trondheim*: 253-258.

Tachibana, Y., Kodama, Y. & Yamada, T. 1991. Variation of air temperature in the Taisetsu Mountains in winter. *Low Temperature Science, Ser. A. Data Report (in Japanese)* 50: 33-45.

Takahashi, N. & Sato, K. 1994. Tail-shaped vegetation patch as an indicator to estimate the winter prevailing wind in the alpine bare ground. *Quarterly Journal of Geograph (in Japanese with English abstract)y* 46: 136-146.

Takahashi, N. & Sone, T. 1988. Palsas in the Daisetsuzan mountains, Central Hokkaido, Japan. *Geographical Review of Japan, Ser. A (in Japanese with English abstract)* 61(9): 665-684.

# Influence of Temperature and Groundwater Fluctuation on LNAPL Migration at Colomac Mine Site

Olumide Iwakun
*Civil and Environmental Engineering Department, University of Alberta, Canada*
Kevin W. Biggar
*BGC Engineering, Edmonton, Alberta, Canada*
David C. Sego
*Civil and Environmental Engineering Department, University of Alberta, Canada*

## Abstract

The ongoing site characterization of spilled petroleum hydrocarbon at the abandoned Colomac gold mine site in a discontinuous permafrost region shows variable distribution of accumulated light non-aqueous phase liquid (LNAPL) in the monitoring wells across the site and over time. The site is adjacent to a lake and has between 0 to 4.6 m of overburden soil underlain by fractured greywacke. Different mechanisms, including groundwater fluctuation and thermal regime, have been proposed to account for spatial and temporal variation of the LNAPL at the site. The measured LNAPL showed increased thickness in the winter period. Multiple linear regression was used to correlate the accumulated LNAPL in one of the most yielding monitoring wells with temperature data from a dedicated thermistor-borehole and measured groundwater elevation. The accumulated LNAPL showed significant correlation with both the temperature data and the groundwater water elevation at the site.

**Keywords:** freeze; LNAPL; migration; mine; permafrost.

## Introduction

Discovery of valuable minerals in the Northwest Territory (NWT) in Canada has led to increased mining activities. The adverse environmental impacts of the mining operations during and after closure are a widespread problem, which has received major attention recently. Many of the mining sites used are located in remote areas where a large percentage of the operating cost is due to logistics of moving and maintaining personnel and materials at the site. To offset some of the logistic issues in transporting petroleum fuel as the main energy source to the site and smooth operation of the mine, large volumes of fuel are stored in tanks on site. The designated area of the site where several fuel storage tanks are located is called the *tank farm*. Accidental fuel spillage during transportation or leakage of the fuel tanks in the tank farm area is a looming problem, which is complicated by the presence of permafrost.

To this effect, various studies have been conducted to understand the behavior of spilled fuel in frozen and freezing environment. Permafrost has been shown to be an effective barrier to water flow but not a barrier to the flow of petroleum hydrocarbons (Biggar et al. 1998, McCarthy et al. 2003). Studies conducted with petroleum hydrocarbon (PHC) contaminated soils in freezing conditions showed that the concept of LNAPL exclusion forward of freezing front is applicable (Konrad & Seto 1991, Tumeo & Davidson 1993, Biggar & Neufield 1996, Chuvilin 1999, Barnes et al. 2004). In addition to the concept of LNAPL exclusion, Barnes et al (2004) stipulated physical displacement of the mobile phase PHC from the pore spaces as water expands on freezing. Chuvilin et al (2001a) showed that spreading and transportation of oil in regions of frozen ground is dependent on oil composition, soil temperature, and type of mineral surface.

Literature on migration of spilled fuel within fractured bedrock in a permafrost environment is limited. Iwakun & Biggar (2007) suggested that a lower groundwater table in the winter period may enhance drainage of mobile free phase PHC as light non-aqueous phase liquid (LNAPL) from the overburden soil and fractured bedrock surface at Colomac mine. However, in this study, the measured petroleum LNAPL thickness was correlated with the measured ground temperature to understand the influence of thermal fluctuation on LNAPL migration at the site.

## Site Background

Colomac mine was an open-pit gold mine located in a discontinuous permafrost region approximately 220 km northwest of Yellowknife in the Northwest Territories. It operated between 1990 and 1997. When it became uneconomical to operate the mine site, it was closed and abandoned in 1999. It is now the responsibility of the Contaminated Site Office (CSO) of Indian and Northern Affairs Canada (INAC) to remediate the site. The site is underlain by fractured bedrock identified as greywacke, and has between 0 to 4.6 m overburden soil made up of sands and gravel. There are different aspects of the site under remediation but this paper will focus on the tank farm area where fuel spillage occurred.

Between 1990 and 2003, over 24 spills of diesel and gasoline around the tank farm were reported at the site (Fig. 1). Of these spills, two were significant. These include 18,000

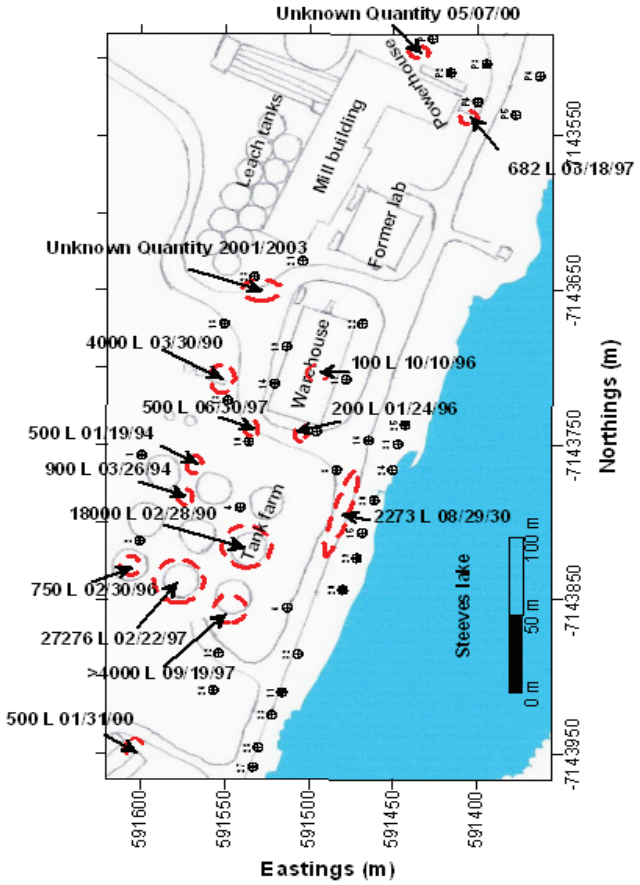


Figure 1. Summary of historical spillage at Colomac mine.

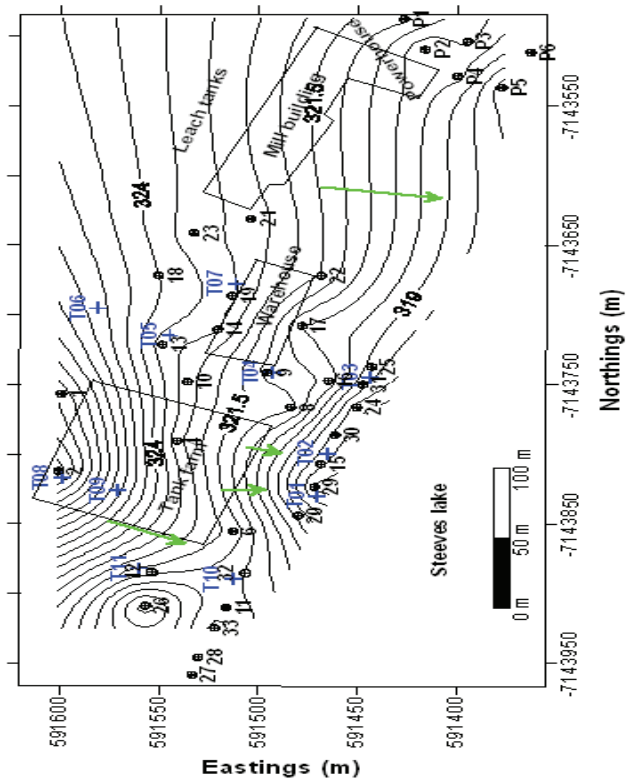


Figure 2. Water table contour for August 2006 showing spatial location of installed monitoring wells and thermistors strings. (Note: thermistor strings are preceeded with T.)

L and 27,276 L in February of 1990 and 1997, respectively, as a result of leakage of one of the fuel storage tanks. After these spills, some measures were taken to curb migration of PHC to Steeves Lake adjacent to the site. These include:

- Installation of 5 m deep interceptor trench lined with corrugated pipe at the west berm of the tank farm in late 1990.
- Placement of skirted boom with absorbent pad along the Shore of Steeves Lake when PHC sheen was observed in late 1990/1991.
- Detailed site characterization and installation of monitoring wells across the site in 2000, shown in Figure 2.
- Replacement of interceptor trench with a frozen soil barrier in 2004 to contain down-gradient migration of mobile phase PHC.
- Removal and biopile treatment of overburden soil at the tank farm area in 2005.

Details of these measures were discussed by Iwakun & Biggar (2007). However, in spite of these measures, petroleum LNAPL is still being observed in some of the monitoring wells across the site. Sheen of PHC at the shore of the lake is also being observed in the summer. Limited effectiveness of these measures shows that knowledge of subsurface behavior of spilled fuel at the site is inadequate. Thus, to improve this understanding, further site investigation was initiated by the University of Alberta Geotechnical Centre and Environment Canada in June 2005.

## Site Investigation

Subsurface investigation at this site includes periodic monitoring of depths to petroleum LNAPL, water, and bottom/ice in the wells; thermistor cable installation and thermal profiling; groundwater sampling; hydraulic testing; borehole imaging; rotary coring; and product recovery. These activities have been discussed by Iwakun & Biggar (2007) and Iwakun et al. (2007). However, for completeness of this paper, summaries of pertinent activities and major findings will be given in this paper with particular emphasis on thermistor installation and monitoring of depths to petroleum LNAPL and water.

*Depths to product and water*

An interface probe was used to measure the depths to petroleum LNAPL, water, and well-bottom. When the measured depth to well-bottom was less than the known depth of the well, ice was inferred at that depth. A summary plot of some of the measurements is shown in Figure 3. The apparent groundwater flow pattern in the summer was inferred from the interpreted isopleths of the groundwater elevation as shown in Figure 2. However, it should be noted that the actual flow pattern may be substantially different from that presented because the fracture networks control the flow direction. In the winter period, apparent flow patterns cannot be inferred because of different thermal distribution at the site as discussed in the subsequent section. Elevated groundwater was noticed in the spring but gradually declined

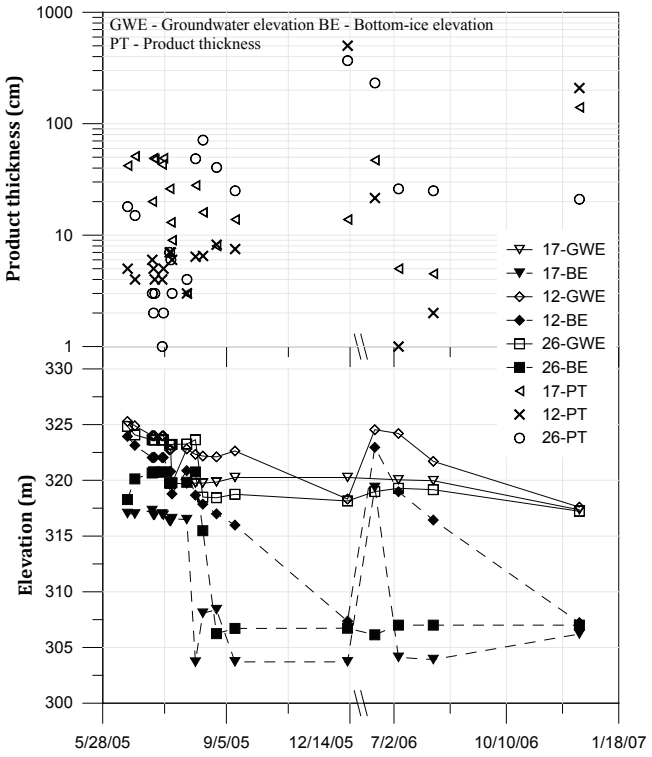

Figure 3. Well-probe data in selected monitoring wells at the site.

as winter approached before freezing.

It was also observed that in early spring, some of the wells were not thawed to well-bottom resulting in an artificial increase in groundwater elevation due to a perched groundwater condition. Thus, at this site, a suprapermafrost water table condition existed from early spring through the summer period. As winter approached, an intrapermafrost water table condition existed across the site except at the warehouse area where the thermal regime was influenced by heat from a generator in the southwest corner of the warehouse building. Due to nearness of the site to the lake, the intrapermafrost water condition may also be influenced by the unfrozen thaw bulb (i.e. talik) adjacent to and beneath the lake.

*Ground temperature profiling*

To understand the influence of the thermal regime on contaminant distribution, Solinst level loggers, barologgers, and thermistor strings were initially installed in some of the wells to corroborate the monitored depths to water and bottom-ice at the site between June 2005 to April 2006. Between April and June 2006, new boreholes with dedicated thermistor strings were installed across the site as shown in Figure 2. Each thermistor string consists of eight sensors at specific depths with battery operated datalogger. The boreholes were backfilled with bentonite pellets and water after installation of thermistor string. Sensitivity of the thermistor strings were tested in the laboratory and found to be within ±0.2°C of actual melting point of ice at 0°C.

*Summary of other pertinent activities*

Some of the wells were hydraulically tested using a packer assembly at discrete intervals in the summer of 2005 and 2006. The results showed higher transmissivity (in the range of $10^{-3}$ to $10^{-6}$ $m^2/s$) within the upper 7 m of the bedrock. At depth, the bedrock has very low transmissivity (in the order of $10^{-9}$ $m^2/s$). Rotary bedrock coring at the site corroborates this inference. The fractured upper section of the bedrock appears localized because the transmissivity varied from one well to the other. Borehole imaging using a Well-Vu camera showed what looks like near vertical and horizontal fractures with depth. However, due to drilling method of most of the wells (i.e. percussion hammer drilling), it is difficult to correlate fracture width from post image analysis to that of the hydraulic test. Fissures observed may be due to well-bore scaring during installation. With borehole imaging, zones with marked discoloration were noticed in the upper section of the bedrock but no pooled free phase PHC was observed at the bottom of the wells.

## Methodology

From the activities stated above, the observed apparent LNAPL thickness in the monitoring wells (MW) showed that MWs 12, 26, and 17 are the highest yielding wells at the site. Of these, MW 12 and 26 are very close (Fig. 2) but MW 12 is closer to the installed thermistor string. MW 17 is close to the warehouse and its thermal profile may be influenced by the heat generated southwest of the warehouse building. Thus, the measured apparent LNAPL thickness of MW 12 and its thermal profile are used for this study.

The measured thermal profile close to MW 12 and 26 is shown in Figure 4. This thermal profile was used for a simple statistical test with the measured apparent LNAPL thickness using multiple linear regression. Since the measured apparent LNAPL also varies with groundwater elevation as shown in Figure 3, a multiple linear regression test with both temperature and groundwater elevation as independent variables was also undertaken. For this study, the temperature value used for the regression analysis was determined by averaging the temperature value in the upper 7 m of the subsurface. This decision was made because other tests conducted at the site including hydraulic tests, bedrock coring, and borehole imaging, showed that the upper section of the bedrock is highly fractured.

The implication of this is that the apparent petroleum LNAPL in the monitoring wells is assumed to come from the overburden soil and fractured upper section of the bedrock.

*Multiple linear regression*

This method of analysis was chosen because of perceived dependency of the measured apparent LNAPL in the wells on temperature and groundwater elevation.

Multiple regression demonstrates the consequence of one independent variable with the other independent variable kept constant. The regression coefficients of the variables are calculated using the equation below:

$$\Sigma X_1 Y = b_1 \Sigma X_1^2 + b_2 \Sigma X_1 X_2$$
$$\Sigma X_2 Y = b_1 \Sigma X_1 X_2 + b_2 \Sigma X_2^2 \quad (1)$$

where $X_j = x_j - x_m$, $Y_j = y_j - y_m$, and both represent deviation of independent and dependent variables ($x$, $y$) respectively; $b_j$ is the regression coefficient of $j$-th variable. The regression coefficients are used to construct equation to the regression plane given by:

$$\bar{y} = b_0 + b_1\bar{x}_1 + b_2\bar{x}_2 \quad (2)$$

where $b_0$ is a constant. Finding $b_1$ and $b_2$ in equation 1 leads to simultaneous equations which can be represented with a matrix of the form AN=B, where $N$ represents a matrix tensor of the unknown regression coefficients and is solved by multiplying the inverse of its coefficient matrix ($A$) with the known vector ($B$); i.e., $N=A^{-1}B$. The tensor of the inverse matrix (i.e., $e_{jj}$ terms) is used in the computation of standard deviation of each regression coefficient ($S_{bj}$) in combination with the residual variance ($S_{y/x}$), and ultimately used in calculating its level of significance using the $t$-test. If the calculated $t$ is greater than the tabulated $t$ (from statistical table), then the null hypothesis that the regression coefficient is insignificant is rejected. The relevant equations are shown below:

$$A^{-1} = \begin{bmatrix} e_{11} & e_{12} \\ e_{21} & e_{22} \end{bmatrix} \quad (3)$$

$$e_{11} = \frac{\Sigma x_2^2}{\Sigma x_1^2 \ \Sigma x_2^2 - (\Sigma x_1 x_2)^2}$$
$$e_{22} = \frac{\Sigma x_1^2}{\Sigma x_1^2 \ \Sigma x_2^2 - (\Sigma x_1 x_2)^2}$$
$$e_{12} = e_{21} = \frac{\Sigma x_1 x_2}{\Sigma x_1^2 \ \Sigma x_2^2 - (\Sigma x_1 x_2)^2} \quad (4)$$

$$S_{y/x}^2 = \frac{\Sigma Y^2 - b_1 \Sigma Y X_1 - b_2 \Sigma Y X_2}{n-3} \quad (5)$$

$$S_{bj} = S_{y/x}\sqrt{e_{jj}} \quad (6)$$

$$t = \frac{b_j}{S_{bj}} \quad (7)$$

An $F$-test was used to test the level of significance of the multiple regression as a whole using the equation below:

$$F = \frac{b_1 \Sigma Y X_1 + b_2 \Sigma Y X_2}{S_{y/x}^2} \quad (8)$$

The computed $F$-value is compared with that given in statistical table at a given level of significance. If the computed value is greater than tabulated value, then the null hypothesis that the partial regression coefficients are insignificant is rejected.

Finally, the degrees of association of the variables were tested using multiple correlation coefficients given by the formula below:

$$r^2 = \frac{b_1 \Sigma Y X_1 + b_2 \Sigma Y X_2}{Y^2} \quad (9)$$

$$r_{yx_j} = \frac{\Sigma x_j Y}{\sqrt{x_j^2 + \Sigma Y^2}} \quad (10)$$

where $r$ and $r_{xyj}$ are sample and any two variable correlation coefficients, respectively. The computed value is also compared with tabulated value in statistical table to draw inference on the null hypothesis as discussed earlier.

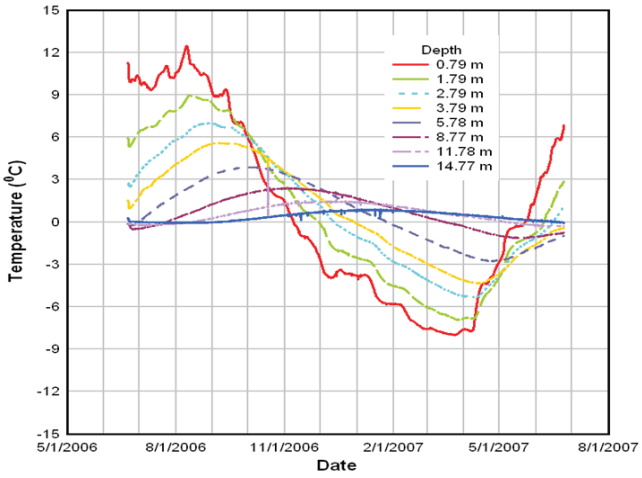


Figure 4. Temperature profile in one of the dedicated thermistor strings "T11" adjacent to MW 12.

## Results

The data used for the regression analysis are shown in Table 1. The averaged integral temperature in the upper 7 m was also divided into two, because there is an inflection in the temperature profile between 3 m and 4 m depths from the ground surface due to heat lag effect as shown in Figure 4. The results of the statistical parameters are shown in Table 2. The calculated F-value of the regression equation and the sample multiple-correlation coefficient are greater than the tabulated value for 5% significant level. Thus, the regression equation is statistically significant, and the measured apparent LNAPL thickness correlates well with groundwater elevation and temperature profile at the site within 95% confidence limit as shown in Figure 5.

The partial regression coefficients of the apparent LNAPL (or product) thickness in the well are negative for both groundwater elevation and temperature. This implies that the product thickness increases with decreasing groundwater elevation and decreasing temperature. The absolute partial regressions of product thickness with groundwater elevation and temperature within the upper 3 m of the subsurface

Table 1. Data from MW 12 used for correlation regression.

| Date | PT (cm) | GWE (m) | T 1-7 (°C) | T 1-3 (°C) | T 3-7 (°C) |
|---|---|---|---|---|---|
| 06/17/05 | 5.0 | 325.3 | 0.240 | 2.414 | -0.793 |
| 06/23/05 | 4.0 | 324.9 | 2.231 | 5.804 | 0.539 |
| 07/07/05 | 6.0 | 324.0 | 3.236 | 6.779 | 1.553 |
| 07/08/05 | 5.0 | 324.0 | 3.283 | 6.795 | 1.614 |
| 07/09/05 | 4.0 | 324.0 | 3.321 | 6.810 | 1.663 |
| 07/15/05 | 4.0 | 324.0 | 3.689 | 7.079 | 2.079 |
| 07/16/05 | 5.0 | 324.0 | 3.772 | 7.210 | 2.139 |
| 07/21/05 | 7.0 | 322.7 | 4.110 | 7.677 | 2.417 |
| 07/22/05 | 7.0 | 322.8 | 4.181 | 7.784 | 2.470 |
| 07/23/05 | 6.0 | 319.7 | 4.261 | 7.894 | 2.535 |
| 08/04/05 | 3.0 | 322.8 | 4.848 | 8.262 | 3.225 |
| 08/11/05 | 6.4 | 322.3 | 5.341 | 9.052 | 3.578 |
| 08/17/05 | 6.5 | 322.2 | 5.486 | 8.828 | 3.898 |
| 08/28/05 | 8.2 | 322.1 | 5.700 | 8.569 | 4.338 |
| 09/12/05 | 7.5 | 322.6 | 5.655 | 7.952 | 4.564 |
| 12/12/05 | 501.0 | 318.3 | 0.220 | -1.909 | 1.231 |
| 06/15/06 | 21.5 | 324.5 | 0.047 | 2.024 | -0.893 |
| 07/06/06 | 1.0 | 324.2 | 3.194 | 6.766 | 1.498 |
| 08/06/06 | 2.0 | 321.7 | 4.997 | 8.523 | 3.320 |
| 12/14/06 | 209.0 | 317.6 | 0.130 | -1.939 | 1.114 |

PT – Product thickness; GWE – Groundwater elevation.
T a-b – Average integral temperature from a-b m depth.

Table 2. Summary of statistical parameters from analysis.

| | | | | | |
|---|---|---|---|---|---|
| b0 | -38.68 | e11 | 0.012 | Sy/x | 85.15 |
| b1 | -6.76 | e22 | 0.003 | Sb1 | 9.45 |
| b2 | 459.61 | e21 | 0.0003 | Sb2 | 4.92 |
| t1 | -4.09 | F-sample | 9.58 | F-table | 3.590 |
| t2 | -1.37 | r-sample | 0.728 | r-table | 0.456 |
| | | | | t-table | 2.110 |

Summary of partial correlation coefficients

| Variables | GWE | T 1-7 | T 1-3 | T 3-7 | PT |
|---|---|---|---|---|---|
| PT | -0.691 | -0.537 | -0.769 | -0.200 | 1.000 |

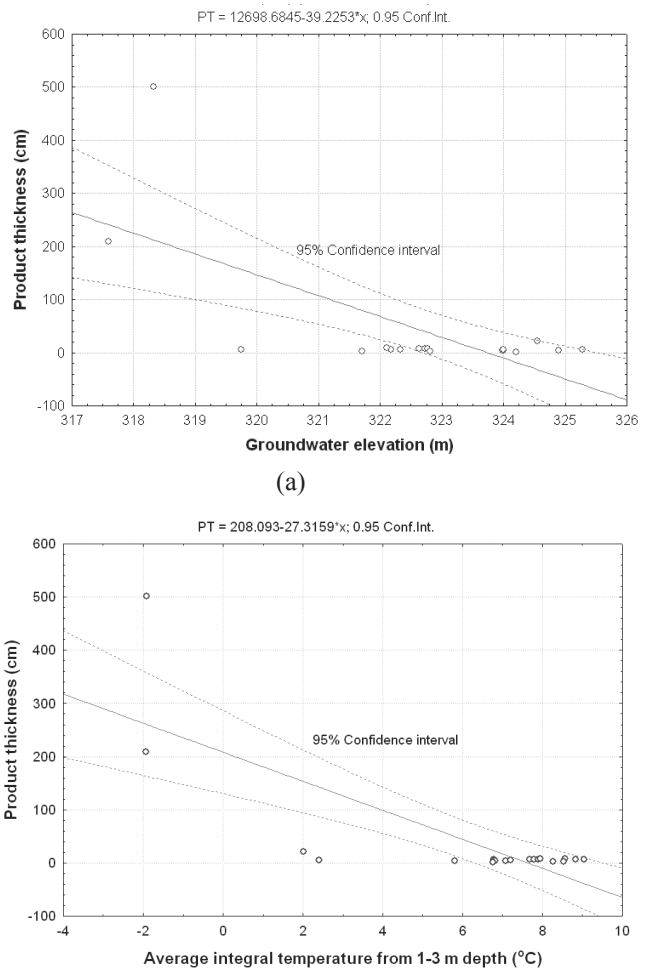


Figure 5. Partial linear correlation regression plots of the product thickness with (a) Groundwater elevation (b) Average integral temperature from 1-3 m depth.

are 0.691 and 0.769, respectively, and above the tabulated regression value of 0.456 from statistical table at 5% significant level (Table 2). The absolute partial regression of integral temperature from 3 to 7 m depth is 0.2, and below the tabulated r-value. Thus, the product thickness is more sensitive to changes in groundwater elevation and temperature within the upper 3 m of the subsurface than that at depth.

## Discussion

Correlation of the product thickness with both the groundwater elevation and temperature profile only depicts association with the variables and does not necessarily imply causation. However, because other tests have been conducted at the site, inference can be drawn on how the decreasing groundwater elevation and temperature contributes to increased product thickness in the monitoring wells. Increased correlation with temperature in the upper 3 m of the subsurface suggests causative active mechanism at that section based on the premise of LNAPL exclusion due to freezing of water in soil matrix (Barnes et al. 2004) and fractures. However, this premise must be further explored experimentally for fissured media under laboratory condition.

Gravity drainage of mobile residual petroleum LNAPL in the formation due to a decrease in groundwater elevation coupled with LNAPL exclusion forward of the freezing front are hereby proposed as active mechanisms contributing to increased product thickness in the monitoring wells. The associative strength of these mechanisms is downplayed because of continual purging of the accumulated petroleum LNAPL from the monitoring wells. The overburden soil around MW 12 is 2.3 m thick and consists of gravel fill with sand. The well-log showed that multiple fractures exist between the upper 0.7 m of the bedrock surface with strong odor of petroleum hydrocarbon (PHC). Previous site characterization at the site by URS (2002) suggested that LNAPL being observed at the site are the residual LNAPL

in the unsaturated zone of the subsurface. Thus, increased correlation of temperature fluctuation in the upper section of the subsurface affirms this.

Lower correlation between the product thickness and averaged integral temperature between 3 and 7 m from the subsurface does not necessarily imply poor influence on the product thickness because other factors such as fracture pattern and network may be masking its association. Though linear regression was used for this analysis, the actual association between the varied parameters may be non-linear. The practical significance of this study is that fluctuation of the groundwater table and freeze thaw cycle may increase recovery of mobile residual petroleum hydrocarbon from the subsurface at this site.

## Conclusions

In this study, accumulated mobile LNAPL thickness in the monitoring well is shown to significantly correlate with the groundwater elevation and temperature at Colomac mine site. The petroleum LNAPL thickness increased with decreasing groundwater elevation and temperature. It was hypothesized that gravity drainage of mobile residual petroleum LNAPL at decreased groundwater elevation coupled with LNAPL exclusion are key mechanisms contributing to the observed behavior. The study suggests that product recovery may be enhanced by engineered fluctuation of the groundwater table and thermal regime at the site.

## Acknowledgments

This study was sponsored by Program for Energy Research and Development (PERD), Indian and Northern Affairs Canada (INAC) and Environment Canada. The contributions by Greg Bickerton and Dale Van Stempvoort of Environment Canada, field assistance provided by Rob Duschene, Ross Neureuther, John Voralek, and Ron Breadmore of INAC are gratefully acknowledged.

## References

Barnes, D.L., Wolfe, S.M. & Filler, D.M. 2004. Equilibrium of petroleum hydrocarbons in freezing ground. United Kingdom. *Polar Record* (214): 245-251.

Biggar, K.W., Haidar, S., Nahir, M. & Jarrett, P.M. 1998. Site investigations of fuel spill migration into permafrost. *Journal of Cold Regions Engineering* 12: 84-104.

Biggar, K.W. & Neufeld, J.C.R. 1996. Vertical migration of diesel into silty sand subject to cyclic freeze-thaw. Cold Regions Engineering: *Proceedings of the Eighth International Conference on Cold Regions Engineering. August 12-16:* 116-127.

Chuvilin, E.M. 1999. Migration of ions of chemical elements in freezing and frozen soils. *Polar Record* 35(192): 59-66.

Chuvilin, E.M., Naletova, N.S., Miklyaeva, E.C., Kozlova, E.V. & Istanes, A. 2001a. Factors affecting the spreadibility and transportation of oil in regions of frozen ground. *Polar Record* 37(202): 229-238.

Iwakun, O. & Biggar, K.W. 2007. Behaviour of spilled petroleum hydrocarbon at Colomac mine site, NWT. Canada. *60th Canadian Geotechnical and 8th joint CGS/IAH-CNC Groundwater Conferences*. Paper No. 565: 8 pp.

Iwakun, O., Biggar, K.W., Van Stempvoort, D. & Bickerton, G. 2007. Fuel contamination characterization in permafrost fractured bedrock at the Colomac mine site. Submitted to Cold Region Science and Technology (CRST-D-06-00119R1). 26 pp.

Konrad, J.M. & Seto, J.T.C. 1991. Freezing of a clayey silt contaminated with an organic solvent. *Journal of Contaminant Hydrology* 8(3-4): 335-356.

McCarthy, K., Walker, L. & Vigoren, L. 2004. Subsurface fate of spilled petroleum hydrocarbon in continuous permafrost. *Cold Regions Science and Technology* 38: 43-54.

Tumeo, M.A. & Davidson, B. 1993. Hydrocarbon exclusion from ground water during freezing. *Journal of Environmental Engineering* 119(4): 715-724.

URS, Norecol, Dames & Moore Inc. 2002. Assessment of hydrocarbons within fractured bedrock at the lakefront and waste oil areas and development of a remedial action plan, Colomac Mine, NWT. Report for Public Works & Government Services Canada. Vancouver, BC: 21 pp. + appendices.

# The Temperature Regime in Boreholes at Nalaikh and Terelj Sites, Mongolia

Ya Jambaljav, A. Dashtseren, D. Solongo, A. Saruulzaya, D. Battogtokh
*Permafrost laboratory at Institute of Geography, MAS, Mongolia*
Y. Iijima, M. Ishikawa, Y. Zhang, H. Yabuki, Ts. Kadota
*Institute of Observational Research for Global Change, JAMSTEC, Japan*

## Abstract

Since 2002, long-term field research of joint Japan-Mongolian IORGC projects have been concentrated and conducted in Nalaikh and in Terelj near Ulaanbaatar, Mongolia. There are two sites in Terelj (Terelj GL, Terelj FA) and one site in Nalaikh. At these sites we have been measuring the meteorological and permafrost parameters. This paper presents the temperature regime from 2003 to 2007 in boreholes located at these sites. The air temperature trend has increased by 1.9°C in Ulaanbaatar since 1969.

**Keywords:** active layer; geocryological; near-surface temperature; permafrost; temperature regime.

## Introduction

Mongolia is a country of predominated by high and middle height mountains with continental climate, which promote the occurrence and development of permafrost. Permafrost underlies almost two thirds of the country and comprises the Province of Hovsgol, the Hangai, Hentei, and Altai mountains, and surrounding areas. Therefore, there is predominately mountain and arid land permafrost from sporadic to continuous distribution which is spread along the southern fringe of the Siberian permafrost region (Sharkhuu 2001). The permafrost in Mongolia is changing very rapidly under the influence of human activities such as open and close-pit coal mining, forest fires, etc. (Sharkhuu 2004).

This paper presents the temperature regimes between 2003 and 2007 from three observation sites (Terelj FA, Terelj GL, and Nalaikh) located near Ulaanbaatar. Long-term field research of joint Japan-Mongolian IORGC projects has been concentrated and conducted in Nalaikh and in Terelj. Nalaikh is located approximately 40 km to the southeast of Ulaanbaatar and is characterized by sparsely grassed pasture plate area. The elevation is about 1420 m a.s.l. Terelj is located approximately 40 km to the east of Ulaanbaatar and approximately 70 km from Ulaanbaatar by main road. Terelj is characterized by mountainous area with heights of 1550–2195 m a.s.l. In Terelj the south facing slopes are characterized by sparsely grassed grasslands with granite appearing in some places. South facing slopes and adjacent valleys have no permafrost. North facing slopes are covered by boreal forest, beneath which the permafrost occurs.

The objectives of this paper are to review the recent temperature regimes and to compare the air, near-surface, and ground temperature curves at selected sites.

*Description of observation sites*

According to the geocryological map of Mongolia (scale 1:1,500,000) the study area is located in an insular and sparsely insular permafrost region (Gravis et al. 1971). The insular and sparsely insular permafrost occupies 1%–50% of the total area. There are 18 observation sites in Terelj and 1 site in Nalaikh. In this paper we used the temperature data from 2 sites in Terelj (Terelj GL, Terelj FA) and from the Nalaikh site (Fig. 1).

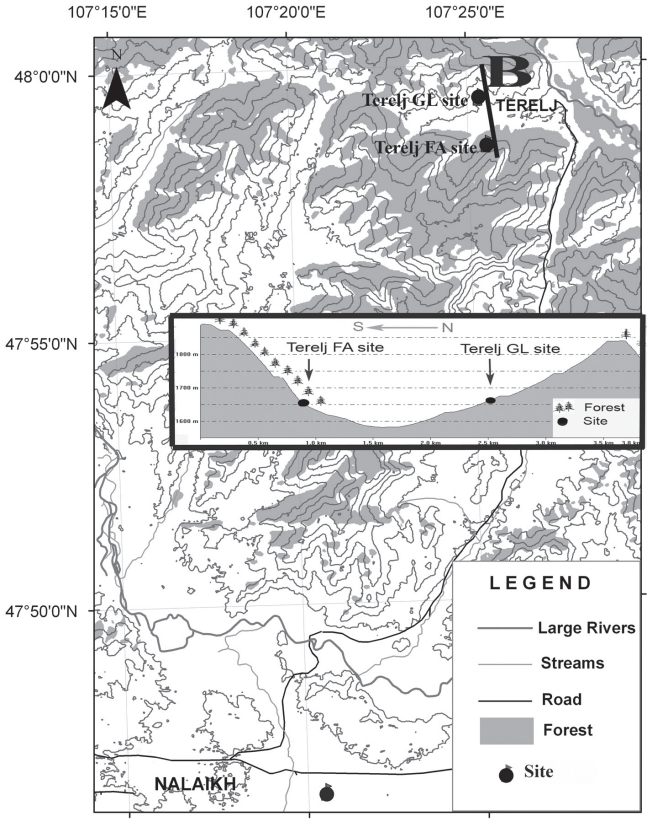


Figure 1. Location of sites. Also the profile along the B line is shown.

Terelj FA site lies on a north facing forested slope of 10°–20°. The upper slope is 25°–40°. The elevation is 1656.5 m a.s.l. A 7.5 m deep borehole was drilled at this site in 2002. The ground temperature has been measured in this borehole using the CR-10X datalogger, datamark, and thermorecorder TR52. Terelj GL site lies on a south facing grassland slope of 10°–15°. The upper slope is 20°–35°. The elevation is 1664.4

m a.s.l. A 10 m deep borehole was drilled at this site in 2002. The ground temperature has been measured in this borehole using the datamark and CR-10X datalogger. The Nalaikh site lies on sparsely grassed pasture plate area of the Nalaikh depression. The elevation is 1420 m a.s.l. Boreholes 30.0 m and 7.0 m deep were drilled at this site in 2002. At these sites we also have measured the meteorological parameters at automatic weather stations (AWS).

*Used data*

In this paper we have used the air temperature and borehole temperature data measured at the Terelj FA and Terelj GL observation sites and at the Nalaikh site. The air temperature has been measured 1 and 2 m above the ground surface at Terelj FA, 1, 2, and 4 m above the ground surface at Terelj GL, and 0.5, 1, 2, and 4 m above the ground surface at Nalaikh. The air temperature data 2 m above the ground surface was used for this paper. Also we have used the temperature data from the 7.0 m deep and 30.0 m deep boreholes at the Nalaikh site, the 7.5 m deep borehole data at Terelj FA, and the 10.0 m deep borehole temperature data at Terelj GL site.

## Climate Condition

According to climate change studies during the last 60 years, the mean annual air temperature has increased by 1.56° in Mongolia. Winter temperature has increased by 3.61° and spring, autumn temperature by 1.4°–1.5°. However the summer temperature has decreased by 0.3° (Natsagdorj 2000).

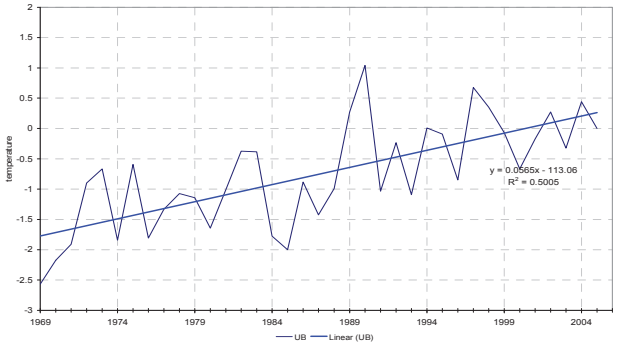


Figure 2. Mean annual air temperature in Ulaanbaatar between 1969 and 2005.

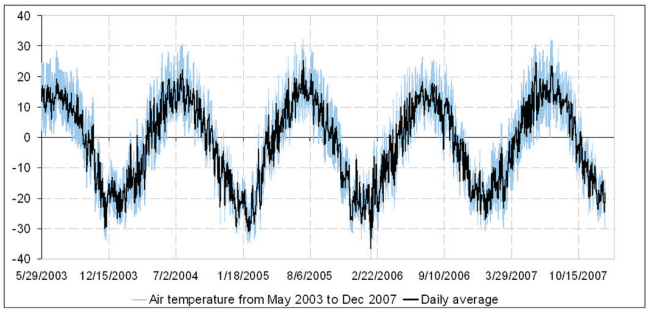


Figure 3. Air temperature at Terelj FA site.

Air temperature trend increased by 1.9° from 1969 to 2005 in Ulaanbaatar (Fig. 2).

## Temperature Regimes of Sites

*Air temperature*

The maximum air temperature has been about +30.0°, and the minimum air temperature about -30.0° for the last 5 years at the Terelj FA site (Fig. 3). The mean annual air temperature was -2.9° for 2003, -2.1° for 2004, -2.97° for 2005, -3.35° for 2006, and -1.69° for 2007.

The maximum air temperature has been about +30.0° and the minimum air temperature is about -30.0° for the last 5 years at the Terelj GL site (Fig. 4). The mean annual air temperature was -1.21° for 2004, -1.36° for 2005, -1.5° for 2006, and +0.63° for 2007.

The maximum air temperature has been about +40.0° and the minimum air temperature is about -35.0° for the last 5 years at the Nalaikh site (Fig. 5). The mean annual air temperature was +0.96° for 2003, +5.82° for 2004, +4.94° for 2005, and +5.41° for 2006.

The air temperature curves are similar for the Terelj sites excepting the mean annual air temperature. But the air temperature curves are significantly different between the Terelj and the Nalaikh sites. The winter air temperature of the Nalaikh site increased rapidly over the last 5 years. At the Nalaikh site over the last 5 years the mean annual air temperature was plus 4.3°, which is disequilibrium with present permafrost in the Nalaikh depression. Mean annual air temperature of the Terelj FA site is minus 2.6° and mean annual air temperature of the Terelj GL site was minus 0.7° for the last 5 years.

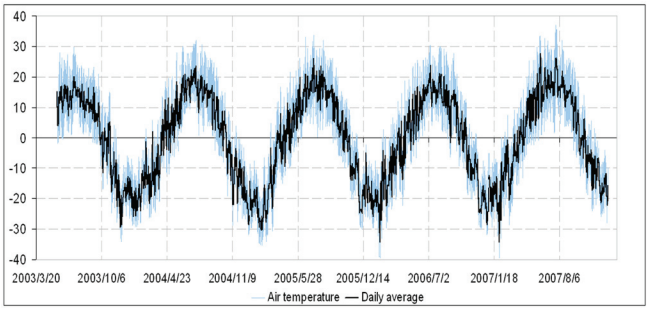


Figure 4. Air temperature at Terelj GL site.

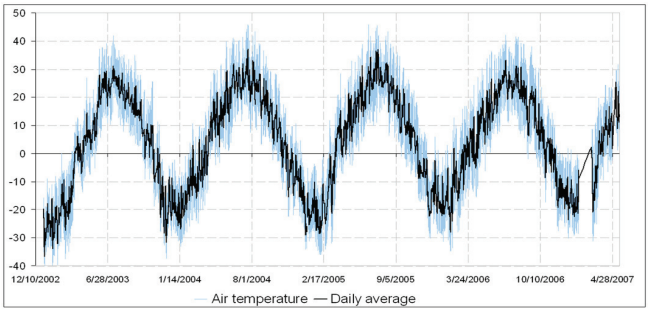


Figure 5. Air temperature at Nalaikh site.

*Near-surface temperature*

In wintertime the day-night temperature fluctuation is smoother than it is in summertime, because the temperature sensors are under the snow in wintertime (Figs. 6, 7, 8). Therefore, the winter near-surface temperature was higher than the winter air temperature. It means that snow cover has a warming effect at all three sites. So the minimum rate of the winter near-surface temperature was about -22°C at Terelj FA, about -19°C at Terelj GL, and about -26°C at Nalaikh.

In summertime day-night temperature fluctuation is higher than it is in wintertime especially at the Nalaikh site because of sparsely grassed area in Nalaikh. The maximum rate of the summer near-surface temperature was about +38°C at Terelj FA, about +35°C at Terelj GL, and about +60°C at Nalaikh.

*Temperature on bottom of seasonally freezing and thawing*

At the Terelj FA site the active layer thickness was about 3.8 m for 2004, 3.5 m for 2005, 3.25 m for 2006, and 3.55 m for 2007. The ground temperature ranged from -2.9°C to +0.1°C at a depth of 3.5 m between 2004 and 2007 (Fig. 9).

At the Terelj GL site the seasonal freezing depth was 3.90 m for 2004, 4.0 m for 2005, 4.2 m for 2006, and 3.85 m for 2007. The ground temperature ranged from -0.3°C to +4.9°C at a depth of 4.0 m between 2004 and 2007 (Fig. 10).

At the Nalaikh site the active layer thickness is more than 7.0 m. As shown on Figure 11, at the Nalaikh site the minimum rate of ground temperature was -0.3°C at a depth of 7.0 m between 2003 and 2007. The maximum rate of ground temperature was not possible to determine due to no data in the summertime.

As shown by Figures 9 and 11 above, the active layer thickness is different due to different topography, ground thermal condition, water content, ice content, and surface cover of the sites. The active layer thickness is about 3.5 m at the Terelj FA site. The Terelj FA site is characterized by north facing forested slope 10°–20°. Active layer thickness is about 7.5 m by borehole with a depth of 30.0 m at the Nalaikh site. The Nalaikh site is characterized by sparsely grassed plate area. As shown in Figure 10, the seasonal freezing depth is about 4.0 m at the Terelj GL site. Therefore the thicknesses of active layer and the seasonal freezing depths are different from place to place within a short distance in the mountain area.

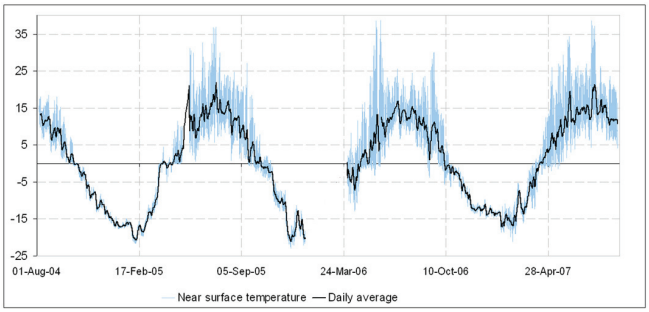


Figure 6. Near-surface temperature at Terelj FA.

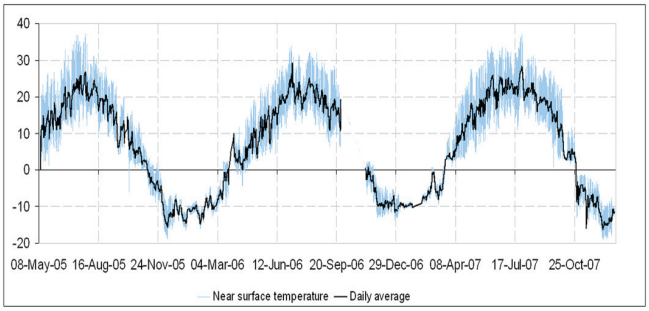


Figure 7. Near-surface temperature at Terelj GL.

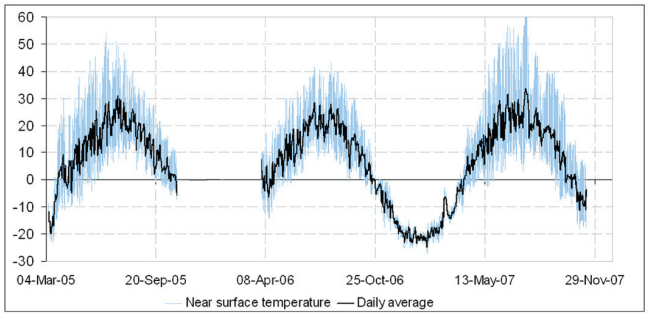


Figure 8. Near-surface temperature at the Nalaikh site.

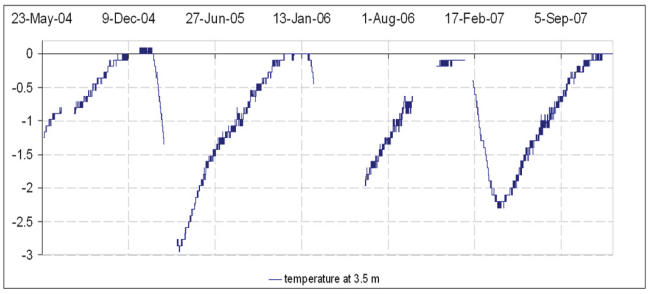


Figure 9. Ground temperature on a depth of 3.5 m at Terelj FA site.

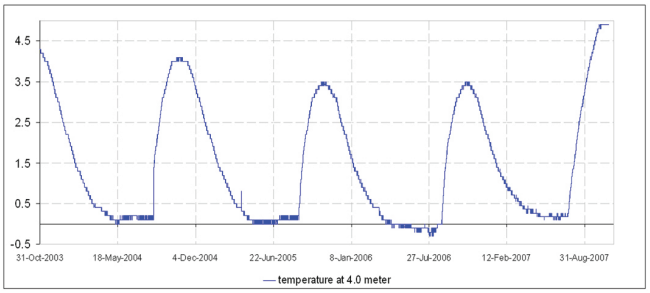


Figure 10. Ground temperature on depth of 4.0 meter at Terelj GL.

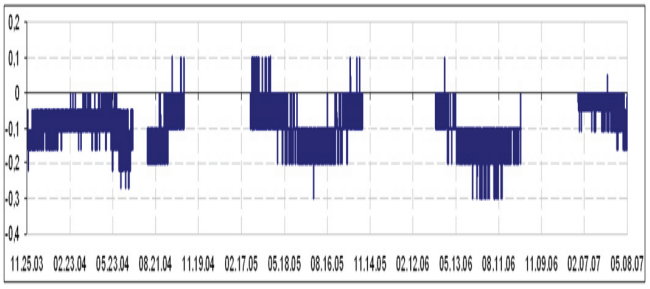


Figure 11. Ground temperature on a depth of 7.0 m at the Nalaikh site.

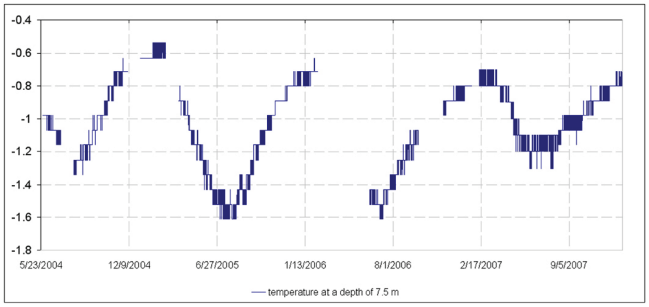


Figure 12. Temperature curve on a depth of 7.5 m from May 2004 to December 2007 at the Terelj FA site.

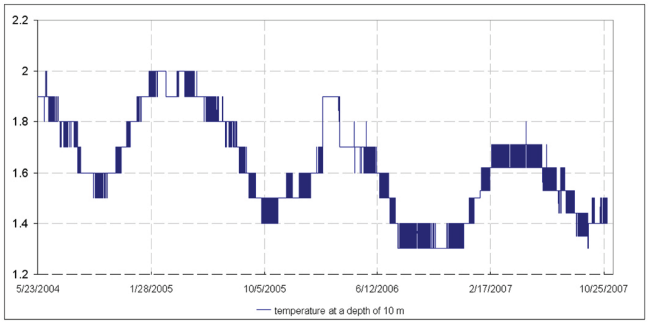


Figure 13. Temperature curve on a depth of 10.0 m from May 2004 to November 2007.

*Deep temperature curves at three sites*

Figure 12 shows the temperature curve on a depth of 7.5 m at the Terelj FA site. As shown in Figure 12, the depth of yearly temperature penetration is more than 7.5 m at the Terelj FA site. The maximum temperature was -0.55°C and the minimum temperature was -1.6°C between 2004 and 2007. The minimum temperatures were higher in 2004 and in 2007 than they were in 2005 and 2006. The maximum temperatures ranged from -0.55°C to -0.7°C.

Figure 13 shows the temperature curve on a depth of 10.0 m at the Terelj GL site. The depth of yearly temperature penetration is more than 10.0 m. The maximum temperature was +2°C in January of 2005. It had decreased between 2004 and 2007.

The minimum temperature was +1.3°C in September of 2006. It also had decreased between 2004 and 2007. Both temperatures (maximum and minimum) decreased from year to year between 2004 and 2007 because the snow thickness and the duration of snow cover became thicker and shorter in this period of time.

Figure 14 shows the temperature profile of the 30 m deep borehole at the Nalaikh site. The temperature below 5.0 m, is close to 0°. As shown in Figure 14, the active layer thickness was 7.5 m. By this temperature profile there are two layers of permafrost. The first layer is from 7.5 m to 11.4 m; the second layer is from 15.5 m down.

## Conclusion

- There are very high amplitudes of air and near-surface temperature at the three sites. Also there are very high day-night fluctuations of air and near-surface temperature. Day-night temperature fluctuation became low in wintertime at the surface, because the sensors lie under the snow cover.
- Near-surface temperature was a little higher than the air temperature in wintertime. So thin snow cover has a warming effect. The snow thickness was about 5–20 cm depending on the topography of the sites.
- The active layer thickness and the seasonal freezing depth are different due to topography, ground thermal conditions, surface cover, water, and ice content. There is a thick active layer at the Nalaikh site.
- Deep temperature is close to 0° at the Nalaikh site. The minimum temperature is -1.6°C on a depth of 7.5 m.
- There are two layers of permafrost at the Nalaikh site.

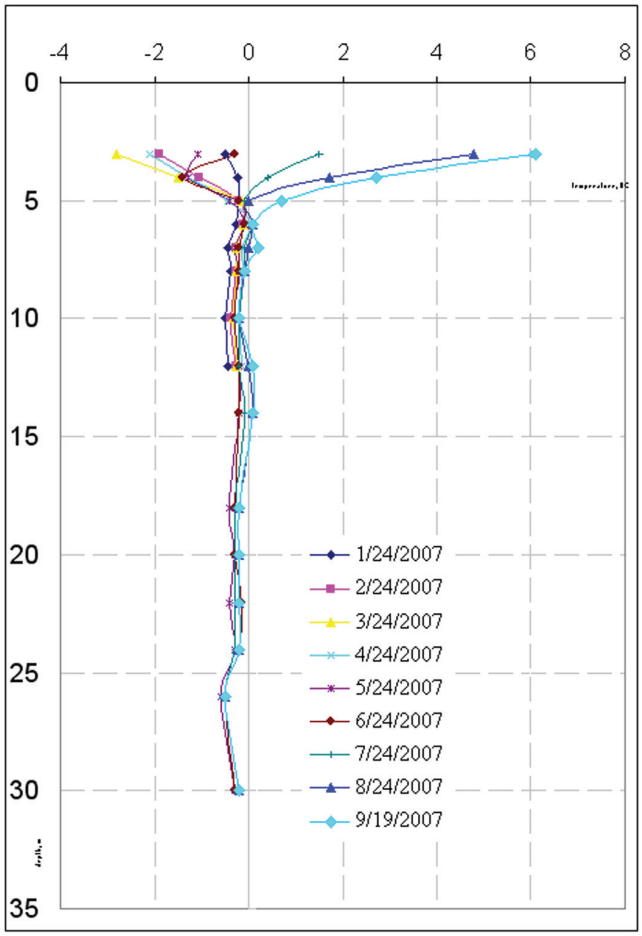


Figure 14. Temperature profile of 30.0 m deep borehole at Nalaikh.

## Acknowledgments

The author wishes to thank the Japan Agency for Marine-Earth Science and Technology and the Institute of Geography of the Mongolian Academy of Sciences who supported this research.

## References

Kudryavtsev, V.A. 1978. *General Geocryology.* Moscow: Moscow University Press, 462 pp.

Ishikawa, M., Sharkhuu, N. & Zang, Y. 2006. Ground thermal and moisture conditions at the southern boundary of discontinuous permafrost, Mongolia. *Permafrost and Periglacial Processes* (Number 2) Volume 16 (ISSN 1045-6740): 209-216.

Sharkhuu, N. 2001a. Permafrost mapping in Mongolia, *Extended abstracts of International Symposium on Mountain and Arid Land Permafrost, Ulaanbaatar, Mongolia, September 2-7, 2001*: 63-67.

Sharkhuu, N. 2001b. Geocryological monitoring in Mongolia, *Extended abstracts of International Symposium on Mountain and Arid Land Permafrost, Ulaanbaatar, Mongolia, September 2-7, 2001*: 63-67.

Sharkhuu, N., Battogtokh, D., Ishikawa, M., Kadota, T. & Zang, Y. 2004. Dynamics of active layer and spring icing at Terelj observation sites, Mongolia *Proceedings of the International Symposium on Terrestrial and Climate Change in Mongolia, Tokyo, Japan, November 9-10, 2004* 5: 29-30.

# Recent Changes in Hydrologic Response Observed in Permafrost Regions of Northwest Canada

J. Richard Janowicz
*Water Resources Section, Yukon Department of Environment, Whitehorse, Yukon Territory, Canada*

## Abstract

Air temperature trends have been observed to change over the last several decades in northern North America. Both summer and winter air temperatures have increased in most regions. An assessment was carried out to determine if corresponding trends of hydrologic response are apparent within permafrost regions of North America. Hydrograph characteristics were assessed using the Mann-Kendall trend test. The greatest changes to hydrologic response were observed with winter low flows. The greatest changes in winter streamflow appear to be occurring within the continuous permafrost zone, where flows from the majority of sampled streams have increased. Winter low flow trends in streams within the discontinuous permafrost zone generally exhibit positive trends, but are more variable. Winter streamflow trends within the sporadic permafrost zone are not consistent. Increasing winter streamflow trends have occurred from some mountainous regions of alpine permafrost. Other streams exhibit no discernable change, while some streams exhibit a negative change.

**Keywords:** continuous; discontinuous; Mann-Kendall; 7-day low flow; sporadic permafrost; trend analysis.

## Introduction

The primary control over hydrologic response in northern regions is permafrost distribution, permafrost thickness, and thickness of the active layer (Hinzman et al. 2005). Thick underlying permafrost and a thin active layer produce short pathways to the stream channel, with little or no interaction with subsurface processes. Ice-rich permafrost restricts rain or snowmelt infiltration to subsurface zones, resulting in surface storage in the form of ponds or wetlands. A thicker active layer enhances infiltration and associated groundwater recharge, which in turn would result in greater groundwater contributions to streamflow. Yukon hydrologic response follows this principle, and is closely tied to the underlying permafrost.

Changing climate appears to be resulting in a likewise change in the permafrost distribution of northern regions, including the Yukon Territory. Increasing air temperatures are resulting in permafrost warming and associated thawing, which in turn results in a thicker active layer. Permafrost degradation is expected to be greatest within the discontinuous and sporadic permafrost zones, since these permafrost classes are warmer; and therefore, more susceptible to thawing (Hinzman et al. 2005). Observations within the discontinuous permafrost regions of Alaska disclose the development of extensive areas of thermokrast terrain due to thawing permafrost (Osterkamp & Romanovsky 1999).

Yukon temperature and precipitation trends have been observed to change over the last several decades (Janowicz 2001). Winter and summer temperatures have increased in all regions, with greater winter temperature increases in northern Yukon, and greater summer increases in southwestern Yukon. Winter precipitation has increased slightly in all regions, while summer precipitation is more variable, decreasing in northern Yukon and increasing in southern Yukon. The greatest changes have occurred in western, mountainous regions where both summer and winter temperatures and winter precipitation have increased significantly. These observed trends are in the general order of projections developed by a Canadian Climate Centre global climate model (GCMII), which is based on a 100 percent increase of $CO_2$ in the atmosphere (Taylor 1997, Intergovernmental Panel on Climate Change 2001).

There have been a number of studies carried out in northern regions of North America on the impact of climate change on hydrologic response (Kite 1993, Burn 1994, Loukas & Quick 1996, 1999, Leith & Whitfield 1998, Whitfield & Taylor 1998, Spence 2002)). Whitfield & Cannon (2000) & Whitfield (2001) assessed climatic and hydrologic variations between two decades (1976–1985; 1986–1995) for stations in British Columbia and Yukon. Hydrologic response was generally found to be characterised by higher year round flows. Mountainous streams were found to have the timing of the freshet advanced, followed by lower summer and fall discharge. Zhang et al. (2001) and Yue et al. (2003) assessed the streamflow records for 243 Canadian hydrometric stations making up the Reference Hydrometric Basin Network, including some Yukon stations, over the period 1967 to 1996. While most of these stations were in southern Canada, they found winter low flows in northern British Columbia and Yukon to have increased significantly. Annual mean and peak flows were observed to have increased in glacerized basins of southern Yukon and northern British Columbia. Burn et al (2004), in the comparison of streamflow of the Liard and Athabasca Rivers in the mountainous, headwater regions of the Mackenzie River basin, found both streams to exhibit increases in winter discharge and some increase in the snowmelt freshet. Dery & Wood (2005) investigated the discharge of 64 arctic or subarctic Canadian rivers from 1964 to 2003. They found a general 10 percent decline in mean annual discharge to the Arctic and North Atlantic Oceans

over that period, which is consistent with a decline in annual precipitation in northern Canada over that period. The decline in streamflow was less pronounced in northwestern Canada, where the results were not statistically significant. Their work indicated there were links between annual discharge and Arctic Oscillation, El Nino/South Oscillation (ENSO), and the Pacific Decadal Oscillation (PDO) at interannual to decadal timescales.

There has been only limited work to date on the impact of climate change specific to Yukon hydrology. Janowicz & Ford (1994) used the CCC GCM temperature and precipitation projections, and a correlation approach to assess the impacts of climate change on the water supply to the upper Yukon River. Their analyses indicated that annual inflows to the glacierized upper Yukon River would increase by 39 percent, primarily in summer months, due to increasing temperature and precipitation. Janowicz (2001) carried out an analysis of streamflow to assess the response of the observed temperature and precipitation changes on peak flows, which normally occur as a result of spring snowmelt. The assessment revealed that there has been a dramatic change in mean annual flood (MAF) in some regions of Yukon over the last 20 years, with a progressive decrease in the parameter moving from south to north. The greatest increases in MAF were observed to occur within the sporadic permafrost zone, from predominantly glacierized systems in western Yukon. Smaller increases were noted in southeastern Yukon. These increases correspond to the observed increase in both summer temperatures and winter and summer precipitation. Peak flows from central and eastern Yukon, within the discontinuous permafrost zone, exhibit very little change. Within the continuous permafrost zone, peak flows were observed to decrease progressively moving northward to the Arctic coast.

This paper summarizes the results of a study carried out to assess apparent trends of annual minimum flows in Yukon and adjacent areas of northwestern Canada over the last few decades.

## Setting and Methodology

The analyses were carried out using data from the Yukon Territory and the western Northwest Territory west of the 125th parallel of longitude, an area covering approximately 920,000 km$^2$. This region consists of three permafrost zones: continuous, discontinuous, and sporadic (Fig. 1). Continuous permafrost areas have greater than 90% coverage; discontinuous areas have between 50 and 90% coverage; and sporadic areas have 10 to 50% coverage (Brown et al. 1997). The continuous, discontinuous, and sporadic zones represent 30, 45, and 25 percent of Yukon, respectively (Natural Resources Canada 1995). Hydrometric data from all active and recently discontinued (<5 years) Environment Canada, Water Survey of Canada (WSC), stations on unregulated streams, with at least 25 years of record were used in the analyses. The data were obtained from the WSC website. Because of numerous station discontinuations in the mid-1990s, only 21 stations were available for analyses. These were equally distributed between the three permafrost classes. The 7-day average minimum annual low flow, which normally occurs in late winter or early spring, was assessed in the present study. The 7-day average low flow parameter is a commonly used, minimum flow measure which reduces the variability over a single value.

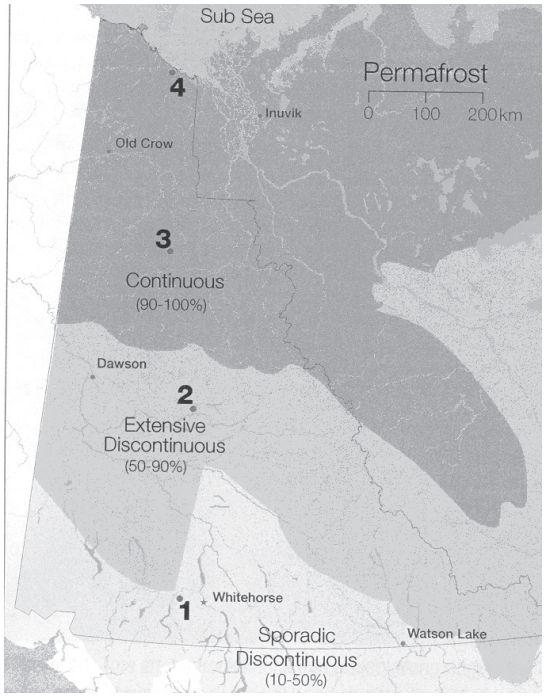


Figure 1. Study area and permafrost zones (from Smith et al. 2004).

*Trend analysis*

The Mann-Kendall trend test was used to assess trends in the 7-day minimum annual low flow parameter. The Mann-Kendall test is a non-parametric test used for the assessment of trends in time series. It is a simple, robust tool which can readily handle missing values. The calculated standard normal variate value (Z) is associated with a specific level of significance. The significance level provides an indication of the strength of the trend. A significance level of 0.001 indicates a very strong trend; 0.01 indicates a strong trend; 0.05 indicates a moderate trend; and 0.1 indicates a weak trend. A level of significance of less than 0.1 indicates there is no discernable trend.

## Results and Discussion

Table 1 provides a summary of the trend analyses. Positive trends in winter low flows are generally evident in all Yukon permafrost regions, with the occurrence of this trend inversely related to latitude. Winter baseflows are also generally related to drainage area. In cold regions, the relationship is more pronounced, with smaller drainages having less groundwater inputs to baseflow; therefore, smaller winter flows. While

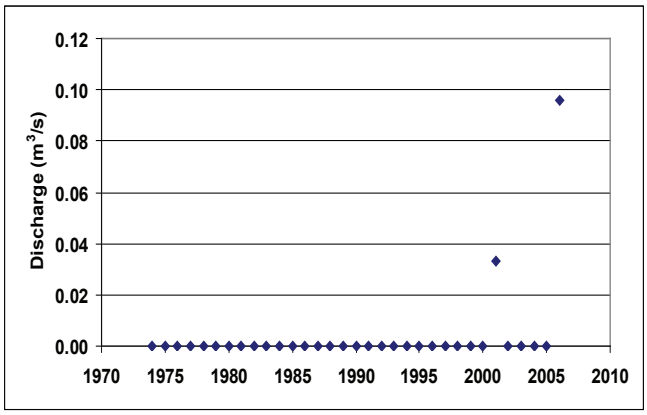


Figure 2. Seven-day average minimum low flow – Rengleng River at Dempster Highway.

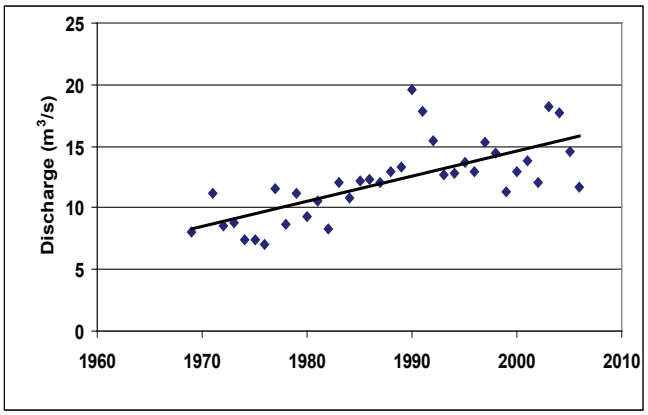


Figure 3. Seven-day average minimum low flow – Arctic Red River at Fort McPherson ($r^2$=0.49).

summer and winter precipitation have generally increased and decreased, respectively, in permafrost regions, annual precipitation has increased slightly, and there has been a corresponding slight observed increase in annual runoff in continuous and discontinuous permafrost regions. Both precipitation and annual discharge increases are slight, and cannot provide the basis for winter low flow increases. Summer and winter air temperatures have been observed to increase in most regions, and may attribute to the increase in winter low flows. Climate warming produces permafrost degradation, which enhances the interaction between surface and groundwater systems, allowing for greater groundwater contributions to baseflow.

The greatest positive trends in winter low flows appear to have occurred in the continuous permafrost zone, where streams with drainage areas in the order of 5,000 km$^2$, generally have streamflow throughout the winter. There is an exception for streams along the Arctic coast, where larger streams often experience "zero" winter flows. It is not possible to statistically validate trends from study streams which have had predominately "zero" winter flows in past decades. As with many statistical techniques, the Mann-Kendall test is not able to handle "zero" flows. Figure 2 provides an illustration of low flow trends for a small stream, the Rengleng River (station number 10LC003), with a drainage area of 1310 km$^2$. Winter low flows in past decades have been nonexistent, while measurable flow during recent winter periods has been observed. The winter flow regime for Caribou Creek (10ND002), with a drainage area of 68.3 km$^2$, has remained unchanged, with "zero" flows throughout the entire 29 year monitoring period.

Figure 3 provides an illustration of the positive winter low flow trend for the Arctic Red River (10LA002), with a drainage area of 18,600 km$^2$.

Trends of winter low flow regimes, with increasing flows, are generally exhibited by streams within the discontinuous permafrost zone. Four of the seven assessed streams have statistically significant positive winter low flow trends. Figure 4 illustrates the increasing trend for the Klondike River (09FA003). Even the smallest streams within the

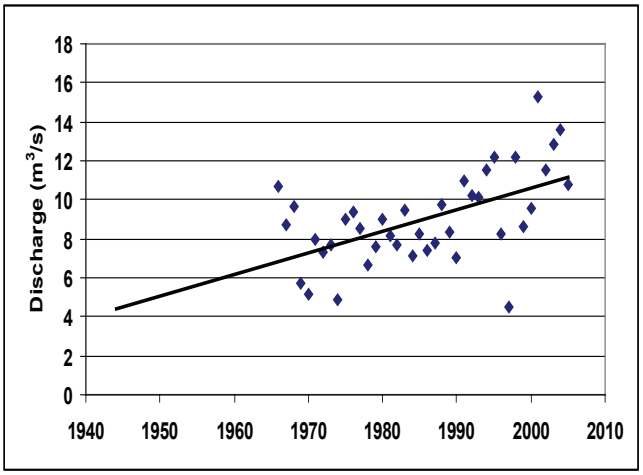


Figure 4. Seven-day average minimum low flow – Klondike River above Bonanza Creek ($r^2$=0.30).

discontinuous permafrost zone normally have winter flows, so drainage area is not as strong a factor in influencing winter streamflow, as in the continuous permafrost zone.

Trends of increasing winter low flows are not generally strong within the sporadic permafrost zone. Two of the seven represented streams have statistically significant positive trends. Both of these streams are transitional with the discontinuous permafrost zone, and one of these drains a mountainous region with significant alpine permafrost. Other streams exhibit no discernable change, while one stream exhibits a negative change.

## Conclusions

An assessment of streamflow response was carried out to determine if there are apparent trends in permafrost regions as a result of observed temperature changes. As permafrost properties change with climate warming, hydrologic response in northern regions would likewise presumably change. Degrading permafrost increases the thickness of the active layer, decreases the overall thickness of the permafrost and, in certain areas, eliminates the presence of

Table 1. Mann-Kendall trend statistics.

| Permafrost Class | Station Name | Drainage Area ($km^2$) | Record Period | n | Z Statistic | Significance Level |
|---|---|---|---|---|---|---|
| Continuous | Old Crow R nr Old Crow | 13900 | 1977-05 | 27 | 0.83 | > 0.1 |
| | Porcupine R nr Border | 59800 | 1962-05 | 40 | 1.81 | 0.1 |
| | Arctic Red R nr Mouth | 18600 | 1969-06 | 37 | 4.89 | 0.001 |
| | Rengleng R bl Hwy #8 | 1310 | 1973-05 | 32 | "0" | - |
| | Caribou Cr ab Hwy #8 | 625 | 1975-06 | 31 | "0" | - |
| | Peel R ab Ft McPherson | 70600 | 1975-06 | 31 | 3.65 | 0.001 |
| | Trail Valley Cr nr Inuvik | 68.3 | 1977-06 | 29 | "0" | - |
| Discontinuous | Ross R at Ross R | 7250 | 1961-05 | 44 | 1.42 | > 0.1 |
| | Pelly R at Pelly Crossing | 49000 | 1953-05 | 52 | 2.12 | 0.1 |
| | Pelly R bl Vangorda Cr | 22100 | 1973-05 | 33 | 2.43 | 0.1 |
| | Stewart R at Mouth | 51000 | 1964-05 | 42 | 1.23 | > 0.1 |
| | Klondike R ab Bonanza Cr | 7800 | 1966-05 | 40 | 3.44 | 0.001 |
| | Flat R nr Mouth | 8560 | 1961-06 | 39 | 0.94 | > 0.1 |
| | S Nahanni R ab Virginia | 14600 | 1964-06 | 42 | 2.3 | 0.1 |
| Sporadic | Dezadeash R at Haines Jnc | 8500 | 1953-05 | 53 | 2.95 | 0.01 |
| | Giltana Cr nr Mouth | 194 | 1981-05 | 25 | 0.82 | > 0.1 |
| | Alsek R ab Bates R | 16200 | 1975-05 | 31 | 0.29 | > 0.1 |
| | Wheaton R nr Carcross | 875 | 1958-05 | 44 | -0.67 | > 0.1 |
| | Takhini R nr Whitehorse | 6930 | 1949-05 | 56 | 1.49 | > 0.1 |
| | White R at Alaska Hwy | 6240 | 1975-05 | 30 | 2.43 | 0.05 |
| | Liard R at Upper Crossing | 33400 | 1961-05 | 45 | 0.73 | > 0.1 |

underlying permafrost entirely. These actions place a greater reliance on the interaction between surface and subsurface processes. Annual minimum flows were assessed, which were represented by the mean 7-day low flow. The Mann-Kendall test was used to statistically validate observed trends. Winter low flow trends have experienced significant apparent changes over the last three decades. The greatest changes in winter low flows appear to be occurring within the continuous permafrost zone, where flows from the majority of sampled streams have increased. Winter low flow trends in streams within the discontinuous permafrost zone generally exhibit positive significant trends, but are more variable. Winter streamflow trends within the sporadic permafrost zone are not consistent. Increasing winter streamflow trends have occurred from some mountainous regions of alpine permafrost. Other streams exhibit no discernable change, while one stream exhibits a negative change.

## Acknowledgment

The work carried out by Cam Malloch in performing much of the data extraction and manipulation is greatly appreciated.

## References

Brown, J., Ferrians, O.J., Heginbottom, J.A. & Melnikov. 1997. *Circum-Arctic map of permafrost and ground ice conditions.* 1:10,000,000. International Permafrost Association.

Burn, D.H. 1994. Hydrologic effects of climate change in west-central Canada. *Journal of Hydrology* 160: 53-70.

Burn, D.H., Cunderlik, J.M. & Pietroniro, A. 2004. Hydrological trends and variability in the Liard River basin. *Hydrological Sciences Journal* 49: 53-67.

Dery, S.J. & Wood, E.F. 2005. Decreasing river discharge in northern Canada. *Geophysical Research Letters* 32:L10401.

Hinzman, L.D., Bettez, N.D., Bolton, W. R., Chapin, F. S., Dyurgerov, M.B., Fastie, C. L., Griffith, B., Hollister, R.D., Hope, A., Huntington, H.P., Jensen, A.M., Jia, G.J., Jorgenson, T., Kane, D.L., Klein, D.R., Kofinas, G., Lynch, A.H., Lloyd, A.H., McGuire, A.D., Nelson, F.E., Nolan, M., Oechel, W.C., Osterkamp, T.E., Racine, C.H., Romanovsky, V.E., Stone, R.S., Stow, D.A., Sturm, M., Tweedie, C.E., Vourlitis, G.L., Walker, M.D., Walker, D.A., Webber, P.J., Welker, J., Winker, K.S. & Yoshikawa K. 2005. Evidence and implications of recent climate change in northern Alaska and other Arctic regions. *Climate Change* 72: 251-298.

Intergovernmental Panel on Climate Change 2001. In: J.T. Houghton et al. (eds.), *Climate change 2001: The Scientific Basis.* Cambridge University Press, 881 pp.

Janowicz, J.R. & Ford, G. 1994. Impact of climate change on water supply in the upper Yukon River. *Proceedings of the 62nd Annual Western Snow Conference, Sante Fe, New Mexico, April 18–21, 1994*.

Janowicz, J.R. 2001. Impact of recent climatic variability on peak streamflow in northwestern Canada with implications for the design of the proposed Alaska Highway gas pipeline. *Proceedings of the 13th Northern Research Basins International Symposium & Workshop, Saariselka, Finland and Murmansk, Russia, August 19–24, 2001*: 161-169.

Kite, G.W. 1993. Application of a land class hydrological model to climate change. *Water Resources Research* 29(7): 2377-2384.

Leith, R.M. & Whitfield, P.H. 1998. Evidence of climate change effects on the hydrology of streams in south-central B.C. *Canadian Water Resources Journal* 23: 219-230.

Loukas, A. & Quick, M.C. 1996. Effect of climate change on hydrologic regime of two climatically different watersheds. *Journal of Hydrological Engineering* 1(2): 77-87.

Loukas, A. & Quick, M.C. 1999. The effect of climate change on floods in British Columbia. *Nordic Hydrology* 30: 231-256.

Natural Resources Canada. 1995. *National Atlas of Canada*. 5th Ed., MCR 4177. Geological Survey of Canada, Terrain Sciences Division, Ottawa.

Romanovsky, V.E. & Osterkamp, T.E. 1999. Evidence for warming and thawing of discontinuous permafrost in Alaska. *Permafrost and Periglacial Processes* 10: 17-37.

Smith, C.A.S., Meikle, J.C. & Roots, C.F. 2004. *Ecoregions of the Yukon Territory – biophysical properties of Yukon landscapes*. Agriculture and Agri-food Canada, PARC Technical Bulletin 04-01, Summerland, British Columbia, 313 pp.

Spence, C. 2002. Streamflow variability (1965–1998) in five Northwest Territories and Nunavut rivers. *Canadian Water Resources Journal* 27: 135-155.

Taylor, B. 1997. Climate change scenarios for British Columbia and Yukon. In: E. Taylor & B. Taylor (eds.), *Responding to global climate change in British Columbia and Yukon, Canada Country Study: Climate Impacts and Adaptation,* Vol. 1. Environment Canada.

Whitfield, P.H. 2001. Linked hydrologic and climate variations in British Columbia and Yukon. *Environmental Monitoring and Assessment* 67: 217-238.

Whitfield, P.H. & Cannon, A.J. 2000. Recent climate moderated shifts in Yukon hydrology. In: D.L. Kane (ed.), *Proceedings AWRA Conference Water Resources in Extreme Environments, Anchorage, Alaska, May 1–3, 2000.*

Whitfield, P.H. & Taylor, E. 1998. Apparent recent changes in hydrology and climate of coastal British Columbia. In: Y. Alila (ed.), *Mountains to Sea: Human Interaction with the Hydrologic Cycle. Proceedings of the 51st Annual Canadian Water Resource Conference*: 22-29.

Yue, S., Pilon, P. & Phinney, B. 2003. Canadian streamflow trend detection: impacts of serial and cross-correlation. *Hydrological Sciences* 48: 51-63.

Zang, X., Harvey, K.D., Hogg, W.D. & Yuzyk, T.R. 2001. Trends in Canadian streamflow. *Water Resources Research* 37: 987-998.

# Factors Contributing to the Long-Term Integrity of Drilling-Mud Sump Caps in Permafrost Terrain, Mackenzie Delta Region, Northwest Territories, Canada

R.E.L. Jenkins
*Water Resources Division, Indian and Northern Affairs Canada, Yellowknife, NT, Canada*
J.C.N. Kanigan
*Department of Geography and Environmental Studies, Carleton University, Ottawa, ON, Canada*
S.V. Kokelj
*Water Resources Division, Indian and Northern Affairs Canada, Yellowknife, NT, Canada*

## Abstract

In this study, we examine the operational and environmental factors associated with the cap performance of 110 drilling-mud sumps constructed between 1965 and 2005 in the Mackenzie Delta region, Northwest Territories. Thawing of ice-rich cover materials can cause cap subsidence and surface ponding, and may increase the potential for migration of sump contents. To control for the effects of degradation over time, we examined data for the 77 sumps constructed between 1968 and 1977. Significant ponding (>20% of cap area) characterized 65% of the sumps in warm permafrost (>-3.9°C) and alluvial terrain. The largest proportion of sumps with good cap integrity were in cold permafrost (<-7.0°C) on tundra uplands. Many sumps that were operated in summer maintained good cap integrity, and were situated in cold permafrost, further highlighting the importance of site environmental conditions. Variable long-term cap performance suggests that a long-term approach to managing sumps in permafrost terrain is necessary.

**Keywords:** cap integrity; drilling-mud sumps; Mackenzie Delta region; permafrost.

## Introduction

Drilling wastes produced during land-based hydrocarbon exploration in the Canadian arctic and subarctic have been disposed of to in-ground sumps (French 1978a, b) in accordance with Federal legislation. Sumps are excavated into permafrost and are generally situated adjacent to the wellhead. Following the completion of the drilling program, the drilling fluids, cuttings and rig wash are deposited to the sump which is then backfilled to form a cap (Fig. 1). The design intent is to confine the active layer within the cover materials and maintain the saline drilling wastes in the underlying permafrost (French 1980, Dyke 2001).

Operational and environmental factors combine to influence sump performance (French 1985). For example, sumps constructed in cold permafrost are more likely to maintain saline drilling fluids in a frozen state even if climate or vegetation conditions change with time. The potential for sump collapse is enhanced where permafrost is ice-rich because thawing of cover materials or adjacent terrain can lead to surface subsidence and ponding. Accumulation of surface water on or around the sump cap may lead to thermal instability promoting additional subsidence. The capping of unfrozen materials can cause fluids to be squeezed out of the sump. Under contemporary practices, the fluids deposited to the sump in winter are assumed to freeze in situ and the wastes are capped prior to warming air temperatures in spring (Fig. 1). Terrain disturbance adjacent to sumps can lead to surface subsidence and ponding around the cap, but impacts can be minimized by operating on a protective ice pad.

Since 1965, about 150 drilling-mud sumps have been constructed in the Mackenzie Delta region. Sump cap collapse and ponding suggests that permafrost, the primary containment medium, has partially degraded and that the drilling wastes are no longer encapsulated by permafrost (Fig. 2) (Kokelj & GeoNorth 2002).

In this paper we summarize information on the construction practices, environmental conditions and cap integrity for 110 drilling-mud sumps constructed over the past 40 years in the Mackenzie Delta region. Our primary objectives are: 1) To provide a summary of sump cap performance; and 2) to examine the influence of construction practices and environmental conditions on long-term sump cap integrity. This investigation is timely because the proposed Mackenzie Gas Pipeline has stimulated renewed hydrocarbon exploration in the region and sumps remain a waste disposal option in the north.

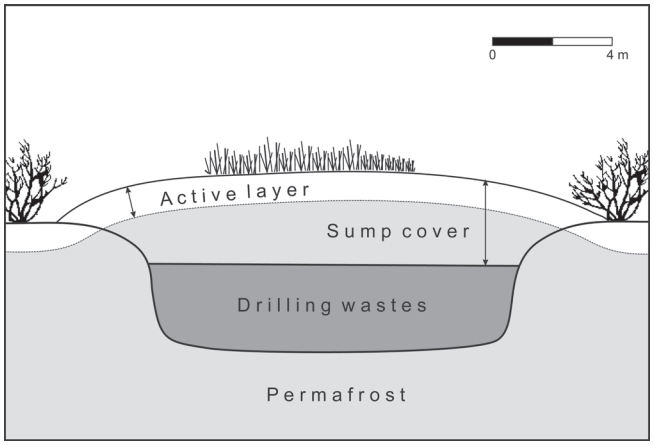


Figure 1. Generalized cross-section of a northern drilling-mud sump.

Figure 2. Drilling-mud sump in the outer Mackenzie Delta. The sump cap has collapsed causing a large pond to form. The arrow indicates submerged willows in the pond. Willows on sump cap in background are approximately 2 m in height.

## Study Area

The drilling-mud sumps we examined are located in the Mackenzie Delta and the adjacent uplands in a diverse range of terrain, permafrost and ecological conditions (Fig. 3). Mean annual air temperatures at Inuvik and Tuktoyaktuk are -8.8°C and -10.2°C, respectively (Environment Canada 2007). Mean annual ground temperatures range from -9°C in upland terrain near the Beaufort Sea coast to above 0°C in point bar willow communities of the Delta (Mackay 1974, Smith 1975).

Most of the drilling-mud sumps in alluvial terrain of the Mackenzie Delta are subject to periodic flooding in spring and those in the low-lying northern delta may also be inundated by storm surges in summer (Fig. 3) (Burn 2002). North of treeline, low shrubs grow along point bars, and sedge wetlands occupy the delta plain. Thermal disturbance associated with the numerous lakes and channels, early removal of snow due to spring flooding, and the growth of tall shrubs and associated deep snow on point bars can account for warmer ground temperatures in the Delta than in the adjacent tundra uplands (Mackay 1974, Smith 1975). Ground temperatures at undisturbed sites in the outer delta range from -2 to -3°C (Mackay 1974). Southward the elevated delta plain is vegetated by spruce forests underlain by permafrost between about -2°C and -4°C (Mackay 1974, Kanigan et al. 2008). In the delta, wedge ice and near-surface aggradational ice is associated with spruce forests and sedge wetlands (Kokelj & Burn 2005, Kokelj et al 2007a).

The uplands east of the Mackenzie Delta, including the Tuktoyaktuk Coastlands, are characterized by low arctic shrub tundra (Ritchie 1984). Mean annual ground temperatures are lower than in the delta due to the absence of flooding and thinner snow cover. Ground temperatures decrease northwards with vegetation height and snow cover, so that permafrost on the Tuktoyaktuk Coastlands and on northern Richards Island may be below -8°C (Mackay 1974). The terrain is hummocky and the fine-grained materials are frost susceptible (Kokelj et al. 2007b). Upland sediments

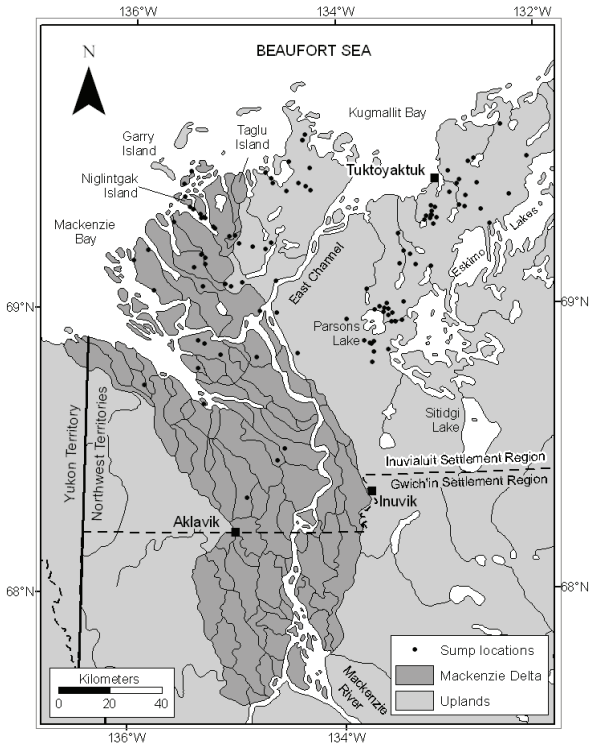


Figure 3. Mackenzie Delta region and drilling-mud sumps examined in this study.

of morainal, glaciofluvial or lacustrine origin contain large volumes of ground ice including massive ice, wedge ice, and near-surface aggradational ice (Mackay 1963, Rampton 1988).

## Methods

We examined operational and environmental data for 110 sumps in the Mackenzie Delta region (Fig. 3). Information on the drilling-mud sumps was extracted from an Indian and Northern Affairs Canada (INAC) compilation of sump data and an inventory of sumps in the Inuvialuit Settlement Region (ISR) funded by the Environmental Studies Research Fund (ESRF) and industry (AMEC Earth and Environmental 2005, Komex International & IEG Environmental 2005). The inventory and field methodologies were developed by an ESRF Technical Advisory Group which included government, Inuvialuit and industry representatives. National Energy Board information on site locations and operating dates was used. The sump information collected via these initiatives is publicly available at (http://nwt-tno.inac-ainc.gc.ca/wrd_e.htm).

Permafrost has been utilized as a primary containment medium in northern drilling-mud sumps (French 1980, Dyke 2001). Sump cap collapse and cap ponding strongly suggest that the underlying permafrost is degrading and that the original design intent is not being achieved. Conversely, a sump cap with no ponding suggests frozen ground has been maintained within and around the sump. Field and aerial photograph based estimates of ponding within the sump

perimeter was grouped into the three categories of 0% to 5% ponding, 6% to 20% ponding and greater than 20% ponding. We suggest that these categories reflected good, moderate and poor cap integrity, respectively.

The timing of sump closure is of interest because the potential for terrain disturbance is greater during the thaw season and air temperatures at the time of capping influence the thermal state of sump contents. Sump construction and closure dates were not recorded but through consultation with industry and regulators it was determined that commencement and completion dates of drilling provide reasonable estimates for the duration that a sump remained open and the subsequent timing of sump closure. In this study, the "summer operating season" was defined as those months in which the Inuvik monthly climate normals from 1971 to 2000 were above 0°C, which includes May 1 to September 30 (Environment Canada 2007). Sumps were grouped by year of construction into those constructed prior to 1980 (1965-1979), those constructed in the 1980s and recently constructed sumps (1990–2005). The intervals are uneven so the few sumps constructed in the 1960s (5) and 2000s (5) could be grouped into adjacent time intervals.

Mean annual permafrost temperatures may be associated with sump performance since areas of cold permafrost are more likely to maintain sump contents in a frozen state and areas with warm permafrost are more susceptible to thawing after disturbance (Smith & Burgess 2004). Sumps were grouped into three ground temperature classes (-1.0 to -3.9°C, -4.0 to -6.9°C, -7.0 to -9.9°C) based on a generalized map of mean annual ground temperatures (Mackay 1974). Historical ground temperature measurements were also obtained from wellheads adjacent to 14 of the sump sites (Taylor et al. 1998).

Associations between sump-cap ponding and environmental and operational variables were determined using an $X^2$ test of independence:

$$X^2 = \sum (O - E)^2 / E \quad (1)$$

where *O* is the observed frequency in the sample, and *E* is the expected frequency in the population (Sokal & Rohlf 1995). A test statistic that is larger than the critical value reflects significant differences between the observed and expected frequencies**,** indicating that there is an association between the two variables.

## Results

Table 1a shows that about half of the sumps had minor ponding, while the other half were characterized by moderate to significant ponding. The majority of sumps were constructed and capped between 1965 and 1979 (Table 1b), and the time period for which a sump is open has decreased over the past four decades (Table 1b). All sumps constructed since 1980 were capped within four months of excavation. Only 20% of all sumps were capped in summer and there have been no summer operations since 1986.

Table 1a. Degree of sump-cap ponding.

| Percent sump- cap ponding | Minor (0-5%) | Moderate (6-20%) | Significant (20%) |
|---|---|---|---|
| Percent of total sumps | 48 (n=53) | 21 (n=23) | 31 (n=34) |

Table 1b. Sump construction practices.

| Year of construction | Percent of total sumps | Sump open >5 mos. (%) | Sump capped in summer (%) |
|---|---|---|---|
| 1965-79 | 73 (n=80) | 25 | 25 |
| 1980-89 | 20 (n=22) | 0 | 10 |
| 1990-2005 | 7 (n=8) | 0 | 0 |

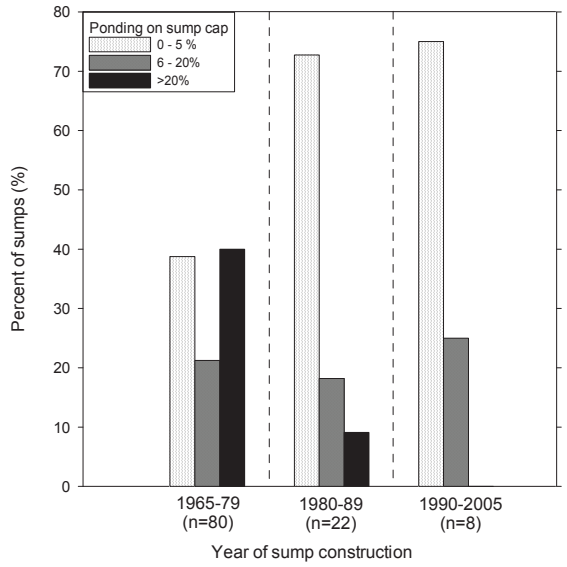


Figure 4. Percentage of sumps affected by minor, moderate and major ponding by period of sump operation. Note that time intervals are uneven.

Sumps constructed since 1990 are characterized by generally good cap integrity in contrast to sumps capped before 1980, most of which have moderate to significant ponding (Fig. 4). There is a statistical association between sump age and cap ponding at the 0.05 level of significance ($X^2_{(4,110)} = 13.569$; $p = 0.009$). The good cap conditions of recently constructed sumps may reflect improvements in site selection, construction and closure practices, but may indicate that sump covers degrade with time (Fig. 2).

To investigate the effects of environmental conditions and operating practices on long-term sump integrity and to control for the influence of sump age we reduced the study scope to 77 drilling-mud sumps constructed between 1968 and 1977. Figure 5 shows that the magnitude of cap ponding decreases with ground temperatures. Over 60% of the sumps in warm permafrost (-1.0°C to -3.9°C), coincident with alluvial terrain, were characterized by significant ponding.

Only 30% of the sumps underlain by cold permafrost in upland terrain have significant ponding, and more than half were well intact (Fig. 5). Sump-cap ponding and mean annual ground temperature are associated at the 0.10 level of significance ($X^2_{(4,77)} = 8.302$; $p = 0.08$).

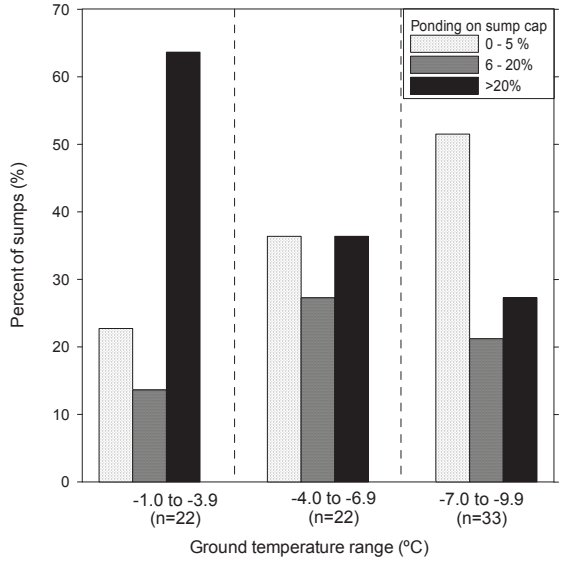


Figure 5. Percentage of sumps affected by minor, moderate and major ponding by mean annual ground temperature class for sumps constructed between 1968 and 1977.

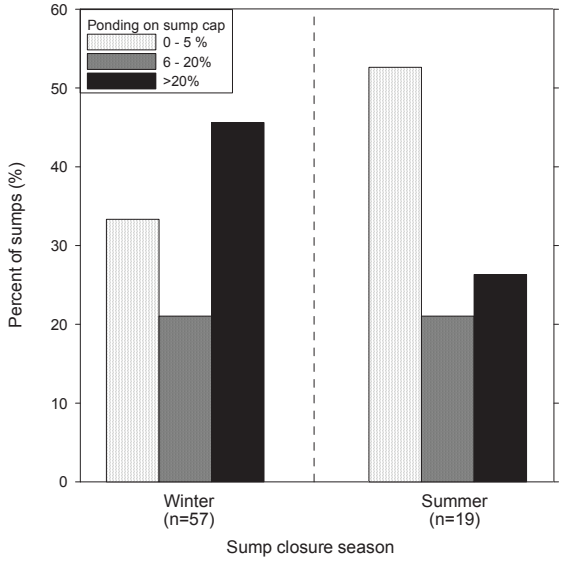


Figure 6. Percentage of sumps affected by minor moderate and major ponding by season of sump closure for sumps constructed between 1968 and 1977.

The sumps constructed from 1968 to 1977 were dichotomized on the basis of the season in which they were closed (summer or winter) (Fig. 6). About 50% of the sumps capped in summer showed minor cap ponding and only 25% were characterized by significant ponding. In contrast, almost half of the sumps capped in winter have significant ponding. Sump-cap ponding is statistically independent of the timing of sump closure ($X^2_{(2,76)} = 2.692$; $p = 0.26$) at the 0.05 level of significance, indicating that the two factors are not associated.

## Discussion

Most of the 110 drilling-mud sumps we examined in Mackenzie Delta region were constructed and capped in the 1970s (Table 1). About 40% of these sumps have ponding on or around the sump cap that exceeds 20% of the cap dimensions (Fig. 4). Cap collapse and ponding indicate that the drilling wastes are no longer completely encapsulated by frozen ground and that the primary waste containment medium has been compromised.

The strong association between cap ponding and sump age can partially be explained by improvements to construction and closure practices since the 1970s. These improvements include: a) a reduction in the amount of fluids utilized during drilling and deposited to the sump; b) more efficient drilling operations and reduction to the length of time a sump is open; c) avoidance of summer operations; and d) minimizing disturbance to terrain adjacent to the sump by operating on a protective ice pad. Irrespective of improved practices, there is evidence that sumps deteriorate with time. Submerged willows in many of the sump ponds suggest that collapse occurred subsequent to cap revegetation, possibly after decades of cap stability (Fig. 2). Sumps covers that are presently intact have the potential to subside if permafrost were to thaw as the result of shrub growth and increased snow accumulation, or due to climate warming (Kokelj & GeoNorth 2002).

Cap subsidence and significant ponding was most common on sumps in warm permafrost of the alluvial delta, whereas the zone of coldest permafrost on northern Richards Island and the Tuktoyaktuk Coastlands had the lowest proportion of sumps with significant ponding, and the highest proportion of intact sump caps (Fig. 5). It appears that potential impacts of high ice content permafrost on sump cap integrity in the northern part of the study region was offset by thermal stability associated with cold permafrost (Mackay 1970, Rampton 1988).

The difficulty of maintaining good sump-cap integrity in a warm permafrost environment is indicated by Figure 5 and corroborated by the poor cap conditions observed at many historical drilling-mud sumps in the central Mackenzie Valley where mean annual ground temperatures are above -3°C (C. Baetz - INAC, pers. com.). In our study area, the warmest permafrost coincides with alluvial terrain of the Mackenzie Delta which is also characterized by naturally poor drainage, probably strengthening the observed association between significant cap ponding and warm permafrost.

No significant association was found between the timing of sump closure and sump-cap ponding (Fig. 6). This result was surprising because various complications have been documented in association with summer operations (French 1980, 1985), including a) thawing and loss of frozen backfill; b) degradation of ice-rich permafrost in exposed sump sidewalls; and c) squeezing and seepage of unfrozen fluids up and out of the sump at the time of capping. Closer inspection of the data reveals that most of the summer sumps were located in cold upland terrain. Only four were located in warm permafrost and alluvial terrain and three of these were

characterized by significant ponding (Fig. 2). Furthermore, some of the summer sumps may have been contoured or recapped in the years immediately following abandonment. The relatively good condition of several summer constructed sumps in cold permafrost highlights the importance of good site selection.

Regardless of site conditions or construction practices there is a strong association between cap ponding and sump age which suggests that sump conditions can deteriorate over time (Fig. 2). Almost 30% of the sumps constructed during winter in cold permafrost between 1965 and 2005 presently have more than 20% of the cover occupied by ponded water. Many sumps constructed under ideal site and operating conditions have degraded, so it is apparent that other factors may lead to the thawing of a sump over time. For example, well-drained exposed mineral soils that characterize the sump cover favour the growth of tall shrubs which trap snow redistributed by winds (Johnstone & Kokelj 2008). Colonization by tall shrubs can transform a cold snow-free cap surface into one with annual snow accumulation of over 1m thickness causing ground warming and possible thawing of sump contents (Johnstone & Kokelj 2008). Natural sites in the study region characterized by mineral soils and deep snow are often associated with a talik (Gill 1972). It is also possible that rising air temperatures and associated ground warming in the western Arctic has contributed to the degradation of sumps (Osterkamp & Romanovsky 1999, Smith et al. 2005).

Decadal scale sump cap performance in the Mackenzie Delta region strongly suggests that if long-term freezing of drilling wastes in permafrost remains an intended waste disposal option, warm permafrost and alluvial terrain must be avoided. Factors that influence the thermal evolution of drilling-mud sumps such as vegetation succession and climate change cannot be directly controlled by best practices, so the necessity for long-term observation and management of sumps in permafrost terrain should be anticipated. Furthermore, the environmental consequences of sump cap collapse should be better understood so that sump cap degradation can be appropriately managed.

## Conclusions

Based on our results and discussion we make the following conclusions:

1. Recent sumps are characterized by good cap integrity, but 40% of sumps constructed prior to 1980 have more than 20% ponding on their surface. The data suggest an improvement of operating and abandonment practices; however this trend may actually reflect the gradual degradation of sump covers over time.

2. For the 77 sumps constructed during the period from 1968 to 1977, poor cap integrity was most prevalent in poorly-drained, alluvial terrain where permafrost temperatures were above -4°C. Sump cap conditions were best at upland sites in cold (<-7.0°C) permafrost. If the objective of a sump is to encapsulate wastes in permafrost, construction in warm permafrost and alluvial environments should be avoided.

3. The season in which a sump was capped was not associated with sump-cap ponding and cap integrity. This is probably because site environmental conditions subsumed the effect of capping season.

4. About one third of the sumps constructed during winter operations in cold permafrost are characterized by significant cap ponding. Factors such as cap revegetation and climate warming may impact long-term sump-cap integrity indicating that a long-term management approach to drilling-mud sumps constructed in permafrost is necessary.

## Acknowledgments

This work was supported by the Aurora Research Institute; Natural Sciences and Engineering Research Council of Canada, Northern Chairs program (C.R. Burn, Carleton University) and the Northern Internship Program; and the Water Resources Division, Indian and Northern Affairs Canada. Data used in these analyses were compiled through an Environmental Studies Research Fund initiative with participation from Indian and Northern Affairs Canada, the Inuvialuit Joint Secretariat, and Industry.

## References

AMEC Earth and Environmental. 2005. Inuvialuit Settlement Region drilling waste disposal sumps study. Submitted to Government of Canada, *Environmental Studies Research Fund, ESRF* 04-046, 54 pp.

Burn, C.R. 2002. Mackenzie Delta. In: S. Black & A. Fehr (eds.) *Natural History of the Western Arctic, Part 1: Land and Water*. Inuvik, Northwest Territories: Western Arctic Handbook Committee, 24-29.

Dyke, L.D. 2001. Contaminant migration through the permafrost active layer, Mackenzie Delta area, Northwest Territories, Canada. *Polar Record* 37 (202): 215-228.

Environment Canada. 2007. *Canada Climate Data* [online], Ottawa. Available from: http://climate.weatheroffice.ec.gc.ca/climateData/canada_e.html [cited 01 August 2007].

French, H.M. 1978a. Terrain and environmental problems of Canadian arctic oil and gas exploration. *Musk-ox* 21: 11-17.

French, H.M. 1978b. *Sump Studies: 1, Terrain Disturbances. Environmental Studies No. 6.* Ottawa: Department of Indian Affairs and Northern Development, 52 pp.

French, H.M. 1980. Terrain, land-use and waste drilling fluid disposal problems, Arctic Canada. *Arctic* 33: 794-806.

French, H.M. 1985. Surface disposal of waste drilling fluids, Ellef Ringnes Island, NWT: short term observations. *Arctic* 38(4): 292-302.

Gill, D. 1972. The point bar environment in the Mackenzie River delta. *Canadian Journal of Earth Sciences* 9: 1382-1393.

Johnston, J. & Kokelj, S.V. 2008. Environmental conditions and vegetation recovery at abandoned drilling-mud sumps in the Mackenzie Delta region, NWT, Canada. *Arctic* (In press).

Kanigan, J.C.N., Burn, C.R. & Kokelj, S.V. 2008. Permafrost response to climate warming south of treeline, Mackenzie Delta, Northwest Territories, Canada (*this proceedings*).

Kokelj, S.V. & Burn, C.R. 2005. Near-surface ground ice in sediments of the Mackenzie Delta, Northwest Territories, Canada. *Permafrost and Periglacial Processes* 16: 291-303.

Kokelj, S.V., Burn, C.R. & Tarnocai, C. 2007b. The structure and dynamics of earth hummocks in the subarctic forest near Inuvik, Northwest Territories, Canada. *Arctic, Antarctic, and Alpine Research* 39(1): 99-109.

Kokelj, S.V. & GeoNorth Limited. 2002. *Drilling Mud Sumps in the Mackenzie Delta Region: Construction, Abandonment and Past Performance.* Submitted to Water Resources Division, Indian and Northern Affairs Canada, Yellowknife, Northwest Territories, 55 pp.

Kokelj, S.V., Pisaric, M.F.J. & Burn, C.R. 2007a. Cessation of ice-wedge development during the 20th century in spruce forests of the Mackenzie Delta, Northwest Territories, Canada. *Canadian Journal of Earth Sciences* 44: 1503-1515.

Komex International & IEG Environmental. 2005. *Inventory of Drilling Waste Disposal Sumps*. Submitted to Imperial Oil Resources, Conoco-Phillips, Shell and BP, 6 volumes.

Mackay, J.R. 1963. The Mackenzie Delta area, Northwest Territories, Geographical Branch, Memoir 8. Department of Mines and Technical Surveys, Ottawa.

Mackay, J.R. 1970. Disturbances to the tundra and forest tundra environment of the western Arctic. *Canadian Geotechnical Journal* 7 (4): 420-432.

Mackay, J.R. 1974. *Seismic Shot holes and Ground Temperatures, Mackenzie Delta Area, Northwest Territories.* In Geological Survey of Canada Paper 74-1, Part A, Report of Activities, April to October 1973. Ottawa: Geological Survey of Canada, Department of Energy, Mines and Resources, 389-390.

Osterkamp, T.E., & Romanovsky, V.E. 1999. Evidence for warming and thawing of discontinuous permafrost in Alaska. *Permafrost and Periglacial Processes* 10: 17-37.

Rampton, V.N. 1988. *Quaternary Geology of the Tuktoyaktuk Coastlands, Northwest Territories, Memoir 423.* Ottawa: Geological Survey of Canada, Department of Energy Mines and Resources Canada.

Ritchie, J.C. 1984. *Past and Present Vegetation of the Far Northwest of Canada*. Toronto: University of Toronto Press, 251 pp.

Smith, M.W. 1975. Microclimate influences on ground temperatures and permafrost distribution, Mackenzie Delta, Northwest Territories. *Canadian Journal of Earth Sciences* 12: 1421-1438.

Smith, S. & Burgess, M. 2004. *Bulletin 579: Sensitivity of Permafrost to Climate Warming in Canada*. Ottawa: Geological Survey of Canada, Natural Resources Canada.

Smith, S.L., Burgess, M.M, Riseborough, D. & Nixon, F.M. 2005. Recent trends from Canadian permafrost thermal monitoring network sites. *Permafrost and Periglacial Processes* 16: 19-30.

Sokal, R.R. & Rohlf, F.J. 1995. *Biometry*, 3rd ed. New York: W.H. Freeman and Co., 887 pp.

Taylor, A., Burgess, M.M., Allen, V. & Wilkinson, A. 1998. *Canadian Geothermal Data Collection: Deep Permafrost Temperatures and Thickness of Permafrost* [online]. Boulder, CO: National Snow and Ice Data Center/World Data Center for Glaciology. Available from: http://nsidc.org/data/docs/fgdc/ggd503_boreholes_ncanada/data.html [cited 01 August 2007].

# Studies on the Cooling Effect of Diatomite in the Protection of Permafrost Embankment

Chen Ji
*State Key Laboratory of Frozen Soil Engineering, Cold and Arid Regions Environment and Engineering Institute, Chinese Academy of Sciences, Lanzhou, China 730000*

Sheng Yu
*State Key Laboratory of Frozen Soil Engineering, Cold and Arid Regions Environment and Engineering Institute, Chinese Academy of Sciences, Lanzhou, China 730000*

Qihao Yu
*State Key Laboratory of Frozen Soil Engineering, Cold and Arid Regions Environment and Engineering Institute, Chinese Academy of Sciences, Lanzhou, China 730000*

Anhua Xu
*Institute for Highway Survey-Design and Research of Qinghai, Xi'ning, China 810000*

Huang Bo
*Institute for Highway Survey-Design and Research of Qinghai, Xi'ning, China 810000*

## Abstract

Preservation of permafrost is one of the principles adopted in permafrost geotechnical engineering. Using a thermal semiconductor can help toward this purpose. The thermal semiconductivity property of water near 0°, diatomite is used for making a kind of thermal semiconductor after it absorbs water. Experiments on the thermal conductivity difference between frozen and unfrozen diatomite, and on the water retention ability of diatomite, were carried out in a laboratory. The results showed that under the condition of water content equal to 140% (its saturation higher than 70%), thermal conductivity of frozen diatomite is about 1.66 times that of thawed diatomite. However, its water retention ability is inferior. For the purpose of improving the long-term cooling effect of saturated diatomite in field experiment engineering, a 0.1 m thick sand layer was covered on the diatomite protection-slope layer. Four years of data monitoring a 120 m long experimental road arranged at Hongtupo section between K391+000 and K391+120 of 214th National Highway, showed that a diatomite slope-protection layer can delay the degradation of the underlying permafrost and improve the stability of the embankment. In order to improve its performance and reduce future maintenance, it is necessary to pay more attention to the construction season, construction techniques, and local climate.

**Keywords:** diatomite; permafrost embankment; thermal semiconductor.

## Background

Preserving permafrost is one of the most basic principles that are adopted in a cold permafrost area. Prethawing techniques can be an alternative for a small portion or shallow, thin permafrost layer, but excepting such conditions, preservation of the permafrost is frequently used in practice. In order to preserve the permafrost, many researchers and engineers have proposed measures which cool down the permafrost by means of adjusting radiation, convection, or conduction. From the point of adjusting conduction, increasing thermal resistance is often used in a cold permafrost area to raise the permafrost table and prevent the frozen soil below the permafrost table from thawing. For example, EPS and PU are often used because of their low conductivity, but warm permafrost dominates the Qinghai-Tibet Plateau. The above measure is very difficult to ensure the stability of a frozen soil ground-foundation. Active cooling measures are essential for preserving permafrost in this area (Cheng 2005, 2007). Construction material with special thermal conductivity features, with conductivity which is higher at low temperatures than at normal temperatures, can be particularly effective in utilizing "thermal offsets" in the active layer soils.

There is a large difference of thermal conductivity between water (0.6 W/m·K) and ice (2.3 W/m·K). Thus, the water can be regarded as a thermal diode with the critical temperature of 0°C. However, as a construction material, it is unsuitable because of its many known disadvantages in foundation engineering. Light, porous media with strong water absorption ability provide an ideal alternative for utilizing the special property of water. For example, peat soil and urea-formaldehyde have been used as thermal semiconductors in arctic and subarctic permafrost regions (Ersoy 1980, Mchattie 1983, Feklistov & Rusakov 1996). Many field experiments and engineering practices have proven their cooling effects (Ma et al. 2002). However, this method has never been applied in the permafrost region in the Qinghai-Tibet Plateau because of the scarcity of those materials (Ma 2005). Diatomite has high porosity and a great capacity for water absorption. Previous tests have shown that the water content of diatomite can easily reach about 200%.

Strong absorption capacity implies its potential as a thermal semiconductor.

## Test on Thermal Conductivity of Diatomite

The testing sample was a kind of coarse-grain diatomite (Fig. 1), produced in Jilin province, China. It has a strong water-absorption capacity and high stability after water saturation. Its bulk density varies from 0.35 to 0.43 g/cm$^3$; its specific gravity is about 2.1. The bulk density of the testing sample is about 0.4 g/cm$^3$. Thermal conductivities of the diatomite with different water contents were measured both in the frozen and unfrozen states. Test results are listed in Table 1.

From Table 1, it can be seen that with the increase of water content, the difference in thermal conductivity of diatomite between frozen and thawed states also increases. When the water content reaches 140% (saturation about 70%), the ratio of thermal conductivities between frozen and thawed diatomite is 1.66.

## Water Retaining Ability of Diatomite

The thermal conductivity ratio between frozen and unfrozen diatomite is associated with its water content. In the engineering practice, it is necessary for the constructor to know its water retaining ability.

Water retaining ability tests were conducted in the laboratory. Ambient temperature was about 20°. Wind was simulated by fan. Wind direction was parallel to the sample's top surface; wind speed was about 5m/s, which is similar to the field environment. Naked diatomite, diatomite covered by a 2 cm thick sand layer, and a 5 cm thick sponge were monitored. From Figure 2, water loss rate all increased with time under the above three experiment conditions. For naked diatomite, the evaporation rate is faster than the one covered by sand or sponge the first four days. Ten days later, all evaporation rates nearly approximate the same value at 55%. Owing to the availability of sand and its early good effect, sand cover was recommended in the field.

Figure1. Diatomite sample for testing.

Table 1. Thermal conductivity test of diatomite with different water content.

| Water content (%) | | 60 | 100 | 140 | 180 | 208 |
|---|---|---|---|---|---|---|
| Saturation (%) | | 30 | 50 | 70 | 90 | 100 |
| Thermal conductivity (w/m·k) | Frozen | 0.26 | 0.53 | 0.76 | 1.08 | 2.33 |
| | Thawed | 0.24 | 0.35 | 0.46 | 0.44 | 0.78 |
| | ratio | 1.08 | 1.51 | 1.66 | 2.47 | 2.98 |

## Introduction of Experiment Engineering

The field experiment was conducted on a northern slope of Hongtupo Mountains between milestone 391+000 and 391+120 along the National Highway 214 (Figs. 3, 4). It was constructed on the upper part of a gentle permafrost slope. The longitude and latitude of the center of experimental section is 98º58.154′E and N35º14.136′N. This section extended 10° SW. The road surface is asphalt paved. On the left, grass grows well, and vegetation coverage is about 70%; on the right, the earth surface is moist, and the vegetation coverage is about 40%. The roadbed is 2.5 m high on the left and 3.5 m high on the right. Annual rainfall is less than 100 mm, and mean annual air temperature is about -4.5 ºC.

The experiment site is located in permafrost area. The volumetric ice content there is 10%–20%. The natural permafrost table is about 2.4 m; the artificial table is about 8.0 m under the road surface; and the mean annual ground temperature is -0.9ºC. The diatomite experimental section has a total length of 50 m. Diatomite layers 0.4 m thick cover both side slopes.

Construction work can be divided into two parts. At the first stage in November 2003, the dry diatomite was laid on the side slope. In April, 2004, water was sprayed for the

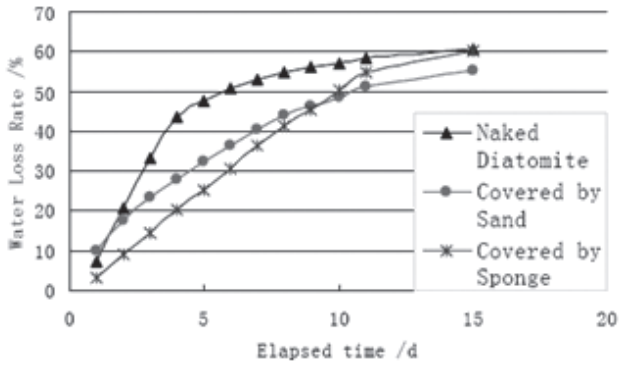


Figure 2. Curves of evaporation ratio changing with time.

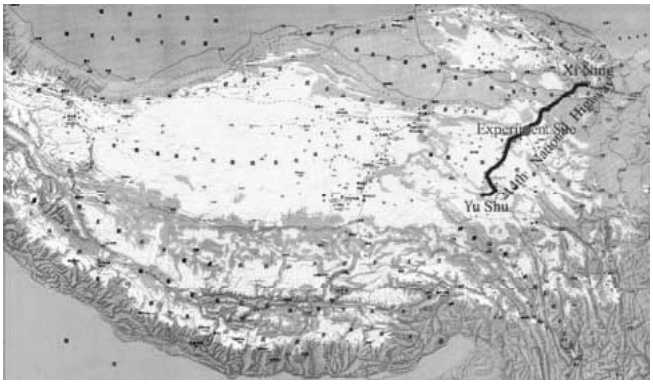


Figure 3. Location of 214th National Highway and the experiment site in the Tibet Plateau.

Figure 4. Experimental section of diatomite protection-slope.

first time. Water content of diatomite reached about 140% at that time. A 0.1 m thick sand soil was put on the diatomite layer to keep the stability of the diatomite cover and reduce evaporation (Fig. 4).

Three monitoring sections were arranged. Two sections (K391+085, K391+100) were the diatomite experiment; another one (K391+050) was a reference. Four monitoring boreholes were drilled for each section. There were located at the east slope-toe, east shoulder, centerline, and left shoulder. Temperature probes were installed in the boreholes at an interval of 50 cm. On both side slopes, 10 temperature probes were installed 50 cm beneath the surface. Monitoring work was conducted between June 2003 and September 2006. Except for a monitoring borehole for measuring natural ground temperatures at K391+085, all monitoring items were identical in the three sections.

## Analysis of the Cooling Effect of the Diatomite

*Surface temperatures of side slopes*

Side slope surface plays a very important role in the thermal balance of a roadbed. High surface temperature is bound to result in the degradation of underlying permafrost. Figure 5 displays the curves of 50 cm deep surface temperature changing with time.

It is evident in Figure 5 that: (1) in a year, slope surface temperatures of reference and diatomite sections behave differently. Compared with the diatomite section, the temperature of the reference section is higher in the summer and lower in the winter. This phenomenon is similar to what happens to the roadbed using EPS or PU. It shows that diatomite can effectively increase the thermal resistance and drop the annual temperature amplitude. Therefore, diatomite can raise the permafrost table and enhance the stability of frozen soil foundation. (2) With time elapsing, the temperature difference between the reference and diatomite sections increased in the summer and declined in the winter. From this point, the diatomite layer served as a thermal insulator and prevented insolation heating from the side slopes into the roadbed in the summer. It served, also, as a thermal conductor and facilitated heat release in the winter.

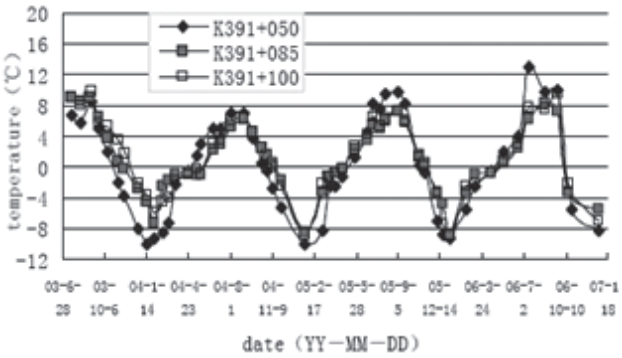

Figure 5. Curves of slope surface temperature changing with the time.

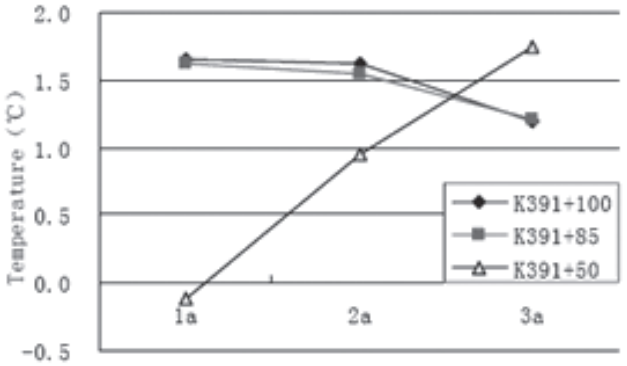

Figure 6. Curves of mean annual temperature of slope surface temperature changing with time.

This phenomenon demonstrates the thermal semiconductor effect of diatomite.

Temperature curves are not adequate proof of the cooling effect of diatomite because the whole year effect is not yet determined. Mean annual temperature is an essential index to affecting the developing trends of the underlying permafrost. In the first two years, the mean annual temperature of the slope surface was lower in the reference section than in the diatomite section, but in the third year, the result was reversed. The mean annual temperature of the diatomite section began to be lower than the reference section (Fig. 6). It can be concluded from the feature of temperature curves that the temperature of diatomite will decline continuously in the next few years, and the temperature difference between the diatomite and the reference section will increase. The cooling effect of the diatomite layer will be confirmed strongly.

*The permafrost table*

A permafrost table is an often-used index to characterize the cooling effect of engineering measures. It can directly indicate the final effect of diatomite. Figure 7 indicates the permafrost table observed in the boreholes in the reference and diatomite sections.

The permafrost table in a natural state changed little from 2003 to 2004. Therefore, the effect of air temperature changes on the cooling effect of diatomite is minor and can be omitted. The permafrost table dropped abruptly beneath the roadbed in the first year. Although the permafrost table

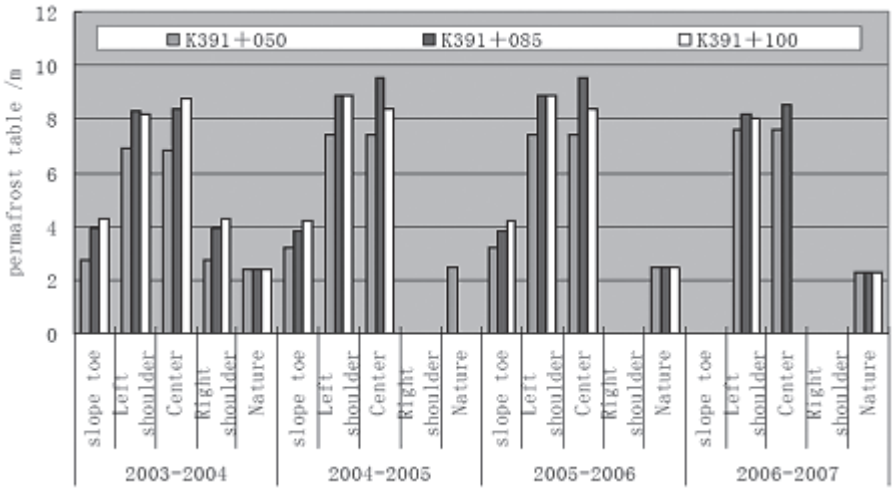


Figure 7. Contrast of the permafrost table between the experiment and comparing section.

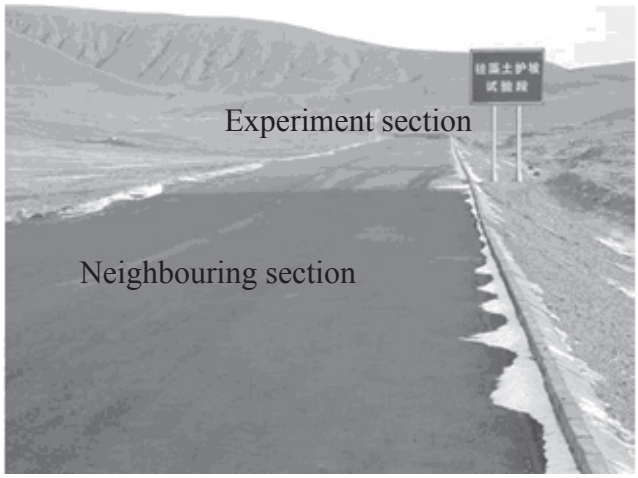


Figure 8. Operational status of experimental section and neighboring section.

in the reference section was higher at the beginning, the trends are more beneficial to the diatomite section than the reference section. In the second and the third year, the permafrost table in the diatomite section fluctuated greatly, but that in the reference section kept lowering. In the fourth year, the permafrost table in the reference section continued to decline, but that in the diatomite section rose. Considering the trend of mean annual surface temperature, the permafrost table will go up continuously over the next several years. The rise of the permafrost table shows that the diatomite layer can act as a good thermal semiconductor when it is saturated with water/ice.

*Operational status*

As of this year, the experimental section with diatomite has worked for four years. The roadbed kept its stability, and the road surface needed little maintenance. This section kept its good performance. However, in the neighboring section, the asphalt pavement has been repaired one time only two years after construction finished (Fig. 8). Investigation at the end of 2006 showed that waves appeared here.

## Problems and Discussions

Although four years of field data prove that the diatomite layer can effectively protect the underlying permafrost, early data are disappointing. It is necessary to analyze the phenomenon in order to avoid future mistakes and to find solutions to problems not previously noticed.

Previous research showed that the construction season plays an important role in the ground temperature under the roadbed and embankment in the initial stage. Its effect can last three or more years (Wen 2006). This is especially true for a roadbed using insulation. In the early spring, ground temperature is relatively low, but topsoils begin to thaw and construction is easier than in the winter. If EPS or PU is added, it can effectively reduce the incoming heat in the coming warm season. On the contrary, if insulation is constructed in the late autumn when ground temperatures are relatively high, it would help prevent heat within the roadway from releasing. In this experiment, diatomite was constructed in the adverse season. Consequently, the permafrost table was deeper and the side slope surface temperature was higher in the diatomite section in the initial several years.

Construction techniques also are important. From November 2003 to April 2004, the diatomite was dry. The dry diatomite is just a thermal insulator and retains the internal heat releasing. Thus, the permafrost table in the diatomite section decreased abruptly in the first year. Furthermore, laboratory test results suggest that the water retaining ability of diatomite is less satisfactory than expected. Due to the lack of maintenance and water-tight measures, the water content changed greatly after April 2004. Investigation in the winter of 2005 and 2006 showed that, although the total water content was more than 100%, the top 3 cm diatomite layer was only about 1%. This layer played a role in insulation during winter. It depressed the semiconductivity performance of diatomite.

Climate also affected the cooling effect of diatomite. The experimental section is located in a cold and arid region. Evaporation potential is far greater than the precipitation.

For diatomite only covered by 10 cm sand, it is impossible to maintain the state of high water content in the diatomite if maintenance is scarce.

## Conclusions

Diatomite can be used as a thermal semiconductor. The performance of a diatomite semiconductor improves with the increase of water content. A diatomite semiconductor can delay the degradation of the underlying permafrost and improve the stability of a road embankment; however, because the period of observation was only four years, its long-term effect needs more validation. This experiment demonstrated that it is necessary to pay more attention to construction season, construction techniques, local climate, and maintenance before a thermal semiconductor is utilized to cool down the permafrost embankment.

## Acknowledgments

This work was supported by the Hundred Young Talented Scientists Program of the Chinese Academy of Sciences granted to Dr. Jilin Qi.

## References

Ersoy T. & Haist G. 1980. Statilization of a Highway embankment in a permafrost area. *Proceedings of the 2nd International Symposium on Ground Freezing. 1980:* 1076-1088.

Feklistov, V.N. & Rusakov, N.L. 1996. Application of foam insulation for remediation of degraded permafrost. *Cold Regions Science and Technology* 24: 205-212.

Guodong C. 2005. A roadbed cooling approach for the construction of Qinghai–Tibet Railway. *Cold Regions Science and Technology* 42(2): 169-176.

Ma, W., Guo-dong, C. & Qing-bai, W. 2002. Preliminary Study on Technology of Cooling Foundation in Permafrost Regions. *Journal of Glaciology and Geocryology* 24 (5): 579-587.

Ma, W., Shi, C., Wu, Q. et al. 2006. Monitoring study on technology of the cooling roadbed in permafrost region of Qinghai–Tibet plateau. *Cold Regions Science and Technology* 44(1): 1-11.

Mchattie, R.L. & Esch, D.C. 1983. Benefits of peat underlay used in road construction on permafrost. *Proceedings of the Fourth International Conference on Permafrost*: 826-831.

Zhi, W. 2006. *Evaluation on the Application of Thermal Insulator in the Embankment in the QTP*. Doctoral thesis for the degree of GUCAS (Graduate University of Chinese Academy of Sciences).

# Identification and Mitigation of Frost Hazards Along the China-Russia Oil Pipeline

Huijun Jin, Jianming Zhang, QihaoYu, Yu Sheng, Zhi Wei, Guoyu Li, Yanjun Ji, Ruixia He, Lanzhi Lü
*State Key Laboratory of Frozen Soils Engineering, 326 W. Donggang Rd., Lanzhou, China 730000*
Jiaqian Hao, Youchang Chen, Wei Wu, Yimin Zhao
*Daqing Oilfield Engineering Company, PetroChina Corporation Limited, Daqing, China 163712*

## Abstract

The China-Russia oil pipeline is designed to transport 603,000 barrels of Siberian crude oil per day using a buried pipeline 914 mm in diameter across 1030 km of permafrost and seasonally frozen ground. Construction was scheduled to be between March 2008 and August 2009. The design was significantly challenged by differential frost heaving and thaw settlement. About 500 boreholes to depths of 5 to 20 m were drilled and cored for analyses, and frozen ground conditions were evaluated. Conventional burial construction modes were adopted after detailed surveys and analyses of permafrost conditions along the pipeline route**.** Permafrost forecasts, thermal and strain/stress analyses, measures to mitigate frost hazards, and a design for long-term monitoring and early detection of developing frost hazards were conducted. Mitigative measures using excavation and backfill of non-frost-susceptible soils, insulation, and drainage control were proposed and adopted. A review of the engineering activities and measures undertaken to address these concerns is presented herein.

**Keywords:** China-Russia oil pipeline; engineering geology; frost heaving; mitigation; permafrost; thaw settlement.

## Introduction

A key component of the Siberian-Pacific oil pipeline is a 1030 km-long, 914 mm-diameter spur pipeline to transport 603,000 barrels of oil daily from Skovorodino, Siberia (54.0°N, 123.6°E, 398 m in elevation) to Daqing, China (46.6°N, 125.0°E, 151 m). The spur pipeline will enter Northeastern China near Mo'he (53.5°N, 122.4°E, 350 m) (Fig. 1) and cross 965 km of permafrost and seasonally frozen ground in China.

Potential pipeline routes were hotly debated in the past 12 years. The Mo'he to Daqing route was chosen because it offered the shortest distance through ice-rich permafrost and wetlands reserves, generally more favorable terrain conditions, and easier access to existing transportation corridors. The pipeline, using conventional burial, is designed to transmit unheated crude oil, with an estimated incoming oil-temperature range of -6°C to +10°C at the Mo'he inlet. It traverses 530 km of warm permafrost, of which about 118 km in China is ice-rich. Permafrost features vary greatly over short distances. In the south, it traverses about 500 km of seasonally frozen ground, with maximum frost penetration depths of 1.8 m to 4.0 m. Preliminary and detailed designs were completed by August and December 2007 respectively. Construction is scheduled in 2008–2009.

The design along an unheated pipeline buried in frozen ground required mitigation of frost heaving in the cold season and thaw settlement in the warm season. A series of resultant environmental impacts and geohazards on pipeline foundation stability needed to be economically minimized after the massive pipeline construction and during the operation period. Therefore, proper designs needed to compromise between long- and short-term investments. Since 2004, the permafrost research activities have been focused on the prediction and mitigation of frost heaving and differential thaw settlement of pipeline foundation soils in order to provide technical support for the pipeline design. This paper reviews the overall research activities and engineering measures addressing these concerns.

## Study Regions

*Topography, geology, and climate*

The pipeline route crosses about 965 km of mountains and plains in Northeastern China. In typical soil profiles, peat and humic soils are underlain by clayey sands and sandy clays. The region along the pipeline route is characteristic of a temperate continental monsoon climate with long, dry, cold winters and short, moist, warm summers. Mean annual air temperatures range from 0°C to 1°C in the south to -5°C to -6°C in the north. Annual precipitation ranges from about 400 to 700 mm, 80%–90% of which falls in summer. The vegetation is comprised of cold to temperate mountain needle-leaf forest. Needle and broad-leaf mixed forests and forest steppes gradually appear when moving southwards into the piedmont area. They are eventually replaced by agricultural land at the southern end of the pipeline route.

*Permafrost features*

Permafrost conditions are characterized by latitudinal and elevational zonation, with local marked variations. The areal extent of permafrost increases northwards from 0% to 65%, and mean annual ground temperatures decrease from 0°C to -2.6°C (Table 1). The observed thickness of permafrost varies from about 1 to 60 m; occasionally permafrost extends to 120 m. Permafrost zones range from isolated patches to widespread discontinuous zones of permafrost. In the northern Da Xing'anling Mountains, tussocks and moss layers are dense, and the thicknesses of surficial deposits are 8–12 m on the shaded slopes of intermontane basins, in wetlands or in lowlands, and on low river terraces. Permafrost

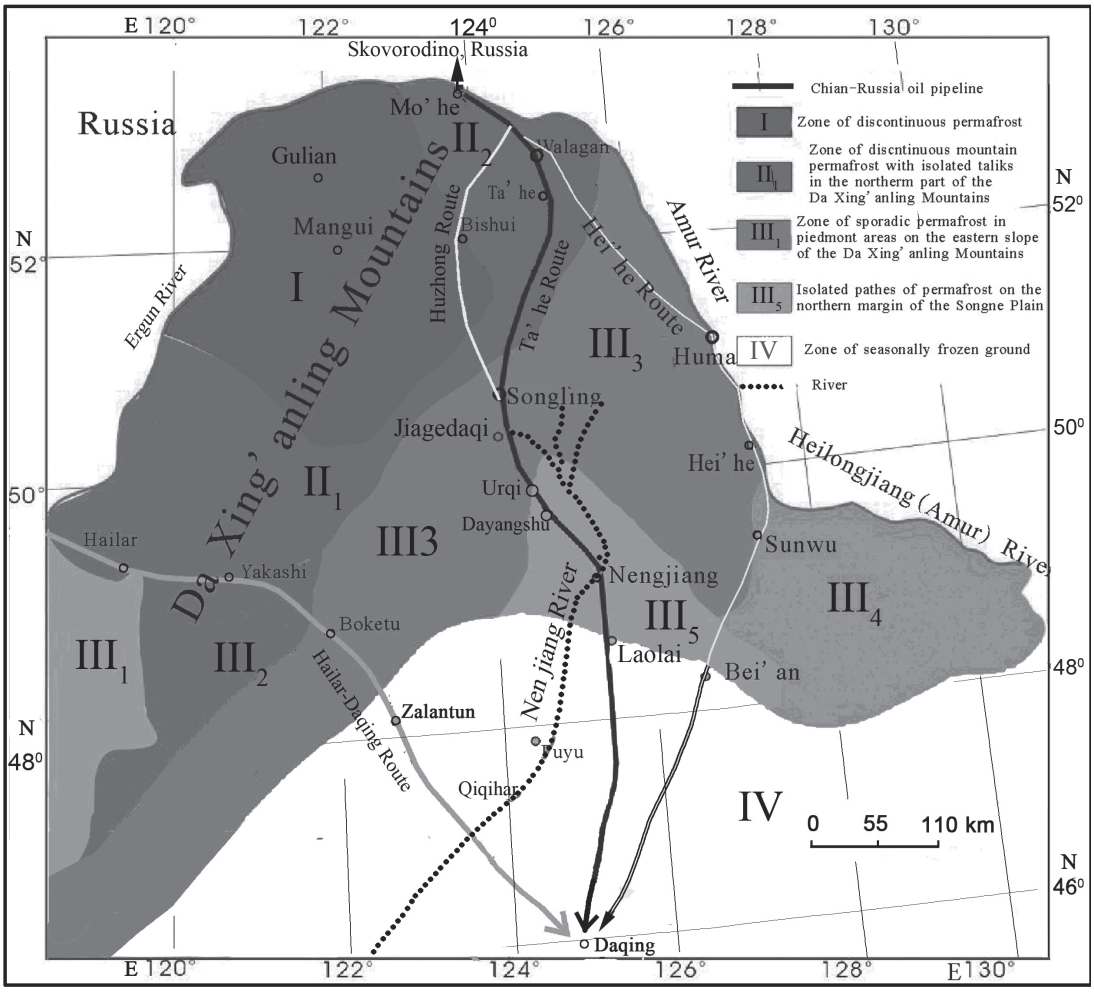


Figure 1. China-Russia oil pipeline routes in Northeastern China (revised from Guo et al. 1981 & Jin et al. 2007a).

can be as thick as about 50 m to 60 m. In contrast, on treeless or sparsely vegetated sunlit slopes with thick surficial deposits, permafrost is either thin or absent. On shaded slopes with dense vegetation, permafrost conditions are intermediate between valley bottom lowlands and sunlit slopes.

*Seasonally frozen ground*

When moving southwards, the maximum thaw depths in river taliks in increasingly fragmented discontinuous permafrost is 2.5 m to 4.0 m, depending on surface cover, soil moisture conditions, and lithology. Seasonally frozen ground largely replaces permafrost from Da'yangshu southwards (Fig. 1). Topographically, this is the transition between the eastern slopes of the Da Xing'anling Mountains and the northern Nen Jiang River Plain. The lithology consists of silt and/or silty clay. The ground water table is generally shallow, and long, cold winters favor frost heaving when moisture and soil conditions suffice. The maximum depth of frost penetration is 1.8 m to 3.5 m, occasionally to 4.0 m.

## Study Methods

*Survey and investigation of permafrost*

The distribution and thickness of warm, ice-rich permafrost; the types, distribution, genesis and features of hazardous periglacial phenomena and assessment of their potentially adverse impacts on pipeline infrastructures were of particular interest in the surveys and investigations (DOE 2007a). During the feasibility, preliminary, and detailed survey stages, about 500 boreholes with depths of 5 m to 20 m were drilled and cored for analyses.

*Assessment and forecast of permafrost conditions*

The assessment and forecast of permafrost included evaluation of the present conditions of permafrost along the pipeline route and their possible changes during the next 50 years (DOE 2007b). The assessment was based on 1951 topographic maps, permafrost data obtained during the 1970s, field engineering explorations in 2006–2007, and aerial mapping at 1:2000 along the pipeline route in 2006–2007. The assessment covered soil strata, topography and geomorphology, permafrost features, engineering geology, classification of frost heaving and thaw settlement of foundation soils, overall assessment, and advice on pipeline construction modes (Jin et al. 2007a). The overall assessment considered the genetic types, water/ice contents, and thaw-sensitivity and/or frost-susceptibility of the pipeline foundation soils.

The zonation has three hierarchical levels: zone, subzone, and section of frozen ground engineering geology (Jin et al.

Table 1. Permafrost features along the pipeline route.

| Location | Lat. (N) | Elev. (m) | M A A T (°C) | MAGT (°C) | PT (m) |
|---|---|---|---|---|---|
| Xing'an | 53°25′ | 260 | | -1.8 | |
| Amur | 52°50′ | 747 | -5.4 | -0.1~-4.2 | 21~120 |
| Station 22 | 52°45′ | 370 | | 2.0 | |
| S of Walagan | 52°30′ | 445 | | -1.8 | |
| JMH K276 | 52°26′ | 410 | | -0.7 | |
| Tafeng | 52°25′ | 560 | -2.8 | -0.3 | 15 |
| N of Cuigang | 52°19′ | 440 | | -0.6 | |
| S of Dawusu | 51°47′ | 500 | | -0.4 | |
| Cuiling | 51°40′ | 1072 | -4.6 | -1.3 | 50 |
| N of Xinlin | 51°40′ | 517 | | -1.2 | |
| N of Tayuan | 51°26′ | 585 | | -2.6 | |
| N of Xintian | 51°08′ | 545 | | -1.2 | |
| JMH K34-35 | 50°41′ | 400 | | 2.0 | |
| Jiagedaqi | 50°23′ | 382 | -4.0 | -0.1 | 7~16 |
| Dayangshu | 50°08′ | 360 | -0.2 | 0.1 | 1~7 |

Note: MAAT—mean annual air temperature; MAGT—mean annual ground temperature; PT—permafrost thickness; N—North; S—South; JMH—Jiagedaqi to Mo'he Highway. The depth of zero annual amplitude of ground temperature, which generally ranges from 10 to 15 m. Air temperatures were based on meteorological data from 1970 to 2005.

2007a in press). Frozen ground along the pipeline route was first divided into zones of seasonally frozen ground, isolated patches, sporadic, and discontinuous permafrost based on the areal extent of permafrost. The zones of permafrost were divided into thermal stability subzones of very unstable (>-0.5°C), unstable (≥-1°C), and stable (<-1°C) permafrost. The 3rd-tier of permafrost zones was based on the soil moisture content. The overall and by-segment assessment synthesized available information.

Changes of permafrost were projected for Northeastern China during the 21st century using GIS-aided equivalent-latitude models (Wei et al. 2008). Possible changes of permafrost conditions at selected sites along the pipeline route were forecasted using the finite-element method. The prediction considered typical boundary and initial conditions based on the observed present conditions along the pipeline route (Jin et al. 2007a). These conditions included air, ground surface, ground temperature and their seasonality; ice-contents, types of permafrost, and a climate warming scenario of 2.4°C during the next 50 years, and influences of anthropogenic activities represented by removal of vegetation and pipeline operation.

*Simulations on pipeline-soil interactions*

According to the best estimation, crude oil temperature will vary from -6°C to +10°C at the Mo'he inlet at the start of oil transmission in August 2009. It was assumed that oil temperatures would have seasonal sinusoidal variations for 50 years, and that the top of the pipeline would be buried at a depth of 1.5 m. Thermal analyses focused on temperatures of crude oil in the pipeline and of foundation soils along the pipeline route; and resultant seasonal and long-term freeze-thaw processes around the buried pipe and along the route, both without engineering measures and with some mitigative measures (insulation, backfill of non-frost-susceptible (NFS) soils, and drainage control). Stress/strain analyses included studies on the coupled thermo-mechanical interactions between the pipeline and foundation soils, possible weak segments along the pipeline with and without the mitigative measures, and checks against the design criteria for steel pipeline integrity, safety, and long-term stability.

*Mitigation of frost hazards*

Engineering measures for mitigation included: 1) stress and strain constraints for pipeline safety; 2) excavation and backfill of NFS-soils at segments with significant frost hazards; 3) drainage and flood controls; 4) insulation; 5) burial depth; 6) transition zones; 7) river and other crossings of linear infrastructures; 8) slope stability; 9) periglacial hazards; and 10) project management in permafrost regions.

*Monitoring of pipeline foundation soils*

Permafrost temperatures along the pipeline route were measured generally on a weekly basis, using thermistor cables fixed in cased boreholes during the 1970–1980s. During 2007–2008, 12 exploratory boreholes with depths of 15 m to 20 m were chosen for ground temperature measurements using thermistor cables (Jin et al. 2007a).

A program for long-term monitoring of pipeline foundation soils was established to ensure pipeline long-term safety through early detection and proactive mitigations of pipeline foundation soil problems. The monitoring elements included ground temperatures, soil moisture contents, and deformation of the pipeline foundation soils, both in the proximity of the pipeline and under natural conditions, for comparison. There were 20 cross-sections designed and they were to be implemented during and/or after pipeline construction.

## Results and Discussions

*Assessment and forecasts of permafrost*

Permafrost along the pipeline route has been in degradation during the past 40 years due to significant climate warming of about 0.9°C to 2.5°C and increased human activity (Jin et al. 2007b). Frozen ground and engineering geology conditions along the pipeline route were inadequately understood for pipeline design prior to the survey in 2006–2007. Recent surveys indicated that about 118 km of warm, ice-rich permafrost along the route needed particular attention. Generally, these segments are associated with wetlands underlain by thick silts or clays.

The major frozen ground zones included: 1) Mo'he-Walagan zone of discontinuous (65% to 80%) permafrost with isolated taliks; 2) Walagan-Songling zone of discontinuous (35% to 65%) permafrost with extensive taliks; 3) Songling-Jiagedaqi zone of sporadic (10% to 35%) permafrost; 4) Jiagedaqi-Dayangshu zone of patchy (<10%) permafrost; and 5) Dayangshu-Daqing zone of seasonally frozen ground (Fig. 1).

The forecast of permafrost conditions considered permafrost types and cover conditions representative of the pipeline route, the removal of forest vegetation during

pipeline construction, and climate warming of about 2.4°C during the pipeline lifespan. It is evident that the permafrost tables will deepen; the rates of temperature increase will slow with operating time, increasing ice contents, and decreasing ground temperatures. However, thaw settlements of pipeline foundations will increase with higher ice contents.

*Thermal analyses*

Oil temperatures at the incoming Mo'he Pump Station and along the pipeline route will be subject to seasonal and interannual variations due to the heat exchanges along the routes in Siberia and China.

Distribution of oil temperatures along the 965 km route during the pipeline lifespan was a key issue to pipeline-soil interactions and pipeline foundation design due to its control on areal extents and developing trends of seasonal and interannual freeze and thaw cylinders around the operating pipeline. These further control the deformations and stresses on the pipeline, and the mitigative measures required. The simulations results indicated that oil temperatures cool southwards in the warm season, but that they warm southwards during the cold seasons (Sheng et al. 2007, 2008). As a result, the amplitudes of seasonal variations will decrease southwards and reach a quasi-stable state at about Km-870 (Fig. 2). Oil temperatures could slightly increase with elapsing time due to climate warming. However, the average annual oil temperature decreases southwards in the north, then starts to increase from about Km-488. This is because ground temperatures along the pipeline route are low before reaching Km-366, roughly 0°C at Km-366 to Km-431, and above 0°C southwards.

The thaw depth beneath the pipeline in the cold (<1.0°C) permafrost area north of Ta'he generally will be small (1.3 m to 2.3 m), but will increase southwards. In the warm (>1.0°C) permafrost area, the thaw depth will increase sharply. With elapsing time, thaw settlement prevails due to thermal impacts from pipeline operation. Changes of the ice-rich permafrost table will be 0.5 m to 2.0 m. The resultant thaw settlement in the north (Km-0 to Km-317) will be large and will need to be mitigated. In the southern part (Km-317 to Km-630), frost heaving in the wetlands will be a major challenge. The depth of ground freezing beneath the pipeline will decrease from about 0.4 m at Km-317 to 0 m at Km-580. By Km-700 minimum oil temperatures will be greater than 0°C.

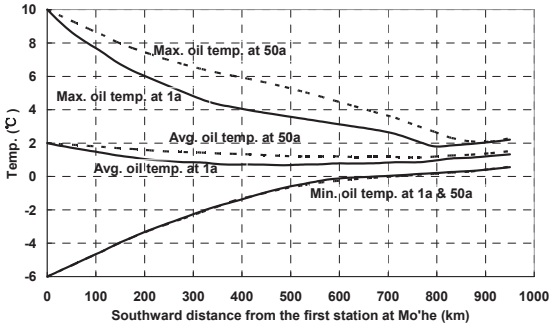


Figure 2. Predicted changes of oil temperatures along the proposed route of un-insulated pipeline.

Two-directional freezing in winter and thawing in summer will occur in soils surrounding the buried pipeline. The thaw cylinder around the pipeline will enlarge with elapsing time but at a decreasing rate with increasing ice contents. The frozen cylinder around the pipeline will diminish with elapsing time, with increasing soil water content, and when moving southwards. Insulation can effectively reduce the development of freeze-thaw cylinders during the early years of operation.

*Strain/stress analyses and pipeline safety constraints*

Frost heaving and differential thaw settlement will result due to spatiotemporal seasonality of oil and soil temperatures and differences of soils and pipelined oil at certain sections (AGRA Earth & Environmental Limited and Nixon Geotech Limited 1999). However, the pipeline is more tolerant of differential thaw settlement than frost heaving. The largest stress would occur in the center of thaw settlement or in the transition zone between frost heaving and non-frost heaving sections; the largest allowable deformation will increase with section length of frost heaving (Sheng et al. 2007). Therefore, frost mounds pose greater threats to the pipeline. The transition zone between frost heaving and thaw settlement is also hazardous. The length of frost-heaving zones has a significant impact on the pipeline bending moment. Any increase in the length of the transition would mitigate frost heaving on the pipeline.

Numerical analyses were conducted on effective stresses on pipeline under various combinations of oil pressure, pipe-wall thickness, length of transition, frost heaving and differential thaw settlement conditions, to determine the maximum allowable deformations under certain combinations of oil pressures and pipe-wall thicknesses (Sheng et al. 2007, 2008).

The stress/strain criteria for designing pipeline foundations were provided according to the best estimates of potential frost heaving and thaw settlement of soils along the pipeline and analytical results of frost heaving and thaw settlement. A linear transition zone model in which the coefficients of frozen and unfrozen ground were 23.4 and 6 MPa, was used, and the length of the transition zone was 40 m. Pipeline foundation safety with and without mitigative measures and its classification under differential deformation, and under various wall thicknesses, oil pressures, and lengths of transition, were analyzed using numerical models for the pipe-soil interactions (Sheng et al. 2007). Reducing the intensity of longitudinal differential deformations using proper insulation, backfill of NFS soils (bedding), and increasing the wall-thickness of the pipe could effectively mitigate the damage from frost hazards (Jin et al. 2007a, Sheng et al. 2007).

*Mitigative measures and construction mode*

During route selection, the engineers chose locations with less-frost-susceptible soils, less soil moisture, deeper ground water tables, and sun-lit slopes. Patchy or sporadic permafrost was avoided or crossed in the shortest distance possible. Other considerations included avoidance of solifluction, icings, frost mounds, wetlands and maintenance of slope stability.

During the design phase, insulation was considered for permafrost areas with high ice contents and susceptibility to frost heaving, to minimize the freeze-thaw extent around the pipeline and thermal impacts of heat exchanges with the underlying permafrost. Differential deformations in interfaces of ice contents, soil types, frost-susceptibility, and construction modes required special attention. In sections with shallow, ice-rich permafrost, backfilling with NFS-soils was accomplished. In the section with thick, ice-rich permafrost, a combination of localized backfill of NFS soils, proper insulation, and drainage control were considered. In sections with extensive frost-susceptible soils, drainage control was critical.

During the construction phase, all designs or changes in design were managed strictly according to the opinions of experienced cold regions engineers. The proper construction season for burial of pipeline in permafrost was in late winter and early spring. Careful examinations of excavated soil profiles were important, as surveys were often inadequate in revealing special permafrost conditions. Removal of vegetation adjacent to the pipeline, operation of large equipment, and necessary drainage were controlled.

The burial depth of the pipeline was designed according to the "*Code for Design of Oil Transportation Pipeline Engineering*" (People's Republic of China National Standard 2003), and to accommodate the local conditions such as thickness of frozen ground, geological conditions, transported oil temperatures, and farmland and woodland. The pipeline was conventionally buried in ice-poor and -medium permafrost areas, or areas with shallowly buried bedrock and the total length is 124.9 km. When passing through forests, the top of the pipe was buried deeper than 1.6 m (below the depth that could be impacted by local forest fires) (Zhou et al. 1994). The pipe ditch was 0.2 m deeper than regular areas, and the fine-grained backfill reached a depth of 0.3 m above the pipe top. In areas north of the Jiagedaqi, the pipe top was buried at depths of 2.2–2.4 m because the measured maximum depth of seasonal frost penetration is 2.6 m to 2.8 m in taliks with frost-susceptible soils.

In the seasonally frozen ground areas south of Jiagedaqithe burial depth of pipeline top was set at the depth of 0.4 m above the maximum local depth of seasonal frost penetration from Jiagedaqi to Ne'he, 1.9 m in Yi'an County, 1.8 m in the Lindian and Daqing areas.

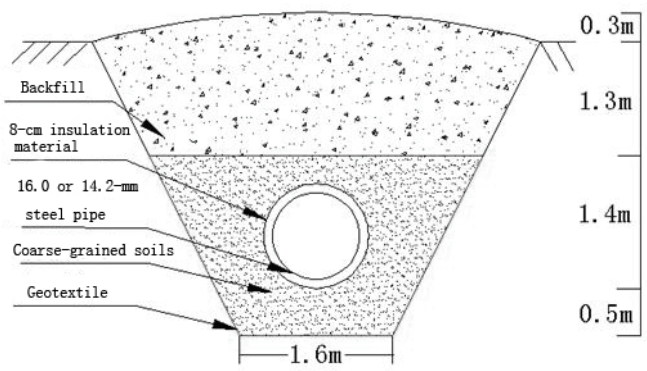


Figure 3. Burial using backfill and insulation for wetlands underlain by thick, high-ice-content permafrost.

The modified burial using coarse-grained (bedding) sand and gravel beneath the pipe was adopted for the ice-saturated and ice-rich permafrost areas. Elevation was not considered because of frequently-occurring forest-fire concerns. The top of the pipe is 1.5 m and the total length of the modified burial is 3.63 km.

In high-ice-content permafrost areas with large active layer thickness, modified burial with insulation and backfill of NFS soils was adopted (Fig. 3) for a total length of 28.3 km. In wetlands underlain by permafrost (total length of 39.2 km), or with frequently-occurring outflow springs (total length of 1.59 km), a similar approach was adopted.

Areas of very ice-rich patchy permafrost, generally less than 3.7 m in thickness, were backfilled with coarse-grained soils (bedding materials). The pipe top was buried 2.0 m. When the thickness of permafrost was large, the pipe top was at 1.8–2.0 m in areas with weakly thaw-sensitive permafrost, or where ice-rich permafrost was partially removed (Tables 2, 3).

Table 2. Results from thermal and strain/stress analyses on backfill and insulation (Sheng et al. 2007).

| Mitigative measures | Wall thickness of pipe | Frozen depth beneath pipe | Stress on pipe (MPa) | Thickness (m) of backfill beneath pipe |
|---|---|---|---|---|
| Backfill, 8-cm Insulation | 16.0 mm | 0.75 m | 315 | 0.3 |
| | 14.2 mm | | 308 | 0.5 |

Table 3. Statistics on mitigative measure for permafrost hazards along the China-Russia oil pipeline..

| Type of frozen ground | Mitigative measures | Length (km) |
|---|---|---|
| Talik (Seasonally frozen ground) | Pipeline top 0.4 m above the local frost penetration; 0.2 m excess backfill of NFS soils beneath pipe. Pipeline top at 1.6 m in bedrocks | 142.86 |
| Ice-poor,-medium permafrost | Conventional burial, pipe top at 1.8 m | 209.46 |
| Ice-rich permafrost (non-wetlands areas) | Pipeline top at 1.6 m, 8-cm-thick insulation around the pipe, 0.5 m backfill of coarse soils beneath pipe of 14.2-mm-wall thickness | 40.73 |
| | Backfill of NFS soils, 14.2-mm-pipe-wall thickness | 21.18 |
| Wetlands with ice-rich permafrost | Pipe top at 1.8 m, 8-cm-thick insulation around pipe, 0.3 m backfill of coarse soils beneath pipe of 16.0-mm-wall-thickness | 42.72 |
| Areas with springs | | 1.59 |

In ice-rich permafrost areas, the top of the pipeline was buried 1.6 m with backfill of NFS-soils, insulation, and other measures. In wetlands underlain by the ice-rich permafrost or with frequent occurrence of outflow springs (potential icings and frost mounds), frost hazards and pipeline floating due to hydrostatic pressure were mitigated using the modified burial with NFS-soil backfill, insulation, and drainage control. If only partial backfill of NFS-soils was required, its depth was chosen based on local engineering geological conditions. When partial backfill of NFS-soils and insulation was required for protection of permafrost and maintenance of a preset, engineered permafrost table, the depths of backfill of NFS soils and insulation parameters were optimized by thermal and strain/stress analyses (Table 2) (Sheng et al. 2007).

## Summary and Conclusions

The China-Russia oil pipeline traverses warm permafrost regions with significant frost hazards in Northeastern China. Significant changes of permafrost were observed or projected along the pipeline route.

Pipeline oil temperatures are expected to generally increase southwards and with time; the effects of climate warming are anticipated to be overshadowed by oil temperature variations; insulation tends to constrain the oil temperature variations and the freeze-thaw cylinder around the pipeline early in the pipeline operation period. Differential thaw settlement is anticipated to have a lesser impact than frost heave on the pipeline.

Conventional burial was chosen for the pipeline in spite of possible significant frost heaving and thaw settlement because of concerns about frequent forest fires, inevitably posing substantial risk to pipeline integrity. Therefore, a system for long-term monitoring and assessment of foundation stability was deemed indispensable for early detection and subsequent proactive mitigation of developing problems.

## Acknowledgments

This study was supported by the Chinese Academy of Sciences (CAS) 100 Talents Program "Stability of linear engineering foundations in warm permafrost regions under a changing climate"; CAS Knowledge Innovation Key Project "Mechanisms and mitigation of frost heaving and thaw settlement of pipeline foundation soils in permafrost regions" (Grant No. KZCX2-YW-311); and PetroChina Technological Development Program on Permafrost Research along the China-Russia Crude Oil Pipeline Route. Dr. Max C. Brewer, Professor Emeritus with the U. S. Geological Survey, Anchorage, kindly English-edited the manuscript.

## References

AGRA Earth & Environmental Limited and Nixon Geotech Limited. 1999. *Monograph on Norman Wells Pipeline Geotechnical Design and Performance.* Geological Survey of Canada Open File 3773, 142 pp.

Daqing Oilfield Engineering (DOE) Co. 2007a. *Report on the Expedition of Frozen Ground Engineering Geology Along the China-Russia Crude Oil Pipeline (Mo'he to Daqing)*. Daqing, China: Daqing Oil Engineering, Company (edited), 122 pp. (in Chinese).

DOE. 2007b. *Review on the Progress of Preliminary Design of the China-Russia Pipeline (Mo'he-Daqing Segment)*. Daqing, China: Daqing Oil Engineering, Company (edited), 428 pp. (in Chinese).

Guo, D.X., Wang, S.L., Lu, G.W., Dai, J.B. & Li, E.Y. 1981. Regionalization of permafrost in the Da- and Xiaoxing'anling Mountains in Northeastern China. *J. Glaciology and Geocryology* 3(3): 1-9 (in Chinese).

Jin, H.J., Zhang, J.M., & Tong, C.J. 2007a. *Final Report on the Assessment and Prediction of Frozen Ground Engineering Geology Along the Mo'he to Daqing Oil Pipeline*. Lanzhou, China: PetroChina Daqing Oil Engineering Company & Chinese Academy of Sciences Cold and Arid Regions Environmental and Engineering Research Institute edited, 309 pp. (in Chinese).

Jin, H.J., Yu, Q.H., Lü, L.Z., Guo, D.X. & Li, Y.W. 2007b. Degradation of permafrost in the Da and Xiao Xing′anling Mountains, Northeastern China. *Permafrost and Periglacial Processes* 18(2): 245-258. Doi: 10.1002/ppp.589.

Jin, H.J., Wei, Z., Yu, Q.H., Lü, L. Z. & Wang, S.L. in press. Assessment of frozen ground engineering geology conditions along the Qinghai-Tibet Highway/Railway, China. *Engineering Geology.*

People's Republic of China. 2003. *Code for Design of Oil Transportation Pipeline Engineering*. PetroChina Co., Ltd. and PRC Ministry of Construction edited, Beijing, China: China Planning Press, 158pp. (in Chinese).

Sheng, Y., Jin H.J., Wen, Z. & Li, G.Y. 2007. *Thermal and Stress Analyses of Foundations Soils Along the Buried Pipeline in Permafrost Regions*. Lanzhou: China: PetroChina Daqing Oil Engineering Company & Chinese Academy of Sciences Cold and Arid Regions Environmental and Engineering Research Institute (edited), 127pp.

Sheng, Y., Wen, Z., Li, G.Y., Hao, J.Q. & Wu, W. 2008. Thaw settlement behavior of permafrost along the proposed China-Russia crude oil pipeline route in Northeastern China. *Proceedings of the Ninth International Conference on Permafrost, Fairbanks, Alaska, June 29–July 3, 2008* (this proceedings).

Wei, Z., Jin, H.J., Zhang, J.M., Ji, Y.J., Yang, S.Z. & He, R.X. 2008. Forecasting changes of permafrost in Northeastern China during the next 50 years using the combination of GIS-aided equivalent-latitude and finite-element models. *Proceedings of the Ninth International Conference on Permafrost, Fairbanks, Alaska, June 29–July 3, 2008* (this proceedings).

Zhou, Y.W., Liang, L.H., Gu, Z.W., Liang, F.X. & Zhang, Q.B. 1994. Changes of thermal regimes of permafrost after forest fires in the northern Da Xing'anling Mountains. In: Q. Zhao, W. Zhang, Y.W. Zhou, & Y. Yang (eds.), *Environmental Impacts of Forest Fires in the Da Xing'anling Mountains and Their Mitigation*. Beijing, China: Science Press, 25-35 (in Chinese).

# Increasing Permafrost Temperatures in Subarctic Sweden

Margareta Johansson
*Dept. of Physical Geography and Ecosystem Analyses, Lund, Sweden and Abisko Scientific Research Station, Abisko, Sweden*
H. Jonas Åkerman
*Dept. of Physical Geography and Ecosystem Analyses, Lund, Sweden*
Christer Jonasson
*Abisko Scientific Research Station, Abisko, Sweden*
Torben R. Christensen
*Dept. of Physical Geography and Ecosystem Analyses, Lund, Sweden and Abisko Scientific Research Station, Abisko, Sweden*
Terry V. Callaghan
*Abisko Scientific Research Station, Abisko, Sweden and Dept. of Animal and Plant Sciences, Sheffield, UK*

## Abstract

This paper reports permafrost temperatures from three peat mires in subarctic Sweden. There were trends of increasing ground temperatures in the boreholes between 1980 and 2002 of 0.04°C $a^{-1}$ to 0.05°C $a^{-1}$ in the upper 1 m and 0.03°C $a^{-1}$ to 0.04°C $a^{-1}$ in the lower 12–15 m. However, no trend was detected in the middle of the profile. To verify the trends from the mires (with scarce temporal resolution), we use ground temperatures from Abisko Scientific Research Station recorded in an area currently nearby permafrost. Here, ground temperatures have increased on an annual basis and at all seasons apart from the summers, where decreasing temperatures were detected. The changes in ground temperatures could be correlated to increasing air temperature and increasing summer precipitation, but surprisingly not with snow depth. At lower depths the increases may be due to possible increased heating from slightly warmer or more freely flowing ground water.

**Keywords:** Abisko; ground temperatures; subarctic Sweden.

## Introduction

Increases in air temperatures in the Arctic region have been almost twice as high as for the rest of the world during the last decades. This arctic amplification is expected to continue (ACIA 2005). These increases have had and will have profound effects on ground temperatures and, hence, on permafrost distribution (Anisimov et al. 2007). Even though it is widely known that there is a mismatch between air and ground temperatures, as there are other parameters of importance to ground temperatures, increasing air temperature in general increases ground temperatures (e.g., Thorn et al. 1999). For time scales up to a decade, the climatic changes of primary importance for ground temperatures are the changes in air temperatures and snow cover (Osterkamp & Romanovsky 1999). Increasing snow depth increases the insulation of ground from prevailing low winter temperatures and, hence, increases the ground temperatures. In contrast, late snowfall decreases soil temperatures due to the high albedo and the consumption of latent heat during snowmelt (Zhang et al. 2001a). In areas of discontinuous permafrost where air temperatures are close to 0°C, shallow permafrost is especially sensitive to climate warming. In such areas, snow depth and duration are particularly important and, together with air temperature, determine the presence or absence of permafrost.

Increasing ground temperatures have been reported from around the Arctic (e.g., Walsh et al. 2005, Romanovsky et al. 2007, Isaksen et al. 2007, Osterkamp & Romanovsky 1999), but information is underrepresented for the lowland discontinuous permafrost area of northern Fennoscandia. This paper reports permafrost temperatures from three peat mires in subarctic Sweden. Here, important changes in permafrost distribution and active layer depth have been recorded in lowland mires (Akerman & Johansson, submitted). We use the relationships between air temperatures, precipitation, and snow depth to explain the recorded changes in ground temperatures found during the last decades.

*Research area*

Abisko is located in subarctic Sweden and lies within the zone of discontinuous permafrost (Brown et al. 1998). Mountain permafrost determined mainly by air temperatures is found approximately above 880 m a.s.l. (Jeckel 1988), whereas at lower elevations permafrost is only likely to exist in peat mires (due to the peat's insulating effect) and underneath wind-exposed ridges (due to lack of snow) (Johansson et al. 2006). Ground temperatures have been recorded in peat mires around Abisko (Storflaket and Kursflaket, Table 1), which is located in an area of rain shadow, with a mean annual precipitation of 303 mm $a^{-1}$ (1913–2006) and a mean annual air temperature of -0.6°C (1913–2006). In similar climatic conditions 6 km west of the mires at the Abisko Scientific Research Station, ground temperatures have been recorded in an area currently without permafrost (Abisko AWS, Table 1).

Table 1. The location, depth of measurements and observation periods for the four sites.

| Site name | Coordinates (Lat/Long) | Measured at depth (m) | Observation period |
|---|---|---|---|
| Storflaket mire | 68º20′51″N 18º57′55″E | 0, 0.5, 1, 1.5, 2, 3, 4, 5, 6, 7, 8, 9, 12 | 1980-1982, 1984-1989, 1994-1997, 2000-2002 |
| Katterjokk mire | 68º25′31″N 18º10′29″E | 0, 0.5, 1, 1.5, 2, 3, 4, 5 | 1980-1982, 1984-1989, 1994-1998, 2000-2002 |
| Kursflaket mire | 68º21′05″N 18º52′42″E | 0, 0.5, 1, 1.5, 2, 3, 4, 5, 6, 7, 8, 9, 12, 15 | 1980-1982, 1984-1989, 1992, 1994-1997, 2000-2002 |
| Abisko AWS (Automatic Weather Station) | 68°21′20″N 18°49′14″E | 0.05, 0.2, 0.5, 1 | 1985 until present |

In addition, ground temperatures have been recorded at a mire located 35 km west of Abisko (Katterjokk, Table 1). Due to a very strong climatic gradient that occurs in the area, this site experiences a maritime climate with a mean annual precipitation of 848 mm $a^{-1}$ and a mean annual air temperature of –1.7°C (1960–1990: Alexandersson et al. 1991). The depth of the peat is similar at all mires ~90 cm and is underlain by silt.

Snow depth in winter has increased by 2 cm/decade from 1913 until present in the area, but no statistically significant trend was detected in the start and end date of the snow season (Kohler et al. 2006).

The depth of permafrost ranges from a few meters in the mire located west of Abisko down to 16 m in the other mires close to Abisko (Akerman & Johansson submitted).

## Methods

*Air temperature monitoring*

Air temperatures have been recorded manually at the Abisko Scientific Research Station from 1913 until present (at the outset, every third hour using the same method as used at the Swedish Meteorological and Hydrological Institute, 2 m screen air temperature). In 1984 an automatic weather station was installed and air temperatures have been recorded automatically every 10 minutes since then.

*Ground temperature monitoring*

At the mires, Copper-Constantan thermocouples were installed in boreholes at depths described in Table 1 and ground temperatures were recorded hourly, the third week of May and September using Campbell loggers.

At Abisko AWS, ground temperatures were recorded using a resistance temperature sensor Pt100 that was connected to an Automatic Weather Station. Data was recorded automatically every 10 minutes.

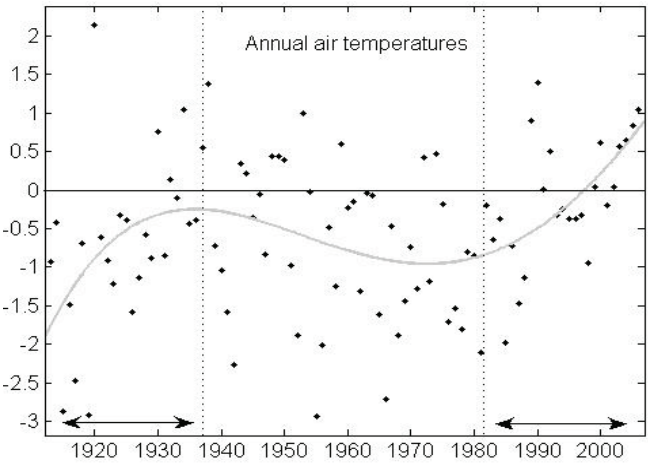


Figure 1. Annual air temperatures and a 4th degree polynomial fit from the Abisko Station, 1913 to 2006. The vertical dotted lines depict the two warming periods for which independent regression analysis was performed.

*Data analysis – determining trends and attributing causes of the observed changes*

Trends were calculated for the ground temperatures from the three mires and from the Abisko Station by using a robust linear regression, as implemented in the software package MATLAB R2006a. Trends were assumed to be significant for $p$ levels $\leq 0.05$. For air temperatures a 4th degree polynomial curve fit was used. To attribute the causes of the observed changes in the ground temperatures, correlation between ground temperatures, air temperatures, snow depth, and precipitation were calculated using multiple regressions (REGRESS) also within the software package MATLAB. All data were normalized and standardized prior to analysis.

## Results

*Air temperatures from Abisko*

The mean annual air temperature at Abisko was -0.6°C between 1913 and 2006. The annual air temperatures at Abisko have during the 20th century experienced an increase in the beginning of the century that lasted until the late 1930s, which was then followed by a slight cooling trend until the mid 1970s and then again followed by an increase that is still ongoing. The regressed mean annual air temperature has been below zero degrees more or less throughout the 20th century, but in the last seven years the regressed annual air temperature has increased above the critical 0°C boundary (Fig. 1). There is an increase in air temperatures during the period of observation of 0.03°C $a^{-1}$ (regression estimate of temperatures). Due to the distinct warming and cooling periods that have occurred throughout the last century, the overall increase in air temperature was not statistically significant ($R^2$ 0.20 *p-value* 0.07). However, when analyzing the two warming periods that correspond roughly with the first 26 years of the record and the last 26 years, statistically significant increases were found (0.09°C $a^{-1}$ for 1913–1938

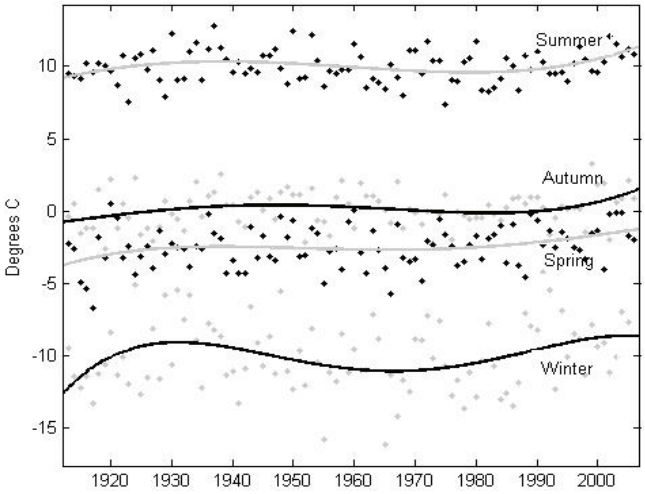


Figure 2. Seasonal air temperatures and a 4th degree polynomial fit from the Abisko Scientific Research Station, 1913–2006.

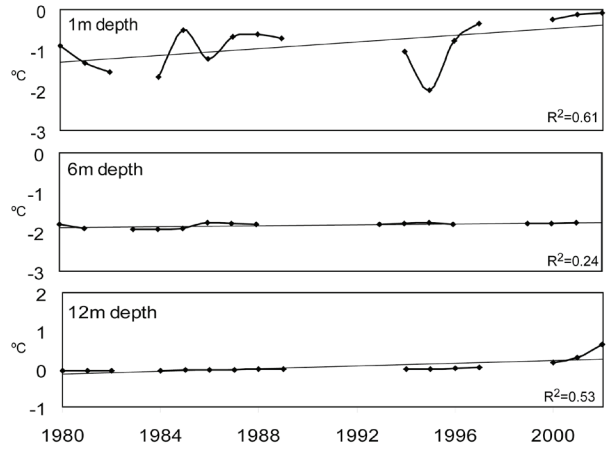


Figure 3. Ground temperatures at 1 m, 6 m, and 12 m depths and linear trends at Storflaket mire measured in September from 1980 to 2002.

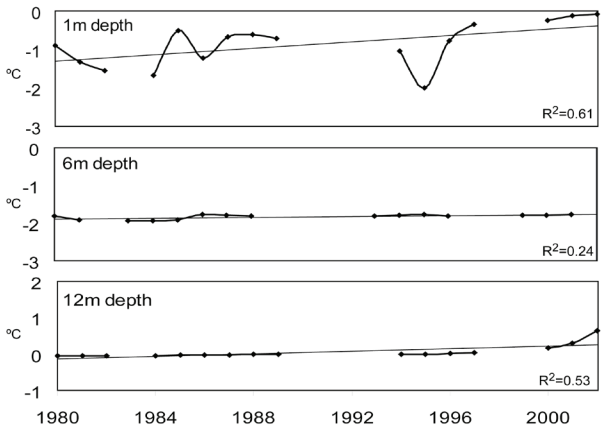


Figure 4. Ground temperatures at 1 m, 6 m, and 15 m depths and linear trends at Kursflaket mire measured in September from 1980 to 2002.

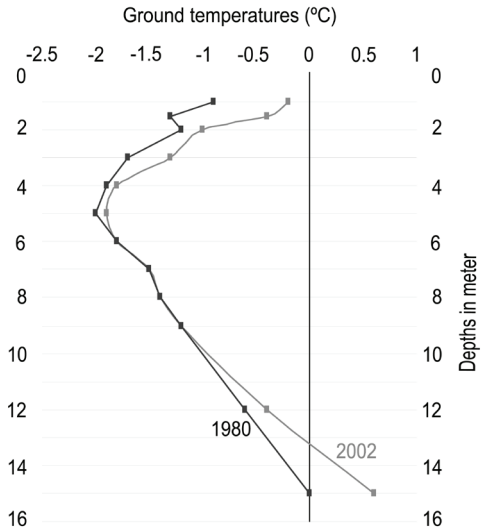


Figure 5. Ground temperatures in September 1980 and 2002 from Kursflaket mire. (Note: There was no subsidence of the ground surface where the temperatures were measured.)

($R^2$ 0.28 *p-value* 0.005) and 0.10°C $a^{-1}$ for 1981–2006 ($R^2$ 0.43 *p-value* 0.001).

For the whole period of observations there has been an increase in air temperatures in all four seasons that follows the same trend as the annual air temperatures (Fig. 2). The largest increases in temperatures are found in winter (December, January and February) 0.04°C $a^{-1}$ (regression estimates), in autumn (September, October and November) and summer (June, July, and August) an increase of 0.02°C $a^{-1}$ was found. Spring (March, April and May) experienced the lowest increase of 0.01°C $a^{-1}$. As the seasonal trends follow the annual trends with increases in the beginning of the century, followed by a cooling period and then again a warming period, the trends in increasing air temperatures are not statistically significant for the whole period of observation at all seasons (MAM $R^2$ 0.06 *p-value* 0.02; JJA $R^2$ 0.003 *p-value* 0.6; SON $R^2$ 0.02 *p-value* 0.19; DJF $R^2$ 0.005 *p-value* 0.48). However, over shorter periods of the temperature records, statistically significant trends, like the increases in the beginning and end of the century can be found. In general it is the lower temperatures that have increased.

*Ground temperatures from the mires*

At Storflaket mire, the ground temperature monitoring has been conducted down to 12 m. There is a statistically significant trend towards warmer September ground temperatures in the upper 1 (0.05°C $a^{-1}$; $R^2$ 0.61 *p-value* 0.004) and the lower 12 m (0.04°C $a^{-1}$; $R^2$ 0.53 *p-value* 0.001) depths. In the middle of the borehole no statistically significant trend could be detected (Fig. 3).

In May, statistically significant increasing trends were found at one (0.09°C $a^{-1}$; $R^2$ 0.38 *p-value* 0.01) and 12 m

Table 2. Regression statistics of ground temperatures between 1985 and 2006 for Abisko AWS including estimates from the regressions of initial and final temperatures and the differences between them.

| Time | Depth (cm) | $R^2$ | *p-value* | Regression estimate of temp °C in 1985 | Regression estimate of temp °C in 2006 | Difference estimated from the regression °C $a^{-1}$ |
|---|---|---|---|---|---|---|
| Annual | 5 | 0.06 | 0.253 | 1.86 | 2.26 | 0.02 |
| | 20 | 0.20 | 0.039 | 1.46 | 2.10 | 0.03 |
| | 50 | 0.29 | 0.009 | 1.44 | 2.23 | 0.04 |
| | 100 | 0.38 | 0.002 | 1.38 | 2.30 | 0.04 |
| Spring (March, April, May) | 5 | 0.01 | 0.744 | -0.56 | -0.40 | 0.007 |
| | 20 | 0.11 | 0.127 | -1.22 | -0.58 | 0.03 |
| | 50 | 0.34 | 0.004 | -1.30 | -0.14 | 0.05 |
| | 100 | 0.49 | 0.000 | -0.84 | 0.28 | 0.05 |
| Summer (June, July, August) | 5 | 0.52 | 0.000 | 9.90 | 7.73 | -0.1 |
| | 20 | 0.40 | 0.002 | 8.23 | 6.45 | -0.08 |
| | 50 | 0.19 | 0.043 | 5.93 | 4.84 | -0.05 |
| | 100 | 0.00 | 0.856 | 3.48 | 3.58 | 0.005 |
| Autumn (September, October, November) | 5 | 0.37 | 0.003 | 1.81 | 3.01 | 0.05 |
| | 20 | 0.48 | 0.000 | 2.07 | 3.41 | 0.06 |
| | 50 | 0.58 | 0.000 | 2.73 | 4.08 | 0.06 |
| | 100 | 0.57 | 0.000 | 3.07 | 4.48 | 0.06 |
| Winter (December, January, February) | 5 | 0.24 | 0.022 | -3.72 | -1.29 | 0.11 |
| | 20 | 0.29 | 0.009 | -3.24 | -0.89 | 0.11 |
| | 50 | 0.34 | 0.004 | -1.59 | 0.14 | 0.08 |
| | 100 | 0.45 | 0.001 | -0.20 | 0.87 | 0.05 |

(0.004°C $a^{-1}$; $R^2$ 0.89 *p-value* 0) depth, but again not for the depths in between.

At Kursflaket mire, ground temperature monitoring has been conducted down to 15 m. The ground temperatures in September have increased in the upper 1 m (0.04°C $a^{-1}$; $R^2$ 0.46 *p-value* 0.003) and in the lower part of the borehole at 12 m and 15 m (0.03°C $a^{-1}$; $R^2$ 0.91 *p-value* 0), while there is no significant trend at depths in between (Figs. 4, 5). In spring no trends were detected at 1 m and 6 m depths. At 15 m there was a statistically significant increasing trend (0.03°C $a^{-1}$; $R^2$ 0.91 *p-value* 0).

At Katterjokk mire the permafrost is very shallow ranging from 2 m to 5 m; hence, no deeper temperature recordings have been made. The same trend as found in the other two mires was detected, with statistically significant increasing ground temperatures in September in the upper 1 m (0.04°C $a^{-1}$; $R^2$ 0.53 *p-value* 0.001); but below no significant trend was detected (Fig. 6). In May, statistically significant trends were detected at both 1 m and 5 m depths, and increases of 0.07°C $a^{-1}$ ($R^2$ 0.66 *p-value* 0.0001) and 0.01°C $a^{-1}$ ($R^2$ 0.71 *p-value* 0), respectively, were recorded.

*Ground temperatures from the Abisko Scientific Research Station*

At the Abisko AWS, the ground temperatures have on an annual basis, increased at all depths (Table 2), but only at 50 cm and 100 cm depth is there a statistically significant trend. In spring, increasing statistically significant trends occur for the same depths, but not in the upper 50 cm. In summer, a decreasing trend in ground temperatures is detected, and down to 50 cm it is statistically significant. In autumn, again we see an increasing trend in ground temperatures, and it is statistically significant for all depths. In winter, there is also an increasing trend that is statistically significant for all depths.

*Correlations of air temperatures and ground temperatures, snow depth and precipitation*

On an annual basis, we could detect a statistically significant correlation between air temperature and ground temperature at Abisko. The highest correlation is found at the 20 cm depth ($R^2$ 0.66) and the lowest, at the 1 m depth ($R^2$ 0.42). The same pattern is detected for the spring. For summer, no correlation could be found between air temperature and soil temperatures. In autumn, statistically significant correlations could be detected at 5 cm ($R^2$ 0.45) and 20 cm ($R^2$ 0.36) depths, but not at lower depths. In winter, statistically significant correlations between air temperature and ground temperature were found at all depths, 5 cm = $R^2$ 0.64, 20 cm = $R^2$ 0.62, 50 cm = $R^2$ 0.55, and 100 cm = $R^2$ 0.45.

No statistically significant correlations were detected between snow depth and the ground temperature in any of the seasons or on an annual basis at the Abisko AWS.

On an annual basis, a weak statistically significant trend could be detected between precipitation and soil temperature at the 20 cm depth, but not at any other depths. In spring, autumn, and winter no correlations between precipitation and ground temperatures were found, but in summer, a statistically significant trend could be detected at 5 cm and 20 cm depths ($R^2$ 0.30 and $R^2$ 0.23).

## Discussion

Mean annual air temperatures at Abisko (Fig. 1) follow the same trend as shown for the Northern Hemisphere (Houghton et al. 2001, IPCC 2007), with a warming period in the beginning of the 20th century continuing until about 1940, followed by slight cooling until the 1970s, and then a second warming period that is still ongoing. Although interannual variation is so large during the last century that the overall increase is not statistically significant, temperature increases are statistically significant in the two warming periods when they are analyzed separately. Similarly, Kohler et al. (2006) did not detect a trend for the whole period (apart from the spring record) but also found statistically significant increases over a shorter time period (1956–2000). The recent increase at the end of the century, mainly due to increases in lower air temperatures, has resulted in a current temperature that is possibly higher than those since at least the Medieval Warm Period (Grudd et al. 2002).

The temporal pattern of mean annual air temperature is repeated in each of the seasons (Fig. 2). For example, Holmgren & Tjus (1996) reported an increase in summer air temperatures from the beginning of the century to about 1940, which was as high as 1.5°C. In addition to the increases in seasonal and mean annual air temperatures, increases in snow depth (Kohler et al. 2006) and active layer depth (Akerman & Johansson Submitted) have occurred in the area.

Increasing ground temperatures could be detected from all four sites, but in the mires, increases in ground temperatures only occurred in the upper and lower parts of the permafrost (Figs. 3, 4). This is accompanied by an increase in active layer depth (Åkerman & Johansson submitted). In the middle, no significant trend was found. Isaksen et al. (2007) also found increases in ground temperatures in mountain permafrost in northern Scandinavia. They detected significant warming down to at least 60 m in depth. Statistically significant correlations were found between the seasonal ground and air temperatures (Isaksen et al. 2007).

We hypothesized that ground temperatures would have been determined by snow depth in addition to air temperatures. This hypothesis was based on studies such as that by Thorn et al. (1999), who worked in a valley close to the Katterjokk mire and concluded that air temperatures could explain as much as 95% of the variance in ground temperatures at shallow depths at some sites. However, at other sites with differing microclimate determined by variation in elevation, aspect, and vegetation cover, air temperatures could only explain as little as 20%. This was suggested to be due to a role of seasonal snow cover (although this was not measured) (Thorn et al. 1999). In addition, Josefsson (1990) found a relationship between ground temperatures and climatic parameters, especially snow cover at four sites near Abisko. Both Thorn et al. (1999) and Josefsson (1991) have interpreted snow cover as one of the most important parameters that determine ground temperatures in our study area.

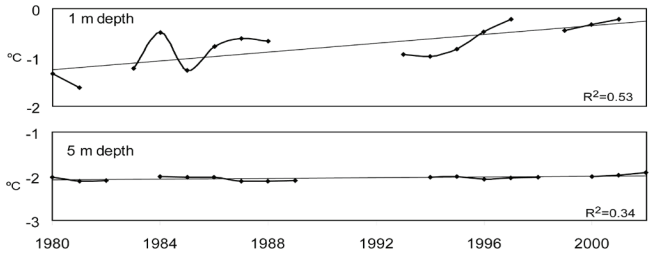


Figure 6. Ground temperatures at 1 and 5 m depth and linear trends at Katterjokk mire measured in September from 1980 to 2002.

We also found correlations between air and ground temperatures. Surprisingly we could not detect any correlation between snow depth and ground temperature even though we used two unique snow datasets from Abisko. Changes in starting and ending dates of snow cover could affect the ground temperatures at Abisko, but no such changes were detected at Abisko (Kohler et al. 2006); hence these cannot explain increases in ground temperatures.

As we found a decrease in summer ground temperatures (Table 2) that could not be correlated to snow depth and air temperature, and the correlations that were found between air temperature and ground temperature explained little of the variance, it can be concluded that other factors also determine the ground temperatures in the Abisko region. The decrease in summer ground temperatures could be caused by a change in vegetation which alters the albedo, shading, and soil moisture. Vegetation has not shifted at the Abisko AWS and, hence, cannot explain the decreasing trend in summer ground temperatures. The decrease in ground temperature was correlated, however, with increases in summer precipitation that have occurred during the last decades. An increase in precipitation increases evaporation which in turn increases the energy consumption resulting in cooler ground temperatures. Similar trends with decreasing summer ground temperatures have been reported from Irkutsk in southcentral Siberia, where they were also attributed to increases in summer precipitation (Zhang et al. 2001b).

The increases in ground temperatures in the lower part of the permafrost might be due to a slight "heat wave" as a result of the warming period at the end of the century. More likely though, there is a possible heating affect from slightly warmer or more freely flowing ground water around and below the frozen bodies of silt and turf. Although, there are no direct measurements of surface and ground water temperatures, temperatures at 12 m and 15 m of just above 0°C indicate that liquid water is flowing at the bottom of the permafrost. However, observations of seasonal variations in ground temperatures at the base of the permafrost are needed to confirm this. If the relatively high temperatures at the base of the permafrost in the mires reflect the movement of liquid water, then the permafrost is even more vulnerable than we first expected because of the influences of warming from above and below.

## Acknowledgments

This work contributes to the IPY "Back to The Future" (BTF; ID No: 512) and we gratefully acknowledge support from the Swedish Environmental Agency (Naturvårdsverket). This work was partly funded by the EU financed project ALARM–Assessing large-scale environmental risks for biodiversity with tested methods, contract no GOCE-CT-2003-506675.

## References

ACIA. 2005. *Arctic Climate Impact Assessment.* Cambridge University Press, 1042 pp.

Akerman, H.J. & Johansson, M. Submitted. Thawing permafrost and deepening active layer in sub-arctic Sweden. *Submitted to Permafrost and Periglacial Processes.*

Alexandersson, H., Karlström, C. & Larsson-McCann, S. 1991. *Temperature and precipitation in Sweden 1961-90 Reference Normals, SMHI Meteorologi Klimasektion* No 81.

Anisimov, O.A., Vaughan, D.G., Callaghan, T.V., Furgal, C., Marchant, H., Prowse, T.D., Vilhjálmsson, H. & Walsh, J.E. 2007. Polar Regions (Arctic and Antarctic). *Climate Change 2007: Impacts, Adaptation and vulnerability*. Contribution of Working Group II to the Fourth Assessment Report of the Intergovernmental Panel on Climate Change. M.L Parry, O.F. Canziani, J.P. Palutikof, P.J. van der Linden & C.E. Hanson, (eds.), Cambridge: Cambridge University Press, 653-685.

Brown, J., Ferrians, O.J., Jr., Heginbottom, J.A. & Melnikov, E.S. 1998. Circum-Arctic Map of Permafrost and Ground-Ice Conditions. In: M. Parsons & T. Zhang (eds.), *International Permafrost Association Standing Committee on Data Information and Communication (comp.)*. 2003. Circumpolar Active-Layer Permafrost System, Version 2.0. Boulder, Colorado: National Snow and Ice Data Center/World Data Center for Glaciology. CD-ROM.

Grudd, H., Briffa, K.R., Karlen, W., Bartholin, T.S., Jones, P.D. & Kromer, B. 2002. A 7400-year tree-ring chronology in northern Swedish Lapland: natural climatic variability expressed on annual to millennial timescales. *Holocene* 12: 657-665.

Holmgren, B. & Tjus, M. 1996. Summer air temperatures and tree line dynamics at Abisko. *Ecological Bulletins* 45: 159-169.

Houghton, J.T., Ding, Y., Griggs, D.J., Noguer, M., van der Linden, P.J., Dai, X., Maskell, K. & Johnson, C.A. (eds.), 2001. *Climate Change 2001: The Scientific Basis*. Cambridge: Cambridge University Press, 881 pp.

IPCC 2007. Climate Change 2007: The Physical Science Basis-Contribution of Working Group I to the Fourth Assessment. In: S. Solomon, D. Qin, M. Manning, Z. Chen, M. Marquis, K.B. Averyt, M. Tignor & H.L. Miller (eds.), *Report of the Intergorvernmental Panel on Climate Change*. Cambridge, United Kingdom and New York, NY, USA: Cambridge University Press.

Isaksen, K., Sollid, J.L., Holmlund, P. & Harris, C. 2007. Recent warming in mountain permafrost in Svalbard and Scandinavia. *Journal of Geophysical Research* 112: F02S04, doi:10.1029/2006JF000522.

Jeckel, P.P. 1988. Permafrost and its altitudinal zonation in N. Lapland. *Proceedings of the Fifth International Conference on Permafrost, Vol. 1, Trondheim, Norway, August 2–5, 1988:* 170-175.

Johansson, M., Christensen, T.R., Akerman, H.J. & Callaghan, T.V. 2006. What determines the current presence or absence of permafrost in the Torneträsk Region, a sub-arctic landscape in northern Sweden. *Ambio* 35: 190-197.

Josefsson, M. 1990. Ground Temperature Variations in a Subarctic Mountain Valley, Abisko, Northern Sweden. *Geografiska Annaler*, Series A 72(2): 179-190.

Kohler, J., Brandt, O., Johansson, M. & Callaghan, T.V. 2006. A long-term Arctic snow depth record from Abisko, northern Sweden, 1913-2004. *Polar Research* 25: 91-113.

Osterkamp, T.E. & Romanovsky, V.E. 1999. Evidence for warming and thawing of discontinuous permafrost in Alaska. *Permafrost and Periglacial Processes* 10: 17-37.

Romanovsky, V.E., Sazonova, T.S., Balobaev, V.T., Shender, N.I. & Sergueev, D.O. 2007. Past and recent changes in air and permafrost temperatures in eastern Siberia. *Global and Planetary Change* 56: 399-413.

Thorn, C.E., Schlyter, J.P.L., Darmody, R.G. & Dixon, J.C. 1999. Statistical relationship between daily and monthly air and shallow-ground temperatures in Kärkevagge, Swedish Lapland. *Permafrost and Periglacial Processes* 10: 317-330.

Walsh, J.E., Anisimov, O., Hagen, J.O.M., Jakobsson, T., Oerlemans, J., Prowse, T., Romanovsky, V., Savelieva, N., Serreze, M., Shiklomanov, A., Shiklomanov I. & Solomon, S. 2005. Cryosphere and hydrology. In: *Arctic Climate Impact Assessment*. Cambridge University Press. 183-242.

Zhang, T., Barry, R.G., Gilichinsky, D., Bykhovets, S.S., Sorokovikov, V.A. & Ye, J. 2001a. An amplified signal of climatic change in soil temperatures during the last century at Irkutsk, Russia. *Climate Change* 49: 41-76.

Zhang, T., Barry, R.G. & Haeberli, W. 2001b. Numerical simulations of the influence of the seasonal snow cover on the occurrence of permafrost at high latitudes. *Norsk Geografisk Tidsskrift* 55: 261-266.

*—Plenary Paper—*

# Permafrost-Related Performance of the Trans Alaska Oil Pipeline

Elden R. Johnson, PE
*Alyeska Pipeline Service Co, Fairbanks, AK*
Lorena A. Hegdal, PE
*Alyeska Pipeline Service Co, Fairbanks, AK*

## Abstract

The Trans Alaska Oil Pipeline System crosses 1287 km (800 mi) of Alaska, from the Prudhoe Bay oil field on the Beaufort Sea (latitude 71°N) to the marine terminal at the ice-free port of Valdez. Approximately 75% of the route consists of permafrost, transecting the full range of conditions from cold, deep and continuous in the north, discontinuous in the interior, and sporadic to frost-free in the south. The pipeline has operated for over 30 years, transporting nearly 2.5 billion cubic meters (16 billion barrels) of warm crude oil in a harsh, technically problematic, and fragile arctic environment. The lifetime operating reliability of the pipeline has been nearly 99%, with only 12 lifetime spills exceeding the 50-barrel definition. This remarkable performance record attests to the functional, environmental and economic success of the project. This paper describes permafrost-related experiences and engineering lessons learned regarding the performance of the pipeline.

**Keywords:** crude oil; lessons; permafrost; pipeline; Trans Alaska Pipeline System (TAPS).

## Introduction

The Trans Alaska Pipeline System (TAPS) is owned by a consortium of major oil companies and operated by the Alyeska Pipeline Service Co, (Alyeska). The route of TAPS spans the full range of permafrost conditions from continuous and cold, to sporadic and marginal. The 48 inch NPS (nominal pipe size, 122 cm diameter) pipeline has transported up to 334 thousand cubic meters per day (2.1 million barrels per day) at peak throughput and currently operates at about 111 thousand cubic meters per day (700 thousand barrels per day). Oil temperatures have ranged from 63ºC (145ºF) at the northern inlet to 7ºC (45ºF) at the southern outlet. TAPS has now transported nearly 2.5 billion cubic meters (16 billion barrels) of crude oil across the State of Alaska since startup in June of 1977. The safe and effective transportation of these huge quantities of warm crude oil over 1287 kilometers (800 miles), 75% of which contains permafrost, was the primary engineering problem faced by the TAPS designers and operators.

Some permafrost related maintenance problems were recognized shortly after startup (Johnson 1983) including buried pipeline settlement; non-condensable gas blockage of thermo-siphons (heat pipes), and buried insulation system failures. Some of these early issues have been resolved as the immediate effect of initial permafrost thawing has diminished over time. Other time-related issues have been corrected by ongoing maintenance programs.

Designing and building a pipeline across the harsh environment of Alaska has distinguished itself as one of the great engineering achievements of history. Many untried and innovative technical solutions were needed. The design was not perfect, however, and has required consistent monitoring and adjustment over the last 30 years. The remarkable success story of TAPS provides important lessons to those planning similar permafrost sensitive pipeline projects in the future.

## Design Challenges

The primary function of the pipeline is to efficiently transport tariff grade crude oil under all environmental and operating conditions experienced over the life of the project. The design life of TAPS was originally stated as 30 years, but as with many infrastructure projects, is now expected to perform well beyond that period (Norton and Miller 2002). In 2004, the federal and state government renewed the grant and lease of pipeline right-of-way for another 30 year period after determining that with proper maintenance the pipeline could safely and efficiently operate for an additional 30 years (Norton et al. 2002).

When oil was first discovered in economic quantities on the North Slope of Alaska in 1968, the pipeline design concept first envisioned consisted of a full length buried pipeline. The pipe itself was purchased assuming a completely buried design. As experts and engineers were engaged, it became clear that warm oil and unstable permafrost were not compatible. The true magnitude of engineering challenge to building a pipeline on permafrost emerged.

The extent and nature of permafrost could not be known until route finding was completed and geotechnical information obtained. Over 5,000 soil borings (1 per 250 m on average) were conducted for characterization and testing of over 15,000 soil samples. Once this information was compiled, frozen and thawed locations could be identified and permafrost found along the route was characterized for engineering purposes as either cold, warm, stable, or unstable.

Permafrost north of the Brooks Range (northern 270 km or 168 miles of the pipeline) was determined to be continuous and cold (Fig. 1). The permafrost temperature on the North Slope is typically about -7ºC near the surface (20ºF) and extends to a depth of nearly 670 meters (2,200 ft). South of the Brooks Range permafrost becomes discontinuous, and then sporadic with varied depth below the active layer.

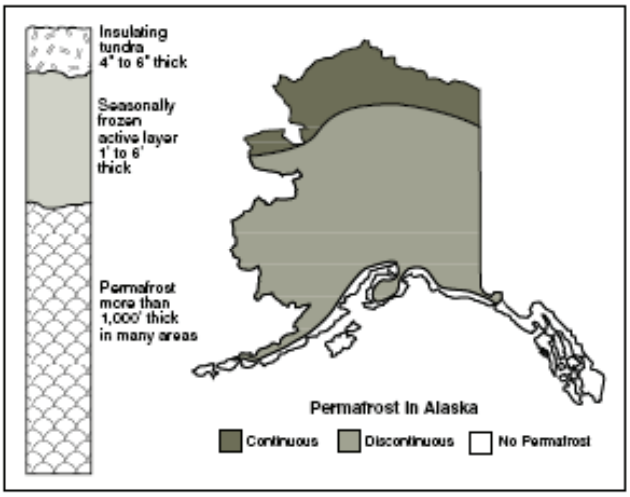


Figure 1. Distribution of permafrost in Alaska.

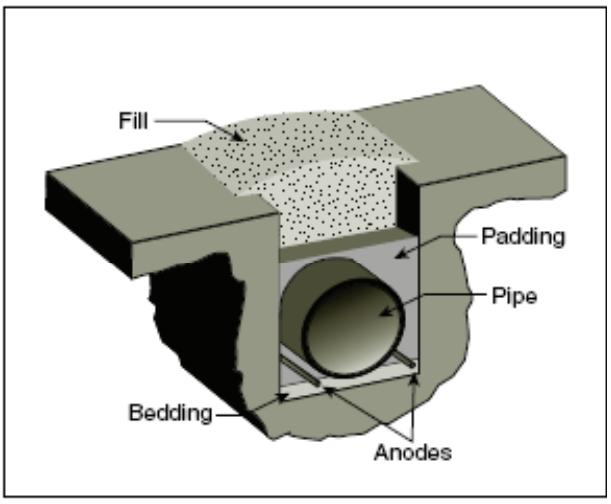


Figure 2. Buried pipeline construction.

Temperatures below the active layer can be near the freezing point and assumed to be -0.3°C (31.5°F) for engineering purposes. Active layer depths vary depending on soil surface material and temperature, from several centimeters to several meters.

Stable permafrost was defined as frozen rock, or clean granular material with no visible ice. Clean granular material was defined as sand or gravel with less than 6% fine material by weight (passing the # 200 sieve). In varied soil profiles, stability was also determined on the basis of a calculated 30-year settlement over the expected depth of thaw of less than 30 centimeters (1 ft).

The key initial design challenge was route finding and mode selection to avoid or minimize the threat to pipeline integrity caused by permafrost. Three basic pipeline design modes were developed and applied depending on permafrost condition (Johnson 1983). These included conventional buried pipelines, above-ground pipeline construction and special insulated buried pipeline construction. Other modes, including bridges and river crossings, special fault crossing, road crossings and animal crossings were employed for unique situations.

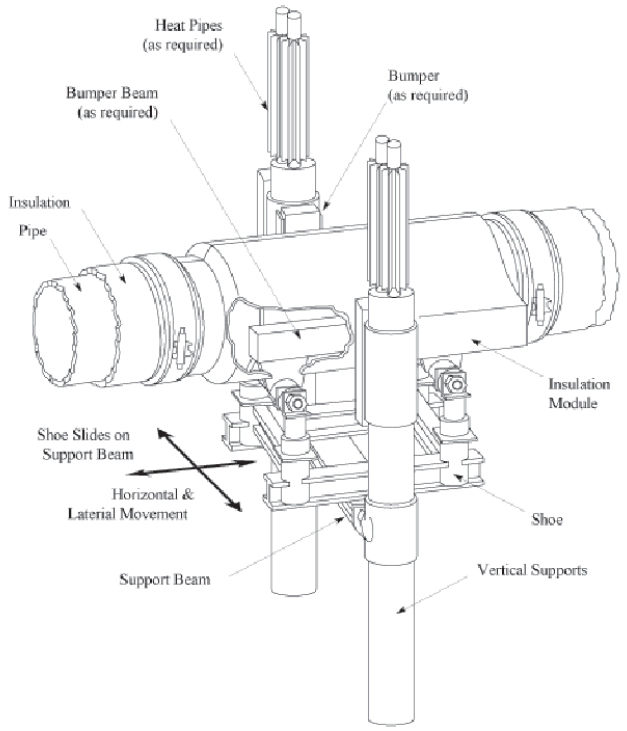


Figure 3. Above-ground pipeline construction.

Buried pipeline construction mode was the preferred mode because it was less costly than others (Fig. 2). The pipeline was buried where thawed or thaw stable ground was encountered. Burial depth averaged 1.5 m (5 ft) and ranged between 1 and 12 m. Buried pipeline required the placement of a cathodic protection system (anodes) to control corrosion. On the North Slope and through mountain passes, the pipeline was often routed along river floodplains because thawed or thaw stable sand and gravel could often be found to allow buried construction. A total of 612 km (380 of 800 miles) or 48% of TAPS was constructed below ground.

The above-ground mode was used where unstable permafrost was encountered. This design avoids permafrost threats by completely bridging over it (Fig. 3). The elegant zigzag configuration (Fig. 4), with thermo-siphon radiators (heat-pipes) often protruding from support pilings visually distinguishes TAPS from all others and makes it one of the most photographed in the world. The zigzag configuration controls the amount of movement associated with thermal expansion, and limited ground movement (static or dynamic). A total of 676 km (420 of 800 miles) or 52% of TAPS was constructed above ground.

Special design constraints dictated the burial of the pipeline at three locations with unstable permafrost which would normally employ an above-ground design. The above-ground mode was thought to interfere with wildlife migration and was not allowed. In this special buried mode, an insulated pipeline was designed with mechanical refrigeration to maintain frozen conditions below the pipe (Fig. 5).

Figure 4. Zigzag configuration of above-ground pipeline.

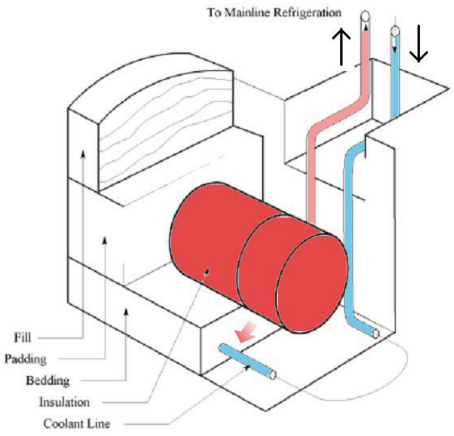


Figure 5. Special buried pipeline construction.

*Other environmental conditions and operating hazards*

A number of additional environmental conditions besides permafrost had to be considered in the design of TAPS. These included natural hazards such as earthquakes, floods, icings, ground movement, extreme weather, fire, corrosion, and material defects. Human related hazards such as incorrect operation, maintenance error, support system structural damage, vehicle or aircraft impact, third party damage, and deliberate sabotage were also considered.

The design of TAPS considered extreme conditions and events which could be expected within the 30-year project life. Design criteria were used to assure the pipeline could withstand normal operating conditions within safe limits, and withstand extreme contingency conditions without failure.

## Operating and Maintenance Experience

Permafrost related operating hazards require ongoing monitoring and maintenance because the nature and magnitude of the threat is constantly changing over time. Alyeska conducts regular monitoring, surveillance, and maintenance activities to inspect the pipeline for changes and to maintain it within specified operating limits. Functional limits are determined for each system component based on principals of Reliability Centered Maintenance (RCM) (Moubray 1997). Monitoring and maintenance strategies are determined based on failure consequence, likelihood, and hazard rate (rate of hazard advance over time such as corrosion or settlement rate).

Monitoring and maintenance strategies are incorporated within written integrity management program procedures. The integrity management plan (IMP) is divided into broad categories for organization and management purposes. The IMP addresses all perceived threats including corrosion, floods, earthquakes, human error, and mechanical breakdown, as well as those related to permafrost. The following integrity management categories are directly or indirectly influenced by permafrost and are described in further detail in the remainder of this paper.

1. Mainline above-ground support systems,
2. Mainline integrity management (curvature, mechanical damage and corrosion),
3. Right of way and facilities civil monitoring,
4. Fuel gas pipeline.

Subject matter experts identified for each program direct scheduled activities, maintain records, assess results and monitor performance. An annual report is prepared to describe previous results, evaluate asset condition, recommend future activities, and recommend improvements in overall program management practice.

*Mainline above-ground support system*

The above-ground support system is a unique component of TAPS which allows it to bridge over unstable permafrost. Were it not for the presence of permafrost, such a support system would not be needed and TAPS would be similar to most other pipelines. Above-ground portions make up 52% of TAPS.

Key system components include the zigzag configuration, intermediate pipeline supports, anchors, vertical support members, and heat-pipes. The zigzag configuration of the pipeline itself (Fig. 4) is designed to allow controlled pipe movement in response to temperature changes or seismic events. Intermediate supports spaced normally every 18 m (60 ft) provide vertical support. Anchors provide for controlled lateral and longitudinal movement and are spaced typically 550 m (1800 ft) apart.

Intermediate supports consist of two vertical support members (VSM) with support brackets, a cross beam, a sliding shoe assembly and intermediate pipe clamp (Fig. 3). The pipe is allowed to slide laterally and longitudinally through the use of low friction Teflon pads. Anchors consist of four vertical support members with support brackets, anchor platform assembly, and anchor clamp. The anchor assembly is designed to release and absorb energy if differential longitudinal loading exceeds the design level.

The primary function of the above-ground system is to support the pipeline under all operating and contingency loadings. Support system components themselves may fail or sustain limited damage during contingency events as long as the pipeline itself does not fail.

Vertical support members (Fig. 6) are the basic units of vertical and lateral support linking the pipe to the ground. VSM consist of 46 cm diameter (18 inch) pipe piles drilled or driven into the ground to a depth which is determined by soil conditions. VSM depths vary between 5 to 15 m (15 to 50 ft) below ground surface with 11 m (35 feet) being the average.

VSM are designed to resist vertical loads in either up or down direction. A typical 2 m (5–7 ft) active layer is assumed to have no load bearing capacity. Upward frost jacking loads are generated in the active layer and control the minimum embedment depth. Vertical loads are resisted in the region below the active layer, by ad-freeze forces where the ground is frozen, and friction forces where thawed. End-bearing resistance is utilized in some cases. The ad-freeze strength used in design is based on a 30 year estimate of viscous creep in frozen soil and depends on permafrost temperature assumptions (warm or cold). A 30-year creep limit of 8 cm (3 inches) of downward movement was used to determine frozen strength.

A total of 78,000 VSM were used in the construction of the above-ground support system. Of these, approximately 97% rely on maintenance of a frozen soil condition for stability. In warm permafrost, heat pipes are used to maintain a permanently frozen condition. VSM with heat pipes are known as thermal VSM (Fig. 6) and make up about 80% of all VSM used. Heat pipes are closed loop, passive heat exchangers, charged initially with ammonia, and now recharged with $CO_2$. They are designed to remove heat in the winter when air temperatures are colder than the ground. They super-cool the soil in the load bearing zone compensating for long term heat loss at the ground surface. A single heat pipe is designed to maintain a frozen condition; two heat pipes are installed in each VSM for redundancy. A total of nearly 124,000 heat pipes were used in the construction of the above-ground pipeline support system.

Above-ground support system components are monitored on a frequency which depends on risk and hazard rate. Monitoring consists of observations which may indicate permafrost degradation such as the following;

1. VSM vertical movement determined by elevation survey, load cell testing, or observed out of level cross beam.

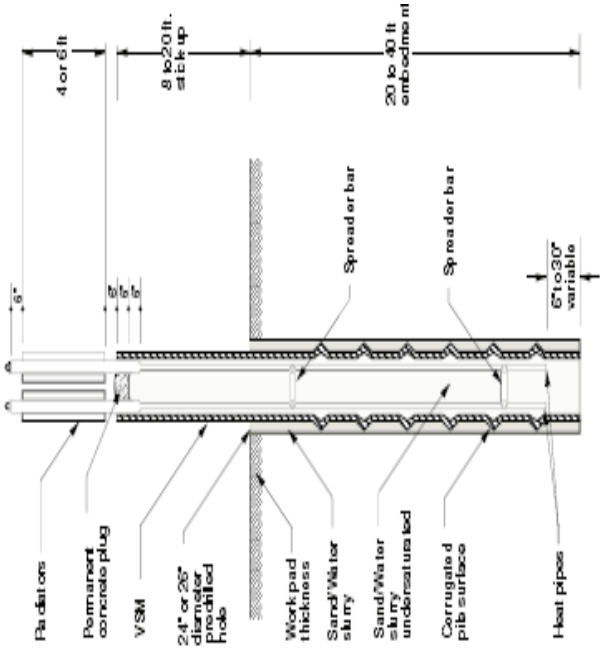


Figure 6. Typical thermal VSM.

2. VSM out of plumb.
3. Heat pipe degradation determined by infrared survey.
4. Tripped anchors, caused by excess lateral load.
5. Intermediate shoes off-center
6. "Floating shoes" not supporting vertical loads.
7. Damaged Teflon sliding base.

Where conditions are observed outside of designated operating limits, maintenance is performed to restore the component to within acceptable parameters. Maintenance may vary from minor adjustments to replacement of system components. A key performance feature of TAPS is its maintainability. Many components are specifically designed for ease of maintenance. The 2007/2008 maintenance year is considered typical of the scale of maintenance activities, consisting of the following;

1. Replace 2 VSM
2. Reposition 4 tripped anchors
3. Load adjust 8 intermediate supports (floating shoes)
4. Repair 9 out-of-location intermediate shoes
5. Replace 1,000 degraded Teflon slide plates
6. Recharge 2,000 degraded heat pipes

Heat pipes have experienced blockage by non-condensable hydrogen gas (a by-product of corrosion). They are monitored by infrared camera able to detect a "cold top" condition indicative of radiator blockage by non condensable gas (Sorensen et al. 2002). Repair of heat pipes is performed by recharging them with $CO_2$. Repairs are prioritized for southern areas where permafrost is marginal, concentrated blockage zones, slopes sensitive to movement, or locations where VSM movement is observed.

The level of maintenance noted above is considered manageable and provides evidence that permafrost degradation is not a current problem in the operation of above-ground portions of TAPS. Increased maintenance

may be anticipated in the future with additional degradation of marginally frozen areas.

*Mainline integrity management*

While the above-ground pipeline avoids most permafrost related risk by bridging over it, the buried pipeline must adapt to differential settlement of the pipeline caused by permafrost thawing. The buried pipeline design required that foundation soils be either thawed or thaw stable. Thousands of pre-construction boreholes and soil tests were conducted to assure that the pipeline was buried only in suitable locations. Boreholes were closely spaced, averaging 250 m (820 ft) along the length of the line, to help detect random pockets of unstable permafrost.

The long-term (30-year) thaw depth for buried TAPS was estimated to vary from 20 to 37 m (70 to 120 ft) depending on soil type and ice content. Frozen soils were not considered thaw stable if calculated thaw settlement exceeded about 30 cm (1 ft). Geologists logged the pipeline ditch during installation to confirm thaw stability of any frozen soil discovered below pipe depth. The pipeline design had to be radically changed to the above-ground mode on multiple occasions due to the discovery of ice-rich or unstable permafrost.

Some areas of unstable permafrost went undetected in spite of all soil data gathered prior to and during construction. In 1979, after 2 years of operation during the most rapid thaw bulb development, the pipe buckled and leaked at two locations. In each case, short pockets of undetected ice rich permafrost caused approximately 1.3 m (4 ft) of pipe settlement over a span of nearly 122 m (400 ft). The pipe was excavated, encapsulated with a steel sleeve and underpinned using a steel support system to prevent further settlement. One leak location was later cut out and replaced. The other is still operating in a safe and stable condition.

Following these initial leaks, an integrity management program (IMP) was developed to detect, measure and assess other potential settlement locations. The program initially consisted of settlement monitoring rods placed on top of the pipe at suspected locations and extended to the ground surface for survey monitoring. Surveys were used to observe the settlement rate and estimate pipe curvature. Pipe curvature was used as the key performance indicator of potential pipe buckling. The program was also supported by numerous additional soil borings to determine subsurface conditions.

A later enhancement incorporated the use of deformation monitoring, in-line inspection (ILI) pigs (instrumented devices) placed in the pipeline which could detect deformation indicative of incipient buckling. The program was instrumental in detecting a dozen locations requiring repair in the decade between 1980 and 1990.

Later in the 1990s, curvature/deformation in-line inspection tools using inertial guidance systems were developed for use on TAPS. These tools are capable of accurately detecting and measuring high curvature areas (Hart et al. 2002).

Settlement repairs initially involved extensive structural support systems, or excavation and replacement in an above-ground mode. One solution involved the use of chemical grouting, and active ground freezing (Thomas et al. 1982) to restore a frozen condition, and then supplemented with numerous free standing heat pipes to permanently maintain the frozen ground. Another solution where the pipe had settled up to 4.6 m (13 ft), involved abandonment of a short section of buried pipeline and replacement with an 800 m (0.5 mile) section of elevated pipe (Simmons & Ferrell 1986). Less severe settlement locations were corrected by excavating the pipe and returning it to a safe curvature using either mechanical lifting or air bags. A detailed description of pipeline settlement repairs is provided by Ferrell and Thomas (1988). Only about 1.5 km out of 612 km (0.9 miles of 380 miles) or 0.25%) of buried pipe required maintenance as a result of permafrost subsidence.

Now with diminished pipeline throughput, the oil takes longer to reach Valdez and thus experiences greater environmental cooling. The thaw bulb below the pipeline has reached its maximum extent and is no longer growing by an appreciable amount. A concern for future low throughput conditions if oil temperatures drop below freezing, is that frost may penetrate to pipe depth, causing increased wax precipitation and freezing of small amounts of water in the oil. In the extreme case, frost jacking forces could develop if frost penetrates below pipe depth.

The special buried insulated pipeline mode presented a different set of permafrost related issues. An annular, shop fabricated, close-celled polyurethane insulation, encapsulated by a fiber reinforced plastic (FRP) outer jacket was used to insulate unstable permafrost from the heat of the pipe. Brine refrigerant is circulated in 15 cm (6 in) diameter refrigeration piping placed below the mainline pipeline (Fig. 5). Refrigeration plants continuously operate to circulate chilled brine. This design relies on the FRP outer jacket to maintain a waterproof pipe environment. This mode is used on about 6 km (4 miles) of the pipeline.

In some cases the FRP outer shell has not effectively prevented water ingress into the insulation. The insulation has become wet, losing its thermal resistance, and causing increased thermal demand on the mechanical refrigeration plants. Refrigeration plants have had to be overhauled and upgraded. Water ingress has also created pipe corrosion concerns that have required excavation, inspection and replacement of the insulation system. Cathodic protection has been added to control corrosion as part of the repair.

*Right of way and facility maintenance*

The pipeline work pad used for access during construction and maintenance was constructed on permafrost, roughly in proportion to the construction mode mix (52% above ground, 48% buried). Five of the 10 original pump stations were constructed on unstable permafrost. Several integrity and maintenance related concerns have been identified in conjunction with permafrost along the right of way and at facilities.

A total of 55 sensitive pipeline slopes were identified where

soil instability could pose a threat to the pipeline. Many of these slopes depend on frozen ground to assure continued stability. Of the 55 sensitive slopes, 6 were deemed high priority and subject to special slope monitoring activities. Maintenance has been required (Tart & Ferrell 2002), including the replacement of several dozen VSM, drainage enhancements and use of surface insulation and heat pipes to maintain permafrost and control down slope movement.

During design of the pipeline, it was divided into segments based on changes in pipeline risk factors. One concern affecting the design was the potential for soil liquefaction under seismic conditions. The preferred solution for buried pipeline was to place the pipeline at a depth below where liquefaction was predicted to occur. In the above-ground mode, the solution was to either avoid liquefiable soils altogether, or maintain them in a frozen condition.

In November 2002, a 7.9 M earthquake, the largest in the world that year, occurred along the Denali Fault which runs directly under the pipeline (Hall et al. 2003). This large earthquake ruptured the ground 5 m (18 ft) laterally and 1.1 m (3.5 ft) vertically at the fault crossing and produced ground motions slightly in excess of design criteria. The pipeline support system was damaged, but the pipe itself did not leak. The pipeline was shut down for 66 hrs for inspection.

Liquefaction was observed at several locations but all above-ground and buried designs performed within expectations. Following the event, an inertial guidance (curvature/deformation) ILI tool was run to identify areas of hidden damage with none found (Johnson et al. 2003). Also, each of the roughly 1500 original design segments deemed sensitive to liquefaction were reassessed in light of the earthquake experience. One concern was that marginally frozen slopes may have thawed over time, creating increased liquefaction risk. This reassessment is now nearly complete with no unstable areas identified at this time.

The gravel work pad constructed alongside the pipeline for access purposes was designed primarily for short term use during the construction period (Metz 1983). A design objective was to minimize use of hard to obtain gravel materials. In some cases, board stock insulation was used either in the work pad itself or around VSM. The purpose of insulation was to reduce thawing of natural materials to maintain trafficability, while minimizing gravel requirements. It was also used around VSM to minimize active layer depth, decrease jacking loads, and increase lateral load resistance.

Insulation used around VSM has been effective in reducing thaw, but adjacent areas of the uninsulated work pad have settled causing depressions, ponding and limiting access. Maintenance has been required to fill some of the deepest depressions in certain areas.

Pump station facilities were built on permafrost at 5 locations (PS 1, 2, 3, 5, and 6). The remaining pump stations were built on thawed or thaw stable ground. Permafrost pump stations were designed with mechanical refrigeration systems to maintain stability of buildings and piping. Routine survey monitoring is used to determine facility settlement. Settlement of buildings and piping has occurred, in some cases requiring maintenance. Free standing heat pipes have been used to maintain permafrost around buildings.

The most serious challenge for the pump stations has been with the buried annular insulated systems similar to those used on the mainline. Water has penetrated the outer jacket, wetting the insulation and creating corrosion concerns. Nearly all buried insulated facility piping has been excavated and replaced with an "insulated box" system (Johnson 1983). This system uses board stock insulation placed under the pipeline but above the refrigeration piping. Board stock insulation is then placed at the sides of the pipe and the annulus filled with a lean mix concrete grout. Cathodic protection anodes and a CP monitoring system are placed within the grout. Board stock is used to cover the box. This reinsulation system has generally performed well, preventing further thaw settlement and inhibiting corrosion since completion in the early 1980's.

*Fuel gas line maintenance*

Alyeska operates a 238 km (148 mile) long fuel gas pipeline to provide natural gas fuel for turbines at the four northern pump stations. The line is 10 inch NPS (nominal pipe size, 25.4 cm diameter) for the first 55 km (34 miles) and 8 inch NPS (20.3 cm diameter) for the last 183 km (114 miles). The line was constructed in winter with a snow and ice work pad. It was buried to a depth of 1 meter (36 in) in cold unstable permafrost. Board stock insulation was placed at the estimated active layer depth of 46 cm (18 inches) over the line to help maintain it in a continuously frozen condition at pipe depth.

The gas line is placed adjacent to the Dalton Highway for much of its route. Disturbance of the surface soil during construction combined with dust from the highway has increased surface heat exchange, and caused a deepened active layer in places. Disturbance of drainage paths has caused some erosion and ponding of water over the line. The gas is chilled to -2ºC (28ºF), but chiller upsets have occasionally allowed periods of above freezing gas temperature (0º–20ºC or 32º–68ºF) in the summer.

The overall affect has been a long term deterioration of permafrost in some locations, subsidence of the surface, and thawing to a depth at or below pipe depth in some places. This has resulted in heaving of the line due to thermal expansion, frost jacking during freeze-back and loss of cover over the pipe. However, there has never been a gas line leak from the pipe.

Maintenance activities have consisted of excavation and reburial of the line to repair heaving locations, and/or replacement of fill over the line to restore depth of cover. Maintenance resulting from permafrost degradation has been required on 10%–20% of the line, primarily where it runs next to the Dalton Highway.

## Lessons Learned: TAPS and Permafrost

Over 30 years ago the owners of TAPS faced the daunting task of engineering and building a pipeline across the breadth of Alaska under harsh arctic conditions along a route consisting mostly of permafrost. A project of this nature had

never before been done. The wisdom of the project was severely questioned at the time, all the way to the President of the United States who authorized it in 1973 only after a tie-breaking vote in Congress. Public expectations were expressed for the highest level of environmental and pipeline safety performance and enforced by strict government agreement and regulation.

The operating history of TAPS now reveals that a warm oil pipeline can be constructed and operated on permafrost. The Trans Alaska Pipeline has been a huge and persistent success over its more than 30 year operating life. It has transported between 10% and 25% of the US domestic crude oil supply, providing a measure of energy security to the people of the United States. It has produced revenues to the State of Alaska to operate the government, generating 80% of the budget, while contributing to a $40 billion Permanent Fund paying annual dividends to Alaska citizens.

Only two pipeline leaks are attributed to permafrost, a 636 cubic meter (4,000 bbl) spill and a 238 cubic meter (1,500 bbl) spill, both occurring in 1979. Careful monitoring and maintenance has been required to mitigate the affects of permafrost hazards. The scale of maintenance attributed to permafrost has been reasonable and manageable, historically estimated to range between 5% and 10% of operating costs. A notable sum, but small compared with the overall benefit generated by the pipeline.

The following lessons regarding TAPS and permafrost are summarized based on the author's experience.

1. The TAPS above-ground design has performed all its functions with relatively minimum maintenance. Its robust and redundant design, built for maintainability, is a beautiful thing in both form and function.
2. The TAPS buried design is more sensitive to permafrost than the above-ground design, requiring comparably more maintenance to address permafrost issues. It is difficult, if not impossible, to find all random pockets of unstable soil using preconstruction boreholes and close construction inspection. Less than 1% of the buried pipeline has required maintenance associated with permafrost subsidence. The advent of inertial instrumented In-Line-Inspection (ILI) tools effectively detects subsidence locations, allowing preventive maintenance to be performed and mitigating subsidence risk.
3. The TAPS special buried, insulated and refrigerated design is maintenance intensive and recommended only as a last resort. Mechanical refrigeration is costly to operate, and buried insulation can not be made reliably waterproof. Wet insulation not only aggravates thaw subsidence, but contributes to corrosion problems which are very difficult to mitigate with cathodic protection. The environmental benefit afforded by this design in facilitating animal migration is questionable.
4. Permafrost related operating hazards require ongoing monitoring and maintenance because the nature and magnitude of the threat is constantly changing over time. An integrity management plan is needed to identify risks, assess condition, and outline permafrost related maintenance options.
5. Any global climate change is not expected to threaten the future operation or integrity of TAPS. Increased maintenance may be expected on above-ground portions, and possibly buried insulated portions especially in marginally frozen southern zones. The above-ground design readily accommodates maintenance and should not experience significantly increased risk. Permafrost risks on buried portions have been largely diminished as thawing has reached its maximum extent.
6. The TAPS fuel gas line provides a small scale view of problems to be anticipated by a larger gas transmission pipeline. More than 10% of the gas line has required permafrost related maintenance attention. The tundra is fragile and is degraded by many construction and operating factors.

Final advice for arctic pipeline engineers is summarized in the words of Dr. Harold Peyton, acclaimed pioneering designer of TAPS: "Engineers must balance the heat flow equation or Mother Nature will do it for them."

## Acknowledgments

The authors wish to thank Alyeska Pipeline Service Company for permission to publish this paper and reviewers for their thoughtful comments and suggestions. Additional details of the history and performance of the pipeline can be found on the corporate web site (Alyeska, the Facts 2007).

## References

Alyeska Pipeline Service Co. 2007. *The Facts, Trans Alaska Pipeline System,* publicly available at Alyeska-pipe.com.

Ferrell, J.E. & Thomas, H.P. 1988. Remedial Solutions for Pipeline Thaw Settlement. International Conference on Pipeline Infrastructure.

Hall, W.J., Nyman D.J., Johnson, E.R. & Norton, J.D. 2003. Performance of the Trans Alaska Pipeline in the Nov 3, 2002 Denali Fault Earthquake. *6th US Conference on Lifeline Earthquake Engineering.* American Society of Civil Engineers (ASCE) Technical Conference, Long Beach CA.

Hart, J.D., Powell G, Hackney, D. & Zulfiqar, N. 2002. Geometry Monitoring of Trans Alaska Pipeline. *11th International Conference on Cold Regions Engineering,* Anchorage AK.

Johnson, E.R., Metz, M.C. & Hackney, D.A. 2003. Assessment of Below Ground Trans Alaska Pipeline Following the Magnitude 7.9 Denali Fault Earthquake. *6th US Conference on Lifeline Earthquake Engineering.* ASCE Technical Conference, Long Beach CA

Johnson, E.R.. 1983. Performance of the Trans-Alaska Oil Pipeline. *Proceedings of 4th International Conference on Permafrost,* Fairbanks AK. National Academy of Sciences, 109-111.

Metz, M.C. 1983. Pipeline Workpads in Alaska. *Proceedings of 4th International Conference on Permafrost,* Fairbanks AK. National Academy of Sciences, 106-108.

Moubray, J. 1997. *Reliability Centered Maintenance,* 2nd Edition, Industrial Press, Inc.

Norton J.D. & Miller J. 2002. Useful Life of Trans Alaska Pipeline, *11th International Conference on Cold Regions Engineering,* Anchorage AK.

Norton, J.D., Jokela, B., Hass, E. & Dugan, R. 2002. Environmental Impact of 25 years of Trans-Alaska Pipeline Operation. *11th International Conference on Cold Regions Engineering,* Anchorage AK.

Simmons, G.G. & Ferrell, J.F. 1986. Alyeska Reroutes Trans Alaska Pipeline at MP 200. *Proceedings of Fourth International Conference on Cold Regions,* ASCE Anchorage, AK.

Sorensen, S., Smith, J. & Zarling, J. 2002. Thermal Performance of TAPS Heat Pipes with Non Condensable Gas Blockage. *11th International Conference on Cold Regions Engineering,* Anchorage AK.

Tart, R.G. & Ferrell, J.F. 2002. Performance of the Squirrel Creek Slopes on Discontinuous Permafrost. *11th International Conference on Cold Regions Engineering,* Anchorage AK.

Thomas, H.P., Johnson, E.R., Stanley, J.M. & Shuster, J.A. 1982. Pipeline Stabilization at Atigun Pass. *Proceedings of the Third International Conference on Ground Freezing,* Hanover NH.

# The Impact of Light-Colored Pavements on Active Layer Dynamics Revealed by Ground-Penetrating Radar Monitoring

Anders Stuhr Jørgensen
*Arctic Technology Centre, Department of Civil Engineering, Technical University of Denmark, DK-2800 Kgs. Lyngby, Denmark.*

Thomas Ingeman-Nielsen
*Arctic Technology Centre, Department of Civil Engineering, Technical University of Denmark, DK-2800 Kgs. Lyngby, Denmark.*

## Abstract

Ground-penetrating radar (GPR) has been used to study the variations in the depth of the frost table throughout a complete thaw-freeze season at Kangerlussuaq Airport, western Greenland. In autumn 2000, three test areas were painted white on the parking area of the airport in order to reduce further development of depressions in the asphalt pavement. One of these areas has been used in the GPR investigations to compare the variations of the frost table underneath a normal dark asphalt surface to that below a more reflective surface. Results clearly indicate a correlation between the use of the reflective surface and a reduced depth of the frost table. In late summer, the difference in the depths of the frost table is approximately 0.9 m. The results should promote interest in the development and use of light-colored pavement materials.

**Keywords:** active layer; ground-penetrating radar; permafrost; reflective surface.

## Introduction

The presence of permafrost is an important aspect in civil engineering in arctic regions. Thawing of ice-rich permafrost leads to consolidation of the active layer above. The construction of road and airport embankments changes the thermal regime of the ground, and may lead to permafrost degradation under or adjacent to such structures. This problem is now amplified by the effects of climate warming. Mapping the lateral and vertical extent of permafrost as well as actual ice-content is, therefore, an important part of geotechnical site investigations in arctic regions. Ground-penetrating radar (GPR) has proved to be a useful method for mapping the distribution of permafrost (Annan 2002, Annan & Davis 1976, Pilon et al. 1992); especially the frost table is often observed as a strong reflection in the GPR data (Jørgensen & Andreasen 2007, Ingeman-Nielsen 2005, Arcone et al. 1998). Thus, repeated GPR surveys can reveal yearly variations in thickness of the active layer.

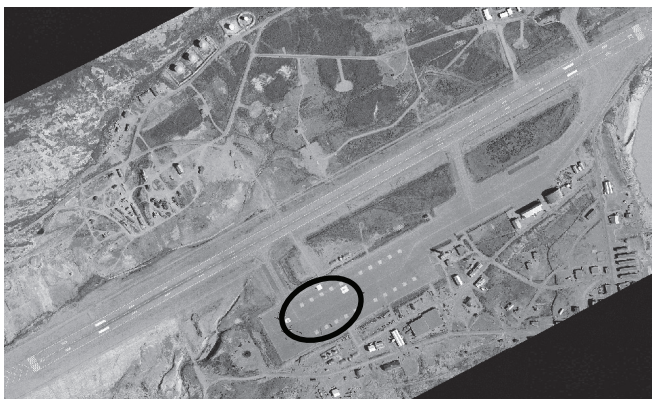

Figure 1. Kangerlussuaq Airport. The investigated area is surrounded by the circle.

This paper is based on repeated GPR investigations from May until October 2007 on the southern parking area at Kangerlussuaq Airport, western Greenland (Fig. 1). The objectives of the measurements were to study variations in the depth of the frost table throughout a complete thaw-freeze season and to compare the differences of the depth underneath a normal dark asphalt and a more reflective surface (a white painted area).

## Site Description

Kangerlussuaq Airport is built on a river terrace (altitude 30–50 m) at the head of the 170 km long fjord, Kangerlussuaq (Søndre Strømfjord), located just north of the Polar Circle at 67°00′N and 50°42′W. In the western part of the area the terrace is made up of fine-grained glaciomarine sediments partly covered with fluvial deposits of sand and gravel. In the eastern part fine-grained marine deposits are absent.

The climatic conditions at Kangerlusssuaq are arctic continental, determined by its northern location and its position in a 2-3 km wide valley surrounded by mountains (plateau altitude 400–600 m). To the east the Greenlandic ice sheet, with altitudes up to 3 km, has a dominant influence on precipitation and winds. These conditions result in a dry sub-arctic climate with winter temperatures down to -40°C (-40°F) and summer temperatures up to 20°C (68°F). From 1977–99, the mean annual temperature was -5.7°C and the mean annual precipitation was 151 mm (Danish Meteorological Institute 2007). Since the middle of the 1990s the mean annual temperature in Kangerlussuaq has increased to -4.0°C (Fig. 2). Nevertheless, Kangerlussuaq is still underlain by 100-150 m of continuous permafrost (Tatenhove & Olesen 1994). The entire active layer is frozen during the winter, but in late summer the depth of the frost

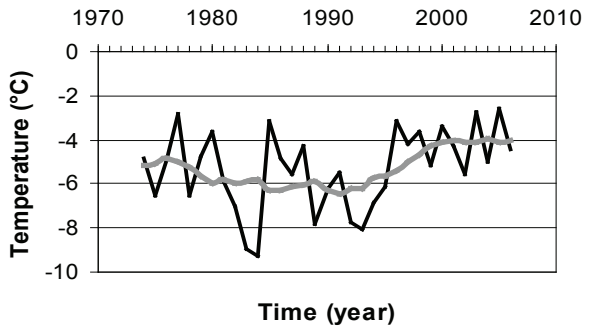


Figure 2. Mean annual air temperature (black) and nine year average temperature (gray) in Kangerlussuaq, 1974-2006 (Danish Meteorological Institute 2007).

table is up to 3.0 m in the open terrain (Ingeman-Nielsen et al. 2007). However, under areas covered with asphalt the depth of the frozen surface is greater, and in some areas this causes melt-water to concentrate under the pavement.

## Methodology

In the period from May until October 2007, eight GPR investigations were carried out at the southern parking area of Kangerlussuaq Airport (Fig. 1). In addition, one investigation was carried out in July 2005 and three investigations were carried out in a period from May until August 2006 (Jørgensen & Andreasen 2007, Jørgensen et al. 2007).

GPR systems produce a short pulse of high frequency electromagnetic energy which is transmitted into the ground. The propagation of the signal depends on electrical properties of the ground, which are mainly controlled by the water content of investigated materials. Changes in the dielectric properties will cause a reflection of parts of the transmitted signal, while the rest of the signal will continue to propagate into the ground. Reflection will occur at each successive interface in the ground, until the signal has been damped by losses in the ground. The reflected signal is detected by the GPR receiver, and travel times for individual radar waves can be used to display the results in a radargram, in terms of received amplitude as a function of travel time.

Results from a GPR investigation give insight into the structural changes in the ground but do not directly show the composition or type of the materials investigated. To calibrate the GPR results from Kangerlussuaq Airport, a borehole was drilled and a trench was dug in August 2005.

We applied a GSSI Model SIR-20 with two ground coupled 400 MHz and 900 MHz (GSSI Model 5103 and GSSI Model 3101) antennas. All measurements were conducted along the same profile (Figs. 3A, 3B) with the antennas towed about 3 m behind a car. The GPR profiles were recorded by survey wheel, and traces were collected every 0.05 m (20 traces per meter).

The post-processing included band-pass trace-filtering to reduce electronic and antenna-to-ground coupling noise, spatial filtering to remove coherent background noise, and

Figure 3A. White painted asphalt surface on the southern parking area of Kangerlussuaq Airport.

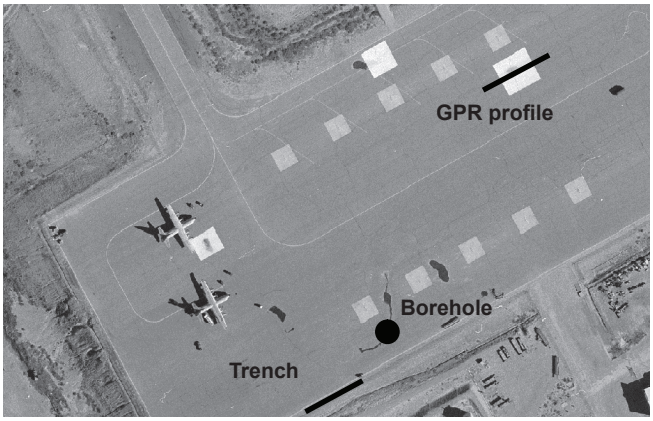


Figure 3B. Placement of GPR measurements across the white painted asphalt surface shown in Figure 3A. The location of the trench and borehole is also shown.

a running average to make a horizontal smoothing of the recorded signal. The processing was carried out using the program ReflexW 3.5 from Sandmeier Scientific Software.

## Results

Figure 4 illustrates the difference in the depth of the frost table underneath the normal black asphalt surface and the more reflective surface (white painted area). The variations of the depth of the frost table throughout the thaw-freeze season are illustrated in Figure 5.

According to borehole data from August 2005, top soils were unsaturated and unfrozen until a depth of 3.5 m. The trench revealed a depth of the frost table close to 4.0 m. The velocity of the radar waves in the unfrozen sediments underneath the southern parking area was estimated to be 0.13 m/ns by combining the GPR results with the results from the borehole logs and the trench.

The GPR results (Fig. 5) illustrate the progressive lowering of the frost table. The results also show the effect of the white surface on the depth to the frost table. The fact that the changes in depth to the strong reflection on the radargrams are aligned with the boundaries of the painted area (26 m wide) confirms that this reflection is actually the interface between the frozen and unfrozen ground.

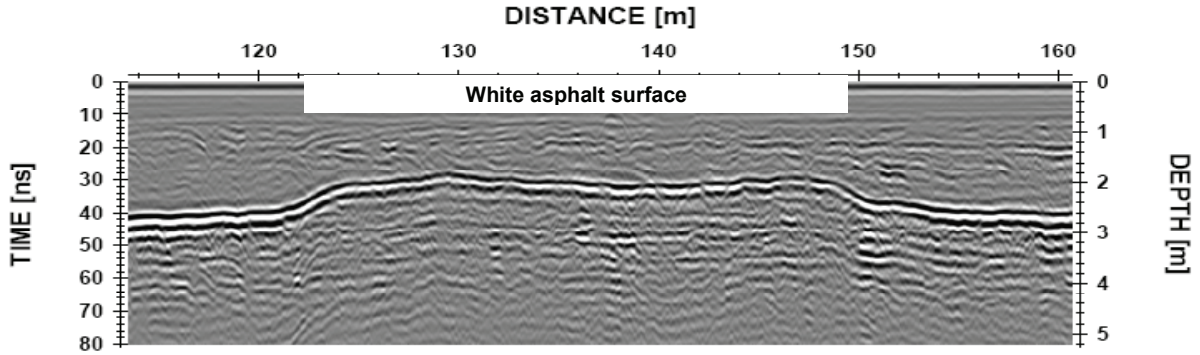


Figure 4. Radargram from July 2007 showing the depth of the frost table. The frost table is seen as a strong reflector in the depth of approximately 2.7 m underneath the normal dark asphalt surface (left and right parts of the radargram) and 2.1 m underneath the white painted area (middle of the radargram).

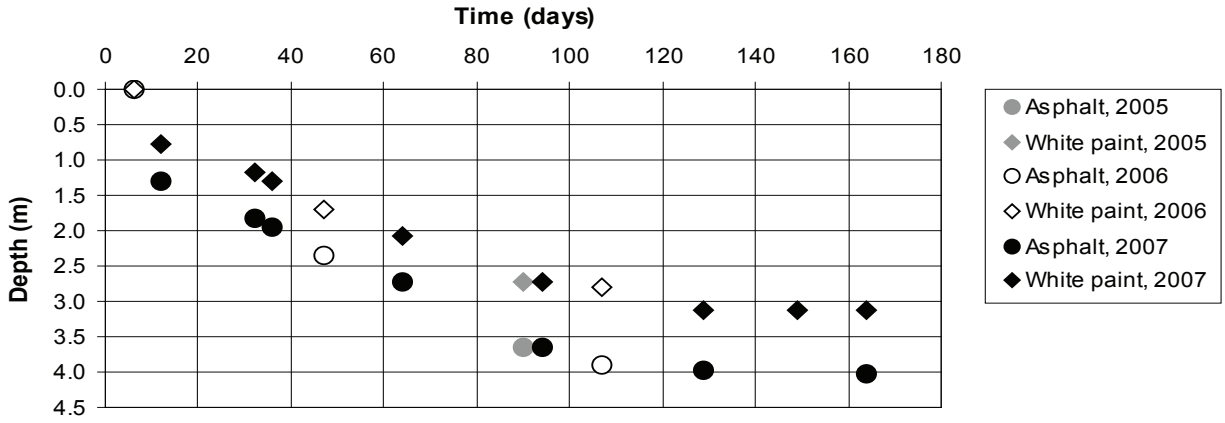


Figure 5. Variations of the depth of the frost table underneath the normal black asphalt surface and the white painted area. The time is shown as number of days from May 1st.

It appears that a stable situation is approached underneath the surfaces between the two measurements carried out in September (Fig. 5). The maximal difference between the depths to the frost table is found as approximately 0.9 m at the end of the thawing period (Fig. 5).

## Discussion

We have performed GPR measurements across a reflective surface (white paint) eight times in the period from May until October 2007. The measurements have shown a clear correlation between the use of the reflective surface and a reduced depth to the frost table. At the end of the thawing period the difference in the depths to the frost table is approximately 15 ns.

Based on borehole information, the measured depth of the frost table (procured by the trench excavation) and GPR data collected at the locations of the borehole and the trench in August 2005, the radar wave velocity in the unfrozen sediments was found to be 0.13 m/ns, which corresponds to a permittivity of 5.3. The top soils at the borehole location were unsaturated sorted sand until a depth of 3.5 m with water content in the range of 2%–5% (Jørgensen and Andreasen, 2007). Using a calibration curve empirically determined by Topp et al. (1980) and soil parameters (density 2.70 g/cm$^3$ and porosity 30%), which is generally used for sandy materials in the area, a permittivity of 5.3 result in a water content of 4.75% for the material. This value lies within the interval of the water content measured in the soil samples from the borehole.

The low water content and well sorted sandy material, which result in a low adherence of the water particles, gives us a situation close to dry conditions and temporal changes in the velocity due to changing pore-water content in the unfrozen sediments were therefore neglected in the present study. An increase in water content will result in an increased permittivity of the material, which will lead to a decreased velocity of the radar waves. A water content of 9.50%, twice the amount of the determined value, would have reduced the maximal difference between the depths to the frost table underneath the two investigated surfaces to approximately 0.2–0.3 m.

Our results have shown that the change in active layer thickness due to the increased reflectivity of surface amounts to approximately 0.9 m in late summer. This constitutes a major difference in the thermal conditions below the reflective surface and the normal dark asphalt surface, and the results should promote interest in the development and use of light-colored pavement materials to reduce settlements under arctic infrastructures caused by the annual thaw-freeze cycle and increasing thickness of the active layer.

## Acknowledgments

This research was mainly funded by the Commission for Scientific Research in Greenland (Kalaallit Nunaani ilisimatuutut misissuinernut kommissioni) and partly funded by the Polar Earth Science Program, Office of Polar Programs, National Science Foundation (ARC-0612533).

We would like to thank the Greenlandic Airport Department (Mittarfeqarfiit) for granting us access to the airport area in Kangerlussuaq, and the Municipality of Sisimiut (Sisimiut Kommunianut) for help with accommodation and transportation.

## References

Annan, P. 2002. GPR – History, Trends, and Future Developments. *Subsurface Sensing Technologies and Applications* 3(4): 253-270.

Annan, P. & Davis, J. 1976. Impulse radar sounding in permafrost. *Radio Science* 11(4): 383-394.

Arcone, S.A., Lawson, D.E., Delaney, A.J., Strasser, J.C. & Strasser, J.D. 1998. Ground-penetrating radar reflection profiling of groundwater and bedrock in an area of discontinuous permafrost. *Geophysics* 63(5): 1573-1584.

Danish Meteorological Institute 2007. Climate data acquired through www.dmi.dk on August 20, 2007.

Ingeman-Nielsen, T. 2005. *Geophysical Techniques Applied to Permafrost Investigations in Greenland*. Ph.D. Thesis. Technical University of Denmark.

Ingeman-Nielsen, T., Clausen, H. & Foged, N. 2007. Engineering geological and geophysical investigations for road construction in the municipality of Sisimiut, West Greenland. *Proceedings, International Conference on Arctic Roads, Sisimiut, Greenland*: 53-61.

Jørgensen, A.S. & Andreasen, F. 2007. Mapping of permafrost surface using ground-penetrating radar at Kangerlussuaq Airport, western Greenland. *Cold Regions Science and Technology* 48: 64-72.

Jørgensen, A.S., Ingeman-Nielsen, T. & Brock, N. 2007. Annual variations of frost table in Kangerlussuaq Airport, western Greenland. *Proceedings, International Conference on Arctic Roads, Sisimiut, Greenland*: 79-83.

Pilon, J. A., Allard, M. & Levesque, R. 1992. Geotechnical Investigations of Permafrost in Ungava with Ground Penetrating Radar. Innovation & Rehabilitation, *Proceedings of the 45th Canadian Geotechnical Conference*, Canadian Geotechnical Society: 19/1-19/9.

Topp, G.C., Davis, J.L. & Annan, A.P. 1980. Electromagnetic determination of soil water content: measurements in coaxial transmission lines. *Water Resources Research* 16(3): 574-582.

Van Tatenhove, F.G.M. & Olesen, O.B. 1994. Ground Temperature and Related Permafrost Characteristics in West Greenland. *Permafrost and Periglacial Processes* 5: 199-215.

*—Plenary Paper—*

# Thermokarst in Alaska

M. T. Jorgenson
*ABR, Inc., Fairbanks, AK 99709*
Y. L. Shur
*Department of Civil Engineering, University of Alaska Fairbanks*
T. E. Osterkamp
*Geophysical Institute, University of Alaska Fairbanks*

## Abstract

Knowledge of the varying surface patterns (landforms), extent, and expansion rate of thermokarst is essential to understanding the response of northern ecosystems to climate change and human impacts. Field studies and airphoto analysis have revealed 22 thermokarst landforms associated with varying heat and mass transfer processes, terrain conditions, and ground ice. These include deep and shallow thermokarst lakes, thaw-lake basins, thaw-lake sinks, thermokarst pits, thermokarst troughs and pits, collapsed pingos, thermokarst shore bogs, thermokarst bogs and fens, thermokarst gullies, thermokarst water tracks, beaded streams, thaw slumps, detachment slides, sink holes and tunnels, glacial thermokarst, collapse-block shores, block landslides, thermokarst conical mounds, irregular mounds, and nonpatterned thawed ground. The extent of permafrost degradation was assessed using airphotos taken across the discontinuous zone, revealing 5% of the area has thermokarst, 62% has permafrost, 21% is unfrozen with no recent permafrost, and 12% remains undetermined. In continuous permafrost of arctic Alaska, thermokarst terrain was evident on 13.5% of the area, and 1.5% was unfrozen under deep non-thermokarst lakes. The rate of degradation based on airphoto analysis at four sites revealed the area affected by thermokarst increased 3.5–8 % over ~50-yr.

**Keywords:** Alaska; classification; degradation; extent rate; permafrost; thermokarst.

## Introduction

Permafrost is an integral component of many northern ecosystems because it supports the ground surface, modifies microtopography, influences soil temperature and moisture, subsurface hydrology, rooting zones, and nutrient cycling (Van Cleve & Viereck 1983, Ford 1987). It is sensitive to climate directly through changes in air temperature, snow cover, or moisture's effects on soil thermal properties, or indirectly from fire frequency or human disturbance with numerous positive and negative feedbacks (Brown and Grave 1979, Osterkamp 1983, Lawson 1986, Esch & Osterkamp 1990, Nelson et al. 2001). Of particular concern for thermokarst, is the warming of permafrost in Alaska by up to 4°C during the last three decades, 2-4°C since the Little Ice Age, and 10°C or more since the end of the Pleistocene (Anisimov & Nelson 1996, Osterkamp 2007). Thawing of ice-rich permafrost can lead to wholesale conversion of ecosystems from terrestrial to aquatic or wetland systems, or conversely cause wetlands to become better-drained (Van Cleve & Viereck 1983, Burn 1998, Osterkamp et al. 2000). In Alaska, 28% of the land has continuous (>90% area), 51% discontinuous, and 8% sporadic/isolated permafrost (Brown et al. 1997).

Where ground ice in fine-grained sediments exceeds the pore space of the soil, thawing of the permafrost can cause the surface to settle or liquefy. The amount of settlement is directly related to the amount and type of ice. These in turn are related to complex interactions of slope position, soil texture, hydrology, and vegetation over time (Shur and Jorgenson 1998). Due to these interactions, the pattern and rate of permafrost degradation can be highly variable. As a result, the nature, extent, and rates of permafrost degradation in Alaska have been poorly quantified.

This paper tries to improve our understanding of thermokarst in Alaska by: (1) classifying and characterizing landforms associated with surface permafrost degradation; (2) estimating the extent of the thermokarst across Alaska, and (3) assessing the rate of degradation in selected areas.

## Thermokarst Landforms

Twenty two thermokarst landforms associated with specific processes of permafrost degradation have been identified based on their microtopography and vegetation characteristics (Shur 1977, Jorgenson & Osterkamp 2005, Jorgenson et al. 2007, Shur & Osterkamp 2007). These are discussed below with respect to their distribution, characteristics, processes, and lateral rates of degradation. Terminology is mostly from Everdingen (1998). We focus here on surface changes, yet recognize that permafrost also can degrade from the bottom and that ice-poor permafrost can degrade without creating visible thermokarst.

Thermokarst lakes (alas lakes) are common throughout Alaska (Wallace 1948, Hopkins 1949, Osterkamp et al. 2000, Yoshikawa & Hinzman 2003, Jorgenson et al. 2006) and northern Yukon (Burn & Smith 1990). In Alaska, they are particularly abundant on the Innoko, Koyukuk, and Yukon Flats in central Alaska, on the Seward Peninsula and Yukon-Kuskokwim Delta in western Alaska, the western

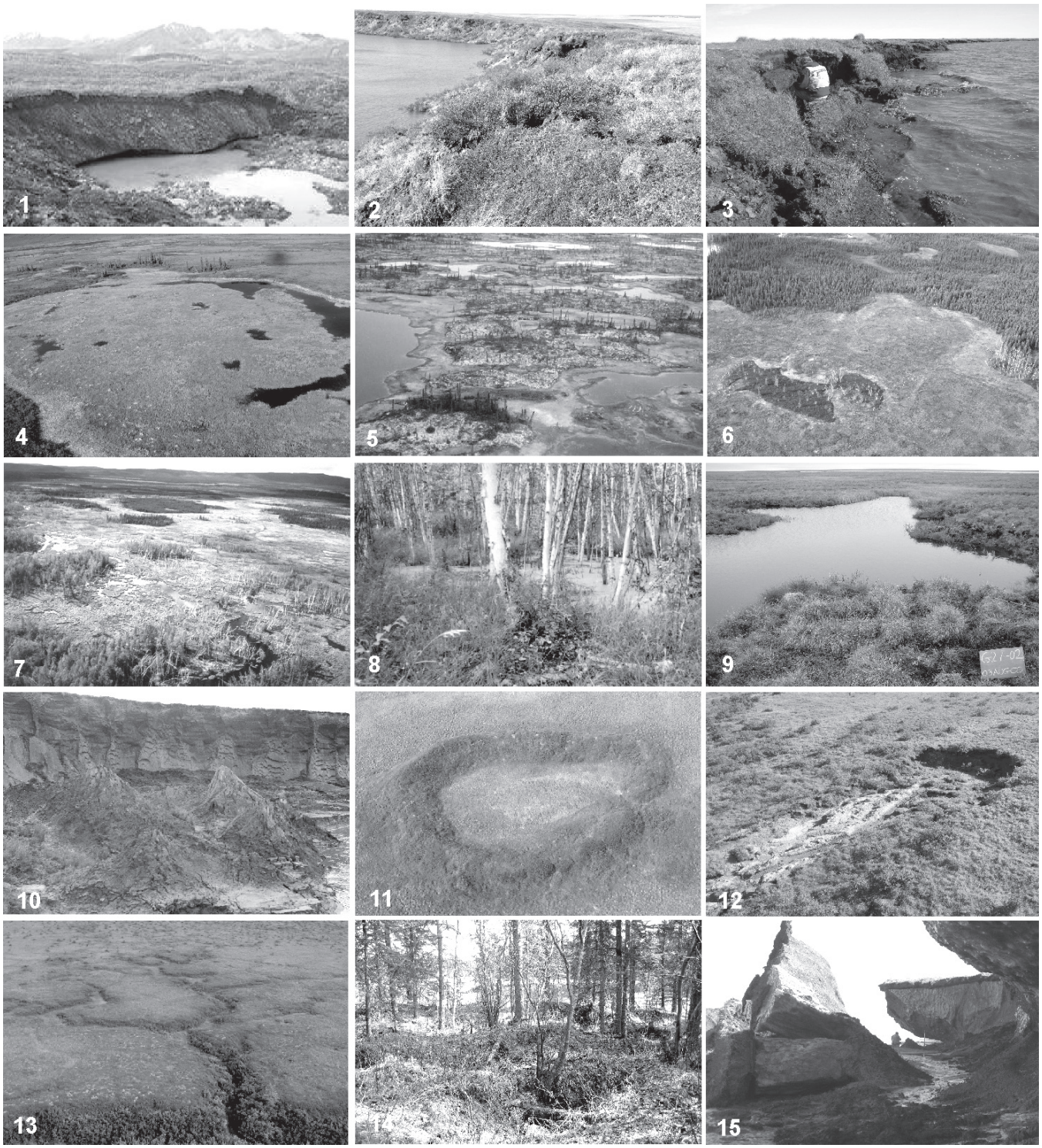


Figure 1. Fifteen thermokarst landforms in Alaska (from left to right on succeeding rows); including: (1) glacial thermokarst on the Muldrow moraine; (2) deep thermokarst lake in yedoma near Cape Espenberg; (3) shallow thermokarst lake near Teshekpuk Lake; (4) thaw-lake basin in Kobuk Valley; (5) thermokarst shore bogs near Innoko River; (6) thermokarst bog in Kobuk Valley; (7) thermokarst fen on Tanana Flats; (8) thermokarst pits on Tanana Flats; (9) polygonal thermokarst trough near Colville Delta; (10) thermokarst conical mounds near Colville River; (11) collapsed pingo near lower Noatak River; (12) thaw slump that started as a detachment slide in Noatak Basin; (13) thermokarst gullies in Kobuk Valley; (14) irregular mounds near Chena River; and (15) collapse blocks undercut by thermo-erosional niche along eroding coast near Cape Halkett.

Beaufort Coastal Plain near Barrow, and the northern Brooks Foothills (Hopkins 1949, Britton 1957, Black 1969, Tedrow 1969, Carter 1988). Permafrost degrades both laterally along the shores, and vertically beneath the water. Rates of lateral degradation range from 0.1 to 2 m/yr depending on ice content, soil texture, and thickness of the surface organic mat, slumping of the banks, and removal of shoreline material by waves. Water depths for shallow thermokarst lakes are typically 1−3 m. Deep thermokarst lakes have water depths >3 m and are classified as a separate thermokarst landform. They typically are found in areas with thick Pleistocene loess deposits, such as at the lower portions of the western Brooks Foothills (Carter 1988) and Seward Peninsula (Hopkins 1949).

Table 1. Thermokarst landforms and processes associated with permafrost degradation.

| Landform | Mass Transfer | Heat Source[1] | Hydrologic Regime | Dominant Ice Type | Typical Size | Settlement (m) | Lateral Rate (m/yr)[2] |
|---|---|---|---|---|---|---|---|
| Deep Thermokarst Lake | Colluvial Waves | Water | Flooded, precip., surface flow | Segregated, ice wedge, other massive ice | 1−1000s ha | 2–10 | 0.5−2 |
| Shallow Thermokarst Lake | Waves | Water | Flooded, precip., surface flow | Segregated and wedge ice | 1−1000s ha | 1–2 | 0.2−2 |
| Thaw-lake Basin | Colluvial Waves | Water | Drained lake, laterally | Same as above | 1−1000s ha | 1–10 | Banks stabilized |
| Thaw-lake Sink | None | Water | Drained out bottom | Same as above | 1−1000s ha | 1–10 | Banks stabilized |
| Thermokarst Pits | None | Still Water | Flooded, precipitation | Ice wedges, thick layered ice | 10s of $m^2$ | 1–2 | na |
| Thermokarst Troughs and Pits | None | Still Water | Partially flooded, precipitation | Ice wedges | 10s of $m^2$ | 0.5–2 | na |
| Collapsed Pingo | None | Still Wat., Air | Flooded to drained | Intrusive Ice | ha | 3–10 | Little after collapse |
| Thermokarst Bogs | None | Still Water | Saturated by precipitation | Thick layered, Reticulate, | ha | 1–2 | 0.1–0.5 |
| Thermokarst Shore Bogs | None | Still Water | Saturated by precipitation | Thick layered, Reticulate, | ha | 1–2 | 0.1–0.5 |
| Thermokarst Fens | None | Flowing water | Groundwater | Thick layered, Reticulate, | 10s of ha | 1–2 | 0.5–1 |
| Thermokarst Water Tracks | None | Flowing Water | Surface flow | Ataxitic, reticulate ice at permafrost surface | 100s of $m^2$ | 0.2–1 | na |
| Thermokarst Gullies | Fluvial | Flowing Water | Surface flow | Ice wedges | 100s of $m^2$ | 1–3 | na |
| Beaded Stream | Fluvial | Flowing Water | Surface flow | Ice wedges | ha | 1–3 | na |
| Sink Holes and Tunnels | Fluvial | Flowing Water | Groundwater | Ice wedges, cave (tunnel) ice | 10s $m^2$ at surface | Pits 2–5 | Little after collapse |
| Thaw Slumps | Colluvial | Air, Water | Surface flow | Ataxitic, reticulate, ice wedges | 100s of $m^2$ | 1−5 | Highly variable |
| Detachment Slides | Colluvial | Air | Drained, surface flow | Ataxitic, reticulate, | 100s of $m^2$ | 0.5–2 | Little after slide |
| Block Landslide | Colluvial | Air | NA | Ice wedges, | 100s of $m^2$ | 3–10 | 2−10 |
| Collapse-block Shore | Colluvial Fluvial | Air | Flowing water, waves | Ice wedges | 10s of $m^2$ | na | 2−10 |
| Conical Thermokarst Mounds | Colluvial | Air | Drained | Ice wedges | 10s of $m^2$ | 2–5 | na |
| Glacial Thermokarst | Colluvial | Air | Flooded by precipitation | Massive glacial ice | 10s of ha | 5–30 | Highly variable |
| Irregular Thermokarst Mounds | None | Air | Drained | Lenticular, Reticulate, Ataxitic | $m^2$ | 0.2–1 | na |
| Nonpatterned Ground (non-thermokarst) | None | Air | Drained, precipitation | Lenticular, Pore | na | <0.2 | na |

[1] Direct solar radiation effects not included. Heat is transferred through soil or sediment in most cases; directly to ice in cliff exposures.
[2] Thaw settlement values, and lateral degradation rates are generalized estimates based on limited data.

Thaw-lake basins develop after a thermokarst lake is breached by stream channels and drained (Britton 1957, Jorgenson et al. 2006). A distinct outlet is evident. They are prevalent in the northern boreal forest transition zone and arctic tundra, in contrast to southern thermokarst lakes, which usually paludify with bog vegetation.

Thaw-lake sink is a special type of thaw-lake basin caused by thawing of permafrost below or surrounding a lake, and drainage through subsurface sediments. These lakes may only partially drain and the water level becomes controlled by groundwater (Yoshikawa & Hinzman 2003). They are particularly abundant on abandoned floodplains on the Yukon Flats, where thick, frozen fine-grained overbank deposits overlie alluvial gravels. Once surface deposits thaw and hydrologic connections are made through the underlying gravel, water drains out the bottom.

Thermokarst pits form as small depressions on ice-rich deposits in the discontinuous zone. They often coalesce to form larger bogs and fens. Degradation is primarily vertical from increases in the active layer, and a talik, the unfrozen zone between the seasonally frozen active layer and the permafrost, quickly develops underneath the pits. Thaw settlement typically is 1−3 m and the pits fill with water.

Thermokarst troughs and pits are abundant in northern Alaska (Black 1969, Billings & Peterson 1980, Jorgenson et al. 2006). They form as a result of the degradation of ice wedges, and at an advanced stage, the thawed ice wedges form a polygonal network of water-filled or drained troughs surrounding high-centered polygons. Degradation occurs vertically as the active layer deepens and melts the underlying ice. Settlement generally is 1−2 m, although in areas where water flow through the trough network reinforces the degradation, settlement may reach 3−4 m. During initial stages of ice-wedge degradation, only scattered pits may be evident where they form at ice-wedge intersections. These features are uncommon in boreal regions due to the sporadic occurrence of ice wedges.

Collapsed pingos form by rapid thawing of massive ice in the cores of the pingos. Water is usually impounded in the center of the collapsed pingo and eventually breaches the rim of thawed material. Pingos are common across northern Alaska (Carter & Galloway 1979), but collapsed pingos are rare, except near the lower Noatak River.

Thermokarst bogs are circular depressions that are widespread on flats throughout central Alaska (Drury 1956, Jorgenson et al. 2001). They are associated with ice-rich, fine-grained soils on abandoned floodplains, lowland loess, and sloping retransported deposits. Vegetation is dominated by ombrotrophic Sphagnum and ericaceous shrubs. Bogs slowly degrade laterally at rates of 0.1−0.5 m/yr and thaw settlement typically is 1−3 m (Jorgenson et al. 2001).

Thermokarst shore bogs occur along slowly degrading margins of shallow thermokarst lakes in the boreal forest region (Drury 1956). Shore bogs are considered distinct because the bogs can expand both into the lake and outward toward the collapsing margin. Thus, the lakes may appear to shrink due to paludification even as the adjacent permafrost continues to degrade.

Thermokarst fens occur on flat to gently sloping terrain where groundwater discharges to surface springs, particularly along the northern foot-slopes of the Alaska Range (Racine & Walters 1994, Jorgenson et al. 2001). The fens are associated with degradation of thick-layered ice in silty abandoned floodplains and lowland loess. They form long, linear depressions often associated with birch forests. Vegetation is dominated by minerotrophic herbaceous vegetation (Racine et al. 1998). Degradation is initiated by lateral degradation at rates of 0.5−1 m/yr and thaw settlement typically is 1−3 m and up to 5 m (Jorgenson et al. 2001). Collapse along the margins of the fens forms a distinctive moat with slowly flowing water.

Water tracks are shallow, linear, parallel depressions that form on gently sloping hillsides in areas with continuous permafrost or on toe slopes with retransported deposits in the discontinuous zone. They are formed by the thawing of ice-rich soils near the surface by supra-permafrost groundwater movement. They are not associated with degrading ice wedges.

Thermokarst gullies form when channelized surface-water flow has deepened the active layer and thawed the ice-rich upper permafrost. They are abundant throughout northern and central Alaska. Where water becomes sufficiently channelized on ice-rich soils, gullies 1−5 m deep may develop that include some mechanical soil erosion (Tsuyuzaki et al. 1999). They are typically associated with thawing ice wedges.

Beaded streams are formed by the melting of wedge ice by flowing water in small lowland streams on flat terrain with formation of pools at the intersection of ice-wedges. They are very identifiable features of arctic lowland terrain with distinctive water quality (Oswood et al. 1989).

Sink holes and tunnels (pipes) occur in gently sloping areas where groundwater flow from hillsides encounters ice-rich colluvium and retransported deposits in the valley bottoms (Carey and Woo 2002, Fortier et al. 2007). Groundwater flow can thaw massive ice (Holocene ice wedges or Pleistocene massive ice deposits) at considerable depth. Removal of the ice leads to rapid collapse (days to weeks except in forests where roots can form a supporting structure for years) of the overlying soil and creation of sink holes. The distribution, extent, and mechanism of these features are not well known.

Thaw slumps are caused by the retrogressive thawing of ice-rich permafrost at a steep head-scarp face. Thaw slumps occur throughout northern and central Alaska and northern Canada (Burn & Friele 1989, Brease 1995, Huscroft et al. 2004, Lantuit & Pollard 2005, Kokelj et al. 2005). They occur on gentle to steep slopes. Typically they are initiated by detachment slides. Removal of the active layer exposes permafrost to rapid thawing. After initial degradation, the thawed area often expands laterally upslope along the exposed headwall. While thaw slumps may be limited in extent they can have important consequences on the water quality of downslope lakes and rivers (Kokelj et al. 2005). They are common adjacent to rivers, lakes, and coastlines.

Detachment slides involved the flow or slide of material

associated with thawing of the ice-rich intermediate layer, increase in pore pressure in the active layer, and subsequent flow of thawed material (Lewkowicz & Harris 2005). Some slides initially can be limited to the active layer without thawing of ice-rich material at the permafrost surface, in cases where heavy rain has increased the soil moisture content and submerged weight. However, after detachment, thawing of the permafrost ensues. Detachment slides often transform into retrogressive thaw slumps. Slides were numerous in both Alaska and the Yukon after extensive forest fires in 2004 (Lipovsky et al. 2005).

Block landslides are created by the cracking and falling of ice-rich blocks of permafrost from tall, steep faces (Dyke 2000). The fallen or sliding blocks thaw or erode away to maintain a steep cliff face.

Collapse-block shores are associated with shoreline erosion that degrades permafrost soils and is common in northern Alaska along the Beaufort and Chukchi seas (Leffingwell 1919, Reimnitz et al. 1988, Jorgenson & Brown 2005, Mars & Houseknecht 2007). In ice-rich soils, thermo-erosional niches are formed by the thermal and mechanical erosion of ice-rich sediments along riverbanks, lake shores, and coastlines (Leffingwell 1919, Walker & Arnborg 1966). The undercut bluffs often crack off in large blocks. Shoreline retreat often is rapid (m/yr).

Conical thermokarst mounds (baydzherakhs) form from thawing of extremely ice-rich permafrost, where the ice wedges are very old and large (UAS 1959). Soil remaining in the center of polygons thaws and slumps into cone-shape mounds. Mounds often disappear in short time. They are indicative of extremely ice-rich, Pleistocene-age permafrost.

Glacial thermokarst forms highly uneven topography and kettle lakes and is common on ice-cored moraines in the Brooks, Alaska, and Chugach ranges. Numerous kettle lakes of early Holocene age and related to retreat of Wisconsin-era glaciers from their terminal moraines are well known throughout previously glaciated regions. Contemporary kettle lakes form in moraines formed during the Little Ice Age, such as at the terminus of the Muldrow Glacier. Water depths are highly variable, ranging from 5 to 30 m, and the water usually is turbid from slumping banks.

Irregular thermokarst mounds are common throughout lowland forests in central Alaska, although they are often indistinct and easily overlooked. They occur on all types of permafrost terrain where soils are ice-poor or where the active layer thaws sufficiently to equilibrate with changed climatic conditions. Usually, the mounds are 0.2−1 m high and 1−3 m across. Where permafrost persists at depth, the mounds become better drained and the lower-lying hollows become wetter. In warmer areas where permafrost has degraded to deep depths, or been entirely eliminated, all microsites become well-drained.

Nonpatterned thawed ground presumably is common on rocky hillsides, gravelly lowlands (abandoned glacial outwash), or gravelly floodplains, where thawing of ice-poor permafrost results in little to no thaw settlement. Detection is difficult because no surface changes are evident, the rocky soils resist penetration for thaw depth or temperature measurements, and evidence of a previously frozen state is often lacking. Permafrost degradation can still cause large ecological changes because increased subsurface drainage improves soil aeration.

The large variation in landforms associated with surface permafrost degradation is a result of the many complex and interacting factors found across the broad geomorphic environments of Alaska (Jorgenson & Osterkamp 2005, Shur & Osterkamp 2007). These include differing climates and rates of warming, physiography, soil texture, mass and heat transfer processes, hydrology, and ice content and morphology. Fire also has a widespread role because changes to the surface energy balance and soil properties are large and instantaneous (Burn 1998, Hinzman et al. 2001).

## Extent

Assessment of the extent of thermokarst features is difficult due to the heterogeneity of ecological responses, diverse spectral characteristics, varying thaw settlement depths, and a wide-range of sizes of thermokarst features, ranging from 1 $m^2$ to 1000s of ha. To overcome these issues, Jorgenson et al. (2007) used airphoto interpretation and point-sampling on 655 airphotos to determine the abundance of thermokarst features across Alaska (Fig. 2).

Interpretation of 387 airphotos from the discontinuous zone (subarctic climate) revealed that 5% of the area has thermokarst terrain, 62% has permafrost unaffected by thermokarst, and 21% is unfrozen with no recent permafrost (e.g., active floodplains, south-facing slopes). In 11.9% of the area, permafrost status could not be determined (primarily bedrock areas that are thaw-stable). When considering only areas where current or recent permafrost was evident (67%), 7% of permafrost-affected areas have degraded. The most common types of thermokarst included: thermokarst fens (1.8% of total area); thermokarst bogs (1.0%); thermokarst lakes (1.0%); thaw-lake basins (0.3%); glacial thermokarst (0.5%); and thermokarst pits (0.3%) within the subarctic zone.

In the continuous permafrost zone, 13.5% of the terrain showed recent or old (early-mid Holocene) permafrost degradation on 268 airphotos. Common landforms included: thaw-lake basins (7.1 %), deep and shallow thermokarst lakes (1.9 %), thermokarst troughs and pits (2.3 %), thermokarst gullies (1.1%), water tracks (0.7%), and beaded streams (0.4%).

Some commonly described thermokarst features, however, were not encountered by the sampling indicating that overall coverage of the features was negligible. Thaw slumps, detachment slides, and thermokarst gullies were not encountered, although they were evident adjacent to a few sampling points. Conical thermokarst mounds, collapse blocks, and sink holes were not encountered.

While photo-interpretation is effective at identifying distinctive thermokarst features, there are two major types of terrain in which permafrost degradation is particularly

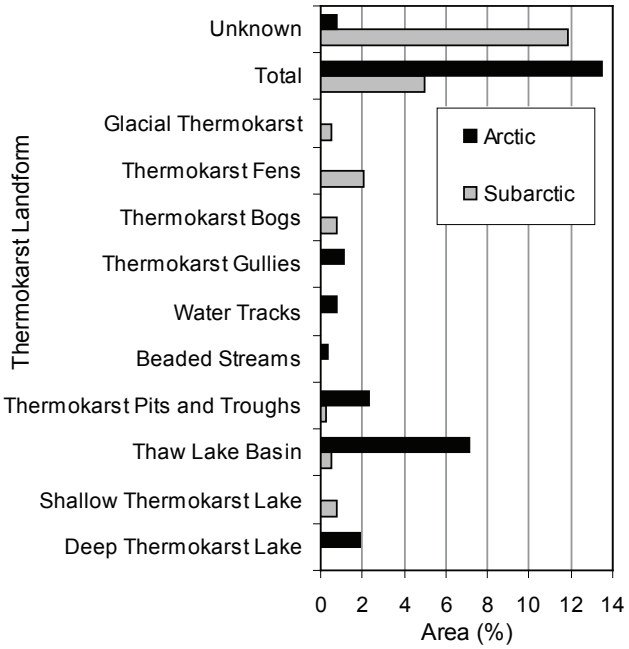


Figure 2. The extent of thermokarst features in arctic and subarctic, Alaska.

problematic to interpret. First, interpretation of thawing of ice-poor, thaw-stable permafrost is not possible because of the lack of thermokarst. This condition is prevalent in bed-rock controlled upland and alpine terrain in the discontinuous zone. In the discontinuous zone, degradation status of 11.9% of the terrain was unknown because of the lack of surface patterns indicative of thermokarst. Second, determination of thermokarst lakes and thaw-lake basins is problematic because not all lakes and basins in permafrost terrain develop from thawing and collapsing of ice-rich permafrost. In particular, lakes occurring in sand dunes and sheets can occur as simple impoundments in low-lying swales. Ground-ice data from Lawson (1983) and Pullman et al. (2007) show that eolian sand has negligible amounts of excess ice and the terrain is not capable of sufficient thaw settlement for thermokarst-lake formation. In addition, many shallow waterbodies are infilling remnant water in drained-lake basins (Jorgenson and Shur 2007). The photo-interpretation indicated 5.1% of the terrain had lakes, but only 1.9% was classified as thermokarst because a large portion of the Beaufort Coastal Plain is covered by eolian sand and slightly pebbly sand sheets. Areas with lakes interpreted to be thermokarst lakes are limited to extremely ice-rich deposits of limited distribution, such as delta overbank and glaciomarine deposits. The Pleistocene loess deposits in the Brooks Foothills have deep thermokarst lakes, but lakes in this hilly terrain are very limited in extent. Similarly, 7.1% of the basins were classified to be of thermokarst origin, while 7.5% to be of non-thermokarst origin.

## Rates

The rate of thermokarst formation has yet to be assessed comprehensively due to the huge area, varying landforms,

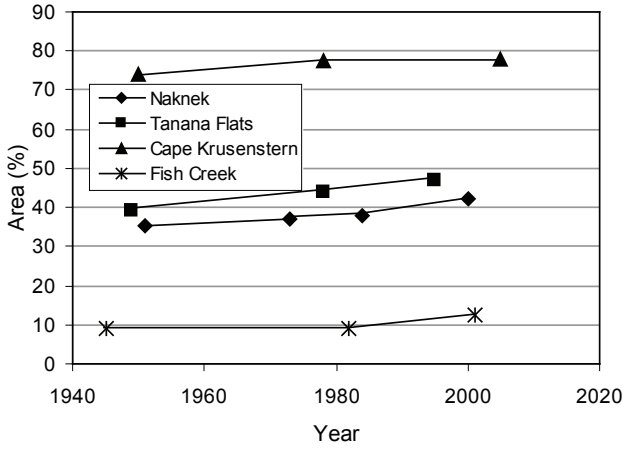


Figure 3. Changes in extent (% area) of thermokarst features from circa 1950 to circa 2000 at four sites in Alaska.

and lack of sufficient high-resolution imagery. Rates determined for a few areas, however, provide insight into degradation rates over the last half century. Below we provide rates across a climatic gradient from the zone of isolated permafrost, where mean annual air temperatures (MAAT) are 2°C, to the continuous zone, where MAATs are as low as -12°C (Fig. 3).

At Naknek in southwestern Alaska, thermokarst bogs have been developing in glacio-lacustrine deposits that have ice-rich permafrost dominated by layers of thick, clear, horizontal ice. Total area with thermokarst features has increased from 35.5% in 1951 to 42% in 2000 within the 9 $km^2$ study area. On the Tanana Flats, where thermokarst fens and bogs are abundant on abandoned floodplain deposits, thermokarst terrain has increased from 39% in 1949 to 47% in 1995 (Jorgenson et al. 2001). On the coastal plain near Cape Espenberg, where thermokarst lakes and thermokarst pits and troughs are abundant on eolian silt and thaw-lake deposits, thermokarst terrain has increased from 73.9% in 1950 to 78.1% in 2005. The high percentage of thermokarst terrain was due to the prevalence of old, drained thaw-lake basins. Finally, tundra near Fish Creek, where thermokarst polygonal troughs are common on flat upland terrain and drained lake basins are common on sandy soils in lowland terrain, thermokarst showed little change between 1945 and 1982 (9%), but had expanded to 12.5% in 2001 due to thawing of the top of ice wedges (Jorgenson et al. 2006). Overall, thermokarst terrain increased in percent area by 3.5 to 8%. The Naknek and Fish Creek areas showed more rapid thermokarst from ~1980 to ~2000, compared to the earlier ~1950 to ~1980 period, while Tanana Flats and Cape Espenberg showed more constant rates of increase between the periods.

## Conclusions

There is a broad diversity of patterns and processes associated with surface permafrost degradation and its ecological consequences. Twenty-two thermokarst landforms have been identified that vary in relation to climate, geomorphic environments and soil texture, hydrologic regime, ice mor-

phology and content. The extent of thermokarst varies from 5% of the surface area in the discontinuous zone to 13.5% in the continuous zone. The age of thermokarst features remains unknown. Overall, thermokarst terrain increased in percent area by 3.5 to 8% at four sites over a ~50-yr period, and at two of the sites the rate of thermokarst development increased during the last 20-25 yrs relative to the first 20-25 yrs since ~1950. This diversity complicates the analysis and modeling of the response of permafrost to climate change.

## Acknowledgments

This research was supported by the Arctic Natural Sciences Program, National Science Foundation (OPP 0454985). We thank Tom George for acquiring the airphotos and for Dorte Dissing's help with GIS. Steve Kokelj and Jim Walters provided many helpful improvements.

## References

Anisimov, O.A. & Nelson, F.E. 1996. Permafrost distribution in the northern hemisphere under scenarios of climatic change. *Glob. Planet. Change* 14: 59–72.

Billings, W.D. & Peterson, K.M. 1980. Vegetational change and ice-wedge polygons through the thaw lake cycle in Arctic Alaska. *Arctic Alpine Research* 12(4): 413–432.

Black, R.F. 1969. Thaw depressions and thaw lakes, a review. *Biuletyn Peryglacjalny* 19: 131–150.

Brease, P.F. 1995. Description, character, and rates of movement of the drunken forest slump-earthflow, Denali National Park and Preserve, Alaska (abstract). *Proceedings of Geological Society of America Meeting, 1995.* Geological Society of America.

Britton, M.E. 1957. Vegetation of the Arctic tundra. In: Hansen, H.P. (ed.) *Arctic Biology*: 18th Biology Colloquium, Oregon State Univ. Press, 67–113.

Brown, J., Ferrians, O.J., Heginbottom, J.A. Jr. & Melnikov, E.S. 1997. Circum-Arctic map of permafrost and ground ice conditions. U.S. Geol. Surv., *CP–45*.

Brown, J. & Grave, N.A. 1979. Physical and thermal disturbance and protection of permafrost. U.S. Army CRREL, Hangover, NH. *Spec. Rep. 79–5.* 42 pp.

Burn, C.R. 1998. The response (1958-1997) of permafrost and near-surface ground temperatures to forest fire, Takhini River valley, southern Yukon Territory. *Canadian Journal of Earth Sciences* 35: 184–199.

Burn, C.R. & Friele, P.A. 1989. Geomorphology, vegetation succession, soil characteristics and permafrost in retrogressive thaw slumps near Mayo, Yukon Territory. *Arctic* 42(1): 31–40.

Burn, C.R. & Smith, M.W. 1990. Development of thermokarst lakes during the Holocene at sites near Mayo, Yukon Territory. *Perm. Peri. Proc.* 1: 161–176.

Carey, S.K. & Woo, M. 2002. Hydrogeomorphic relations among soil pipes, flow pathways, and soil detachments within a permafrost hillslope. *Physical Geography* 23(2): 95-114.

Carter, L.D. 1988. Loess and deep thermokarst basins in arctic Alaska. *Proceedings Fifth International Conference on Permafrost, Trondheim, Norway.* Tapir Publishers, 706–711.

Carter, L.D. & Galloway, J.P. 1979. Arctic Coastal Plain pingos in National Petroleum Reserve in Alaska. K. M. Johnson, and J.R. Williams (eds.). *The U.S. Geological Survey in Alaska; accomplishments during 1978, U. S. Geological Survey Circular 804-B.* U.S. Geological Survey, 804-B: B33–B35.

Drury, W.H. 1956. Bog flats and physiographic processes in the upper Kuskokwim River region, Alaska. *Contributions from the Gray Herbarium of Harvard University, No. CLXXVIII*, 130 pp.

Dyke, L.D. 2000. Stability of permafrost slopes in the Mackenzie Valley. In: Dyke, L.D. & Brooks, G.R. (eds.). *The physical environment of the Mackenzie Valley, Northwest Territories: a base line for the assessment of environmental change*. Geological Survey of Canada, Bulletin 547: 177–186.

Esch, D.C. & Osterkamp, T.E. 1990. Cold regions engineering: climatic warming concerns for Alaska. *Journal Cold Regions Engineering* 4: 6–14.

Everdingen, R. van (ed.). 1998. Multi-language glossary of permafrost and related ground-ice terms. National Snow Ice Data Center for Glaciology, Boulder, CO.

Ford, J. & Bedford, B.L. 1987. The hydrology of Alaskan wetlands, USA.: A review. *Arct. Alp. Res.* 19: 209–229.

Fortier, D., Allard, M. & Shur, Y. 2007. Observation of rapid drainage system development by thermal erosion of ice wedges on Bylot Island, Canadian Arctic Archipelago. *Permafrost Periglacial Proc.* 18: 229–243.

Hinzman, L., Yoshikawa, K., Fukuda, M., Romanovsky, V., Petrone, K. & Bolton, W. 2001. Wildfire in the subarctic boreal forests, ecosystem impacts and response to a warming climate. *Tokohu Geophysical Journal* 36(2): 119–131.

Hopkins, D.M. 1949. Thaw lakes and thaw sinks in the Imuruk Lake area, Seward Peninsula, Alaska. *Journal of Geology* 57: 119–131.

Huscroft, C.A., Lipovsky, P.S. & Bond, J.D. 2004. A regional characterization of landslides in the Alaska Highway Corridor, Yukon. Yukon Geol. Surv., Whitehorse. *Open File Rep. 2004–18*, 61 pp.

Jorgenson, M.T., Pullman, E.R. & Shur, Y.L. 2003. Geomorphology of the Northeast Planning Area of the National Petroleum Reserve-Alaska, 2002. Second Annual Report prepared for Phillips Alaska, Inc., Anchorage, AK, by ABR, Inc., Fairbanks, AK, 67 pp.

Jorgenson, M.T. & Osterkamp, T.E. 2005. Response of boreal ecosystems to varying modes of permafrost degradation. *Can. J. Forest Research* 35: 2100–2111.

Jorgenson, M.T. & Shur, Y. 2007. Evolution of lakes and basins in northern Alaska and discussion of the thaw lake cycle. *Journal of Geophysical Research* 112:F02S17, doi 10.1029/2006JF000531.

Jorgenson, M.T. & Brown, J. 2005. Classification of the Alaskan Beaufort sea coast and estimation of sediment and carbon inputs from coastal erosion. *GeoMarine* 482: 32–45.

Jorgenson, M.T., Racine, C.H., Walters, J.C. & Osterkamp, T.E. 2001. Permafrost degradation and ecological changes associated with a warming climate in central Alaska. *Climatic Change* 48: 551–579.

Jorgenson, M.T., Shur, Y. & Pullman, E.R. 2006. Abrupt increase in permafrost degradation in Arctic Alaska. *Geophysical Res. Letters* 33: L02503, 2005GL024960.

Jorgenson, M.T., Shur, Y.L., Osterkamp, T.E. & George, T. 2007. Nature and extent of permafrost degradation in the discontinuous zone of Alaska. *Proceedings of Seventh International Conference on Global Change.* University of Alaska, Fairbanks, AK. pp. 120–125

Kokelj, S.V., Jenkins, R.E., Milburn, D., Burn, C.R. & Snow, N. 2005. The influence of thermokarst disturbance on the water quality of small upland lakes, Mackenzie Delta region, Northwest Territories, Canada. *Permafrost and Perigla. Process.* 16: 343-353.

Lantuit, H. & Pollard, W.H. 2005. Temporal stereophotogrammetric analysis of retrogressive thaw slumps on Herschel Island, Yukon Territory. *Natural Hazards and Earth System Science* 5: 413-423.

Lawson, D.E. 1983. Ground ice in perenially frozen sediments, northern Alaska. *Proceedings Fourth International Conference on Permafrost.* National Academy Press, Washington, D.C., 695-700.

Lawson, D.E. 1986. Response of permafrost terrain to disturbance: a synthesis of observations from northern Alaska, U.S.A. *Arctic and Alpine Research* 18: 1–17.

Lewkowicz, A.G. & Harris, C. 2005. Frequency and magnitude of active-layer detachment failures in discontinuous and continuous permafrost, northern Canada. *Permafr. Periglacial Proc.* 16(1): 115-130.

Leffingwell, E. de K. 1919. The Canning River region of northern Alaska. U.S. Geol. Surv., Washington, D.C. *Prof. Pap. 109*, 251 pp.

Lipovsky, P.S., Coastes, J., Lewkowicz, A.G. & Trichim, E. 2005. Active-layer detachments following the summer 2004 forest fires near Dawson City, Yukon. *Yukon Exploration and Geology 2005*. Yukon Geological Survey, Whitehorse, Yukon: 175-194.

Mars, J.C. & Houseknecht, D.W. 2007. Quantitative remote sensing study indicates doubling of coastal erosion rate in past 50 yr along a segment of the Arctic coast of Alaska. *Geology* 35: 579–582.

Nelson, F.E., Anisimov, O.E. & Shiklomonov, O.I. 2001. Subsidence risk from thawing permafrost. *Nature* 410: 889–890.

Osterkamp, T.E. 1983. Response of Alaskan permafrost to climate. *Permafrost Fourth International Conference Proc.* National Academy Press, Wash., D.C., 145–152.

Osterkamp, T.E. 2007. Characteristics of the recent warming of permafrost in Alaska. *J. Geophys. Res*. 112, F02S02, doi 10.1029/2006JF000578.

Osterkamp, T.E., Viereck, L., Shur, Y., Jorgenson, M.T., Racine, C., Doyle, A. & Boone, R.D. 2000. Observations of thermokarst and its impact on boreal forests in Alaska, USA. *Arc. Ant.. Alp. Res.* 32: 303–315.

Oswood, M.W., Everett, K.R. & Schell, D.M. 1989. Some physical and chemical characteristics of an arctic beaded stream. *Holarctic Ecology* 12(3): 290-295.

Pullman, E.R., Jorgenson, M.T. & Shur, Y. 2007. Thaw settlement in soils of the Arctic Coastal Plain, Alaska. *Arctic, Antarctic, and Alpine Research* 39(3): 468-476.

Racine, C.H., Jorgenson, M.T. & Walters, J.C. 1998. Thermokarst vegetation in lowland birch forests on the Tanana Flats, Interior Alaska, U.S.A. *Proceedings Seventh International Conference on Permafrost.* Collection Nordicana 57: 927–933.

Racine, C.H. & Walters, J.C. 1994. Groundwater-discharge fens in the Tanana lowlands, Interior Alaska, U.S.A. *Arctic and Alpine Research* 26: 418–426.

Reimnitz, E.S., Graves, M. & Barnes, P.W. 1988. Map showing Beaufort Sea coastal erosion, sediment flux, shoreline evolution, and the erosional shelf profile. U.S. Geol. Surv., Denver, CO. *Misc. Invest. Series Map I-1182-G:* 22

Shur, Y.L. 1977. *Thermokarst*. Moscow: Nedra Publishing House (in Russian).

Shur, Y. & Osterkamp, T.E. 2007. Thermokarst. Institute of Northern Engineering, University of Alaska Fairbanks, Fairbanks, AK. *Rep. INE06*.11, 50 pp.

Shur, Y.L. & Jorgenson, M.T. 1998. Cryostructure development on the floodplain of the Colville River Delta, northern Alaska. *Proceedings Seventh International Conference on Permafrost.* Collection Nordicana 57: 993–1000.

Tedrow, J.C.F. 1969. Thaw lakes, thaw sinks, and soils in northern Alaska. *Biuletyn Peryglacjalny* 20: 337–345.

Tsuyuzaki, S., Ishizaki, T. & Sato T. 1999. Vegetation structure in gullies developed by the melting of ice wedges along Kolyma River, northern Siberia. *Ecological Research* 14: 385–391.

Van Cleve, K. & Viereck, L.A. 1983. A comparison of successional sequences following fire on permafrost-dominated and permafrost-free sites in Interior Alaska. *Proc. Fourth International Conference on Permafrost.* National Acad. Press, Wash.,D.C., 1292–1297.

USSR Academy of Sciences (UAS). 1959. *Fundamentals of Geocryology (Permafrost Science).* Moscow, 431 pp.

Walker, H.J. & Arnborg, L. 1966. Permafrost and ice-wedge effect on riverbank erosion. *Proceedings, Permafrost, International Conference.* National Academy of Sciences, Washington, D.C., 164–171.

Wallace, R.E. 1948. Cave-in lakes in the Nabesna, Chisana, and Tanana River Valleys, eastern Alaska. *Journal of Geology* 56(3): 171–181.

Yoshikawa, K. & Hinzman, L. 2003. Shrinking thermokarst ponds and groundwater dynamics in discontinuous permafrost. *Permafrost Perigla. Proc.* 14: 151–160.

# Thermal Processes in the Active Layer of the Larsbreen Rock Glaciers, Central Spitsbergen, Svalbard

Håvard Juliussen
*The University Centre in Svalbard (UNIS)*
Ole Humlum
*Institute of Geosciences, University of Oslo, Norway*
Lene Kristensen
*The University Centre in Svalbard (UNIS)*
Hanne H. Christiansen
*The University Centre in Svalbard (UNIS)*

## Abstract

A recent scientific focus on the thermal regime of openwork blocky deposits has lead to the conclusion that air circulation in the pore spaces and exchange with the atmosphere may be particularly important processes of heat transfer in such materials. This contradicts our data from the coarse openwork active layer of the Larsbreen rock glaciers. Visual observations and temperature data give inconsistent results on air circulation activity at this site, and we conclude that this process seems less important here compared to what is reported from other areas. Other thermal processes at the site, in addition to conduction, include water vapour transport and subsequent sublimation, and meltwater infiltration followed by several refreezing and melting events. More data is needed to understand the complex process pattern in the coarse active layer of these rock glaciers, and further instrumentation is planned as part of the IPY-project 'TSP Norway – Thermal State of Permafrost in Norway and Svalbard.'

**Keywords:** active layer; coarse debris; heat transfer; non-conductive processes; rock glacier; Svalbard.

## Introduction

In openwork blocky debris such as rock glaciers, coarse talus deposits, and block fields, reported mean annual temperatures are often lower than in adjacent finegrained material (Harris & Pedersen 1998, Hanson & Hoelzle 2005). A recent scientific focus has lead to the conclusion that this temperature anomaly is due to air exchange between the blocky debris and the atmosphere and circulation of air within the material (Harris & Pedersen 1998). Circulation could be by free or forced convection (Nield & Bejan 2006). Free convection is driven by temperature-induced density differences of the air and may operate in gravel-sized materials or coarser if the degree of water saturation is less than about 40% (Johansen 1975), while forced convection is driven by pressure gradients as, for example, induced by high wind speeds (Ping et al. 2007). However, the general importance of this process is still largely unknown (cf. Juliussen & Humlum, in press) as many studies consider extreme cases with large pore spaces (Gorbunov et al. 2004) and steep slopes (Delaloye et al. 2003).

In this paper, we identify and discuss thermal processes operating in the coarse openwork active layer of some rock glaciers near the glacier Larsbreen in Svalbard (Fig. 1), based on visual observations from the active layer in Spring 2006 and temperature data from the active layer 2005–06.

## Study Site

In Svalbard, low mean annual air temperatures (MAAT) of -5.1 to -7.1°C (1961–1990, ©Norwegian Meteorological Office) result in continuous permafrost except beneath temperate parts of glaciers. The permafrost is typically some tens of meters to 100 m thick in major valley bottoms and close to the sea, but up to 400–500 m thick in the mountains (Humlum et al. 2003).

Rock glaciers are common features in Svalbard (Sollid & Sørbel 1992). At the study site, rock glaciers are creeping out from the talus slope in front of and in a lateral position to the Larsbreen glacier (78°12′N, 15°36′E, 250 m a.s.l.) (Fig. 1). The rock glaciers in front of the glacier were deformed by the glacier advance during the Little Ice Age, but still each individual rock glacier can be traced back to the talus cone from which it is creeping, while the longitudinal furrows separating the rock glaciers are all associated with inter-cone depressions.

In the winter, snow accumulates in the depressions to depths of several meters. The rock glacier fronts, on the other hand, are covered by only a thin and sporadic snow cover. Avalanches are frequent in the study area, and cover the rooting zone of the rock glaciers with snow in the winter. By bringing snow and rock debris to the rock glacier rooting zone, they are probably a driving factor for the rock glacier development at this site (Humlum et al. 2007).

The rock debris in the rock glacier is talus material composed of Tertiary sandstones and shales (Hjelle 1993). Average clast size (b-axis) is 15.0 cm at the surface and 8.5 cm close to the permafrost table, and the clasts are slabby (c:a axial ratio of 0.24 to 0.32 and b:a axial ratio of 0.66 to 0.73, see also Fig. 2). The active layer is openwork, and the pore volume is filled with air in summer and a mix of air

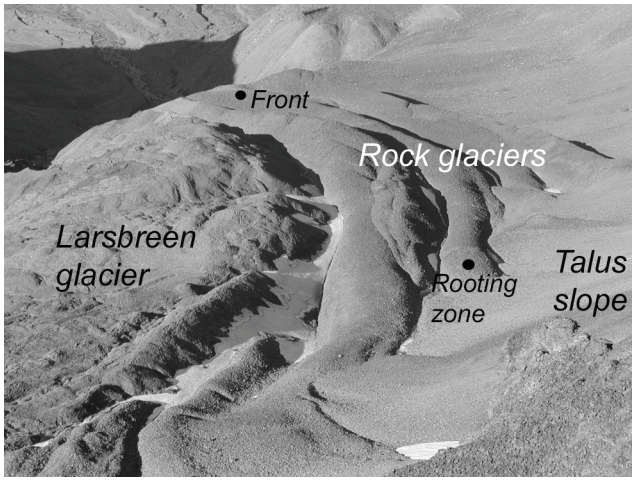


Figure 1. Photo showing the debris-covered front of the Larsbreen glacier, the rock glaciers, and the sites with active layer temperature measurements at the front and at the rooting zone.

and ice in the winter. The active layer is about one meter thick on the rock glaciers, and less than half a meter in the depressions between the rock glaciers.

## Methods

*Visual observations*

The active layer was manually excavated at irregular time intervals during Spring 2006 to visually observe spatial and temporal changes in ice content and the structure of the ice during the melting season.

*Temperature measurements*

The active layer thermal regime on the rock glacier has been monitored close to the front (at the surface and at depths 0.35 m, 0.70 m, and 0.90 m) since Autumn 1999 and just below the rooting zone (at the surface and at depths 0.30 m, 0.60 m, and 1.15 m) since Summer 2005 (Fig. 1). Air temperature at the site was measured in a 0.15 m high naturally-ventilated stone cairn. Tinytag miniloggers with a precision of ±0.2°C were used both for air and active layer temperature monitoring. Temperature was logged at hourly intervals.

Since active layer temperatures were logged at two sites only, ground surface temperatures below the snow cover were measured manually at irregular time intervals through the winter and Spring 2006 to detect any spatial variability not recorded in the logger series. High spatial variability in winter ground surface temperature may reflect zones with rising and sinking pore air within individual convection cells (e.g., Goering 2002), while low variability would be against a hypothesis of effective, distinct convections cells.

*Calculation of Rayleigh numbers*

The potential for free air convection in a porous medium can be explored by estimating the Rayleigh number, which determines if heat transfer in a fluid is mainly by convection or conduction (Nield & Bejan 2006). It is given by:

$$Ra = \frac{C\beta gKH\Delta T}{\nu k} \quad (1)$$

where $C$, $\beta$, and $\nu$ are the volumetric heat capacity, expansion coefficient, and kinematic viscosity of the pore fluid (in this case air); $g$ is gravitational acceleration; $K$ is the intrinsic permeability of the blocky debris layer; $H$ is the thickness of the layer; $\Delta T$ is the temperature difference between the top and bottom of the layer (warmer boundary below); and $k$ is the effective thermal conductivity.

Free convection can be expected if the Rayleigh number exceeds a critical value. In the case of closed upper and lower boundaries, such as represented by a continuous snow cover and the permafrost table, respectively, this critical value is $4\pi^2 \approx 40$ (Nield & Bejan 2006). When there is no snow, and the pore volume is open to the atmosphere (open boundary), the critical value is 27 (Serkitjis & Hagentoft 1998).

The Rayleigh number is estimated from the temperatures logged at the front and at the rooting zone. The effective thermal conductivity was estimated with an empirical relationship to porosity $n$ (Johansen 1975):

$$k = 0.039n^{-2.2} \quad (2)$$

A value of 0.3 was used for the porosity. The hydraulic permeability was estimated with the approach of Fair & Hatch (1933), also used by Goering (2002):

$$K = \frac{1}{5}\left[\frac{(1-n)^2}{n^3}\left(\frac{\alpha}{100}\sum\frac{p}{d_m}\right)^2\right]^{-1} \quad (3)$$

where $\alpha$ is a particle shape parameter; $p$ is the percentage of particles held between adjacent size limits; and $d_m$ is the geometric mean size of those limits. These parameters are estimated from clast size measurements. The Rayleigh number estimates are conservative, as a minimum estimate of the hydraulic permeability was used.

## Results

*Visual observations*

Visual observations from the active layer excavations in spring indicated that several types of non-conductive heat transfer processes had operated in the previous winter: infiltration and refreezing of meltwater, and sublimation of water vapour, the latter forming delicate hoar.

Interstitial ice was found in distinct zones, filling the open pore spaces or forming icicles (Fig. 2). Ice accumulations were largest beneath thin snow. Initially, the ice accumulations occurred in distinct zones as extensions of localized meltwater pathways through the snowpack (e.g., Conway & Benedict 1994, Albert et al. 1999). Thus, the ice formed by refreezing of infiltrating surface meltwater reaching the cold active layer. As the melting season progressed, ice accumulations became more widespread. After the snow cover was completely melted, the ice in the active layer started to melt from the surface.

Figure 2. Photos showing icicles and interstitial ice in the pore volume of the active layer. Vertical section of ruler is 17 cm. Photos taken 26.04.2006 (left) and 04.05.2006 (right).

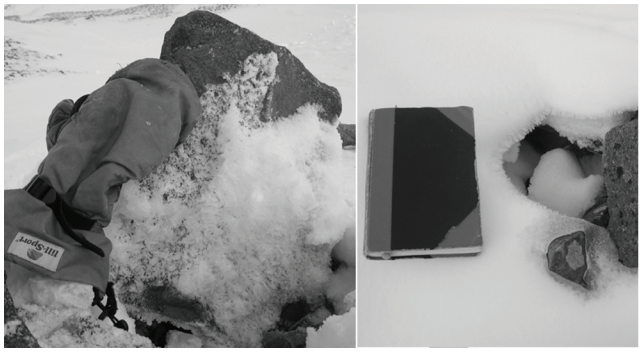

Figure 3. Left panel: Large hoar crystals occupying the pore volume and the base of the tilted block. Glove for scale. Photo taken 24.04.2006. Right panel: Funnel through the snow cover. Note the hoar on the funnel rim. Notebook (width 10cm) for scale. Photo taken 10.05.2006.

Well-developed hoar was found in the upper part of the active layer, in places filling the entire pore volume, and on snow funnel rims (Fig. 3). The hoar crystals were largest and most common near the surface of the rock glaciers where snow was thin or absent and active layer cooling was most effective. Hoar was also superimposed on some of the icicles, but not all, suggesting several episodes, both in the early winter and in the spring, of meltwater infiltration and refreezing. The prevalence of hoar suggests transport of water vapour in the pore volume towards the colder upper part of the active layer and subsequent sublimation.

Funnels through thin snow covers were frequently observed after snowfall (Fig. 3). Funnels indicate exchange of air between the pore volume and the outside (Keller & Gubler 1993).

*Active layer temperatures*

Average daily temperature in the air (at 15 cm height) and in the active layer at the rock glacier front and at the rooting zone for the period Sept. 2005–June 2006 are given in Figure 4. Active layer freeze-back occurred in the middle of September and was immediate, due to the lack of water in the coarse materials. At the front, negative temperatures prevailed in the active layer until May, and active layer temperatures followed the ambient air temperature throughout the winter. The shift to positive temperatures in May was immediate down to 0.35 m depth, but at 0.70 m depth there was a zero curtain period (stable temperature at 0°C) of about a week. This indicates that the upper 0.35 m was more or less free of ice, while some ice existed deeper in the active layer that required energy to melt before the temperature could switch to positive values.

At the rooting zone, the temperatures followed the air temperature until the onset of December, when the site was covered with avalanche snow. For the rest of the winter, the active layer temperatures followed only the main trends in the air temperature as high-frequency fluctuations were masked by the snow. The temperature curves from both sites show several episodes of sudden temperature increase, indicating meltwater infiltration and refreezing during the winter season, forming the observed ice accumulations (Fig. 2). These episodes occurred in periods of warm weather in the autumn, in January during an unusually warm and wet period, and in the spring melt season. In May and June, a snowmelt and zero curtain period of at least one month delayed active layer warming at the rooting zone. The zero curtain period started more or less at the same time at all depths, reflecting the abrupt nature of the infiltration process. The zero curtain period was significantly longer at 1.15 m depth, reflecting that melting occurs from the surface only and possibly indicating a higher ice content than at shallower depths.

The estimated Rayleigh numbers are also given in Figure 4. Since the Rayleigh number is a function of the active layer temperature gradient, it fluctuated in rhythm with the active layer temperatures through the winter. At the front, the theoretical critical Rayleigh number (open boundary) was frequently exceeded, indicating possible episodes of free convection at this site. The estimated Rayleigh numbers for the period 2000–2005 were of comparable size (not shown).

At the rooting zone, the Rayleigh number fluctuated in rhythm with that at the front and with the ambient air temperature, with the highest values well above the critical value (open boundary), until the site was covered by avalanche snow. Below avalanche snow, the Rayleigh number increased to a maximum just above the critical value (closed boundary) and showed less fluctuation than at the snow-free site. Keeping in mind that the Rayleigh number estimate was conservative, there is a potential for free convection also at this site.

*Ground surface temperatures (GST)*

The manually measured ground surface temperatures are displayed in Figure 5 as average values for each date with one standard deviation. Between 7 and 22 measurements were made at each visit. Continuous ground surface temperature measurements at two sites within 20–30 m from the rooting zone profile are also given (GST1 and GST2), along with the surface temperatures at the rooting zone and air temperature. The standard deviation of the manual measurements was mostly below 1°C, even when Rayleigh number estimates show a potential for convection. This suggests that there were no highly effective convection cells. Moreover, the temporal evolution of the ground surface temperatures was

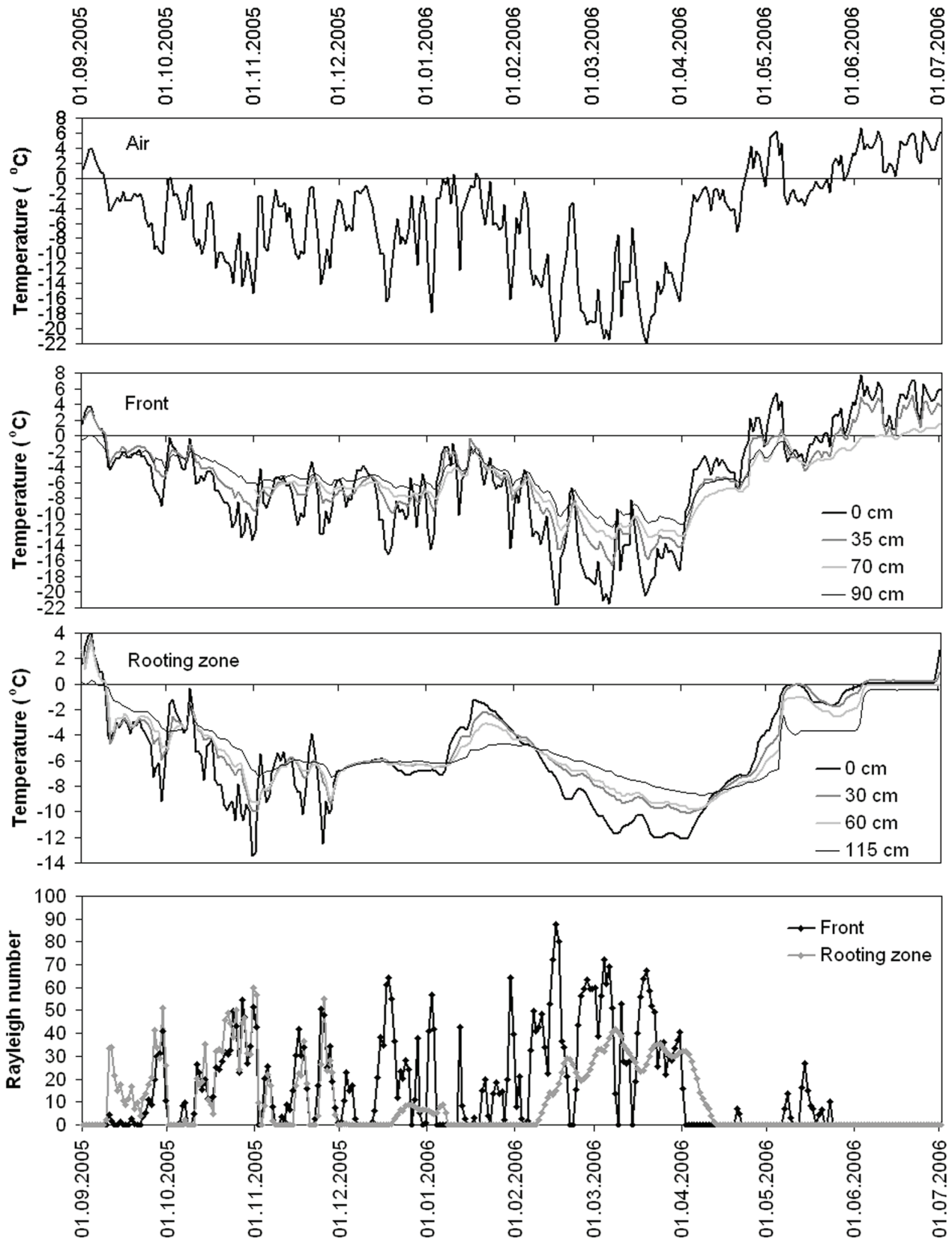


Figure 4. Daily air temperatures (at 15 cm height), active layer temperatures and estimated Rayleigh numbers at the front and at the rooting zone for the period Sept. 2005 – June 2006.

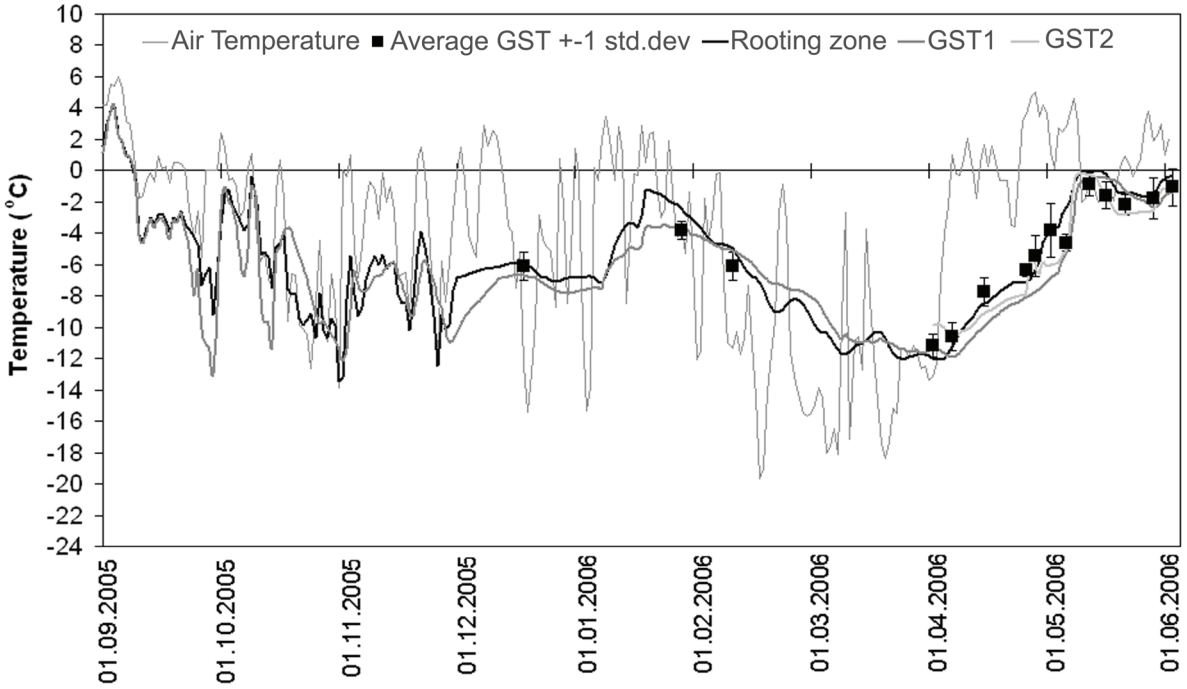


Figure 5. Average GST ± one standard deviation, based on measurement campaigns at irregular time intervals. Continuous ground surface temperatures at two sites with thick snow (GST1 and GST2), surface temperature at the rooting zone and air temperature (official temperatures from Svalbard airport, provided by the Norwegian Meteorological Office) are also given. GST2 starts on April 1.

the result of heat conduction through snow, as shown by snow temperature measurements, rather than by circulation of pore air in the active layer. The highest spatial variability in manually measured ground surface temperatures was due to a differential snowmelt pattern.

## Discussion

Considering air convection in the active layer, the Rayleigh number and the spatially distributed GST revealed inconsistent results. While convection should be expected according to the Rayleigh number, both under open and closed boundary situations, no distinct convection cells were identified in the GST data. Funnels indicate that air exchange with the atmosphere is operating where the snow cover is thin (<10 cm). No funnels were found in thick snow covers. A possible explanation for the discrepancy between the Rayleigh number estimate and the GST data could be that the convection process is less efficient than described by e.g., Goering (2002), so that it is not detected in the spatially distributed GST data. Preservation of the delicate hoar supports that. The convection process may, perhaps, rather be viewed as a series of releases of 'heat bubbles' as described by Hanson & Hoelzle (2004), having negligible influence on the thermal regime. Instead, conduction is probably the main thermal process (cf. Gruber & Hoelzle 2008).

The presence of hoar in the upper part of the active layer indicates transport of water vapour and subsequent sublimation. Transport of water vapour may be by diffusion or air convection. Test measurements of relative humidity in the active layer pore volume, show saturated conditions for most of the winter, except for three shorter periods totalling 11–12 days, when the relative humidity decreases to 93–98% in the upper 0.35 m. Some upward vapour diffusion can be expected, at least during these periods, but it is at present not known to which degree this process can explain the amount of hoar in the upper part of the active layer. The drops in relative humidity nicely give the timing of air exchange between the pore volume and the atmosphere.

As the snow melts in spring, meltwater infiltrates the highly permeable active layer. The (initially small amount of) meltwater will first refreeze close to the surface in the active layer due to the cold content of the active layer. The observed icicles and extensions of meltwater pathways through the snow pack (Fig. 2) are formed in this way. As more meltwater is released and the cold content of the active layer decreases, the meltwater may infiltrate deeper into the active layer and eventually reach the base of the active layer, where it refreezes due to the colder permafrost below. Sawada et al. (2003) measured an accumulation of about 0.2 m of ice in only a few days in a block slope in Japan. This ice requires energy to melt and further delays active layer development (cf. Woo & Xia 1996).

Other processes, such as wind-forced convection (Humlum 1997) and heat radiation (Johansen 1975), may also be important for the thermal regime of coarse-grained active layers. Lack of relevant data precluded a discussion of these processes here.

Further studies are planned at the site as part of the IPY-project "TSP Norway—Thermal State of Permafrost in Norway and Svalbard." This involves an attempt to measure relevant energy fluxes (cf. Smith & Burn 1987, Rist & Phillips 2005).

## Conclusions

Heat transfer processes in the coarse-grained active layer of the Larsbreen rock glaciers in Svalbard have been discussed based on visual observations of ice in the active layer and temperature data. The following conclusions can be drawn:

- Considering air convection in the active layer, the Rayleigh number and the spatially distributed GST data reveal inconsistent results. Convection of air in the pore volume of blocky debris seems less important here compared to what is reported from other areas. Winter air exchange between the pore volume of the blocky layer and the atmosphere may operate through snow covers thinner than about 10 cm.
- Hoar in the upper part of the active layer indicates transport of water vapour, by diffusion or air convection, and subsequent sublimation.
- Water from snowmelt infiltrates and refreezes in the active layer. Melting of this ice delays active layer development.

## References


Albert, M., Koh, G. & Perron, F. 1999. Radar Investigations of Meltwater Pathways in a Natural Snowpack. *Hydrological Processes* 13: 2991-3000.

Conway, H. & Benedict, R. 1994. Infiltration of Water into Snow. *Water Resources Research* 30: 641-649.

Delaloye, R., Reynard, E., Lambiel, C., Marescot, L. & Monnet, R. 2003. Thermal Anomaly in a Cold Scree Slope (Creux du Van, Switzerland). *Proceedings of the Eighth International Conference on Permafrost, Zürich, Switzerland, July 21–25, 2003*: 175-180.

Fair, G.M. & Hatch, L.P. 1933. Fundamental Factors Governing the Streamline Flow of Water through Sand. *Jour. American Water Works Assoc.* 25: 1551-1565.

Goering, D.J. 2002. Convective Cooling in Open Rock Embankments. *Cold Regions Engineering*: 629–644.

Gorbunov, A.P., Marchenko, S.S. & Severskiy, E.V. 2004. The Thermal Environment of Blocky Materials in The Mountains of Central Asia. *Permafrost and Periglacial Processes* 15: 95-98.

Gruber, S. & Hoelzle, M. 2008. The Cooling Effect of Coarse Blocks Revisited. *Proceedings of the Ninth International Conference on Permafrost, Fairbanks, Alaska, June 29- July 3, 2008* (this proceedings).

Hanson, S. & Hoelzle, M. 2004. The Thermal Regime of the Active Layer at the Murtèl Rock Glacier Based on Data from 2002. *Permafrost and Periglacial Processes* 15: 273-282.

Hanson, S. & Hoelzle, M. 2005. Installation of a Shallow Borehole Network and Monitoring of the Ground Thermal Regime of a High Alpine Discontinuous Permafrost Environment, Eastern Swiss Alps. *Norwegian Journal of Geography* 59: 84-93.

Harris, S.A. & Pedersen, D.E. 1998. Thermal Regimes beneath Coarse Blocky Materials. *Permafrost and Periglacial Processes* 9: 107-120.

Hjelle, A. 1993. *Geology of Svalbard*. Oslo: Norsk Polar-Institutt. 162 pp.

Humlum, O. 1997. Active Layer Thermal Regime at Three Rock Glaciers in Greenland. *Permafrost and Periglacial Processes* 8: 383-408.

Humlum, O., Instanes, A. & Sollid, J.L. 2003. Permafrost in Svalbard: a Review of Research History, Climatic Background and Engineering Challenges. *Polar Research* 22: 191-215.

Humlum, O., Christiansen, H.H. & Juliussen, H. (2007). Avalanche-derived Rock Glaciers in Svalbard. *Permafrost and Periglacial Processes* 18(1)*:* 75-88.

Johansen, Ø. 1975. *Varmeledningsevne av jordarter. (Thermal Conductivity of Soils),* Trondheim: NTH (Norw. Tech. Univ.) Licentiat-Thesis. 231 pp. (in Norwegian).

Juliussen, H. & Humlum, O. In press. Thermal Regime of Openwork Block Fields on the Mountains Elgåhogna and Sølen, central-eastern Norway. *Permafrost and Periglacial Processes* 19(1).

Keller, F. & Gubler, H. 1993. Interaction between Snow Cover and High Mountain Permafrost, Murtel-Corvatsch, Swiss Alps. *Proceedings of the Sixth International Conference on Permafrost, Beijing*, 332-337.

Nield, D.A. & Bejan, A. 2006. *Convection in Porous Media*. New York: Springer Science and Business Media Inc, 640 pp.

Ping, H., Zhao, Z., Guodong, C. & Hui. B. 2007. Ventilation Properties of Blocky Stones Embankments. *Cold Regions Science and Technology* 47(3): 271-275.

Rist, A. & Phillips, M. 2005. First Results of Investigations on Hydrothermal Processes within the Active Layer above Alpine Permafrost in Steep Terrain. *Norwegian Journal of Geography* 59(2): 177-183.

Sawada, Y., Ishikawa, M. & Ono, Y. 2003. Thermal Regime of Sporadic Permafrost in a Block Slope on Mt. Nishi-Nupukaushinupuri, Hokkaido Island, Northern Japan. *Geomorphology* 52, 121-130.

Serkitjis, M. & Hagentoft, C.E. 1998. The Influence of Natural Convection on the Heat Transfer in an Air Filled Porous Medium Bounded by an Air Layer. *Nordic Journal of Builduing Physics* 1: 1-24.

Smith, M.W. & Burn, C.R. 1987. Outward Flux of Vapour from Frozen Soils at Mayo, Yukon, Canada: Results and Interpretation. *Cold Regions Science and Technology* 13: 143-152

Sollid, J.L. & Sørbel, L. 1992. Rock glaciers in Svalbard and Norway. *Permafrost and Periglacial Processes* 3: 215-220.

Woo, M. & Xia, Z. 1996. Effects of Hydrology on the Thermal Conditions of the Active Layer. *Nordic Hydrology* 27: 129-142.

# Water Balance for a Low-Gradient Watershed in Northern Alaska

Douglas L. Kane
*Water and Environmental Research Center, University of Alaska Fairbanks, USA*
Robert E. Gieck
*Water and Environmental Research Center, University of Alaska Fairbanks, USA*
Larry D. Hinzman
*International Arctic Research Center, University of Alaska Fairbanks, USA*

## Abstract

Water balance computations are a tool for developing a better understanding of hydrologic processes and their interaction for all types of environments. In this case study, water balance computations are carried out for an Arctic watershed characterized by continuous permafrost, lack of trees, low hydraulic gradient, negative mean annual temperature, and a snow cover for eight to nine months. The Putuligayuk River is a north draining river that drains 471 km$^2$ and empties into the Arctic Ocean. The snowmelt event, in late May or early June, is the major hydrologic runoff event of the year that results in 80% of the snowpack leaving the basin as surface flow. During the summer months, evapotranspiration (ET) exceeds precipitation with 60% of rainfall precipitation leaving the basin as ET and 40% as runoff. Annually, 60% leaves as runoff and 40% as ET.

**Keywords:** Arctic; evapotranspiration; continuous permafrost; precipitation; runoff; surface storage; water balance.

## Introduction

It is abundantly clear that the Arctic is undergoing change from permafrost warming (Lachenbruch & Marshall 1986) to glacier mass wasting (Arendt et al. 2002), to snow cover reduction (Robinson et al. 1993), to reduction in sea ice extent (Maslanik et al. 1999, Vinnikov et al. 1999), to increasing shrub abundance (Sturm et al. 2001), to later freeze-up and earlier break-up (Magnuson et al. 2000), to many other changes (Hinzman et al. 2005). Hinzman et al. (2005) summarizes numerous kinds of evidence of environmental change, what the climatic drivers are and what are the implications. During this environmental change, hydrologist struggle with quantifying various hydrologic fluxes to improve our understanding of the Arctic hydrologic cycle with methods prone to error and considerable year-to-year natural variability. Water balance computation, generally at the small watershed scale, is one tool used to advance our knowledge of Arctic hydrology (Kane & Yang 2004). Unfortunately these studies are of short duration (no trends observed) and only at the small catchment scale (~400 km$^2$ or smaller).

Both the domestic and industrial demand for water and the impact that climate change is having on the hydrologic cycle in the Arctic warrants that we improve our hydrologic understanding. The number of hydrologic stations in the Arctic is quite low, the longevity of these stations is relatively short (except in Russia), and most stations are located at low elevations along the coasts or major drainages. Since 1999, we have been monitoring the runoff from the Putuligayuk River, including other complementary hydrologic and meteorological data. Reported here is the seasonal water balance for this 471 km$^2$ low-gradient catchment (Fig. 1) draining into the Arctic Ocean.

## Setting

The Putuligayuk River (Fig. 1) is part of a nested watershed study (Kane et al. 2000) on the North Slope of Alaska that drains an area south of the Prudhoe Bay oil field

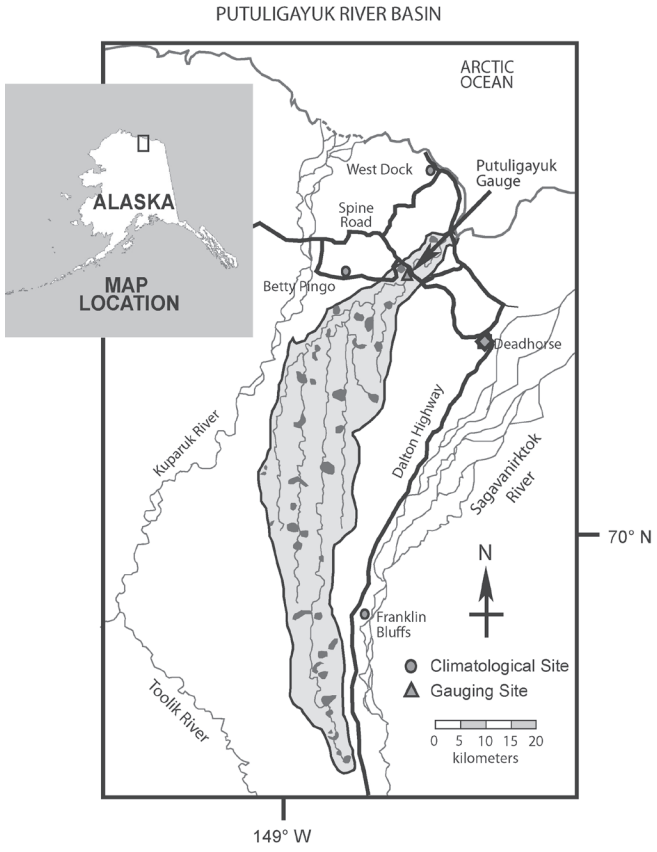


Figure 1. Location map of the north–draining Putuligayuk watershed on the North Slope of Alaska.

before flowing northward through the middle of the field and into the Arctic Ocean. It is a patchwork of lakes, drained lakes, and numerous other permafrost features such as high and low centered polygons, pingos, strangmoor ridges, frost boils, and hummocky terrain. This is an area of continuous permafrost with a maximum measured depth of 600 m, treeless and mostly vegetated with sedges with some shrubs in riparian areas. The elevation at the top of the watershed is 109 m and at the gauging site, 7 m. The active layer is typically around 35 to 55 cm at summer's end (Hinzman et al. 1998) and is composed of surficial organic soils (~20 cm although quite variable) over mineral soils.

Flow ceases in this basin during the winter months with breakup occurring in late May or the first two weeks in June, just prior to the summer solstice. The snowmelt breakup is the biggest runoff event of the year; this is substantiated by the U.S. Geological Survey, which first gauged this stream from 1971 through 1986 (1980 and 1981 missing). Little or no other complementary data were collected during this gauging period. For the past few years, snowfall precipitation has averaged about 40% of the annual precipitation. Redistribution by wind is a major component of the hydrologic cycle of this region. Elevational depressions (drainages, drained lakes, ponds, etc.) are depositional areas for blowing snow, and exposed areas are eroded. Snow damming in the river and smaller drainages (including lake outlets) delays the runoff event by several days; typically the tundra snowcover is almost completely absent before any runoff of significance is measured at the gauge.

During the summer months, evapotranspiration exceeds precipitation. This means that the surface storage of water in the ponds, wetlands and lakes decreases over the summer. Some late summer precipitation may replenish some of this deficit; however, most of the deficit will be made up during the following spring break-up (Bowling et al. 2003). In the summer, as the watershed dries out, the drainage network becomes fragmented. This explains why there is minimal runoff response during the summer months to precipitation, although it comprises 60% of annual precipitation.

## Methods

Since 1999, we have been collecting hydrologic and meteorological data on the central coastal plain on the North Slope of Alaska in the near vicinity of the Arctic Ocean. One objective of this data was to perform a water balance determination of a low-gradient watershed that is in an area of continuous permafrost. The three main features of the water balance equation are the input (P), changes in various storage terms (ΔS), and outputs (ET and R); if we ignore storage terms, this equation can be simplified to:

$$P - ET - R \pm \Delta S = \eta \quad (1)$$

where

P = precipitation, both snowfall and rainfall (possibly condensation)
ET = evapotranspiration (possibly sublimation)
R = discharge throughout the entire period of flow
ΔS = Change in surface storage
η = error term on closure

Summer liquid precipitation gauges exist at three sites (Fig. 1) immediately adjacent the Putuligayuk catchment: at Franklin Bluffs, Betty Pingo and West Dock. In addition there are meteorological measurements at each of these sites that collect 10 m profiles of air temperature, relative humidity and wind speed profiles; incoming and outgoing long- and short-wave and net radiation fluxes, wind direction, soil temperature, barometric pressure, and soil moisture data are also measured. Snow surveys of snow water equivalent (SWE) on the ground are carried out the last week of April. For the Putuligayuk catchment there are several measurements sites (number varied from year to year) where 50 snow depth and 5 density measurements are made at each site to get an estimate of the average SWE for that area.

The Putuligayuk River is gauged on the Prudhoe Bay oilfield where it crosses the Spine Road. A stage-discharge relationship has been developed with the stage being measured continuously during the warm summer season with both a float-type water level recorder and a pressure transducer, both located in a stilling well in the center of the river. During break-up the stage-discharge relationship is not reliable as there is some ice and considerable wind redistributed snow in the channel that slowly erodes as flows increase during the ablation season. Snow damming, both at the outlet of lakes and in the river channel, is an important hydrologic process as it delays the runoff response by several days. Typically, most of the shallow snow cover on the tundra disappears before the runoff has increased significantly (initially there is some local runoff along the roadway). The flow is gauged each day during the breakup once the flow seriously starts to increase. Once the flow starts to significantly increase during ablation, the flow continues to increase and peak even if a cold period sets in (Bowling et al. 2003). Historically, there are several years of stream gauging data as this site was operated from 1970 to 1979 and 1982 to 1986 by the U.S. Geological Survey. From the work by Bowling et al. (2003), it is clear that meltwater from the snowpack is responsible for recharging the copious number of lakes in the catchment and also producing the observed runoff. The flow gradually recedes over the summer with only small peaks in response to summer precipitation.

Studies carried out by researchers associated with the Water and Environmental Research Center at the University of Alaska (Rovansek et al. 1996, Mendez et al. 1998, Bowling et al. 2003) have demonstrated that in this part of the Arctic, it is common for summer evapotranspiration (ET) to exceed precipitation. Therefore a drying of the watershed (shrinkage of wetlands, ponds, and lakes) and fragmentation of the drainage network takes place during the summer. Meteorological data are collected so estimates of ET can be made over the basin as reported on by several groups working

in the area (Kane et al. 1990, Rovansek et al. 1996, Mendez et al. 1998). Shutov et al. (2006) also presents methods conveniently adapted for calculating evaporation when detailed information on the hydrology and meteorology is missing.

Here we are going to use the Priestley-Taylor (Priestley & Taylor 1972) method to estimate the catchment ET:

$$-Q_e = \alpha(\Delta/(\Delta + \gamma))\ (Q_{net} + Q_g) \quad (2)$$

where

$\alpha$ = empirical parameter elating actual and equilibrium evaporation
$\Delta$ = slope of saturated pressure curve
$\gamma$ = psychometric constant
$Q_{net}$ = net radiation
$Q_g$ = ground heat flux
$Q_e$ = latent heat flux

The amount of water lost over the catchment from the watershed is equal to:

$$ET = Q_e/(\rho_w * \lambda) \quad (3)$$

where

ET = evapotranspiration
$\rho_w$ = density of water
$\lambda$ = latent heat of vaporization

The value of $\alpha$ varies with both space and time (Mendez et al. 1998); it was highest for lakes, intermediate for wetlands, and lowest for uplands; for wetlands and uplands it decreases during the summer.

It is very difficult to make field estimates of storage changes in this watershed at the seasonal or annual time scale. The numerous lakes, ponds, and wetlands represent a distributed storage reservoir for both rainfall and snowmelt. The amount of snowmelt water stored in a watershed each spring depends upon the ET and precipitation amounts the previous summer. In this water balance analyses we assume that the difference between the incoming precipitation (both rainfall and snow on the ground at winter's end) and export from the watershed (runoff and ET) represent the change in storage. Or it is assumed that there is no closure error.

## Results and Discussion

Table 1 shows the water balance computations for the Putuligayuk catchment for a 9-year period from 1999 to 2007. An examination of the runoff hydrographs for the years gauged (Kane et al. 2000, Bowling et al. 2003) shows a significant runoff response to snowmelt, with very little response to summer precipitation; typical snowmelt and summer hydrographs for 3 years are shown in Figure 2. The hydrograph for 2003 shows a very high peak runoff that corresponds to the maximum SWE measured in the watershed. Also the average of the runoff from snow divided by SWE or the snow runoff ratio (0.78) is much greater than the average rainfall runoff ratio (0.36). This is true for each year also.

Although, the 9-year averages of SWE at winter's end (9.5 cm) and summer rainfall (8.5 cm) are very similar, a majority of the runoff is generated from snowmelt. Of the total precipitation, 60% left the basin as runoff over the 9-year period. This is considerably higher than found in more temperate climates and is partially due to the continuous permafrost in the basin. The global average for runoff has been reported as 36% (Baumgartner & Reichel 1975). However, there was considerable year-to-year variation in annual runoff, from 33% to 79% of annual precipitation. Part of this annual variation can be explained by changes in surface storage, magnitude of SWE and summer rainfall, and the timing of some of these events. If one looks at the data in Table 1, it can be seen that in the summer of 2005, with the second lowest warm season precipitation, the runoff ratio the following year was the second lowest for the 9-year duration. This is due to snowmelt water going back into surface storage after the previous dry summer when ET was equivalent to the summer precipitation. Wet years generally have high runoff ratios and dry years just the opposite; this is due to limited storage. In addition to the amount of precipitation, the timing is important; SWE is more likely to run off while summer precipitation is more likely to result in ET that produces a surface storage deficit. Late summer precipitation when ET is low can also significantly reduce the surface storage deficit that can develop over the summer when ET exceeds precipitation. The likelihood is that the wettest month of the year will be at the end of summer; however in any single year it can be September, July, or even June.

SWE at the end of winter averaged 9.5 cm and varied from a low of 8.2 cm to a high of 11.2 cm. Summer precipitation has averaged 8.5 cm the past 9 years; the range is quite wide as it ranges from 1.5 to 13.7 cm. There were three years when the summer precipitation was very low and produced drought conditions, at least for part of the summer: 6.0 cm in summer 2000, 5.0 cm in summer 2005 and 1.5 cm in summer 2007. The importance of the low summer precipitation is reflected in the amount of water stored in the watershed, both as surface and subsurface stores, and the deflated hydrologic runoff response to snowmelt the next year.

It is not clear why both the snow and rainfall runoff ratios are so low the first summer in 1999. As we were not monitoring the hydrology and meteorology in 1998, we have to rely on limited data from outside the catchment. There is some evidence that 1998 was a dry summer, but that does not explain the low rainfall runoff ratio. One weakness of this study is our inability to quantify the surface storage in the myriad of lakes, ponds, and wetlands that cover this landscape. Bowling et al. (2003) showed that in a 3-year period, 1999 to 2001, 24% to 42% of the snowmelt water went into storage. This water is lost back to atmosphere over the following summer, mainly to ET.

Table 1. Water balance components for Putuligayuk watershed, North Slope of Alaska, 1999 to 2007.

| Year | SWE (cm) | Rainfall (cm) | ET (cm) | Snowmelt Runoff (cm) | Summer Runoff (cm) | Total Runoff (cm) | Storage Change (cm) | Total Runoff Ratio | Snow Runoff Ratio | Rainfall Runoff Ratio |
|---|---|---|---|---|---|---|---|---|---|---|
| 1999 | 10.4 | 10.0 | 5.6 | 5.1 | 1.6 | 6.7 | 8.1 | 0.33 | 0.49 | 0.16 |
| 2000 | 9.9 | 6.0 | 5.8 | 9.7 | 2.8 | 12.5 | -2.4 | 0.79 | 0.98 | 0.47 |
| 2001 | 8.4 | 7.5 | 5.4 | 6.8 | 2.3 | 9.1 | 1.3 | 0.57 | 0.81 | 0.31 |
| 2002 | 9.4 | 13.7 | 6.3 | 7.4 | 6.3 | 13.7 | 3.1 | 0.59 | 0.79 | 0.46 |
| 2003 | 11.2 | 10.8 | 5.4 | 10.5 | 6.8 | 17.3 | -0.8 | 0.79 | 0.94 | 0.63 |
| 2004 | 9.2 | 11.1 | 6.3 | 7.6 | 7.1 | 14.8 | -0.8 | 0.73 | 0.83 | 0.64 |
| 2005 | 8.9 | 5.0 | 5.0 | 8.4 | 0.5 | 8.8 | 0.0 | 0.64 | 0.94 | 0.10 |
| 2006 | 9.5 | 10.7 | 8.0 | 5.5 | 2.8 | 8.3 | 3.9 | 0.41 | 0.58 | 0.26 |
| 2007 | 8.2 | 1.5 | 6.6 | 5.2 | 0.3 | 5.5 | -2.5 | 0.57 | 0.63 | 0.21 |
| Max. | 11.2 | 13.7 | 8.0 | 10.5 | 7.1 | 17.3 | 8.1 | 0.79 | 0.98 | 0.64 |
| Min. | 8.2 | 1.5 | 5.0 | 5.1 | 0.3 | 5.5 | -2.5 | 0.33 | 0.49 | 0.10 |
| Ave. | 9.5 | 8.5 | 6.1 | 7.4 | 3.4 | 10.8 | 1.1 | 0.60 | 0.78 | 0.36 |
| Std. Dev. | 0.9 | 3.8 | 0.9 | 1.9 | 2.7 | 4.0 | 3.4 | 0.16 | 0.17 | 0.20 |

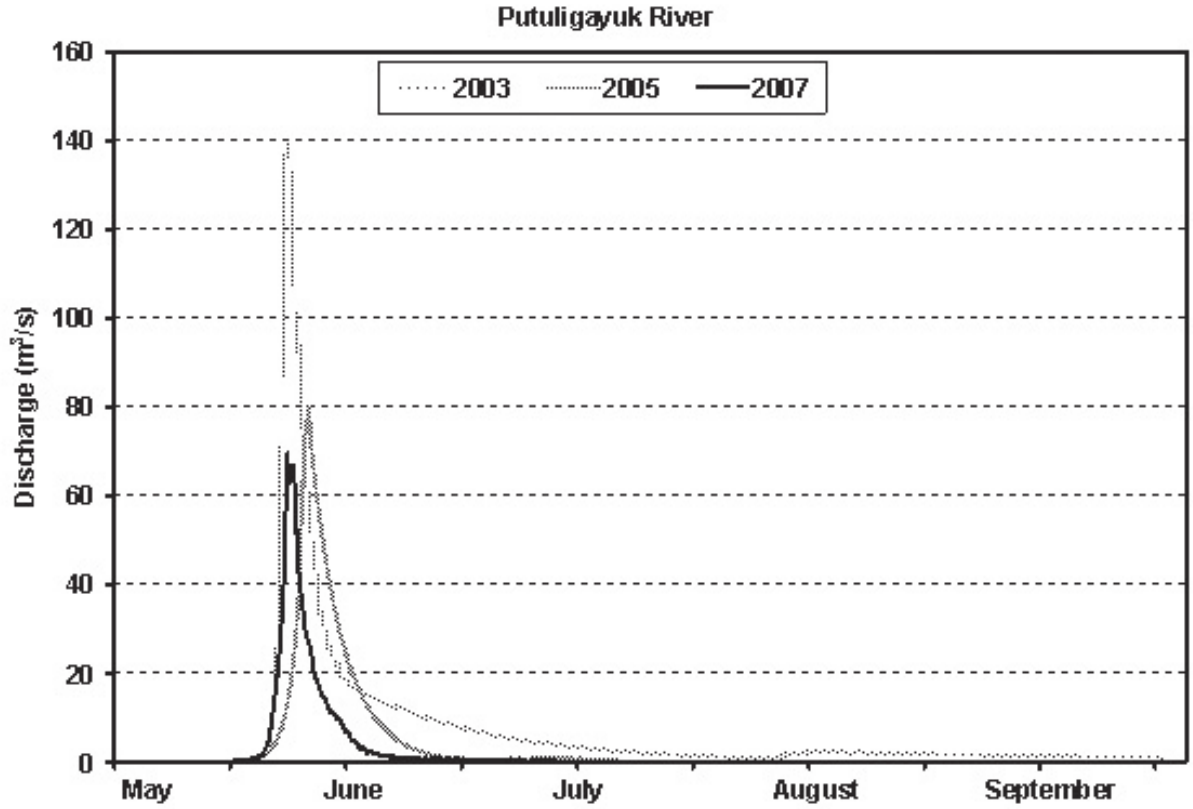


Figure 2. Typical annual hydrographs demonstrating the dominance of snowmelt runoff in the annual hydrologic cycle for the Putuligayuk River catchment.

There have been several water balance determinations for what is referred to as the nested watersheds of the Kuparuk basin (Lily et al. 1998, Kane et al. 2004), although the Putuligayuk catchment is just outside to the east. There are similarities in the water balance of other neighboring watersheds (Imnavait, Upper Kuparuk and Kuparuk) and this watershed; however there are also interesting contrasts. It can be anticipated that snowmelt will be a significant runoff event in these watersheds with average runoff ratios exceeding 0.5 and for individual years near 0.8 (Table 2). One interesting feature of the Putuligayuk catchment is the high average runoff ratio of 0.8 for the snowmelt period. This value is both surprising because this is a low-gradient watershed and it has much more surface storage (lakes, ponds, and wetlands) than the other three watersheds mentioned above.

It is clear that the snowmelt runoff response of the Putuligayuk catchment depends on the timing and amounts of precipitation the previous summer. Typically precipitation increases monthly throughout the summer and any deficits that develop in storage are partially replenished by summer precipitation, particularly at summer's end when ET is minimal. Significant precipitation at the end of summer produces high runoff response the next spring, while summer

Table 2. Summary of runoff ratios for 3 watersheds on the North Slope of Alaska.

| Basin | Total Runoff Ratio | Snow Runoff Ratio | Rainfall Runoff Ratio |
|---|---|---|---|
| Putuligayuk River [1] (n = 9 years) | 0.60 | 0.80 | 0.40 |
| Upper Kuparuk River [2] (n = 7 years | 0.62 | 0.49 | 0.68 |
| Imnavait Creek [2] (n = 19 years) | 0.50 | 0.66 | 0.41 |
| Kuparuk River [3] (n = 4 years) | 0.58 | 0.86 | 0.35 |

1. This paper 2. Kane et al. (2004) 3. Lilly et al. (1998)

drought conditions will result in a low runoff yield during the following ablation.

The summer runoff response of the Putuligayuk River can only be described as not impressive (Fig. 2). From the end of snowmelt to summer's end, the discharge is generally in recession with only a few very small responses to precipitation. Kane et al. (2003) discussed how permafrost land forms could retard surface runoff, and McNamara et al. (1998) described how the active layer slowly yields water during the summer and results in an extended recession that lasts through freeze-up in the fall. Otherwise the stream would cease flowing during the summer; this is actually a possibility in the summer of 2008 because of the extreme drought conditions of the summer of 2007.

## Conclusions

This low-gradient river has a surprisingly high runoff ratio, both annually and during snowmelt. A majority of this runoff leaves the basin during and immediately after snowmelt, but first any surface storage deficit from the previous warm season must be replenished. Summer runoff response is minimal and generally ET exceeds P, which results in drying out of the basin and fragmentation of the drainage network. This is particularly true earlier in the summer when the probability of precipitation is lower than at the end of summer. Drought conditions during a summer result in lower than expected runoff response the following year. Storage is the most significant unknown in this computation; we just do not have adequate tools for getting quantitative estimates of subsurface (active layer) and surface storage. However, it is clear that the amount of surface storage is low in terms of average annual precipitation. Estimates of ET spatially over the watershed could be improved with more data, but the likelihood of this happening is quite low. With the record low summer precipitation in 2007, it is predicted that the snow runoff ratio for 2008 will be quite low unless the SWE is considerably above the 9-year average of 9.5 cm.

## Acknowledgments

This paper is based on work supported by the National Science Foundation, Office of Polar Programs, Grants OPP-9814984 and OPP-0335941. We are also grateful to all faculty, staff, and students who helped collect the data that made these computations possible.

## References

Arendt, A.A., Echelmeyer, K.A., Harrison, W.D., Lingle, C.S. & Valentine, V.B. 2002. Rapid wastage of Alaska glaciers and their contribution to rising sea level. *Science* 297: 382-386.

Baumgartner, A. and Reichel, E. 1975. The world water balance. Elsevier Scientific Publishing Company, New York, U.S.A.

Bowling, L.C., Kane, D.L., Gieck, R.E. Hinzman, L.D. & Lettenmaier, D.P. 2003. The role of surface storage in a low-gradient Arctic watershed. *Water Resources Research* 39(4): 1087.

Hinzman, L.D., Goering, D.J. & Kane, D.L. 1998. A distributed thermal model for calculating soil temperature profiles and depth of thaw in permafrost. *Journal of Geophysical Research* 103(D22):28,975-28,991.

Hinzman, L.D., Bettez, N., Boulton, W.R., et al. 2005. Evidence and implications of recent climate change in northern Alaska and other Arctic regions. *Climatic Change* 72: 251-298.

Kane, D.L., Gieck, R.E. & Bowling, L.C. 2003. Impacts of surficial permafrost landforms on surface hydrology.

Kane, D.L., Gieck, R.E. & Hinzman, L.D. 1990. Evapotranspiration from a small Alaskan Arctic watershed. *Nordic Hydrology* 21: 253-272.

Kane, D.L., Hinzman, L.D., McNamara, J.P., Zhang, Z. & Benson, C.S. 2000. An overview of a nested watershed study in Arctic Alaska. *Nordic Hydrology* 31(4/5): 245-266.

Kane, D.L., Gieck, R.E., Kitover, D.C., Hinzman, L.D., McNamara, J.P. & Yang, D. 2004. Hydrological cycle on the North Slope of Alaska. In: *Northern research basins water balance.* Kane, D.L & Yang, D. Eds., IAHS Publication 290, pp. 224-239.

Kane, D.L. & Yang, D. (eds.). 2004. *Northern research basins water balance.* International Association of Hydrological Sciences, IAHS Publication 290, 271 pp.

Lachenbruch, A.H. & Marshall, B.V. 1986. Changing climate: geothermal evidence from permafrost in the Alaskan Arctic. *Science* 234: 689-696.

Lilly, E.K., Kane, D.L., Hinzman, L.D. & Gieck, R.E. 1998. Annual water balance for three nested watersheds on the North Slope of Alaska. Proc., Permafrost, Seventh International Conference, Yellowknife, Canada, pp. 669-674.

Magnuson, J., Robertson, D. Son, B., Wynne, R., Livingstone, D., Arai, T., Assel, R., Barry, R., Card, V., Kuusisto, E., Grannin, N., Prowse, T., Steward, K. & Vuglinski, V. 2000. Historical trends in lake and river ice cover in the Northern Hemisphere. *Science* 289: 1743-1746.

Maslanik, J.A., Serreze, M.C. & Agnew, T. 1999. On the record reductions in western Arctic sea ice cover in 1998. *Geophys. Res. Lett.* 26(13): 1905-1908.

McNamara, J. P., Kane, D.L. & Hinzman, L.D. 1998. An analysis of stream flow hydrology in the Kuparuk River basin, Arctic Alaska: A nested watershed approach. *Journal of Hydrology* 206:39-57.

Mendez, J., Hinzman, L.D. & Kane, D.L. 1998. Evapotranspiration from a wetland complex on the Arctic coastal plain of Alaska. *Nordic Hydrology* 29(4/5): 303-330.

Priestley, C.H.B & Taylor, R.J. 1972. On the assessment of surface heat flux and evaporation using large scale parameters. *Monthly Weather Review* 100(1):81-92.

Robinson, D.A., Dewey, K.F. & Heim, R.R. 1993. Global snow cover monitoring: an update. *Bull. Am. Meteorol. Soc.* 74: 1689-1696.

Rovansek, R.J., Hinzman, L.D. & Kane, D.L. 1996. Hydrology of a tundra wetland complex on the Alaskan Arctic coastal plain, U.S.A. *Arctic and Alpine Research* 28(3): 311-317.

Shutov, V., Gieck, R.E., Hinzman, L.D. & Kane, D.L. 2006. Evaporation from land surface in high latitude areas: a review of methods and study results. *Nordic Hydrology* 37(4/5): 393-411.

Sturm, M., Racine, C. & Tape, K. 2001. Increasing shrub abundance in the Arctic. *Nature* 411: 546-547.

Vinnikov, K.Y., Robock, A., Stouffer, R.J., Walsh, J.E., Parkinson, C.L., Cavalieri, D.J., Mitchell, J.F.B., Garrett, D. & Zakharov, V.K. 1999. Global warming and Northern Hemisphere sea ice extent. *Science* 286: 1934-1937.

# Detailed Cryostratigraphic Studies of Syngenetic Permafrost in the Winze of the CRREL Permafrost Tunnel, Fox, Alaska

Mikhail Kanevskiy
*University of Alaska Fairbanks Institute of Northern Engineering, Fairbanks, Alaska, USA*
Daniel Fortier
*University of Alaska Fairbanks Institute of Northern Engineering, Fairbanks, Alaska, USA*
Yuri Shur
*University of Alaska Fairbanks Department of Civil and Environmental Engineering, Fairbanks, Alaska, USA*
Matthew Bray
*University of Alaska Fairbanks Department of Civil and Environmental Engineering, Fairbanks, Alaska, USA*
Torre Jorgenson
*ABR, Inc., Fairbanks, Alaska, USA*

## Abstract

The CRREL Permafrost Tunnel is a well-known location for studies of Late Pleistocene syngenetic permafrost. Our detailed cryostratigraphic mapping in the winze of the tunnel was based on study of cryogenic structure, ice content of the sediments, and different types of massive ice. The results show that original ice-rich syngenetically frozen silts were partly reworked by thermal erosion, which proceeded mainly along the large ice wedges. Gullies and underground channels, formed at various depths, were filled with ice and sediments, the structure and properties of which differ from the original syngenetic permafrost. In the winze, thin peat layers underlain by distinct ice lenses were observed. These layers mark the former positions of the permafrost table during peat accumulation, which occurred during slower sedimentation periods.

**Keywords:** Alaska; cryofacial analysis; cryostructure; mapping; syngenetic permafrost; thermal erosion.

## Introduction

The well-known CRREL Permafrost Tunnel located near Fairbanks, Alaska, offers exposures of the Late Pleistocene syngenetically frozen silts with large ice wedges. The tunnel, constructed more than 40 years ago, consists of a main horizontal adit, which reaches 110 m in length, and an inclined winze 45 m long.

Ice-rich silts exposed in the tunnel belong to Goldstream Loess Formation of Wisconsinan age and are underlain by the gold-bearing Fox Gravel (Péwé 1975, Long & Péwé, 1996). Silts of eolian origin were partly reworked and retransported by slope and fluvial processes (Péwé 1975, Hamilton et al. 1988).

Similar syngenetic ice-rich permafrost with huge ice wedges was observed in many unglaciated areas of Siberia and Northern America. In Russian literature they are known as "Yedoma" or "Ice Complex" sediments (Katasonov 1978, Popov et al. 1985, Romanovskii 1993). Such permafrost has been studied in the continuous permafrost zone, and its occurrence in central Alaska is a rare phenomenon.

The tunnel, and particularly its adit, has been extensively studied by geologists and recently by permafrost scientists. Sellmann (1967) made general sketches of the exposures and characterized the stratigraphy and main types of ground ice observed in the tunnel. Detailed geological and paleoenvironmental studies of Quaternary sediments in the tunnel were performed by Hamilton et al. (1988).

Shur et al. (2004) identified features related to original syngenetic permafrost and showed the impact of thermo-erosion processes on the structure of the permafrost. Bray et al. (2006) performed mapping of permafrost in the main adit. Both works were focused on identification of differences between original permafrost and later modifications of it. However, in-depth understanding of syngenetic permafrost formation requires more detailed studies of permafrost properties and cryogenic structures. This paper presents detailed cryostratigraphic studies performed in the winze, where the original syngenetic permafrost is preserved better than in the main adit.

The main goals of our study were: (a) to compile a cryostratigraphic map of the winze, (b) to describe cryostructures of the permafrost, (c) to reconstruct events of the permafrost and sedimentary history of the study area, and (d) to estimate the ice content of the sediments.

## Methods

The section of the winze 38 m long and from 12 to 18 m below the surface was studied in 2005–2006. The cryostratigraphic mapping used a cryofacial analysis proposed by Katasonov (1978). This analysis is based on the close relationship between cryostructure assemblages and specific terrain units, and reveals the way permafrost was formed. Cryofacial analysis has been especially useful for study of syngenetic permafrost (Katasonov, 1978).

The mapping of one wall and ceiling of the winze was performed in the scale 1:20; several sections were studied

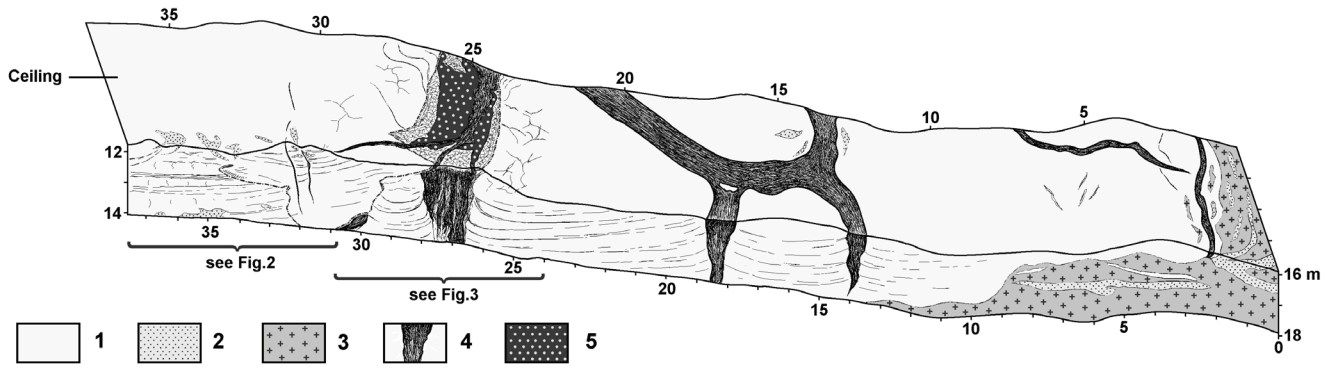


Figure 1. General view of the left wall and the ceiling of the winze. 1–silt; 2–sand; 3–Fox Gravel; 4–ice wedge; 5–thermokarst-cave ice.

greater detail (scale 1:4). Figure 1 shows the general view of the winze; more detailed fragments are shown in Figures 2 to 4. AMS radiocarbon dating (Fig. 2) was performed at the University of Arizona.

## Results

The permafrost soils in the winze are mainly silts with sand lenses. The main cryostructure is micro-lenticular (Shur et al. 2004, Bray et al. 2006), which is characterized by occurrence of very small sub-horizontal (sometimes wavy) discontinuous ice lenses. The thickness of uniformly distributed ice lenses (and vertical spacing between them as well) usually does not exceed 0.5 mm.

Several varieties of micro-lenticular cryostructure can be distinguished in the winze (e.g., latent micro-lenticular, micro-braided). Micro-lenticular cryostructure (including all its varieties) is the most typical cryostructure of syngenetic permafrost; usually it occupies not less than 50–60% of the entire thickness of such sections (Kanevskiy 1991, 2003).

In the winze, gravimetric moisture content of the sediments with micro-lenticular cryostructure varies from 100% to 240% (Fig. 4a, Ssection 1). The similar range (80–180%, average 130%) was found in the adit of the tunnel (Bray et al. 2006). Organic content of the sediments varies from 3.3% to 9.5% by weight (Fig. 4a); the greatest values are specific to the organic-rich layers. The radiocarbon dates for these layers vary from 31, 000 to 35,000 y BP (Fig. 2).

Seven thin organic-rich horizons were observed in the upper part of the winze, at a depth of 12–14 m from the ground surface (Fig. 2). At the depth of about 0.4 to 0.6 m below each peat horizon, there are distinct ice (or ice-rich) layers (referred to as *belts* in the Russian literature). Numerous thin cracks partially filled with ice (ice veins) extend downward from the peat layers to a depth of up to 0.5 m. These cracks form polygons up to 0.5 m across.

Numerous sites of former gullies and underground channels were observed at various depths. They had been cut by running water in the silty sediments and afterwards filled with thermokarst-cave ice and soils, the structure and properties of which differ from the original syngenetic permafrost (Shur et al. 2004, Bray et al. 2006, Fortier et al. 2008).

In the winze, the gully filled with sediments was observed at the interval 29–35 m (Figs. 1 to 3). A truncated ice wedge affected by thermal erosion is located under this gully. The sediments filling the gully are mostly ice-poor stratified silts with lenses of sands. They contain numerous inclusions of organic material, which were interpreted as having been reworked by water. The organic content of the sediments in the gully varies from 7.0% to 22.8% and is much higher in comparison with the original permafrost (Fig. 4b).

Cryostructures in the lower part of section 2 (Fig. 4b, 60-165 cm) vary from latent micro-lenticular to porous. The gravimetric moisture content of this part of section 2 varies from 70% to 100% which is smaller than the water content of the original syngenetic permafrost. Such water content is unusual for sediments with very small amount of visible ice. It can be attributed to the higher organic content (Fig. 4b). Sediments with an organic content of 9–12% have a gravimetric moisture content of 70–80%, whereas sediments with organic content of 14–16% have a moisture content of 90–100%.

The cryostructures and ice contents of the upper part of the section 2 (Fig. 4b, 0–60 cm) are similar to those of the original permafrost; the gravimetric moisture contents here vary from 110% to 140%. This indicates change of sedimentation mode and decrease of sedimentation rate at the last stages of gully infilling.

Ice wedges observed in the winze have width of up to 1.8 m; their apexes terminate at the stratigraphic contact between the silts and the underlying alluvial gravels (Fig. 1). The exposure of ice wedges at the ceiling of the winze allows for an estimation of the shape and size of polygons, which reaches 8–12 m.

A horizontal body of thermokarst-cave ice crosscutting the ice wedge is exposed on the ceiling in the upper part of the winze (Fig. 3, section A-B). Its thickness varies from 0.2 to 0.35 m and it is underlain by a silt layer (0.1–0.4 m thick) with a reticulate-chaotic cryostructure (Shur et al. 2004, Fortier et al. 2008). This ice body is aligned with the ice wedge; however, it is wider than the wedge and therefore incised in the permafrost surrounding the ice wedge. The thermokarst-cave ice body is crossed by numerous sub-vertical ice veins, forming a small secondary ice wedge (Fig. 3, section A-B). Similar structures were observed in the adit (Shur et al. 2004, Bray et al. 2006).

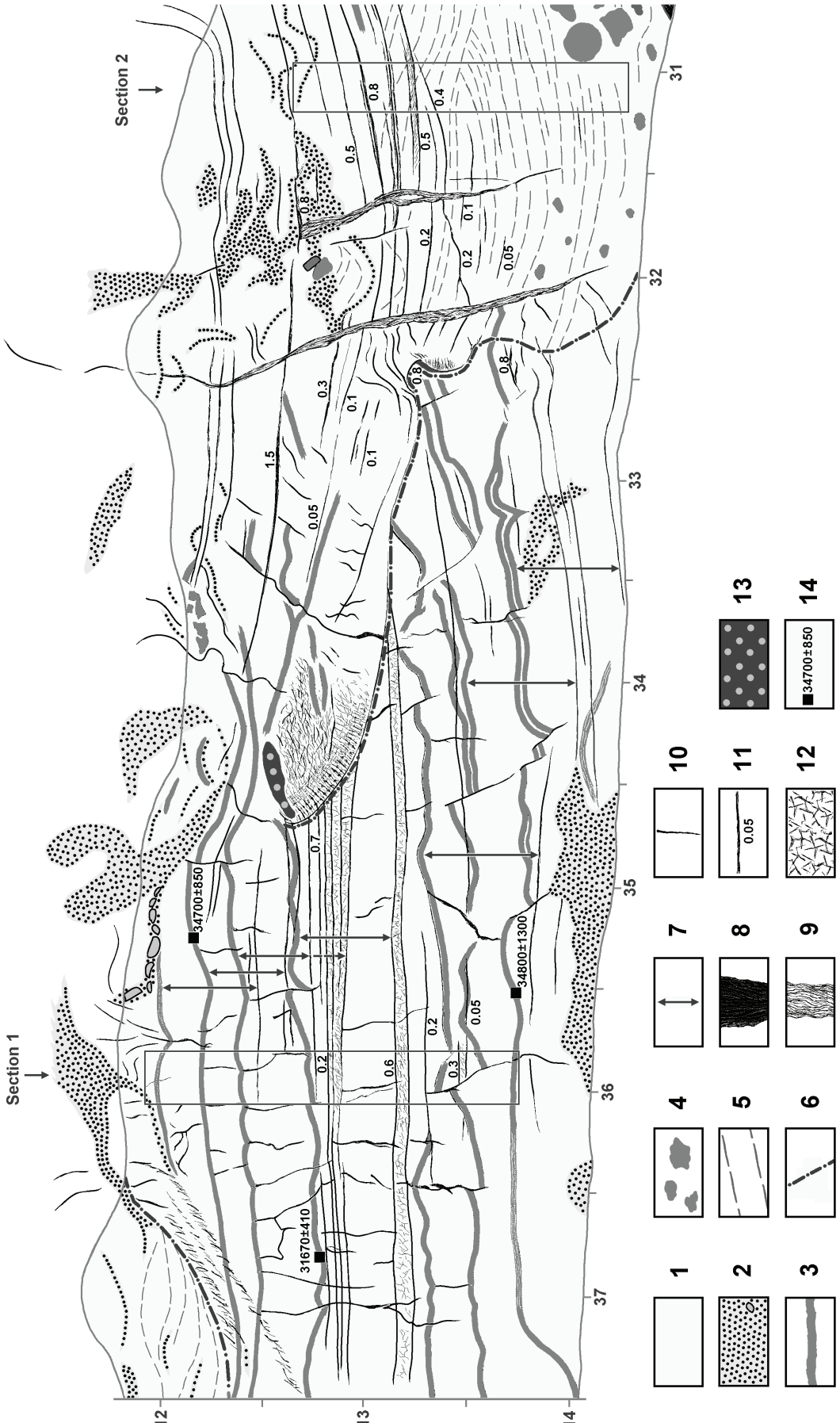


Figure 2. Cryostratigraphic map of the left wall of the winze, interval 31–37 m. 1–silt; 2–sand, gravel inclusion; 3–in situ peat layers; 4–inclusions of re-transported organic matter; 5–lamination in silt; 6–erosion boundary; 7–approximate position of active layer at the periods of slower sedimentation; 8–ice wedge; 9–composite wedge (ice/silt); 10–isolated ice vein; 11–ice layer (belt), thickness in cm; 12–reticulate-chaotic cryostructure; 13–thermokarst-cave ice; 14–uncalibrated radiocarbon age in y BP.

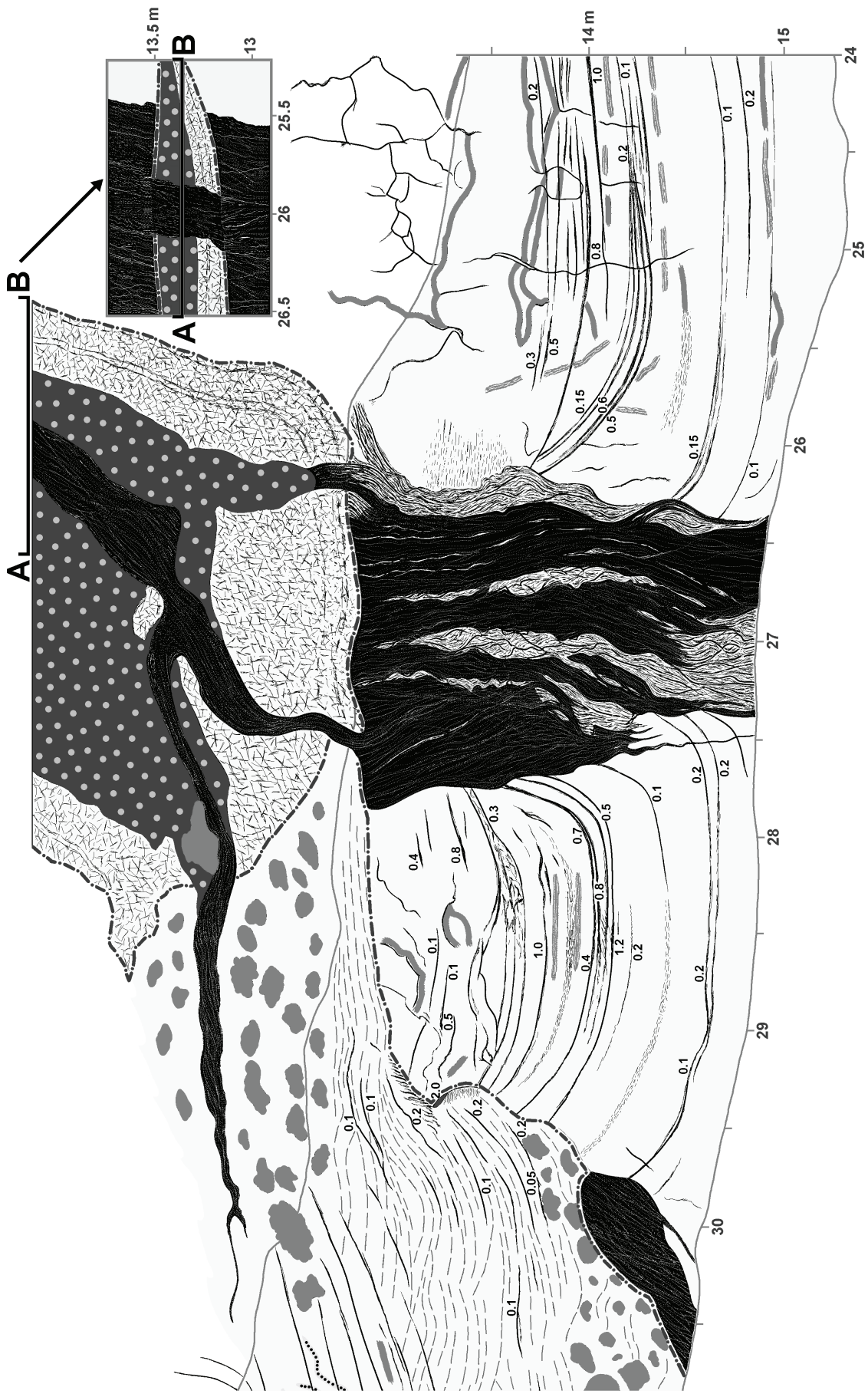


Figure 3. Cryostratigraphic map of the left wall of the winze, interval 24–31 m. For the legend, see Figure 2. A–B–schematic reconstruction of vertical section through the thermokarst-cave ice body, located at the ceiling of the winze.

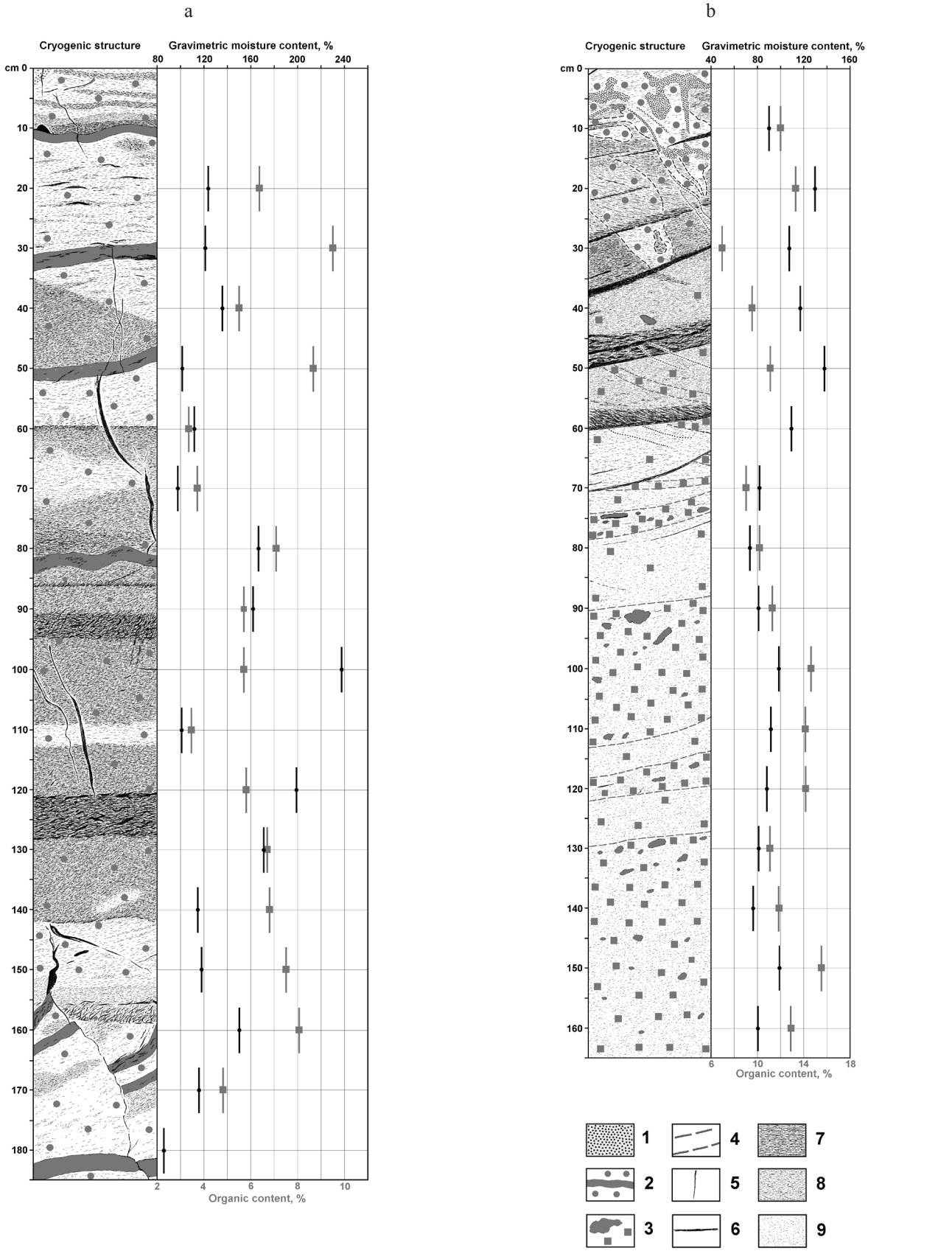


Figure 4. Details of cryogenic structure and properties of sections 1 (a) and 2 (b); location of sections is shown at Figure 2. 1–sand; 2–*in situ* peat layer and inclusions of organic matter; 3–inclusions of retransported organic matter; 4–lamination in silt; 5–isolated ice vein; 6–distinct ice layer (belt); 7–micro-braided cryostructure; 8–micro-lenticular cryostructure; 9–latent micro-lenticular/porous cryostructure.

## Discussion

The study shows the prevalence of ice-rich syngenetically frozen silts with some areas partly reworked by thermal erosion, which proceeded mainly along large ice wedges. The evidences of syngenetic freezing, including undecomposed tiny rootlets and the prevalence of a micro-lenticular cryostructure, were observed directly above the contact between silts and poorly sorted alluvial gravels. The occurrence of micro-lenticular cryostructure varieties is typical for syngenetic permafrost, and is mostly linked to different rates of sedimentation (Kanevskiy 1991, 2003). The great variability of gravimetric moisture content of silts can be associated with the different cryostructures.

We associate the ice layers (belts), located beneath organic-rich horizons (Fig. 2), with the bottom of the active layer at the periods of temporary stabilization of the ground surface which occurred during periods of slower sedimentation favorable to peat accumulation. Approximate positions of the active layer at this time are denoted with arrows in Figure 2. During periods of very slow sedimentation, small polygons were formed due to shallow cracking at the stabilized surface.

There are several lines of evidence to suggest thermal erosion processes were going simultaneously with syngenetic permafrost formation. First, the occurrence of ice veins in the thermokarst-cave ice body suggests that the ice wedge continued to grow after its partial destruction by thermo-erosion and the subsequent formation of the thermokarst-cave ice. Second, the cryogenic structure of the upper part of the "gully" section (Fig. 4b) is identical to the cryogenic structure of the original permafrost.

## Conclusions

Mapping in the winze of the CRREL permafrost tunnel shows the prevalence of ice-rich syngenetically frozen silts with micro-lenticular cryostructure. Periods of slow sedimentation were marked by peaty horizons and distinct ice layers, located at a depth of about 0.4 to 0.6 m below every peat horizon. These ice layers show the former positions of the permafrost table during the peat accumulation. Small ice veins extend downward from peaty horizons, forming polygons up to 0.5 m across.

The original syngenetic permafrost was partly reworked by thermal erosion, which proceeded mainly along ice wedges. No clear evidence of thermokarst was observed. Thaw unconformities are connected with the development of gullies and underground channels. These cavities were filled with water and soils, which froze back in situ, and which differ in structure and properties from the original syngenetic permafrost. Thermal erosion processes were going simultaneously with accumulation of syngenetically frozen silts and ice wedge development.

## Acknowledgments

We thank the Cold Regions Research and Engineering Laboratory (CRREL) and its Fairbanks office for the opportunity to perform our studies in the tunnel. We are grateful to Margaret Cysewski, Eva Stephani, and Matthew Dillon for their field and laboratory assistance. This work was supported by the National Science Foundation under grant ARC-0454939 and Alaska EPSCoR, funded by the NSF award #0701898 and the state of Alaska. Any opinions and findings expressed in this material are those of the authors and do not necessarily reflect the views of the NSF.

## References

Bray, M.T., French, H.M. & Shur, Y. 2006. Further cryostratigraphic observations in the CRREL permafrost tunnel, Fox, Alaska. *Permafrost and Periglacial Processes* 17(3): 233-243.

Fortier, D., Kanevskiy, M. & Shur, Y. 2008. Genesis of reticulate-chaotic cryostructure in permafrost. *Proceedings of the Ninth International Conference on Permafrost*, *Fairbanks, Alaska, June 29–July 3, 2008* (this proceedings).

Hamilton, T.D., Craig, J.L. & Sellmann P.V. 1988. The Fox permafrost tunnel: a late Quaternary geologic record in central Alaska. *Geological Society of America Bulletin* 100: 948-969.

Kanevskiy, M.Z. 1991. The role of quasi-syngenesis in formation of Quaternary sediments cryogenic structure in Northern Yakutia. In: P. Melnikov, & Y. Shur, (eds.), *The Upper Horizon of Permafrost.* Moscow: Nauka, 47-63 (in Russian).

Kanevskiy, M. 2003. Cryogenic structure of mountain slope deposits, northeast Russia. *Proceedings of the Eighth International Conference on Permafrost*, *Zurich, Switzerland, July 21-25, 2003*: 513-518.

Katasonov, E.M. 1978. Permafrost-facies analysis as the main method of cryolithology. *Proceedings of the Second International Conference on Permafrost*, *July 13-28, 1973*, *USSR Contribution*. Washington: National Academy of Sciences, 171-176.

Long, A. & Péwé, T.L. 1996. Carbon dating by high-sensitivity liquid scintillation counting of wood from the Fox permafrost tunnel near Fairbanks, Alaska. *Permafrost and Periglacial Processes* 7(3): 281-285.

Péwé, T.L. 1975. *Quaternary geology of Alaska. Geological survey professional paper 835*. Washington,D.C.: United States Government Printing Office, 145 pp.

Popov, A.I., Rozenbaum, G.E. & Tumel, N.V. 1985. *Cryolithology*. Moscow: Moscow University Press, 239 pp. (in Russian).

Romanovskii, N.N. 1993. *Fundamentals of cryogenesis of lithosphere*. Moscow: Moscow University Press, 336 pp. (in Russian).

Sellmann, P.V. 1967. *Geology of the USA CRREL permafrost tunnel, Fairbanks, Alaska.* Hanover, New Hampshire: US Army CRREL Technical Report 199, 22 pp.

Shur, Y., French, H.M., Bray, M.T. & Anderson, D.A. 2004. Syngenetic permafrost growth: cryostratigraphic observations from the CRREL Tunnel near Fairbanks, Alaska. *Permafrost and Periglacial Processes* 15(4): 339-347.

# Interactive Stress Between Frost Bulb and Chilled Pipe by an Axis-Symmetric Freezing Experiment

Shunji Kanie
*Graduate School of Engineering, Hokkaido University, Sapporo, Japan*
Satoshi Akagawa
*Graduate School of Engineering, Hokkaido University, Sapporo, Japan*
Motohiro Sato
*Graduate School of Engineering, Hokkaido University, Sapporo, Japan*
Hikaru Okamoto
*Graduate School of Engineering, Hokkaido University, Sapporo, Japan*

## Abstract

It has been known that a chilled gas pipeline buried in frost susceptible soil can be subjected to frost heave deformation. Frost heave itself has been studied by various researchers, but experimental observations of the mechanical interaction between the gas pipeline and the surrounding frost bulb has been rarely reported. The purpose of this study is to experimentally observe the interactive behavior between a chilled pipe and frost bulb under simplified conditions. The authors carried out an axis-symmetric freezing experiment which promotes formation of a concentric frost bulb. It is obviously difficult to measure the interactive stress, as well as the stress distribution, in the specimen. Therefore, the authors adopted complementary calculations for stress evaluation. Though the specimen is assumed elastic and homogeneous in the calculation, changes in the interactive stress between frost bulb and the pipe are estimated during frost bulb formation based on the observation results and analysis.

**Keywords:** experiment; frost bulb; mechanical modeling; pipeline; stress.

## Introduction

A chilled gas pipeline installed underground may be subjected to frost heave, since a frost bulb forms around the pipe in frost-susceptible soil. This phenomenon has been studied by numerous researchers. Even in recent studies, Razaqpur and Wang (1996) proposed their practical models for frost heave estimation considering water migration based on the Clausius-Clapeyron equation; for example. Mikkola (2001) demonstrates the applicability of a mathematical model in which a physicochemical structure of the soil is described by using remeshing techniques for the Galaerkin method. As an engineering approach, various evaluation methods applying the segregation potential theory have been developed by Nixon (1982, 1987a-b), Konrad (1987), Shen & Ladanyi (1991), and Selvadurai & Shinde (1993). The authors also have been studying engineering estimation based on Takashi's equation, as a practical evaluation method with a beam on an elastic foundation model. Though frost heave behavior of the pipe with growth of a frost bulb has been researched, interactive stress acting between the frost bulb and chilled pipe has been rarely measured directly.

The purpose of this study is to experimentally observe the interactive behavior under a simplified condition and to consider an engineering evaluation method for interactive stress estimation. The axis-symmetric experiment proposed in this paper aims to promote concentric formation of the frost bulb and to measure stresses acting on the pipe with the growth of the frost bulb. Since it has been known that volumetric change in the frost bulb shows anisotropic properties and is affected by the constraining stress acting in the growing direction of ice lens, the pipe and the surrounding specimen were set vertically to exclude the effect of the force of gravity. As a result, the formation of a concentric frost bulb could be expected in the horizontal plane. Considering the difficulty in measuring the interactive stress at the boundary between the frost bulb and the pipe, the authors adopted a mechanical model for reasoning the interactive stress with known boundary conditions at the inner surface of the pipe and at the periphery of the specimen.

This mechanical model was also applied to examine the anisotropic properties in frost heave ratio during freezing. The calculated stresses on the inner surface of the pipe were compared with the observed stresses and the anisotropic properties of frost heave are discussed.

## Axis-Symmetric Freezing Experiment

In multi-dimensional freezing of frost-susceptible soil, frost heave ratio is depending on the direction of freezing and the constraining stress. If the pipe is set horizontally and frost bulb forms in vertical plane, concentric formation of frost bulb cannot be expected, because the constraining stresses vary with the location in the vertical plane due to gravity force. In order to consider the interactive behavior between pipe and frost bulb, simplified condition without the effect of gravity force is preferable for both empirical and analytical evaluations. Therefore, the pipe and the cylindrical specimen surrounding the pipe were set vertically to promote concentric frost bulb formation in the horizontal plane to realize a quasi-one-dimensional behavior.

Table 1. Experimental conditions for consolidation.

| Material | Kaolin | |
|---|---|---|
| Specific gravity of particle | 2.64 | g/cm$^3$ |
| Water content Before consolidation | 70 | % |
| Water content After consolidation | 50 | % |
| Amplitude of load | 80 | kPa |
| Time for consolidation | 170 | hrs |

*Consolidation phase*

First, frost susceptible material, kaolin, is filled in the mold and vertical load is applied from the top of specimen. Water contained in the specimen is drained from the top and the bottom through porous stones. The temperature of the laboratory is kept at +1°C during consolidation, and the temperature of the specimen is expected to be the same at anywhere in the specimen at the beginning of the freezing phase. The experimental conditions are tabulated in Table 1.

*Freezing phase*

After the consolidation, the outer mold is removed. The specimen keeps its position with constraint by a rubber membrane covering the outer surface of the specimen. Then, cold antifreeze starts to run through the pipe to promote the formation of the frost bulb. In the freezing phase, the top plate of the specimen is replaced with a thick acrylic plate to prevent vertical growth of a frost heave and to observe the formation of a horizontal frost bulb. The temperature of cold antifreeze is controlled to gradually decrease to keep the freezing rate in radial direction of 1 mm/hr based on the heat transfer analysis in advance. The final temperature of cold antifreeze was set at -10°C. Photo 1 shows the experimental apparatus during the consolidation phase and the freezing phase.

*Measurement and observation*

On the inner surface of the pipe, four sets of strain gauges for circumferential and vertical directions were set at the middle height of the specimen. The temperature distribution within the specimen was measured by four thermo-meters to confirm the growth of the frost bulb.

The change in peripheral length of the specimen was recorded by a wire gauge and was used for estimating the constraining stress at the outer boundary based on the spring coefficient of rubber membrane. In addition, frost bulb formation can be observed through the acrylic top plate.

If one wants to directly observe the interactive stress between the outer surface of the pipe and the inner surface of the specimen, installing a pressure gauge at the boundary may be a solution. However, the contact condition for adfreeze strength is affected by the gauge. In this paper, the authors adopt a mechanical model for reasoning interactive stresses using known boundary conditions at the inner surface of the pipe and the periphery of the specimen. This mechanical model will be introduced in the following section.

*Experimental result*

Pictures of the specimen during the freezing phase and after the experiment are shown in Photo 2. The size of the frost bulb was almost the same as that anticipated by thermal analysis, and the final outside diameter of the frost bulb became about 150 mm.

(a) Consolidation phase

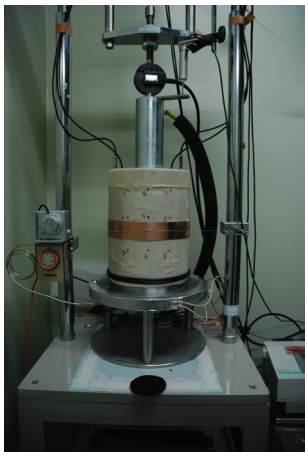

(b) Freezing phase

Photo 1. Experimental apparatus.

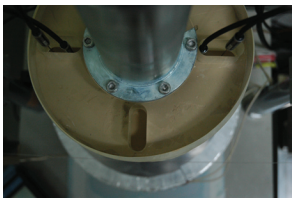

(a) During the freezing

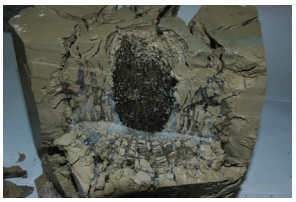

(b) After the freezing

Photo 2. Observed frost bulb: Picture (a) was taken during the freezing phase. Picture (b) is a photo after the freezing.

The stress in circumferential direction on the inner surface of the pipe varies with the growth of the frost bulb. Figure 1 illustrates the change in circumferential stress with time, and it can be found that tensile stress is gradually increasing. The interactive stress between the pipe and the frost bulb will be discussed with the evaluation model introduced in the following section.

The pipe was set at the center before removing, and the front upper part of the specimen was cut out to confirm ice lens formation within the specimen. It is found that a concentric frost bulb was successfully formed.

## Mechanical Model and Analysis

The cylindrical specimen including the pipe is completely axis-symmetric so that a quasi-one-dimensional model with polar coordinates on a horizontal plane was applied. Because the material is assumed homogeneous and isotropic, nonlinear large deformations such as tensile cracks cannot be evaluated. However, anisotropic property in frost heave ratio is considered by giving appropriate radial and circumferential strains for corresponding volumetric change.

*Formulation for stress evaluation*

It can be assumed that the displacement in circumferential direction is zero and no body force is acting. Then, the equilibrium equation is expressed by equation (1).

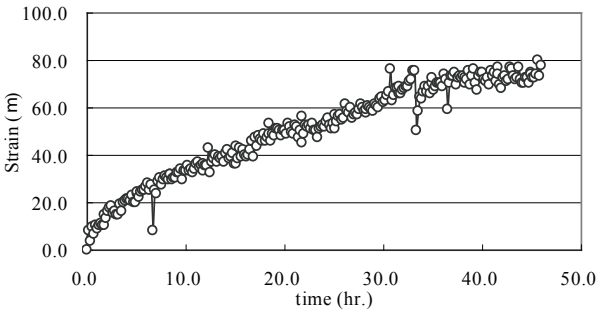


Figure 1. Change in circumferential stress on the inner surface of the pipe with the growth of the frost bulb.

$$\frac{d\sigma_r}{dr}+\frac{1}{r}(\sigma_r-\sigma_\theta)=0 \tag{1}$$

where $r$ stands for the radial coordinate, and $\sigma_r$, $\sigma_\theta$ are stresses in radial and circumferential directions. The stress strain relation is given as follows.

$$\begin{Bmatrix}\varepsilon_r\\ \varepsilon_\theta\end{Bmatrix}=\frac{1+\nu}{E}\begin{bmatrix}(1-\nu) & -\nu\\ -\nu & (1-\nu)\end{bmatrix}\begin{Bmatrix}\sigma_r\\ \sigma_\theta\end{Bmatrix}+\begin{Bmatrix}\varepsilon_{rt}\\ \varepsilon_{t\theta}\end{Bmatrix} \tag{2}$$

$\varepsilon_r$, $\varepsilon_\theta$ are strains in radial and circumferential directions. $E$ and $\nu$ are elastic modulus and Poisson's ratio, respectively. The strains are defined with displacements as equation (3).

$$\varepsilon_r=\frac{du}{dr},\ \varepsilon_\theta=\frac{u}{r} \tag{3}$$

Introducing equations (2) and (3) into (1), we can get the following equation (4).

$$\frac{d}{dr}\left[\frac{1}{r}\frac{d(ru)}{dr}\right]=0 \tag{4}$$

If equation (4) is integrated twice, the displacement $u$ is described as a function of $r$ with two constants.

$$u=\frac{1}{2}C_1r+C_2\frac{1}{r} \tag{5}$$

Introducing a discrete model in the radial direction, the two constants can be related with the displacements at two nodes next to each other. The radial coordinates for those nodes are assumed as $a$ and $b$ respectively. The strains at $r$ between two nodes are given by the following equation.

$$\begin{Bmatrix}\varepsilon_r\\ \varepsilon_\theta\end{Bmatrix}=\frac{1}{a^2-b^2}\begin{bmatrix}1/2 & -1/r^2\\ 1/2 & 1/r^2\end{bmatrix}\begin{bmatrix}2a & -2b\\ -ab^2 & a^2b\end{bmatrix}\begin{Bmatrix}u_a\\ u_b\end{Bmatrix} \tag{6}$$

In order to take the anisotropic property in frost heave ratio into consideration, parameter β, the ratio of inflation strain in θ direction to that in $r$ direction, is introduced.

$$\beta=\varepsilon_{t\theta}/\varepsilon_{tr},\ \varepsilon_v=\varepsilon_{tr}+\varepsilon_{t\theta} \tag{7}$$

$\varepsilon_v$ is the volumetric strain. Finally, we can get the following equation (8) for the discrete model.

$$\begin{Bmatrix}\sigma_r(a)\\ -\sigma_r(b)\end{Bmatrix}=[K]\begin{Bmatrix}u_a\\ u_b\end{Bmatrix}-\frac{\alpha}{1+\beta}\begin{Bmatrix}1-\nu(1-\beta)\\ -1+\nu(1-\beta)\end{Bmatrix}\varepsilon_v \tag{8}$$

Where

$$[K]=\alpha\frac{1}{a^2-b^2}\begin{bmatrix}a+(1-2\nu)b^2/a & -2(1-\nu)b\\ -2(1-\nu)a & b+(1-2\nu)a^2/b\end{bmatrix}$$

$$\alpha=\frac{E}{(1+\nu)(1-2\nu)}$$

Two boundary conditions are necessary for solving the discrete model. At the inner surface of the pipe, no radial stress is assumed because the pressure due to antifreeze is negligible. As another boundary condition, the constraining stress due to the membrane is adopted at the periphery of the specimen

*Volumetric strain*

If no water migration is considered, and contained water in the specimen is completely frozen, the volumetric strain is easily determined based on the water content and inflation ratio of ice. In this study, we applied Takashi's equation for estimating the volumetric strain. Takashi's equation was originally derived from numerous one-dimensional experiments to relate the frost heave ratio with the constraining stress and freezing rate as equation (9).

$$\xi=\xi_0+\frac{\sigma_0}{\sigma}\left(1+\sqrt{\frac{U_0}{U}}\right) \tag{9}$$

$\xi$ : frost heave ratio, $\sigma$ : constraining stress, $U$ : freezing rate and $\xi_0$, $\sigma_0$ and $U_0$ are constants for the material obtained by experiment regulated by Japan Geomechanical Standard.

Though the frost heave ratio in Takashi's equation stands for volumetric change in one-dimensional frost heave, it is also introduced as volumetric strain $\varepsilon_v$ in this study with the anisotropic parameter β. The constraining stress σ varies with the growth of the frost bulb. Then, it was calculated by the mechanical model with the growth and was applied into Takashi's equation to decide the volumetric change. The calculation conditions are tabulated in Table 2.

## Evaluation of Results

*Circumferential stress of pipe*

The observed circumferential stress acting on the inner surface of the pipe has already been introduced in Figure 1. The estimated stresses by the mechanical model are added to the observation results as shown in Figure 2. In this figure, estimations with several variations in β based on Takashi's equation (case 1 to case 3) are illustrated, as well as the estimation results (case 0) in which in-situ freezing without water migration is assumed with isotropic inflation due to freezing. As shown in the figure, the estimation by Takashi's equation with β=0.0 shows good coincidence with the observation.

Table 2. Calculation conditions.

| | | | |
|---|---|---|---|
| Radius | pipe | | 20 mm - 25 mm |
| | specimen | | 25 mm - 100 mm |
| Elastic Modulus | pipe | | 210 GPa |
| | specimen | unfrozen | 150 MPa |
| | | frozen | 300 MPa |
| Poisson's ratio | pipe | | 0.3 |
| | specimen | unfrozen | 0.2 |
| | | Frozen | 0.2 |
| Number of element | | | 76 |

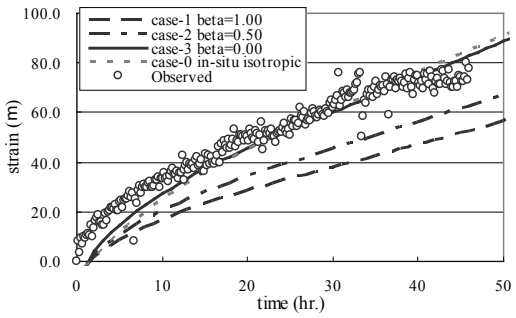


Figure 2. Estimated circumferential stress.

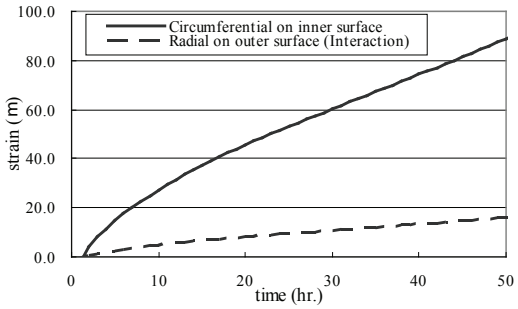


Figure 3. Estimated interactive radial stress.

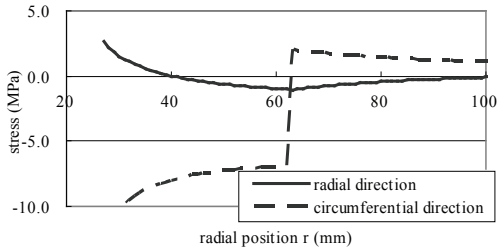


Figure 4. Stress distribution in the specimen (36 h after freezing).

Though the setting of appropriate β requires further study, it is understood that the estimation based on Takashi's equation may give satisfactory estimation for stress interaction.

*Interactive stress between the frost bulb and the pipe*

Figure 3 shows the estimation results for interactive stress in the radial direction between the frost bulb and the pipe based on Takashi's equation with β=0.0. It can be found that the radial interactive stress is tensile and is increasing with time. However, the amplitude of tensile stress is about 20% of the circumferential stress in the pipe. It may be that the frost bulb prevents stress transfer in the radial direction with its inflation. In this analysis, perfect continuity condition at the boundary for the interaction has been assumed, so that further discussion including adfreeze strength at the boundary may be necessary.

Figure 4 shows the stress distribution within the specimen estimated by the mechanical model. It is found that tensile stress in a radial direction is acting near the pipe, and its value reaches the maximum compression at the freezing front. On the other hand, circumferential stress is compressive in the frost bulb, and it becomes tensile in unfrozen soil.

## Conclusion

Important findings obtained through this study are summarized as follows:

The newly-developed axis-symmetric freezing apparatus contributes to concentric formation of a frost bulb, and the interactive stress between frost bulb and pipe is successfully examined.

Evaluation of stress acting on the pipe shows good coincidence with the observation result by introducing Takashi's equation to the estimation of frost heave ratio.

In this study, introducing anisotropic property to frost heave yields better estimation in stress evaluation.

The interactive stress between frost bulb and pipe is tensile stress in the radial direction and is increasing with the growth of the frost bulb.

In this experiment, the specimen was covered with a rubber membrane, and the constraining stress due to the membrane was comparatively small due to its low spring coefficient. For further study, experiments under higher constraint pressure are preferable to scrutinize the interactive action.

## References

Konrad, J.M. 1987. Procedure for determining the segregation potential of freezing soils. *Geotechnical Testing Journal, ASTM* 10: 51-58.

Konrad, J.M. & Shen M. 1996. 2-D frost action modeling using the segregation potential of soils. *Journal of Cold Regions Science and Technology* 24: 263-278.

Mikkola, M. & Hartikainen, J. 2001. Mathematical model of soil freezing and its numerical implementation. *International Journal for Numerical Methods in Engineering* 52: 543-557.

Nixon, J.F. 1982. Field frost heave predictions using the segregation potential concept. *Canadian Geotechnical Journal* 19: 526-529.

Nixon, J.F. 1987a. Thermally induced frost heave beneath chilled pipelines in frozen ground. *Canadian Geotechnical Journal* 24: 260-266.

Nixon, J.F. 1987b. Pipeline frost heave prediction using the segregation potential frost heave method. *Proceedings of Offshore Mechanics and Arctic Engineering* 1-6.

Razaqpur, A.G. & Wang, D. 1996. Frost-induced deformations and stresses in pipeline. *International Journal of Pres Ves & Piping* 69: 105-118.

Selvadurai, A.P.S. & Shinde, S.B. 1993. Frost heave induced mechanics of baried pipelines. *Journal of Geotechnical Engineering, ASCE* 119: 1929-1951.

Shen, M. & Ladanyi, B. 1991. Soil-pipeline interaction during frost heave around a buried chilled pipeline. In: D.S. Sodhi (ed.), *Cold Regions Engineering, ASCE 6th International Specialty Conference*. ASCE Publications, New York, 11-21.

# Permafrost Response to Climate Warming South of Treeline, Mackenzie Delta, Northwest Territories, Canada

J.C.N. Kanigan
*Department of Geography and Environmental Studies, Carleton University, Ottawa, Canada*
C.R. Burn
*Department of Geography and Environmental Studies, Carleton University, Ottawa, Canada*
S.V. Kokelj
*Water Resources Division, Indian and Northern Affairs Canada, Yellowknife, Canada*

## Abstract

The mean annual ground temperature (MAGT) at two sites in the Mackenzie Delta, south of treeline, has increased by 0.3°C and 0.7°C over the past 40 years. This ground warming is less than reported from the adjacent tundra uplands. The hypothesis that MAGTs in the boreal forest region of the delta may have a reduced response to climate warming due to the thermal influence of numerous water bodies has been investigated with an equilibrium geothermal model. The model indicates that water bodies have a warming influence on MAGTs up to 750 m from the lake or channel. If lake-bottom temperatures do not respond to climate warming, or warm more slowly than ground surface temperatures, then MAGTs at sites close to water bodies will warm more slowly than sites located greater than 750 m away. This may partly explain the apparent dampening of ground thermal responses to climate change in the delta.

**Keywords:** climate warming; ground temperature; Mackenzie Delta; modeling; thermal regime; water bodies.

## Introduction

This paper examines the sensitivity of permafrost to climate change in an area where different surfaces may vary in their response to warming. The southern and central Mackenzie Delta is forested, and approximately 40% of the area is occupied by water bodies (Mackay 1963, Emmerton et al. 2007) (Figs. 1, 2). The delta region is experiencing relatively rapid climate warming, and the annual mean air temperature has increased from about -10°C to -7°C between 1960 and 2005 (Fig. 3) (Environment Canada 2007). Ground temperatures at 24 to 29 m depth at three shrub tundra sites northeast of the delta have responded to this warming, increasing by 0.2°C, 0.4°C, and 0.8°C between 1990 and 2002 (Smith et al. 2005). We hypothesize that mean annual ground temperatures (MAGT) in the delta may differ in their response to climate warming from those in the tundra uplands due to the physical characteristics of the forest cover, and the thermal influence of the more numerous water bodies. Annual mean lake-bottom temperatures may be more stable over time than similar land-surface temperatures because the climatic warming is dominantly in winter, when lakes are ice covered and lake-bottom temperatures remain close to 0°C and are insensitive to fluctuations in air temperature (Maxwell 1997, Burn 2002).

In this paper we report recent ground temperature change in the boreal forest regions of the Mackenzie Delta. Ground temperatures measured in 2006 at two forested sites near Inuvik and Reindeer Station (Fig. 1) are compared with data collected in 1961 and 1969. Previous studies have acknowledged that ground temperatures are higher in the delta than in the adjacent tundra uplands due to the thermal influence of water bodies, and have attempted to remove this influence by situating ground temperature measurement sites away from water (Mackay 1974). In this study, an equilibrium model was used to determine the distance from water bodies at which the thermal disturbance is negligible, and a spatial analysis was conducted to quantify the area

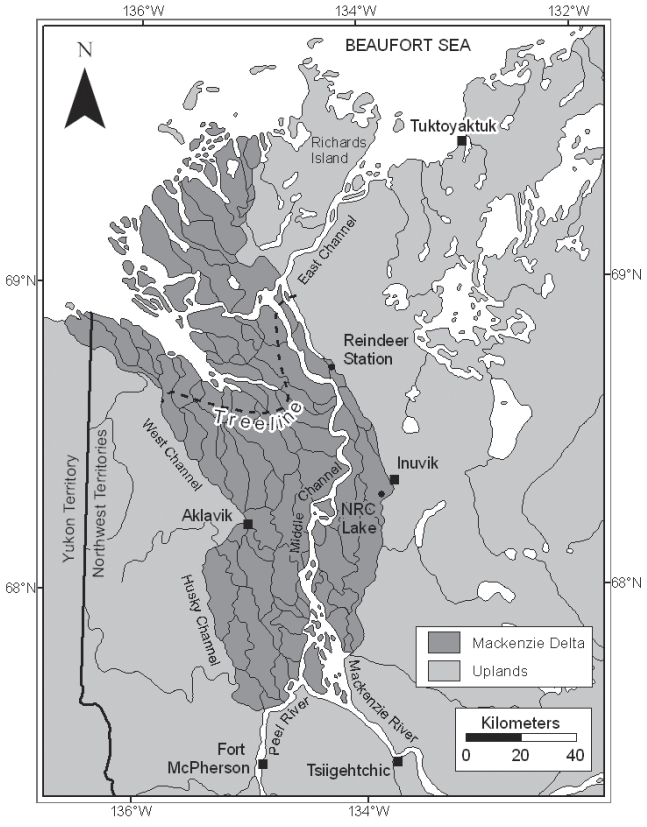


Figure 1. Mackenzie Delta region. Dark grey shading bounds the delta, and treeline is delimited by the dotted line (Mackay 1963).

Figure 2. Mackenzie Delta south of treeline. Land surfaces dominated by spruce forest are separated by channels and lakes.

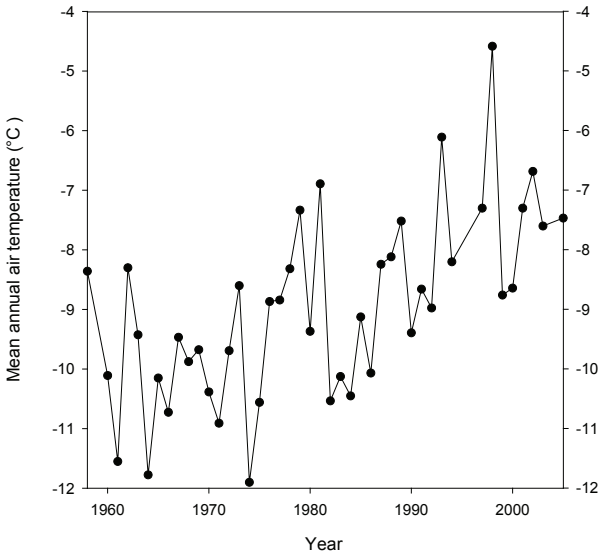


Figure 3. Mean annual air temperatures at Inuvik, 1958 to 2005. Data from Environment Canada (2007).

of the delta which is unaffected by the warming of water. We discuss whether ground temperatures in the delta will respond less to climate warming than in upland terrain, where there is a lower density of lakes.

## The Mackenzie Delta Region

A variety of permafrost and terrain conditions exist in the Mackenzie Delta region, with a principal distinction between the alluvial delta and the shrub-tundra uplands to the east (Fig. 1). The delta is flooded annually by waters from the Mackenzie and Peel Rivers. Infiltration of flood water contributes to higher MAGT in the delta (-2°C to -4°C) than in the tundra uplands northeast of the delta (-6°C to -9°C) (Mackay 1974). The deposition of nutrients during the flood contributes to a northern extension of treeline, which forms the boundary between the central and northern delta (Fig. 1) (Mackay 1963).

The ground is warmer in the delta than in the surrounding uplands principally due to the high density of lakes and channels (Smith 1975). The late winter ice thickness on lakes in the central delta is less than 1 m, and most lakes do not freeze through (Mackay 1963, Marsh & Lesack 1996). As a result, an unfrozen talik forms in the sediments underneath most lakes of the Mackenzie Delta. The ground temperature beside lakes and channels is affected by heat flowing from the warmer sediments under the water body to the surrounding permafrost (Williams & Smith 1989).

South of treeline, white spruce (*Picea glauca*) communities occupy the majority of the land surface above the level of annual flooding. These communities are associated with colder permafrost than lower elevation sites because of surface conditions related to reduced flooding, including a thicker organic layer and a thinner snow cover due to canopy interception (Mackay 1974, Smith 1975, Pearce et al. 1988). The uppermost 1 to 2 m of permafrost in most spruce-forest communities are characterized by high ground-ice content, and, in places, syngenetic ice wedges (Kokelj & Burn 2005). Land surfaces of the central and southern delta located well away from water bodies have been used to measure ground temperatures that are relatively undisturbed by warming related to the presence of water (Mackay 1974).

## Methods

*Field methods*

Ground temperatures were measured at two spruce-forest sites in the east central delta for comparison with data collected in 1961 and 1969 (Fig. 1) (Johnston & Brown 1964, Smith 1973). The site near Reindeer Station is located 101 m from the nearest lake, and 110 m from a channel, and the site at NRC Lake is located 77 m from the nearest lake and 72 m from a channel. These sites are representative of forested surfaces in the delta. Both sites were re-instrumented in 2004 by drilling a hole with a water-jet within 50 m of the original location and installing thermistors at comparable depths. Steel pipe was used to case the hole, which was filled with low conductivity silicone oil, and seven calibrated thermistors were installed at 0.5, 1.0, 3.0, 5.0, 7.0, 9.0, 11.0, 13.0, and 15.0 m depths. Steel pipe was used because it is sufficiently robust to withstand environmental stresses in the field. Temperatures at 15 m depth were of interest since this is near the depth of zero annual amplitude (Mackay 1974). It is assumed that the conductivity of the black iron pipe has a minimal influence at 15 m. The temperature at this depth corresponds with the MAGT and responds to long-term changes in air temperature or surface conditions, rather than seasonal fluctuations. Temperature measurements were made in 2006 to ensure that thermal equilibrium had re-established after drilling.

*Analytical methods*

The warming effect of water bodies on ground temperatures was modeled using equations developed by Lachenbruch (1957) and modified by Burn (2002). In the absence of water bodies, the undisturbed ground temperature profile is:

$$T_z = T_g + z/I \quad (1)$$

where $T_z$ is the temperature (°C) at depth z (m), $T_g$ is the mean annual ground surface temperature (°C), and I is the geothermal gradient (m°C$^{-1}$).

In the delta, the configuration of land and water can be modeled as a strip of a specified width of land that is bounded by a wide channel on one side, and a large lake on the other (Fig. 4). This is a conservative approach, as it assumes that the permafrost is a disturbance to ambient conditions governed by water bodies, not vice-versa. Many diagrams of the distribution of permafrost in the delta are consistent with this position (e.g. Smith & Hwang 1973, Fig. 4; Smith 1976, Fig. 14). This is a simplified representation of field conditions as modeled by Brown et al. (1964), who required a specific configuration for water bodies surrounding the site. In this paper, we are interested in a more general case. Under steady-state conditions, the ground temperature profile at a point on this strip of land is:

$$T_z = T_w + z/I + [(T_g - T_w)/\pi] [\tan^{-1}(H_{p1}/z) + \tan^{-1}(H_{p2}/z)] \quad (2)$$

(modified from Burn 2002, eq. 4) where $T_w$ is the mean annual water temperature (°C), $H_{p1}$ is the width (m) of the strip of land from the lake to the point of measurement, and $H_{p2}$ is the width (m) of the strip of land from the point of measurement to the channel. Current conditions are described by $T_g$ = -3°C, $T_w$ = 6°C, and I = 45 m°C$^{-1}$ (Burn 2002). Ground temperatures were measured at 50 cm below the ground surface at the two delta spruce forest sites at Reindeer Station and NRC Lake between January 2005 and December 2006 to obtain $T_g$. The $T_w$ was estimated from the mean annual lake-bottom temperature at NRC Lake, a small lake near Inuvik, measured from August 2005 to August 2007. NRC Lake is representative of the size and depth of most lakes in the delta (Johnston & Brown 1964, Marsh et al. 1999, Emmerton et al. 2007), and is representative of the flooding frequency of approximately 33% of lakes in the central delta, which is about once in five years (Marsh & Hey 1989). Smith (1976) reports less than 1°C difference between the $T_w$ for a delta lake-bottom and $T_w$ in channels.

A GIS analysis of topographic maps of the central and southern delta was conducted to determine the extent of terrestrial surfaces influenced by water bodies using ArcMap™ version 9.2. (Environmental Systems Research Institute 2007). National Topographic Database 1:50,000 scale vector data were used (Canada Center for Topographic Information, http://maps.nrcan.gc.ca), applying delta boundaries and treeline defined by Mackay (1963) (Fig. 1). Most aerial photographs used to generate the maps were taken during the early 1950s. Buffers were placed around channels and lakes in order to calculate the percentages of land in the delta located greater than 0, 50, 75, 100, 150, 300, 500, and 750 m away from a water body.

## Results

*Field results*

To characterize the current thermal regime, maximum and minimum ground temperatures recorded between January 2005 and December 2006 are presented in Figures 5 and 6. The 15 m ground temperature at the NRC Lake site increased from -3.5°C in May 1961 to -2.8°C in April 2006, a total increase of 0.7°C, or about 0.2°C per decade. At the site near Reindeer Station, ground temperature at 15 m depth increased by about 0.1°C per decade, from -2.3°C in September 1969 to -2.0°C in September 2006, a total increase of 0.3°C. Surface conditions at the time of the historical measurements were similar to those at present (Johnston & Brown 1964, Smith 1973); so it is likely that climate warming has contributed to the higher present day ground temperatures. Based on these two sites, it appears that ground temperatures in the delta have increased at a slower rate than on the adjacent shrub tundra (Smith et al. 2005). Data from the shrub tundra were obtained from below the depth of zero annual amplitude (24 and 29 m), and it is likely that even greater increases would have been recorded at the depth of zero annual amplitude.

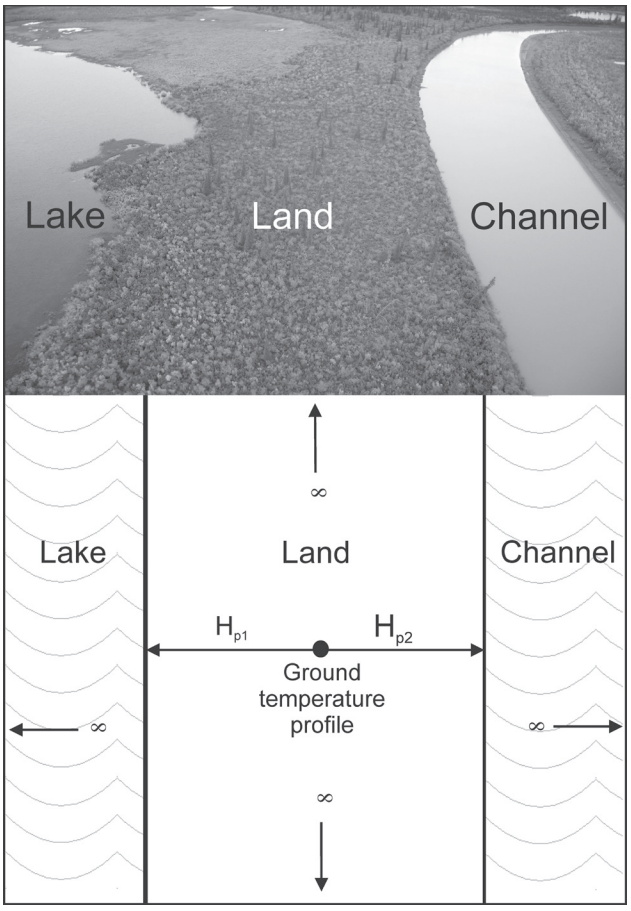

Figure 4. Configuration of ground and water bodies for simplified calculation of thermal disturbance from water in the delta environment.

*Analytical results*

Comparison of 15 m depth ground temperatures for various horizontal distances from water bodies with the undisturbed ground temperature are presented in Figure 7. The results indicate that in close proximity to water bodies ($H_{p1}$=$H_{p2}$ = 0 to 200 m) the warming influence of the water decreases greatly as the horizontal distance from

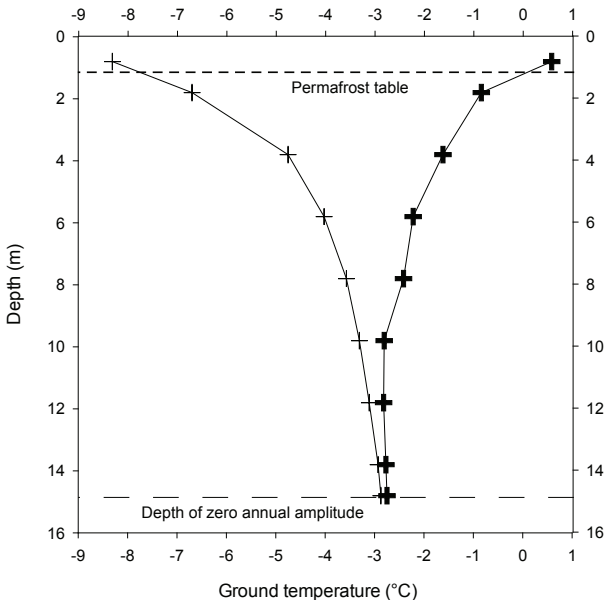


Figure 5. Ground temperature envelope from NRC Lake site, January 2005 to December 2006.

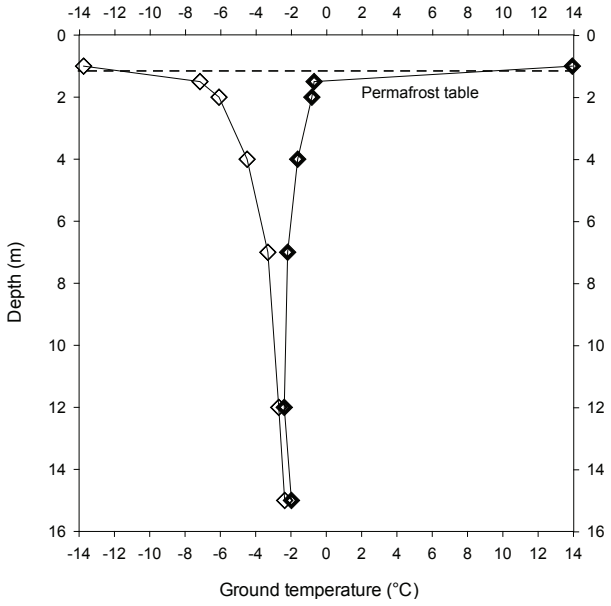


Figure 6. Ground temperature envelope from Reindeer Station site, January 2005 to December 2006.

water bodies increases. With further increases in horizontal distance ($H_{p1}$=$H_{p2}$ = 200 to 1000 m), the ground temperature decrease is much reduced. If the distance from one water body remains small ($H_{p1}$ = 50 m), as the distance from the second water body ($H_{p2}$) is increased, then the 15 m depth ground temperature remains above the undisturbed ground temperature despite further increases in $H_{p2}$, due to the close proximity of the first water body. The undisturbed ground temperature is approached where there is a large distance from both water bodies ($H_{p1}$=$H_{p2}$ = 750 m).

Figure 7 shows that the difference between the disturbed and undisturbed ground temperature at 15 m depth is 0.1°C, 750 m from a water body. This difference approximates the precision of a thermistor, so at this distance the warming

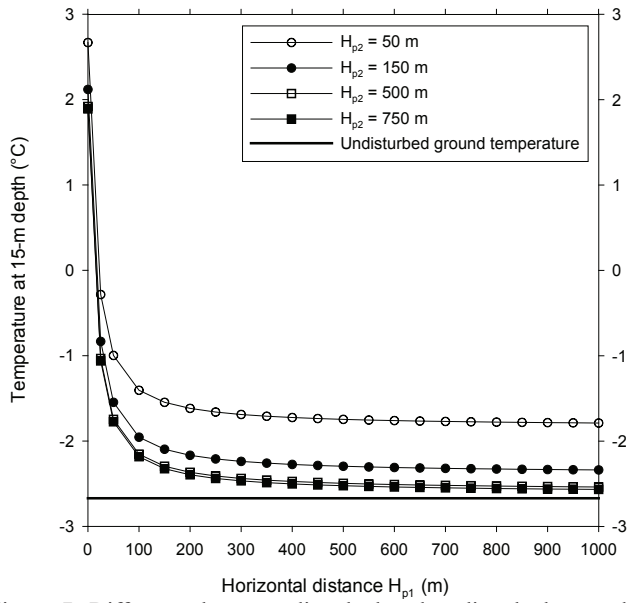


Figure 7. Difference between disturbed and undisturbed ground temperature as distances from channel and lake increase.

effect of water bodies is not detectable. The thermal influence of water bodies is detectable up to distances of about 750 m.

Spatial analysis of the central and southern delta indicated a total area of approximately 7900 km², of which about 58% is land. Only about 2% of land surfaces in the central and southern delta are located more than 750 m away from a water body (Fig. 8). This suggests that in the delta south of treeline, almost all ground temperatures at 15 m depth are affected to some extent by the thermal disturbance of water. The thermal effect is significant for most land areas, since a large proportion (81%) of terrestrial surfaces in the delta are located less than 150 m from a water body. The calculated 15 m depth ground temperature at a site located 150 m from a water body, given current $T_g$ and $T_w$, is 0.6°C higher than the undisturbed ground temperature.

To test the hypothesis that ground where the temperature is affected by water bodies will warm less than unaffected ground, the equilibrium model was used to simulate the response of ground temperatures at 15 m depth to changes in $T_g$ and $T_w$. Sites 50 and 150 m away from water bodies were used to simulate disturbed ground, and sites 750 m from water bodies to simulate undisturbed ground (Table 1). Data in Table 1 indicate that if the $T_g$ and $T_w$ are increased by the same amount, there is an equivalent increase in the temperature at 15 m depth, regardless of the horizontal distance from water bodies. So if ground and water temperatures respond to climate warming at the same rate, then MAGTs will respond uniformly throughout the delta.

The remaining scenarios simulate different responses of ground and water to climate warming. If $T_g$ increases but $T_w$ remains constant, the full increase in $T_g$ is propagated to 15 m at sites located 750 m away from water bodies. However, the unchanged $T_w$ is important at sites located 150 m or less from water bodies. The second scenario in Table 1 describes an increase of 1°C in $T_g$, and no change in $T_w$. At a site

located 150 m from a water body, the temperature at 15 m depth is 0.1°C less than the corresponding temperature when $T_g$ and $T_w$ are both increased by 1°C. There is a reduction in the warming at 15 m depth, but at 150 m, this effect is comparable to the precision of measurement. A greater difference is produced when the $T_g$ is increased by scenario, at 150 m from water, the 15 m ground temperature 3°C while the $T_w$ remains unchanged (#4, Table 1). In this scenario at 150 m from water, the 15 m ground temperature is 0.2°C less than if $T_g$ and $T_w$ are both increased by 3°C. This is a physically significant effect since approximately 81% of land in the southern delta is located less than 150 m from a water body (Fig. 8).

The impact of no change in water temperatures is amplified at a distance of 50 m from a water body. At this distance, an unchanged $T_w$, coupled with a $T_g$ increase of 1°C (#2, Table 1) leads to a 15 m ground temperature 0.2°C less than if the $T_w$ also increased by 1°C. Similarly (#4, Table 1), under a $T_g$ increase of 3°C, the 15 m ground temperature is 0.6°C less than if the $T_w$ had also increased by 3°C. It appears that the response of water bodies to climate warming is physically significant at 50 m from a water body, and by implication, also at lesser distances. Such distances represent approximately 34% of the terrestrial area in southern delta (Fig. 8).

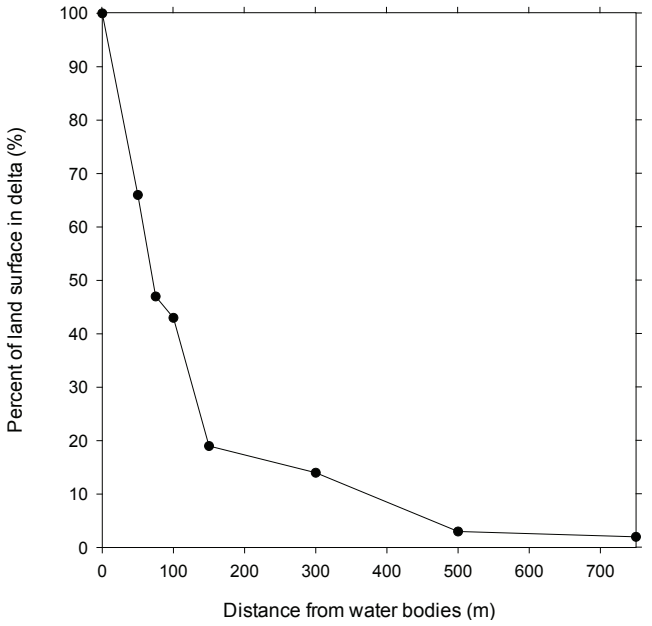


Figure 8. Percentages of land surface in the central and southern Mackenzie Delta that are located at distances greater than those specified from water bodies.

In the previous scenarios, $T_w$ remained unchanged despite warming air temperatures in order to provide a distinction between the response of $T_g$ and $T_w$ to climate warming. It is perhaps more likely that water temperatures will respond to climate warming, but at a slower rate than ground temperatures. In the fifth scenario, the $T_w$ was increased by half the change in $T_g$. The reduction in 15-m temperature of 0.1°C at 150-m distance may be undetectable due to instrument precision, but the reduction of 0.3°C at 50-m distance is measurable.

When water temperature warms more slowly than ground temperature, the modeling indicates that the thermal effect of water dampens the effect of climate warming, and that the dampening increases with proximity to the water body. In the Mackenzie delta, lakes are relatively static features, but the channels shift following bank erosion during the spring flood. There is a characteristic vegetation succession on point bars opposite cut banks which has been associated with various stages of permafrost aggradation (Smith 1975). Many sites within 50 m of channels may not support an equilibrium thermal regime, and at these locations the departure from undisturbed conditions will be greater than the equilibrium results presented in Table 1.

## Conclusions

Field evidence from two sites in the forested Mackenzie delta indicates that recent ground temperature change in the delta, has been less than at three sites in the adjacent shrub tundra. Ground temperature modeling and spatial analysis indicate that almost all of the land in the delta is affected to some degree by water bodies. The reduced ground temperature changes measured in the delta may be related to the slow response of lakes to climate warming.

Based on the results that have been presented, the following conclusions are made:

1. Ground temperatures at 15 m depth have increased by 0.3°C and 0.7°C at two spruce-forest sites in the southern Mackenzie Delta since the 1960s. The warming rates of 0.1°C and 0.15°C per decade are slower than in the adjacent upland.

2. An equilibrium model for 15 m ground temperatures shows that the warming effect of water bodies extends to distances of 750 m from water bodies.

Table 1. Ground temperatures and ground temperature change in brackets at 15 m depth calculated at 50, 100, and 750 m from water bodies using equation 2, assuming different warming scenarios.

| Horizontal distance from Water bodies $H_{p1}=H_{p2}$ (m) | Current conditions $T_g$=-3ºC $T_w$=6ºC (ºC) | 1 $T_g$=-2ºC(+1) $T_w$=7ºC (+1) (ºC) | 2 $T_g$=-2ºC(+1) $T_w$=6ºC (0) (ºC) | 3 $T_g$=0ºC(+3) $T_w$=9ºC (+3) (ºC) | 4 $T_g$=0ºC(+3) $T_w$=6ºC (0) (ºC) | 5 $T_g$=0ºC(+3) $T_w$=7.5ºC (+1.5) (ºC) |
|---|---|---|---|---|---|---|
| 50 | -1.0 | 0.0 (+1) | -0.2 (+0.8) | 2.0 (+3) | 1.4 (+2.4) | 1.7 (+2.7) |
| 150 | -2.1 | -1.1 (+1) | -1.2 (+0.9) | 0.9 (+3) | 0.7 (+2.8) | 0.8 (+2.9) |
| 750 | -2.6 | -1.6 (+1) | -1.6 (+1) | 0.4 (+3) | 0.4 (+3) | 0.4 (+3) |

3. Spatial analysis indicates that about 2% of terrestrial surfaces in the delta are located at distances greater than or equal to 750 m from a water body, and therefore, almost all terrestrial sites in the delta experience the thermal influence of water bodies to some extent.

4. Results from an equilibrium model indicate that if lake-bottom temperatures do not respond to climate warming, or warm more slowly than ground surface temperatures, then mean annual ground temperatures at sites close to water bodies will warm more slowly than undisturbed sites. This may explain why ground thermal responses to recent climate warming appear to be damped in the Mackenzie Delta in comparison with the adjacent tundra uplands.

## Acknowledgments

The research was supported by the Natural Sciences and Engineering Research Council of Canada, the Polar Continental Shelf Project (Natural Resources Canada), the Aurora Research Institute, and the Water Resources Division and Northern Scientific Training Program, Indian and Northern Affairs Canada. We thank Douglas Esagok, Larry Greenland, William Hurst, Les Kutny, and Thai Nguyuen for field assistance, and M.F.J. Pisaric and D.W. Riseborough for comments on the M.Sc. from which this work developed. This paper is Polar Continental Shelf Project contribution number 00908.

## References

Brown, W.G., Johnston, G.H. & Brown, R.J.E. 1964. Comparison of observed and calculated ground temperatures with permafrost distribution under a northern lake. *Canadian Geotechnical Journal* 1: 147-154.

Burn, C.R. 2002. Tundra lakes and permafrost, Richards Island, western arctic coast, Canada. *Canadian Journal of Earth Sciences* 39: 1281-1298.

Emmerton, C.A., Lesack, L.F.W. & Marsh, P. 2007. Lake abundance, potential water storage, and habitat distribution in the Mackenzie River Delta, western Canadian Arctic. *Water Resources Research* 43: W05419.

Environment Canada 2007. Canada climate data [online]. Ottawa, Canada. Available from http://climate.weatheroffice.ec.gc.ca/climateData/canada_e.html [accessed 08 August 2007].

Johnston, G.H. & Brown, R.J.E. 1964. Some observations of permafrost at an arctic lake in the Mackenzie Delta, N.W.T., Canada. *Arctic* 17: 163-175.

Kokelj, S.V. & Burn, C.R. 2005. Near-surface ground ice in sediments of the Mackenzie Delta, Northwest Territories, Canada. *Permafrost and Periglacial Processes* 16: 291-303.

Lachenbruch, A.H. 1957. *Three-dimensional Heat Conduction Beneath Heated Buildings.* U.S. Geological Survey Bulletin 1052-B. U.S. Geological Survey.

Mackay, J.R. 1963. *The Mackenzie Delta area, Northwest Territories, Geographical Branch, Memoir 8*. Ottawa: Department of Mines and Technical Surveys.

Mackay, J.R. 1974. Seismic shot holes and ground temperatures, Mackenzie Delta area, Northwest Territories. *Geological Survey of Canada Paper 74-1, Part A, Report of Activities, April to October 1973*. Ottawa: Geological Survey of Canada, Department of Energy, Mines and Resources, 389-390.

Marsh, P. & Hey, M. 1989. The flooding hydrology of Mackenzie Delta lakes near Inuvik, NWT, Canada. *Arctic* 42: 41-49.

Marsh, P. & Lesack, L.F.W. 1996. The hydrologic regime of perched lakes in the Mackenzie Delta: potential responses to climate change. *Limnology and Oceanography* 41: 849-856.

Marsh, P., Lesack, L.F.W. & Roberts, A. 1999. Lake sedimentation in the Mackenzie Delta, NWT. *Hydrological Processes* 13: 2519-2536.

Maxwell, B. 1997. Responding to global climate change in Canada's Arctic. *The Canada Country Study: Climate Impacts and Adaptation. Vol. 2*. Downsview, Ontario: Atmospheric Environment Service, Environment Canada.

Pearce, C.M., McLennan, D. & Cordes, L.D. 1988. The evolution and maintenance of white spruce woodlands on the Mackenzie Delta. *Holarctic Ecology* 11: 248-258.

Smith, M.W. 1973. *Factors Affecting the Distribution of Permafrost, Mackenzie Delta, N.W.T.* Ph.D. thesis. Vancouver, B.C.: Department of Geography, The University of British Columbia.

Smith, M.W. 1975. Microclimate influences on ground temperatures and permafrost distribution, Mackenzie Delta, Northwest Territories. *Canadian Journal of Earth Sciences* 12: 1421-1438.

Smith, M.W. 1976. *Permafrost in the Mackenzie Delta, Northwest Territories*. Geological Survey of Canada Paper 75-28. Ottawa: Geological Survey of Canada, Department of Energy, Mines and Resources.

Smith, M.W. & Hwang, C.T. 1973. Thermal disturbance due to channel shifting, Mackenzie Delta, N.W.T., Canada. *Permafrost: The North American Contribution to the Second International Conference*: 51-60.

Smith, S.L., Burgess, M.M, Riseborough, D. & Nixon, F.M. 2005. Recent trends from Canadian permafrost thermal monitoring network sites. *Permafrost and Periglacial Processes* 16: 19-30.

Williams, P.J. & Smith, M.W. 1989. *The Frozen Earth: Fundamentals of Geocryology*. Cambridge: Cambridge University Press, 360 pp.

# Near-Surface Permafrost Conditions near Yellowknife, Northwest Territories, Canada

K.C. Karunaratne
*Ottawa-Carleton Geoscience Centre, Carleton University, Ottawa, Canada*
S.V. Kokelj
*Water Resources Division, Indian and Northern Affairs Canada, Yellowknife, Canada*
C.R. Burn
*Department of Geography and Environmental Studies, Carleton University, Ottawa, Canada*

## Abstract

Yellowknife, NWT, lies in the discontinuous permafrost zone, in the southern portion of the Slave Geologic Province of the Canadian Shield. There are few data on permafrost temperature from the Yellowknife area. Thermistors connected to miniature dataloggers were installed to measure air, near-surface, and permafrost temperatures at nine sites in four peatlands near Yellowknife, for two years. Annual mean ground surface temperatures were above 0°C at all sites, but annual mean temperatures in permafrost ranged from -1.9 to -0.2°C. The presence of permafrost at these sites is therefore due to the thermal offset, which ranged between 1.3 and 4.0°C. Annual mean air temperature was about 4.5°C higher in the second year and the surface offset declined by 2.6°C. The thermal offset increased by 1.2°C.

**Keywords:** n-factors; peatlands; permafrost; surface offset; thermal offset; Yellowknife.

## Introduction

The city of Yellowknife, NWT, is located at the southern boundary of the Slave Structural Province of the Canadian Shield. The area is known for its Archean bedrock and the long history of mining. Currently, the region is experiencing rapid industrial development and the effects of global warming, which both affect and are affected by permafrost. Our understanding of permafrost conditions near Yellowknife is based largely on Brown (1973) and Wolfe (1998). The purposes of this paper are (1) to present field measurements of air and ground temperatures at several peatlands in the Yellowknife area for two consecutive years; and (2) to discuss the spatial variation in the surface and thermal offsets over the period of record. The field data presented in this paper were collected at sites along the Ingraham Trail up to 70 km east of the city.

## Climate and Permafrost

The climate-permafrost system can be described by the difference between the annual mean temperatures of the air ($Ta_a$) and ground surface ($Ts_a$), the surface offset, and the difference between $Ts_a$ and the annual mean temperature at the top of permafrost ($Tp_a$), or the thermal offset (Lachenbruch et al. 1988, Smith & Riseborough 1996). The surface offset is a function of the surface energy balance and therefore varies with vegetation, moisture, snow, and soil thermal properties (Klene et al. 2001, Karunaratne & Burn 2004). In winter, the surface offset is controlled by snow cover, and the latent heat released during ground freezing (Karunaratne & Burn 2004). The thermal offset is controlled by seasonal differences in the thermal conductivity of the active layer and the extent of winter cooling (Romanovsky & Osterkamp 1995, Riseborough 2002). The thermal conductivity of soil increases upon freezing because the thermal conductivity of ice is four times that of liquid water. Thus soil moisture content controls the difference between frozen and thawed conductivities of a soil, and thereby, the thermal offset as well. The thermal offset is negligible in bedrock and relatively high in peat. A large thermal offset can result in the presence of permafrost where annual mean surface temperature is greater than 0°C (Burn & Smith 1988).

Numerical models of the climate-permafrost relation have been developed that parameterize the surface and thermal offsets. The TTOP model, proposed by Smith & Riseborough (1996), represents the surface offset through freezing and thawing n-factors. The n-factor is a ratio of surface to air freezing or thawing indices (e.g., degree-days) (Karunaratne & Burn 2004). In the literature, thawing n-factors ($n_t$) range from 0.26 at a fen, to greater than 1.0 at open sites with well-drained mineral surfaces, and freezing n-factors ($n_f$) from 0.12 for wet sites with thick snow covers, to 0.48 for dry sites with little snow (Karunaratne & Burn 2004, Klene et al. 2001, Taylor 1995). The thermal offset depends on the ratio of thawed to frozen thermal conductivity (Romanovsky & Osterkamp 1995, Riseborough 2002), which can be estimated from soil characteristics.

## Study Area

Yellowknife has a continental climate, with a mean annual air temperature (MAAT) of -4.6ºC (Environment Canada 2007). The mean daily maximum temperature for July is 21°C but can reach 30°C, while the mean daily minimum temperature for January is -31°C, and has dropped as low as -51°C (Environment Canada 2007). The mean total annual precipitation is 280 mm, of which more than half arrives as rain. Snow cover develops in October, persists until

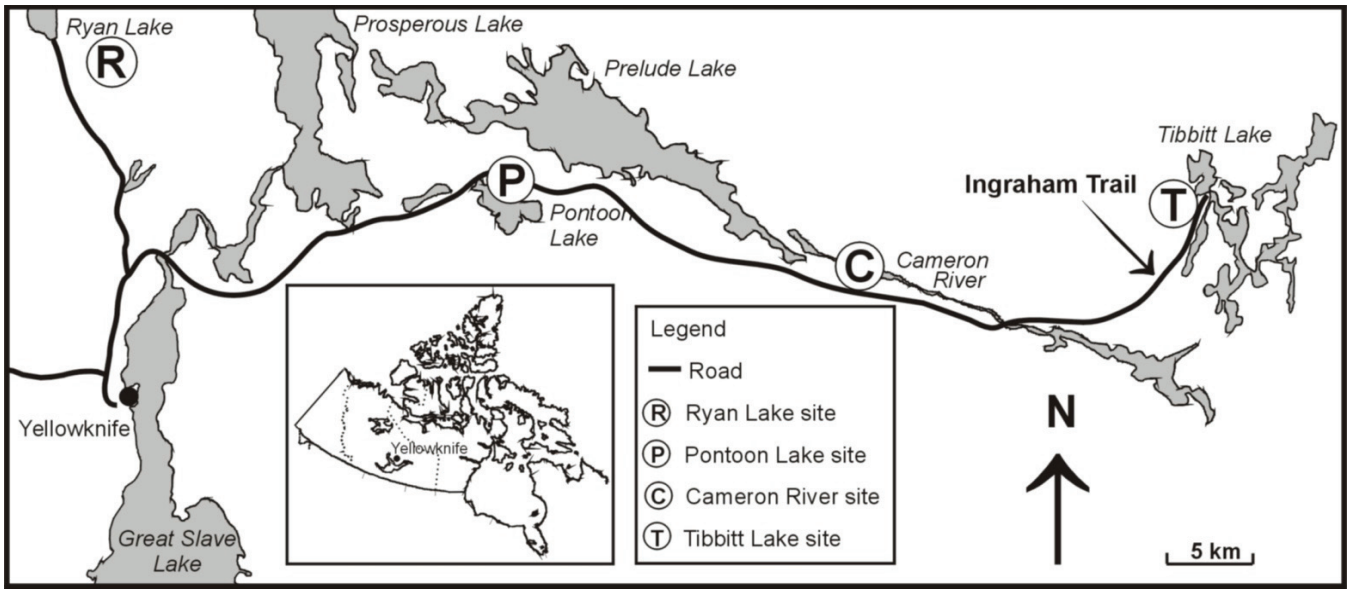


Figure 1. Location of peatland sites near Yellowknife.

the end of April, and approaches a depth of 40 cm in late winter (Environment Canada 2007). The terrain surrounding Yellowknife predominantly consists of peatlands populated by *Picea mariana*, and upland bedrock outcrops colonized by *Pinus banksiana*. The area lies in the extensive discontinuous permafrost zone (Heginbottom et al. 1995). Brown (1973) determined that permafrost is encountered near Yellowknife in peatlands, but not in outcrops or unconsolidated material. He recorded permafrost 50 m thick beneath a 30–cm active layer in a black-spruce peatland, and 30 m thick beneath a 68–cm active layer in a sedge peatland. In both cases the surficial peat was more than 1 m thick. Permafrost was absent in a nearby burnt peatland where the organic horizon was only 30 cm thick. Brown (1973) determined that mean annual ground temperatures were interannually variable, possibly due to differences in snow cover.

*Study sites*

Four sites were chosen along the Ingraham Trail east of Yellowknife to examine near-surface permafrost conditions. The sites were near Ryan Lake (R), situated 10 km north of Yellowknife, and at Pontoon Lake (P), Cameron River (C), and Tibbitt Lake (T), which were 30, 50, and 70 km east of Yellowknife respectively (Fig. 1). The sites were located in peatlands with *Sphagnum sp*. mosses and *Cladina sp*. lichens, and open-canopy *Picea mariana* forest. Low-lying shrubs commonly included *Ledum groenlandicum*, *Vaccinium vitis-idaea*, *Andromeda polifolia*, and *Empetrum nigrum*. *Rubus chamaemorus* was also ubiquitous. Although the peatlands are classified as basin bogs under the Canadian Wetland Classification System (1997), for the most part, the moss surface was dry, and the base of the active layer was commonly saturated. However, moisture conditions varied spatially and interannually.

*Study period*

The study period consisted of two years from October 2004 to September 2005, and from October 2005 to September 2006. Precipitation differed between the years at the Yellowknife Airport. Summer 2004 was dry, receiving only 61mm of rain. The following summers were wetter, with 232 mm of rain in 2005, and 180 mm in 2006.

Snowfall was similar for both years but higher than normal, with maximum snow depth at the airport of 66 cm in both years.

## Field Methods

Thermistors connected to miniature dataloggers were installed in 2003 and 2004 to measure air and near- surface temperatures at the peatlands. In total, nine sets of thermistors were installed at the four peatlands. Air temperatures were measured in radiation shields 1.5 m above the ground surface at peatlands T, C, and R. The thermistors measuring near-surface and ground temperatures were mounted on a wooden dowel and inserted into an augered hole. Near-surface temperatures were measured 2 to 5 cm beneath the living moss layer, and ground temperatures were measured at 50 and 100 cm depths. Temperature was recorded every 2 hours (Onset Computing, HOBO®, H08-006-04). The thermistors had a precision of ±0.38°C at 20°C, but random error associated with instrument precision is reduced in long-term averages because of the number of individual measurements (4380 measurements $year^{-1}$). The accuracy of the thermistors was reported to be ±0.5°C, but was found to be ±0.3°C of 0°C when they were calibrated in an ice bath.

In September 2006, soil samples of known volume were collected at each instrumented site at 10, 20, 30 and 50 cm depths. The soil samples were dried for 48 hours at 105°C to determine the volumetric soil moisture. Surveys of vegetation within 10 $m^2$ of each site were conducted in 2005, and included visual estimates of the canopy cover. Active-layer depths were determined at each of the instrumented sites in late summer by probing to resistance. In April 2005, snow depths were measured nine times along a 4x4 m cross-transect centered on the point of ground temperature measurements.

Table 1. Active layer depths , and the mean annual ground temperature at 50 cm ($T_{50a}$) and 100 cm ($T_{100a}$), and the annual maximum temperature at 100 cm ($T_{100max}$) for 2004–05 and 2005–06.

| Site | Active Layer Depth (cm) | $T_{100max}$ (°C) | $T_{100a}$ (°C) | $T_{50a}$ (°C) | $T_{100a}$ - $T_{50a}$ (°C) |
|---|---|---|---|---|---|
| 2004-05 | | | | | |
| T-01 | 50 | -0.6 | -1.9 | -1.9 | 0.1 |
| C-02 | 60 | -0.6 | -0.7 | -0.2 | -0.4 |
| C-03 | 61 | -0.2 | -0.2 | 0.7 | -0.8 |
| C-04 | 44 | -0.6 | -1.7 | -1.9 | 0.2 |
| P-05 | 54 | | - | -1.3 | |
| P-06 | 40 | -0.2 | -1.2 | -1.6 | 0.4 |
| R-07 | 48 | -0.6 | -0.8 | -0.9 | 0.1 |
| R-08 | 44 | -0.6 | -1.8 | -1.8 | 0.0 |
| R-09 | 40 | -0.6 | -1.8 | -1.8 | 0.0 |
| Mean | 49 | -0.5 | -1.3 | -1.2 | -0.1 |
| 2005-06 | | | | | |
| T-01 | 59 | -0.6 | -1.0 | -0.8 | 0.3 |
| C-02 | 68 | -0.6 | -0.6 | 0.3 | 0.9 |
| C-03 | 70 | -0.2 | -0.2 | 0.9 | 1.0 |
| C-04 | 50 | -0.6 | -0.7 | -0.4 | 0.2 |
| P-05 | 62 | - | - | 0.3 | |
| P-06 | 45 | -0.2 | -0.3 | -0.5 | 0.2 |
| R-07 | 61 | -0.6 | -0.6 | 0.2 | 0.8 |
| R-08 | 57 | - | -1.1 | -0.1 | 1.0 |
| R-09 | 45 | - | -1.1 | -0.1 | 1.0 |
| Mean | 57 | -0.5 | -0.7 | 0.0 | 0.7 |

## Permafrost at the Sites

Permafrost was established in the peat, but its thickness and that of the peat was unknown. Active-layer depths varied spatially and interannually and ranged from 40 to 70 cm (Table 1). The annual maximum temperature at 100 cm was below 0°C for both years at all the sites, indicating the presence of permafrost (Table 1). In 2004–05, the mean annual temperature at 100 cm ($T_{100a}$) ranged from -0.2°C at C-02 to -1.9°C at T-01; a difference of 1.7°C (Table 1). $T_{100a}$ was between 0.7 and 1.0°C colder in 2004–05 than in 2005–06 except at C-02 and C-03 where it was nearly the same temperature in both years. At the coldest site, T-01, freezeback of the active layer did not occur until mid-January 2005 and until late February 2006, as indicated by a sudden decrease in the temperature at 50 and 100 cm depth (Fig. 2). At C-03, the warmest site, the temperature at 100 cm remained at -0.2°C throughout both years.

## Air Temperature

$Ta_a$ (October to September) at Yellowknife Airport (YZF) was -5.1°C for 2004–05, slightly below the MAAT of -4.6°C. The following year was warmer, with $Ta_a$ of -0.6°C. The mean air temperature for the freezing (October to April) season ($Ta_f$) was 5.5°C lower in 2004–05 than in 2005–06, while the mean air temperature for the thawing (May-September) season ($Ta_t$) was 3.3°C lower in 2005 than in 2006 (Table 2). On average YZF was 0.9°C warmer than the study sites throughout the year, due to differences in microclimate conditions between the airfield and peatlands. The maximum difference between the peatlands for $Ta_a$ and seasonal average temperatures ($Ta_f$ and $Ta_t$) in both years was 0.8°C, but it was usually less than 0.3°C. The air temperatures at the study sites were similar, with differences in air temperature amongst the study sites, for the most part, within the accuracy of the instruments. Deviations in $Ta_a$ beyond ±0.3°C were not consistent between sites, years, or seasons.

Table 2. Annual (October to September) mean air temperature ($Ta_a$), mean air temperature for the freezing season ($Taf$) and thawing season ($Ta_t$) for the Yellowknife Airport (YZF), and the Ryan Lake (R), Cameron River (C), and Tibbitt Lake (T) sites for 2004–05 and 2005–06.

| | $Ta_a$ (°C) | | $Ta_f$ (°C) | | $Ta_t$ (°C) | |
|---|---|---|---|---|---|---|
| Site | 2004-05 | 2005-06 | 2004-05 | 2005-06 | 2004-05 | 2005-06 |
| YZF | -5.1 | -0.6 | -16.0 | -10.5 | 10.1 | 13.3 |
| R | -5.7 | -1.3 | -16.6 | -11.2 | 9.3 | 12.4 |
| C | -6.1 | -1.4 | -17.1 | -11.2 | 9.1 | 12.0 |
| T | -6.1 | -1.3 | -17.4 | -11.3 | 9.5 | 12.6 |
| Mean | -5.8 | -1.2 | -16.8 | -11.1 | 9.5 | 12.6 |

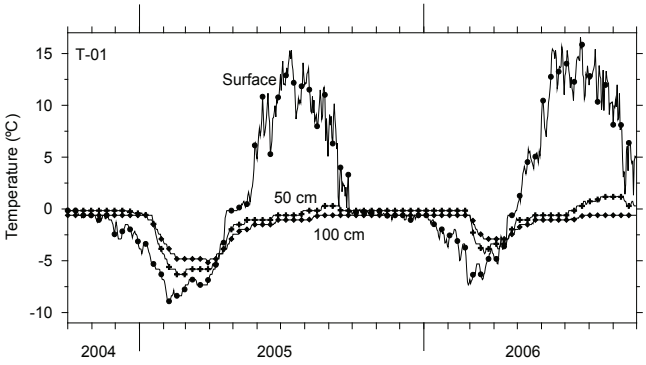


Figure 2. Mean daily surface and ground temperatures at 50 and 100 cm at site T-01 from October 2004 to September 2006. For clarity, the symbols are presented every 10 days while the plot is continuous throughout the two years.

## Surface Temperature

The temperature of the surface is common to both the surface and thermal offsets and therefore is integral to the climate-permafrost relation. Surface temperature is measured at the base of the living mosses, approximately 2 to 5 cm from the ground surface to avoid radiative heating. This method is attractive because it positions the sensor close to the relatively warm ground surface during the summer, and is appropriate for measuring winter surface temperature,

Table 3. Mean near-surface temperatures for the year ($Ts_a$), freezing season ($Ts_f$) and thawing season ($Ts_t$), in 2004-05, and associated site characteristics.

| Site | $Ts_a$ (°C) | $Ts_f$ (°C) | $Ts_t$ (°C) | Snow Depth (cm) | Soil Moisure (g $cm^{-3}$) | Canopy Cover (%) |
|---|---|---|---|---|---|---|
| T-01 | 0.8 | -3.8 | 7.3 | 60 | 0.69 | 6-15 |
| C-02 | 2.4 | -1.6 | 7.9 | 56 | 0.74 | 6-15 |
| C-03 | 2.0 | -1.6 | 7.0 | 62 | 0.74 | 1-5 |
| C-04 | 0.1 | -4.0 | 5.9 | 45 | 0.70 | 51-75 |
| P-05 | 1.0 | -4.3 | 8.4 | 60 | 0.44 | 16-30 |
| P-06 | 0.4 | -5.1 | 8.2 | 42 | 0.41 | 51-75 |
| R-07 | 1.9 | -2.9 | 8.6 | 60 | 0.68 | 1-5 |
| R-08 | 0.3 | -4.1 | 6.5 | 41 | 0.67 | 51-75 |
| R-09 | -0.5 | -5.0 | 5.8 | 41 | 0.67 | 76-100 |

Table 4. Rank order of the sites by annual mean surface temperature ($Ts_a$), and the mean surface temperature for the freezing season ($Ts_f$) and thawing season ($Ts_t$) for 2004–05 and 2005–06.

| 2004–05 | | 2005–06 | |
|---|---|---|---|
| $Ts_a$ (°C) | | | |
| R-09 | -0.5 | R-09 | 2.3 |
| C-04 | 0.1 | C-04 | 2.5 |
| P-06 | 0.4 | P-06 | 2.5 |
| T-01 | 0.8 | T-01 | 2.7 |
| C-02 | 2.4 | C-02 | 3.3 |
| Mean | 0.6 | Mean | 2.7 |
| Range | 2.9 | Range | 1.1 |
| $Ts_f$ (°C) | | | |
| P-06 | -5.1 | T-01 | -2.2 |
| R-09 | -5.0 | P-06 | -2.0 |
| C-04 | -4.0 | C-04 | -2.0 |
| T-01 | -3.8 | R-09 | -1.9 |
| C-02 | -1.6 | C-02 | -1.1 |
| Mean | -3.9 | Mean | -1.8 |
| Range | 3.5 | Range | 1.0 |
| $Ts_t$ (°C) | | | |
| R-09 | 5.8 | R-09 | 8.1 |
| C-04 | 5.9 | C-04 | 8.8 |
| T-01 | 7.3 | T-01 | 9.6 |
| C-02 | 7.9 | C-02 | 9.6 |
| P-06 | 8.2 | P-06 | 9.6 |
| Mean | 7.0 | Mean | 9.1 |
| Range | 2.4 | Range | 1.5 |

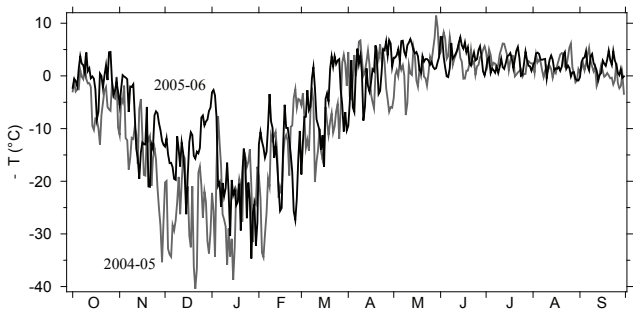


Figure 3. Difference between air and surface mean daily temperature at site C-02 for 2004–05 and 2005–06.

near the peat-snow interface. Such data can also be used to compare organic and exposed mineral surfaces.

*Spatial variability of surface temperature*

Annual mean and seasonal mean near-surface temperatures at each of the sites for 2004–05 are presented in Table 3, along with snow depth, mean volumetric soil moisture of the active layer, and estimated canopy cover. One measurement site was located in peatland T (T-01); three sites were in peatland C (C-02, -03, -04); two sites were in peatland P (P-05, -06); and three were in peatland R (R-07, -08, -09).

The range in $Ts_a$ was 2.9°C among all nine sites, and 2.3°C among the sites at C and 2.4°C among the sites at R. Similarly, the variation in $Ts_f$, and $Ts_t$ within peatlands C and R was no less than 60% of the total variation between peatlands. This suggests that the surface thermal regime was the same amongst the peatlands, and that variations in surface temperature among the instrumented sites were due to differences in microclimate.

The lowest $Ts_a$, and $Ts_f$, were measured at sites with over 50% canopy cover, and with thinner snow covers in winter due to interception of snow (Table 3). At sites where the snow depth was ≤ 45 cm, $Ts_a$ were 0±0.5°C, and at sites with more than 50 cm of snow, $Ts_a$ were between 0.8 and 2.4°C. The lowest $Ts_t$ were also found at sites with high canopy cover, except at sites P-05 and P-06 which had the lowest soil moistures (Table 3). Canopy cover appears to control surface temperatures in peatlands through shading in summer and its influence on snow distribution in winter.

*Interannual variation in surface temperature*

Surface temperatures for 2004–05 and 2005–06 were examined at T-01, C-02, C-04, P-06 and R-09 to determine the year-to-year variability (Table 4). The surface temperature sensors at R-07, R-08, C-03, and P-05 did not produce reliable records in 2005-06 and were eliminated from this analysis. The average $Ts_a$, $Ts_f$, and $Ts_t$ at the sites were 2.0°C lower in 2004–05 than in the following year (Table 4). The difference in annual mean surface temperature between the years was less than half of that for air temperature (Table 2). This is likely due to both the impact of snow cover in

Table 5. Surface offset ($Ta_a$-$Ts_a$), and freezing ($n_f$) and thawing ($n_t$) n-factors calculated from freezing and thawing degree-days at the sites.

| | Surface Offset (°C) | | $n_f$ | | $n_t$ | |
|---|---|---|---|---|---|---|
| Site | 2004-05 | 2005-06 | 2004-05 | 2005-06 | 2004-05 | 2005-06 |
| T-01 | 6.8 | 4.1 | 0.22 | 0.19 | 0.79 | 0.76 |
| C-02 | 8.4 | 4.7 | 0.09 | 0.10 | 0.85 | 0.76 |
| C-03 | 8.0 | - | 0.09 | - | 0.75 | - |
| C-04 | 6.1 | 3.9 | 0.24 | 0.18 | 0.64 | 0.70 |
| P-05 | 7.0 | - | 0.25 | - | 0.90 | - |
| P-06 | 6.5 | 3.9 | 0.30 | 0.18 | 0.88 | 0.68 |
| R-07 | 7.9 | - | 0.17 | - | 0.93 | - |
| R-08 | 6.5 | - | 0.24 | - | 0.64 | - |
| R-09 | 5.3 | 3.7 | 0.29 | 0.14 | 0.51 | 0.62 |
| Mean | 6.9 | 4.0 | 0.21 | 0.16 | 0.76 | 0.70 |

buffering the ground from variations in the air temperature regime, and to the impact of permafrost in restricting increases in surface temperature (Karunaratne & Burn 2004). The rank order of the five sites by $Ts_a$ and $Ts_t$, was the same for both years (Table 4). The rank order of the sites by $Ts_f$, was similar for both years because the differences between four of the sites in 2005–06 did not exceed 0.3°C; the accuracy of the thermistors. Thus the interannual differences in surface temperature are consistent between the instrumented sites. $Ts_a$ for all the sites was above 0°C for both years, except for R-09 in 2004–05. This indicates that the presence of permafrost in the Yellowknife area is due to the thermal, rather than the surface, offset. The thermal offset causes mean annual ground temperatures to decrease with depth through the active layer allowing permafrost to exist with mean annual surface temperatures above 0°C. Without the thermal offset, mean annual ground temperatures would increase with depth and therefore never extend below the mean annual surface temperature.

## Surface Offset

The surface offset and the freezing ($n_f$) and thawing ($n_t$) n-factors were calculated for 2004–05 and 2005–06 based on surface temperatures measured at the sites and the average air temperature from T, C, R (Table 5). In 2004–05, the surface offset ranged from 5.3°C at R-09 to 8.4°C at C-02. The following year the surface offset was lower; between 3.7 and 4.7°C. The differences in surface offset between the two years can be attributed to differences between air and surface temperatures in early winter, since snow conditions were similar. In 2004–05, air temperatures had dropped below -20°C by mid-November, before the active layer had refrozen, which resulted in large differences between air and surface temperature (Fig. 3). In 2005–06, air temperatures were consistently higher than -20°C until the beginning of January, and thus closer to the surface temperature during freeze-back of the active layer.

Table 6. Thermal offsets calculated with ground temperatures at 50 cm ($T_{50a}$) and 100 cm ($T_{100a}$) for 2004–05 and 2005–06.

| | $T_{Sa}$-$T_{50a}$ (°C) | | $T_{Sa}$-$T_{100a}$ (°C) | |
|---|---|---|---|---|
| Site | 2004-05 | 2005-06 | 2004-05 | 2005-06 |
| T-01 | 2.5 | 3.3 | 2.7 | 3.8 |
| C-02 | 2.4 | 2.7 | 3.0 | 4.0 |
| C-03 | 1.1 | - | 2.2 | - |
| C-04 | 1.8 | 2.8 | 1.8 | 3.2 |
| P-05 | 1.9 | - | - | - |
| P-06 | 1.9 | 3.0 | 1.6 | 2.8 |
| R-07 | 2.6 | - | 2.7 | - |
| R-08 | 2.0 | - | 2.3 | - |
| R-09 | 0.8 | 2.3 | 1.1 | 2.4 |
| Mean | 1.9 | 2.8 | 2.2 | 3.2 |

Values of $n_f$ ranged from 0.09 at C-02 and C-03 to 0.30 at P-06, and for $n_t$ from 0.51 at R-09 to 0.93 at R-07 (Table 5). Both $n_f$ and $n_t$ for the study sites are within the range of n-factors reported in the literature for spruce peatlands (Jorgenson & Krieg 1988, Taylor 1995, Karunaratne & Burn 2004). Wet sites with thick active layers had the lowest values of $n_f$, and high values of $n_f$ were calculated for sites with high canopy cover and subsequent thin snow covers. Values of $n_t$ were related to canopy cover, with shaded sites having lower $n_t$ than open sites. Sites P-05 and P-06 had higher $n_t$ than their canopy cover would suggest possibly because of their low soil moisture. This suggests that moisture availability has a strong influence on $n_t$ in peatlands.

## Thermal Offset

The annual mean temperature at the top of permafrost ($T_{Pa}$) is required to calculate the thermal offset, but since the depth of the active layer varies spatially and interannually (Table 1), it is difficult to measure $T_{Pa}$. Fortunately, ground temperatures within the uppermost metres of permafrost can be used instead, as the ground warms very slowly with depth in this part of the temperature profile (Willams & Smith 1989), and temperatures several metres below the top of permafrost are similar to that at the top of permafrost. In 2004–05, slightly more than half of the sites had active layers thinner than 50cm, and the mean annual temperatures at 50 and 100 cm depths ($T_{50a}$ and $T_{100a}$) were generally within 0.5°C, except at C-03 which had the deepest active layer (Table 1). The following year, most of the sites had active layers that were thicker than 50 cm, and the difference between $T_{50a}$ and $T_{100a}$ was 0.4°C higher than in 2004–05 (Table 1). The average difference in the thermal offset between that calculated with $T_{50a}$ as opposed to $T_{100a}$ was 0.1°C for the sites with active layers thinner than 50 cm, and 0.9°C for the sites with active layers thicker than 50 cm (Table 6). Thus the thermal offset calculated with $T_{100a}$ is more appropriate to compare values between sites and years. The thermal offset ($T_{Sa}$-$T_{100a}$) was lower in 2004–05 than the following year for all of the sites; between 1.1 and 3.0°C in

2004–05 and between 2.4 and 4.0°C in 2005–06 (Table 6). The rank of the sites by the thermal offset was the same both years, with the highest value found at C-02 and the lowest at R-09. Sites with thick active layers had large thermal offsets (Table 1).

## Conclusions

Air, surface and ground temperatures were measured in four peatlands near Yellowknife during 2004–05 and 2005–06. The following are the principal results of the study:

(1) The lowest annual mean surface temperatures were measured at sites with high canopy cover.
(2) The mean annual mean permafrost temperature among the sites was -1.3°C in 2004–05 and 0.7°C the following year.
(3) The mean surface offset among the sites was 5.9°C.
(4) The mean thermal offset among the sites was 2.6°C.
(5) Since the mean annual ground surface temperature in the peatlands was above 0°C, permafrost near Yellowknife is sustained by the thermal offset.

## Acknowledgments

The research has been supported by the Natural Sciences and Engineering Research Council of Canada, and the Northern Scientific Training Program of Indian and Northern Affairs Canada. Field assistance from numerous individuals, especially Jesse Farlane and Krystal Thompson, is acknowledged with gratitude.

## References

Brown, R.J.E. 1973. Influence of climatic and terrain factors on ground temperatures at three locations in the permafrost region of Canada. *Proceedings of the Second International Conference on Permafrost, North American Contribution, Yakutsk, U.S.S.R., July 13-28, 1973*: 27-34.

Burn, C.R. & Smith, C.A.S. 1988. Observations of the 'Thermal Offset' in near-surface mean annual ground temperatures at several sites near Mayo, Yukon Territory, Canada. *Arctic* 41: 99-104.

Environment Canada. 2007. Available from http://climate.weatheroffice.ec.gc.ca/.

Heginbottom, J.A., Dubreuil, M.A. & Harker, P.A. 1995. Canada-Permafrost. In: *National Atlas of Canada 5th Edition*. Ottawa: National Atlas Information Service, Natural Resources Canada, Plate 2.1 MCR 4177.

Jorgenson, M.T. & Kreig, R.A. 1988. A model for mapping permafrost distribution based on landscape component maps and climatic variables. *Proceedings of the Fifth International Conference on Permafrost, Trondheim, Norway, August 2-5, 1988*: 176-182.

Karunaratne, C.K. & Burn, C.R. 2004. Relations between air and surface temperature in discontinuous permafrost terrain near Mayo, Yukon Territory. *Canadian Journal of Earth Sciences* 41: 1437-1451.

Klene, A.E., Nelson, F.E. & Shiklomanov, N.I. 2001. The N-factor in natural landscapes: variability of air and soil-surface temperatures, Kuparuk river basin, Alaska, U.S.A. *Arctic, Antarctic and Alpine Research* 33: 140-148.

Lachenbruch, A.H., Cladouhos, T.T. & Saltus, R.W. 1988. Permafrost temperature and the changing climate. *Proceedings of the Fifth International Conference on Permafrost, Trondheim, Norway, August 2-5, 1988*: 9-17.

National Wetlands Working Group. 1997. *The Canadian Wetland Classification System, Second Edition.* B.G. Warner & C.D.A. Rubec (eds.), Waterloo, Ontario: Wetlands Research Centre, University of Waterloo, 68 pp.

Riseborough, D.W. 2002. The mean annual temperature at the top of permafrost, the TTOP Model, and the effect of unfrozen water. *Permafrost and Periglacial Processes* 13: 137-143.

Romanovsky, V.E. & Osterkamp, T.E. 1995. Interannual variations of the thermal regime of the active layer and near surface permafrost in Northern Alaska. *Permafrost and Periglacial Processes* 6: 313-335.

Smith, M.W. & Riseborough, D.W. 1996. Permafrost monitoring and detection of climate change. *Permafrost and Periglacial Processes* 7: 301-309.

Taylor, A.E. 1995. Field measurements of n-factors for natural forest areas, Mackenzie Valley, Northwest Territories. *Geological Survey of Canada, Current Research, 1995-B*: 89-98.

Williams, P.J. & Smith, M.W. 1989. *The Frozen Earth: Fundamentals of Geocryology.* New York: Cambridge University Press, 306 pp.

Wolfe, S.A. 1998. *Living with frozen ground: A field guide to permafrost in Yellowknife, Northwest Territories*. Geological Survey of Canada, Miscellaneous Report No. 64. 71 pp.

# The Schmidt-Hammer as a Relative Age Dating Tool for Rock Glacier Surfaces: Examples from Northern and Central Europe

Andreas Kellerer-Pirklbauer
*Institute of Geography and Regional Science, University of Graz, Austria*

## Abstract

This paper presents new data of measurements of Schmidt-hammer rebound values (*R*-values) on rock glacier surfaces and adjacent landforms from one site in northern Norway (Lakselv) and two sites in central Austria (Dösen and Weissenkar). The obtained *R*-values reveal long and complex rock glacier formation histories with initiations in the early Holocene. At least the large studied rock glaciers were formed continuously during most of the Holocene, whereas for small rock glaciers this is more difficult to prove. This implies that the Schmidt-hammer method seems to be a powerful tool in surface dating, particularly for large rock glaciers where multiple measurement sites along a longitudinal profile are possible to sample. *R*-values from such profiles enable the establishment of relative chronologies with high temporal resolution. Reliable absolute dating is possible when surfaces of known age with similar vegetation and climate history and comparable lithology are available. The more surfaces of known age are available, the better is a resulting age-calibration curve.

**Keywords:** Holocene landscape development; rock glacier formation; rock glacier surface dating; Schmidt-hammer.

## Introduction

Rock glaciers originate from thick debris accumulations (talus and/or till) in high-relief environments that are under cryogenic conditions for a substantial period of time. Surface morphology, extent, and shape are the cumulative result of their entire genesis and thus climatic past. Temporal dates regarding their initiation and evolution period are the key to valuable palaeoclimatic information. Precise dating of rock glaciers is difficult but can be best achieved by applying an integrated approach, using a combination of relative—thereby distinguishing between fieldwork-based approaches (Schmidt-hammer rebound value, lichenometry, and weathering-rind thickness) and photogrammetry-based approaches (displacement rates and interpolated streamlines)—and absolute (luminescence, exposure/cosmogenic, and radiocarbon) dating methods (Haeberli et al. 2003). Absolute dating methods for rock glacier surfaces are still at an initial stage (Haeberli et al. 1999), are time-consuming, and have their own suites of assumptions and errors (cf. Shakesby et al. 2006), whereas relative dating methods are used more frequently (e.g., Haeberli et al. 2003, Frauenfelder et al. 2005, Kellerer-Pirklbauer et al. 2007). The combination of the Schmidt-hammer and photogrammetry-based approaches seems to be a powerful relative age-dating approach allowing—up to a certain extent—also absolute age estimations (Frauenfelder et al. 2005, Kellerer-Pirklbauer et al. 2007). However, Kellerer-Pirklbauer et al. (2007) pointed out that the main drawback of photogrammetry-based calculations of displacement rates and, derived from that, interpolated streamlines, is the crude assumption of constant velocity during the entire period of formation. Age estimations derived from Schmidt-hammer measurements seem to substantially reduce this drawback.

In this study the Schmidt-hammer method was applied at five rock glaciers and adjacent landforms in different environmental and geological settings. Results and age estimates are presented and compared with each other. The study areas are located at the following sites in Europe:

(1) One rock glacier near Lakselv, Gaissane Mountains, northern Norway (69°57′N, 24°47′E). Age dating based on cosmogenic isotope analysis is currently in progress from surface samples of a nearby rock glacier (LA-B in Fig. 1A) by Frauenfelder (pers. com.). No results are available so far.

(2) Three rock glaciers in the Dösen Valley, Ankogel Mountains, central Austria (46°59′N, 13°26′E). No detailed age estimations have been reported previously from there.

(3) One rock glacier in the Weissenkar Cirque, Schober Mountains, central Austria (46°57′N, 12°45′E). Crude age estimations were reported previously by Buchenauer (1990) suggesting a postglacial formation age.

## Study Areas

*Northern Norway – Lakselv*

The study area near Lakselv, Gaissane Mountains, is characterised by a steep escarpment (caused by faulting) with some hundreds of meters in vertical dimension. This escarpment separates a high plateau from the broad glacially modified Balgesvag´gi valley (Fig. 1A). The high plateau is gently dipping towards the west with smooth summits reaching elevations above 800 m a.s.l. The bedrock at the study area consists of Precambrian and Palaezoic sandstones and silts. A number of gravitationally induced landforms can be identified at the foot of this escarpment reaching a lower elevation of ca. 380–400 m a.s.l. Such landforms are in particular two talus-derived, lobated rock glaciers (LA-A and LA-B in Fig. 1A) and four distinct avalanche boulder tongues (ABT in Fig. 1A). At this study area the intact (i.e. containing permafrost but presumably no current movement; Farbrot 2007), monomorphic and lobated rock glacier LA-A with a surface area of 0.09 km² was studied. For a detailed site description refer to Farbrot (2007).

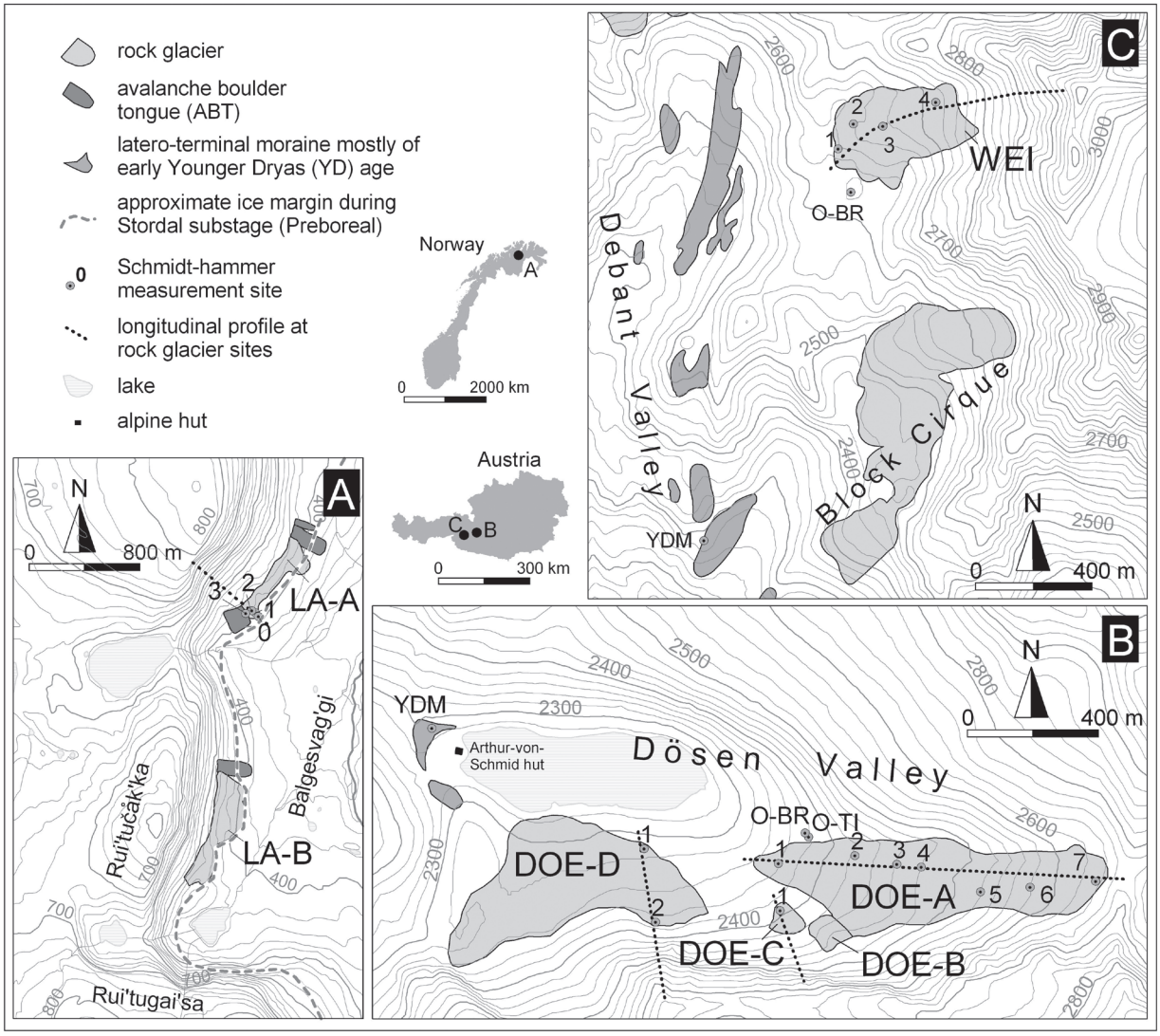


Figure 1. The study areas near (A) Lakselv, Gaissane Mountains in northern Norway and (B) Dösen Valley and (C) Weissenkar Cirque, both in central Austria: (A) Both rock glaciers (LA-A and LA-B=rock glacier Lakselv A and B) occur in close vicinity to avalanche boulder tongues indicating their close genetic relationship. Two Schmidt-hammer measurement sites are located at LA-A (1 & 2) and two nearby (0 & 3). The margin of the Fennoscandian Ice Sheet during the Stordal substage (Preboreal) was at the foot of the escarpment coming from east as indicated in the map. Age dating based on cosmogenic isotope analysis is currently in progress at LA-B. (B): Schmidt-hammer readings were carried out at two active, monomorphic, tongue-shaped (DOE-A and DOE-B) and one intact, monomorphic, lobated rock glacier (DOE-D) in the Dösen Valley. Dots at the rock glaciers, near rock glacier DOE-A (O-BR=bedrock outside rock glacier; O-TI=till boulders outside rock glacier) and at the terminal moraine of early Younger Dryas age (YDM) indicate sites of Schmidt-hammer measurements. (C) Schmidt-hammer readings were carried out at the surface of Weissenkar Rock Glacier (WEI), slightly outside the rock glacier at a roche moutonée (O-BR) and at a latero-terminal moraine ridge of early Younger Dryas age (YDM). Depicted landforms based on (A & B) field work and aerial photograph interpretation, and on (C) Buchenauer (1990). Dotted lines in the maps indicate longitudinal profiles.

*Central Austria – Dösen*

The second study area is situated in the Ankogel Mountains at the inner part of the glacially shaped, E-W trending Dösen Valley. This part of the valley is characterised by four north-to-west facing rock glaciers, a cirque floor with a tarn lake, and distinct terminal moraines (Fig. 1B). The moraines were presumably formed during the Egesen-maximum advance and are thus of early Younger Dryas (YD) age (Lieb 1996). The elevation ranges between 2270 m a.s.l. at the cirque threshold to more than 3000 m a.s.l. at the nearby Säuleck peak. The four rock glaciers predominantly consist of granitic gneiss (Kaufmann et al. 2007). Three of these rock glaciers (DOE-A, B, and C in Fig. 1B) are considered to be active, and one (DOE-D in Fig. 1B) is regarded as climatic inactive (Lieb 1996). In this study, the focus was on the two active and monomorphic rock glaciers, DOE-A (0.19 km²) and DOE-C (0.007 km²), and on the inactive and monomorphic rock glacier DOE-D (0.17 km²). Previous permafrost research—including velocity measurements—focused particularly on the rock glacier DOE-A (for details see Lieb 1996 or Kaufmann et al. 2007).

*Central Austria – Weissenkar*

The third study area is located in the Schober Mountains

at a west-exposed cirque in the Debant Valley. As indicated by the high number of rock glaciers ($n$=126), the Schober Mountains provide suitable topoclimatic and geological (crystalline rocks) conditions for rock glacier formation (Lieb 1996). The cirque is dominated by the tongue-shaped Weissenkar Rock Glacier (WEI in Fig. 1C) which is fed by active scree slopes. Until the late 1990s, the rooting zone of WEI was occupied by a large perennial snow field. WEI consists of an active upper lobe overriding an inactive lower lobe. Different types of mica schist form the lithological component of the rock glacier. WEI is characterized by well developed furrows and ridges at its entire lower half, a lower limit at 2615 m a.s.l., a length of 500 m, and a surface area of 0.11 km². WEI creeps from the cirque to a plateau-like area composed of roches moutonées. Latero-terminal moraine ridges of Late Glacial age are frequent in the area. At this study area the rock glacier, one roche moutonée, and a distinct moraine ridge of supposed Egesen/early YD age located at the lower end of the Block Cirque were studied (cf. Buchenauer 1990, Lieb 1996, Kaufmann et al. 2006).

## Methods

A Schmidt-hammer (or sclerometer) is a light and portable instrument traditionally used for concrete stability testing by recording a rebound value ($R$-value) of a spring-loaded bolt impacting a surface. Beginning in the 1980s (e.g., Matthews & Shakesby 1984, McCarroll 1989), this method has been increasingly applied in glacial and periglacial studies for relative rock surface dating. The obtained $R$-value is proportional to the compressive strength of the rock surface and gives a relative measure of the surface hardness and thus provides information on the time since surface exposure and the degree of weathering. High values are indicative of a lower age and vice-versa.

Analogue L-type Schmidt-hammers have been used at all three study areas using products of the companies "PROCEQ," Switzerland (Norwegian site) and "Controls," Italy (Austrian sites). On each of the larger rock glaciers (LA-A, DOE-A, DOE-D, and WEI), two to seven locations close to the central flow line between the frontal ridge and the rooting zone were measured. Sites were kept as small as possible. Measurements on rock glaciers were made on ridge crests and high spots to minimise the possible influence of late-lying snow on weathering rates.

Complementary measurements were carried out on a smaller rock glacier (DOE-C), on boulders at the active talus of the rooting zone of DOE-A, on an active ABT (LA-A3), and at outside sites located adjacent or down-valley from the rock glacier termini. These outside sites were located twice on bedrock (2 x O-BR: Dösen and Weissenkar) and four times on glacigenic boulders (LA-A0, O-TI and 2 x YDM: Dösen and Weissenkar). Sampled stable boulders and bedrock sites in each of the three study areas were selected on the basis of comparable lithology with dry, flat and clean surface, free of lichens, visual fissures and cracks (McCarroll 1989, Haeberli et al. 2003, Shakesby et al. 2006).

Arithmetic means of 50 individual readings (4 impacts per boulder; only the two middle values were noted) with 95% confidence interval were examined at all sites (Matthews & Shakesby 1984, Shakesby et al. 2006). Arithmetic means are representative for the effective hardness of the analyzed surface. The 95% confidence interval is indicative for the standard error and statistically significant age differences between measurement sites.

## Results

The Schmidt-hammer results of all three study areas are summarised in Fig. 2A to 2C. Frequency distribution of only one sample shows low bimodality (LA-A3), and skewness is generally low to moderate. Negative skewness may point to a somewhat lower mean $R$-value (higher age) than observed; positive skewness may indicate a somewhat higher mean $R$-value (lower age) than observed.

*Rock glaciers near Laksekv*

Mean $R$-values range from 48.8 outside LA-A (LA-A0) to 54.8 at the active ABT (LA-A3) adjacent to the rock glacier with low 95% confidence limits. The four samples cover a $R$-value range of only 6.0. $R$-values taken at the rock glacier surface are significantly higher than the ones taken from the outside site close to a moraine ridge of Preboreal age, and they are significantly lower than the ones from the ABT.

*Rock glaciers in the Dösen Valley*

Mean R-values range from 29.7 at the YDM site to 47.7 at the active talus above DOE-A (DOE-A7) covering a $R$-value range of 18.0. The 95% confidence limits are generally below ±1.00. A decrease in $R$-values can be discerned at the inactive rock glacier DOE-D and, in particular, at the active rock glacier DOE-A (δ$R$-value 12.3).

*Rock glacier in the Weissenkar Cirque*

Mean $R$-values range from 21.5 at the YDM site to 38.0 at site WEI4 located in the active rooting zone of the rock glacier covering a $R$-value range of 16.4. The rooting zone was occupied by a glacier during the Little Ice Age (~1850 AD) and a large perennial snow field until the late 1990s indicating a rather young age of the deposits at site WEI4. The 95% confidence limit at site WEI4 (1.77) is the highest of all 23 measured sites. A clear decrease in $R$-values can be discerned at the rock glacier WEI (δ$R$-value 13.5).

## Discussion

When analyzing Schmidt-hammer literature, it becomes obvious that $R$-value decrease over time is quite heterogeneous in alpine climates and in different lithologies. However, $R$-value differences of >10 suggest time periods of some thousands to more than ten thousand years even in competent rocks such as gneiss (e.g., Aa & Sjåstad 2000, Frauenfelder et al. 2005, Kellerer-Pirklbauer et al. 2007).

*Rock glaciers near Lakselv*

The formation of the studied rock glaciers in Lakselv

(LA-A) was initiated sometime after the retreat of the Fennoscandian Ice Sheet from the study area. During the YD period, the site of the rock glacier LA-A was situated well inside the glacier limit (Sollid et al. 1973). Marginal moraine ridge systems belonging to the Post-Main (Stordal) substages (Sollid et al. 1973) of suggested Preboreal age (9-10 ka BP, uncalibrated $^{14}$C years; Andersen 1979) were deposited in very close vicinity to the present rock glaciers LA-A and LA-B (see Fig. 1A). Later these moraine ridges acted as natural barriers for the development of both lobated rock glaciers and were partly incorporated into them.

The interpretation of the obtained *R*-values is difficult, and the dating here is very speculative. Aa & Sjåstad (2000) calculated for a site in southern Norway that the *R*-value was reduced by 20.5 over a period of 9730 a. Their study site is to some extent climatically comparable to the Lakselv site but with different lithology (gneiss). They inferred a (hypothetical) linear surface weakening rate of 2.1 *R*-values per 1 ka. However, complications arise because the increase in the degree of weathering over time (i.e. weathering rind thickness) and the role of flaking of the weathering rind are not easy to quantify. Schmidt-hammer mean values seem to correlate with weathering rind thickness almost linearly (Laustela et al. 2003) allowing good comparison. Weathering rind thickness increases nonlinearly with time although this nonlinear weathering-time relationship seems to occur on very long timescales often exceeding 100 ka (Skakesby et al. 2006). The role of flaking of weathering rinds might be more important for shorter time periods (Etienne 2002). The *R*-value differences of 3.4 between LA-A1 and LA-A3 (site at the ABT) and 2.6 between LA-A1 and LA-A0 (site close to the Preboreal moraine ridge) is statistically significant. They allow the conclusion that the rock glacier surface is significant younger than Preboreal but significant older than the currently still active ABT. The low δ*R*-value of 6.0 between the ABT site and the site adjacent to the moraine ridge also might be explained by occasional dispersing of rock material over the entire rock glacier LA-A and its foreland by powerful debris-charged snow avalanches. Judging from the morphology of the rock glacier itself, the glacial and periglacial landforms in close vicinity, and the considerations by Kääb (2005) – total age of rock glaciers might be 2–5 times higher than the minimum age obtained for the surface – a long and complex formation history and a rock glacier initiation soon after the Preboreal is suggested.

*Rock glaciers in the Dösen Valley*

The initiation of all rock glaciers in this study area occurred after the Egesen advance in the early YD period as indicated by the moraines downvalley from the four rock glaciers. In Austria, the early YD is 10Be-dated to around 12.3–12.4 ka (Kerschner & Ivy-Ochs 2007). Thus the maximum and the minimum R-values in this study area can be absolute dated to 12.3–12.4 ka at the YDM site and ~0 a at the active talus site DOE-A7. In this regard, one should not forget the time lag between initial crack formation in the rock face above the rock glacier (exposure to weathering) and the eventual release of a clast to the talus below. Quantification of this period is difficult.

By using a linear relationship between *R*-value and time, a tentative age-calibration curve with a mean decrease of 1.46

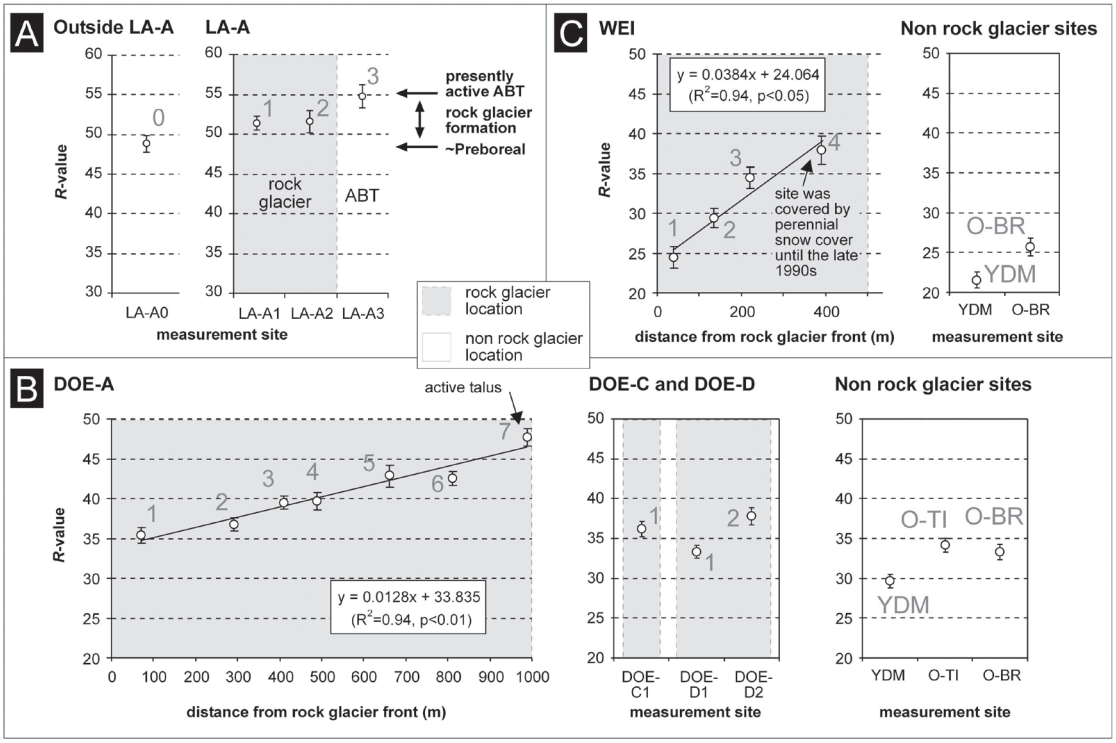


Figure 2. Results of the Schmidt-hammer measurements at the studied rock glaciers and nearby non-rock glacier locations in (A) northern Norway (LA-A) and (B-C) in central Austria (DOE-A, DOE-C, DOE-D and WEI): *R*-values show the arithmetic mean and 95% confidence limits at each measurement site. At the large monomorphic rock glaciers, DOE-A and WEI, *R*-values are plotted against distance from rock glacier front. Best-fit correlations are indicated. Numerals in the graph refer to locations in Figure 1. Estimated age ranges for (A) are given.

*R*-values per 1 ka can be inferred (Fig. 3A). Skakesby et al. (2006) introduced a simple method to investigate the likely size of error of the absolute age estimates derived by the linear relationship. According to their approach, error limits for the predicted ages are determined separately for the YD and present sites from the corresponding 95% confidence intervals of *R*-values by a straight line. The error limits in the predicted age based on this approach is ±607 years for YDM and ±774 years for DOE-A7. Thus a predicted age error of ca. ±0.7 ka for all sites should be considered.

A substantially and statistically significantly lower mean *R*-value at the YDM site compared to all other sites ($\delta \geq 3.6$) suggests that during the YD and Preboreal periods, the head of the Dösen Valley was covered by a glacier terminating between the YDM and the present rock glacier front. The following glacier retreat deglaciated the bedrock site O-BR and deposited the coarse boulders at site O-TI. Identical *R*-values from site DOE-D1 suggest that the rock glacier DOE-D reached its lower end at a similar time. This further suggests that due to its lower position along the valley axis, this valley stretch was not glaciated in the preceding Preboreal period but allowed the formation of DOE-D.

The insignificant *R*-value difference between the outside site O-TI and the lowest site on DOE-A is difficult to interpret when considering the assumption that the total age of a rock glaciers is 2–5 times higher than the minimum age obtained for the surface (Kääb 2005). The obtained minor difference suggests that the surface and total landform age of DOE-A seems to be similar. The same seems to be true for DOE-C and DOE-D. Explanations might be: (a) a less effective "conveyor belt" mechanism (Haeberli et al. 2003), (b) debris-covered glacier tongues which were later incorporated in the rock glacier, (c) mineral variations in the bedrock, or (d) differences in the surface weakening rate between sites due to different vegetation /snow cover histories in the Holocene.

The regression line at DOE-A indicates that this rock glacier was formed continuously during most of the Holocene. Recent velocity data (1954–2005) from the rock glacier DOE-A show mean annual velocity rates of 13.4–37.4 cm $a^{-1}$ (Kaufmann et al. 2007). If these velocities are taken as (questionable) constant over time and combined with the length of DOE-A, ages of 2.7–7.5 ka are calculated. These age values are lower than the age estimate of the lowest rock glacier site (DOE-A1) obtained by the tentative age-calibration curve presented in Fig. 3A (8.4±0.7 ka).

*Rock glacier in the Weissenkar Cirque*

The *R*-values from the third study area suggest a comparable landscape history to the one from the Dösen Valley. The initiation of the rock glacier WEI occurred after the Egesen advance in the early YD period as indicated by the YD moraines downvalley from the cirque. The linear relationship between the *R*-value of the YD moraine site (YDM: 21.5) and the uppermost measurement site in the rooting zone of the rock glacier (WEI4: 38.0) reveals a mean decrease of 1.33 R-values per 1 ka (Fig. 3B).

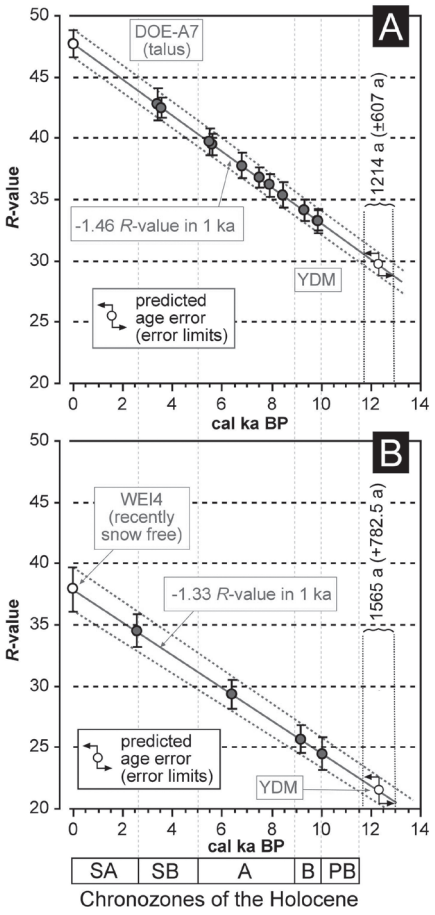


Figure 3. Tentative age-calibration curves for the *R*-values of the study areas Dösen (A) and Weissenkar (B) based on two surfaces of known age indicated as open circles. The calculation of predicted age error including error limits is illustrated for the YDM locations. Grey circles indicate calculated ages based on this approach. Holocene chronozones: SA=Subatlantic, SB=Suboreal, A=Atlantic, B=Boreal and PB=Preboreal.

This rate is only slightly less than the one from the Dösen Valley which indicates that the reduction in the mean *R*-value during the Holocene in central Austria was similar for granitic gneiss (Dösen) and mica schist (Weissenkar) despite substantially different absolute *R*-values.

At Weissenkar Cirque the bedrock site just outside the rock glacier (O-BR) suggests a younger age than the lowest site at the rock glacier (WEI1). Reasons for that might be explanations (a) to (d) presented above. The statistically significant decrease in R-values along a profile at WEI points to a long formation history of the landform starting in the early Holocene. At WEI, the lowest measurement site reveals an age of about 10 ka (cf. Fig. 3B). Therefore, WEI might be even older than the large rock glacier DOE-A in the Dösen Valley. Recent velocity data (1974–2004) from WEI were summarised by Kaufmann et al. (2006) showing low mean annual velocity rates of 1.6–11.6 cm $a^{-1}$. Assuming constant velocities and using a length of 500 m, rock glacier ages of 4.3–31.1 ka can be estimated. This maximum age is certainly far too high, highlighting the weakness of the assumption of constant surface velocity.

## Conclusions

The Schmidt-hammer method seems to be a powerful tool in rock glacier dating, particularly for large rock glaciers where multiple measurement sites along a longitudinal profile are sampled. *R*-value data from such profiles enable the establishment of relative chronologies with high temporal resolution. For small and short rock glaciers this method is more difficult to apply, and additional palaeoclimatic information is required to constrain age estimates. At the study sites in Austria it was possible to estimate relatively accurately the age for Holocene features. However, possible incorporation of older clasts in the rock glacier surface or dispersing of "fresh" rock material by powerful debris-charged snow avalanches can lead to errors. Furthermore, mineral variations in the bedrock or differences in the rate of surface weakening between sites due to different vegetation/ snow cover histories might significantly influence *R*-values. Reliable absolute surface age dating is only possible when surfaces of known age with similar vegetation and climate history, and comparable lithology are available. The more surfaces of known age are available, the better is a resulting age-calibration curve.

## Acknowledgments

This study was carried out within the project ALP-CHANGE (www.alpchange.at) financed by the Austrian Science Fund (FWF) and by an international research scholarship by the Research Council of Norway. Research at the Weissenkar site was supported by students of my institute who are kindly acknowledged. The comments of both reviewer and the editor were highly appreciated.

## References

Aa, R. & Sjåstad, J.A. 2000. Schmidt hammer age evaluation of the moraine sequence in front of Bøyabreen, western Norway. *Norsk Geologisk Tidsskrift* 80: 27-32.

Andersen, B.G. 1979. The deglaciation of Norway 15 000–10 000 BP. *Boreas* 8: 79–87.

Buchenauer, H.W. 1990. Gletscher- und Blockgletscher-geschichte der westlichen Schobergruppe (Osttirol).- *Marburger Geographiche Schriften* 117: 276 pp.

Etienne, S. 2002. The role of biological weathering in periglacial areas: a study of weathering rinds in south Iceland. *Geomorphology* 47: 75-86.

Farbrot, H. 2007. *Distribution, thermal regime and geomorphic significance of mountain permafrost in northern Europe - examples from Iceland, northern Norway & Svalbard.* PhD. Thesis. University Oslo, 141 pp.

Frauenfelder, R. Laustela, M. & Kääb, A. 2005. Relative dating of Alpine rockglacier surfaces. *Zeitschrift für Geomorphologie* 49: 145-166.

Haeberli, W., Kääb, A., Wagner, S., VonderMühll, D., Geissler, P., Haas, J.N., Glatzel-Mattheier, H. & Wagenbach, D. 1999. Pollen analysis and 14C age of moss remains in a permafrost core recovered from the active rock glacier Murtèl-Corvatsch, Swiss Alps: geomorphological and glaciological implications. *Journal of Glaciology* 45: 1-8.

Haeberli, W., Brandovà, D., Burga, C., Egli, M., Frauenfelder, R., Kääb, A. & Maisch, M. 2003. Methods for absolute and relative age dating of rock-glacier surface in alpine permafrost. *Proceedings of the Eighth International Conference on Permafrost, Zurich, Switzerland, July 21-25, 2003:* 343-348.

Kääb, A. 2005. Remote sensing of mountain glaciers and permafrost creep. *Schriftenreihe Physische Geographie Glaziologie und Geomorphodynamik* 48: 266 pp.

Kaufmann, V., Ladstädter, R. & Lieb, G.K. 2006. Quantitative assessment of the creep process of Weissenkar rock glacier (Central Alps, Austria). *Proceedings of the Eight International Symposium High Mountain Remote Sensing Cartography, La Paz, Bolivia, March 21–28, 2005:* 77-86.

Kaufmann, V., Ladstädter, R. & Kienast, G. 2007. 10 years of monitoring of the Doesen rock glacier (Ankogel group, Austria) - A review of the research activities for the time period 1995-2005. *Proceedings of the Fifth Mountain Cartography Workshop, Bohinj, Slovenia, March 29–April 1, 2006:* 129-144.

Kellerer-Pirklbauer, A., Wangensteen, B., Farbrot, H. & Etzelmüller, B. 2007. Relative surface age-dating of rock glacier systems near Hólar in Hjaltadalur, Northern Iceland. *Journal of Quaternary Science* 23 (2): 137-151.

Kerschner, H. & Ivy-Ochs, S. 2007. Palaeoclimate from glaciers: Examples from the Eastern Alps during the Alpine Lateglacial and early Holocene. *Global and Planetary Change* 60(1-2): 58-71.

Laustela, M., Egli, M., Frauenfelder, R. & Haeberli, W. 2003. Weathering rind measurements and relative age dating of rock-glacier surfaces in crystalline regions of the Swiss Alps. *Proceedings of the Eighth International Conference on Permafrost, Zurich, Switzerland, July 21-25, 2003:* 627-632.

Lieb, G.K. 1996. Permafrost und Blockgletscher in den östlichen österreichischen Alpen. *Arbeiten aus dem Institut für Geographie, Univerisät Graz* 33: 9–125.

Matthews, J.A. & Shakesby, R.A. 1984. The status of the 'Little Ice Age' in southern Norway: relative-dating of Neoglacial moraines with Schmidt hammer and lichenometry. *Boreas* 13: 333-346.

McCarroll, D. 1989. Potential and limitations of the Schmidt hammer for relative dating. Field tests on Neoglacial moraines, Jotunheimen, southern Norway. *Arctic and Alpine Research* 21: 268-275.

Shakesby, R.A., Matthews J.A. & Owen, G. 2006: The Schmidt hammer as a relative-age dating tool and its potential for calibrated-age dating in Holocene glaciated environments. *Quaternary Science Reviews* 25: 2846-2867.

Sollid, J.L., Andersen, S., Hamre, N., Kjeldsen, O., Salvigsen, O., Sturod, S., Tveita, T. & Wilhelmsen, A. 1973. Deglaciation of Finnmark, North Norway. *Norsk Geografisk Tidsskrift* 27: 233-325.

# Scaled Centrifuge Modeling of Solifluction in Permafrost and Seasonally Frozen Soils

Martina Kern-Luetschg
*Cardiff University, School of Earth Sciences, Cardiff CF10 3YE,UK*
Charles Harris
*Cardiff University, School of Earth Sciences, Cardiff CF10 3YE,UK*
Peter Cleall
*Cardiff University, School of Engineering, Cardiff, CF24 3AA, UK*
Yuchao Li
*Cardiff University, School of Engineering, Cardiff, CF24 3AA, UK*
Hywel Thomas
*Cardiff University, School of Engineering, Cardiff, CF24 3AA, UK*

## Abstract

The technique of centrifuge modeling allows accurate simulation of full-scale geotechnical processes in small-scale models under correct self weight. Here we report results from two scaled 10 g centrifuge modeling experiments, designed to simulate solifluction processes associated with one-sided and two-sided freezing of an active layer of 1 m thickness at prototype scale. A distinct dry intermediate layer was observed in the two-sided experiment where only very small displacement and thaw settlement occurred. The overall rate of thaw in the two-sided model was significantly slower compared to the one-sided experiment. The total soil deformation profiles after five freeze-thaw cycles show a plug-like sliding component immediately above the permafrost table in the two-sided experiments, but shear strain decreasing with depth in the one-sided experiment. Data from these experiments are currently being used to calibrate and validate newly developed numerical constitutive modeling algorithms designed to predict soil behavior during solifluction.

**Keywords:** active layer; centrifuge modeling; solifluction.

## Introduction

Here we present first results of scaled centrifuge simulation of solifluction processes associated with one-sided and two-sided soil freezing, allowing detailed comparison of hydrothermal processes and downslope displacement rates. These experiments are part of a research program designed to predict styles and rates of periglacial solifluction and their relationship to factors such as climate, hydrology, geology, and topography. New process-based numerical models are being developed and validated against well-controlled full-scale simulations (Harris et al., this volume) and reduced-scale centrifuge modeling.

Freezing and thawing of frost-susceptible, soil-covered slopes cause slow downslope soil movement which is highly significant to slope evolution. In areas of warm or no permafrost, seasonal freezing is from the surface downwards (one-sided freezing), whereas in cold permafrost areas, large thermal gradients in the uppermost permafrost layer can cause active layer freezing in two directions: from the permafrost table upwards and from the ground surface down (two-sided freezing) (e.g., Lewkowicz 1988, Shiklomanov & Nelson 2007). Bottom-upward freezing is most widespread where mean ground temperatures are below -5°C and usually precedes freezing from the surface (Shur 1988). In the case of one-sided freezing, ice lens formation occurs near the ground surface, but during two-sided freezing, ice lenses accumulate in a transition zone that includes the basal zone of the active layer and the upper part of the permafrost (Shur et al. 2005). Thaw penetration into this zone causes deeper soil movements and "plug-like" solifluction (Mackay 1981, Lewkowicz & Clarke 1998).

Numerous field studies of solifluction processes have emphasized the factors controlling spatial variability, and a global review is given by Matsuoka (2001). More detailed exploration of the mechanisms of periglacial solifluction under one-sided freezing has been achieved in large-scale laboratory simulations with controlled soil properties and boundary conditions (Coutard et al. 1988, Harris et al. 1996). The potential of using geotechnical centrifuge modeling technique for the simulations of mass movement processes in thawing slopes has been demonstrated in recent studies (Harris et al. 2001, Harris et al. 2003a,b, Harris et al. 2008). The present experiments were designed to simulate solifluction following one-sided and two-sided freezing conditions under correct slope self weight in the centrifugally accelerated gravity field and under well-controlled soil and boundary conditions.

## Numerical Modeling

For stability problems in cold regions, such as periglacial solifluction, it may be difficult to accurately measure the field stresses in thawing soils with the limitation of current

instruments and methods. The rates and styles of periglacial solifluction apparently depend to some degree on the depth at which ice lenses develop during frost heaving, (Matsuoka 2001). An accurate prediction of ice lensing is therefore of great importance to model the process of periglacial solifluction. A fully coupled thermo-hydro-mechanical numerical approach for modeling solifluction in freezing and thawing soils is under development, based on the existing software, COMPASS (Cleall et al. 2007). Numerical models will be calibrated against laboratory physical models, including centrifuge studies, and assessed via simulation of field data from monitored natural slopes in Svalbard and Norway (Harris et al. 2007).

## Centrifuge Modeling Technique

Geotechnical centrifuge modeling allows detailed studies of real processes under defined boundary conditions, providing an excellent tool for verifying numerical methods. In the rotating centrifuge, a $1/N$ scaled model is subjected to a centrifugal force equivalent to $N$ gravities ($g$) which increases the self-weight of the soil and thus generates a gravitational stress distribution in the model, which is equal to that in the prototype. In a centrifuge test at $Ng$, model linear dimensions scale as $1/N$, area $1/N^2$, stress 1/1, temperature 1/1, time for convective and conductive heat transfer $1/N^2$, and time for seepage force similarity $1/N^2$ (Croce et al. 1985, Savidou 1988). A 1/10 scale centrifuge model tested at 10 g therefore extrapolates to the correct prototype scale.

Accurate scaled modeling requires similitude in soil properties between model and prototype, which is achieved by using the same soil with the same stress history. In the present context, the thaw consolidation theory (Morgenstern & Nixon 1971) provides a framework for the analysis of effective stress within thawing ice-rich soils, the governing factors being thaw penetration rate (controlling rate of meltwater release) and consolidation rate (controlling rate of dissipation of excess pore-water pressure). Since time for seepage force similarity and for heat transfer both scale as $1/N^2$, no scaling conflicts arise in modeling the thaw consolidation process, and model time is reduced by a factor of $N^2$ (Harris et al. 2000, 2001).

However, the time scaling factor for viscous flow is 1/1, so potential temporal scaling conflicts arise if the dynamic response of the thawing soil to gravitational stress is a function of its viscosity. A series of "modeling of models" centrifuge experiments, in which solifluction processes were simulated at different scales and gravitational accelerations, showed virtually identical profiles of shear strain and identical soil transport rates in all models when scaled to prototype, leading to the conclusion that shear strains during solifluction reflect an elasto-plastic response of the thawing soil to gravitational stress, controlled by pore-water pressures, and not fluid flow controlled by viscosity (Harris et al. 2003a). Thus, no significant scaling conflicts arise during centrifuge modeling. An additional advantage of the method is that processes which would take many days or months at prototype scale can be simulated in a few hours.

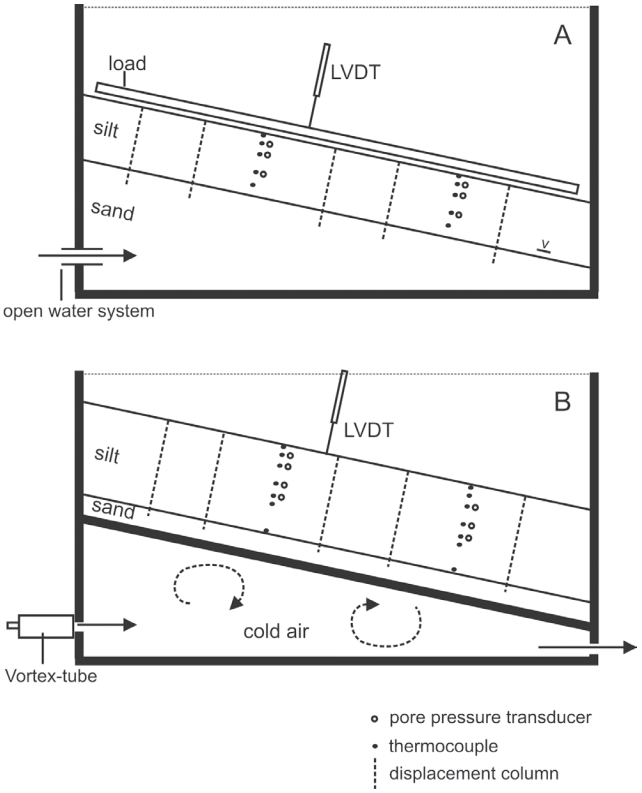


Figure 1. Experimental design during model freezing on the lab floor. (A) one-sided freezing and (B) two-sided freezing. The sides and base of the test box were surrounded in polystyrene insulation, and the surface temperature lowered to between -5°C and -10°C.

## Design of Centrifuge Experiments

The Cardiff University geotechnical centrifuge consists of a beam centrifuge of 2.7-m radius for testing model packages of up to 1000 kg at an acceleration of up to 100 gravities. 1/10 scale slope models with gradient 12° were constructed in Perspex boxes of internal dimensions 0.74 m x 0.45 m x 0.44 m (Fig. 1) using the same silty soil that was used for equivalent full-scale laboratory simulations (see Harris et al., this volume). For this study, two different model types were prepared to simulate (a) the response of the thawing soil to ice distribution generated by seasonal one-sided freezing and (b) the response of the thawing soil to ice distribution generated by two-sided freezing under cold permafrost conditions. Soil was placed over a basal sand layer forming a 9-cm-thick model (scaling to 90 cm) for the one-sided experiments and a 14-cm-thick model (scaling to 140 cm) for the two-sided experiment.

In each, 2 vertical arrays of 5 and 7 type-K thermocouples, respectively, and three Druck pore pressure transducers were inserted. Thermocouples were placed at 5 cm above the box for air temperatures and at depths 0, 1, 3.5, 6, and 7 cm in the one-sided and at 0, 2, 3.5, 6, 8, and 9 cm in the two-sided model. Columns of 5 mm plastic cylinders were inserted perpendicular to the slope surface to measure soil deformation. A regular grid of 1 cm circular markers was distributed on the surface to monitor surface downslope displacement during thawing.

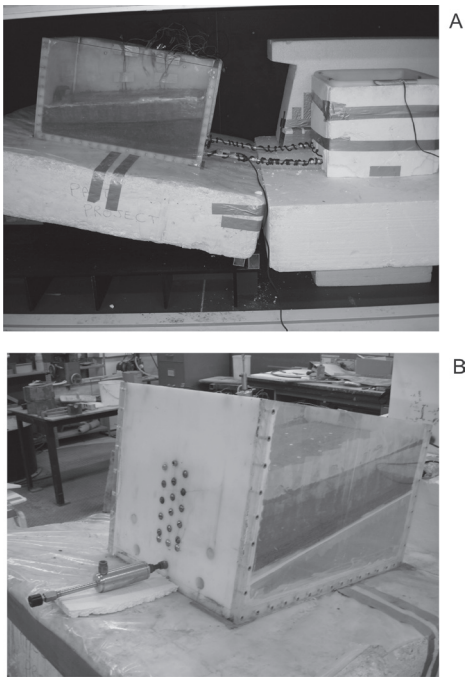


Figure 2. Model preparation. (A) One-sided set-up for freezing with an open-water system. (B) Two-sided freezing with a basal cooling system using vortex tubes.

Two linear voltage transducers (LVDT, LDC 1000C) were placed perpendicular to the soil surface to monitor frost heave during freezing. The model boxes were thermally insulated with polystyrene, and the soil slopes were frozen from the surface downwards at air temperatures between -5°C and -10°C in a freezing chamber under 1 g.

The one-sided model was frozen from the top under a confining load of 1.5 kPa and with an open-water system through the basal sand layer allowing ice segregation in the soil layer. During freezing, the model was tilted to give a horizontal soil surface, and water level was maintained at the sand-soil interface (Fig. 2A). In the two-sided model, a cold permafrost table was simulated using a basal cooling system of cold compressed air generated by three vortex tubes (Fig. 2B). During each cycle of two-sided freezing, summer heave was simulated by sprinkling water on the surface with air temperatures above 0°C and with the basal cooling system running, maintaining base temperatures around -3°C. Pore-water pressures, soil temperatures, air temperature, and frost heave were monitored through the data logger (Campbell CR1000).

The frozen model slopes were placed in the centrifuge gondola and thawed under a gravitational field of 10 gravities. Thawing was from the soil surface downwards at air temperatures between 10°C and 15°C and with an open drainage system. A laser (OADM20) was mounted above the slope surface to monitor thaw settlement. Every 30 minutes the grid of surface markers was captured by an automatic camera to trace the ground surface downslope displacement during thawing. During each freezing cycle, all sensors were monitored at 10-s intervals via the on-board centrifuge data logging system (Campbell CR10X). Each model was subjected to 5 freeze-thaw cycles.

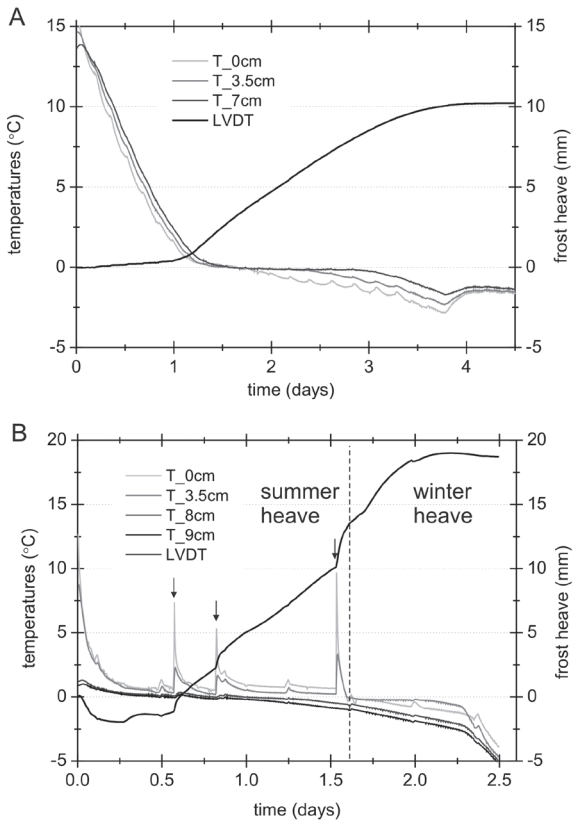


Figure 3. Frost heave and soil temperatures. (A) One-sided freezing experiment showing progressive frost heave over time and freezing from the surface downwards. (B) Two-sided freezing experiment in which heave can be divided into summer and winter components with active layer freezing from the surface downwards and from the permafrost table upwards. For summer, heave water was added to the surface (marked by arrows).

## Results

*Thermal regime and frost heave*

During freezing of the soil models at 1g, the one-sided experiment showed a significant difference in frost heaving rate and thermal regime compared to the two-sided experiment, illustrated in Figure 3. Surface-downwards freezing of the one-sided model over a four-day period is indicated by the temperature-time series at depths 0, 3.5, and 7cm. Ice segregation occurred throughout the soil layer, reflected by uniform frost heaving rates (LVDT) over the freezing period (Fig. 3A). In the two-sided experiment, where basal temperatures were maintained below zero, active layer freezing took place over two days (Fig. 3B) and total heave was due (a) to summer heave with positive air temperatures and ice accumulation at the active layer base followed by (b) winter heave with active layer freezing from the surface downwards and from the permafrost table upwards.

A total of 10 mm (scaling to 10 cm at prototype) frost heave was measured in the one-sided and 19 mm (scaling to 19 cm) in the two-sided experiment. Heaving ratios (i.e., frost heave divided by thickness of the frozen layer) for different depths are listed in Table 1.

Table 1. Frost heave and thaw settlement measurements from the one-sided and two-sided experiment.

| Test | Thaw depth (m) | Thaw settlement (mm) | Heaving ratio | Thaw rates (mm/hr) | Displacement (mm) | Ratio displacement/ settlement |
|---|---|---|---|---|---|---|
| 1-sided | 0 | 10.8 | - | 0.72 | 7.8 | 0.72 |
| | 0.1 | 31.3 | 0.24 | 0.33 | 9.3 | 0.30 |
| | 0.35 | 17.2 | 0.06 | 0.23 | 6.0 | 0.35 |
| | 0.6 | 22.4 | 0.08 | 0.39 | 3.9 | 0.18 |
| | 0.7 | 49.3 | 0.33 | 0.23 | 1.1 | 0.02 |
| 2-sided | 0 | 7.1 | - | 0.28 | 0.0 | 0.0 |
| | 0.2 | 29.9 | 0.23 | 0.30 | -3.1 | -0.11 |
| | 0.35 | 6.4 | 0.04 | 0.07 | 3.8 | 0.60 |
| | 0.6 | 4.0 | 0.02 | 0.03 | -0.7 | -0.18 |
| | 0.8 | 5.4 | 0.03 | 0.02 | 2.5 | 0.45 |
| | 0.9 | 63.3 | 0.39 | 0.25 | 17.0 | 0.27 |

*Thaw rates and thaw settlement*

In Figure 4, thaw-penetration and thaw-settlement rates are shown during thawing at 10 g of the one-sided and the two-sided experiments in the centrifuge. Nearly linear thaw-settlement rates were monitored in the one-sided experiment. However, temperature profiles showed an apparent deceleration of thaw penetration close to the surface and between 0.6 and 0.7 m depths (prototype scale), associated with depths of slightly increased ice formation in the model. For each thawed layer (i.e., between two instrumentation depths), total thaw settlement, average thaw rates (i.e., thaw settlement per time), and heave ratio (i.e., thaw settlement per frozen layer thickness) are listed in Table 1. In the two-sided experiment, higher settlement rates were monitored near the surface and between depths 0.8 and 0.9 m (prototype scale) (Fig. 4B). In the relatively drier ice-poor layer (i.e., small heave ratios) between depths 0.35 and 0.6 m, lower rates of thaw settlement were measured. A very similar pattern was observed in recent field measurements on a permafrost solifluction slope in Svalbard (Harris et al. 2006) where moisture migration upwards and downwards during two-sided freezing had also left an ice poor central layer.

*Rates of surface movement and displacement profiles*

Table 1 shows surface displacement (at prototype scale) for each thaw depth during the one-sided and the two-sided experiment, based on time-lapse photographs of the displacement of one marker located in the center part of the model, where minimal boundary effects were expected. In the one-sided experiment, more than three-quarters of total displacement occurred during thaw of the uppermost 0.35 m, whereas in the two-sided experiment, most displacement occurred during thaw below 0.6 m. At these depths, highest ratios of displacement to thaw settlement were observed. However in the two-sided cycle, at depths between 0.2 to 0.6 m apparent upslope and downslope displacements were observed, which could have been caused by soil desiccation and crack formation during thaw progression into the relatively drier layers at these depths. From the displacement values in Table 1, and assuming that surface displacements were due to displacement of the thawed layer immediately above the thaw front, subsurface displacement profiles were derived. Figure 5(a) shows profiles after one freeze-thaw cycle, (b) after five cycles of repeated freezing and thawing. The one-sided profiles show highest displacement near the surface, whereas in the two-sided experiment displacement occurs at deeper depths generating profiles similar to the plug-like movement of an active layer over an ice-rich basal shear zone as was described by Mackay (1981), Lewkowicz & Clarke (1998), and Matsuoka (2001).

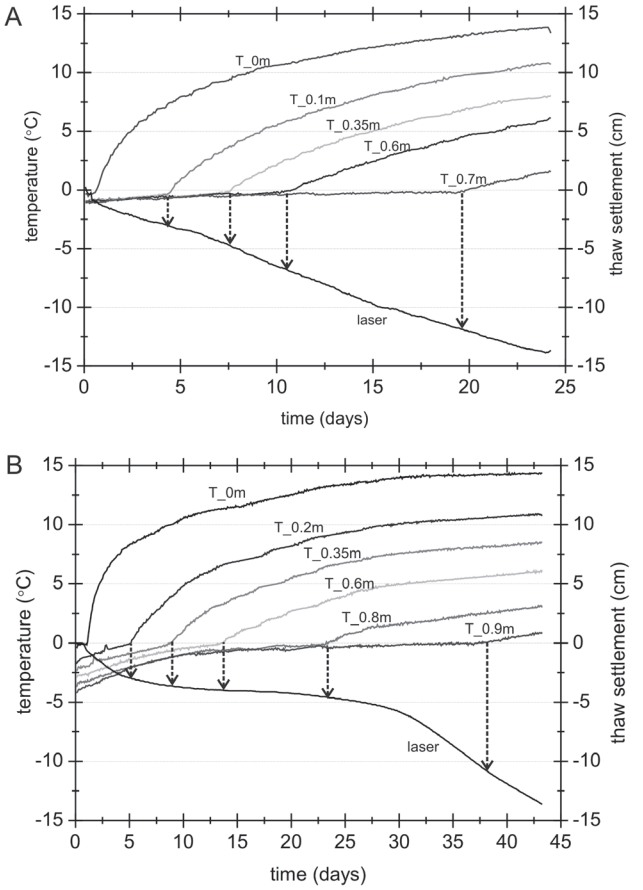


Figure 4. Temperature and settlement measured during thawing in the centrifuge for (A) the one-sided and (B) the two-sided experiment.

Displacement columns were excavated after 5 freeze thaw

cycles. Figure 6 shows an example for each experiment: the one-sided (a) and the two-sided (b). Although reflecting the generic shape of the calculated profiles (Fig. 5), the profile shapes exhibited by the columns also show some deviations especially for the two-sided experiment. This is due to the fact that the freezing cycles are not exactly reproducible: cycle-to-cycle variation in frost heave and depths of ice accumulation cause variation in total displacement and in the location of main displacement horizon (Fig. 6B). It should be noted that the active-layer thickness simulated in the two-sided freezing experiment was 9–10 cm model scale, 90–100 cm prototype. This is marked by an arrow in Figure 6B. Disturbance of the marker column below this depth reflects the final thawing of the model following the five-cycle experiment.

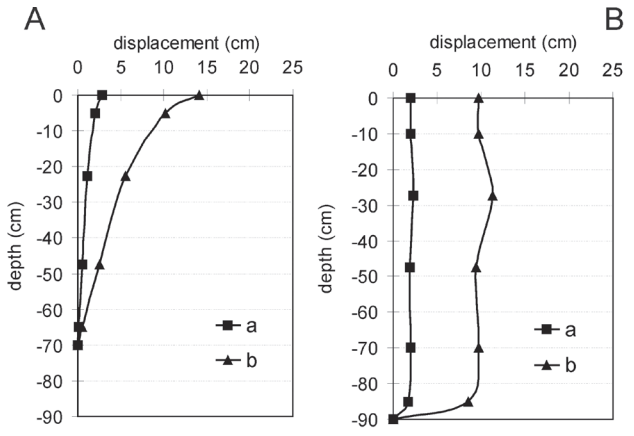


Figure 5. Calculated displacement profiles after (a) one freeze-thaw cycle and (b) five repeated cycles for (A) the one-sided and (B) the two-sided experiment.

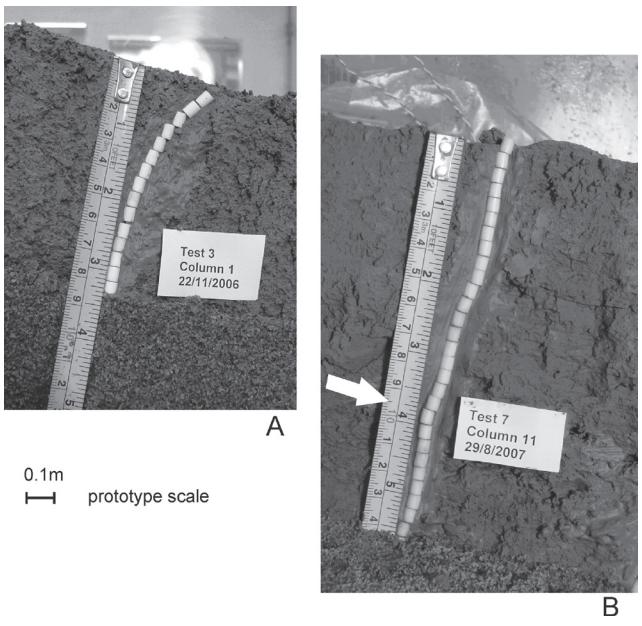


Figure 6. Observed subsurface displacement following five cycles for (A) the one-sided and (B) the two-sided experiment. The base of each column corresponds to the base of the model and top of the underlying sand layer.

## Discussion

Subsurface displacement profiles resulting from the one-sided and two-sided experiments presented above exhibit significant differences regarding the depths where main displacement took place (Fig. 6). Matsuoka (2001) classified shapes of displacement profiles from field observations into four subgroups: needle ice creep, diurnal frost creep, annual frost creep with possible gelifluction, and plug-like flow. The typically convex shaped displacement profiles developed during five freeze-thaw cycles in our one-sided experiment (Fig. 6A) are similar to the one-sided seasonal freezing, gelifluction type of displacement profiles described by Matsuoka (2001). This profile shape typically originates from shear strain concentrated in the uppermost few centimeters to decimeters, depending on the duration of the freeze-thaw period which controls the depth of ice lens formation during freezing. In contrast, the two-sided experiments typically show concave-shaped profiles (Fig. 6B) similar to the plug-like displacement reported from cold permafrost areas where the basal active layer is ice-rich. In the two-sided freezing experiment (and in nature), the maximum summer active layer depth varied from cycle to cycle, leading to basal displacements occurring over a depth range of around 15 mm at model scale, or 15 cm at prototype scale, rather than being concentrated in one distinct layer. In general, the scaled experiments show similar shapes to those observed in full-scale experiments of one-sided and two-sided freezing and thawing (Harris et al., this volume). Scaled displacement rates and depths are in the same order of magnitude as field observations of solifluction in both seasonal frost and cold permafrost areas (see for instance Matsuoka & Hirakawa, 2000).

## Conclusion

1. From these first results, we may conclude that the principle processes of solifluction associated with two-sided and one-sided active layer freezing were successfully physically modeled in small-scaled centrifuge experiments.
2. In the two-sided experiments, a distinct ice-poor intermediate layer was associated with very little thaw settlement downslope displacement.
3. Significantly different shapes of the one- and two-sided displacement profiles can be related to distribution of soil ice in the frozen models and subsequent consolidation during thaw. First qualitative comparisons indicate that scaled displacement rates and profile shapes are consistent with displacement profiles observed in field and full-scale laboratory experiments.
4. The geotechnical centrifuge modeling technique has proven an important tool for further systematic investigations of active layer behavior under controlled and repeatable conditions.
5. Further detailed validation through the principle of modeling of model analysis (Ko 1988) is in process and being produced in the near future.

6. Calibration and validation of numerical modeling with the scaled centrifuge physical modeling are in process, and further simulations of field monitoring and full-scale laboratory simulation experiments will be conducted.

## Acknowledgments

This research was funded by the British Engineering and Physical Sciences Research Council Research Grant GR/T22964. Technical support from Harry Lane in the geotechnical centrifuge laboratory is gratefully acknowledged.

## References

Cleall, P.J., Seetharam, S.C. & Thomas, H.R. 2007. Inclusion of some aspects of chemical behaviour of unsaturated soil in thermo/hydro/chemical/mecha-nical models. I: Model development. *ASCE Journal of Engineering Mechanics* 133(3): 338-347.

Coutard, J.-P., Van Vliet-Lanoe, B. & Auzuet, A.V. 1988. Frost heaving and frost creep on an experimental slope: results for soil structures and sorted stripes. *Zeitschrift fur Geomorphologie, Supplementband* 71: 13-23.

Croce, P.V., Pane, V., Znidarcic, D., Ko, H-Y., Olsen, H.W. & Schiffman, R.L. 1985. *Applications of Centrifuge Modelling to Geotechnical Design*, W.H.Craig, Ed. Balkema, Rotterdam, 381-401.

Harris, C., Davies, M.C.R. & Coutard, J.-P. 1996. An experimental design for laboratory simulation of periglacial soliflucton processes. *Earth Surf. Process. Landforms* 21: 67-75.

Harris, C., Rea, B.R. & Davies, M.C.R. 2000. Geotechnical centrifuge modelling of gelifluction processes: validation of a new approach to periglacial slope studies. *Annals of Glaciology* 31:263-268.

Harris, C., Rea, B.R. & Davies, M.C.R. 2001. Scaled physical modeling of mass movement processes. *Permafrost and Periglacial Processes* 12:125-136.

Harris, C., Davies, M.C.R. & Rea, B.R. 2003a. Gelifluction: viscous flow or plastic creep? *Earth Surf. Process. Landforms* 28: 1289-1301.

Harris, C. & Smith, J.S. 2003b. Modelling gelifluction processes: the significance of frost heave and slope gradient. *Proceedings of the Eighth International Conference on Permafrost, Zurich, Switzerland. Balkema, Lisse*: 355-360.

Harris, C., Luetschg, M., Murton, J.B., Smith, F.W. Davies, M.C.R., Christiansen, H.H. & Ertlen-Font, M. 2006. Solifluction processes in Arctic permafrost: Results of laboratory and field experiments. *EOS Trans., AGU, 87*(52), Fall Meeting Supplement, Abstract C43A-03.

Harris, C., Luetschg, M., Davies, M.C.R. Smith, F., Christiansen, H.H. & Isaksen, K. 2007. Field instrumentation for real-time monitoring of periglacial solifluction. *Permafrost and Periglacial Processes* 18: 105-114.

Harris, C., Smith, J.S., Davies, M.C.R. & Rea, B. 2008. An investigation of periglacial slope stability in relation to soil properties based on physical modelling in the geotechnical centrifuge. *Geomorphology* 93: 437-459.

Harris, C., Kern-Luetschg, M., Murton, J., Font, M., Davies, M. & Smith, F. 2008. Full-scale physical modeling of solifluction processes associated with one-sided and two-sided active layer freezing. *This volume.*

Ko, H.-Y. 1988. Summary of the state of the art in centrifuge model testing. In: W.H. Craig, R.G. James, & A.N. Schofield (eds.), *Centrifuges in Soil Mechanics*. Rotterdam: Balkema, 11-18.

Konrad, J.M., & Morgenstern, N.R. 1980. A mechanistic theory of ice lens formation in fine-grained soils. *Canadian Geotechnical Journal* 17: 473-486.

Lewkowicz, A.G. 1988. Slope processes. In: M.J. Clark (ed.), *Advances in Periglacial Geomorphology*. Chichester: Wiley, 325-368.

Lewkowicz, A.G. & Clarke, S. 1998. Late summer solifluction and active layer depths, Fosheim Peninsula, Ellesmere Island, Canada. *Proceedings the Seventh International Conference on Permafrost, Yellowknife, Canada*, 641-646.

Mackay, J.R. 1981. Active layer slope movement in a continuous permafrost environment, Garry Island, Northwest Territories, Canada. *Canadian Journal of Earth Sciences* 18: 1666-1680.

Matsuoka, N. & Hirakawa, K. 2000. Solifluction resulting from one-sided and two-sided freezing: field data from Svalbard. *Polar Geosci.* 13: 187-201

Matsuoka, N. 2001. Solifluction rates, processes and landforms: A global review. *Earth-Science Reviews* 55: 107-134.

Morgenstern, N.R. & Nixon, J.F. 1971. One-dimensional consolidation of thawing soils. *Canadian Geotechnical Journal* 8: 558-565.

Savidou, C. 1988. Centrifuge modelling of heat transfer in soil. *Centrifuge 88*. Rotterdam: Balkema, 583-591.

Shur, Y.I. 1988. The upper horizon of permafrost soils. *Proceedings of the Fifth International Conference on Permafrost*, *Trondheim, Norway,* 867-871.

Shur, Y., Hinkel, K.M. & Nelson, F.E. 2005. The transient layer: Implications for geocryology and climate-change science. *Permafrost and Periglacial Processes* 16: 5-17.

Shiklomanov, N.I. & Nelson, F. 2007. Active layer processes. In: S.A. Elias (ed.), *Encyclopedia of Quaternary Science,* Vol. 3, Oxford: Elsevier, 2138-2146.

# Snow and Temperature Relationships on Polygonal Peat Plateaus, Churchill, Manitoba, Canada

G. Peter Kershaw
*Department of Earth & Atmospheric Sciences, University of Alberta, Edmonton, AB, Canada, T6G 2E3*

## Abstract

Polygonal peat plateaus are a common landform in the Hudson Bay Lowlands and are diagnostic of continuous permafrost. The polygons are formed by ice wedge troughs that have different surface water and plant cover characteristics. In winter the low troughs accumulate more snow than the raised wind-deflated centers. This variation in snowpack drives temperature differences that can be dramatic. When thermokarst subsidence results from ice wedge melting, the snow accumulation is greater and the enhanced insulation traps more of the heat gained in summer. The mean annual temperature beneath the snow can rise above 0°C and the potential for a positive feedback occurs where further thermokarst subsidence traps more insulating snow. Ice wedges cease cracking and after degradation of the ice wedges, the raised polygon centres or baydjarakh have an external morphology that has resulted in them being mistakenly identified as palsas.

**Keywords:** baydjarakh; frost cracking; ice wedge polygon; microclimate; snowpack; temperature; thermokarst.

## Introduction

Polygonal peat plateaus are relatively flat-topped features that have been dissected by ice wedge polygons and that often rise <2 m above the surrounding terrain (Brown 1970, van Everdingen 2005, Zoltai & Tarnocai 1975). The polygons are the ice wedge troughs that often have a different plant community from that which dominates the polygon centres.

One of the first descriptions of polygonal patterns was from Siberia by Figurin in 1823 (Washburn 1979). Since then they have been described from around the circumpolar North (French 1996, Mackay & Black 1973, Washburn 1979). They are formed by thermal contraction of the host sediments during winter followed by water entering the crack to freeze and form an ice veinlet that, given enough time for the cycle to repeat, develop into ice wedges (Fortier & Allard 2005, Fortier & Allard 2004, Kerfoot 1972, Lachenbruch 1966, Lachenbruch 1962, Leffingwell 1915, Mackay 1993, Mackay 1986, Mackay 1974, Mackay & Burn 2002, Mackay & MacKay 1974).

Thermal contraction has been observed with air temperature declines of 14°C $d^{-1}$ over 34 h to 3.7°C $d^{-1}$ over 102 h in peaty sands of northern Québec (Allard & Kasper 1998); 12°C $d^{-1}$ over 18 h in peaty silts on Bylot Island, Nunavut (Fortier & Allard 2005); and 1.8°C $d^{-1}$ over 96 h in ice-rich peat on islands in the Mackenzie Delta, NWT (Mackay 1993). In his 1993 paper Mackay concluded there was little correspondence between the mean daily air temperature and cracking of ice wedges; however, he noted that ice wedge cracking occurs when the mean minimum temperatures at 50 cm depth fall between -17°C and -23°C (the number and dates of readings were not specified).

Several factors can affect the magnitude and frequency of cracking, but there is a consensus that snowpack is a critical variable. One must be careful since in some studies the polygons are low-centered so that the snow insulates the polygon centres as well as the depressed ice wedge troughs (Allard & Kasper 1998, Fortier & Allard 2005). In high-centered polygons such as those at Churchill, the snowpack is thinner in the centers than the bordering ice wedge troughs. In general, a deeper, more continuous and long-lasting snowpack will insulate the ground against heat loss in winter (Goodrich 1982, Nicholson & Granberg 1973, Smith 1975).

*Study area*

The study features were ~2 km apart at similar elevation (~15 m a.s.l.) (Fig. 1). They were within the forest-tundra ecotone between the open forest and tundra near the Churchill Northern Studies Centre.

Excavations at one site in 1997 revealed ice nipples (Péwé 1962) extending from the tops of the larger ice wedges. These secondary wedges were more vein shaped—consistently ~2 cm thick and extending approximately 15 cm above the main wedge. Due to their morphology and lack of indications of

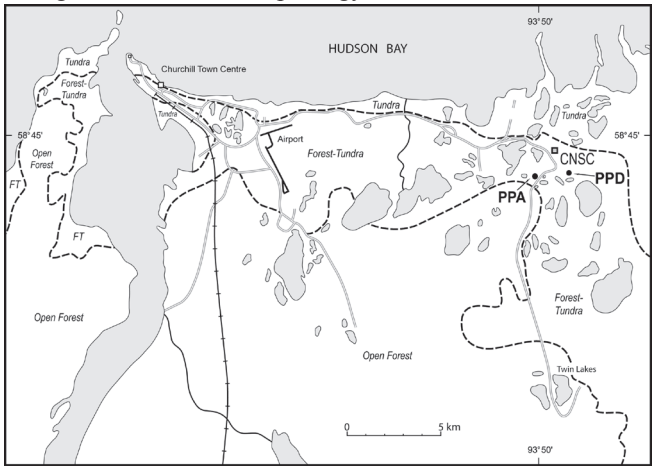


Figure 1. The study features were ~20 km east of the town of Churchill. Polygonal peat plateaus with degrading ice wedges (PPD) and aggrading ice wedges (PPA) were ~2 km south of the Churchill Northern Studies Centre (CNSC).

rapid peat accumulation, they were interpreted as evidence of active layer thinning and so can be classified as epigenetic ice wedges (Dostovalov & Popov 1966, French et al. 1982, Mackay 1974). The shallow (~20 cm) depressions over the ice wedges and the ice nipples are evidence of permafrost aggradation (Mackay 1976).

The ice wedges at the other site were degrading, as evidenced by the linear thermokarst depressions (0.8–1.5 m deep and 2–7 m wide) surrounding isolated remnant polygon centres (baydjarakhs). As with the aggrading site, the polygon centers were at the same height and flat topped. However, at the degrading site, the edges of intact and former ice wedge troughs were steep-sided, ending in a sedge wetland. When viewed from the air, the pattern of the original ice wedges was clearly polygonal. At both sites the polygons were 5–10 m in diameter. In 1997, and annually since 2002, ground-penetrating radar and coring at both sites have confirmed the presence of ice wedges within frozen peat of 1.25–2.5 m depth overlying marine sediments (clasts imbedded in a silty clay matrix) topped by a thin to 15 cm layer of poorly-decomposed marine algae. Coring confirms that the peat is dominantly well-decomposed to poorly-decomposed sedge peat with minor amounts of fine woody material, probably dwarf shrubs. Given the isostatic history (Dredge 1992), internal characteristics, basal marine algae deposits, and setting, the site history is probably much like reported for similar polygonal peat plateaus on Devon Island (Somr & King 1990).

Thaw depths were measured with a graduated probe in October 2007 at both sites. The polygon centers had 45.7 (n = 98) and 41.6 (n = 108) cm active layer on the polygonal peat plateau degrading and aggrading respectively. The mean active layer depth on the ice wedges at the aggrading peat plateau was 37 (n = 20) cm. Thaw depth in the troughs around the baydjarakhs could not be reliably determined since the underlying marine sediments were stony which prevented deep probing. Ground-penetrating radar surveys suggest a 10 to 12 m active layer between the remnant polygon centers.

In most cases the raised polygon centers were dominated by lichens (*Alectoria nigricans, A. ochroleuca, Cetraria nivalis, C. cucullata, Cladina* spp. and *Cladonia* spp.), dwarf ericaceous shrubs (*Ledum decumbens, Rhododendron lapponicum*) and the forb *Rubus chamaemorus*. The depressed ice wedge troughs on the aggrading permafrost site were dominated by mosses (*Sphagnum* spp. and *Dicranum* spp.), *Betula glandulosa*, *L. decumbens, Rubus chamaemorus* and *Salix* spp. On the degrading permafrost site the drier subsided troughs have similar plant cover to the aggrading site but where they extend to the water table the plants are dominated by wetland species (*Calliergon* spp. and *Carex aquatilis*).

## Methods

Midwinter snowpack surveys were conducted over eight days in February each year from 2002 to 2007. Although the data collection included full snowpit stratigraphic descriptions, the data presented here are from the snow core (Adirondack) sampling. Sampling was stratified by microsite on the two polygonal peat plateaus–polygon centre and wedge troughs. Annual sample sizes varied between 30 and 132 and over the six years a total of 475 to 558 samples were taken on the four microsites–polygon centres and ice wedge troughs at both the aggrading and degrading polygonal peat plateaus.

Temperature was monitored with Campbell Scientific International CR10X data loggers and type T thermocouples connected through a multiplexer in the enclosure with the logger (AM416 or AM16/32) with reference junction on the 10X wiring panel. Readings were taken every 5 min with the mean daily temperature used in this analysis. Air temperature was recorded at 1.5 m height while surface temperatures were at 0 cm, shielded by moss or lichen. Near-surface permafrost temperature was measured at 80 cm depth; however, at the degrading permafrost site the sensor was severed by an animal after installation so no mean could be calculated for 2004.

A microclimate station was installed at the aggrading polygonal peat plateau in June 2001 and at the degrading polygonal peat plateau in June 2003. Mean annual temperatures were calculated for only those years where there was a full record: 2002–2006 and 2004–2006 for the aggrading and degrading sites, respectively.

A synthetic value was derived to facilitate comparison of the potential for heat conduction through the snowpack (Kershaw 2001). The Heat Transfer Coefficient (HTC) uses depth and density to estimate the potential heat loss from the soil; higher values indicate greater heat conduction and less insulation.

$$HTC = k/d \quad (1)$$

where $k$ is the thermal conductivity (Abel's 1893) of the snowpack and $d$ is the snowpack depth

$$k = (2.94\ 10^{-6}\ W\ m^{-1}\ °K^{-1})(\rho)^2 \quad (2)$$

where $\rho$ is snowpack density (kg $m^{-3}$)

Mean annual temperatures were calculated from the daily means during the year. Freezing degree-day totals were calculated by accumulating the mean daily values <0°C for the year.

## Results

Interannual snowpack characteristics of depth and the potential for heat conduction were rarely significantly different (Figs. 2, 4). Consequently, comparisons among microsites were made with means of the six years of data.

*Snowpack depth*

Comparing microsites, snowpack depth varied little among years (Fig. 2). However, there were great differences between polygon centres and ice wedge troughs at both study sites. In the subsided ice wedge troughs at the degrading

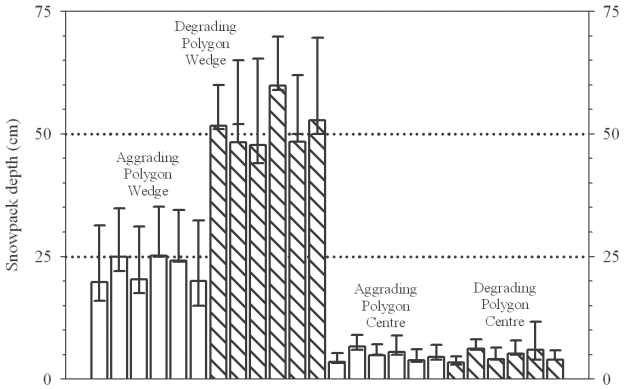


Figure 2. Midwinter snowpack depth 2002–2007 for the two ice wedge troughs and polygon centres on aggrading and degrading polygonal peat plateaus. Mean with capped lines for median (bottom) and standard deviation (top).

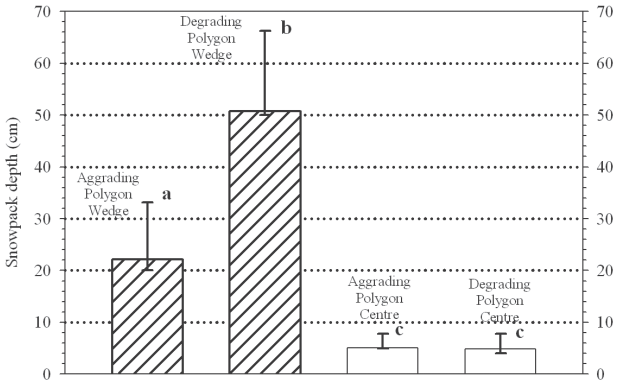


Figure 3. Midwinter snowpack depth (mean of six years) for the two ice wedge troughs and polygon centres on aggrading and degrading polygonal peat plateaus. Mean with capped lines for median (bottom) and standard deviation (top). Significantly different ($p < 0.05$) values have different letters.

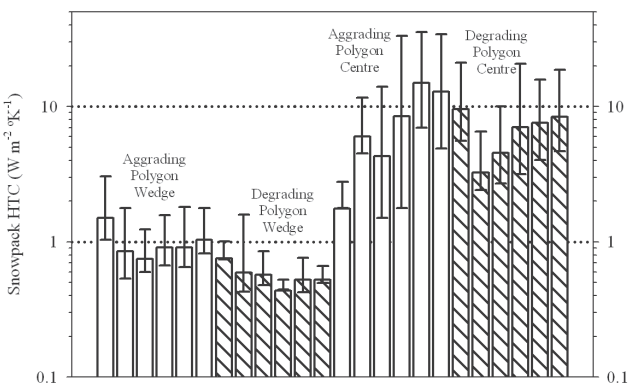


Figure 4. Midwinter snowpack heat transfer coefficient (HTC) (2002–2007) for the two ice wedge troughs and polygon centres on aggrading and degrading polygonal peat plateaus. Mean with capped lines for median (bottom) and standard deviation (top).

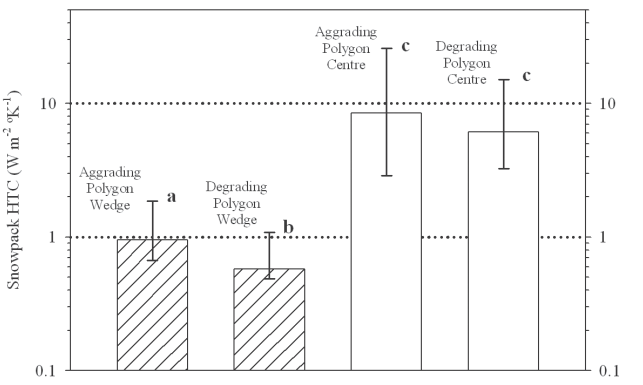


Figure 5. Midwinter snowpack heat transfer coefficient (HTC) (mean of six years) for the two ice wedge troughs and polygon centres on aggrading and degrading polygonal peat plateaus. Mean with capped lines for median (bottom) and standard deviation (top). Significantly different ($p < 0.05$) values have different letters.

polygonal peat plateau there was ~10x more snow than on the adjacent polygon centres. At the aggrading polygonal peat plateau there was 4x–5x more snow in the troughs. The polygon centre snowpack was similar between the two sites while the ice wedge troughs had significantly deeper snow (Fig. 3).

*Snowpack heat conduction*

Regardless of the year, there was ~10x higher potential for heat loss from the polygon centers compared to the adjacent ice wedge troughs (Fig. 4). The potential for heat loss from the wedge troughs on the degraded peat plateau was 40% lower that on the aggrading features (Fig. 5).

*Temperature characteristics*

Except for 2004, the mean annual air temperature was similar for the two sites (Fig. 6). Both the mean annual polygon centre surface temperatures and the near-surface permafrost temperatures were very similar. However, the mean annual surface temperatures of the ice wedge troughs differed by 5.5 to 6.5°C with the degrading ice wedges having mean annual temperatures well above 0°C at 2 and 3.5°C.

Freezing degree-days were greatest in 2004 and least in 2006 (Fig. 7). The polygon centres and the near-surface permafrost had similar values. Despite similar air temperatures, the ice wedge troughs were much colder on the aggrading peat plateau.

## Discussion

The two study sites were close enough to share the same climatic characteristics and yet differed greatly in their geomorphic status—aggrading vs. degrading permafrost.

*Snowpack – temperature relations*

Snowpack on the polygon centres was similar in depth and potential heat conduction on the two sites (Figs. 3, 5). As a result, their surface temperature characteristics were similar with the same freezing degree-day totals (Figs. 6, 7). The mean annual temperature of the near-surface permafrost differed by only 0.2°C (Fig. 6).

The main difference between the sites was the snowpack and temperature characteristics of the ice wedge troughs. With at least double the snowpack and almost half the heat conduction, the degrading ice wedges had mean annual

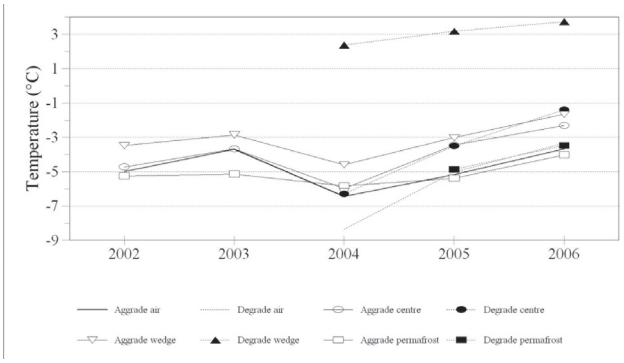


Figure 6. Mean annual temperature on polygonal peat plateau with aggrading permafrost (Aggrade) and degrading permafrost (Degrade). Temperatures measured at 150 cm height (air), ground surface of polygon ice-wedge trough (wedge) and ground surface of polygon centre (centre).

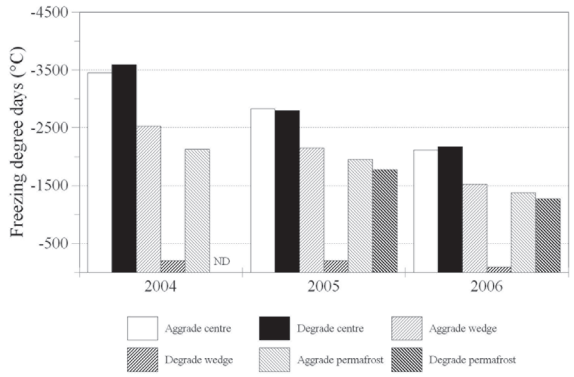


Figure 7. Accumulated freezing degree-days (<0ºC) on polygonal peat plateaus with aggrading permafrost (Aggrade) and degrading permafrost (Degrade). Temperatures measured at 150 cm height (Air), ground surface of polygon ice wedge trough (wedge) and ground surface of polygon centre (centre). No 2004 data available for near-surface permafrost on the degrading peat plateau.

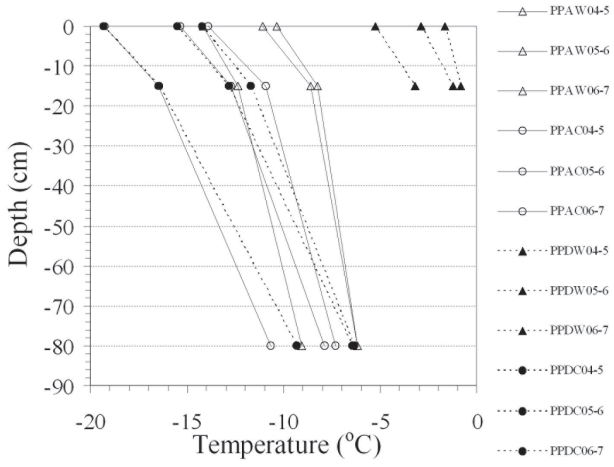


Figure 8. November to March mean temperatures for three winters (2004–2007) on polygonal peat plateaus with aggrading (PPA) and degrading (PPD) ice wedges (W) and their associated polygon centres (C). Measurements at the ground surface, 15 and 80 cm depth except for depressions associated with degraded ice wedges (PPDW).

surface temperatures above 0°C (Fig. 6). Winter temperatures (November–March) confirm that the degrading wedges were warmer than the polygon centres and the wedges on the aggrading site (Fig. 8). There was an average gradient of between 6.6°C and 10°C between the ground surface and 80 cm depth on the polygon centres.

The plant cover and near-surface peat characteristics were similar at both sites on the polygon centres but differed on the adjacent ice wedge troughs. The polygon centres had a thin snowpack with high heat conduction potential and consequently surface temperatures were similar to the air (Figs. 3, 5, 6). In 2003 open thermal contraction cracks were observed on the aggrading site but no cracks have ever been found at the degrading site. With no difference in polygon centre characteristics it must be the ice wedge trough characteristics that allow cracking to occur and the degrading site no longer possess these characteristics. The snowpack characteristics appear to set the limits to thermal contraction cracking.

*Geomorphic implications*

It is clear that the current state of the features is heavily influenced by surface topography interactions with snowpack and its thermal characteristics.

At the degrading site, it appears that a threshold has been achieved in the thermokarst depressions whereby thermal-contraction cracking has ceased. The snowpack prevents the magnitude and rate of cooling required for cracking of the residual ice wedges. It is also the case that many of the ice wedges have completely melted (Fig. 9). As thermokarst subsidence occurs the trough's ability to trap insulating snow increases and winter soil heat loss declines. Further degradation of the ice wedges eventually drops the surface to that of the surrounding fen and the local water table. The snow insulates so effectively that the mean annual temperature was from 7°C to 10.7°C warmer beneath the snow resulting in a mean annual surface temperature that was well above 0°C (Fig. 7). In contrast, on the aggrading site the difference was 1.9°C to 2.2°C with the mean annual surface temperature well below 0°C (Fig. 7).

Between ice wedge aggradation and complete degradation, there is a shift in snowpack characteristics over the wedges from offering little resistance to heat loss to effective insulation. At Churchill the study features provide examples of the two endpoints of this continuum. Given the dramatic differences between the two sites it might be that the switch between the two states occurred abruptly (a few years) after a threshold of snow thermal properties was achieved.

## Conclusions

Two polygonal peat plateaus that were <2 km apart had similar plant cover, internal composition and mesoclimate; however, they differed in that one had degrading while the other had aggrading ice wedges. The ice wedge troughs in the baydjarakh field were often >1 m deeper than the aggrading site due to thermokarst subsidence.

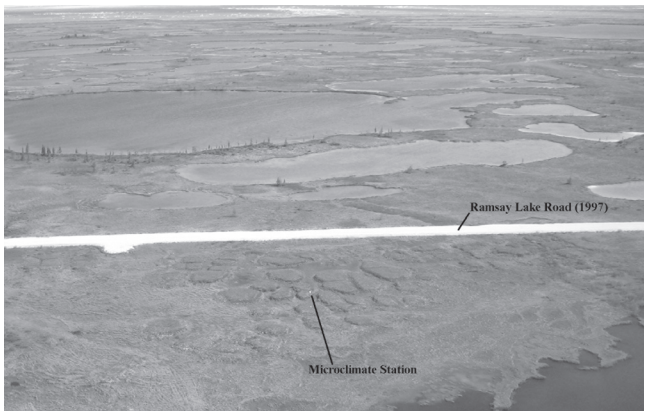


Figure 9. The former ice wedge pattern is still apparent at the degrading ice wedge site. The baydjarakh field developed as the original ice wedges degraded several decades prior to the construction of the Ramsay Lake Road. Hudson Bay is visible on the horizon.

The midwinter snowpack over the degrading ice wedges insulated against heat loss to the extent that the mean annual temperature was 2°C to 3°C above 0°C. Under these circumstances the ice wedges cannot reform. A new paradigm prevails at this site where the residual polygon centers remain elevated with shallow active layers and internal temperatures similar to the aggrading ice wedge site. The thermal contraction that would normally cause ice wedge cracking can occur on the raised mound of the residual polygon centre without affecting the area that surrounds it and which is under >50 cm of insulating snow. Under these circumstances the raised polygon centres are stable unless other processes such as change in plant cover or deflation of the peat lead to a change in their thermal state.

The residual polygon centres or baydjarakh (Czudek & Demek 1970) have been locally incorrectly identified as palsas. Their external morphology resemble palsas but their origin precludes this classification (van Everdingen 2005).

Polygonal peat plateaus are ubiquitous in the Hudson Bay Lowland (Dredge & Mott 2003) and are common throughout the rest of Canada (Tarnocai & Zoltai 1988, Zoltai et al. 1988). They are also common in Russia (Romanovskij 1985). Where they are sustaining thermokarst subsidence, interactions with increasing snowpack and its ability to trap summer heat could amplify the degradation process to the point that the ice wedges completely melt out. This positive feedback would be arrested if the polygon centre was lowered through such processes as deflation of the peat by wind (Seppälä 2004). However, it appears that progression of the process to a point whereby the ice wedges completely degrade is facilitated by snowpack interactions. In the area where polygonal peat plateaus are common and where future climate warming starts thermokarst subsidence, snowpack feedbacks could amplify the process and accelerate the effects of climate warming.

## Acknowledgments

Earthwatch Institute volunteer teams along with students from the University of Alberta and Churchill Northern Studies Centre staff collected the snowpack data. In 1997 Dr. Michel Allard and Stewart Brown conducted initial excavations of the ice wedges and the first GPR surveys. Funding for this research has been through Earthwatch Institute, Churchill Northern Studies Centre, NSERC, IPY PPS Arctic Canada, and Canadian Circumpolar Institute.

## References

Abel's, G. 1893. Daily variation of temperature in snow and the relation between the thermal conductivity of snow and its density. *Meteorologicheskii Vestnik* 3.

Allard, M. & Kasper, J.N. 1998. Temperature conditions for ice wedge cracking: field measurements from Salluit, northern Québec. In: A.G. Lewkowicz & M. Allard (eds.), *Proceedings of the 7th International Permafrost Conference, Collection Nordicana, No. 57*. Québec: Centre d'études nordiques, Université Laval.

Brown, R.J.E. 1970. Occurrence of permafrost in Canadian peatlands. *Proceedings of the Third International Peat Congress,Quebec*. Ottawa: National Research Council Canada.

Czudek, T. & Demek, J. 1970. Thermokarst in Siberia and its influence on the development of lowland relief. *Quaternary Research* 1(1): 103-120.

Dostovalov, B.N. & Popov, A.I. 1966. Polygonal systems of ice wedges and conditions of their development. *Proceedings Permafrost International Conference*, *Lafayette, Indiana.*

Dredge, L.A. 1992. *Field guide to the Churchill Region, Manitoba: glaciations, sea level changes, permafrost landforms, and archeology of the Churchill and Gillam areas, Miscellaneous Report 53*. Ottawa: Geological Survey of Canada.

Dredge, L.A. & Mott, R.J. 2003. Holocene pollen records and peatland development, Northeastern Manitoba. *Géographie Physique et Quaternaire* 57(1): 7-19.

Fortier, D. & Allard, M. 2005. Frost-cracking conditions, Bylot Island, Canadian Arctic Archipelago. *Permafrost and Periglacial Processes* 16: 145-161.

Fortier, D. & Allard, M. 2004. Late Holocene syngenetic ice-wedge polygons development, Bylot Island, Canadian Arctic Archipelago. *Canadian Journal of Earth Sciences* 41: 997-1012.

French, H.M. 1996. *The Periglacial Environment*. Essex, England: Addison Wesley Longman Limited.

French, H.M.; Harry, D.G. & Clark, M.J. 1982. Ground ice stratigraphy late-Quaternary events, southwest Banks Island, Canadian Arctic. *Proceedings Fourth Canadian Permafrost Conference*, *Calgary, Alberta*.

Goodrich, L.E. 1982. The influence of snow cover on the ground thermal regime. *Canadian Geotechnical Journal* 19: 421-432.

Kerfoot, D.E. 1972. Thermal contraction cracks in an Arctic tundra environment. *Arctic* 25: 142-150.

Kershaw, G.P. 2001. Snowpack characteristics following wildfire on a simulated transport corridor and adjacent subarctic forest, Tulita, N.W.T., Canada. *Arctic, Antarctic, and Alpine Research* 33(2): 131-139.

Lachenbruch, A.H. 1966. Contraction theory of ice-wedge polygons: a qualitative discussion. *Proceedings Permafrost International Conference, Lafayette, Indiana*. U.S. National Academy of Sciences, Publication 1287.

Lachenbruch, A.H. 1962. *Mechanics of thermal contraction cracks and ice-wedge polygons in permafrost. GSA Special Paper* 70, 69 pp.

Leffingwell, E.D.K. 1915. Ground-ice wedges: the dominant form of ground-ice on the north coast of Alaska. *Journal of Geology* 23: 635-654.

Mackay, J.R. 1993. Air temperature, snow cover, creep of frozen ground, and the time of ice wedge cracking, Western Arctic Coast. *Canadian Journal of Earth Sciences* 30: 1720-1729.

Mackay, J.R. 1986. The first seven years (1978–1985) of ice-wedge growth, Illisarvik experimental drained lake site, western Arctic coast. *Canadian Journal of Earth Sciences* 23(11): 1782-1795.

Mackay, J.R. 1976. Ice-wedges as indicators of recent climatic change, Western Arctic coast. *Geological Survey of Canada, Report of Activities, Paper 76-1A*: 233-234.

Mackay, J.R.1974. Ice-wedge cracks, Garry Island, Northwest Territories. *Canadian Journal of Earth Sciences* 11: 1366-1383.

Mackay, J.R. & Black, R.F. 1973. Origin, composition, and structure of perennially frozen ground and ground ice: A review. *Permafrost: North American Contribution, Second International Conference*, *Yakutsk*.

Mackay, J.R. & Burn, C.R. 2002. The first 20 years (1978–1979 to 1998–1999) of ice-wedge growth at the Illisarvik experimental drained lake site, western Arctic coast, Canada. *Canadian Journal of Earth Sciences* 39: 95-111.

Mackay, J.R. & MacKay, D.K. 1974. Snow cover and ground temperatures, Garry Island, N.W.T. *Arctic* 27(4): 287-296.

Nicholson, F.H. & Granberg, H.B. 1973. Permafrost and snowcover relationships near Schefferville. *North American Contribution Permafrost Second International Conference*. *Yakutsk.*

Péwé, T.L. 1962. Ice wedges in permafrost, lower Yukon River area, near Galena, Alaska. *Biuletyn Peryglacjalny* 11: 65-76.

Romanovskij, N.N. 1985. Distribution of recently active ice and soil wedges in the USSR. In: M. Church & O. Slaymaker (eds.), *Field and Theory Lectures in Geocryology*. Vancouver: University of British Columbia.

Seppälä, M. 2004. *Wind As a Geomorphic Agent in Cold Climates*. Cambridge: Cambridge University Press.

Smith, M.W. 1975. Microclimatic influences on ground temperatures and permafrost distribution, Mackenzie Delta, Northwest Territories. *Canadian Journal of Earth Sciences* 12: 1421-1438.

Somr, C.H. & King, R.H. 1990. Origin of polygonal peat plateaus under conditions of continuous permafrost, Truelove Lowland, Devon Island, N.W.T. In: M.M. Burgess, D.G. Harry & D.C. Sego (eds.), *Permafrost, Canada, Proceedings of the Fifth Canadian Permafrost Conference, Collection Nordicana 54*. Québec: Centre d'études nordiques, Université Laval.

Tarnocai, C. & Zoltai, S.C. 1988. Wetlands of Arctic Canada. In: C.C.A. Rubec (ed.), *Wetlands of Canada*. Montreal: Polyscience Publications Inc..

van Everdingen, R.O. (ed.). 2005. *Multi-Language Glossary of Permafrost and Related Ground-Ice Terms*. Boulder: National Snow and Ice Data Center/World Data Center for Glaciology.

Washburn, A.L. 1979. *Geocryology: A Survey of Periglacial Processes and Environments*. London: Edward Arnold Publishers Ltd.

Zoltai, S.C. & Tarnocai, C. 1975. Perennially frozen peatlands in the western Arctic and Subarctic of Canada. *Canadian Journal of Earth Sciences* 12(1): 28-43.

Zoltai, S.C., Tarnocai, C., Mills, G.F. & Veldhuis, H. 1988. Wetlands of Subarctic Canada. *Wetlands of Canada*. Montreal: National Wetlands Working Group, Canada Committee on Ecological Land Classification, Polyscience Publications.

# Changes in Surface Topography and Active Layer Following Partial Gravel Removal in the Prudhoe Bay Oilfield, Alaska

Janet G. Kidd
*ABR, Inc. – Environmental Research & Services, Fairbanks, AK, USA*

## Abstract

To promote the development of wetland plant communities on abandoned sites in the Prudhoe Bay Oilfield, Alaska, gravel has been partially removed to create suitable soil and hydrological conditions. This study focused on changes in surface topography and thermal regime following gravel removal at 6 sites over the past 17 years. We established transects across each site to monitor the relative surface elevation and depth of the active layer. The sites range in age from 4–16 years, and the depth of residual gravel fill varies from 8–60 cm. Results varied widely among the sites surveyed, with changes in surface topography and thaw depth ranging from minimal to extensive. In some cases, thaw settlement continued for more than 15 years after gravel removal. The deep thaw penetration likely was preserved due to the absence of an insulative surface organic mat. Despite the potential for promoting thermokarst, gravel removal is an effective approach for creating wetland ecosystems on disturbed sites.

**Keywords:** active layer; gravel fill; relative surface elevation; thaw depth; thermokarst; wetlands.

## Introduction

Over the past 30 years, research has been conducted in the Prudhoe Bay Oilfield to develop strategies for rehabilitating land disturbed by oil extraction and oilfield operations (e.g., Mitchell 1979, Moore & Wright 1991, unpubl., McKendrick 1991, Jorgenson & Joyce 1994, Jorgenson 1997, Jorgenson et al. 2003a). Part of this effort has involved assessing the potential for restoring tundra wetland plant communities by removing gravel from abandoned sites and applying plant materials (Jorgenson & Joyce 1994, Kidd et al. 2004, 2006). Removing the gravel reestablishes a hydrologic connection with adjacent, undisturbed tundra communities and improves site characteristics for plant establishment and growth.

Although gravel removal can help facilitate the restoration of wetland plant communities on disturbed sites, the disruption of the thermal regime following gravel removal, and the resulting subsidence, can limit vegetation recovery in some cases (Jorgenson & Joyce 1995, Kidd et al. 2004, 2006). The absence of a thick, insulative gravel layer or tundra vegetative mat subjects the underlying permafrost to melting. In some cases, ponding is extensive, with water levels too deep to support emergent plant species. Compression of the underlying tundra soil by the weight of gravel fill also can result in the creation of impoundments (Kidd et al. 2004). When the gravel is removed, the depression that remains promotes the impoundment of water, which can further promote thaw subsidence by conducting and convecting heat away from the ground (Hopkins 1949).

To better predict the extent of changes in surface topography and permafrost following gravel removal and the effect on restoration efforts, we surveyed the relative surface elevation and depth of the active layer (thaw depth) of 6 gravel removal sites in the Prudhoe Bay Oilfield. The sites range in age from 4–16 years and include abandoned airstrips, access roads, an operations pad, and an exploratory well site (Fig. 1).

The survey sites are located in a variety of landscape settings, including Old Alluvial and Alluvial-Marine terraces and Basin Complexes (Jorgenson et al. 2003b, unpubl.). Adjacent plant communities include Moist Sedge-Shrub Tundra, Fresh Sedge and Grass Marsh, and Wet Sedge Meadow Tundra. Dominant plant species are *Carex aquatilis*, *C. bigelowii*, *Eriophorum* spp., *Arctophila fulva*, and *Salix* spp. Large waterbodies also are present near many of the sites. Based on data collected at Deadhorse and Prudhoe Bay (1990–2007), mean annual air temperature in the study area is -11°C, and mean annual total precipitation is 17.6 cm (National Climate Data Center 2007). The mean depth of the active layer in tundra ranges from 30.5–60.6 cm, based on measurements collected near West Dock (Fig. 1) and Deadhorse (1995–2005) (Streletskiy et al. 2008).

## Methods

Prior to gravel removal, the gravel fill thickness at all sites was approximately 1.5 m, which is typical for roads and pads in the Prudhoe Bay Oilfield. After gravel removal, the residual gravel fill thickness ranged from 8–60 cm, except at the North Prudhoe Bay State No. 2 Exploratory Well Site (hereafter referred to as North State 2) and the Mobil W/Z airstrip. Shallow and deep basins were excavated in portions of these sites, resulting in complete gravel removal. Gravel was removed in winter or early spring, and the following summer, various plant cultivation treatments were applied. Treatments included applying fertilizer alone, seeding native-grass cultivars, transplanting tundra plugs, and seeding indigenous (locally collected) species. Fertilizer was applied with all the planting treatments. At one site, an area was left untreated as a control. Note that not all of the treatments listed above were applied at each site.

Relative surface elevations and thaw depths were measured from 1990–2006 along permanent transects established in each gravel removal area. The transects varied in number

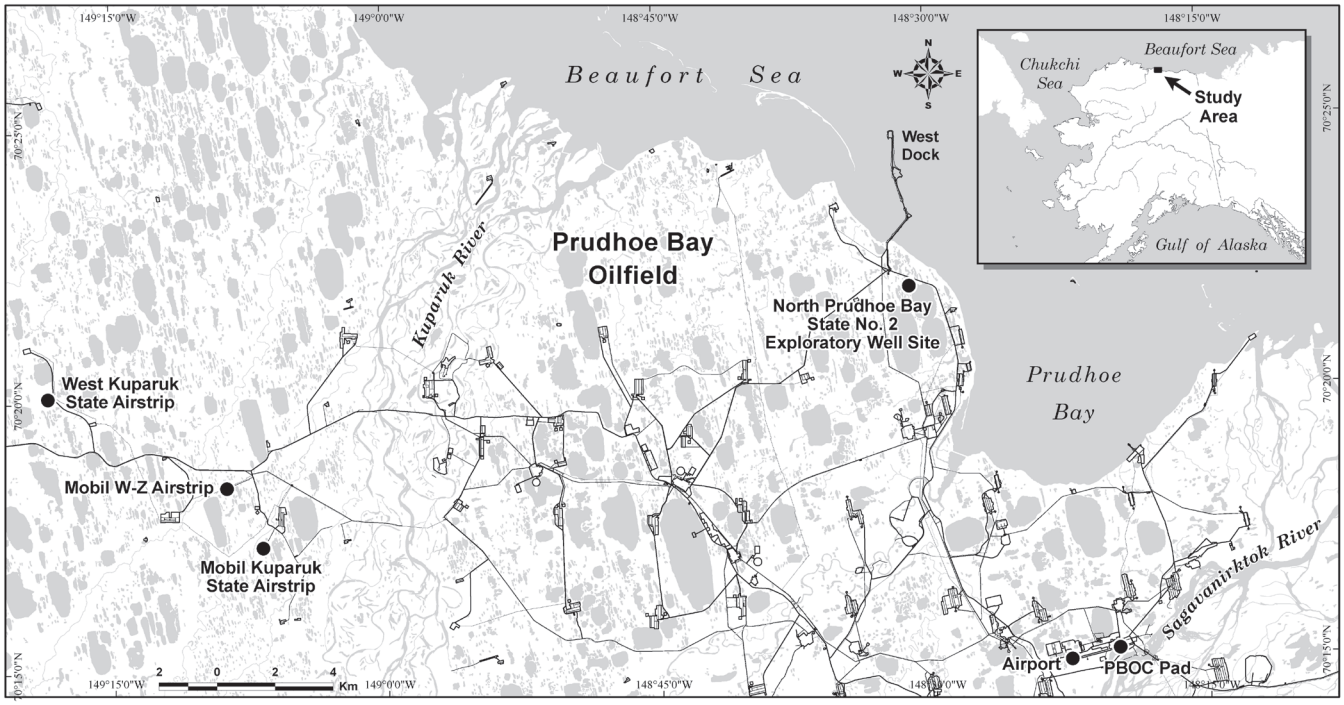


Figure 1. Locations of gravel removal sites surveyed for surface elevation and thaw depth, Prudhoe Bay Oilfield, Alaska, USA, 1990–2006.

and length, depending on the size of each site, and extended into the adjacent, undisturbed tundra approximately 5–10 m. Elevations were recorded at 1–2 m intervals along a meter tape using an auto-level or a laser level and survey rod. Thaw depths generally were measured every 5 m to the depth of resistance using a steel probe, which follows the methodology used in the Circumpolar Active Layer Monitoring (CALM) Program (Nelson et al. 1996). Additional thaw-depth measurements were made at prominent terrain breaks in the gravel removal areas and in the adjacent, undisturbed tundra in later years. The surveys were conducted in early to mid-August. Permanent benchmarks were not available at each location, so elevations were tied to the mean surface elevation of the adjacent, undisturbed tundra. Collection of geotechnical and ground temperature data was beyond the scope of this study.

## Results and Discussion

Changes in surface elevation and thaw depth following gravel removal varied widely among the 6 sites surveyed, and were independent of site age (Figs. 2–5 & 7; Table 1). The greatest thaw settlement measured occurred at Mobil Kuparuk State Airstrip (-0.55 m, Fig. 2), where only 4 years had lapsed since gravel removal. In contrast, at North State 2, the southern transect only subsided 0.15 m in the 16-year period following gravel removal (Fig. 3). The topography of the 2 basins excavated also changed very little during this period. Changes in surface elevation on the northern transect were more notable, and included the development of several deep ponds.

The presence of deep troughs and depressions at Mobil Kuparuk Airstrip, the northern transect at North State 2, the

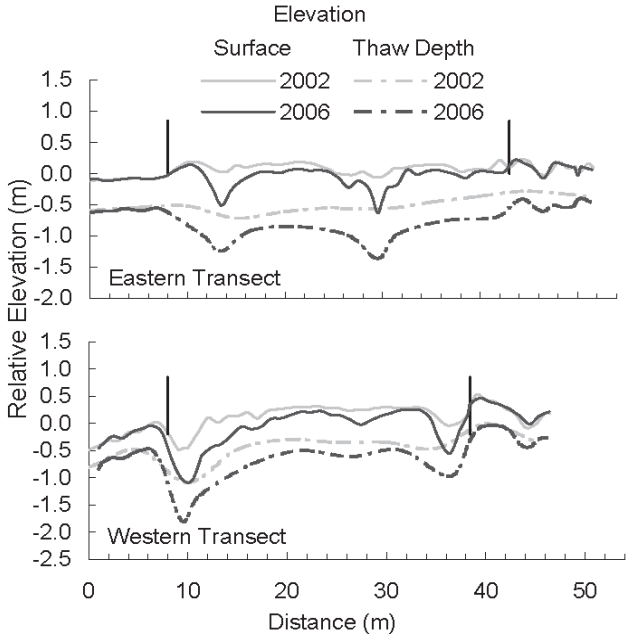


Figure 2. Profiles of relative surface and thaw depth elevation across Mobil Kuparuk State airstrip, 2002 & 2006. Brackets indicate boundaries between gravel removal areas and adjacent, undisturbed tundra.

Airport (Road 2, Fig. 4), and PBOC Pad (Fig. 5), indicate that ice wedges are present and in the process of melting. Flooded polygons form in response to the thawing wedges and are particularly evident at the Airport (Fig. 6). Elsewhere, more moderate subsidence has occurred (Fig.7), although the active layer is deep at all sites. Mean thaw depths range from 0.7–1.2 m (Table 1) and have yet to stabilize, even at the oldest sites (Airport, PBOC, North State 2). Mean thaw

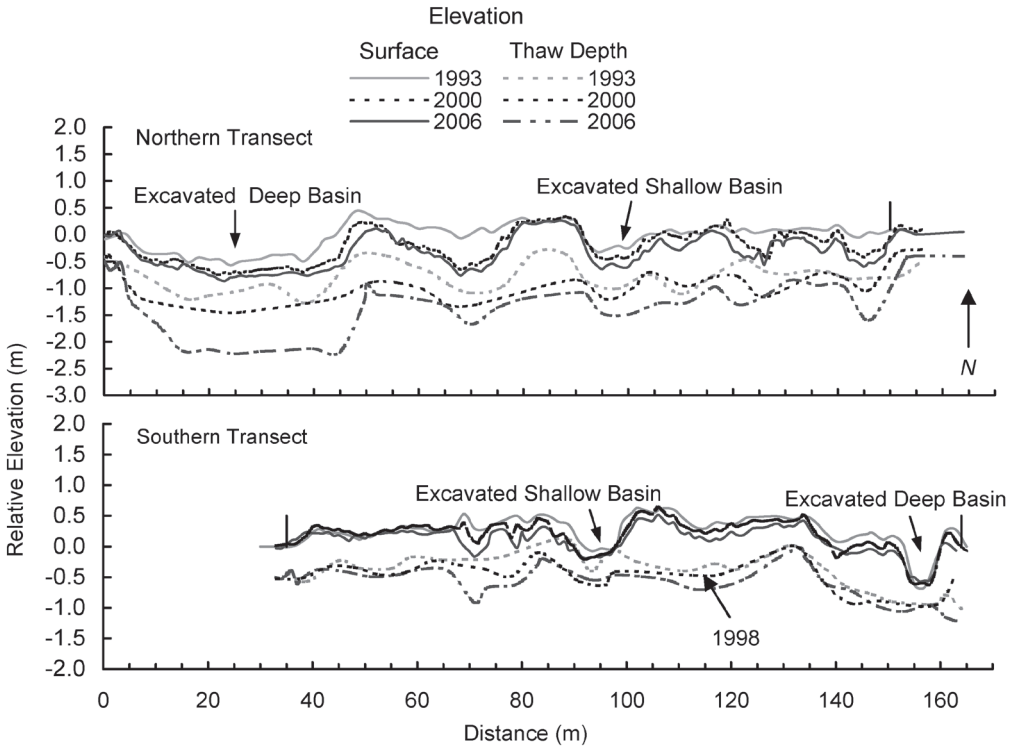


Figure 3. Profiles of relative surface and thaw depth elevation across North State 2, 1993, 2000, & 2006. Brackets indicate boundaries between gravel removal area and adjacent, undisturbed tundra.

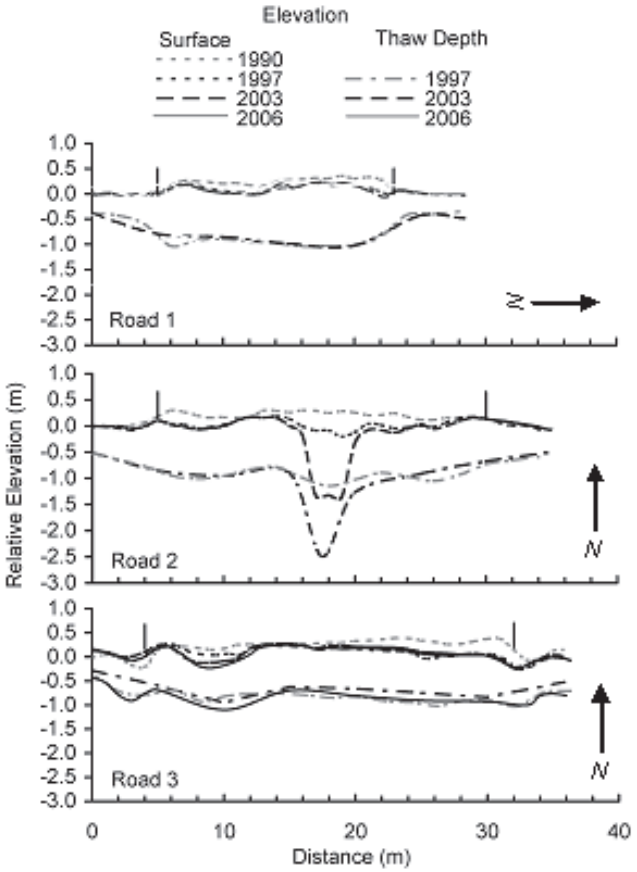


Figure 4. Profiles of relative surface and thaw depth elevation across Airport access roads 1990, 1997, 2003, and 2006. Brackets indicate boundaries between gravel removal areas and adjacent, undisturbed tundra.

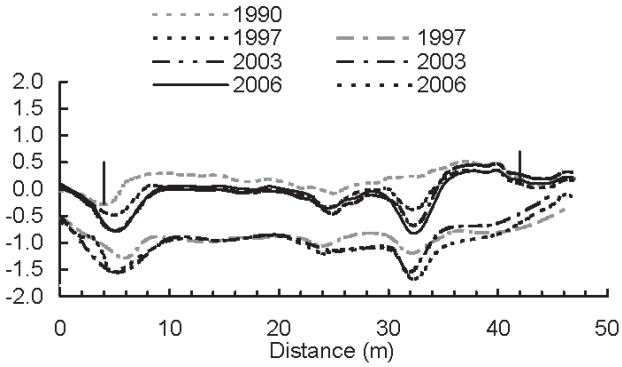


Figure 5. Profiles of relative surface and thaw depth elevation across PBOC Pad, 1990, 1997, 2003, & 2006. Brackets indicate boundaries between gravel removal areas and adjacent, undisturbed tundra.

depth in adjacent, undisturbed tundra in 2006 ranged from 0.49 m (± 0.02 m, n = 35) at Mobil W-Z to 0.73 m (± 0.03 m, n = 8) at the Airport.

The thawing and subsequent settlement of ice wedges at some of the sites is consistent with what has been observed elsewhere in terrain with similar characteristics. The 3 airstrips and the Airport access roads are all located in fine-grained, abandoned floodplain deposits, which are known to be ice rich (Jorgenson et al., 1996, unpublished). Compared with other terrain units in the region, the alluvial marine deposits associated with North State 2 are known to have some of the highest volumes of both ground and wedge ice (Pullman et al. 2007); this partly explains the extensive thermokarst on the northern half of the site. The southern

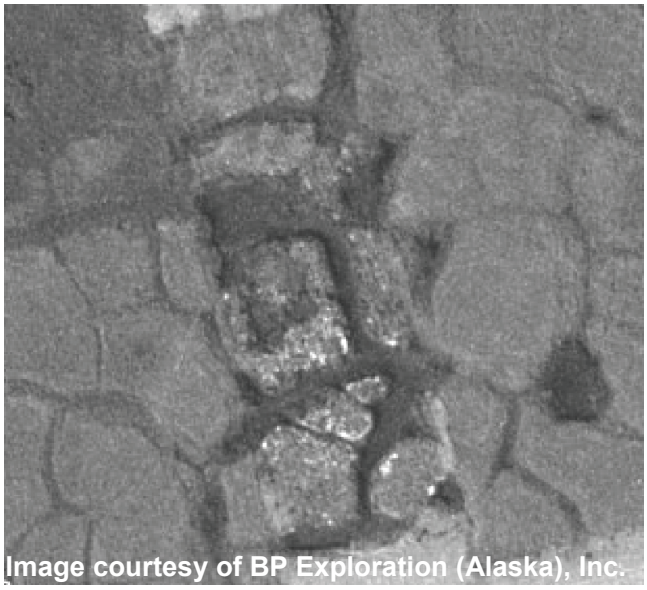


Figure 6. Aerial view of Road 3, Airport, showing deep, flooded polygon troughs, 2006.

half has experienced considerably less thaw settlement, however, suggesting that the processes governing surface stability at North State 2 are complex. The site is located in an old drained-lake basin, and the uneven thermokarst pattern probably reflects an irregular distribution of wedge ice in the sediments.

The differential settlement reveals the importance of varying types of ice. The settlement in the polygon centers between the ice wedges, which have varying forms of segregated ice, usually was only 10–30 cm. This is consistent with the thaw settlement estimates of 8–53 cm for a range of terrain types (Pullman et al. 2007). Settlement of the centers probably has achieved equilibrium with the new surface thermal regime. In contrast, the surface over ice wedges settled as much as 1.5 m. Ice wedges are particularly sensitive to disturbance (and climate change) because the wedge ice lies immediately below the active layer, and thus, there is little additional soil that can be thawed and added to the active layer to achieve a new stable equilibrium (Jorgenson et al. 2006). In addition, impoundment of water provides a positive feedback on heat gain and melting of ice. Jorgenson et al. (2006) found that aquatic sedges can rapidly colonize and stabilize the troughs within 30–50 yr, but troughs in the gravel removal areas are slow to vegetate. Consequently, they may be slower to stabilize until the wedge ice is almost completely melted out.

The absence of a deep organic soil layer has probably also played an important role in the maintenance of deep active layers and continued thaw settlement at these sites. Although productive communities of mosses and vascular plants have established in some of the treatment areas at the oldest sites, soil development has been minimal. The top 15–60 cm is still composed almost exclusively of coarse gravel, with varying amounts of sand. In addition,

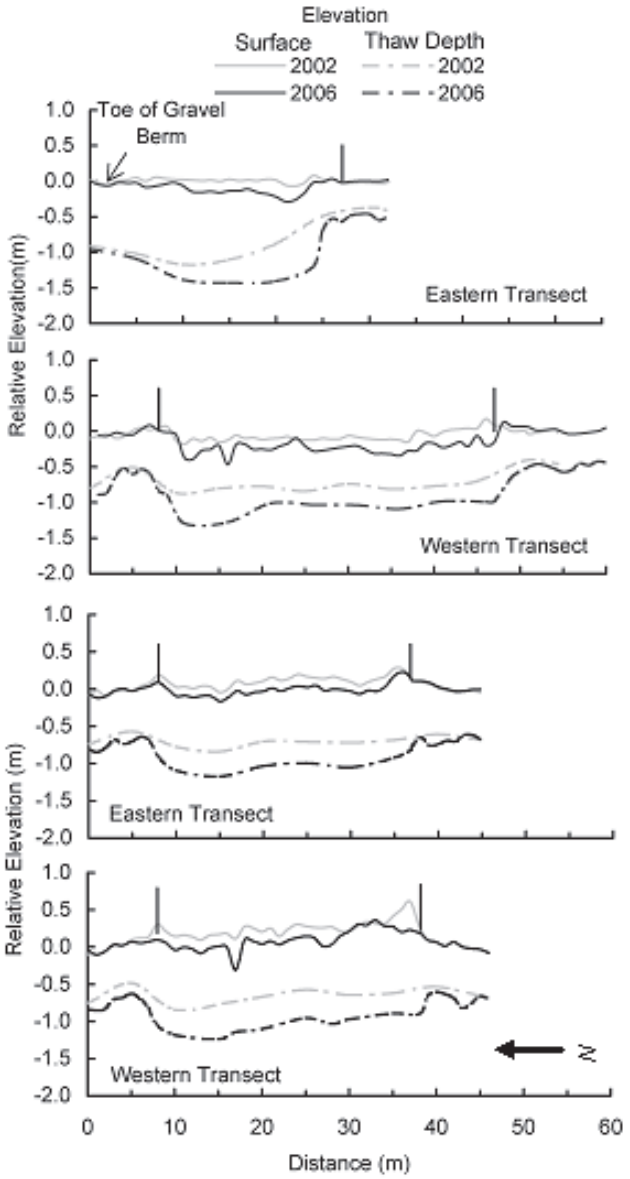


Figure 7. Profiles of relative surface and thaw depth elevation across Mobil W-Z (a) and West Kuparuk State (b) airstrips, 2002 and 2006. Brackets indicate boundaries between gravel removal areas and adjacent, undisturbed tundra.

plants have been unable to establish in deep ponds and troughs. As a result, during the relatively warm summers, heat can penetrate deeply into the exposed soil. The soils are saturated, and the high water content also serves as an excellent conductor of heat. Given the poor soil conditions and short growing season of the Arctic, it likely will be several decades before a sufficient moss and sedge peat mat develops on these sites to effectively insulate the soil. Consequently, we can expect that the volume of wedge ice will be substantially reduced before the sites become thermally stable.

Table 1. Mean (± SE) relative surface elevations and thaw depths for six study sites, Prudhoe Bay Oilfield, Alaska, 1990–2006.

| Site | Surface Elevation (m) | | | | Thaw Depth (m) | | | |
|---|---|---|---|---|---|---|---|---|
| | Initial | | Final | | Initial | | Final | |
| Airport | Mean (±SE) | n[a] | Mean (±SE) | n | Mean (±SE) | n | Mean (±SE) | n |
| Road 1 (1990, 2003) | 0.26 (0.01) | 16 | 0.09 (0.02) | 19 | 0.98 (0.22) | 22 | 1.06 (0.02) | 3 |
| Road 2 (1990, 2003) | 0.22 (0.01) | 24 | -0.22 (0.10) | 25 | 0.80 (0.25) | 24 | 0.98 (0.05) | 5 |
| Road 3 (1990, 2006) | 0.49 (0.01) | 26 | 0.10 (0.03) | 27 | 0.85 (0.23) | 25 | 0.93 (0.02) | 7 |
| PBOC Pad (1990, 2006) | 0.22 (0.02) | 36 | -0.11 (0.05) | 36 | 0.93 (0.22) | 30 | 0.94 (0.04) | 11 |
| North State No. 2 Exploratory Well Site (1993, 2006) | | | | | | | | |
| North | -0.03 (0.03) | 80 | -0.36 (0.03) | 149 | 0.81 (0.04) | 16 | 1.11 (0.04) | 33 |
| South | 0.26 (0.03) | 70 | 0.11 (0.02) | 130 | 0.66 (0.04) | 27 | 0.70 (0.04) | 32 |
| Mobil Kuparuk State Airstrip (2002, 2006) | | | | | | | | |
| East | 0.10 (0.01) | 38 | -0.07 (0.03) | 40 | 0.64 (0.05) | 8 | 0.81 (0.03) | 10 |
| West | 0.44 (0.04) | 31 | -0.11 (0.06) | 34 | 0.62 (0.01) | 6 | 0.66 (0.04) | 7 |
| Mobil W-Z Airstrip (2002, 2006) | | | | | | | | |
| Middle | 0.01 (0.01) | 24 | -0.11 (0.02) | 24 | 1.04 (0.06) | 5 | 1.16 (0.07) | 5 |
| West | -0.08 (0.01) | 37 | -0.23 (0.02) | 39 | 0.70 (0.01) | 8 | 0.80 (0.02) | 9 |
| West Kuparuk State Airstrip (2002, 2006) | | | | | | | | |
| East | 0.11 (0.01) | 28 | -0.04 (0.02) | 28 | 0.84 (0.03) | 6 | 1.03 (0.02) | 6 |
| West | 0.26 (0.02) | 31 | 0.10 (0.02) | 31 | 0.92 (0.03) | 6 | 1.11 (0.04) | 8 |

[a] n = sample size.

## Conclusions

The results of long-term monitoring of surface stability and permafrost of gravel removal sites indicate that the observed changes in the thermal regime are long lasting and should be considered when planning land rehabilitation efforts to promote vegetation recovery. At sites where the probability of extensive thermokarst and thaw settlement occurring is high, the application of plant-cultivation treatments should be postponed until conditions are relatively stable. This delay will allow plant materials to be established in areas where conditions are likely to remain suitable over the long term. This effort can be assisted by assessing the terrain characteristics and the pattern of change in surface topography at each site following gravel removal. For many sites, the network of ponds and troughs that form is apparent relatively soon after gravel removal (within the first 3 years), although determining the ultimate water depth of ponds and troughs is more challenging.

Despite the potential for promoting thermokarst, gravel removal is an effective approach for creating wetland ecosystems on disturbed sites, for several reasons. First, a hydrologic connection with the adjacent, undisturbed tundra is established, facilitating the exchange of nutrients, seeds, plant propagules, and soil microbes. Second, the wetland hydrology encourages colonization by tundra plant species, primarily sedges and grasses. Finally, the heterogeneous surface topography that results from thermokarst creates a range of site conditions from moist to wet to ponded, allowing for the establishment of a diversity of plant species, with varying life-history characteristics. This diversity helps ensure some plasticity in the plant communities that establish, allowing them to respond to changing surface conditions while the thermal regime stabilizes. A potential concern is that the thermokarst associated with gravel removal sites might destabilize adjacent areas. However, although some thaw settlement is evident along the margins of gravel removal sites, we have not observed any dramatic changes in the surface stability of these areas.

## Acknowledgments

Funding for this study was provided by BP Exploration (Alaska), Inc., and managed by Bill Streever, Environmental Studies Leader. Initial financial support for data collection was provided by ARCO Alaska, Inc. Torre Jorgenson designed the land rehabilitation studies that are the sources of the long-term datasets and provided a valuable technical review. Sue Bishop assisted with fieldwork and reviewed the manuscript. Additional field support and graphical assistance was provided by Tim Cater, Kate Beattie, and Allison Zusi-Cobb.

## References

Hopkins, D.M. 1949. Thaw lakes and thaw sinks in the Imuruk Lake area, Seward Peninsula, Alaska. *Journal of Geology* 57: 119-131.

Jorgenson, M.T. 1997. Patterns and rates of, and factors affecting natural recovery on land disturbed by oil development in arctic Alaska. *Disturbance and Recovery in Arctic Lands: an Ecological Perspective*. NATO ASI Series 2 Environment, Vol. 25, Dordrecht: Kluwer Academic Publishers, 421-442.

Jorgenson, M.T. & Joyce, M.R. 1994. Six strategies for rehabilitating land disturbed by oil development in the arctic Alaska. *Arctic* 47: 374-390.

Jorgenson, M.T., Aldrich, J.W., Pullman, E.R., Ray, S.R., Shur, Y., Smith, M.D., Stickney, A.A. & Walker, H.J. 1996. Geomorphology and hydrology of the Colville River Delta, Alaska, 1995. Final report prepared for ARCO Alaska, Inc., Anchorage, AK, by ABR, Inc. and Shannon & Wilson, Inc., Fairbanks, AK, 136 pp.

Jorgenson, M.T., Kidd, J.G., Cater, T.C., Bishop, S.C. & Racine, C.H. 2003a. Long-term evaluation of methods for rehabilitation of lands disturbed by industrial development in the Arctic. In: R.O. Rasmussen & N.E. Koroleva (eds.), *Social and Environmental Impacts in the North*. Dordrecht: Kluwer Academic Publishers, 173-190.

Jorgenson, M.T., Roth, J.E., Emers, M., Schlentner, S.F., Swanson, D.K., Pullman, E.R., Mitchell, J.S. & Stickney, A.A. 2003b. An ecological land survey in the Northeast Planning Area of the National Petroleum Reserve–Alaska, 2002. Final report prepared for ConocoPhillips Alaska, Inc., Anchorage, AK, by ABR, Inc., Fairbanks, AK, 124 pp.

Jorgenson, M.T., Shur, Y.L. & Pullman, E.R. 2006. Abrupt increase in permafrost degradation in Arctic Alaska. *Geophysical Research Letters* 33: L02503, doi:10.1029/2005GL024960.

Kidd, J.G., Streever, B., Joyce, M.R. & Fanter, L.H. 2004. Wetland restoration of an exploratory well on Alaska's North Slope: a learning experience. *Ecological Restoration* 22: 30-38.

Kidd, J.G., Streever, B. & Jorgenson, M.T. 2006. Site characteristics and plant community development following partial gravel removal in an arctic oilfield. *Arctic, Antarctic, and Alpine Research* 38(3): 384-393.

McKendrick, J.D. 1991. Arctic tundra rehabilitation—observations of progress and benefits to Alaska. *Agroborealis* 23(1): 2-40.

Mitchell, W.W. 1979. *Three varieties of native Alaskan grasses for revegetation purposes.* University of Alaska, Alaska. Alaska Agricultural Experiment Station Circular 32.

Moore, N. & Wright, S.J. 1991. *Revegetation with Arctophila Fulva, 1985–1989*. Final report prepared for ARCO Alaska, Inc., Anchorage, AK, by Plant Materials Center, Alaska Dept. Natural Resources, Palmer, AK.

National Climate Data Center. 2007. U.S. Dept. of Commerce. Website address (accessed February 2007): http://www.ncdc.noaa.gov/oa/ncdc.html

Nelson, F., Brown, J., Lewkowicz, T. & Taylor, A. 1996. Active Layer Protocol. In: U. Molau & P. Molgaard (eds.), *ITEX Manual,* 2nd Ed. Danish Polar Center.

Pullman, E.R., Jorgenson, M.T. & Shur, Y. 2007. Thaw settlement in soils of the Arctic Coastal Plain, Alaska. *Arctic, Antarctic and Alpine Research* 39: 468-476.

Streletskiy, D.A., Shiklomanov, N.I. & Nelson, F.E. 2008. 13 years of observations at Alaskan CALM sites: long-term active layer and ground surface temperature trends. *Proceedings of the Ninth International Conference on Permafrost, Fairbanks, Alaska, June 29–July 3, 2008* (this proceedings).

# Vegetation Differentiation Across a Topographic Yedoma–Alas Transect in the High Arctic Tundra of Oyogos Yar, East Siberia

Frank Kienast
*Research Institute and Museum for Natural History Senckenberg, Research Station for Quaternary Palaeontology Weimar, Weimar, Germany*
Lutz Schirrmeister
*Alfred Wegener Institute for Polar and Marine Research, Potsdam, Germany*
Sebastian Wetterich
*Alfred Wegener Institute for Polar and Marine Research, Potsdam, Germany*

## Abstract

Excessive moisture is regarded as the main cause for the fall of Pleistocene tundra-steppe and the rise of modern tundra. The arctic tundra of Oyogos Yar is low in diverse plant species (ca 100). The floral composition is mainly the result of differences in moisture or drainage, respectively. We describe a vegetational profile recorded in August 2007 along a 10 km transect from the top of a yedoma ridge down to the adjacent alas depression between 40 m to 10 m a.s.l. Six main landscape units are described with respect to their floristic composition: yedoma top with thermokarst mounds, mud boils, yedoma slopes, small thermokarst ponds, thermo-erosional valleys, and the bottom of thermokarst depressions. Arctic thermokarst landscapes with yedoma ridges and alas depressions can be well-classified according to their vegetation. The main constituents of the plant cover at well-drained sites are grasses and polar willows, whereas excessively wet sites are occupied by sedges, cotton grass, and peat moss.

**Keywords:** alas depression; bioindication; moisture regime; thermokarst; tundra vegetation; yedoma elevation.

## Introduction

The arctic vegetation cover reflects very well the small-scale periglacial landscape differentiation. Detailed surveys of plant associations are essential for the understanding of biotic responses to changes in permafrost landscapes. Around Beringia, the great influence of topography on arctic vegetation has been described from Alaska (Walker 2000, Kade et al. 2005) and from the Taymyr Peninsula (Matveyeva 1994). Such studies of modern tundra vegetation are, however, little-known from Arctic Yakutia. Within the frame of the joint Russian-German expedition, "Lena–New Siberian Islands 2007," we studied relief-vegetation interactions at the coast of the Dimitrii Laptev Strait in August 2007.

## Regional Setting

Oyogos Yar is the name of the mainland coast of the Dimitrii Laptev Strait (Fig. 1) between the mouth of the Kondrat'eva River in the east and Cape Svyatoy Nos in the west. This landscape is part of the Yana-Indigirka Lowland in Northeastern Siberia. Up to 500 m thick continuous permafrost and wide spread thermokarst characterize the coastal lowland. Oyogos Yar's topography is dominated by extremely flat plains covered by mires and shallow lakes.

There are two main topographic elements: low elevations, so-called yedoma, which represent the Pleistocene ground level, and thermokarst depressions (alases), which formed as a result of thermal degradation of the ice-rich permafrost that constitutes the yedoma.

According to Aleksandrova (1980), Oyogos Yar belongs

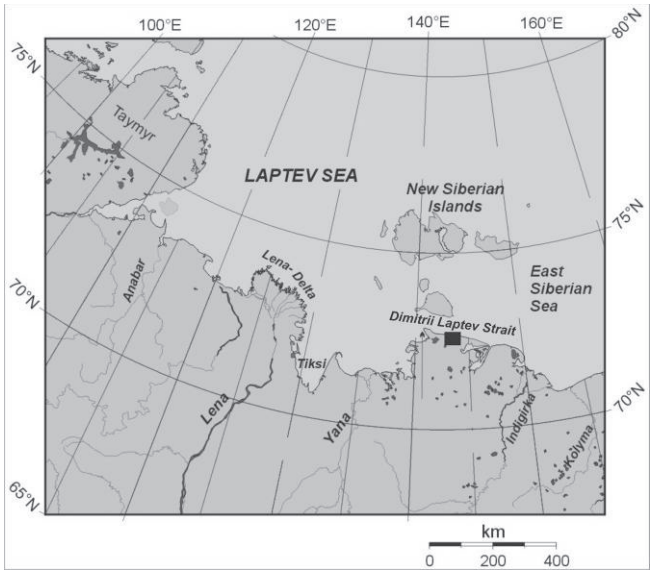


Figure 1. Position of the study area (black square corresponds to Fig. 2) at the mainland coast of the Dimitrii Laptev Strait.

to the Sellyakh Inlet–Indigirka Delta district of the East Siberian province of the southern arctic tundra characterized by the dominance of *Alopecurus alpinus* and *Salix polaris*, the presence of *Carex ensifolia* ssp. *Arctisibirica,* and the absence of subarctic elements like *Betula nana* s.l. According to the Circumpolar Arctic vegetation map (CAVM Team 2003), the study area is covered with sedge/grass, moss wetland (W1) with *Carex aquatilis*, *Arctophila fulva*, *Dupontia*, and *Eriophorum* spp.

The study area is located about 8 km west of the Kondrat'eva River mouth (Fig. 2) opposite to Cape

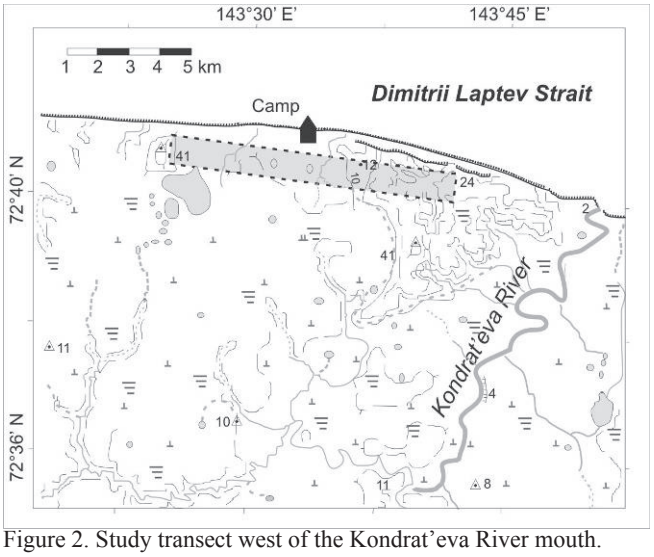

Figure 2. Study transect west of the Kondrat'eva River mouth.

Shalaurova, the eastern edge of Bol'shoy Lyakhovsky Island. The climate is characterized by cold winters, cool summers, and low precipitation. Climate data from the weather station Cape Shalaurova, about 80 km north of the study site, reflect a mean July air temperature of 2.8°C, a mean January air temperature of -32.2°C, and an annual precipitation of 253 mm (Rivas-Martínez 1996–2004).

## Site Description

The study transect extends across the bottom of a large alas depression about 10 km in diameter (5 to 10 m a.s.l.) and the adjacent slope and top areas of a yedoma hill of up to 40 m in height (Figs. 2, 3). The alas bottom dominantly consists of polygonal wetland tundra with a 0.5 to 1.0 m thick peat cover. The thermokarst depression is cut by the coast of the Dimitrii Laptev Strait in the north, and additionally intersected by several thermo-erosional valleys that drained to the coast.

Within the recorded transect, the following six main landscape units are described with respect to their floristic composition: the yedoma with thermokarst mounds, mud boils, yedoma slopes, small thermokarst ponds, thermo-erosional valleys, and the bottom of thermokarst depressions.

## Vegetation Characteristics

*Thermokarst mounds on the yedoma*

Thermokarst mounds are the best-drained habitats in the study area (Fig. 4). Their plant cover is mainly composed of *Salix polaris*, *Dryas punctata,* and *Alopecurus alpinus*. Other grasses, such as *Festuca brachyphylla* and *Deschampsia borealis,* and dicots, like *Potentilla hyparctica, Oxyria digyna, Papaver polare,* and *Valeriana subcapitata,* also occur.

*Mud boils*

Mud boils are the result of cryoturbation caused by frost pressing. In consequence, muddy soil flooded the ground.


Figure 3. View from the alas bottom to the yedoma hill.


Figure 4. Thermokarst mounds on the yedoma at Oyogos Yar.

The substrate is silty and well-drained. Mud boils occur at places most exposed and windswept on the Yedoma. Plants occur here only between such mud spots; the coverage is consequently very low with 20 to 40% (Fig. 5). *Potentilla hyparctica, Salix polaris,* and low growing grasses, and rushes like *Festuca brachyphylla, Deschampsia borealis,* and *Luzula confusa* are the main constituents of such habitats In addition, herbs such as *Lloydia serotina, Cardamine bellidifolia, Androsace triflora*, and *Tephroseris atropurpurea* occur in lower abundance.

This vegetation is similar in composition to cryptogam, herb barren (B1) or to the gramioid tundra (G1), described in the Circumpolar Arctic vegetation map (CAVM Team 2003).

*Yedoma slopes*

At yedoma slopes, the coverage is in general >80%. In the upper parts of slopes in SW exposition, *Dryas punctata* is one of the main constituents. *Salix polaris* and several grass species (*Alopecurus alpinus, Deschampsia borealis,* and *Festuca brachyphylla)* and *Luzula confusa* are characteristic of yedoma slopes. In lower parts of the slopes, where it is less drained and, consequently, moister, *Arctagrostis latifolia, Petasites frigidus,* several saxifrages (*S. nelsoniana, S. cernua, S. hieracifolia*) and other herbs (*Gastrolychnis apetala, Tephroseris atropurpurea, Ranunculus spp.*) are typical (Fig. 6).

Figure 5. Mud boil at the top of the yedoma visible in Figure 3.

Figure 6. Lower part of a yedoma slope with dominating *Arctagostis latifolia.* In the background, a thermo-erosional valley with reddish spectral signature (here: dark) is visible.

Figure 7. Thermokarst pond with dominating *Pleuropogon sabinei* growing immersed in the water (inserted photo).

*Small thermokarst ponds*

In small depressions on the yedoma, ponds with *Pleuropogon sabinei* and on the shore, *Arctophila fulva*, *Arctagrostis latifolia, Ranunculus hyperboreus, Dupontia fischeri*, *Eriophorum polystachion,* and *E. scheuchzeri* occur (Fig. 7).

Interestingly, genuine aquatics were widely lacking. Only *Hippuris vulgaris* was solitarily found in a sterile form. The white-flowered *Ranunculus pallasii* and *Caltha palustris* grew immersed in some ponds within the Alas depressions.

Figure 8. Thermo-erosional valley intersecting the yedoma of Oyogos Yar. Main constituent here is *Eriophorum scheuchzeri* causing a green spectral signature.

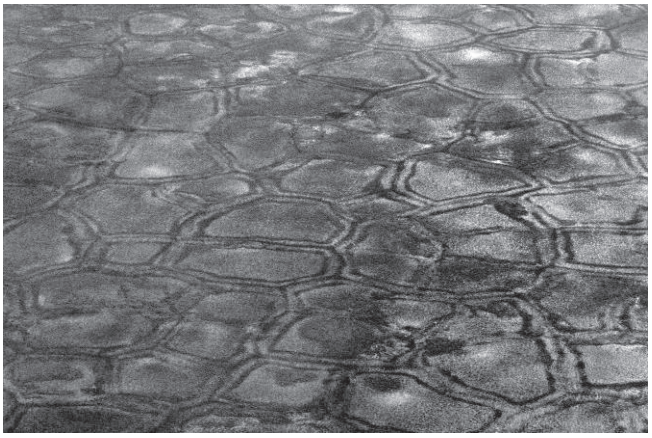

Figure 9. Bottom of a thermokarst depression with a water table above the ground. The polygonal surface patterns are visually strengthened by vegetational differentiation (compare Fig. 10).

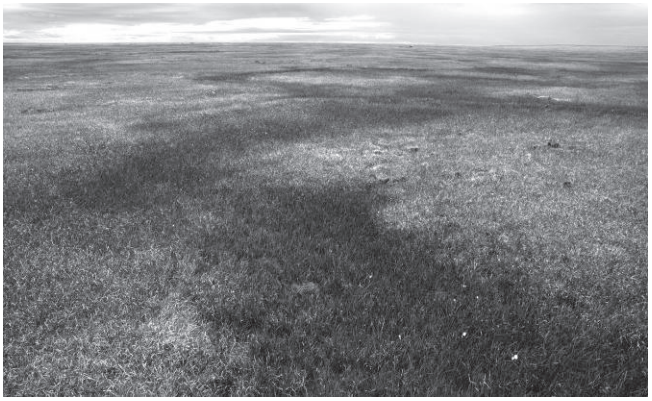

Figure 10. The wettest places in high center polygonal wetland tundra are the inter-polygonal trenches. Here, *Eriophorum polystachion* is the main constituent, causing a reddish (here dark) pattern.

*Thermo-erosional valleys*

Thermo-erosional valleys are permanently supplied by running water. They are characteristically colored and recognizable from a far distance (Fig. 6). Dark green and reddish signatures are mainly caused by different *Eriophorum* species: green – *E. scheuchzeri*, and red – *E.*

*polystachion* (Figs. 6, 8). Other plants of thermo-erosional valleys are *Petasites frigidus* and several crowfoot and grass species (*Dupontia fischeri, Calmagrostis holmii*).

*Bottom of thermokarst depressions*

The bottom of thermokarst depressions, alases, is in contrast to thermo-erosional valleys characterized by stagnant water and covered mainly with sedges (*Carex ensifolia* ssp. *arctisibirica*) and cotton grass (*Eriophorum polystachion*).

The vascular plant diversity here is the lowest in the study area. *Sphagnum* moss is widely present, causing irregular pale green spots in polygonal wetlands where the surface of water is above the ground (Fig. 9).

At sites outside water bodies, rushes (*Luzula nivalis, L. confusa*) cover large areas, together with several grasses (*Dupontia fischeri, Calamagrostis holmii, Poa alpigena,* and *Arctophila fulva*). The wettest places are almost exclusively occupied by *Eriophorum polystachion*, which produces reddish patterns on the ground indicating the water trenches between polygons from afar (Figs. 9, 10).

## Conclusions

The main landscape units in thermokarst-affected landscapes can be well distinguished by their vascular plant cover.

Moisture or drainage, respectively is the most important ecological factor in the study area resulting in the strongest vegetation differentiation.

Subordinate factors are exposure and declination. There were no really dry places in the study area.

Excessive wetness is well-indicated by plants with characteristic spectral properties and, therefore, visible from far distances.

The plant species composition can alter quickly on short distances reflecting moisture changes resulting from the damming effect of the frozen ground.

The existence of such small-scale variations in the plant cover has important implications for the interpretation of palaeobotanical records.

## Acknowledgments

We thank all participants of the joint Russian-German expedition, *Lena–New Siberian Islands 2007*, who helped us collecting, drying, and preparing the plants for the herbarium. The studies were supported by the German Science Foundation (KI 849/1).

## References

Aleksandrova, V.D. 1980. The Arctic and Antarctic: their division into geobotanical areas. Cambridge University Press, Cambridge.

CAVM Team. 2003. Circumpolar Arctic Vegetation Map. 1:7,500,000. Conservation of Arctic Flora and Fauna (CAFF) Map No. 1. Anchorage, Alaska: U.S. Fish and Wildlife Service.

Kade, A., Walker, D.A.& Raynolds, M.K. 2005. Plant communities and soils in cryoturbated tundra along a bioclimate gradient in the Low Arctic, Alaska. *Phytocoenologia* 35(4): 761-820.

Matveyeva, N.V. 1994. Floristic classification and ecology of tundra vegetation of the Taymyr Peninsula. Northern Siberia. *Journal of Vegetation Science* 5: 813-828.

Rivas-Martínez, S. 1996–2004. Climate diagrams, Worldwide. *Bioclimatic Classification System*. Phytosociological Research Center, Spain. Online database, http://www.globalbioclimatics.org/plot/ru-mys-s.htm.

Walker, D.A. 2000. Hierarchical subdivision of Arctic tundra based on vegetation response to climate, parent material and topography. *Global Change Biology* 6 (Suppl. 1): 19-34.

# A Two-Dimensional Numerical Heat Transfer Solution for Frost Heave Prediction Using the Segregation Potential Concept

Koui Kim
*Dept. of Civil and Environmental Engineering, University of Alaska Fairbanks, Fairbanks, AK, USA*
Wei Zhou
*Dept. of Geology and Geological Engineering, Colorado School of Mines, Golden, CO, USA*
Scott L. Huang
*Dept. of Mining and Geological Engineering, University of Alaska Fairbanks, Fairbanks, AK, USA*

## Abstract

The Segregation Potential (SP) concept has been widely used to predict frost heaving for engineering projects, such as the design of buried chilled gas pipelines or ground freezing. It is of utmost importance for the SP concept to calculate an accurate temperature gradient in the frozen fringe. The authors developed a modified apparent heat capacity method using temperature-dependent unfrozen water contents. The model was implemented using the finite element method (FEM) with very fine mesh. The numerical results of the model have shown satisfactory accuracy as compared with the analytical solution. In addition, the model eliminates oscillations of the temperature gradient in the frozen fringe.

**Keywords:** chilled gas pipeline; frost heave; phase change; segregation potential.

## Introduction

Frost heave is a mass and heat transfer phenomenon. The ice lens grows behind the freezing front. The transitional partially frozen zone between the ice lens and the unfrozen soil is called the *frozen fringe* (Miller 1972). Secondary frost heave theory (Miller 1978) is based on well-established principles of soil physics, hence it is the most popular theory. The secondary frost heave theory was successfully developed for numerical modeling (O'Neill & Miller 1985). However, the input parameters are difficult to obtain. Konrad & Morgenstern (1980, 1981) developed the Segregation Potential (SP) concept to overcome this problem. The SP concept succeeded in obtaining the overall frozen fringe characteristics including the suction gradient and the hydraulic conductivity through laboratory frost heave tests. The velocity of the pore water migrating to the frozen fringe, $v$, was proportional to the temperature gradient in the frozen fringe, grad$T_{ff}$, provided the suction at the pore-freezing front was constant:

$$v = \frac{P_w - P_u}{d} K_{ff} = \left( \frac{P_w - P_u}{T_s - T_f} K_{ff} \right) \text{grad} T_{ff} = \text{SP} \times \text{grad} T_{ff} \quad (1)$$

where $P_w$ = suction pressure at the active ice lens; $P_u$ = suction at the freezing front; $K_{ff}$ = overall hydraulic conductivity of the frozen fringe; $d$ = thickness of the frozen fringe; $T_s$ = segregation temperature; $T_f$ = freezing temperature; and SP = segregation potential.

It was confirmed in a previous study by Konrad & Morgenstern (1982) that the SP value near thermal steady state is dependent on the following variables:

$$\text{SP} = \text{SP}\left(\dot{T}_f, P_u, P_e, etc\right) \quad (2)$$

where $T_f$ = the cooling rate of the frozen fringe; $P_e$ = confining pressure acting on the freezing front.

The cooling rates are very small in the field condition. It is reasonable to apply the cooling rates at the formation near thermal steady state obtained by constant temperature boundary frost heave tests for the field condition (Konrad & Morgenstern 1984). From Equation 1, the SP value decreases with increasing $P_u$. In most field conditions, $P_u$ is fairly small as long as the freezing front is below the water table. Therefore, it would be reasonable to use the SP value determined by a laboratory frost heave test in which the warm plate temperature is close to freezing point, because the thermal boundary condition creates a small $P_u$ value due to the short unfrozen soil length. The effect of $P_e$ is taken into account empirically by Konrad & Morgenstern (1982):

$$\text{SP} = \text{SP}_0 \exp\left(-aP_e\right) \quad (3)$$

where $a$ = a soil constant; $\text{SP}_0$ = the maximum value of segregation potential that occurs at zero external pressure.

Since the proposed model is based on the SP concept, the migrated water amount depends on the temperature gradient, the rate of cooling, and the stress state. To simplify the simulation process, numerically uncoupled temperature solution from the stress–strain analysis or mass transfer solution can be applied. For any particular time step, the non-linear temperature distribution is first calculated with an iterative procedure, and then this temperature solution is used to determine the location of the freezing front. With the freezing front position determined, the SP concept is then used to calculate the volume of water flow to the segregation freezing front.

The precise calculation of the temperature gradient in the

frozen fringe is of utmost importance for the SP concept. Also, the coupled stress state has a strong dependence on thermal regime. Therefore, a numerical procedure for the transient heat transfer is first presented in this paper. Second, the verification of the developed heat transfer model is described. Finally, a new technique to calculate the temperature gradient in the frozen fringe is discussed.

## Heat Transfer Model with Phase Change

*Governing differential equation*

The three basic modes of heat transfer are conduction, convection, and radiation. Heat conduction is the primary mode in soils (Konrand & Shen 1996). Although heat convection was considered in some models (e.g. Harlan 1973), it is usually negligible in soil heat transfer studies (Farouki 1981). Nixon (1975) reported that the convection component is two or three orders of magnitude smaller than the conduction component. Radiation components hardly contribute to the amount of heat transfer at all. Radiation accounts for less than 1% of the total heat transfer in sands and even less in fine-grained soils (Farouki 1981).

For the above mentioned reason, the developed two-dimensional heat transfer model with isotropic thermal properties is based on conduction only and is governed by the following equation:

$$C\frac{\partial T}{\partial t}+L=\frac{\partial}{\partial x}\left(k\frac{\partial T}{\partial x}\right)+\frac{\partial}{\partial y}\left(k\frac{\partial T}{\partial y}\right) \tag{4}$$

where $C$ = volumetric heat capacity of soil; $L$ = volumetric latent heat; $T$ = soil temperature; $t$ = time; and $k$ = effective thermal conductivity of soil.

Alternatively, Equation 4 can be expressed as:

$$C_a\frac{\partial T}{\partial t}=\frac{\partial}{\partial x}\left(k\frac{\partial T}{\partial x}\right)+\frac{\partial}{\partial y}\left(k\frac{\partial T}{\partial y}\right) \tag{5}$$

where $C_a$ = the apparent volumetric heat capacity.

The traditional apparent heat capacity is defined as:

$$C_a=C+\frac{L}{TI} \tag{6}$$

where $TI = T_f - T_s$ : the temperature interval.

In this study, unfrozen water effect is taken into account in the phase change.

$$C_a=C+L'\rho_w\frac{\partial\theta_w}{\partial T} \tag{7}$$

where $L'$ = latent heat of fusion per unit mass of water ($3.337*10^5$ J/kg); $\rho_w$ = density of water (1000 kg/m$^3$); and $\theta_w$ = volumetric fraction of water.

This method is applied for fine-grained soils (Nixon 1983, Shen 1988). This method produces latent heat release over a range of subfreezing temperature.

*Unfrozen water content in Fairbanks silt*

Anderson and Morgenstern (1973) described a two-parameter power equation to determine unfrozen water content as:

$$w_u=m\times\left(T_f-T\right)^n \tag{8}$$

where $w_u$ = unfrozen water content; $m,n$ = characteristic soil parameters.

Michalowski & Zhu (2006) developed a first order exponential decay function:

$$w_u=w_1+\left(w^t-w_1\right)\exp\left(\frac{T-T_f}{b}\right) \tag{9}$$

where $w^t$ = the water content in an unfrozen state; $w_1$ = the asymptotic value; and $b$ = the rate of decay.

With decreasing temperature, the unfrozen water content reaches the asymptotic value.

Equations 8 and 9 can describe the unfrozen water content of the soil, with which a clayey soil would be expected to have a relatively high unfrozen water content. However, the laboratory results of Fairbanks silt at the UAF pipeline experiment site showed a relatively low unfrozen water content and a very steep gradient around the freezing temperature (Huang et al. 2004). Therefore the authors applied a second order exponential decay given by:

$$\begin{cases} w_u=w_1+w_2\exp\left(\dfrac{T-T_f}{t_1}\right)+w_3\exp\left(\dfrac{T-T_f}{t_2}\right) \\ w_1+w_2+w_3=w^t \end{cases} \tag{10}$$

where $t_1$,$t_2$ = rate of decay.

Figure 1 shows the comparison between the calculated unfrozen water content curve and the measured results of Fairbanks silt at the UAF pipeline experiment site. The unfrozen water affects the soil's thermal properties.

## Verification of Proposed Model

As shown in Equation 1, the precise calculation of the temperature gradient in the frozen fringe is the most important step for the SP concept. Nixon (1986) developed a two-dimensional geothermal model, named HAL, and conducted quadratic function fitting through three temperature points near the freezing front to determine grad$T_{ff}$. However, the proposed method produced oscillations of grad$T_{ff}$ (Carlson & Nixon 1988). Coutts (1991) proposed that grad$T_{ff}$ should be determined at the segregation temperature, which is the coldest temperature in the phase change range. This

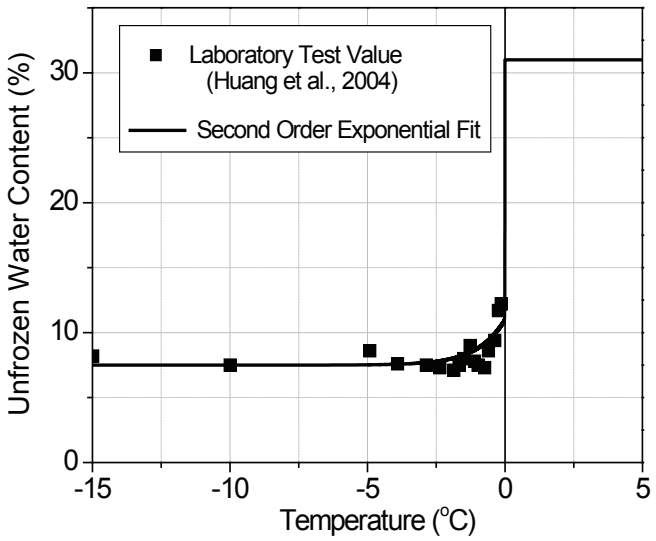


Figure 1. Unfrozen water contents of Fairbanks silt.

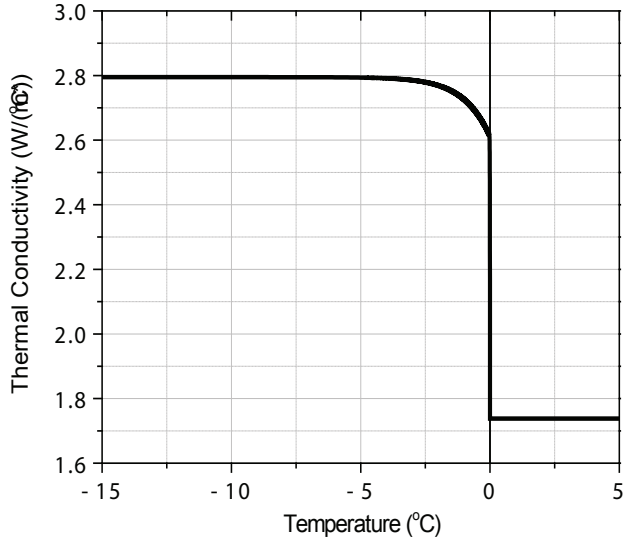


Figure 2. Thermal conductivity of Fairbanks silt for the proposed solution.

approach, however, could not eliminate oscillations. Konrad and Shen (1996) modified Coutts's model, and eliminated oscillations of grad$T_{ff}$ using forced mesh adjustment. However, the procedure was very complicated to manage. Also, the adjusted mesh had numerical instability, because the stiffness term of the adjusted mesh had a very large range compared with that of the unfrozen or totally frozen mesh (Hawlader et al. 2004). The authors propose a new approach applying a fine mesh and considering the effects of unfrozen water.

The proposed model is implemented by ABAQUS/Standard-6.7 finite element code. The soil geometry is a 0.0005 m by 10 m column. The two-dimensional four-node linear heat transfer element (DC2D4) is applied. The soil is divided into 0.0005 m square meshes. The mesh is only one element wide. The initial soil temperature is 1°C. The temperature boundary at the top is set at –1°C, and kept constant for 2000 hours. Zero heat flux is applied at the bottom and side boundaries. For the boundary conditions defined above, the two-dimensional heat transfer model is verified as a one-dimensional solution.

The unfrozen water contents shown in Figure 1 are taken into account in the thermal conductivities and volumetric heat capacities. Figures 2 and 3 show thermal conductivities and volumetric heat capacities of the Fairbanks silt at the UAF pipeline site, respectively. Thermal conductivity values were obtained by the thermal conductivity needle-probe method, then calibrated using the correlations of Johansen (1977). Those values are applied for the proposed model using the apparent heat capacity in Equation 7.

The proposed model is compared with the case using the traditional apparent heat capacity method with Equation 6, and verified against the Neumann solution. The Neumann solution is not valid for non-linear thermal properties but rather for materials that exhibit constant values in both the frozen and unfrozen states. Frozen thermal properties are determined at the asymptotic point. Latent heat generation

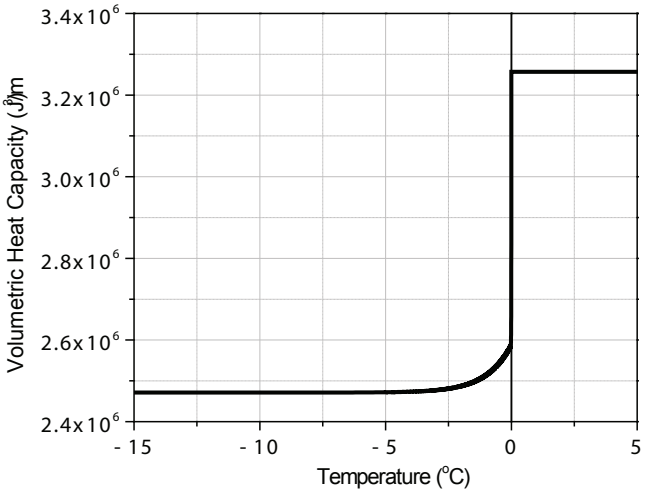


Figure 3. Volumetric heat capacity of Fairbanks silt for the proposed solution.

was a concern in the frozen water amount from the freezing temperature to the asymptotic point (= $w^t - w_1$). The thermal conductivities of the frozen and unfrozen phase are determined as 2.79 and 1.74 W/(m*°C), the volumetric heat capacities were $3.26*10^6$ and $2.47*10^6$ J/(m$^3$*°C), respectively. The volumetric latent heat is $1.16*10^8$ J/m$^3$. Those constant properties are also used for the traditional apparent heat capacity method. The calculations are made by $TI$ = 0.01°C, 0.05°C, and 0.1°C.

The freezing front penetration in each case is compared in Figure 4. While the traditional apparent heat capacity method for the case of $TI$ = 0.01°C is identical to the result obtained from the Neumann solution, its accuracy is sensitive to the magnitude of $TI$. With increasing $TI$, the freezing front penetrates deeper.

Figure 5a shows the temperature profiles of Neumann and the proposed solution at 2000 hours. The proposed solution agrees

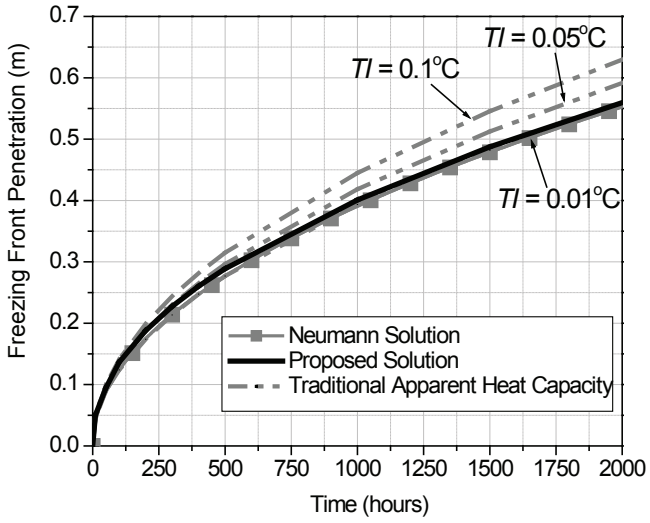


Figure 4. Comparison of freezing front penetration.

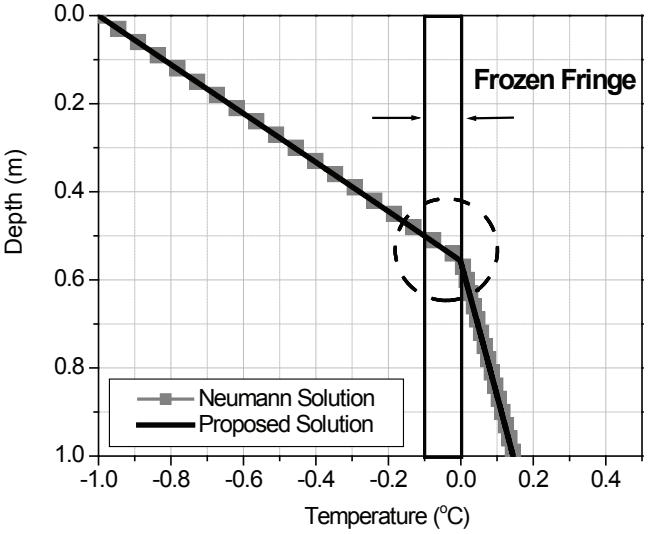


Figure 5a. Comparison of temperature distribution at 2000 hours.

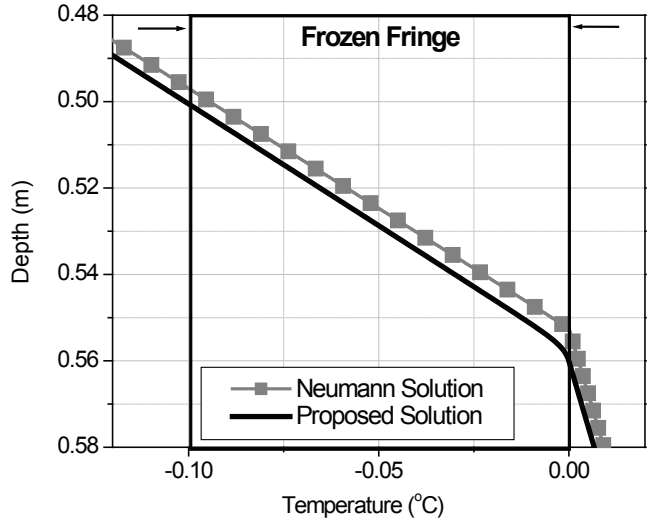


Figure 5b. Comparison of temperature distribution in frozen fringe at 2000 hours.

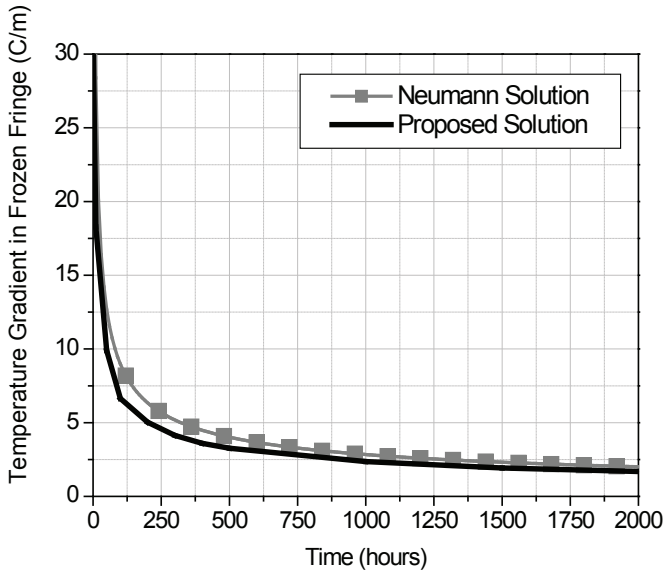


Figure 6. Comparison of temperature gradient in frozen fringe between Neumann and the proposed solution.

well with the Neumann solution. Figure 5b shows the close-up view of temperature distribution in the frozen fringe. $T_s$ is assumed as –0.1°C to define the frozen fringe. Since the square mesh size is 0.0005 m, there are approximately 100 points in the frozen fringe. The effect of the fine mesh gives two advantages. First, it is the accuracy of the temperature distribution in the frozen fringe. The freezing front of the proposed solution is slightly deeper than that of Neumann solution as shown in Figures 4 and 5b. Also, the temperature distribution of the proposed solution is non-linear. This is due to the non-linear thermal properties of the unfrozen water content. The second advantage is the elimination of oscillations of grad$T_{ff}$. The history of grad$T_{ff}$ between the proposed and Neumann solution is shown in Figure 6. The precision of the proposed solution is quite satisfactory and stable. Because of the precise and stable grad$T_{ff}$, it will be possible to adequately conduct water migration prediction using the SP concept.

It is true that the proposed solution requires considerable calculation time because of the fine mesh size. However, this issue was solved by using an IBM p690 computer at the Arctic Region Supercomputing Center in the University of Alaska Fairbanks.

The proposed solution was used to simulate the UAF frost heave experiment. Figures 7 and 8 show the finite element mesh and simulated temperature distribution with a deformed mesh in a steady state, respectively. The details of the mechanical model coupling and simulation results will be presented in a future paper.

## Conclusion

A transient heat transfer model was developed to determine the temperature gradient in the frozen fringe with high precision using the SP concept. The proposed approach was implemented using a FEM model with a

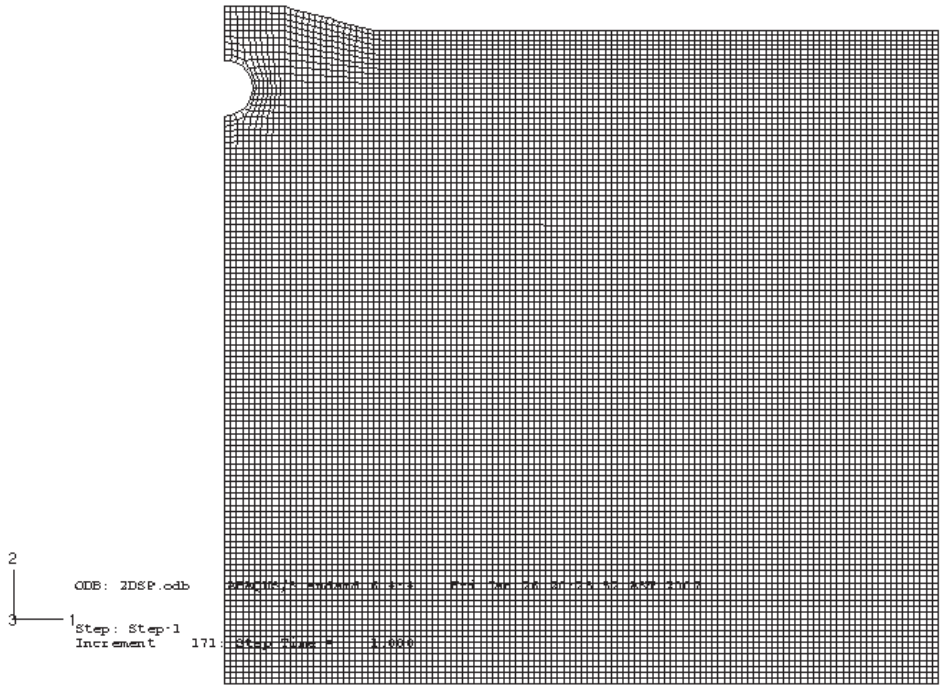


Figure 7. Finite element mesh for the simulation of the UAF pipeline experiments.

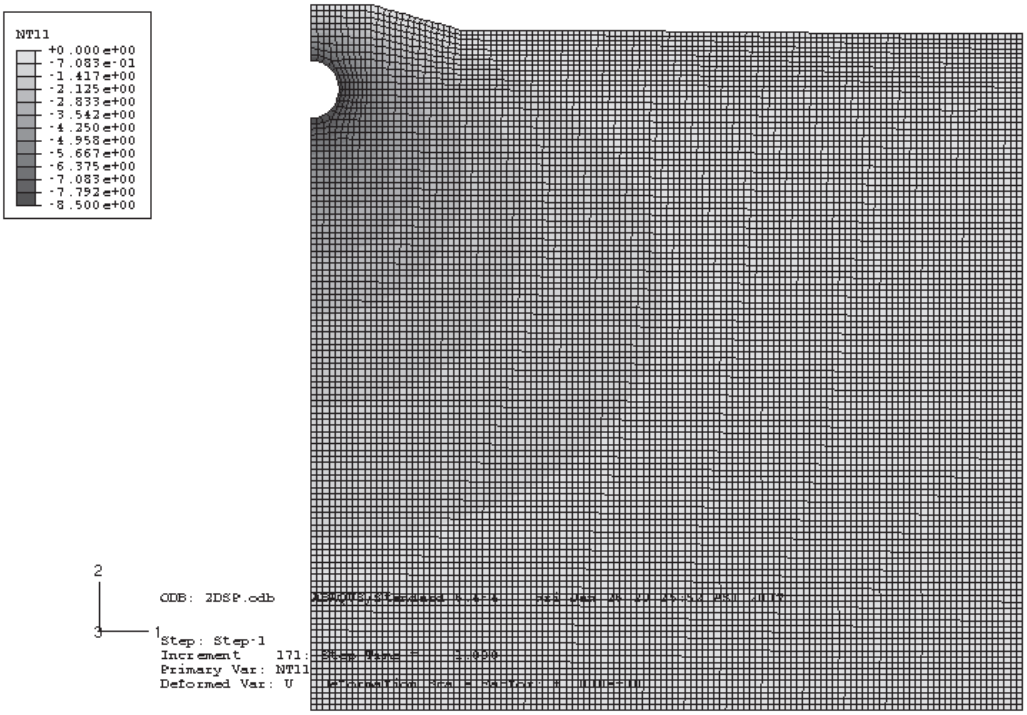


Figure 8. Simulated deformed mesh and temperature distribution in steady state.

fine mesh. A modified apparent heat capacity method considering unfrozen water contents was applied in the model. The model developed in this study has achieved the following improvements:

1. The proposed method can properly simulate the non-linear temperature distribution in the frozen fringe.
2. The calculated grad$T_{ff}$ does not exhibit oscillations.
3. The simulated results agree well with the Neumann solution.

## Acknowledgments

The numerical simulation of the study was supported by an Alaska EPSCoR Graduate Research Fellowship. The financial assistance is appreciated. The authors would also like to thank Dr. Xiong Zhang, University of Alaska Fairbanks, for his suggestions regarding the numerical simulation.

## References


Anderson, D.M. & Morgenstern, N.R. 1973. Physics, chemistry and mechanics of frozen ground. *Proceedings of 2nd International Conference Permafrost, Yakutsk, Russia*: 257-288.

Carlson, L.E. & Nixon, J.F. 1988. Subsoil investigation of ice lensing at the Calgary, Canada, frost heave test facility. *Canadian Geotechnical Journal* 25: 307-319.

Coutts, R.J. 1991. *Development of Two-dimensional Finite Element Model to Calculate Temperatures and Stresses in Frost Susceptible Soils around a Chilled Pipeline.* M.S. Thesis. Ontario, Canada: University of Waterloo.

Farouki, O.T. 1981. *Thermal Properties of Soils*. CRREL Monograph 81-1. Hanover, NH: U.S. Army Cold Regions Research and Engineering Laboratory.

Harlan, R.L. 1973. Analysis of coupled heat-fluid transport in partially frozen soil. *Water Resources Research* 9: 1314-1323.

Hawlader, B.C., Morgan, V. & Clark, J. 2004. A simplified solution for frost heave prediction of chilled pipelines. *Proceedings of the Cold Regions Engineering & Construction Conference & Expo, Alberta, Canada.*

Huang, S.L., Bray, M.T., Akagawa, S. & Fukuda, M. 2004. Field investigation of soil heave by a large diameter chilled gas pipeline experiment, Fairbanks, Alaska. *Journal of Cold Regions Engineering* 18: 2-34.

Johansen, O. 1975. *Thermal Conductivity of Soils.* Draft translation 637, Hanover, NH: U.S. Army Cold Regions Research and Engineering Laboratory.

Konrad, J.M. & Morgenstern, N.R. 1980. A mechanistic theory of ice lens formation in fine-grained soils. *Canadian Geotechnical Journal* 17: 473-486.

Konrad, J.M. & Morgenstern, N.R. 1981. The segregation potential of a freezing soil. *Canadian Geotechnical Journal* 18: 482-491.

Konrad, J.M. & Morgenstern, N.R. 1982. Effect of applied pressure on freezing soils. *Canadian Geotechnical Journal* 19: 494-505.

Konrad, J.M. & Morgenstern, N.R. 1984. Frost heave prediction of chilled pipelines buried in unfrozen soils. *Canadian Geotechnical Journal* 21: 100-115.

Konrad, J.M. & Shen, M. 1996. 2-D frost action modeling using the segregation potential of soils. *Cold Regions Science and Technology* 24: 263-278.

Michalowski, R.L. & Zhu, M. 2006. Frost heave modelling using porosity rate function. *International Journal for Numerical and Analytical Methods in Geomechanics* 30: 703-722.

Miller, R.D. 1972. Freezing and heaving of saturated and unsaturated soils. *Highway Research Record* 393: 1-11.

Miller, R.D. 1978. Frost heaving in non-colloidal soils. *Proceedings of 3rd International Conference on Permafrost, Edmonton, Alberta, Canada*: 708-713.

Nixon, J.F. 1975. The role of convective heat transport in the thawing soils. *Canadian Geotechnical Journal* 12: 425-429.

Nixon, J.F. 1983. Practical application of a versatile geothermal simulator. *Journal of Energy Resources Technology* 105: 442-447.

Nixon, J.F. 1986. Pipeline frost heave predictions using a 2-D thermal model. *ASCE Research on Transportation Facilities in Cold Regions*: 67-82.

O'Neill, K. & Miller, R.D. 1985. Exploration of a rigid ice lens model of frost heave. *Water Resources Research* 21: 281-296.

Shen, M. 1988. Numerical analysis of temperature field in a thawing embankment in permafrost. *Canadian Geotechnical Journal* 25: 163-166.

# Methane Emission from Siberian Wet Polygonal Tundra on Multiple Spatial Scales: Process-Based Modeling of Methane Fluxes on the Regional Scale, Lena Delta

Stefanie Kirschke
*German Aerospace Center, German Remote Sensing Data Center, Wessling, Germany*
Kurt P. Guenther
*German Aerospace Center, German Remote Sensing Data Center, Wessling, Germany*
Klaus Wisskirchen
*German Aerospace Center, German Remote Sensing Data Center, Wessling, Germany*
Torsten Sachs
*Alfred Wegener Institute for Polar and Marine Research, Potsdam, Germany*
Stefan Dech
*German Aerospace Center, German Remote Sensing Data Center, Wessling, Germany*

## Abstract

Uncertainties in the carbon budget of high latitude ecosystems are partly due to difficulties in assessing the spatially and temporally highly variable methane emissions of permafrost soils. $CH_4$ contributes significantly to global warming. Arctic regions are most critically influenced by a changing climate. Modeling approaches are important tools to determine $CH_4$ fluxes of arctic environments. We present two process-based models to calculate methane emission from permafrost soils. Model forcing consists of ECMWF (European Center for Medium-Range Weather Forecasts) meteorological data which are validated against field measurements. Auxiliary input data is derived from satellite imagery and field measurements. A MERIS-FR land classification scheme is used to upscale emissions. Model results are validated using methane flux measurements on the landscape and small scale carried out in 2006 in the Lena Delta (72°N, 126°E) by Alfred Wegener Institute for Polar and Marine Research. The study site is characterized by arctic tundra ecosystems and continuous permafrost.

**Keywords:** Arctic; climate change; methane emissions; modeling; permafrost; tundra.

## Introduction

*Introduction*

The radiative forcing due to methane—the second largest of the long-lived greenhouse gases after carbon dioxide—and its Global Warming Potential (GWP), which is about 20 times higher than the GWP of $CO_2$ (IPCC 2001), demonstrate the significant contribution of methane to warming of the atmosphere. The global atmospheric methane concentration has risen from a pre-industrial value of about 715 ppb to a current value of about 1774 ppb (IPCC 2007).

The observed increase in methane concentrations is very likely due to anthropogenic activity, mainly agriculture, burning of fossil fuels, and landfills. Contributions of further sources to the global atmospheric methane budget are not well determined yet (IPCC 2007) due to the difficulty in assessing the global emission rates of the natural sources, the strengths of which are highly variable in space and time (IPCC 2001).

Permafrost soils represent a large carbon reservoir, with an estimated carbon pool of about 900 Gt for frozen yedoma (ice-rich soils with high labile carbon content [Walter et al. 2003]) and non-yedoma soils excluding peatlands. The permafrost carbon reservoir exceeds that of the atmosphere (~730 Gt) and vegetation (~650 Gt) (Zimov et al. 2006).

Due to high sensitivity of the arctic soil carbon reservoir to increasing temperatures and to the large surface area, arctic regions are most critically influenced by changing climate. In thawed permafrost soils, methane is produced by specially adapted microbes under anaerobic conditions and released into the atmosphere. Extensive thawing of permafrost will release the carbon contained in the soils, hence further affecting the global carbon cycle. Model scenarios predict a severe degradation of permafrost in the Northern Hemisphere, including a northward shift of the permafrost boundary as well as an increase in active layer depth (Lawrence & Slater 2005, Zhang et al. 2007).

Studies on measuring methane flux on the landscape scale using the eddy covariance technique have been conducted by only by a few research groups (Fan et al. 1992, Friborg et al. 2000, Hargreaves et al. 2001, Harazono et al. 2006, Wille et al. 2007). Very few studies on modeling methane emission in Siberian permafrost regions on the regional scale have been performed (Bohn et al. 2007).

This study aims at modeling the methane budget of a high latitude permafrost-affected region for determining source strength, and at understanding emission patterns on a regional scale. Remote sensing techniques and ground-truth measurements are used to derive information needed as input for process-based models and to upscale modeling from single point to regional scale. We present a new approach where the methane model by Walter (1998) is modified for permafrost conditions and applied to a study site characterized by continuous permafrost.

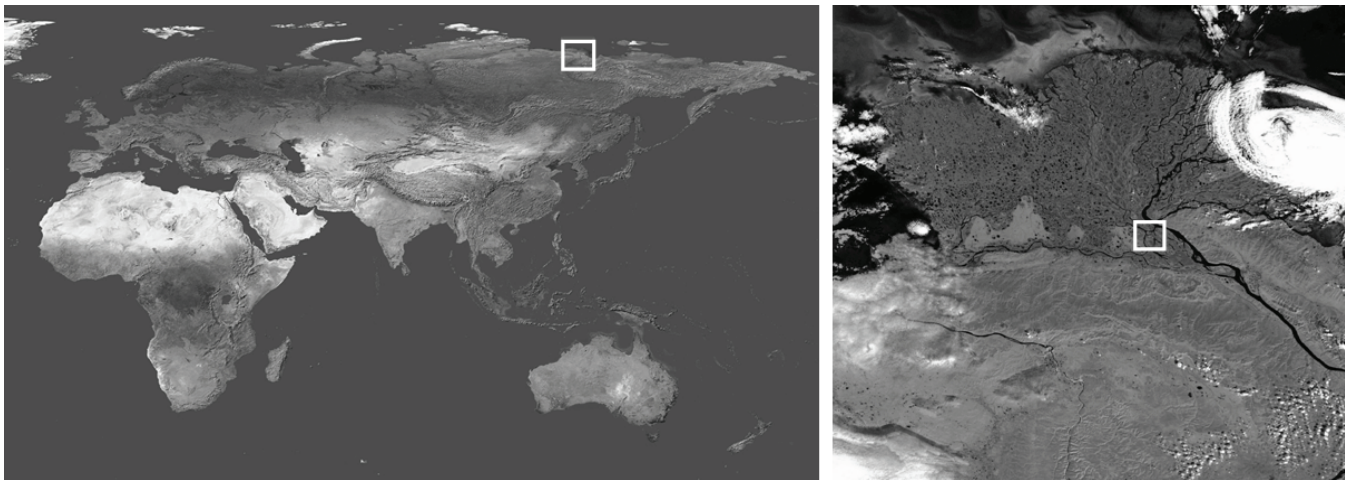

Figure 1. Geographical settings of the Lena River Delta and Samoylov Island shown in boxes (left panel: RGB composite of the globe based on MODIS data; right panel: RGB image for August 26, 2006, based on MERIS-FR data).

## Materials and Methods

*Study site*

The Lena River Delta is located at the Laptev Sea coast in northeast Siberia (Fig. 1). It is considered a key region for understanding the underlying processes of the development and dynamics of permafrost in the Arctic under a warming climate. The region is characterized by arctic tundra ecosystems and is underlain by deep continuous permafrost.

The delta, situated at the north coast of Siberia, is the largest delta in the Arctic and one of the largest in the world (Walker 1998). It is characterized by a highly heterogeneous landscape of smaller and wider river branches and channels, as well as more than 1500 islands of various sizes on an area of about 32,000 km$^2$ (Walker 1998). Three major fluvial terraces with different geomorphological characteristics form the delta (Schwamborn et al. 2002). The 30-year (1961–1990) averages of mean air temperature and total precipitation measured at the meteorological station in Tiksi (eastern delta) are -13.5°C and 323 mm, respectively (Roshydromet 2004). The vegetation is mainly characterized by sedge/grass/moss wetland and sedge/moss/dwarf-shrub wetland, as well as dwarf-shrub tundra (CAVM Team 2003). The growing period is short, lasting for 60–80 days (Grigoriev 1993). The surface is characterized by wet polygonal tundra with a pronounced micro-relief (Wille et al. 2007).

Since 1998, yearly expeditions have been conducted by Alfred Wegener Institute for Polar and Marine Research, Potsdam (AWI) to study carbon dynamics and involved microbial processes and communities as well as the energy and water budget of Arctic tundra. Campaigns have been carried out on Samoylov Island (Fig. 1). Samoylov (72°22′N, 126°28′E) is representative of the active and youngest part of the Lena Delta and covers an area of approximately 7 km$^2$.

*Model description*

The methane emission model (Walter 1998) is a one-dimensional process-based climate-sensitive model to derive methane flux from natural wetlands. The processes leading to methane emission are modeled within a one-dimensional soil column which is discretized in 1 cm thick soil layers. Three different transport mechanisms that contribute to methane release from soils are taken into account and modeled explicitly; namely diffusion, ebullition, and plant-mediated transport.

Methane production strongly depends on the position of the water table (Roulet et al. 1992, Bubier et al. 1995), which is a measure for dividing the soil column into an anaerobic and aerobic zone (Fig. 2). Methane is only produced under the absence of oxygen and, hence, only in water-saturated parts of the soil column (Fig. 2a). The production of methane by methanogenic bacteria is a function of substrate availability, pH and temperature (Walter 1998). The temperature dependence of methane production rates can be described by $Q_{10}$ values which depict the relative increase in activity after a temperature rise of 10°C (van Hulzen et al. 1999). The gas is then transported to the soil/water interface by molecular diffusion, ebullition and, if vascular plants occur, by plant-mediated transport. When the water table drops below the soil surface, oxygen can enter the soil pores, and the methane produced in lower, still water saturates (anaerobic) parts of the soil body and is transported upwards and oxidized in the aerobic zone by methanotrophic bacteria (Fig. 2b). Methane oxidation can be described by Michaelis-Menten kinetics (Bender & Conrad 1992).

The model is driven by meteorological data and needs auxiliary input data, such as vegetation and soil characteristics, land classification schemes, fraction of cover, and Net Primary Productivity (NPP). NPP is parameterized as a measure for substrate availability and, thus, is an important input parameter. Since the model was modified for permafrost conditions, many parameters are time-dependent with successive thawing of the soil body, and only a few fixed parameters are used in the simulation runs.

NPP of high latitude tundra ecosystems is calculated by the process-based vegetation model BETHY/DLR (Biosphere Energy Transfer Hydrology Model) (Knorr 1997,

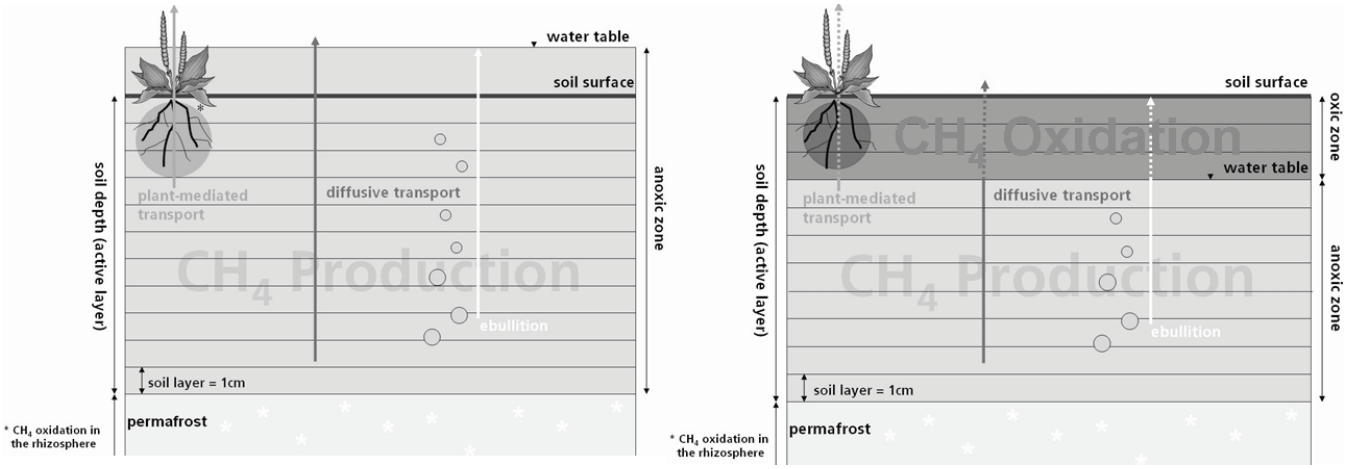


Figure 2. Schematic presentation of a soil column in the methane model. (a) Methane production and different transport mechanisms under water saturated conditions (anaerobic); (b) methane production and consumption as well as different transport mechanisms under partly aerobic conditions.

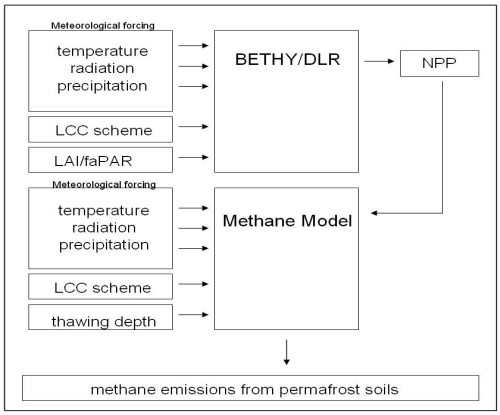


Figure 3. Flow chart illustrating the coupling of the BETHY/DLR model (NPP), the methane model, and their required input data.

Wisskirchen 2005). For simulations with BETHY/DLR, information about the state of vegetation is required; for example, time series of LAI (Leaf Area Index). Figure 3 shows the methodical structure of how the two models are coupled to work as a stand-alone package for modeling methane emission in permafrost regions.

*Data*

Both models need meteorological forcing data. Datasets provided by the European Centre for Medium Range Weather Forecast (ECMWF) are applied in modeling NPP and methane fluxes.

Auxiliary input data must be provided for both models. For simulations with the vegetation model BETHY/DLR, information about vegetation type and the state of vegetation (time series of LAI) is required. Running the methane model, additional input data such as vegetation parameters (e.g., rooting depth), soil characteristics (e.g., pore volume), land classification schemes (e.g., wetland distribution), fraction of cover, and NPP are needed.

Thawing of permafrost is described in the model by using measurements of active layer depth taken during field campaigns. Thawing/freezing is accounted for in order to characterize permafrost-related processes more realistically. The simulation starts with the first thawing of permafrost soil. Methane emission increases with increasing thawing depth, subsequently slowly decreases, and eventually comes to an end with permafrost re-freezing.

During the field campaign "System Laptev Sea – LENA2006" carried out from May to September 2006, Medium Resolution Imaging Spectrometer Full Resolution (MERIS-FR) data were acquired for the full growing season. MERIS-FR data were processed to derive information on vegetation characteristics needed as model input.

*Vegetation characteristics*

Vegetation characteristics play an important role in the presented modeling approach. In the vegetation model BETHY/DLR, LAI is used to describe the seasonal development of vegetation. It is needed as a continuous input variable to assess NPP.

In order to obtain realistic time series of LAI for the growing season 2006 of the Lena Delta, an approach using the MERIS Global Vegetation Index (MGVI), also called Top of the Atmosphere Vegetation Index (TOAVI), was used. FAPAR (Fraction of Absorbed Photosynthetically Active Radiation) can be retrieved by remote sensing techniques with acceptable accuracy using TOAVI values (Gobron et al. 2004) and can subsequently be used to estimate LAI. For homogeneous vegetation cover, $LAI_{\mathrm{hom}}$ is calculated using the equation (Monteith & Unsworth 1990):

$$LAI_{\mathrm{hom}_i} = LAI_{\max} \cdot \frac{\log\left(1 - FAPAR_i\right)}{\log\left(1 - FAPAR_{\max}\right)} \qquad (1)$$

$LAI_{\max}$ is chosen according to in situ measurements (Eq. 3). $FAPAR_i$ and $FAPAR_{\max}$ are derived from MGVI values.

During the field campaign 2006, field spectral measurements were taken using a portable ASD FieldSpecFR spectrometer (Analytical Spectral Devices Inc.). The spectrometer covers a wide spectral range from 350–2500 nm. Due to

the highly heterogeneous surface patterns of wet polygonal tundra, different plant communities with different vegetation cover have evolved on a small scale in high and low center polygons and polygon rims, depending on changes in substrates and hydrologic regimes. Spectral measurements were taken in order to derive data on vegetation characteristics such as NDVI (Normalized Difference Vegetation Index) and LAI which can then be used to differentiate between plant communities as well as to validate satellite data.

Spectra have been processed using ENVI software. Processing is inevitable in order to correct for sensor properties and reference measurements using a spectralon panel. Biophysical indices (NDVI and LAI) were calculated and compared with NDVI and LAI values derived from MERIS-FR data.

NDVI was calculated from spectral data using the equation (Rouse et al. 1974):

$$NDVI = \frac{\left(R_{864} - R_{671}\right)}{\left(R_{864} + R_{671}\right)} \quad (2)$$

where $R_{864}$ and $R_{671}$ denote the reflectance at wavelengths 864 nm (near infrared) and 671 nm (red), respectively.
LAI was then calculated after Gardner & Blad (1986):

$$LAI = -1.248 + 5.839 * NDVI \quad (3)$$

$LAI_{max}$ in equation (1) was set according to *LAI* values derived from equation (3).

## Results and Discussion

*Leaf Area Index (LAI)*

Figure 4 shows results of the two approaches described above and presents a comparison between LAI calculated from field spectra and remote sensing data, respectively. The datasets compare reasonably well with slightly higher LAI values derived from in situ measurements. Additionally, a steeper slope can be observed in the in situ dataset. Possible explanations might be (1) an inaccurate atmospheric correction of MERIS-FR data due to high sun zenith angles and (2) the spatial resolution of MERIS-FR data (300 m) being unable to capture the high spatial heterogeneity of wet polygonal tundra.

However, it can be seen that the temporal variation of LAI during the vegetation period of 2006 is represented realistically. After slowly increasing at the beginning of the growing season, LAI reaches its maximum in mid-August (DOY 229) and then starts decreasing again. This agrees with ground truth observations from field campaigns in the delta.

Handling optical satellite data for high-latitude regions is often problematic due to high cloud contamination and high sun zenith angles. Here it is shown that for arctic regions like the Lena River Delta, information on vegetation characteristics can be retrieved from optical satellite-based measurements. Ground-truth data are useful for validating satellite-derived plant biophysical parameters. Working with

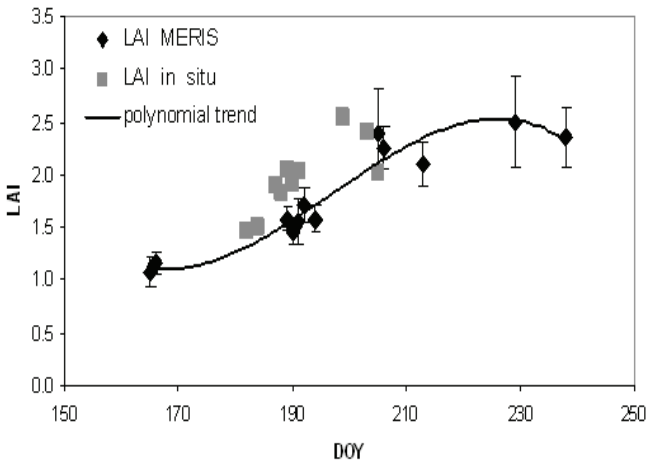


Figure 4. Time series of LAI for Samoylov Island for the growing season 2006. Diamonds: seasonal course of LAI derived from MERIS FAPAR values and polynomial fit, error bars indicate SD; triangles: LAI derived from field spectral measurements.

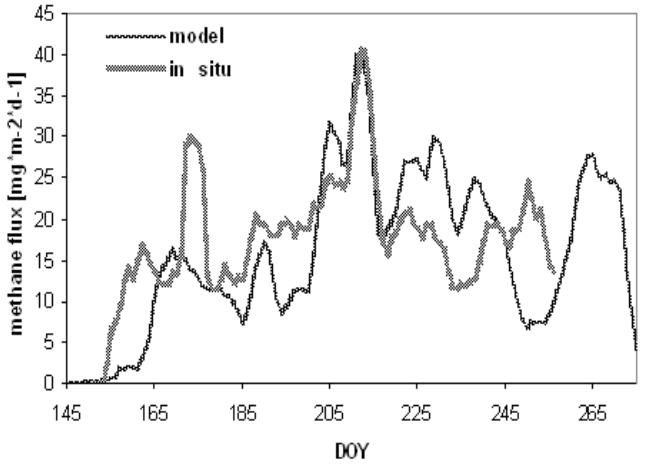


Figure 5. Measured and modeled methane fluxes (5-day running means) from a one-dimensional model run for the growing season 2006 and model coordinates 72°N, 126°E (Samoylov Island).

both ground-truth and remote sensing approaches as presented here provides a powerful tool to estimate vegetation characteristics on the small scale and to upscale these characteristics to the regional scale.

Realistic time series of plant canopy characteristics like LAI can be used as model input and to validate literature values when information about the state and seasonal variation of vegetation is required (BETHY/DLR).

*Methane flux modeling*

Methane flux was modeled one-dimensionally for the growing seasons of 2003–2006. Figure 5 shows a comparison of measured and modeled fluxes for the growing season of 2006. Flux measurements on the landscape scale using eddy covariance technique were carried out on Samoylov Island from June 9, 2006, through September 19, 2006, (Sachs et al. 2008). An eddy flux tower 3.6 m in height was used for methane flux measurements as well as for additional mete-

orological measurements. The seasonal course of modeled methane fluxes is limited by soil thawing and freezing.

In situ flux time series are used to validate the methane model and adjust model parameters, like $Q_{10}$ values characterizing methane reduction and oxidation, to the study site. Between DOY 151 and 256, during overlap of the two curves, modeled methane flux is in good accordance with observed data. Flux integrals for both curves for the overlapping period are 1686 mg $CH_4$ $m^{-2}$ (model) and 1895 mg $CH_4$ $m^{-2}$ (measurements), respectively, which indicates a model underestimation of about 10%. This result agrees well with other studies using the same methane emission model; for example, when applied in Western Siberia (Bohn et al. 2007).

As can be seen in Figure 5, the time series of modeled methane emission shows less variation between days than the measured flux. This difference in seasonal fluctuation is due to the high variability of methane emission, both spatially and temporally (Joabsson et al. 1999, Wagner et al. 2003) and can be explained by the main factors controlling methane release. Wille et al. (2007) identified soil temperature and near-surface turbulence to be the driving parameters of methane emission in the Lena Delta.

The observed small-scale variability shown in the in situ data cannot fully be represented in the model results. Model input data on soil temperatures derived from ECMWF have a spatial resolution of 0.5°, and thus, variations in soil temperature due to the micro-relief of wet polygonal tundra cannot be taken into account.

Additionally, no data on wind distribution, wind direction, and wind speed are considered in the methane model.

However, since the project aims at quantifying methane emission on a regional scale, well-founded knowledge of small-scale process variability is an important factor for model understanding but cannot be fully implemented in the model.

## Conclusions

For the growing season 2006, methane fluxes were modeled using two process-based models, a vegetation, and a methane emission model. Simulated methane fluxes are in agreement with in situ flux measurements ($r^2 = 0.63$). Time-integrated fluxes are 1686 mg $CH_4$ $m^{-2}$ (model) and 1895 mg $CH_4$ $m^{-2}$ (measurements), respectively. This indicates a model underestimation of about 10% which agrees with results of a study conducted in Western Siberia using the same methane emission model, where a model underestimation of about 10% was observed as well (Bohn et al. 2007).

Leaf Area Index needed as input for the vegetation model was calculated using two different approaches. LAI was derived (1) from satellite-based measurements and (2) by processing field spectral measurements. In situ data were applied in validating satellite data. It could be shown that information about the state and seasonal variation of the vegetation in arctic regions can be retrieved by remote sensing techniques. Used for deriving time series of LAI for the study site, the satellite measurements provide realistic results and compare reasonably well with LAI calculated from in situ spectral measurements.

The results demonstrate the important role of modeling techniques in assessing methane emissions for High Arctic permafrost-influenced ecosystems. Understanding of micro-scale processes studied through scientific field work is absolutely necessary when applying process-based models.

## Acknowledgments

This project is conducted in the frame of the Helmholtz Research Network “Integrated Earth Observing System” (Helmholtz-EOS). Thanks to colleagues from AWI Potsdam for their in situ measurements and for getting the chance to participate in the LENA2006 campaign. Thanks to Dr. Dirk Wagner (AWI) who graciously provided data on $Q_{10}$ values. The MERIS-FR data presented in this paper were acquired within the ESA-AO 3909.

## References

Bender, M. & Conrad R. 1992. Kinetics of $CH_4$ oxidation in oxic soils exposed to ambient air or high $CH_4$ mixing ratios. *FEMS Microbiology Ecology* 101: 261-270.

Bohn, T.J, Lettenmaier, D.P., Sathulur, K. & Bowling, L.C. 2007. Large scale modeling of wetland methane emissions. *Integrated Land Ecosystem – Atmosphere Processes Study Newsletter* 4: 40-42.

Bubier, J.L., Moore, T.R., Bellisario, L., Comer, N.T. & Crill M.C. 1995. Ecological controls on methane emissions from a northern peatland complex in the zone of discontinuous permafrost, Manitoba, Canada. *Global Biogeochemical Cycles* 9(4): 455-470.

CAVM Team, 2003. Circumpolar Arctic Vegetation Map. Scale 1:7,500,000. Conservation of Arctic Flora and Fauna (CAFF) Map No. 1. U.S. Fish and Wildlife Service, Anchorage, Alaska.

Fan, S.M., Wofsky, S.C., Bakwin, P.S. & Jacob, D.J. 1992. Micrometeorological Measurements of $CH_4$ and $CO_2$ exchange Between the Atmosphere and Subarctic Tundra. *Journal of Geophysical Research* 97(D15): 16627-16643.

Friborg, T., Christensen, T.R., Hansen, B.U., Nordstroem, C. & Soegaard, H. 2000. Trace gas exchange in a high-arctic valley 2. Landscape $CH_4$ fluxes measured and modeled using eddy correlation data. *Global Biogeochemical Cycles* 14(3): 715-723.

Gardner, B. & Blad, B. 1986. Evaluation of spectral reflectance models to estimate corn leaf area while minimizing the influence of soil background effects. *Remote Sensing of Environment* 20:183-193.

Gobron, N., Mélin, F., Pinty, B., Taberner, M. & Verstraete, M.M. 2004. MERIS Global Vegetation Index: Evaluation and Performance. *Proceedings of the MERIS User Workshop, Frascati, Italy, November 10-13, 2003*.

Grigoriev, M.N. 1993. Cryomorphogenesis in the Lena Delta. Yakutsk (in Russian), 173 pp. In: J. Schneider, 2005, *Bilanzierung von Methanemissionen in Tundragebieten am Beispiel des Lena-Deltas, Nordostsibirien, auf der Basis von Fernerkundungsdaten und Gelaendeuntersuchungen*. Alfred Wegener Institute for Polar and Marine Research, Research Unit Potsdam, Master Thesis, 103 pp.

Harazono, Y., Mano, M., Miyata, A., Yoshimoto, M., Zulueta, R.C., Vourlitis, G.L., Kwon, H. & Oechel, W.C. 2006. Temporal and spatial differences of methane flux at arctic tundra in Alaska. *Mem. Natl Inst. Polar Res., Spec. Issue* 59: 79-95.

Hargreaves, K. J., Fowler, D., Pitcairn, C.E.R. & Aurela, M. 2001. Annual methane emission from Finnish mires estimated from eddy covariance campaign measurements. *Theoretical and Applied Climatology* 70: 203-213.

IPCC 2001. Climate Change 2001: The Scientific Basis. Contribution of Working Group I to the Third Assessment Report of the Intergovernmental Panel on Climate Change. J.T. Houghton, Y. Ding, D.J. Griggs, M. Noguer, P.J. van der Linden, X. Dai, K. Maskell, & C.A. Johnson (eds.), Cambridge, UK & New York, NY: Cambridge University Press, 881 pp.

IPCC 2007. Climate Change 2007: The Physical Science Basis. Contribution of Working Group I to the Fourth Assessment Report of the Intergovernmental Panel on Climate Change S. Solomon, D. Qin, M. Manning, Z. Chen, M. Marquis, K.B. Averyt, M. Tignor & H.L. Miller (eds.), Cambridge, UK & New York, NY: Cambridge University Press, 996 pp.

Joabsson, A., Christensen, T.R. & Wallén, B. 1999. Vascular plant controls on methane emissions from northern peat forming wetlands. *Trends in Ecology & Evolution (TREE)* 14(10): 385-388.

Knorr, W. 1997. Satellitengestützte Fernerkundung und Modellierung des globalen CO2-Austauschs der Landbiosphäre: Eine Synthese. Max-Planck-Institute for Meteorology, Examensarbeit Nr. 49 (in German), Hamburg, Germany.

Lawrence, D.M. & Slater, A.G. 2005. A projection of severe near-surface permafrost degradation during the 21st century. *Geophysical Research Lett*ers 32: L24401.

Monteith, J.L. & Unsworth, M.H. 1990. Principles of environmental physics. In: E. Arnold (ed.), London, 291 pp. In: P.J. Sellers, S.O. Los, C. Tucker, C.O. Justice, D.A. Dazlich, G.J. Collatz & D.A. Randall, 1996. *A Revised Land Surface Parameterization (SiB2) for Atmospheric GCMs.* Part II: The Generation of Global Fields of terrestrial Biophysical Parameters from Satellite Data. *Journal of Climate* 9(4): 706-737.

Roshydromet, Russian Federal Service for Hydrometeorology and Environmental Monitoring (2004). http://www.worldweather.org/107/c01040.htm.

Roulet, N., Moore, T.R., Bubier, J.L. & Lafleur, P. 1992. Northern fens: methane flux and climatic change. *Tellus* 44(B): 100-105.

Rouse, J.W., Haas, R.H., Schell, J.A. & Deering, D.W. 1974. Monitoring vegetation systems in the Greta Plains with ERTS. *Proceedings of the Third Earth Resources Technology Satellite-1 Symposium, Greenbelt, NASA SP-351,*301-317.

Sachs, T., Giebels, M., Wille, C., Kutzbach, L. & Boike, J. 2008. Methane emission from Siberian wet polygonal tundra on multiple spatial scales –vertical flux measurements by closed chambers and eddy covariance, Samoylov Island, Lena Delta. (this proceeding).

Schwamborn, G., Rachold, V. & Grigoriev, M.N. 2002. Late Quaternary sedimentation history of the Lena Delta. *Quaternary International* 89: 119-134.

Van Hulzen, J.B., Segers, R., van Bodegom, P.M. & Leffelaar, P.A. 1999. Temperature effects on soil methane production: an explanation for observed variability. *Soil Biology and Biochemistry* 31: 1919-1929.

Wagner, D., Kobabe, S., Pfeiffer, E.-M. & Hubberten , H.-W. 2003. Microbial Controls on Methane Fluxes from a Polygonal Tundra of the Lena Delta, Siberia. *Permafrost and Periglacial Processes* 14: 173-185.

Walker, H. J. 1998. Arctic deltas. *Journal of Coastal Research* 14(3): 718-738.

Walter, B. 1998. Development of a process-based model to derive methane emissions from natural wetlands for climate studies. Max-Planck-Institute for Meteorology, Examensarbeit Nr. 60, Hamburg, Germany, 160 pp.

Walter, K. M., Chapin III, F.S., White, D.M. & Zimov, S.A. 2003. Stratification of Thermokarst Lakes in NE Siberia based on Diffusive $CH_4$ Emissions. *Proceedings of the Arctic System Science Program All-Hands Workshop, Seattle, Washington, February 20–23, 2002:* 222.

Wille, C., Kutzbach, L., Sachs, T., Wagner, D. & Pfeiffer, E.-M. 2007. Methane Emission from Siberian arctic polygonal Tundra: Eddy Covariance Measurements and Modeling. *European Geosciences Union General Assembly 2007*, Abstract No. EGU2007-A-10277.

Wisskirchen, K. 2005. Modellierung der regionalen CO2-Aufnahme durch Vegetation. Dissertation (in German), Meteorologisches Institut der Rhein. Friedr.-Wilh.-Universität Bonn, 129 pp.

Zhang, Y., Chen, W. & Riseborough, D.W. 2007. Transient projections of permafrost distribution in Canada during the 21st century under scenarios of climate change. *Global and Planetary Change* (in press).

Zimov, S.A, Schuur, E.A.G. & Chapin III, F.S. 2006. Permafrost and the Global Carbon Budget. *Science* 312(5780): 1612-1613.

# Interannual Variability of Winter N-Factors in the Kuparuk River Basin, Alaska

Anna E. Klene
*Department of Geography, University of Montana, Missoula, MT 59812, USA*
Frederick E. Nelson, Nikolay I. Shiklomanov, Dmitry A. Streletskiy
*Department of Geography, University of Delaware, Newark, DE 19716, USA*

## Abstract

Hourly air and soil temperatures were monitored using arrays of miniature data loggers within eight 1-ha plots representing natural land cover types in northern Alaska's Kuparuk River watershed between 1995 and 2006. For each plot, mean daily air and soil temperatures were used to calculate mean winter *n*-factors, the ratio of seasonal freezing degree-day sums at the ground surface to those in the air. Mean 12 year *n*-factors ranged from 0.32 to 0.58 within the various plots, with ranges of 0.18 to 0.28 over the period of record. A distinct latitudinal gradient of *n*-factor values exists along this continentality gradient. Although direct measurements of snow cover are not available at the sites, temperature patterns indicate that snow cover is a major determinant of winter *n*-factor values.

**Keywords:** air temperature; Alaska; n-factor; permafrost; snow cover; soil-surface temperature.

## Introduction

Transfer of heat between the atmosphere and ground in arctic environments can be complex. Large differences in vegetation and soil characteristics can occur over very short distances, leading to highly variable near-surface soil temperatures. In permafrost regions, however, it is often critical to be able estimate soil temperatures over large geographic areas. The *n*-factor, the ratio of freezing (or thawing) degree-day sums at the soil surface to those in the air at standard instrument height, was proposed (Carlson 1952) as a way of summarizing the seasonal winter (or summer) surface energy balance. Although the n-factor was introduced for engineering purposes, there has been considerable recent interest in its application to natural surfaces (Taylor 1995, Klene et al. 2001a, Karunaratne & Burn 2003, 2004, Kade et al. 2006). This, in turn, has led to its use in modeling exercises (e.g., Buteau et al. 2004, Juliussen & Humlum 2007).

Most previous studies have focused on series of plots in different latitudes, soil, and vegetation types over one or two seasons. This study utilizes multiple soil temperatures within a series of plots and examines the mean *n*-factor for each plot over 12 winter seasons to reveal information about interannual variability.

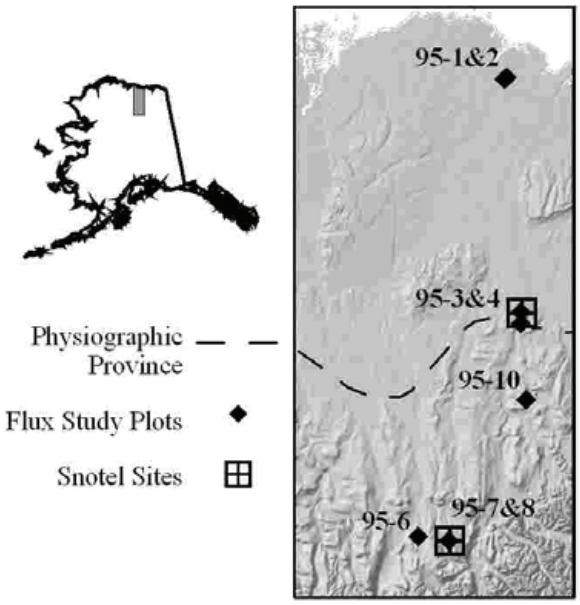


Figure 1. A shaded relief map of the study area showing locations of the Flux Plots, SNOTEL sites (see text), and the physiographic boundary between the coastal plain in the north and foothills in the south are depicted.

## Study Area and Background

The Kuparuk River Basin of northern Alaska stretches from the Brooks Range to the Beaufort Sea, just west of the Dalton Highway (Fig. 1). This watershed was the focus of the U.S. National Science Foundation's (NSF) Arctic System Study Flux Project, an integrated mid-1990s study of the flux of greenhouse gases from terrestrial to atmospheric and marine environments (Kane & Reeburgh 1998).

Several of the projects utilized the "Flux Plots," a series of ten 1-ha plots arrayed along a climatic gradient from north to south. These plots were selected to represent common land-cover/soil associations and detailed vegetation and soil characterization was done on each. During the years the Flux Study was operating, these plots were incorporated into the NSF-funded Circumpolar Active-Layer Monitoring (CALM) program, allowing climate and active layer thickness measurements to continue in subsequent years. One plot on an island in the Sagavanirktok River was abandoned after flooding washed away the instrumentation, and another was discontinued due to difficulty in accessing a mountain top.

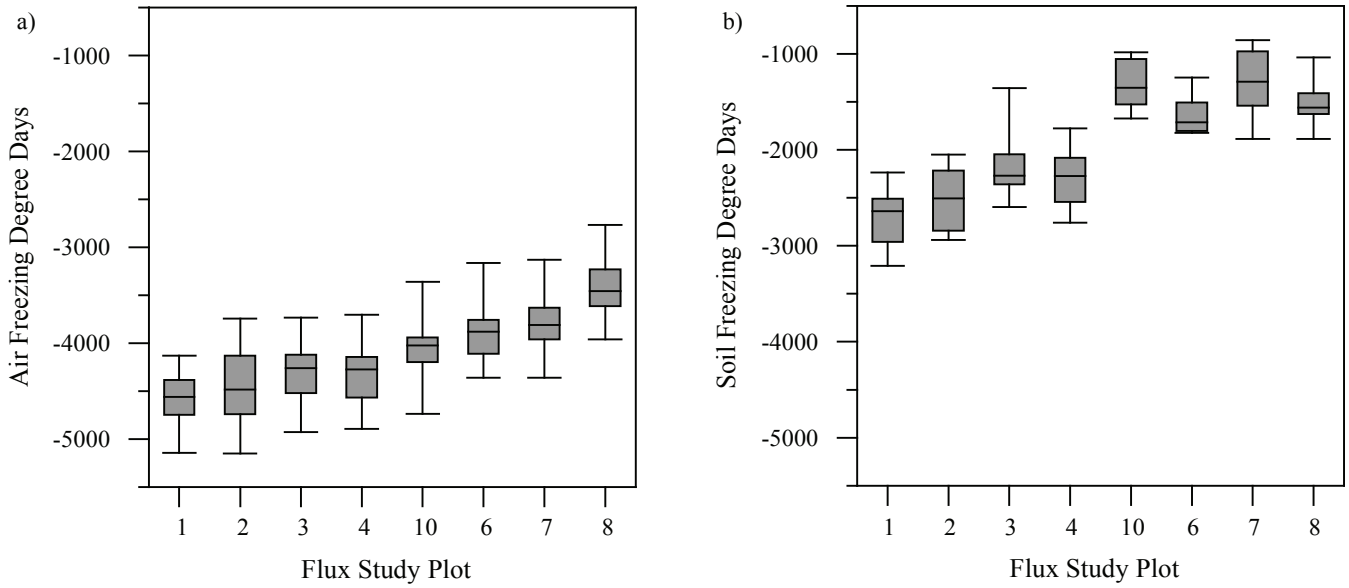


Figure 2. Box-and-whisker plots show the median, quartiles, and range of freezing degree-day sums in the air (a) and soil (b) at each of the eight Flux Plots observed between 1995 and 2006. Sites are arranged by latitudinal position; a distinct north-to-south (left-to-right) progression of values is apparent.

Elevations at the Flux plots used here ranged from 12 to 938 m a.s.l. Ten-year mean February and July air temperatures ranged from -18.3°C to -28.2°C and 7.3°C to 10.8°C, respectively, at the plots observed. Snow depths measured along a N-S transect in 1994–1996 varied from 0 m to 2 m within the basin (Taras et al. 2002). Permafrost underlies the entire region, with depths of about 600 m reported near Prudhoe Bay (Lachenbruch et al. 1982). Mean active layer thickness at the Flux Plots ranged from 42.2 cm to 60.3 cm during the 1995–1997 period (Klene et al. 2001). Vegetation was classified into four main categories: wet tundra, moist acidic tundra, moist nonacidic tundra, and shrublands (Walker & Bockheim 1995). Mean vegetation heights within the eight plots examined here ranged from 2.2 cm to 13.8 cm. Organic layer thickness ranged from 0 cm to 34 cm at the Flux Plots. Physiographically, the plots lie in the Arctic Coastal Plain province in the north and the Arctic Foothills province in the south (Wahrhaftig 1965). Observed soils included pergelic cryaquepts, cryorthents, cryoborolls, and histic pergelic cryaquolls (Walker & Bockheim 1995).

Klene et al. (2001) examined within- and between-plot variability of summer *n*-factors calculated for 1995–1997 at these plots. They found that mean n-factors within plots were robust when more than five soil-surface temperatures were available, and that the values were systematically related to land cover type. Mean summer *n*-factors calculated from 3 seasons of data ranged from 0.73 to 1.00 at the eight Flux Plots examined in this study (Klene et al. 2001).

## Methodology

As part of the Flux Study, ten Stowaway© data loggers were installed at each Flux Plot in 1995. One monitored air temperature inside a six-gill radiation shield at standard screen height (1.8 m) while nine recorded soil-surface temperature in a range of microenvironments (Klene et al. 2001). The Stowaway loggers have gradually been replaced with five two-channel HoboPro© data loggers. The two-channel loggers have an accuracy of ±0.2°C and precision of 0.02°C at the freezing point. Thermistors at ground level were positioned approximately immediately below the ground surface to measure near-surface soil temperature. This placement was generally within an organic soil, though this varied from plot to plot. Water infiltration and animal damage led to high attrition rates initially, but recent records have generally been more reliable, although animal damage still causes losses each year. Observations were taken hourly until 1998, when a two-hour interval was adopted to extend battery life.

The hourly observations were summarized into daily means from which freezing degree-day sums (DDF) were calculated from air and soil records for the winter season, defined as 15 Sept to 15 May (243 days), following Hinkel et al. (2008). Adoption of this protocol results in inclusion of the entire snow cover period for most years. Statistics were computed for each winter season when more than 165 days with at least five of the nine soil-surface measurements were available at each plot. Freezing degree days (DDF) are calculated by summing mean daily temperatures for those days in which the mean was less than 0°C. Units are °C·days. Winter *n*-factors are based on freezing degree-day sums, thus warmer soil temperatures will lead to smaller winter *n*-factors, often attributable to the insulating effects of the snowpack. This is in contrast to thawing (summer) *n*-factors which are calculated using thawing degree days, which results in warmer soils leading to larger n-factors.

Snow depth is usually cited (e.g., Benson 1969; Goodrich 1982) as an important determinant of winter soil-surface temperatures and thus *n*-factors. However, snow depth records are rare in the Arctic. Two SNOTEL stations have

Table 1. Summary statistics for mean winter 1995–1996 through 2006–2007 at the eight Flux Plots.

| | Flux 1 | Flux 2 | Flux 3 | Flux 4 | Flux 6 | Flux 7 | Flux 8 | Flux 10 |
|---|---|---|---|---|---|---|---|---|
| N winters | 10 | 10 | 12 | 12 | 12 | 12 | 10 | 10 |
| Minimum | 0.49 | 0.47 | 0.33 | 0.42 | 0.33 | 0.22 | 0.30 | 0.24 |
| Mean | 0.58 | 0.56 | 0.51 | 0.54 | 0.43 | 0.35 | 0.44 | 0.32 |
| Median | 0.58 | 0.55 | 0.51 | 0.54 | 0.43 | 0.37 | 0.46 | 0.33 |
| Maximum | 0.70 | 0.64 | 0.61 | 0.68 | 0.51 | 0.48 | 0.54 | 0.42 |
| Range | 0.21 | 0.18 | 0.28 | 0.26 | 0.18 | 0.26 | 0.24 | 0.18 |
| Stand. Dev. | 0.05 | 0.05 | 0.07 | 0.07 | 0.06 | 0.08 | 0.08 | 0.05 |

been operating within the study area over the period of record at the Sagwon Hills and Imnavait Creek. These sites are part of the SNOwpack TELemetry program run by the U.S. Natural Resources Conservation Program. Direct snow depth observations were unavailable but accumulated monthly precipitation has been archived (NRCS 2007). Precipitation was summed from October to May and used as a crude estimate of winter snowfall. Although this does not account for local variability resulting from vegetation, drifting, or scouring, it provides a basis for initial assessment.

## Results and Discussion

The basic components of the n-factor are air and soil degree-day sums. These are plotted in Figure 2 to illustrate the variability of these parameters over the 12 winter seasons at each of the Flux Plots. The climatic gradient of colder air temperatures on the coastal plain and warmer inland temperatures is readily apparent (Fig. 2a). The air-temperature gradient is a simple manifestation of the north-south continentality gradient in the region; the fact that the surface-temperature gradient shows a corresponding trend indicates that air and surface temperatures are more strongly coupled than elsewhere on Alaska's North Slope (Hinkel et al. 2008).

The soil degree-day sums (Fig. 2b) are systematically warmer than the air temperatures by approximately 2000°C·days. Twelve-year mean differences ranged from 1897°C·days at Plot 1 to 2756°C·days at Flux 10. They also reveal a distinct warming from north to south. The four most southerly sites are more similar in their soil DDF ranges and means than were the air degree-day sums.

Analysis of mean winter n-factors at each plot revealed a substantial interannual variability considering that the soil temperatures were averages from multiple individual microsites within each 1-ha plot. Table 1 lists summary statistics. Mean values at the more northerly sites are larger (0.51 to 0.58) while the southerly sites have mean values of 0.32 to 0.44. Ranges in the mean winter *n*-factors at each plot varied from 0.18 to 0.28.

Box and whisker plots were calculated for the mean winter *n*-factors at each site and revealed, once again, a strong gradient from north to south (Fig. 3). A broader distribution of mean *n*-factors at the four southerly sites is reflected in the increased area within the quartile box. While the latitudinal

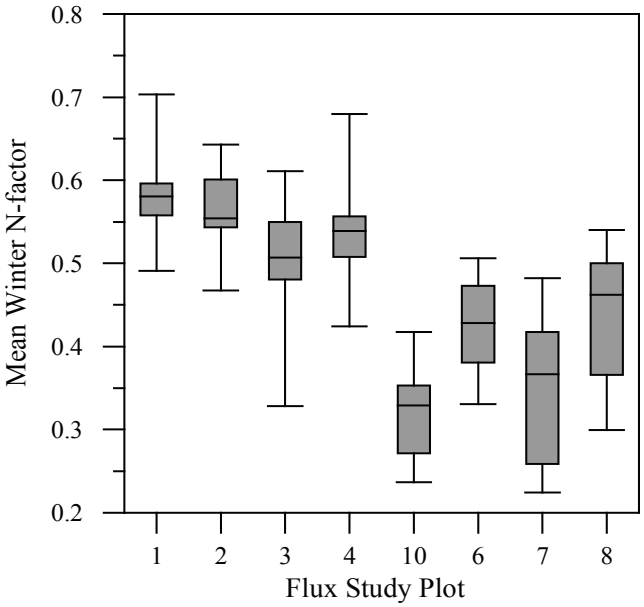


Figure 3. Box-and-whisker plots show the median, quartiles, and range of mean winter *n*-factors at each of the eight Flux Plots observed between 1995 and 2006.

gradient appears very distinct, snow depth at regional and microtopographic scales is an important factor determining ground temperature (Benson 1967, Gold 1967, Goodrich 1982). Vegetation should also be examined, as it can act to "trap" snow and prevent it from further displacement by wind gusts.

To examine these relationships, mean winter n-factors were plotted against the air and soil degree-day sums from which they were calculated (Fig. 4). $DDF_{air}$ values show general trends of warmer air temperatures, leading to higher n-factors (Fig. 4a). The magnitude of the n-factor varies strongly by site (Plot 1 having the largest and Plots 6 and 10 the smallest) while $DDF_{air}$ varies over a similar range. It is clear, therefore, that air temperature is not the sole determinant of the latitudinal gradient apparent in Figures 2 and 3.

The plot of $DDF_{soil}$ (Fig. 4b) indicates that soil temperature constitutes a much stronger control over mean *n*-factor values. The data have an almost linear relationship, with warmer soils corresponding to lower *n*-factors. The data cluster tightly by plot, with northern sites having larger *n*-factor values and southern sites being lower.

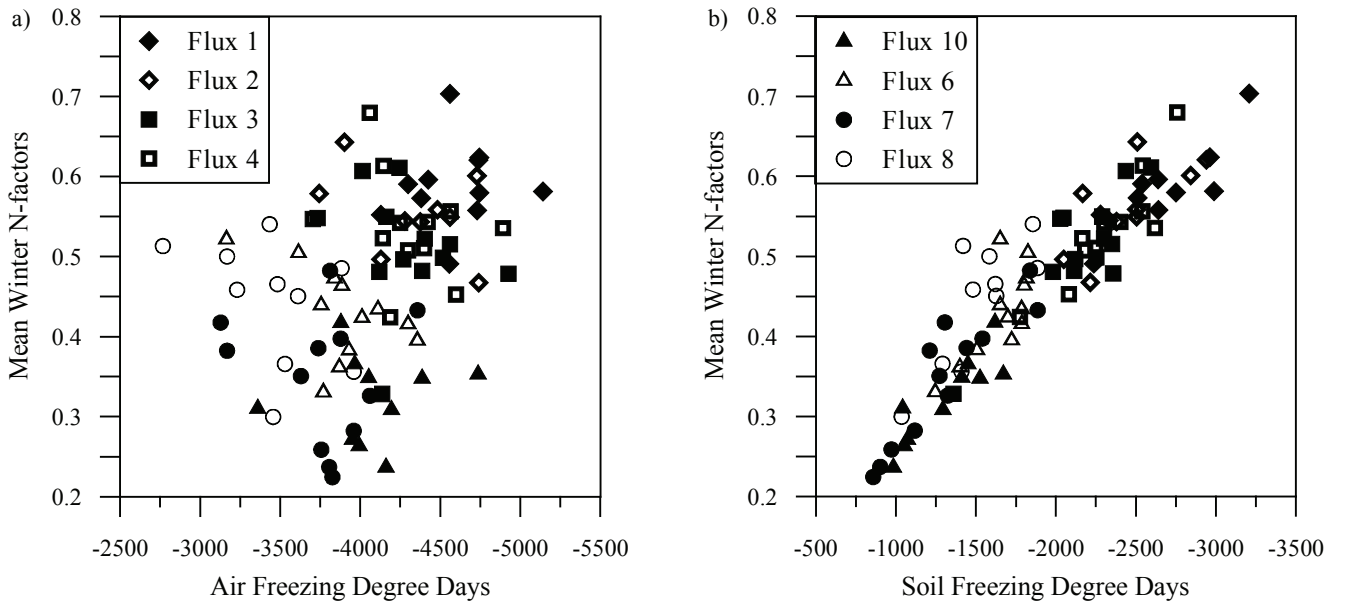


Figure 4. Mean winter air (a) and soil (b) degree days of freezing measured at each Flux Plot and graphed against mean winter n-factors. While air temperatures show no clear relationship, soil temperatures are directly related, reflecting the thermal influence of snow. X-axes have the same scale but different ranges.

Land cover within the region shows a general trend from moist nonacidic and wet sedge tundra complexes on the flat coastal plain, to a mix of acidic and shrub tundras in the foothills. The Flux Plots reflect these patterns (Walker & Bockheim 1995). Flux Plots 1 and 2 were chosen to include moist and wet complexes on the coastal plain. Plots 3 and 4 were selected as homogenous 1-ha areas of nonacidic and acidic tundra within close geographic proximity to each other (Walker & Bockheim 1995). The nonacidic tundra is characterized by the presence of Carex, Dryas, Eriophorum, and Hylocomium, while the acidic tundra has Eriophorum, Ledum, Betula, Hylocomium, and Salix with distinct tussock development (Walker & Bockheim 1995). Plots 6 and 8 are mixed acidic and shrub tundra and were included because of previous research done at those locations. Plot 7 is an acidic wetland. Site 10 was selected to represent a water-track, a shrubby wet first-order stream channel complex. The lower soil DDFs and n-factors at Plots 7 and 10 reflect their higher soil moisture contents. In the foothills, all 4 sites have the potential for drifting and scouring of snow, with slope angles ranging from 0° (Plot 7 in the bottom of a valley) to 15° at Plot 8. Sites 3, 6, 8, and 10 have slopes of more than 3°.

Taras et al. (2002) found that snow depth means and standard deviations were lower and less variable on the coastal plain than in the foothills. They were also able to categorize the amount of decoupling between air and soil temperatures using snow depth classes: 0–25 cm (highly coupled), 25–80 cm (coupled), and 80–200 cm (decoupled).

Although several studies have examined snow patterns on the North Slope, plot-level data were not available. Two SNOTEL sites, Sagwon and Imnavait, are located within the study area and have records covering the period 1995–2006. Each of these lies in close proximity to a pair of Flux Plots, in the Sagwon Hills (Plots 3, 4) and at Imnavait Creek (Plots 7, 8). Table 2 presents summary statistics of the accumulated precipitation (Oct–May) between 1995 and 2006 at these sites. While the mean winter precipitation at these sites is similar (approximately 8.7 cm), the range at Sagwon is just 1.0 while the Imnavait site range is 6.4 in.

Table 2. Summary statistics of the winter precipitation (Oct–May) accumulated at the available SNOTEL sites (cm). Seasons missing any monthly accumulation data were not used.

| | Sagwon | Imnavait |
|---|---|---|
| N | 6 | 10 |
| Minimum | 6.9 | 4.3 |
| Mean | 8.4 | 9.0 |
| Median | 8.8 | 7.2 |
| Maximum | 9.4 | 20.6 |
| Range | 2.5 | 16.3 |
| Stand. Dev. | 0.9 | 5.0 |

A crude assumption was made that the Sagwon site could represent general winter snow conditions in the northern portion of the study area while the Imnavait site would represent the southern. The Sagwon Hills are effectively the end of the coastal plain and beginning of the foothills province. Figure 5a shows the relationship between accumulated winter precipitation at Sagwon and mean winter n-factors at the four northern sites, while Figure 5b shows Imnavait and the southern sites.

Interestingly, the coastal sites furthest away from the Sagwon site seemed most closely related to interannual changes in snow depth. This presumably reflects that regional differences are important in areas that tend to be wind-blown with relatively shallow snowpack. In the south, no clear relationship is apparent. The documented variability of snow depth in the foothills (Taras et al. 2002) resulting

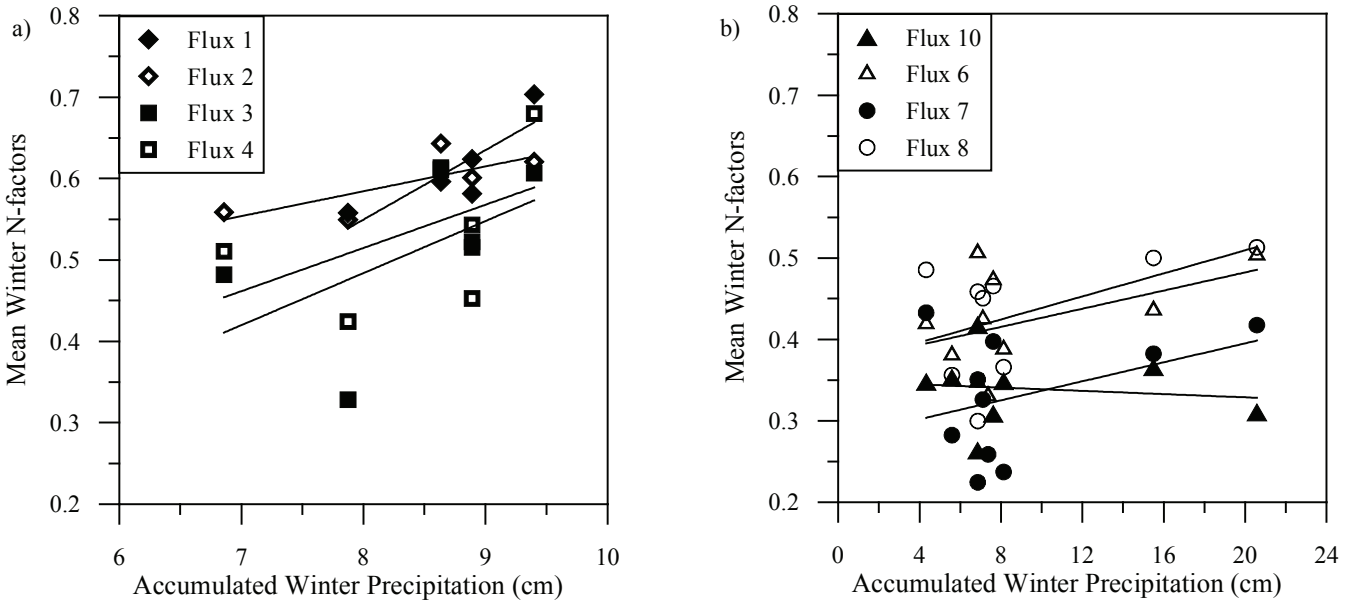


Figure 5. Accumulated winter precipitation (Oct–May) at SNOTEL sites plotted against mean winter *n*-factors in the northern (a) and southern (b) portion of the study area, represented by the Sagwon and Imnavait SNOTELs, respectively. The *x*-axes differ in scale.

from microtopography, vegetation, and wind-action is obfuscating the general interannual variability in snowpack conditions.

In comparison to previous work, the mean winter n-factors are higher than those found by Carlson (1952) and Taylor (1995) in central Alaska and the Mackenzie River Valley but similar to those observed by Karunaratne and Burn (2003, 2004) and Kade et al. (2006) in the Yukon Territory and northern Alaska. Snow depths may be thicker at Carlson's and Taylor's sites. In the study by Karunaratne and Burn (2003) in the Yukon between 1997 and 2000, n-factors ranged between 0.3 and 0.5 while the mean maximum snow depth observed ranged from 19–28 cm. Kade et al. (2006) calculated n-factors at a transect of three sites in northern Alaska overlapping the central and northern portions of the study area and found values of 0.3 and 0.6 at tundra sites bracketing the locations of Plots 3 and 4 and Sites 1 and 2.

## Conclusions

The unusual set of geographically diverse observations used in this study allowed interannual quantification of n-factor variability at a range of tundra sites over 12 winter seasons. The latitudinal gradient in mean winter *n*-factors values are related not just to air temperatures, but also to vegetation and snow depth, as previous work and theory suggest. However, the lack of in situ snow depth measurements prevents further detailed analysis of within-plot variability. Future work should consider methods for improving quantification of snowpack characteristics, both spatially and temporally in the region.

## Acknowledgments

This work was supported by the National Science Foundation under grants OPP-0095088 and 0352958. Opinions, findings, conclusions, and recommendations expressed in this paper are those of the authors and other CALM investigators, and do not necessarily reflect the views of the National Science Foundation. We are grateful for assistance with fieldwork from J. Riverstone (Mueller) and many graduate students and colleagues over the years.

## References

Benson, C.S. 1969. *The Seasonal Snow Cover of Arctic Alaska*. Washington D.C.: Arctic Institute of North America, 96 pp.

Buteau, S., Fortier, R., Delisle, G. & Allard, M. 2004. Numerical simulation of the impacts of climate warming on a permafrost mound. *Permafrost and Periglacial Processes* (15)1: 41-47.

Carlson, H. 1952. Calculation of depth of thaw in frozen ground. In: *Frost Action in Soils: A Symposium*, Highway Research Board Special Report 2 Washington, DC: National Research Council, 192-223.

Gold, L.W. 1967. Influence of surface conditions on ground temperature. *Canadian Journal of Earth Sciences* 4: 199-208.

Goodrich, L.E. 1982. The influence of snow cover on the ground thermal regime. *Canadian Geotechnical Journal* 19: 421-432.

Juliussen, H. & Humlum, O. 2007. Towards a TTOP ground temperature model for mountainous terrain in central-eastern Norway. *Permafrost and Periglacial Processes* (18)2: 161-184.

Kade, A., Romanovsky, V.E. & Walker, D.A. 2006. The n-factor of nonsorted circules along a climate gradient in Arctic Alaska. *Permafrost and Periglacial Processes* 17(4): 279-289.

Kane, D.L. & Reeburgh, W.S. 1998: Introduction to special section: Land-Air-Ice Interactions (LAII) Flux Study. *Journal of Geophysical Research* 103: 28913-28915.

Karunaratne, K.C. & Burn, C.R. 2003. Freezing n-factors in discontinuous permafrost terrain, Takhini River, Yukon Territory, Canada. In: *Proceedings of the 8th International Conference on Permafrost. Zurich: University of Zurich-Irchel*: 519-524.

Karunaratne, K.C. & Burn, C.R. 2004. Relations between air and surface temperature in discontinuous permafrost terrain near Mayo, Yukon Territory. *Canadian Journal of Earth Sciences* 41: 1437-1451.

Klene, A.E., Nelson, F.E., Shiklomanov, N.I. & Hinkel, K.M. 2001. The n-factor in natural landscapes: variability of air and soil-surface temperatures, Kuparuk River Basin, Alaska. *Arctic, Antarctic, and Alpine Research* 33(2): 140-148.

Lachenbruch, A.H., Sass, J.H., Marshall, B.V. & Moses, T.H. Jr. 1982. Permafrost, heat flow, and the geothermal regime at Prudhoe Bay, Alaska. *Journal of Geophysical. Research* (87)B11: 9301-9316.

NRCS 2007. *Accumulated Precipitation for Sagwon, Alaska.* URL: http://www.ak.nrcs.usda.gov/ Snow/snowsites.html.

Sturm, M., McFadden, J.P., Liston, G.E., Chapin, F. S. III, Racine, C.H. & Holmgren, J. 2001. Snow-shrub interactions in Arctic tundra: A hypothesis with climatic implications. *Journal of Climate* 14: 336-344.

Taras, B., Sturm, M. & Liston, G.E. 2002. Snow-ground interface temperatures in the Kuparuk River Basin, arctic Alaska: measurements and model. *Journal of Hydrometeorology* (3):44, 377-394.

Taylor, A.E. 1995. Field measurements of n-factors for natural forest areas, Mackenzie Valley, Northwest Territories. In: *Geological Survey of Canada, Current Research,* 1995-B: 89-98.

Wahrhaftig, C. 1965. *Physiographic Divisions of Alaska.* Washington, DC: United States Geological Survey.

Walker, D.A. & Bockheim, J.G. 1995: *Vegetation-Soil Characterization at the 12 Flux Tower Sites. ARCSS/ LAII/Flux Study.* LAII Science Management Office, University of Alaska Fairbanks, Fairbanks, AK.

# Geophysical Mapping of Isolated Permafrost Lenses at a Sporadic Permafrost Site at Low Altitude in the Swiss Alps

Christof Kneisel
*Department of Physical Geography, University of Würzburg, Germany*
Daniel Schwindt
*Department of Physical Geography, University of Trier, Germany*

## Abstract

Results of geophysical mapping of isolated permafrost lenses at a vegetated scree slope below the timberline using electrical resistivity tomography and refraction seismics are presented. In total, 20 geoelectrical and 10 seismic surveys were performed. Using 5 m spacing, survey length resulted in 175 m and 265 m arrays for the geoelectrical surveys and 115 m for the refraction seismic surveys. With respect to the large heterogeneity of the permafrost distribution, tomographic inversion schemes were used for data analyses and interpretation. Both electrical resistivity and refraction seismic surveys showed isolated anomalies of high resistivity and high velocity within the subsurface, especially in the lower parts of the scree slope. P-wave velocities of the isolated anomalies were between 1700-4300 m/s in a host material with velocities between 1000-1500 m/s. In most cases these locations coincide with the high-resistivity anomalies of the 2D resistivity tomography.

**Keywords:** electrical resistivity tomography; geophysical mapping; isolated permafrost; refraction seismics; scree slope; Swiss Alps.

## Introduction

The Upper Engadine is one of the mountain regions in Switzerland with widespread alpine permafrost occurrence. Discontinuous permafrost is encountered above 2400 m a.s.l. Below the timberline, sporadic permafrost is assumed to exist only at very shaded sites. One of these special places is situated in the Bever valley, which represents one of the few sites in Switzerland where isolated permafrost lenses could be confirmed by several geophysical techniques (Kneisel et al. 2000, Kneisel 2003, Kneisel & Hauck 2003). For a detailed geophysical mapping of the sporadic permafrost distribution joint application of electrical resistivity tomography and seismic refraction surveys have been applied.

There are several publications concerning joint application of geoelectrical surveys and refraction seismics for sounding of rock glacier permafrost using one-dimensional techniques (e.g., Vonder Mühll 1993, Wagner 1996, Ikeda 2006). Similar to electrical resistivity tomography, a tomographic variant of seismic refraction which has become increasingly important in the past few years can be applied yielding two-dimensional velocity distributions of the subsurface (e.g., Musil et al. 2002, Kneisel & Hauck 2003, Hauck et al. 2004, LeBlanc et al. 2004, Maurer & Hauck 2007).

With respect to the known small-scale heterogeneity as many as 20 geoelectrical and 10 seismic surveys were performed, of which characteristic profiles are shown. This paper significantly extends the earlier studies presented by the author (see above) by introducing a larger number of 2D geophysical surveys using tomographic inversion schemes for data analyses allowing for more detailed interpretation and conclusions.

## Site Description

The sporadic permafrost site below the timberline is located in the Bever Valley, a trough-shaped valley with bottom elevation between 1730 m and 1800 m a.s.l. at its lower end. Both the north- and south-exposed valley sides are wooded. At present the upper timberline is between 2200 m and 2300 m a.s.l. Larch (*Larix decidua*) and cembra pine (*Pinus cembra*) are the dominant tree species of the forest. Most parts of the scree slopes which occur below the rock walls are well covered with vegetation (Fig. 1). The soils are poorly developed and covered by an organic layer up to 30 cm thick. Below the organic layer, only a few centimeters of mineral soil exist. Mean annual air temperature at a nearby climate station in the Bever village at 1710 m a.s.l. is +1°C.

## Methods

*Electrical resistivity tomography (ERT)*

Since geoelectrical methods are most suitable for


Figure 1. North-exposed vegetated scree slopes in the Bever valley. Lines indicate location of survey profiles.

investigating a subsurface with distinct contrasts in conductivity and resistivity, geoelectrical soundings constitute one of the traditional geophysical methods which have become standard in permafrost research to detect mountain permafrost. Since a marked increase of the electrical resistivity occurs at the freezing point, the method is expected to be most suitable to detect, locate, and characterize structures containing frozen material. Based on the number of scientific publications in the last decade and the large variety of applications, the tomographic variant of the method (electrical resistivity tomography, ERT) is maybe the most universally applicable method in mountain studies (Kneisel & Hauck 2008).

Resistivity values of frozen ground can vary over a wide range depending on the ice content, the temperature, and the content of impurities. The dependence of resistivity on temperature is closely related to the amount of unfrozen water. Perennially frozen silt, sand, gravel, or frozen debris with varying ice content show resistivity values between 5 kOhm.m to several hundred kOhm.m (e.g., Haeberli & Vonder Mühll 1996, Hauck & Kneisel 2008).

For the presented research the two-dimensional (2D) electrical surveys were performed using the Wenner and Wenner Schlumberger configurations with 5 m spacing and an IRIS SYSCAL Junior Switch resistivity-meter. The measured apparent resistivities are used to build up a vertical contoured section showing the lateral and vertical variation of resistivity over the section. The conventional method of plotting the results for the interpretation is the so-called pseudosection which gives an approximate image of the subsurface resistivity distribution. High gradients in the subsurface resistivity distribution usually indicate interfaces between different layers. The measured sets of apparent resistivities were inverted using the software package RES2DINV. This inversion software tries to reduce the difference between the calculated and measured apparent resistivity values by adjusting the resistivity of the model blocks. Topographic corrections can be incorporated into the inversion algorithm which is an essential point for studies in alpine periglacial environments with often complex and heterogeneous topography. Further details on different array geometries and data processing are given for instance in Reynolds (1997) and Kneisel (2006).

*Refraction seismics*

Similar to the resistivity investigated by electric methods, the sharp increase of the seismic primary wave (P-wave) velocity at the freezing point is used to differentiate between frozen and unfrozen material. The P-wave velocity distribution can be used as a complementary indicator to resistivity for the presence of frozen material. The method is especially useful to determine the top of the permafrost layer, as the contrast for the P-wave velocity between the unfrozen top layer (= active-layer, 400-1500 m/s) and the permafrost body (2000-4000 m/s) is usually large. On the other hand, the values for most common rock types (e.g., gneiss or granite) are similar to the values for ice, so the detection of mountain permafrost is often difficult by using refraction seismic data alone. From this it becomes clear that for some permafrost applications refraction seismic has to be combined for instance with electric methods, in order to get unambiguous results in terms of permafrost delineation. A Geometrics Geode 24-channel seismograph and a cable with 5 m spacing were used for data acquisition. A total number of 10 shot points enabled the data set to be inverted with tomographic inversion schemes. The Pickwin and Plotrefa software was used for data processing and analyses. To create the starting model for each profile a 1D-time-term inversion was performed. The tomographic inversion scheme is based on a least squares algorithm. Topographic corrections were incorporated into the inversion algorithm. Further details on seismic data analyses are given in Palmer (1986) and Reynolds (1997).

## Results and Discussion

Profile L1 is situated in a clearing (Fig. 1) where the thickness of the organic layer varies between 15 and 25 cm. Two isolated high resistivity anomalies with a thickness of 10-15 m and a horizontal extent between 10-20 m are present in the ERT (Fig. 3). Maximum resistivities of more than 160 kOhm.m point to permafrost. This interpretation is confirmed by the results of the refraction seismic tomography with P-wave velocities of 4300 m/s for the lower anomaly. Though the upper anomaly shown in the ERT is not completely displayed in the refraction seismic tomogram, relatively warm permafrost (-0.2°C) is confirmed by temperature measurements in an 8 m deep borehole at this location (Fig. 2).

Both tomograms show a thin active-layer of 2-4 m depth, which is due to the isolating properties of the thick organic layer. This modelled active-layer depth compares well with the temperature measurements in the borehole. Measured in late October 2006, the maximum thaw depth had been reached.

High velocities and resistivities usually indicate high ice

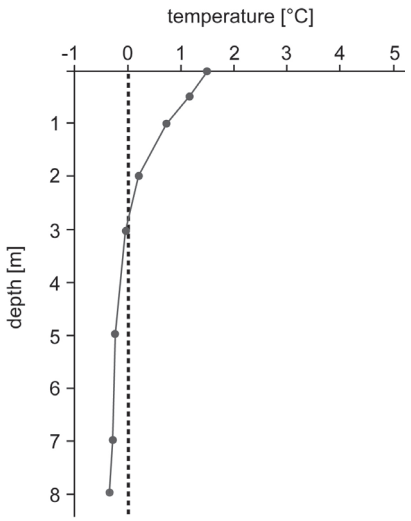


Figure 2. Borehole temperatures measured on 25.10.2006.

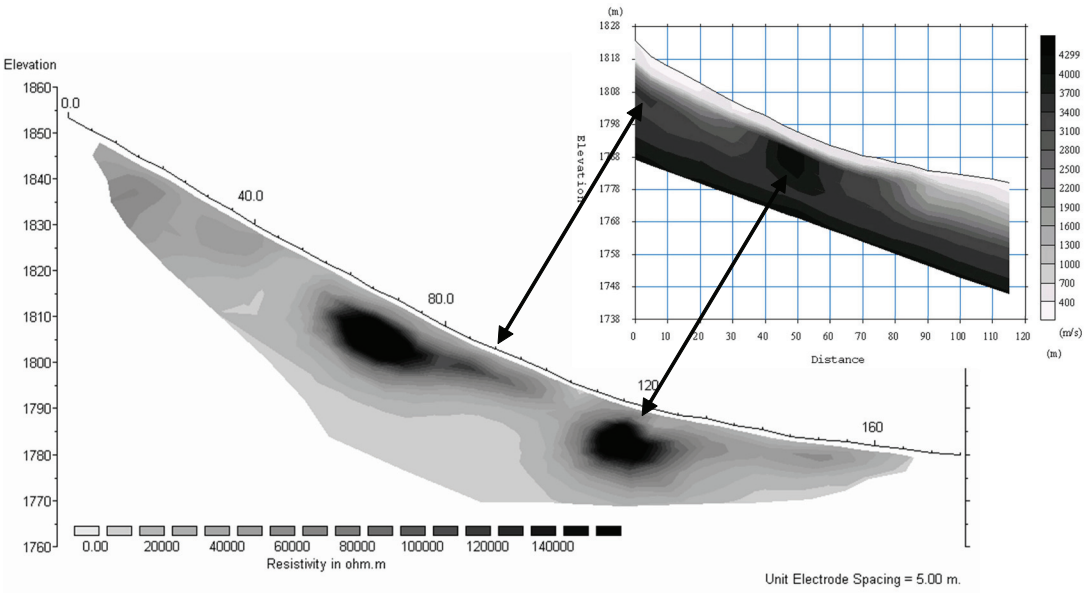


Figure 3. Electrical resistivity and refraction seismic tomograms of profile L1.

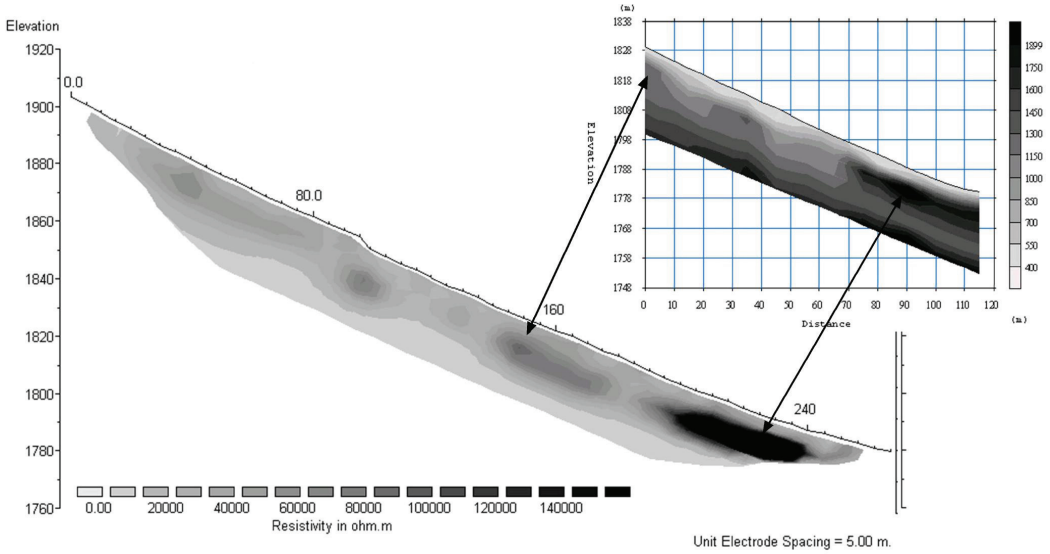


Figure 4. Electrical resistivity and refraction seismic tomograms of profile L3.

contents. Despite permafrost temperatures of only -0.2°C, the unfrozen water content is assumed to be relatively low, in the areas of the high resistivity and high velocity anomalies. The nearly linear decrease of resistivity values at greater depth indicates increasing unfrozen water content due to rising temperatures.

The ERT profile L3 (Fig. 4) shows two elongated high resistivity anomalies in the lower part of the scree slope. With resistivities of more than 160 kOhm.m the anomaly between 205 and 240 m of the ERT array is, situated in an area of coarse blocky material with low rates of fine grained material, covered with a thick organic layer of up to 30 cm. Despite relatively low P-wave velocities of 1900-2000 m/s this anomaly is assumed to represent permafrost. Low P-wave velocities at this place are most likely due to high contents of air filled voids. Profile L3 is assumed to be situated at the margin of a permafrost lens (Fig. 7). This is supported by results of a cross- and a parallel-measured profile, not shown in this paper.

The anomaly between 145 and 180 m of the ERT array and resistivities of 80-100 kOhm.m can be correlated with two anomalies in the refraction seismic tomogram. Unlike the lower parts of the profile, this area can be characterized by higher rates of fine grained material and an organic layer of about 20 cm. Despite of low P-wave velocities between 1500-1600 m/s permafrost can be assumed. If the high resistivities in this area were only due to air filled voids, seismic velocities should be much lower.

Without further research the anomalies above 1820 m a.s.l. in profile L3 cannot clearly be confirmed as permafrost, however the high resistivities are probably due to air filled voids and permafrost also in the upper parts of the scree slope.

The organic layer thickness in the area of profile L5 is comparatively thin, varying from 10-15 cm. In the ERT of profile L5 (Fig. 5) three anomalies with comparatively low resistivities of 60-100 kOhm.m are shown. The lower anomaly between 90 and 150 m can be compared with a more homogeneous area of high velocities (3000-3200 m/s) in the refraction seismic tomogram, hence are interpreted as permafrost. Below a depth of 10-15 m resistivities decrease nearly linear, indicating a decrease in ice content and/or increasing unfrozen water content. Ice rich, but "warm" permafrost can be assumed. High P-wave velocities exclude high amounts of air filled voids. The lower resistivities as compared to the other profiles could be due to comparatively higher unfrozen water content. Due to comparable conditions, concerning surface and subsurface properties, permafrost can also be assumed for the anomalies in the upper parts of the profile.

Very shaded conditions and a homogenous subsurface, with higher amounts of blocky material and an organic layer of about 20 cm is found in most parts of profile L7. Both, the ERT and the refraction seismic tomogram of profile L7 show an elongated high resistivity/high velocity anomaly between 1780 and 1815 m a.s.l., confirming probably ice-rich permafrost (Fig. 6). A thin active-layer of less than 2 m is

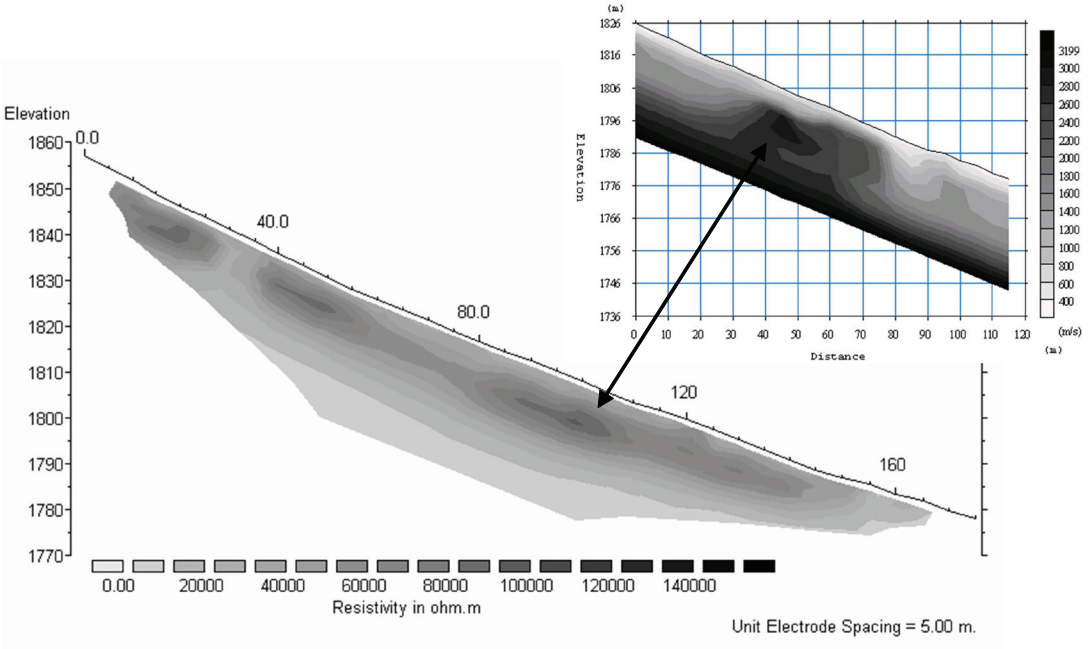


Figure 5. Electrical resistivity and refraction seismic tomograms of profile L5.

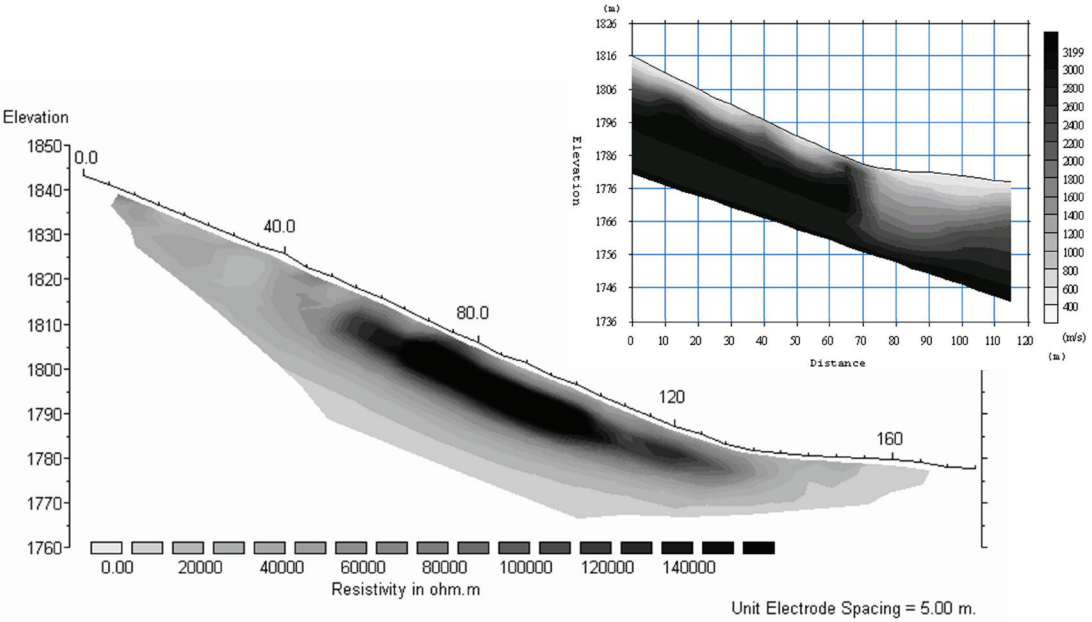


Figure 6. Electrical resistivity and refraction seismic tomograms of profile L7.

detected. However, these profiles had been measured in May 2007 and maximum thaw depth had not yet been reached. In contrast to the ERT, where resistivities slowly decrease up and down slope from the center of the permafrost lens, a sharp decrease to lower velocities is shown in the refraction seismic tomogram. Low resistivities and gradually increasing low P-wave velocities in the gently inclined lower parts of the profile could point to higher amounts of fine grained material in the subsurface.

Permafrost has been detected all over the investigated scree slope below 1840 m a.s.l. by extensive geophysical mapping (Fig. 7) however, permafrost distribution and characteristics are heterogeneous. In profiles L1 and L7 high resistivity/high velocity permafrost is present (Table 1, Fig. 7). Ice-rich permafrost with low amounts of unfrozen water and air cavities can be assumed. Lower resistivities but high P-wave velocities in profile L5 can be interpreted as ice-rich but warm permafrost with higher amounts of unfrozen water reducing the electrical resistivity. High resistivity/low velocity permafrost is to be found in profile L3. Due to very low amounts of fine grained material between the boulders many air cavities lead to high resistivities but low P-wave velocities.

Table 1. Comparison of maximum resistivities and P-wave velocities.

| Profile | maximum resistivity (kOhm.m) | maximum P-wave velocity (m/s) |
|---|---|---|
| L1 | >160 | 4100 |
| L3 | >160 | 1900-2000 |
| L5 | 90-100 | 2900 |
| L7 | 140->160 | 3100 |

## Conclusions

Joint application of electrical resistivity and refraction seismics has proven to be a useful approach at this heterogeneous permafrost site as they provide complementary information about the subsurface. With respect to the large heterogeneity of the permafrost distribution, tomographic inversion schemes were used for data analyses and interpretation for both methods.

Both, electrical resistivity and refraction seismic surveys showed isolated anomalies of high resistivity and high velocity within the subsurface, especially in the lower parts of the scree slope. P-wave velocities of the isolated anomalies were between 1700-4300 m/s in a host material with velocities between 1000-1500 m/s. These locations coincide with the high-resistivity anomalies of the 2D resistivity tomography. Due to the P-wave velocities between 1700-4300 m/s, the high-resistive anomalies can be characterised as permafrost lenses, because air cavities would result in much smaller P-wave velocities. In most cases the results of both techniques coincide very well. Results of the refraction seismic tomography also point to a thin active-layer, especially in the lower parts of the scree slope. This can be due to the isolating properties of the thick layers of organic material which is, among other factors, responsible for the occurrence of this sporadic permafrost at low altitude.

The ground thermal regime is assumed to be a result of the interaction of climatic conditions with topography (northern exposure, small amount of incoming radiation, frequent temperature inversions in winter, distribution and duration of snow cover) as well as surface and subsurface factors (organic layers, coarse blocky material).

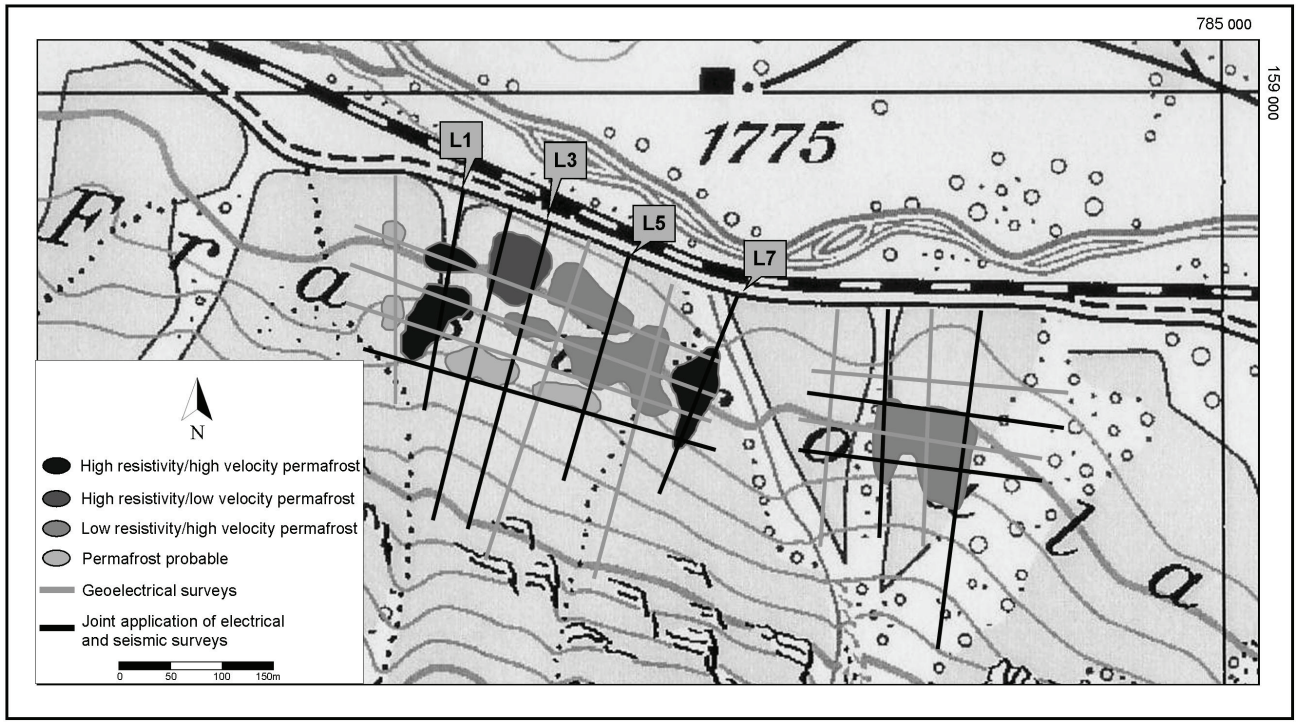


Figure 7. Location of geophysical surveys and inferred permafrost lenses in the Bever Valley.

## References

Haeberli, W. & Vonder Mühll, D. 1996. On the characteristics and possible origins of ice in rock glacier permafrost. *Zeitschrift für Geomorphologie* N.F. Suppl. 104: 43-57.

Hauck, C., Isaksen, K., Vonder Mühll, D. & Sollid, J.L. 2004. Geophysical surveys designed to delineate the altitudinal limit of mountain permafrost: an example from Jotunheimen, Norway. *Permafrost and Periglacial Process* 15(3): 191-205.

Hauck, C. & Kneisel, C. 2008. *Applied geophysics in periglacial environments.* Cambridge University Press, in press.

Ikeda, A. 2006. Combination of conventional geophysical methods for sounding the composition of rock glaciers in the Swiss Alps. *Permafrost and Periglacial Processes* 17: 35–48.

Kneisel, C. 2003. Sporadic and discontinuous mountain permafrost occurrence in the Upper Engadine, eastern Swiss Alps. *Proceedings of the 8th International Conference on Permafrost*, *Zurich, Switzerland*: 561-566.

Kneisel, C. 2006. Assessment of subsurface lithology in mountain environments using 2D resistivity imaging. *Geomorphology* 80: 32-44.

Kneisel, C., Hauck, C. & Vonder Mühll, D. 2000. Permafrost below the timberline confirmed and characterized by geoelectrical resistivity measurements, Bever Valley, eastern Swiss Alps. *Permafrost and Periglacial Processes* 11(4): 295-304.

Kneisel, C. & Hauck, C. 2003. Multi-method geophysical investigation of a sporadic permafrost occurrence. In: L. Schrott, A. Hoerdt, & R. Dikau (eds.), Geophysical methods in geomorphology. *Zeitschrift für Geomorphologie*, Suppl. 132: 145-159.

Kneisel, C. & Hauck, C. 2008. Electrical methods. In: C. Hauck & C. Kneisel (eds.), *Applied Geophysics in Periglacial Environments*. Cambridge University Press, in press.

LeBlanc, A.M., Fortier, R., Allard, M. & Cosma, C.G. 2004. Seismic cone penetration test and seismic tomography in permafrost. *Canadian Geotechnical Journal* 41: 796-813.

Maurer, H. & Hauck, C. 2007. Geophysical imaging of alpine rock glaciers. *Journal of Glaciology* 53(180): 110-120.

Musil, M., Maurer, H., Green, A.G., Horstmeyer, H., Nitsche, F., Vonder Mühll, D. & Springman, S. 2002. Shallow seismic surveying of an Alpine rock glacier. *Geophysics* 67(6): 1701-1710.

Palmer, D. 1986. Refraction Seismics. In: Helbig & Treitel (eds.), *Handbook of Geophysical Exploration. Seismic Exploration 13*. London-Amsterdam: Geophysical Press.

Reynolds, J.M. 1997. *An Introduction to Applied and Environmental Geophysics*. Chichester: Wiley.

Vonder Mühll, D. 1993. Geophysikalische Untersuchungen im Permafrost des Oberengadins. - Mitt. Versuchsanst. Wasserbau, Hydrologie und Glaziologie, ETH Zürich, 122: 222 pp.

Wagner, S. 1996. DC resistivity and seismic refraction soundings on rock glacier permafrost in northwest Svalbard. *Norsk Geografisk Tidsskrift* 50: 25-36.

# Thawing Permafrost and Temporal Variation in the Electrical Conductivity of Water in Small Tundra Lakes, Mackenzie Delta Region, N.W.T., Canada

S.V. Kokelj
*Water Resources Division, Indian and Northern Affairs Canada, Yellowknife, NT, Canada*
B. Zajdlik
*Zajdlik and Associates, Inc.*
M.S. Thompson
*Water and Climate Impacts Research Centre, Department of Geography, University of Victoria, Victoria, Canada*
R.E.L. Jenkins
*Water Resources Division, Indian and Northern Affairs Canada, Yellowknife, NT, Canada*

## Abstract

Temporal variation in the late summer water quality of 21 small tundra lakes in the Mackenzie Delta region was investigated from 2003 to 2007. Ten lakes were undisturbed, eight had thaw slump scars in their catchments, and three were impacted by highly active thaw slumps. The electrical conductivities (EC) of lake waters from 2003–2007 varied significantly between most lakes. The greatest differences were between the disturbed lakes with elevated EC and undisturbed lakes with relatively low EC. Over the study period, the lowest and highest late-summer lake water EC were recorded in 14 of 21 lakes in association with the wettest preceding year (2006), and driest preceding winter (2003), respectively. This suggests that the chemistry of small tundra lakes is sensitive to variations in the annual water balance. Over time, the greatest relative variation in EC within lakes was associated with undisturbed lakes with unique catchment characteristics and lakes with large active thaw slumps. Intense slumping caused lake water EC to increase, and stabilization was associated with a decreasing trend.

**Keywords:** climate change; lake chemistry; Mackenzie Delta region; retrogressive thaw slumping; tundra lakes.

## Introduction

Impacts to northern aquatic systems are anticipated with climate warming due to the modification of hydrological processes, increases in water temperature and terrestrial biomass, and intensification of disturbance regimes (Rouse et al. 1997, Jorgenson et al. 2006, Lantz & Kokelj, 2008). It is well documented that water in small tundra lakes is generally low in ionic concentration because runoff derived from snowmelt and rainfall is rapidly transported through a thin nutrient-poor active layer (Quinton & Marsh 1999, Kokelj & Burn 2005). Interannual variations in precipitation and catchment runoff should then influence the chemistry of these lakes (Rouse et al. 1997). Furthermore, there is a geochemical contrast between the leached active layer soils and the underlying ion-rich permafrost so that degradation of near-surface permafrost due to -active layer deepening or thaw slumping (Fig. 1) may modify the chemistry of soils, slope runoff, and waters in adjacent lakes and ponds (Kokelj & Lewkowicz 1999, Kokelj et al. 2002, Kokelj et al. 2005, Keller et al. 2007).

The physical and chemical characteristics of small lakes affected by retrogressive thaw slumps and adjacent undisturbed tundra lakes were described by Kokelj et al. (2005), and here we examine temporal variations in the electrical conductivity (EC) of water in these lakes from 2003 to 2007. Since runoff from areas affected by thawing permafrost is solute-rich (Kokelj & Lewkowicz 1999), we hypothesized that the ionic concentrations as indicated by EC would increase with time in lakes affected by active thaw slumps, whereas the stabilization of a slump may cause lake water ionic concentration to stabilize or decrease. It is reported that solute concentrations in lakes with stable thaw slumps are elevated with respect to undisturbed lakes (Kokelj et al. 2005), but relative interannual variability of the two populations may be similar due to the influence of regional climate conditions. To test these hypotheses, the chemical characteristics of water in the ten undisturbed lakes and the 11 lakes affected by recently stabilized and active slumps between Inuvik and Richards Island were evaluated in late summer from 2003 to 2007 (Fig. 2). Temporal patterns in EC are examined with respect to precipitation patterns and disturbance status. The implications of climate-induced permafrost degradation on lake chemistry are discussed and variability in water quality conditions is considered with respect to defining baseline water quality conditions for assessing environmental impacts of northern development.

## Environmental Setting

The study lakes are in upland terrain east of the Mackenzie River Delta between Inuvik and the Beaufort Sea coast (Fig. 2). Kokelj et al. (2005) described the study area so that only a brief overview is provided here. The region is characterized by thousands of small lakes and ponds, most of which occur in glaciogenic deposits derived from carbonate and shale bedrock of the Mackenzie Basin (Rampton 1988, Mackay 1992, Burn 2002). As a result, calcium and sulphate are dominant ionic constituents of lake water (Kokelj et al. 2005).

Figure 1. Large, recently stabilized retrogressive thaw slump, Lake 10B. The thaw slump scar is about 7 ha in area. Note active slumps are developing in the scar zone in the upper part of photograph.

Lakes occupy between 10 and 20% of the landscape in the vicinity of the study lakes and median lake areas are on the order of a few hectares (Kokelj et al. 2005). Terrain is underlain by ice-rich permafrost and thaw slumps are common throughout the region (Fig. 1) (Mackay 1963, Rampton 1988). From 8 to 17% of water bodies in the vicinity of the study lakes are influenced by thermokarst slumping (Kokelj et al. 2005).

## Study Lakes

Twenty-one study lakes between Inuvik and Richards Island were selected following analysis of aerial photographs and field reconnaissance in 2002 (Fig. 2). Small lakes with first-order catchments were selected (Table 1). Catchment, lake. and thaw slump disturbance areas were estimated by digitizing respective parameters on georeferenced, orthorectified, 1:30,000 scale, colour aerial photographs from 2004. Field reconnaissance and re-correction of aerial photographs has resulted in minor modifications to the aerial estimates of catchment and disturbance areas reported in Kokelj et al. (2005) (Table 1).

The lakes are in shrub and low shrub tundra environments in rolling terrain (Ritchie 1984). The small lakes (1 to 18 ha) are within headwater catchments that range from 7 to 92 ha. Eleven of the catchments (Lakes 1B to 11B) contain retrogressive thaw slumps, which occur on slopes surrounding the study lakes and occupy from 4 to 35% of the respective watershed areas (Fig. 1, Table 1). Lakes 5B, 9B and 10B were impacted by highly active slumping for at least a portion of the five-year study period. Slumping at 5B and 10B stabilized in 2004 and 2003, respectively, with activity at 10B increasing again in 2007. Lake 9B had a large and highly active slump for the first three years of study, but as the slump grew upslope, the headwall diminished and activity decreased in 2006 and 2007. Ten undisturbed lakes (Lakes 1A to 11A) are situated near disturbed catchments (Fig. 2). Time series data were not available for Lake 7A. The

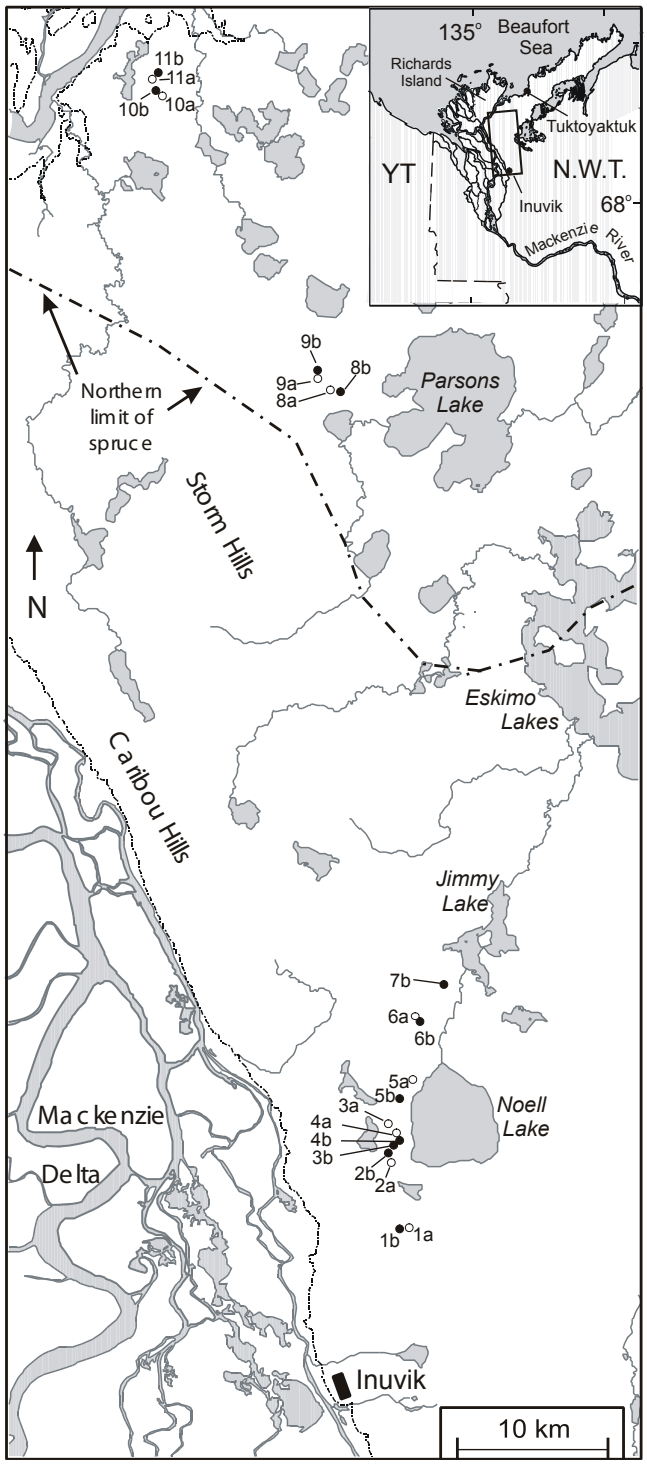


Figure 2. Map of tundra upland study lakes east of Mackenzie Delta, NWT.

southern portion of the study area was burned by wildfire in 1968, affecting catchments 1A, 1B, 2A, 2B, 3A, 3B, 4A, and 4B (Landhäuser & Wein 1993, Mackay 1995). Burned areas are colonized by dense alder and willow bush and active-layeractive layer thicknesses are generally greater than in the nearby tundra (Landhäuser & Wein 1993). Lake depth, determined at the centre of each lake, ranged from 11.3 m at Lake 3B to 1.6 m at Lake 8A, but the deepest parts of

small lakes and ponds may be located away from the centre. Maximum late winter ice thickness in 2003 and 2007 did not exceed 1.5 m, and therefore, even the shallowest lakes did not freeze to the bottom. Profiles obtained during late summer surveys suggest that portions of lakes over about 6 m deep may be thermally and chemically stratified in late summer (Kokelj et al. 2005, Fig. 3).

## Methods

From 2003 to 2007, during late August or the first week of September, surface water samples were obtained from the centre of each lake using a helicopter equipped with floats. Water samples were collected in 1 L polyethylene bottles rinsed three times with sample site water prior to collection. Sampling depth was about 50 cm. Following collection, sample bottles were placed in a cooler with ice packs and returned to the laboratory for analysis. Water samples were analyzed following standard methods taken from Clesceri et al. (1998). Specific EC and total alkalinity were measured on unfiltered samples in the laboratory using a Titralab radiometer. Anions and cations were evaluated by ion chromatography and hardness was calculated as the sum of inorganic calcium and magnesium using:

$$\text{Hardness (mg/L)} = 2.497 \times \text{Ca(mg/L)} + 4.117 \times \text{Mg(mg/L)}$$

Potential effects of lake and year on EC in undisturbed and disturbed lakes were tested using a randomized complete block design with years as blocks (Sokal & Rohlf 1995) followed by *post hoc* multiple comparisons using Tukey's test to control the experiment-wise Type 1 error rate. As lakes were not replicated, the interaction between year and lake could not be tested. Since multiple comparisons of means among lakes collapse data over years, the assumption of no year-lake interaction must be met if there is a significant effect. Although this assumption could not be tested, time series graphics of EC by lake provide no evidence of lake-year interaction. Residual diagnostics including Shapiro-Wilk's test of normality, visual assessment of leverage, plot residuals versus observed values, and a plot of fitted versus observed values indicate no concerns with assumptions of the statistical model (Sokal & Rohlf 1995). Relative variation in the conductivity of individual lakes over time was described by the coefficient of variation (CV) (Sokal & Rohlf 1995). Relations between water quality parameters and temporal variation in EC between lakes were explored using Spearman's rank correlations (Sokal & Rohlf 1995). Interpretation of the correlation results were regarded as tentative due to the likely low power of the between-lake EC tests because of small sample size and the large number of tests which adversely affect Type 1 error rate. Statistical analyses were conducted in R (R Development Core Team, 2007).

## Results

*Lake water ionic concentrations, 2003–2007*

Electrical conductivity (EC) in late summer surface water samples collected from 2003–2007 was strongly correlated with major ions (Ca, Mg, K, Na, and $SO_4$; $P < 0.0001$) (also, see Kokelj et al. 2005; Table 3). This indicates that EC is a good descriptor of ionic strength in the water of the study lakes. In the undisturbed lakes, the highest late summer conductivities from 2003–2007 were observed in Lake 3A (160 to 185 µS/cm), which is one of the more southerly catchments and was burned in 1968 (Fig. 3). The lowest conductivities over this period were observed in Lake 9A (38.9 to 44.2 µS/cm), located in hilly upland tundra on the eastern slope of the Storm Hills (Fig. 2). The mean EC of undisturbed lakes from 2003 to 2007 was 104.5, 94.7, 93.2, 87.2, and 96.7 µS/cm, respectively. Analysis of variance shows that EC in undisturbed lakes varies significantly with year and lake, with the largest variation being associated with between lake differences (Table 2a, Fig. 3). Tukey's honest significant difference procedure indicates that, with four exceptions, the disturbed lakes, across years, are significantly different from one another. The *post hoc* testing also showed that in 2003, the mean EC of undisturbed lakes was significantly higher than in 2004 through 2006, but not 2007, and that EC in 2006 was significantly lower than that in 2007.

Ionic concentrations in lakes affected by retrogressive thaw slumping were always elevated with respect to undisturbed lakes (Figs. 3 & 4) (Kokelj et al. 2005). Lake 10B, had the highest lake water EC of any disturbed lake

Table 1. Lake area and catchment characteristics and coefficients of variation (CV) of late summer EC, 2003–2007, for ten undisturbed lakes and 11 lakes affected by retrogressive thaw slumping, tundra uplands, Mackenzie Delta region.

| Lake No. | Lake area (ha) | Catchment area (ha) | Slump area (ha) | Slump status Active - A Stable - S | CV |
|---|---|---|---|---|---|
| *Undisturbed* | | | | | |
| 1A | 1.1 | 10.9 | - | - | 0.0737 |
| 2A | 2.0 | 17.2 | - | - | 0.1007 |
| 3A | 1.3 | 13.1 | - | - | 0.0669 |
| 4A | 1.2 | 15.5 | - | - | 0.0979 |
| 5A | 2.9 | 20.9 | - | - | 0.0799 |
| 6A | 3.6 | 19.7 | - | - | 0.1144 |
| 8A | 2.1 | 24.4 | - | - | 0.0947 |
| 9A | 3.1 | 29.3 | - | - | 0.0547 |
| 10A | 2.3 | 26.3 | - | - | 0.0475 |
| 11A | 9.8 | 70.1 | - | - | 0.1034 |
| *Disturbed* | | | | | |
| 1B | 18.0 | 91.6 | 3.3 | A/S | 0.0644 |
| 2B | 4.9 | 15.9 | 0.9 | S | 0.0397 |
| 3B | 4.0 | 15.3 | 3.6 | S | 0.0499 |
| 4B | 5.0 | 17.8 | 2.5 | S | 0.0495 |
| 5B | 2.8 | 27.7 | 2.0 | A | 0.1418 |
| 6B | 1.2 | 7.5 | 0.8 | S | 0.0349 |
| 7B | 3.1 | 34.7 | 1.0 | A/S | 0.0600 |
| 8B | 6.5 | 32.7 | 4.0 | A/S | 0.0482 |
| 9B | 3.6 | 7.2 | 2.5 | A | 0.0650 |
| 10B | 11.4 | 23.3 | 7.2 | A/S | 0.0318 |
| 11B | 10.5 | 39.4 | 2.5 | A/S | 0.0378 |

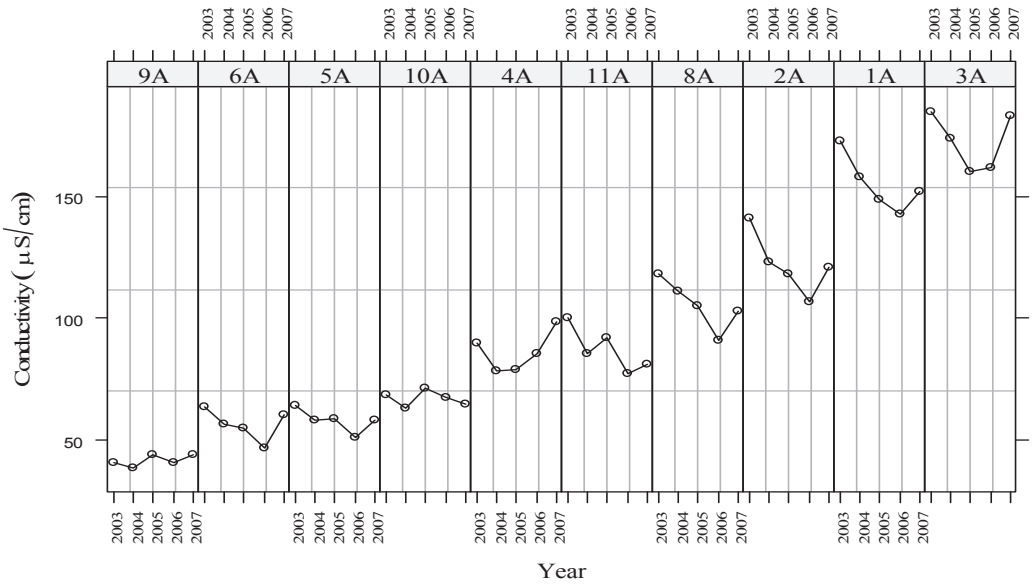


Figure 3. Electrical conductivity of lake water, undisturbed lakes 2003–2007, Mackenzie Delta region.

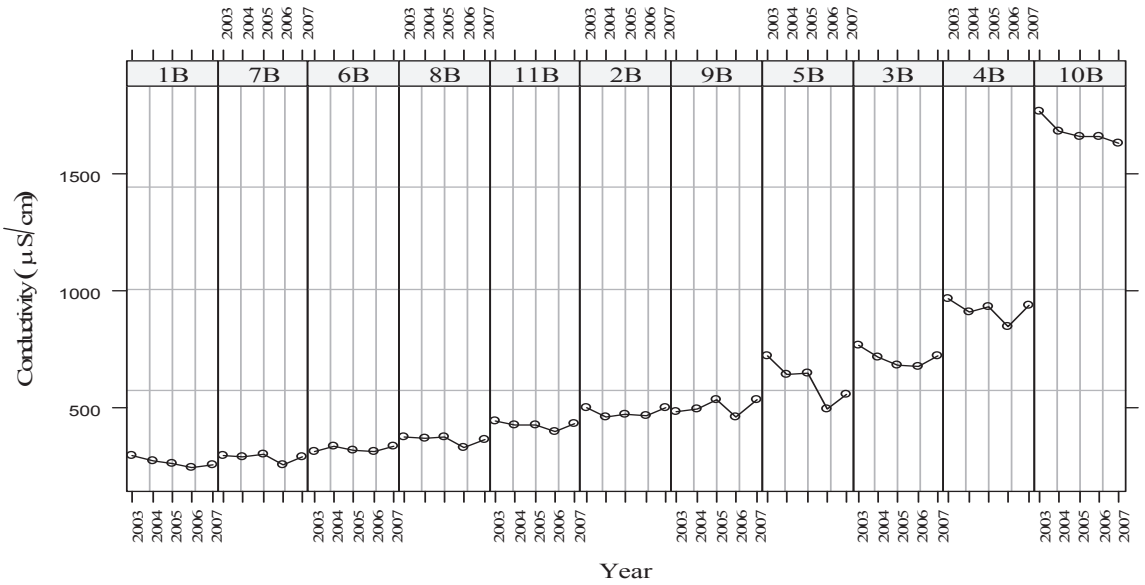


Figure 4. Electrical conductivity of lake water, lakes affected by slumping 2003–2007, Mackenzie Delta region.

and the greatest proportion of catchment area affected by slumping (Fig. 4, Table 1). The most southerly lake, 1B, had the smallest proportion of catchment area influenced by slumping and the lowest EC values. Yearly mean EC of the 11 lakes impacted by slumping from 2003 to 2007 was 631.7, 600.8, 602.5, 561.0, and 597.0 µS/cm, respectively. Table 2b shows that both lake and year are significant factors describing conductivity in the disturbed lakes and as expected the effect of lake (Kokelj et al. 2005) is much larger than that of year. The *post hoc* testing indicated that most lakes are significantly different from one another and that conductivity in 2006 is significantly lower than in 2003 through 2005.

Spearman's rank correlations of late summer lake water EC from 2003 to 2007 indicated significant positive associations between 36 pairs of lakes (Figs. 3, 4). It is also interesting to note the highest late summer EC was measured in 2003 for 14 of the 21 lakes, and the lowest lake water EC was also measured in 14 of 21 lakes in summer 2006 (Figs. 3, 4). Variability in late summer EC over years was described for each of the 21 lakes by calculating their CV (Table 1). Electrical conductivities of lakes 6A and 11A had the highest CV for the undisturbed population. The EC of lakes affected by retrogressive thaw slumping appear to be less variable than the undisturbed lakes, but this is due to the much higher ionic concentrations in disturbed lakes (Figs. 3, 4, Table 1) (Kokelj et al. 2005). Among the disturbed lakes, the highest CV for EC occurred in lakes 5B, 9B, and 1B. The first two lakes were characterized by large areas of highly-active slumping, and Lake 1B is in the largest study catchment and has a relatively large slump that reactivated in 2006 (Table 1).

Table 2. ANOVA table for conductivity in a) undisturbed lakes and b) lakes affected by thaw slumping.

| Source | Degrees of freedom | Mean square | F-statistic | P-value |
|---|---|---|---|---|
| *a)Undisturbed lakes* | | | | |
| Lake | 9 | 9488 | 9.8968 | <0.0001 |
| Year | 4 | 391 | 240.0757 | <0.0001 |
| Error | 36 | 40 | | |
| *b)Disturbed lakes* | | | | |
| Lake | 10 | 836065 | 874.3637 | <0.0002 |
| Year | 4 | 6964 | 7.2826 | <0.0001 |
| Error | 40 | 956 | | |

## Discussion

In the study region, tundra lakes are characterized by low ionic concentrations typically less than 100 µS/cm (Pienitz et al. 1997, Kokelj et al. 2005). Local variations in terrain and catchment conditions contribute to between lake differences in the EC of lake water (Figs. 3, 4, Table 2). For example, amongst undisturbed lakes, the highest lake water EC (1A, 2A, 3A) was associated with catchments that were burned in 1968 (Kokelj et al. 2005). Active layer deepening and thawing of near-surface permafrost can release soluble materials which may be transported to the lakes by surface runoff. Amongst the undisturbed lakes, the greatest relative variation in late summer EC (Table 1) was associated with lakes that possess unique catchment characteristics, including the influence of periodic icings and flooding by a nearby stream (6A), and large catchment areas which may experience interannual variation in contributory areas (11A).

End of summer EC from 2003–2007 covaried between many disturbed and undisturbed lakes (Figs. 3, 4). Although we interpret these results cautiously, the correlations suggest the influence of a regional driver. Mean conductivities of both disturbed and undisturbed lakes were notably high in 2003 and low in 2006. The minimum end of summer EC occurred in 14 of 21 lakes in August 2006, which was preceded by the wettest summer and year (Fig. 5). In contrast, EC highs in 14 of 21 individual lakes were recorded in August 2003, which was preceded by the driest winter. These observations suggest that the ionic chemistry of these lakes is sensitive to annual variations in the seasonal water balance.

Regardless, Table 2 emphasizes that between-lake differences have a greater relative influence over EC than does year. Figures 3 and 4 highlight the importance of permafrost degradation on between lake differences in EC as well as on the temporal variations in the chemistry of disturbed lakes. Lakes affected by retrogressive thaw slumping possess elevated ionic concentrations and EC with respect to undisturbed lakes because soluble materials released from thawing permafrost are transported to the lakes by surface runoff (Figs. 3, 4) (Kokelj et al. 2005). The intensity of ionic effects on lake water is positively associated with the proportion of catchment area affected by disturbance (Kokelj et al. 2005). Slumping also appeared to influence temporal variability in lake water EC. The highest coefficients of variation in late summer EC of disturbed lakes were associated with lakes affected by active slumping (Table 1). As hypothesized, intense slumping activity was associated with increasing EC (9B, 2003–2005) because thaw slumping exposes soluble materials that may be transported from disturbed slopes to the lake by surface runoff (Kokelj & Lewkowicz 1999). Stabilization of large active slumps was associated with a decreasing trend in EC, likely because the source of soluble materials is diminished with time (5B, 2005–2007; 10B, 2003–2007) (Fig. 4). It should be pointed out that temporal variation in ionic strength of water in the lakes 9B and 10B did not correlate with any of the other study lakes. In these lakes, effects of slumping subsumed the effects of a regional driver which appears to be influencing the EC of many other study lakes.

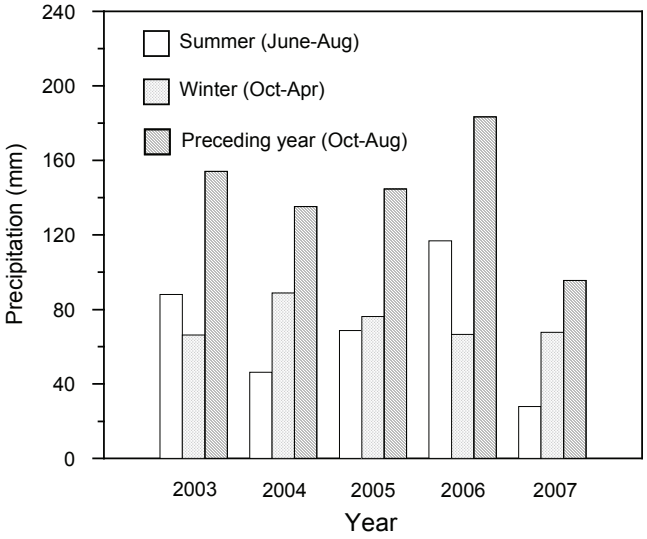


Figure 5. Precipitation for preceding summer, winter and year, Tuktoyaktuk, NWT (Environment Canada 2007).

Permafrost temperatures are rising in response to 20th Century climate warming in Alaska and northwestern Canada and the frequency and magnitude of terrain disturbances associated with thawing permafrost is increasing (Serreze et al. 2000, Jorgenson et al. 2006, Lantz & Kokelj, 2008). An acceleration of thermokarst activity in conjunction with the geochemical response of lakes to slump growth (Fig. 4) suggests that permafrost disturbance could grow in importance as a driver of lake water chemistry.

In addition to anticipating impacts of climate change on tundra lakes, understanding factors that influence temporal variation in water chemistry is critical to establishing baseline water quality conditions for aquatic effects-monitoring programs. These programs are becoming regulatory requirements for assessing impacts and determining effectiveness of mitigations associated with resource development projects in Canada's North. The study lakes highlight the importance of considering catchment characteristics such as thaw slumping and lake sensitivity to interannual variations in the water balance when selecting reference lakes for the establishment of baseline conditions.

## Conclusions

From these results the following conclusions are drawn:

1. Small lakes affected by thermokarst slumping have elevated EC relative to undisturbed lakes.

2. The largest degree of temporal variation in ionic strength of undisturbed tundra lakes occurred in association with unique catchment characteristics.

3. Patterns of variation in late summer EC appeared to be similar amongst many small tundra lakes. End of summer lake water EC may be sensitive to the annual water budget.

4. Amongst the disturbed lakes, those influenced by active slumping showed the greatest degree of variability in lake water EC. Increasing lake water EC was observed in a lake with a large rapidly growing slump and a decline in lake water EC was observed in lakes where large slumps have recently stabilized.

## Acknowledgments

This work was supported by the Department of Indian Affairs and Northern Development, the Inuvialuit Joint Secretariat, the Natural Sciences and Engineering Research Council of Canada, the Northern Chair, C.R. Burn, and the Aurora Research Institute. Field assistance by Douglas Esagok and Nathen Richea is gratefully acknowledged.

## References

Burn, C.R. 2002. Tundra lakes and permafrost, Richards Island, western Arctic coast, Canada. *Canadian Journal of Earth Sciences* 39: 1281-1298.

Clesceri, L.S., Greenberg, A.E. & Eaton, A.D. 1998. *Standard methods for the examination of water and wastewater, 20th Edition*. American Public Health Association. Washington, D,C.: United Book Press.

Environment Canada. 2007. *Canadian climate data online*. Available from http://www.climate.weatheroffice.ec.gc.ca/climateData/monthlydata_e.html

Jorgenson, M.T., Shur, Y.L. & Pullman, E. R. 2006. Abrupt increase in permafrost degradation in Arctic Alaska. *Geophysical Research Letters* 33.

Keller, K., Blum, J.D. & Kling, G.W. 2007. Geochemistry of soils and streams on surfaces of varying ages in Arctic Alaska. *Arctic, Antarctic and Alpine Research* 39: 84-98.

Kokelj, S.V. & Burn, C.R. 2005. Geochemistry of the active layer and near-surface permafrost, Mackenzie delta region, Northwest Territories, Canada. *Canadian Journal of Earth Sciences* 42: 37-48.

Kokelj, S.V., Jenkins, R.E., Milburn, D., Burn, C.R. & Snow, N. 2005. The influence of thermokarst disturbance on the water quality of small upland lakes, Mackenzie Delta region, Northwest Territories, Canada. *Permafrost and Periglacial Processes* 16: 343-353.

Kokelj, S.V. & Lewkowicz, A.G. 1999. Salinization of permafrost terrain due to natural geomorphic disturbance, Fosheim Peninsula, Ellesmere Island. *Arctic* 52: 372-385.

Kokelj, S.V., Smith, C.A.S. & Burn, C.R. 2002. Physical and chemical characteristics of the active layer and permafrost, Herschel Island, western arctic coast, Canada. *Permafrost and Periglacial Processes* 13: 171-185.

Lantz, T.C. & Kokelj, S.V. 2008. Increasing rates of retrogressive thaw slump activity in the Mackenzie Delta region, N.W.T. Canada. *Geophysical Research Letters* (in press).

Landhäusser, S.M. & Wein, R.W. 1993. Postfire vegetation recovery and tree establishment at the Arctic treeline: climate-change-vegetation-response hypotheses. *Journal of Ecology* 81: 665-672.

Mackay, J.R. 1963. The Mackenzie Delta area, N.W.T. Geographical Branch, Department of Mines and Technical Surveys, Ottawa, Canada, Memoir 8.

Mackay, J.R. 1992. Lake stability in an ice-rich permafrost environment: examples from the western Arctic coast. In *Aquatic Ecosystems in Semi-Arid Regions: Implications for Resource Management*. Robarts RD, Bothwell ML. (eds.) N.H.R.I. Symposium Series 7, Environment Canada, Saskatoon. 1-25.

Mackay, J.R. 1995. Active layer changes (1968 to 1993) following the forest-tundra fire near Inuvik, N.W.T., Canada. *Arctic and Alpine Research* 27: 323-336.

Pienitz, R., Smol, J.P. & Lean D.R.S. 1997. Physical and chemical limnology of 59 lakes located between the southern Yukon and the Tuktoyaktuk Peninsula, Northwest Territories (Canada). *Canadian Journal of Fisheries and Aquatic Science* 54: 330-346.

Quinton, W.L. & Marsh, P. 1999. A conceptual framework for runoff generation in a permafrost environment. *Hydrological Processes* 13: 2563-2581.

R Development Core Team. (2007). *R: A language and environment for statistical computing, V.2.3.1*. Vienna, Austria: R Foundation for Statistical Computing. ISBN 3-900051-07-0. http://www.R-project.org.

Rampton, V.N. 1988. *Quaternary geology of the Tuktoyaktuk Coastlands, Northwest Territories*. Memoir 423. Geological Survey of Canada.

Ritchie, J.C. 1984. *Past and present vegetation of the far northwest of Canada.* Toronto: University of Toronto Press, 251 pp.

Rouse, W., Douglas, M., Hecky, R., Kling, G., Lesack, L., Marsh, P., McDonald, M., Nicholson, B., Roulet, N. & Smol, J.P. 1997. Effects of climate change on freshwaters of Region 2: Arctic and sub-arctic North America. *Hydrological Processes* 11: 873-902.

Serreze, M.C., Walsh, J.E., Chapin, F.S., III, Osterkamp, T., Dyurgerov, M., Romanovsky,V., Oechel, W.C., Morison, J., Zhang, T., & Barry, R.G. 2000. Observational evidence of recent change in the northern high-latitude environment. *Climate Change* 46: 159-207.

Sokal, R.R. & Rohlf, F.J. 1995. *Biometry*. 3rd edition. New York: W.H. Freeman and Company, 876 pp.

# Cryolithosphere on Mars and the Thickness of Frozen Rock

Ilya Komarov
*Moscow State University, Faculty of Geology, Department of Geocryology, Russia*
Vladislav Isaev
*Moscow State University, Faculty of Geology, Department of Geocryology, Russia*
Oleg Abramenko
*Moscow State University, Faculty of Geology,Department of Geocryology, Russia*

## Abstract

The primary conceptualization of a cryolithosphere on Mars and a thickness of frozen rocks were introduced by Kuzmin (1983), Krass and Merzlikin (1990), and Clifford and Parker (2001). All evaluations of thickness of the Martian cryolithosphere were based on a stable temperature field model. The thickness of frost rocks ($H_m$) was found following the profile of gradual temperature distribution with depth for one- and two-layered lithological models. The average annual surface temperature, temperature of phase transition for water, temperature of heat transfer, and heat flux to the lower permafrost boundary were taken into account. The revised estimates of the frozen rock thickness are much reduced.

**Keywords:** cryolithosphere; heat transfer; modeling; temperature field; thermal conductivity coefficient.

## Introduction

The greater distance of Mars from the Sun (1.5 times more than Earth) and strong rarefaction of the Martian atmosphere determines the existence of a large region with negative temperatures—a cryosphere. It begins at a height of 130–140 km above the surface, and extends deep inside across the entire planet. Many relief forms can be interpreted by the presence of a thick layer of frozen rock and consequent cryological processes. The relief is characterized by highly elongated forms which are up to 10 times larger in size then their terrestrial analogues. Considerable differences in the ice formation processes within the frozen rocks, and the scale of ice-saturated layers destruction on Mars and on Earth, could possibly explain such a significant difference in size.

Current ideas about the cryolithosphere of Mars and a frozen rock layer are mainly based on the work of Kuzmin (1983), Krass and Merzlikin (1990), and Clifford and Parker (2001). It has been estimated based on a stable thermal field model.

The thickness of a massive frozen rock layer ($H_м$) was found by the profile of stationary distribution of temperature $T$ (K) with depth for models with one- and two-layered lithological cross-sections. The average surface temperature $T_{av}$ and the temperature of phase transition of water, $T_{ph}$ , and values of heat flux to the lower boundary of the cryolithosphere, $q$, are known. The main differences in these calculations were caused by the choices the various authors have made for the following parameters.

Coefficient of thermal conductivity ($\lambda$) for the upper rock layers. $\lambda_m$=1.8 W m$^{-1}$ K$^{-1}$ according to Merzlikin, and $\lambda_m$ = 2.0 W m$^{-1}$ K$^{-1}$ according to Parker. In both calculations, a correction for the influence of temperature on the thermal conductivity of ice and upper layer porosity (0.35±0.15) has been used. Kuzmin set an average of $\lambda_m$=2.1 8 W m$^{-1}$ K$^{-1}$, and using $\lambda_{min}$ =0.59 and $\lambda_{max}$ =3.47 8 W m$^{-1}$ K$^{-1}$.

The magnitude of heat flux from depth ($q$) is 0.04 W m$^{-2}$ or $q$ = 0.03 W m$^{-2}$ according to Krass and Clifford, respectively. $q$ = 0.039 W m$^{-2}$ (minimum = 0.022; maximum =0.055 W m$^{-2}$).

The average surface temperature ($T_{av}$) is equal to - 63°C. $T_{av}$ = -29°C at the equator and $T_{av}$ = -90°C at the poles in the works of Kuzmin, while $T_{av}$ = - 82.5°C; $T_{av}$ = -55°C at the equator and $T_{av}$ = -119°C at the poles in the work of Clifford and Parker.

The presence of water-saturated layers in a cross-sectional model was considered by Kuzmin, Clifford, and Parker in their last publications.

The resulting average thickness of frozen rock varies from 2.7 km (Krass & Merzlikin 1990) to 3.23 km (Kuzmin 1983), changing from 1.5 km to 2.3–4.7 km in equatorial regions to 5 km (Kuzmin 1983) to 6.5–13 km (Clifford and Parker) under the polar caps.

According to the data of remote probing obtained recently (Mars Climate Database of the European Space Agency), and according to our ideas, it seems reasonably to precict the depth of the cryolithosphere and to reduce the estimated thickness of the frozen rock layer on Mars.

For the final evaluations, the following data were taken into account: (a) corrected means of surface temperature observed along meridians; (b) the pressure of upper layers on the lower boundary of frozen rock; (c) the presence on the surface of a dehydrated regolith layer with a thickness from 0.2 to 2.0 m. This layer is characterized by extremely low thermal conductivity (thermal resistance of a 1.5 m thick layer of regolith is equal to 5–10 m of freshly deposited snow); and (d) mineralization of pore solutions, taking the presence of highly mineralized solutions on Mars as a vital hypothesis. There appear to be salty "crusts" in study areas observed by landing craft such as Viking 1 and 2, and the Mars Pathfinder. Also, x-ray spectrometer (APXS) in the

Ares valley, and spectrometer Mossbauer in Gusev crater, registered high salinity in areas where the Mars Rovers, the Mars Pathfinder, and the Spirit landed.

The actual thickness of the frozen rock cryolithosphere on Mars is estimated to average around 2300 m, which is less than what was earlier assumed and similar to values observed on Earth. Frozen rocks contain cryohydrates that have no analogues on Earth.

For the analysis and interpretation of properties of Martian surface rocks, a set of laboratory experiments was carried out for terrestrial samples across a wide range of negative temperatures (from -60 to -120°C); these included measurement of thermal conductivity, heat capacity, and coefficient of linear expansion.

## Discussion

*Temperature conditions on the surface of Mars*

The Martian Global Database (MGD) (www.lmd.jussieu.fr/mars.html) was used for evaluation of spatiotemporal mutability of components of surface energy (radiation-heat) balance, the surface temperature, and the temperature of the near-surface atmospheric zone for high latitude regions of Mars based on General Circulation Models (GCM) to model climate and atmosphere circulation. GCMs are also widely used for weather predication and climate research on Earth.

The Martian version of GCM is the result of cooperative work of LMD (Laboratoire de la Meteorologie Dynamique du CNRS, LMD, Paris) and AOPP (Atmospheric, Oceanic and Planetary Physics, Department of Physics, Oxford University, Oxford, England UK). They are based on actual data received from orbital stations and landing rovers from Mars Pathfinder, Mars Global Surveyor, and Viking 1 and 2.

The influence of atmosphere dustiness and dust storms were taken into account by adding some corrections for different scenarios: "dust" year and "clear" year, average and strong global dust storms The database is an information-searching system equipped with a calculation module for receiving current data on climatic parameters and during a period for a precise site, region, or across the planet.

The analyses of temperature conditions on the surface and in the near-surface atmosphere layers show that the dynamics of seasonal temperature have some characteristic features (Table 1). Maximum temperatures were observed at the end of the Martian summer, while the warmest season is autumn (for the North hemisphere).

Winter temperature tends to decrease with some variations for different areas. It is the coldest period for the region 64°N, 48°E with the peak of negative temperatures at -128.9°C. The coldest time for more southern areas 58°N, 48°E, as well as for 64°N, 30°E, is spring with the temperatures around -123°C.

In the extremely cold period (Ls = 330–360), diurnal temperature fluctuates within 1°C for the area 65°N, 68°N, within 50°C for the latitudes 47°N, and reaches the most significant values up to 100°C at latitude 43°N. Diurnal surface temperature for latitudes 65°N, 68°N achieve a minimum at 10 a.m. and a maximum at 12 p.m. The lower latitudes 43°N, 47°N are characterized by a minimum at 8 a.m., while maximums are differentiated according to the albedo. The lowest temperatures on the Utopia area (43°N, 91°W), for example, were observed at mid-day and the highest temperature at 18 a.m.; with 100°C of temperature fluctuation. In the areas of low albedo, temperatures are minimal at 8 a.m. and maximal at 14–16 p.m., and vary some 40–50 degrees.

*Existence of dry soft regolith on the Martian surface*

In accordance with data from the High Energy Neutron Detector (HEND) (Feldman et al. 2002), there is a dry soft regolith layer on the surface of Mars. The depth varies from 0.2 m close to the polar caps to 1.5–2.0 m on the equator. It was formed by physical weathering and has andesite or andesite-basaltic composition. The regolith layer at the Viking-1 landing site is composed mainly of clay particles or dusty fraction up to 60% (from 0.05–0.001 to less 0.001 mm), and by a sand fraction of up to 30% (from 0.1 to 2 mm). Some stone-like rounded inclusions with a size of 3–4 cm were noticed.

The thermal inertia (I) is the main thermal parameter of rocks, where $I = (\lambda C_{vhc})^{1/2}$. Here, $C_{vhc}$ is the volumetric heat capacity in J $cm^{-3}$ $K^{-1}$). Maps of thermal inertia compiled with the help of MCD and the data received by rovers (Jakovsky et al. 2000) allows generalizing a character of varying thermal inertia.

In particular, a significant increase of *I* values was observed from background values 100 J $m^{-2}$ $K^{-1}$ $s^{-1/2}$ (for 80% of the surface) to 400 J $m^{-2}$ $K^{-1}$ $s^{-1/2}$ for areas in northern latitudes from 86ºN, and to 2000 J $m^{-2}$ $K^{-1}$ $s^{-1/2}$ for some regions in the Southern Hemisphere.

As the data on thermal inertia is a *sine qua non* condition for regolith thermal conductivity, some experimental data obtained by differential scanning calorimetry (Komarov 2003, Isaev et al. 2006) for terrestrial samples were used in mathematic modeling of the thermal fields.

Values of volumetric heat capacity ($C_{vhc}$) do not depend on rarefaction and forces of gravitation. Samples of rocks were tested in an air-dry state because analyses of spectral lines of water in the short-wave part TES spectrums of the Martian surface showed that the amount of water in regolith is less than 0.1–0.2 weight percent (Christensen et al. 2001).

According to the data from neutron spectroscopy collected by the Mars Odyssey (Feldman et al. 2002), the total water content in the regolith layer on Mars is only up to first percents. Therefore, it appears to be chemically bound water.

Values of thermal inertia (I) vary between 330–380 J $m^{-2}$ $K^{-1}$ $s^{-1/2}$, the rock density (ρ) between 1.0–1.6 g $cm^{3}$ for areas of Viking-1 and 2 landings. Taking into account the magnitude of the volumetric heat capacity (C) as 0.42 kJ $kg^{-1}$ $K^{-1}$, and the dependence of C on the temperature, theoretical values of the thermal conductivity coefficient λ were in the range of 0.12 to 0.2 W $m^{-1}$ $K^{-1}$ were realized.

These estimates are similar to those actually evaluated on Mars by landing stations. For other sites located in middle and high latitudes of the Northern Hemisphere, values of λ are between 0.07–0.15 W $m^{-1}$ $K^{-1}$.

Therefore, in spite of the shallow thickness and owing to the low thermal conductivity, the thermal resistance of the regolith layer is very high and could be compared to the resistance of a fresh snow on the Earth with a thickness of 3–5 m.

*Results of laboratorial measurements of properties of terrestrial rocks at subzero temperatures*

For the analysis and interpretation of rock properties of the subsurface layer on Mars, along with the data on heat capacity (C) obtained for terrestrial samples, it is possible to use experimental measurements of thermal conductivity and the coefficient of linear expansion (Komarov 2003, Isaev et al. 2006). It was determined for a wide range of negative temperatures (down to -120°C) by calorimeter and dilatometer equipment. Values of thermal conductivity for terrestrial rocks were re-estimated in accordance with the average value of near-surface atmospheric pressure (6 mbar). An account was based on the method of Dulnev and Zarichnyak (1974) under the conditions of transitional mode of gaseous medium flux ($2 \geq Kn \geq 0.1$, where Kn os the Knudsen criterion). The coefficient of accommodation was taken for the $CO_2 - SiO_2$ system (for the Martian atmosphere the main constituent is $CO_2$ – 95%).

This, with some corrections for rarefaction, corresponds to the coefficient of thermal conductivity of dusty particles.

According to our point of view, the thermal conductivity of the subsurface layer corresponds to coefficient values for dusty particles with a density in the range of 1.15 ± 0.15 g $cm^{-3}$. The density of surface rocks evaluated by orbital stations, and based on thermal inertia, is 1.2 g $cm^{-3}$. According to polarimetric analysis, it is 1.0 g $cm^{-3}$ for the layer of some part of mm. Radar shows 1.4 g $cm^{-3}$, while the analyses of dielectric permittivity estimates 1.2 $cm^{-3}$ for waves in the range of 3.8 to 70 cm.

Calculated evaluations of the thermal conductivity of ice-saturated rocks on Mars by Clifford and Parke were based on the generalized conductivity method. It was taken into account the dependence of ice thermal conductivity on the temperature which is, by far, significantly increased with the lowering of temperature. In our opinion, the value of λ was dramatically overestimated and, as a consequence, the thickness of permafrost was overestimated as well. As provided by experimental data ,some increase of λ can be noted exclusively for the pure hexagonal polycrystalline ice in a volume.

Among the possible explanations for actual decrease of λ in spite of the increase in conductivity of ice, are the following reasons:

(1) Loss of plastic properties of ice and formation of micro cracks within the body of ice starting at -12°C;

(2) Under low temperatures, a different coefficient of linear expansion (α) for ice and for mineral structures plays an important role, resulting in the formation of micro cracks at the mineral-ice interface; and

(3) A coefficient of linear expansion (α) specific to different minerals leads also to the formation of micro cracks.

The total effect of these processes becomes dominant and drives to decreasing of bulk thermal conductivity λ (Komarov 2003, Isaev et al. 2006).

*The upper boundary of frozen rocks and ice content in the upper layers*

The upper boundary of the frozen rocks was determined by the "impact method" developed in the analyses of surface images of Mars (scale from 1:5000000 to 1:250000) that were collected by Mariner-9, Mars-5 and Viking-1 and -2. This method is based on geomorphologic criterion. Morphological impact features revealed an alteration of upper layers of frozen rocks at different latitudes.

Thus, it was found that geologically young impact sites are often surrounded by radial fluid-like fluxes. It seems to be a result of a melting process in the underlying ice-saturated rocks that appeared after meteoritic explosion in ice-containing rocks. Evaluation of comparative ice-content was proposed by Kuzmin & Zabalueva (2002), who set up the ratio of the debris flow area to the diameter of the impact crater itself. A depth of frozen rock confining layers was also mapped (Kuzmin & Zabalueva 2002). Along with the data from the HEND equipment collected during the Mars Odyssey mission (Feldman et al. 2002), it has been used in our work for the evaluation of ice content in the frozen rocks.

This data shows a significant decrease of epithermal neutrons flux (energy rate 1eV - 0.1 MeV) in the areas of high latitudes caused by the presence of water ice within the subsurface rocks. The water content in a 2 m surface layer was evaluated as 40% by weight for Northern Hemisphere and 23% for Southern hemisphere (for 1-layer model), and to 55% (for two-layer model where dry regolith layer with 2% of water content overlies the subsurface strata).

*Influence of overlying rock layers on the occurrence of low margin of frost rocks*

Due to well-known peculiarities of ice formation in capillary-pore medium and in independent volume, a modified equation of Claiperon–Clauzius was used for evaluation of pressure (P) on temperature of phase transfer between water and ice. The equation takes into account the possibility of phase equilibrium for the phases under different pressure. In other words, it was assumed that ice of water can be liberated under the Martian atmospheric pressure while the water is subjected by the pressure of overlying layers.

This situation is characteristic for Mars, where strongly dissected basalts and andesites are abundant in subsurface layers due to impact activity. High rarefaction on Mars results in increasing density in liquid and solid phases during the process of degassing, though it makes a negligible correction in evaluations. Therefore, in the estimation of

Table 1. Monthly temperature on Mars according to latitude and season.

| Ls | 0-30 | 30-60 | 60-90 | 90-120 | 120-150 | 150-180 | 180-210 | 210-240 | 240-270 | 270-300 | 300-330 | 330-360 | T av. K | T av. C |
|---|---|---|---|---|---|---|---|---|---|---|---|---|---|---|
| 90 N | 148 | 155 | 184 | 217 | 208 | 174 | 152 | 148 | 148 | 148 | 148 | 148 | 165 | -108 |
| 60 N | 174 | 212 | 222 | 224 | 218 | 204 | 186 | 160 | 150 | 150 | 150 | 151 | 183 | -90 |
| 30 N | 220 | 225 | 220 | 220 | 220 | 220 | 215 | 210 | 205 | 205 | 205 | 215 | 215 | -58 |
| 0 | 215 | 215 | 210 | 210 | 215 | 230 | 230 | 230 | 230 | 225 | 225 | 220 | 221 | -52 |
| 30 S | 215 | 205 | 194 | 194 | 205 | 220 | 235 | 245 | 245 | 245 | 240 | 230 | 223 | -50 |
| 60 S | 178 | 150 | 147 | 146 | 146 | 146 | 152 | 210 | 242 | 242 | 228 | 205 | 183 | -90 |
| 90 S | 145 | 145 | 145 | 144 | 143 | 143 | 144 | 145 | 168 | 239 | 223 | 171 | 163 | -110 |
| average | 185 | 187 | 189 | 194 | 194 | 191 | 188 | 193 | 198 | 208 | 203 | 191 | 193 | -80 |

Table 2. Estimated thickness (m) of frosty, frost, and frozen rocks.

| Coordinate | Close to North polar cap | 60N | 30N | 0 | 30S | 60S | Close to South pole cap |
|---|---|---|---|---|---|---|---|
| Average temperature of surface, ºC | -119 | -94 | -62 | -55 | -63 | -96 | -123 |
| Average thickness of regolith, m | 0 | 0.6 | 1.5 | 1.8 | 1.5 | 0.6 | 0 |
| Average thickness of frosty rock, m | 0 | 0 | 150 | 300 | 150 | 0 | 0 |
| False thickness of frost rock (evaluate on value of thermal resistance), m | 0 | 25 | 210 | 370 | 210 | 25 | 0 |
| Average thickness of frozen cryohydrate-content rocks, m | 2520 | 1470 | 0 | 0 | 0 | 1550 | 2680 |
| Average thickness of frozen ice-content rocks, m | 1250 | 1250 | 1100 | 570 | 1140 | 1250 | 1250 |
| Average summarized thickness of frost rocks, m | 3770 | 2720 | 1100 | 570 | 1140 | 2800 | 3930 |
| Average thickness of cryolithosphere (with average thickness of cooled rocks 600 m), m | 4370 | 3320 | 1850 | 1470 | 1890 | 3400 | 4530 |

the temperature on the low margin of frozen rocks and cryolithosphere, terrestrial values were taken for the density of ice and water. The effect of low gravitation on Mars was taken into account when the pressure of overlying strata was evaluated. By operation of the additivity rule, the influence of overlying layer pressure and mineralization of pore solutions could be calculated. The possibility of potential presence of gas hydrates within the frozen rocks was not appreciated.

*Effect of mineralization of pore solutions (based on the hypothesis of the existence of brines at depth on Mars)*

Salt crusts found by Viking 1 and 2 and by Mars Pathfinder evidence the existence of brines close to the surface. It is characterized by high chlorine and sulfur content in comparison with background rocks. Salt crust formation can be explained by the mechanism of capillary inflow of salty solutions up to the layer subjected to summer temperature fluctuations, as well as by irregular frost penetration. The latter leads to the formation of closed volumes of mineralized brines.

This formation is accompanied by increasing hydrostatic pressure and by subsequent cracking of frost rocks under mechanical stress. Mineralized solutions can be discharged on the surface forming salty crusts after evaporation.

Mineralization of surface layers was observed by Mars Pathfinder and Spirit rovers equipped by alfa-proton spectrometer (APEX) (Rieder et al. 1997) and by Mossbauer spectrometer in Ares valley and in the area of the Gusev impact.

Seasonal monitoring of radar reflectivity in the area of Solar Gulf also confirms the presence of brines in the frozen rocks.

In our opinion, the mechanism of formation of "martian cryopegs" is similar to the terrestrial analogues observed in regions of Central Yakutia, where considerable cryogenic concentration of pore solutions was taking place due to strong evaporation. Salt migration down along the sequence is forced out by frost penetration as a result of the "piston mechanism". Accumulation of mineralized solutions leads to the formation of cryopegs characterized by high salt concentrations that exceed 250 ml/l.

The composition of these brines is presumably magnesium-chlorine-sulfate: ice $H_2O + CaCl_2 \times 6H_2O + MgCl_2 \times 12\ H_2O$

(the point of the eutectic is around 217K). This isotherm (217K) can be selected as a potential boundary between the zone of frozen $H_2O$- ice contained and frost cryohydrate contained rocks. It has no analogues on Earth.

The existence of mineralized waters set conditions for the zone of cooled rocks with no ice-content close to the low boundary of frozen rocks which is determined by the 273K isotherm. The upper boundary can be evaluated as additive value of temperature of ice to water phase transfer - 258 K (overlying rocks pressure and mineralization of pore solutions were taken into account).

## Conclusions

Based on the estimated values of rocks which are tabulated (Table 2), it is concluded:

1. The average thickness of the frozen rock layer (cryolithosphere) is 2300 m, with some corrections caused by heat flux inflow. This value exceeds the terrestrial analogue but is significantly less than assumed earlier. A hypothesis of the existence of highly mineralized brines on Mars, the influence of the thermal resistance of a dry surface layer of regolith and overlying rocks on the temperature of water-ice formation, was taken into account.

2. The sequence is constrained by layers (from surface): frosty (thickness up to 300 m), frost (thickness up to 3900 m); cooled rocks (thickness up to 600 m) and thawed rocks. Within the frost rocks a cryohydrate-contained layers were identified. It has not been observed on Earth.

The presence of gas hydrates in the frozen rocks of Mars was not discussed due to lack of data.

## References


Christensen, P.R. et al. 2001. The Mars Global Surveyor Thermal Emission Spectrometer experiment: Investigation description and surface science results. *J. Geophys. Res*. 106: 23823–23871.

Clifford, S.M. & Parker, T.J. 2001. *Icarus* 154: 40-78.

Dulnev G.N. & Zarychnyak Y.P., 1974, Heatconductivity of fusions and composed materials. *Energia*, 261 pp.

Feldman, W.C., Boynton W. V. & Tokar, R. L.. 2002, Global distribution of neutrons from Mars: results from Mars Odyssey, *Science* 297: 82-84.

Isaev, V.S., Komarov I.A. & Abramenko, O.N. 2006. *Planetary Chronology Workshop*, Abstract #6009.

Jakovsky, B.M. et al. 2000. The thermal inertia of Mars from the Mars Global Surveyor Thermal Emission Spectrometer. *J. Geophys. Res*. 105: 9643.

Komarov, I.A. 2003. *Proceeding of Third Mars Polar Science Conference*, Abstract #8015.

Komarov, I.A. 2003. Thermodynamic and heat mass transfer in disperse frozen grounds. *Scientific Worlds*. 608 pp.

Krass, M. & Merzlikin, V. 1990. *Hydrometeoizdat*, p. 361.

Kuzmin, R.O. 1983. *Cryolithosphere of Mars.* Moscow: Science.

Kuzmin, R.O. & Zabalueva, E.V. 1999 *LPSC*, Abstract 2104.

Kuzmin, R.O. & Zabalueva E.V. 2002. *Computational modeling of ice redistribution process in subsurface layer of Martian regolith on equator under quasi periodical fluctuations of planet axial inclination.* Herald of the Academy of Sciences Department of Geoscience, 1(20).

Rieder, R., Economou, T., Wanke, H. et al. 1997. The chemical composition of Martian Soil and Rocks returned by the Mobile Alpha Proton x-ray spectrometer: Preliminary results from x-ray Mode. *Science* 228: 1771-1774. www.lmd.jussieu.fr/mars.html.

# Geocryological Problems Associated with Railroads and Highways

V.G. Kondratiev
*TransEGEM, Moscow, Russia*

## Abstract

Over the last 10 years, significant new construction of railroads and highways has occurred in Transbaikal and the adjacent territories, including China. Examples of geocryological problems associated with selected railroad and highway locations are presented. Operational reliability, assessment, and monitoring needs are discussed. Emphasis is given to providing comprehensive geocryological exploration efforts, utilizing innovative and intelligent design solutions, allowing for timely and quality construction procedures as well as making provisions for necessary ongoing maintenance. Experience with anti-deformation measures, used for both the Russian and Chinese railroads and highways, utilizing both active and passive methods for strengthening the embankments on ice-rich permafrost, is also presented. In addition, technical solutions involving anti-frost heaving devices for electrical contact-line railway and power line tower supports, is reviewed.

**Keywords:** embankments; geocryological monitoring; highways; permafrost; railroads; thaw settlement.

## Introduction

The history of railways constructed in permafrost regions exceeds more than 100 years: Transbaikalian, Amur, Alaska, Norilsk, Gudson, Labrador, Baikal–Amur (BAM), Amur–Yakut (АЯМ), Yamal, and some other railways in Russia, the USA, and Canada. Construction of each of these railroads provides examples of frozen-ground construction and attempts to provide stable subgrade soils in areas of permafrost and deep seasonal freezing.

Construction in China of the Qinghai–Tibet Railway along the Golmud–Lhasa segment occurred in 2000–2006. This is the newest stage of major railway construction, involving conditions of permafrost and deep seasonal freezing of the soils. The project has included new, large-scale attempts to solve some of the specific problems.

The author was involved with Chinese experts on addressing problems of geocryological concerns along the Qinghai–Tibet Railway and the Qinghai–Tibet Highway over the last 14 years, and in Russia, has been actively engaged in these problems since 1986. Results of his research are reflected in more than 60 technical papers and reports, as well as 5 monographs published in the USSR, Russia, the USA, Canada, Norway, China, Japan, and Finland. Information from these projects and various studies are briefly reviewed in this paper.

## Geocryological Problems Associated with Railroads

There has been very limited success in building a railway line that would not undergo deformations resulting from thawing of ice-rich soils or frost heave, induced by freezing of wet foundation soil. These problems are characteristic for all railroads regardless of the length of time in operation. The Transbaikalian Railroad has been in operation more than 100 years, the BAM and the Amur–Yakutsk Main Line, well over tens of years, and the connecting lines Chara–Cheena and Ulak–Elga, only several years. The Qinghai–Tibet Railway has only recently been completed.

Figure 1. Deformations of a track and power line tower support along an electrified section of the Transbaikalian Railroad, km 6278, November 2006.

One of the major problem areas on the Transbaikalian Railroad, located at route segment 6277 to 6278 km, is shown in Figure 1. This segment is known as the "golden" kilometer. At this location, continuing deformation of the embankment and rail-sleeper grating have been occurring since 1949. Train speed limitations of 40 km/h, and sometimes as low as even 15 km/h, have been imposed since 1969, while addition of ballast and rail adjustments are executed annually.

In some places, the ballast has already subsided 5 to 6 m, and subsidence of the railbed has not ceased. This condition is expected to continue for many years, since the embankment was constructed on permafrost soils having a thickness of 25 to 30 m.

On the East Siberian Railroad, in the region of the Kazankan sidings at 1374 km on the BAM, major railway track deformation has been taking place for nearly two decades. From the original four-track lines on this segment, only one remains in service; however, as shown in Figure 2, it also requires nearly-continual maintenance and recurrent refitting. For the last 7 years, 360 million rubles (about 15

Figure 2. Area of severe deformation on the East Siberian Railroad at 1374 km of BAM, September 2003 (photo by E.A. Kozyreva).

Figure 3. Track and power line tower deformation along the Chara–Cheena Railroad, October 2003.

million dollars) have been spent to refit this section of the railroad, but the problem of stabilization remains unsolved. Train speeds are still limited to 15 to 40 km/h, since the threat of unacceptable deformation of the track on this side hill-slope remains. Since this segment of the BAM is electrified, it is critical that the electric contact net and supporting power line towers be repaired as well.

To the north of the Transbaikalia, the Chara–Cheena Railroad was constructed in 2001. The route extends over an area having extremely complex engineering-geocryological conditions involving ice-rich permafrost. In some areas, the underground ice has a thickness of 5 to 10 m. An example of this railway track deformation, occurring under the adverse influence of cryogenic warming processes, is shown in Figure 3.

## Sun-Precipitation Protective Sheds

The thawing of permafrost soil under railroad and highway embankments is usually caused by: 1) increased absorption of solar radiation into the subgrade when compared to the natural surface; 2) the infiltration of precipitation through the embankment; 3) an increase in the thickness of snow cover at the base of the embankment and adjacent area; and 4) the migration of surface and subsurface water into the body and base of the subgrade in side-hill slope areas.

Figure 4. Sun-precipitation protective sheds on the Qinghai–Tibet Railway, August 2006.

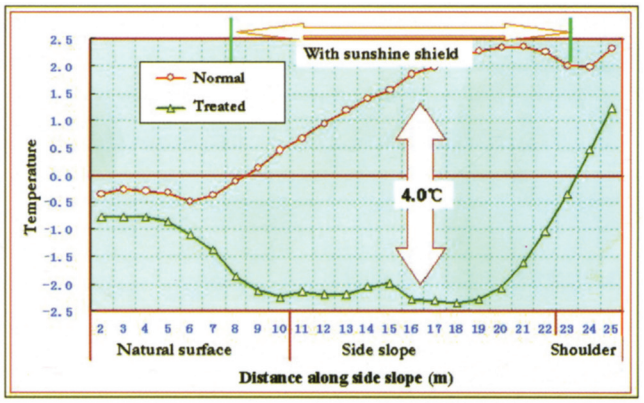


Figure 5. Cooling influence of the sun-precipitation protective sheds, constructed on the embankment slopes of the Qinghai–Tibet Railway.

Several methods of strengthening the base of embankments on ice-rich permafrost have been developed. These methods cause a decrease in the average annual temperature of soils and assist in preserving the permafrost state in a way that reduces warming and improves cooling impacts.

These technical solutions have been presented in articles, reports, and monographs, both in domestic and foreign publications (Kondratiev 1994, 1996, 1998, 2002, 2004, & 2006). The solutions have been applied on experimental projects while constructing the Amur–Yakutia trunk line and the connecting Ulak–Elga Railroad, and while preparing a feasibility study of stabilization measures for use on the Transbaikalian Railroad. Some of these solutions have been applied also on the Qinghai–Tibet Railway in China. An example of the sun-precipitation protective shed applied to side slopes is shown in Figure 4. Data from observations at the full-scale site indicates temperature reductions ranging from 3 to 5ºC in the subgrade soil. This cooling influence, as shown in Figure 5, serves to improve the stability of the subgrade soil on the highly ice-rich permafrost soil (Niu & Shen 2006).

Application of sun-precipitation protective sheds has also been accomplished on Russian railways and highways. On the Amur–Yakut Railway at the approach to the Lena River for tens of kilometers of the railroad, there exists a so-called ice complex, having a thickness of several tens of meters. Excavation or mechanical pre-thawing of this ice thickness is considered to be impractical. Therefore, it has

been concluded that this section should be protected from thawing during all periods of railroad operation.

In 2007, a technical study of the application of sheds for preventing degradation of ice-rich permafrost, at the base of an embankment along the Tommot–Kerdem Railway, was initiated at five separate sites. These involved three embankments having heights of 3.48, 6.64, and 7.31 m and two excavations having depths of 2.38 and 5.5 m.

For comparison, at the same sites, thermotechnical calculations of the cooling influence of convective stone/rock covering on the embankments and excavated slopes were executed. Results were found to show a higher efficiency with the sun-precipitation protective sheds for cooling soils in the subgrade of an embankment and prevention of degradation in the underlying permafrost soil, particularly when used in combination with dolomite powder (light-reflecting painting) placed on the surfaces of the basic platform and employment of an antifiltering membrane underneath. Results further indicate that:

• On slopes of both embankments and excavations, the shed-only application provided a decrease of 10 to 31% (average 22.4%) in the depth of the bedding and cover over the permafrost soils along the axis in comparison with the rock covers.

• On the slopes of both embankments and excavations, use of sheds in combination with dolomite powder painted on the surface of the basic platform provided a 25 to 35% (average 30.6%) decrease in the depth of the bedding and cover over the permafrost soils along the axis in comparison with the rock covers.

• On the slopes of both embankments and excavations, use of sheds in combination with the dolomite power painted on the surface of the basic platform and with placement of an antifiltering membrane underneath provided a 28 to 40% (average 34.6%) decrease in the depth of the bedding and cover over the permafrost soils along the axis in comparison with the rock covers. In this case, cooling of the embankment and subgrade soil occurs more rapidly than at sites having rock covers. After only 5 years, the subgrade soils and a substantial part of the body of the embankment exist in the permafrost state, whereas under the rock covers the embankment remained unfrozen, and complete freezing will only occur after 50 years.

Thermotechnical calculations for the Amur–Yakut Highway, as well as experimental research in Tibet, demonstrate that sun-precipitation protective shed applications represent an effective treatment as an anti-deformation device for embankments on railroads and highways at sites containing icy permafrost soils. The positive effect of the shed application is accomplished by both allowing the intensive winter cooling of the embankment and its subgrade, and by both the reduction in infiltration of summer precipitation and the exclusion of direct solar radiation. This helps to preserve the higher strength properties of the frozen soils in the subgrade during all periods. Thus, the design of an embankment becomes simpler, traffic volume and safety improves, and maintenance and repair needs decrease.

Figure 6. Adverse deformation of power line tower supports along the electrified section of the Transbaikalian Railroad, August 2001.

## Operational Reliability and Monitoring

Operational reliability of railways and highways in regions of permafrost is predetermined by the choice of constructive-technological solutions and methods of effective execution during construction and subsequent maintenance operations. Constant protection of roads from adverse engineering-geocryological processes, particularly in areas of ice-rich soil, is important in order to provide stability and maintain traffic design speeds. To be most effective, such protection needs to be carried out systematically with emphasis on engineering and geocryological monitoring of the routes. This includes providing regular reviews and controls, technical analysis, and estimations and forecasts of changes in freezing conditions. Such a procedure allows detection and mitigation of undesirable and adverse cryogenic processes. The concept of such a monitoring system was developed for the constructed Berkakit–Tommot–Yakutsk Railroad (Kondratiev and Pozin 2000). In 2001, the concept and process were presented in Beijing and then applied to the Qinghai–Tibet Railway route.

## Anti-Frost Heaving Tower Supports

The provision and effective utilization of basic facilities of railways in areas of a permafrost and deep seasonal soil freezing is associated with significant difficulties. As an example, on the Transbaikalian Railroad during the past 10 years (1997 to 2006) at least 17,192 power line tower supports required corrective repairs and 3,294 were replaced. In most cases deformation of support structures were caused by frost jacking within wet friable sediments of seasonally thawed (STL) or seasonally frozen (SFL) layers. Figure 6 provides an example of the extent of tower deformation.

In responding to this problem, a patented solution for an anti-frost heaving measure was developed for the purpose of decreasing the influence of frost heaving forces. This is accomplished by the simultaneous increase in lateral forces on the tower support in STL by freezing and by cooling within long-term frozen soils by means of (a) thermosyphon support in STL, inserted into a hollow reinforced concrete support or metal base; (b) wrapping of an anti-frost heaving sleeve made of nonfreezing grease and a protective casing

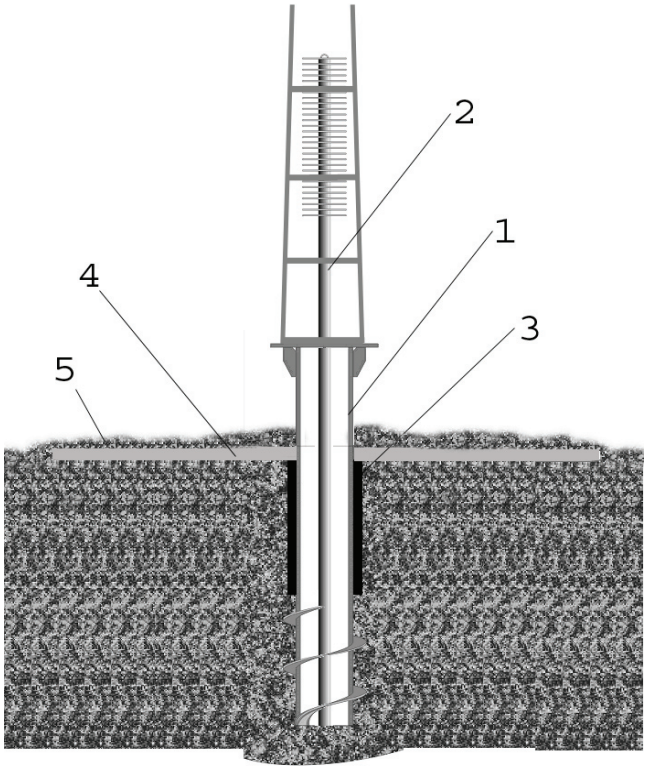


Figure 7. Metal support with screw base (1), with thermosyphon inset (2), anti-frost heaving sleeve (3), thermal insulation (4), and a covering soil layer (5).

made of frost-resistant material; (c) placement of heat and hydroinsulation at the soil surface around the support; and (d) inclusion of a sun-precipitation protective shed around the support and anti-frost heaving sleeve (Kondratiev, 2005).

The anti-frost heaving device design for a metal tower support having a screw base (as shown in Fig. 7) consists of three basic elements: the thermosyphon, the thermal insulation, and the anti-frost heave sleeve.

In October 2003, anti-frost heaving devices consisting of the thermosyphon structure and a 1.25 m long anti-frost heaving sleeve were installed on five tower support pile bases along the Erofey–Pavlovich–Sgibievo segment of the Transbaikalian Railroad.

Work on placing the insulation layer around the support bases and protective soil cover was performed in April 2004, after allowing maximum winter freezeback of the soil around the metal support bases. The elevated portion of the supports was then painted with a white cover.

Analysis of the data recovered since November 2004 shows that, owing to the cooling influence of the thermosyphons, soil freezing near the base (at 0.1 to 0.2 m from the surface) occurred more quickly than at 0.55 to 0.65 m. Around one support, the frozen soil mass, which normally thaws to a depth of 2.5 to 4 m by late autumn, was found to preserve the soil in a constantly-frozen state around the lower portion of the support at a depth of 1.5 to 3 m.

Periodic level surveys were conducted on the top part of the tower supports and have shown that the tower bases having anti-frost heaving devices have remained stable under varying conditions of soil freezing and thawing cycles. Measurements indicate that the vertical movement does not exceed 10 mm, based on a measurement accuracy of a Class III level survey. Whereas, 20 to 30% of the tower bases not having anti-frost heaving devices have begun to heave after 2 to 3 years following installation. Their vertical moving for 5 annual cycles of freezing-thawing have ranged from 10 to 280 mm.

Following verification of the experimental anti-frost heaving devices for the tower support bases, applications have now been extended to electrified rail line projects such as the Karimakaya–Borzya, Burinda–Magdagachi, Mogocha–Amazar, Chernovskaya, and Karimskaya stations. This solution also has the potential for use on other types of tower structures such as signal system devices, high voltage transmission lines, communication structures, and elevated pipelines which are exposed to the negative influence of soil frost heaving.

## Geocryological Problems Associated with Highways

Problems with embankment stability of subgrade soils are characteristic for highways within permafrost regions as well. Particularly for the newer "Amur" Highway extending from Chita to Khabarovsk (shown in Figs. 8–10) and the Qinghai–Tibet Highway (shown in Fig. 11).

The federal "Amur"–Chita to Khabarovsk Highway is one of the largest contemporary construction efforts in Russia. Construction of the road, having a length of 2165 km, began in 1978 and is planned for completion in 2010. However, even now, many sections of the road are subject to constant repairs that are not always successful. As an example, the high embankment on the "Amur" Highway, where it passes over Chichon Stream at 247 km, is presented. Here, the uneven subsidence of the 20 m high embankment has been observed since May 2001, soon after the delivery of this highway section. Since that time, as shown in Figure 8, subsidence of the road surface in some places has approached about 2 m, in spite of the periodic addition of soil and the re-leveling to profile grade.

Both transverse and diagonal cracks, having widths of up to 15 to 20 cm, are opening within the roadway, shoulders, and embankment slopes. The pavement surface is also highly deformed. This highway section is in a very distressed condition. The traffic speed for vehicles is now limited to 40 km/h for this section, while the designated design speed is 100 km/h.

During September 2006, the innovative repairs of this 200 m of failing section, as shown in Figure 9, was completed.

Almost 10 million rubles have been spent on repairs to date; however, as shown in Figure 10, deformation of the embankment section continues. The subgrade soil in this section consists of 15 to 20 m of permafrost, with the larger part being ice-rich soils that settle and flow upon thawing. As a result, permafrost degradation and corresponding deformation of the road under the prevailing conditions is

expected to continue indefinitely.There are a number of other such examples along the "Amur" Highway. Since much of the route passes through the southern fringe of discontinuous permafrost and also lies within a region of deep seasonal soil freezing, it is evident that an ongoing change in permafrost conditions and deep seasonal freezing will continue. Thus, it is important to identify permafrost conditions along the route, develop systematic means to address or control the cryogenic dynamics that adversely influence elements of the roadway, and initiate the timely application of protective measures. Therefore, in order to provide for a more effective operation of this highway, the system of engineering-geocryological monitoring of the "Amur" Highway was developed under the designation SIGMA "Amur."

In 2006, the TransEGEM organization developed and submitted to Rosavtodor the concept of SIGMA "Amur." Following is a summary of the developed concept (Kondratiev et al. 2007):

• The SIGMA "Amur" structure includes information gathering, processing and analysis of information, assessment and information storage, forecasting and projection of protective measures, and application of protection (implementation of protective measures).

• The operating scheme of SIGMA "Amur" provides for a number of regular procedures arranged into cycles for data gathering and processing, assessment of hazardous engineering-geocryological processes, forecasting their future development, and management of unfavorable processes.

• The operating structure of SIGMA "Amur" consists of several subsystems designed for different purposes: hierarchical, project monitoring, and operating subsystems, productive work, and methodical and technical support.

• Primary subjects of SIGMA "Amur" engineering-geocryological inquiry consists of three interrelated parts: geology-geographical, permafrost, and highway conditions.

• The overall program of the SIGMA "Amur" organization emphasizes optimal structure and consistency in practical operations, both with regard to organization and function.

• The plan is to implement a complex program with the aim to set up SIGMA "Amur." The program has three stages: preliminary stage, setup of information database, and the SIGMA "Amur" operation stage.

• Address proposals on the organization of SIGMA "Amur" operation.

The early creation and functioning of SIGMA "Amur" was intended to provide a more reliable and safe highway that will reduce less unproductive expenditures and improve its operations. Without application of such a concept, the "Amur" Highway will be subject to continuing repairs, constant traffic speed limitations for vehicles, and major financial and material losses.

In the 1950s the Qinghai–Tibet Highway was constructed with a gravel-crushed stone coating. In the 1980s, it was reconstructed, and in may sections, asphalt pavement was applied. This black pavement surface accelerated degradation of permafrost within the subgrade, producing

Figure 8. A section of road on the "Amur"–Chita to Khabarovsk Highway, km 247, before repairs, July 2006.

Figure 9. Same section of road on the "Amur"–Chita to Khabarovsk Highway, km 247, one month after completing innovative repairs, October 2006.

Figure 10. Same section of road on the "Amur"–Chita to Khabarovsk, km 247, eighteen months after completing innovative repairs, March 2008.

Figure 11. Deformation and displacement of an embankment slope on the Qinghai–Tibet Highway as a result of permafrost degradation outside the influence area of the thermosyphons, August 2006.

significant surface deformations in those sections having ice-rich soils. Also, those subgrades having frost heaving soils were adversely impacted (Wu et al. 1988). Recently the highway was reconstructed to meet contemporary high-speed vehicle standards. The highway, in essence, traverses parallel with the Qinghai–Tibet Railway. The highway has

a hard-surfaced pavement and utilizes anti-frost heaving measures in the sections having ice-rich soils. At some of these locations, thermosyphons have been placed in the form of one or two lines along roadway shoulders; however, as can be seen in Figure 11, some embankment problems have begun to occur. It is also expected that the thermosyphons will not protect the road from thermokarsts because of their limited radius of cooling.

## Conclusions

In conclusion, it is felt that the above information again demonstrates that, in order to achieve stable and reliable transportation routes in regions of permafrost and deep seasonal frozen soils, it is critical that a system be utilized which provides comprehensive geocryological exploration and evaluation, uses innovative and intelligent design solutions, allows timely and quality construction procedures, and provides for necessary ongoing maintenance.

## References

Kondratiev, V.G. 1994. Strengthening of roadbed base on very icy permafrost soils. *Abstracts of International Conference on Arctic Margins, Magadan, 1994.*

Kondratiev, V.G. 1996. Strengthening railroad roadbed bases constructed on icy permafrost soils. *Proceeding of Eighth International Conference on Cold Regions Engineering, Fairbanks, Alaska, 1996*.

Kondratiev, V.G. 1998. Measures to control deformation of roadbeds on icy rich permafrost. *Proceeding 8th Congress of International Association for Engineering Geology and the Environment. Vol. V. Vancouver, Canada, 1998:* 3365-3371.

Kondratiev, V.G. 2002. Design and experience controlling railroad embankment deformation on ice-rich permafrost. *Proceeding of the Eleventh International Conference, Cold Regions Impacts on Transportation and Infrastructure, Anchorage, 2002:* 467-482.

Kondratiev, V.G. 2004. Problems and ways of permafrost preservation in the roadbed basis. *Journal of Glaciology and Geocryology* (26) Supplement Aug. 2004: 8-11.

Kondratiev, V.G. 2005. Stabilization of roadbed and contact-line and air line supports on permafrost. Chita: Chitgu, 241 pp. (in Russian).

Kondratiev, V.G. 2006. The active methods of stabilization of roadbed and contact-line and air line supports on permafrost. *Abstracts of Asian Conference on Permafrost. Lanzhou, China, August 7–9, 2006:* 57-58.

Kondratiev, V.G. & Pozin V.A. 2000. *Concept of the System of Engineering-eocryological Monitoring of the Berkakit–Tommot–Yakutsk Railway.* Chita: Zantrans, 84 pp. (in Russian).

Kondratiev, V.G., Soboleva, S.V. & Dementiev A.D. 2007. Concept of the engineering-geocryological monitoring of the Chita–Khabarovsk federal highway "Amur." *Proceedings of the 8th International Symposium on Cold Region Development. Tampere, Finland, September 25–27, 2007:* 199-200.

Niu, F. & Shen, Y. 2006. *Guide of Field Excursion after Asian Conference on Permafrost (August 10–16, 2006)*. Lanzhou, China.

Wu, Z. et al. 1988. *Roadbed Engineering in Permafrost Regions*. Lanzhou University.

# The Influence of the Winter Season on Active Layer Depth in Taiga Landscapes, the Yakutsk Vicinity, East Siberia

P.Y. Konstantinov
*Melnikov Permafrost Institute SB RAS, Yakutsk, Russia*
R.N. Argunov
*Melnikov Permafrost Institute SB RAS, Yakutsk, Russia*
E.Y. Gerasimov
*Melnikov Permafrost Institute SB RAS, Yakutsk, Russia*
I.S. Ugarov
*Melnikov Permafrost Institute SB RAS, Yakutsk, Russia*

## Abstract

This paper presents the results of investigations on interannual variability of seasonal thaw depth in the taiga landscapes on the Lena-Kenkeme watershed in the vicinity of Yakutsk (East Siberia). The results of our investigations indicate that the depth of seasonal thaw is more strongly related to the interannual variation of winter ground heat loss than to the interannual variation of air thawing index or total summer precipitation.

**Keywords:** active layer; ground heat storage; ground temperature; seasonal thaw depth; soil moisture content.

## Introduction

The necessity of considering wintertime heat losses from the ground when analyzing seasonal thaw patterns is dictated by the specifics of the heat balance of the ground layer in contact with the atmosphere. The greater the winter heat loss from the ground (within the entire depth of annual heat exchange), the larger the amount of heat required for preliminary ground warming in the summer. Correspondingly, there will be some reduction in the proportion of the heat expended on phase transformation of soil moisture, and hence less energy will be available for deep summer thawing of the soil.

The winter heat loss from the ground shows strong variations from year to year. It is greater in years with thin snow cover and lower in those with deep snow. There are, however, no accurate methods for measuring or estimating this quantity. The intensity of winter cooling can be qualitatively characterized by the mean annual ground temperature at the active layer–permafrost boundary ($t_\xi$), because in permafrost areas the winter season plays a decisive role in the development of the ground thermal regime. Compared to the amount of ground heat exchange, $t_\xi$ is easier to determine experimentally and is found by standard measurements with temperature sensors permanently installed in the ground. The $t_\xi$ value is lower in the years of increased winter heat losses from the ground and is higher in years with reduced winter heat losses. Thus, the effect of variations in the winter ground heat loss on summer thaw depth can be estimated by investigating the relationship between thaw depth and interannual variation in mean annual ground temperature.

## Methods

A modified design of the Danilin-type frost gage developed for Russian weather stations was used in this study. This device determines the 0°C isotherm within the ground from the position of the thawed/frozen interface in the measuring tube with distilled water, which is removed for reading from the pipe that is permanently installed in the ground. The Danilin frost gage has two important advantages. First, determination of the 0°C isotherm in the surrounding ground from phase change of water in the measuring tube provides a sufficiently reliable measurement, requires no preliminary calibration, and has virtually unlimited time stability. Even if there is some difference between the position of the 0°C isotherm determined by the frost gage and the actual position of the phase boundary (or the top of plastic frozen soil in clay material) due to different freezing points of the soil and the tube water, this will not affect statistical parameters of the time series since the error will be systematic. Second, the use of the frost gage ensures that measurements are made at the same location each year; this eliminates the potential effects of spatial variation.

Many years of experience have shown that the Danilin frost gage provides accurate estimates of thaw depth, but that it is not satisfactory for the study of active layer freezing. Therefore, a considerably simplified design of the Danilin frost gage intended exclusively for determination of summer thaw depth has been used in this study. This design does not use an extractable measuring tube, eliminating air convection into the soil. The simplified version of the frost gage consists of a polypropylene tube with an outer diameter of 25 mm and an inner diameter of 20 mm, whose length exceeds the maximum possible thaw depth at a site. The tube is waterproof and sealed at the bottom. The sealed bottom is lowered into a small-diameter hole drilled for thaw depth measurement. The annulus is backfilled and thoroughly compacted. Then the tube is filled with distilled water to the ground surface level. The position of the 0°C isotherm in the ground is determined by a metal tape whose end is lowered

into the frost gage tube to the water/ice interface at the time of measurement.

Experimental investigations were conducted in taiga landscapes in the vicinity of Yakutsk (East Siberia, 62°N, 129°E). The thermal research program was initiated in 1996 (Konstantinov et al. 2001, Konstantinov & Fukuda 2001, Fedorov et al. 2003).

Experimental sites 1, 2, and 3 are located on the erosional plain (southern part of the study area) where the active layer consists predominantly of fine-grained sands (dry density 1100-1800 kg/m$^3$; 75%–85% sand, 8%–11% silt, and 6%–15% clay) and silty sands (dry density 1200–1750 kg/m$^3$; 61%–67% sand, 25%–29% silt and 6%–10% clay). Sites 4, 5, and 6 are located in the erosional-aggradational plain (northern part of the study area) where the soils consist mainly of silts (dry density 960-1700 kg/m$^3$; 19%–47% sand, 41%–66% silt, and 7%–20% clay).

Experimental site 1: Middle part of a long, gentle north-facing slope. Soils: sands and silty sands. Vegetation: *Laricetum arctouso-vacciniosum*.

Experimental site 2: Ridge crest. Soils: sands. Vegetation: *Lariceto-pinetum limnoso-arctostaphylosum*.

Experimental site 3: Upper part of a long, gentle north-facing slope. Soils: sands and silty sands. Vegetation: *Lariceto-betuletum limnoso-vacciniosum*.

Experimental site 4: Inter-alas surface surrounded by mature and growing thermokarst depressions. Soils: silts. *Mixtoherboso-graminosum* meadow.

Experimental site 5: Dry area on the bottom of a large thermokarst depression (alas). Soils: silts. *Mixtoherboso-graminosum* meadow.

Experimental site 6: Inter-alas surface. Large clear-cut area in larch forest where tree stands were removed in the early 1990s. Soils: silts. Vegetation: secondary growth of grasses and fragments of the low-shrub layer.

## Results

The values of basic meteorological variables for the period of investigation are presented in Table 1, using a provisory year starting from 1 October and ending on 30 September, so that one winter season would not fall in two different calendar years. Double figures are used; e.g., 1997/1998, 1998/1999, etc. The data indicate that the main meteorological parameters have strong interannual variability in the study area, resulting in significant interannual variations of mean annual ground temperature (Table 2). The maximum difference in $t_\xi$ has been 1.5°C–3.2°C in absolute values.

Interannual variations in maximum annual thaw penetration at experimental sites are given in Table 3. For the observation period, the standard deviation of thaw depth is 0.07–0.14 m, and the coefficient of variation is 0.04 to 0.09. As is seen, seasonal thaw depth is less variable than mean annual ground temperature, whose coefficient of variation is 0.25–0.47 for the same period. This fact imposes more stringent requirements on the instruments and methods used in field experiments. The use of only mechanical probing or soil temperature profiles in the study of interannual variation in seasonal thawing can result in errors, since these methods give less accurate estimates than the frost gage. This is especially critical in southern permafrost regions where active layer thicknesses exceed 1 m.

Tables 1 and 3 show that there is no obvious relationship between the active layer thickness and the air thawing index. Data for the period 2005–2007 confirm this conclusion. Interannual variations in the degree-days sum at the ground cover surface (May-September) are plotted in Figure 1. It is seen that the surface thawing index decreased in 2005–2007, but the depth of thaw and the mean annual ground temperature increased.

There is also no strong relationship between the seasonal thaw depth and the total summer precipitation. The years with the deepest (1999/2000) and shallowest (2000/2001) thaw penetration had total summer rainfall of 126 and 68 mm, respectively. The effect of precipitation on seasonal thaw depth appears not to be a major determinant here with this small difference in precipitation totals, considering that their range over the observation period was 68 to 256 mm. A distinct relationship between thaw depth and summer precipitation was only observed at Site 1 located in the middle part of a long, gentle slope with a larch stand on sandy soils (Tables 1, 3). In 1998/1999, 2004/2005, 2005/2006, and 2006/2007 high suprapermafrost groundwater flow occurred at this site after heavy rains, resulting in the deepest thaw.

Tables 2 and 3 and Figure 1 show that seasonal thaw depth increased in years with higher mean annual ground temperatures (1999/2000, 2004/2005, 2005/2006, and 2006/2007) and decreased in years with lower $t_\xi$ (2000/2001, 2001/2002, 2002/2003, and 2003/2004). During the period of observations, $t_\xi$ was warmest in 1999/2000. In that year most sites experienced maximum thaw depths, while air thawing indices and rainfall totals were within the average range of the series variation. The best agreement between the interannual variability of thaw depth and that of mean annual temperature was observed at sites with the minimum $t_\xi$ difference over the observation period (Site 6).

If we compare thaw development in four years with the coldest ground temperatures (2000/2001, 2001/2002, 2002/2003, and 2003/2004), it is seen that the depth of thaw was not shallowest in the coldest year 2002/2003. This discrepancy can be explained if one compares pre-summer soil moisture contents in these years, which were 1.5–1.8 times higher in 2000/2001 and 2003/2004 compared to 2001/2002 and 2002/2003 (Fig. 2). This is the reason for minimum thaw in 2000/2001 and 2003/2004: greater heat loss is required for phase change of soil moisture under the conditions of increased seasonal ice content in the active layer. Shallower thaw depth at Site 2, which experienced warmer ground temperatures in 2006/2007 compared to 2005/2006 can also be attributed to the effects of variations in seasonal ice content. Many investigators have shown that opposite trends in thaw depth can occur over short distances. One possible explanation is the effect of seasonal ice content in the active layer, because ground conditions vary greatly over

Table 1. Meteorological parameters over the observation period.

| Meteorological parameter | 1997 / 1998* | 1998 / 1999* | 1999 / 2000* | 2000 / 2001* | 2001 / 2002* | 2002 / 2003* | 2003 / 2004* | 2004 / 2005* | 2005 / 2006* | 2006 / 2007* |
|---|---|---|---|---|---|---|---|---|---|---|
| $\Sigma_{-t}$ | -5051 | -5341 | -5026 | -5529 | -4658 | -5022 | -5109 | -5394 | -5053 | -4709 |
| $\Sigma_{+t}$ | 2158 | 1964 | 1941 | 2014 | 2139 | 1996 | 1821 | 2087 | 2034 | 2019 |
| $t_{m.a.}$ | -8.0 | -9.4 | -8.6 | -9.8 | -7.0 | -8.4 | -9.2 | -9.2 | -8.4 | -7.5 |
| $R_s$ | 146 | 196 | 126 | 68 | 89 | 243 | 128 | 199 | 256 | 191 |
| $h_{sn}$ | 0.27-0.29 | 0.29-0.32 | 0.32-0.38 | 0.16-0.20 | 0.22-0.25 | 0.10-0.16 | 0.15-0.18 | 0.40-0.45 | 0.38-0.42 | 0.36-0.40 |
| $h_{sn\ max}$ | 0.40-0.45 | 0.43-0.48 | 0.40-0.45 | 0.27-0.30 | 0.42-0.48 | 0.26-0.29 | 0.30-0.38 | 0.50-0.60 | 0.43-0.47 | 0.50-0.55 |

Explanations: * - the annual period from 1 October to 30 September; $\Sigma_{-t}$, $\Sigma_{+t}$ - sum of freezing and melting degree-days (Yakutsk station); $t_{m.a.}$ - mean annual air temperature (Yakutsk station), °C; $R_s$ - summer precipitation, mm (Yakutsk station); $h_{sn}$ - depth of snow cover at the experimental sites (data are as December 1), m; $h_{sn\ max}$ - maximum depth of snow cover at the experimental sites (data are as March 1), m.

Table 2. Mean annual ground temperature at experimental sites over the observation period.

| Site | Mean annual ground temperature, °C | | | | | | | | | | Average value | Standard deviation | Coefficient of variation |
|---|---|---|---|---|---|---|---|---|---|---|---|---|---|
| | 1997 / 1998 | 1998 / 1999 | 1999 / 2000 | 2000 / 2001 | 2001 / 2002 | 2002 / 2003 | 2003 / 2004 | 2004 / 2005 | 2005 / 2006 | 2006 / 2007 | | | |
| 1 | -2.5 | -2.6 | -1.6 | -2.9 | -3.0 | -3.4 | -3.2 | -2.6 | -1.4 | -1.2 | **-2.4** | **0.77** | **0.32** |
| 2 | -1.7 | -1.7 | -0.9 | -2.2 | -2.0 | -2.7 | -2.4 | -1.7 | -1.0 | -0.6 | **-1.7** | **0.68** | **0.40** |
| 3 | -1.6 | -1.6 | -0.8 | -1.9 | -1.9 | -2.3 | -2.2 | -1.8 | -0.9 | -0.6 | **-1.6** | **0.59** | **0.38** |
| 4 | -2.2 | -2.0 | -1.5 | -1.8 | -1.7 | -2.7 | -2.3 | -1.6 | -1.5 | -1.1 | **-1.8** | **0.47** | **0.25** |
| 5 | -2.6 | -2.4 | -1.4 | -2.5 | -2.6 | -3.2 | -3.0 | -2.0 | -1.5 | -0.8 | **-2.2** | **0.76** | **0.35** |
| 6 | -1.8 | -2.0 | -1.2 | -2.8 | -3.4 | -4.4 | -3.4 | -2.1 | -1.4 | -1.1 | **-2.4** | **1.10** | **0.47** |

Table 3. Maximum depth of summer thaw at experimental sites over the observation period.

| Site | Depth of summer thaw, m | | | | | | | | | | Average value | Standard deviation | Coefficient of variation |
|---|---|---|---|---|---|---|---|---|---|---|---|---|---|
| | 1997 / 1998 | 1998 / 1999 | 1999 / 2000 | 2000 / 2001 | 2001 / 2002 | 2002 / 2003 | 2003 / 2004 | 2004 / 2005 | 2005 / 2006 | 2006 / 2007 | | | |
| 1 | 1.50 | 1.57 | 1.52 | 1.46 | 1.52 | 1.54 | 1.37 | 1.62 | 1.60 | 1.67 | **1.54** | **0.09** | **0.06** |
| 2 | 2.01 | 1.97 | 2.08 | 1.91 | 1.92 | 2.01 | 1.94 | 2.12 | 2.17 | 2.10 | **2.02** | **0.09** | **0.04** |
| 3 | 1.83 | 1.88 | 1.91 | 1.73 | 1.83 | 1.80 | 1.71 | 1.90 | 1.97 | 1.98 | **1.85** | **0.09** | **0.05** |
| 4 | 1.85 | 1.77 | 2.07 | 1.63 | 1.86 | 1.81 | 1.79 | 1.96 | 2.00 | 2.03 | **1.88** | **0.14** | **0.07** |
| 5 | 1.76 | 1.80 | 1.84 | 1.66 | 1.77 | 1.76 | 1.71 | 1.82 | 1.84 | 1.90 | **1.79** | **0.07** | **0.04** |
| 6 | 1.53 | 1.49 | 1.66 | 1.39 | 1.43 | 1.44 | 1.39 | 1.62 | 1.65 | 1.77 | **1.54** | **0.13** | **0.09** |

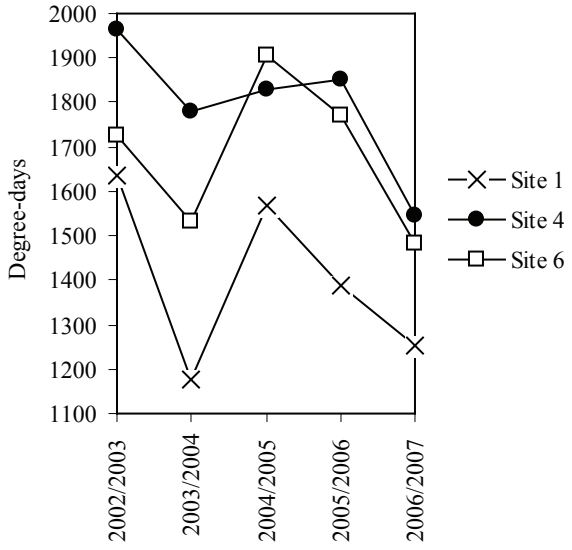


Figure 1. Interannual variations of degree-days sum at the ground cover surface.

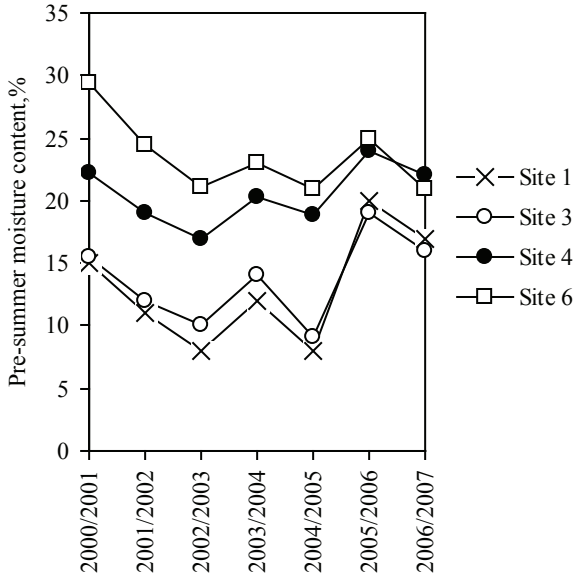


Figure 2. Interannual variation in the pre-summer moisture contents of the active layer (averages for the entire active layer profile).

space. Adjacent sites can therefore experience very different thaw rates if they show dissimilar variations in seasonal ice content from year to year. These examples demonstrate that soil moisture is an important consideration in the study of interannual variability of seasonal thaw depth.

Data on the effect of winter factors on active layer thickness are available mostly for the regions with a continental climate, such as Central Yakutia and northern Tian Shan (Blagoobrazov 1964, Skryabin et al. 1998, Marchenko 2002, Konstantinov et al. 2006). For the coastal regions of the permafrost zone, the depth of thaw has been found to be more sensitive to summer factors, mainly the thawing index (Brown et al. 2000, Leibman 2001, Fedorov-Davydov et al. 2004, Mazhitova & Kaverin 2007).

## Conclusions

The results of our investigations indicate that in the taiga landscapes of the Yakutsk area, the depth of seasonal thaw is more strongly related to the interannual variation of winter ground heat loss than to the interannual variation of the air thawing index or total summer precipitation. This suggests that in years with warmer summers, the heat surplus at the ground surface is largely expended to increase eddy heat flux and latent heat flux, with only a small portion spent on heat flow into the soil. One of the major factors controlling seasonal thaw depth is soil moisture content in the active layer, which deserves a more in-depth study to develop a better understanding of the problem.

The findings of this study and other studies indicate that the relationship of active layer depth to winter factors is much stronger in the continental areas than in the coastal regions.

## Acknowledgments

This study received partial financial support from Japan Science and Technology Corporation (JST) and Japan Agency for Marine-Earth Science and Technology (JAMSTEC).

## References

Blagoobrazov, V.A. 1964. Seasonal and long-term fluctuations of the permafrost table in flatlands of Central Tien Shan. In: *Glaciological Investigations in Tien Shan.* Frunze: Kyrghyz Academy of Sciences Press, 65-76.

Brown, J., Hinkel, K.M. & Nelson, E.F. 2000. The Circumpolar active layer monitoring (CALM) program: research designs and initial results. *Polar Geography* 24(3): 165-258.

Fedorov, A.N., Gavriliev, P.P. & Konstantinov, P.Y. 2003. Study of permafrost-landscape dynamics at Spasskaya Pad. *J. Nauka I Obrazovanie* 3: 62-65.

Fedorov-Davydov, D.G., Davydov, S.P. & Davydova, A.I. 2004. Spatial and temporal regularities of soil seasonal thawing in the north of the Kolyma lowland. *Kriosfera Zemli* VIII(4): 15-26.

Konstantinov, P.Y., Argunov, R.N. & Gerasimov, E.Y. 2006. On the relationship between seasonal thaw depth and interannual variation of mean annual ground temperature. *Kriosfera Zemli* X(3): 15-22.

Konstantinov, P.Y., Rusakov, V.G. & Fukuda, M. 2001. Thermal Regime of the Upper Permafrost Layers in Taiga Landscapes, Yakutsk Area, 1996-2000. *Proceedings of the 9th Symposium on the Joint Siberian Permafrost Studies between Japan and Russia in 2000*. Sapporo: Hokkaido University, 204-209.

Konstantinov, P.Y. & Fukuda, M. 2001. Temperature Regime of the Upper Permafrost in the Yakutsk Area *Proceedings of the Second International Workchop on Global Change: Connection to the Arctic.* Sapporo: Hokkaido University, 103-106.

Leibman, M.O. 2001. Active-layer dynamics and measurement technique at various landscapes of central Yamal. *Kriosfera Zemli* V(3): 17-24.

Marchenko, S.S. 2002. Results of monitoring of active layer in the northern Tien Shan Mountains. *J. Kriosfera Zemli* VI(3): 25-34.

Mazhitova, G.G. & Kaverin, D.A. 2007. Thaw depth dynamics and soil surface subsidence at a Circumpolar active layer monitoring (CALM) site, the European north of Russia. *Kriosfera Zemli* XI(4): 20-30.

Skryabin, P.N., Varlamov, S.P. & Skachkov, Y.B. 1998. *Interannual Variations in the Ground Thermal Regime, Yakutsk Area.* Novosibirsk: SB RAS Press, 144 pp.

# Landscape Geochemical Features and Peculiarities of $^{137}Cs$ Distribution in Tundra Landscapes of the Lower Pechora Reaches

E.M. Korobova
*Vernadsky Institute of Geochemistry and Analytical Chemistry, Russian Ac. of Sciences*
N.G. Ukraintseva
*All-Russia Research Institute for Pipelines*
V.V. Surkov
*Moscow State University*

## Abstract

Distribution of natural and man-made chemical elements in soils and vegetation of modern landscapes of the Lower Pechora floodplain and the adjacent terrace was studied along landscape transects crossing the floodplain and terrace zones at different distances from the coast (Bolvansky Cape) to the settlement of Bol'shaya Sopka to reveal peculiarities due to landscape structure and natural migration processes. River water was characterized by low salinity (35–131 mg/l) and hydrocarbonate-calcium composition, while groundwater was comparatively enriched in magnesium, sodium, chlorine ions (39, 26, 31 meq%) and water-soluble organics (peaty areas, 540–2450°, Pt-Co scale). The concentration of $^{137}Cs$ in soils and vegetation was within the global fallout level, but varied considerably (2.5–215 Bq/kg and 24–365 Bq/kg dry weight, correspondingly) in relation to hydrological, landscape, and soil features of the area, the plant species enabling discussion of the recent history of migration processes in landscapes after man-made contamination.

**Keywords:** $^{137}Cs$ in soils and plants; landscape geochemistry; Lower Pechora; radioecology; radionuclide profiles.

## Introduction

Draining vast areas, the rivers of the Arctic basin play an important role in its material balance on its margins rich in bioresources. The Pechora River basin belongs to an area with minor man-made impact and is, therefore, of interest for monitoring global man-made contamination and its history in high-latitude permafrost regions. Being a ubiquitous artificial marker of contamination, $^{137}Cs$ has been included in natural processes for more than 50 years and can serve as the tracer of spatial transformation of aerial contamination in modern landscapes. The objectives of this study were to reveal landscape heterogeneity and peculiarities of $^{137}Cs$ redistribution in the Lower Pechora area. The two main morphological elements, namely the floodplain and terrace area, were selected to compare the river transport and in situ migration with permafrost impact.

## Study Area and Methods

Field studies were performed in the area of the Lower Pechora basin in 2003 and 2004. The strategy of investigation was similar to that applied in the Lower Yenisey reaches (Korobova et al. 2007). A series of landscape transects crossing the floodplain and terrace zones were located at different distances from the coast: Cape Bolvansky, Yushino settlement on the right river side, the upper delta Ekushnaky (EK) and Kermundei (KM) Islands, the right river side near Naryan Mar, and on the left high terrace near Bol'shaya Sopka (Table 1). Soil, water, and plant samples were taken at the selected sites characterizing the two main geomorphological levels. They correspond to terraces and flooding zones in order to compare radiocesium distribution in landscape components under atmospheric water migration and river transport. The location of study sites in a meridional seaward direction was to follow the marine impact and the delta island formation.

Soil profiles were sampled continuously, with sampling increments ranging from 2–10 cm to a depth of 40–100 cm. Vegetation was described by species composition and abundance and sampled at 0.25 $m^2$ plots located over the soil profiles. Surface and groundwater samples collected at selected points of the cross section were filtered, sealed, and preserved in a dark freezer (-5°C) for transportation to the laboratory. Ion composition of water samples was determined with the help of ion selective electrodes ($NO_3^-$, $Cl^-$), titrimetry ($HCO_3^-$), nephelometry ($SO_4^{2-}$), photometry ($NH_4^+$, $PO_4^{3-}$) techniques and AES-ICP (cations). Accuracy of determination did not exceed 5%.

$^{137}Cs$ and $^{40}K$ were determined in soil and plant samples with the help of a Canberra gamma-spectrometer with an HPGe detector. $^{137}Cs$ determination error equaled on the average 31% and 33% (soils and plants), $^{40}K$ – 19% (soils), correspondingly, depending upon the concentration level.

## Chemical Composition of the Surface and Ground Water on Terrace and Flood Plain

Water samples were analyzed to characterize $^{137}Cs$ water migration conditions (Sanchini 1988). Salinity and colority of water, as well as suspended load, considerably varied in their type, landscape position, and distance from the sea

Table 1. Sampling plots location.

| Location | Sampling plots indices | Geomorphology | Soil and vegetation cover | Active layer depth, cm | Sampling depth, cm |
|---|---|---|---|---|---|
| Cape Bolvansky, 3,5 south from the Pechora mouth | A3p | III marine terrace, top of the hill | Polygonal undershrub-lichen tundra | 110 | 120 |
| | A11 | Terrace backslope | Shrubby tundra, peaty soil on buried peaty gley | >180 | 180 |
| | P1 | Alluvial-marine floodplain, flat ridge on its shoulder | Polygonal undershrub-lichen tundra, lichen polygon with alluvial humus-peaty gley soil | 80 | 30 |
| | P2 | Inter-ridge depression on the riverside coastal floodplain | Willow with horsetail-reedgrass-sedge tussock cover on humus-peaty soil with buried humus-peaty layer | Bed talik | 30 |
| Lower delta, near set. Yushino | Yu1 | Low glacial-marine terrace, flat rise on the summit | Polygonal lichen tundra with undershrub, peaty gley loamy soil with detritus | >90 | 70 |
| | Yu2 | The talf close to the edge of the terrace | Undershrub-sphagnum-lichen peat on humus-peaty soil | 42 | 45 |
| Lower delta, Gluboky Island | Gl1 | Frontal part of the plain 1.5 m above low water level (LWL) | Willow stand with horsetail-reedgrass-meadow sweet overground cover on soddy-gley sandy loam soil | Bed talik | 125 |
| Southern suburbs of Naryan Mar | NM2-03 | II High terrace | A fragment of the old spruce forest with thick moss-lichen cover on tundra forest sandy soil | >80 | - |
| Medium delta, 200 m from set. Iskateli | NM3 | I high terrace, 11.6 m above LWL | Birch-larch elfin forest with moss-lichen cover on oddy-weakly podzolized soil developed on humus-podzolic illuvial-ferrugenous sandy soil | >140 | 120 |
| | NM6 | Sandy dunes on the edge of the terrace 4.3 m above LWL | Exposed profile Aeolian sand covering buried soddy-podzolic soil | >400 | 125 |
| Medium delta, right side coastal floodplain | NM4 | Inter-ridge abandoned channel 1,0 m above LWL | Willow shrubs sedge-herbaceous on soddy laminated loamy sand soil | Bed talik | 30 |
| | NM5 | Riverside alluvial ridge of the low level floodplain | Willow shrubs with pioneer herbages on primitive weakly soddy laminated sandy soil | Bed talik | 50 |
| | NM1a | Inter-ridge depression | Herbaceous-sedge wet meadow with horsetail and willow restoration on silty-gley soil | Bed talik | 80 |
| Medium delta, Ekushansky Island | EK1 | Exposed profile of the low level floodplain | Light herbaceous-grass cover (surface coverage – 10%), soddy sandy soil on laminated alluvium | Bed talik | 190 |
| | EK2 | Exposed profile of the medium-level coastal floodplain | Herbaceous-grass meadow with high willow, soddy sandy soil overlain buried soody gley soil underlain by peaty silty gley soil | Bed talik | 66 |
| Medium delta, Kermundej Island | KM1 | Edge of abandoned channel between the two former isles, 27 cm above LWL | Wet tussock sedge meadow on silty-gley soil | Bed talik | 67 |
| | KM2 | Western toeslope to central depression | Herbaceous-reedgrass-sedge meadow on soddy-gley loamy soil on sandy alluvium | Bed talik | 85 |
| | KM3 | Riverside ridge of the high floodplain 3,90 m above LWL | Thin high willow with horsetail stand on primitive weakly sod laminated soil | Bed talik | 90 |
| | KM4 | Wide inter-ridge depression. | Bushy willow thicket with grass and horsetail on soddy gleyish loamy soil on sandy and loamy alluvium | Bed talik | 125 |
| | KM5 | Ridge on the medium-level floodplain abruptly sloping to the young depression | Bushy willow with herbaceous-leguminous-grassy cover on soddy light loamy laminated soil on sandy alluvium | Bed talik | 90 |
| | KM6 | Medium level floodplain 3,6 m above LWL. | High willow with alder and herbaceous-leguminous-grassy cover stand on soddy sandy loam soil | Bed talik | 90 |
| Near set. Bolshaya Sopka | BS1 | High terrace on the left riverbank | Polygonal moss-lichen tundra with undershrubs on peaty gley soil developed on pebbled moraine loams | 86 | 90 |
| | BS2 | Flat shallow depression on the terrace | Undershrub-lichen-moss peat on humus-peaty-gley soil | 43 | 53 |

(Table 1). The Pechora River water was characterized by neutral pH value, low salinity (0.07–0.13 g/l) and colority except for its deep inlet at Kermundej Island (Table 2). Water salinity was the highest in the soil water on Cape Bolvansky terrace (0.193 g/l) close to the sea aquatory. The adjacent terrace foot and the lower floodplain groundwater were much fresher (<0.06 g/l) due to river impact. Low water salinity not exceeding 0.05 g/l was observed on the peaty watersheds upstream, while soil water of the islands and the river water were two times the value. Salinity correlated

Table 2. General characteristics of water samples

| Sampling places | Water type | Suspension, g/l | Colority, grad | Salinity, mg/l |
|---|---|---|---|---|
| 1. Cape Bolvansky | r* | | | 70 |
| 2. Gluboky Shar | r | 0,172 | 35 | 131 |
| 3. Gorodetsky Shar | r | 0,116 | 16 | 129 |
| 4. Kermundej Island | r | 0,106 | 35 | 131 |
| 5.Creek at Kermundej Island | r | 0,099 | 135 | 109 |
| 6. Naryan Mar (2003 year) | r | | | 94 |
| 7. Naryan Mar (2004 year) | r | 0,083 | 26 | 131 |
| 8. Naryan Mar | tap | - | 10 | 118 |
| 9. Yushino terrace (Yu2)** | gr | 0,891 | 2450 | 39 |
| 10. Yushino terrace peat | pt | 0,141 | 620 | 45 |
| 11. Yushino Lake | l | 0,165 | 82 | 35 |
| 12. Kermundej low floodplain (KM1)** | gr | 0,420 | 26 | 164 |
| 13. Kermundej Island , abandoned channel | l | 0,120 | 55 | 113 |
| 14. Ekushansky Island, Rybnoe Lake | l | 0,121 | 45 | 87 |
| 15. Bolshaya Sopka peat | pt | 0,419 | | 70 |

* r – *Pechora River*; l – *lake*; pt - *peat*; gr –*ground*.
** Sampling plots indices – see Table 1.

with pH ($r$=0.701, $n$=14) and water hardness ($r$=0.895). A tendency of negative relation was observed between salinity and colority ($r$=-0.528, n=13).

Peaty areas were noted for enhanced colority of water (up to 2450º, Pt-Co scale) due to soluble organic substances most abundant in the active layer of tundra humic gley soils. Suspended load determined varied from 0.1 to 0.8 g/l and increased in the groundwater of organic soils (Tables 1, 2).

*Ion composition*

Ion composition of ground-water presented in Figure 1 proved considerable leaching of the former marine sediments developed on Cape Bolvansky terrace. However, relatively high chlorine, magnesium, and low hydro-carbonate ion content indicate the marine contribution. The Pechora water near Cape Bolvansky was relatively enriched in sodium. A higher percentage of sodium and potassium ion content was found in the groundwater of Yushino soils. Pechora River water was relatively enriched in chlorine (up to 0.4 meq/l) and sodium (maximum 0.28 meq1/l) as compared to groundwater collected from soil cuts on the adjacent coastal zone and terraces (0.23 meq/l and 0.17 meq/l correspondingly). Chlorine, sulphate ions, and strontium content in the river water slightly decreased upstream, while potassium concentration in river water increased upstream (from 0.6 mg/l to 1.1 mg/l) being in general lower as compared to groundwater (up to 1.7 mg/l in the latter).

Terrestrial water compared to the river was noted for enhanced content of $NH_4^+$ (0.4–2.6 mg/l) and $PO_4^{3-}$, the highest nitrate ion amount $NO_3^-$ (0.03–013 meq/l), and a large value of chemical oxygen demand (130–433 $mgO_2$/l,) in

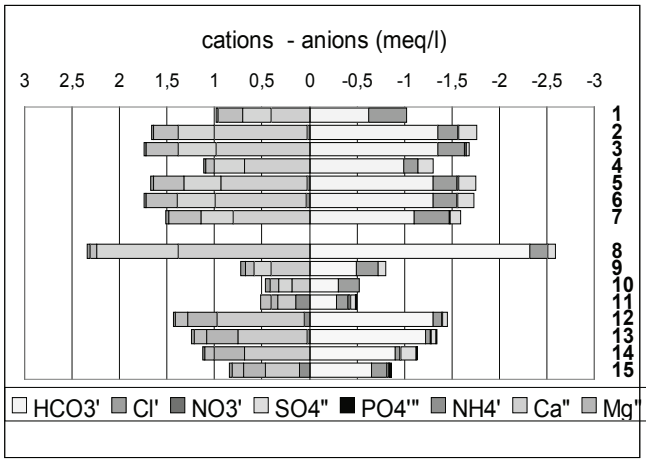


Figure. 1. Chemical composition of water samples positioned in southward direction. 1–15 - sampling places, see Table 2.

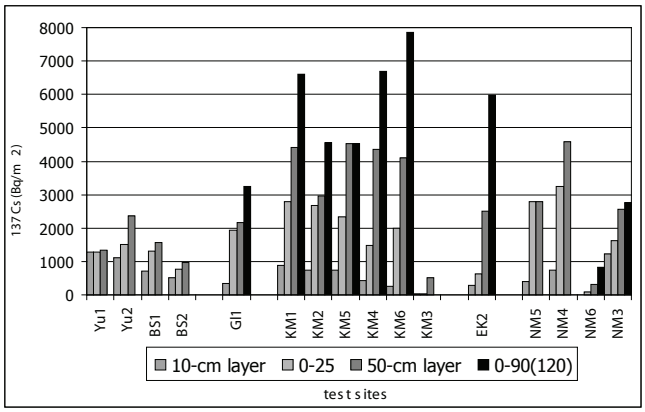


Figure 2. $^{137}$Cs inventory in soil layers of different thickness. Sampling plots indices – see Table 1.

water of the peaty terraces (Pechora–17 mg/l, determination by V. Filonenko). It was at least twice as rich in silicon and iron as compared to the river. Performed analysis showed chemical signatures of the increasing influence of the marine environment that can be direct (aerial and water) and indirect (marine sediments) on both the terrace landscapes and river water and a considerable enrichment of the Pechora tundra terrace soils in water-soluble organic compounds and mobile iron. Similar water migration conditions due to vicinity of the sea seaward increase of salinity, chlorine and sodium in water and soil water extractions) and cryogene concentration of salts (enrichment of the tundra soils in water-soluble organic compounds and iron) were found earlier for the Lower Yenisey landscapes (Ivanov & Vlasov 1974, Korobova et al. 2003, 2004).

## $^{137}$Cs Distribution in Soils

*$^{137}$Cs inventory in soils*

$^{137}$Cs activity determined in 203 samples collected from different soil layers was within the global fallout level and varied from 0.58 to 215 Bq/kg (dry weight – dw).

Radiocesium contamination density varied within sixteen studied plots from 0.8 to 7.8 kBq/m$^2$, V = 57% (Fig. 2). Mean

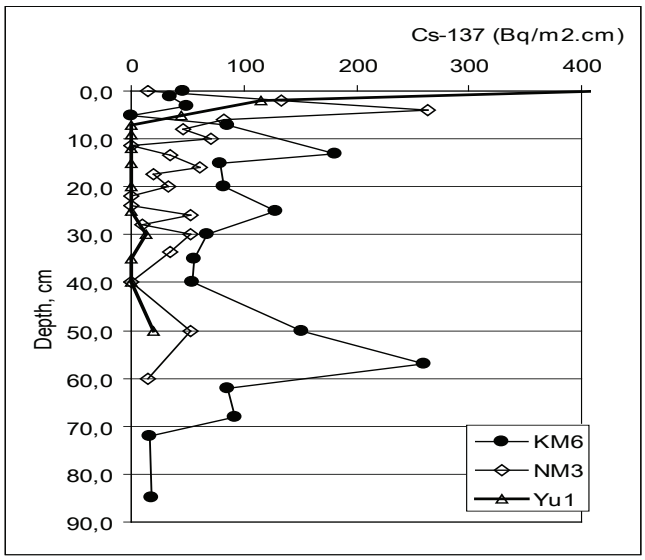


Figure 3. Three main types of $^{137}$Cs profiles at the studied in Lower Pechora region. Sampling plots indices – see Table 1.

value equaled 4.8 ± 0.6 kBq/m$^2$ that corresponded to the data published in the *Atlas of Radioactive Contamination of Russia* (*Atlas* 1998, Wright et al. 1997, Strand et al. 1998).

Topsoil layers were most contaminated at watersheds (over 1 kBq/m$^2$, plots Yu1, 2; NM3, terrace landscapes). However, the contamination density within the total sampled depth was found the highest for the floodplain plots. The floodplain soils appeared to contain in total several times the amount of $^{137}$Cs determined in the active layer of the terrace soils (Kermundej Island, Fig. 2).

$^{137}$Cs is known to be easily adsorbed by clay particles via ion exchange of interlayer cations or on the mineral edge defects (Evans et al. 1983, Cornell 1993, Bostick et al. 2002). Therefore, it seemed interesting to compare its inventory with that of natural $^{40}$K since in sands, potassium concentration is in general three times lower than that in clay sedimentary rocks.

$^{40}$K inventory was the lowest in fresh sandy deposits of the medium-level sandy bars (KM3, NM6). In the organic soils of the peaty terraces, especially most distant from the coast (plot BS), $^{40}$K inventory was the lowest. Positive correlation was established between $^{137}$Cs and $^{40}$K in 10–25 cm soil layer for all plots (0.760, *n*=14), in the lower (50–130 cm) mineral layers (0.640, *n*=8) and the total layer (0–130 cm, 0.708, *n*=9) in floodplain landscapes. In the top 10–cm layer of floodplain $^{137}$Cs and $^{40}$K relation was negative, while in watershed top organic horizons it had a positive tendency (*r*=0.653, *n*=5).

*$^{137}$Cs profiles in terrace and floodplain soils*

Our earlier investigations performed in the Lower Yenisey River basin showed that distribution in soil profiles significantly depended upon the origin of contamination (global fallout or regional river discharge) and geomorphological position of the plot (Korobova et al. 2004, 2007). In the Lower Pechora reaches the highest $^{137}$Cs values were characteristic for terrace landscapes (215 Bk/kg, Yu2; 65–120 Bq/kg, NM3). Specific $^{137}$Cs activity of the floodplain soil layers did not exceed 20 Bq/kg, reaching maximum in the buried

Table 3. Fraction and $^{137}$Cs distribution in pedon NM3 (see Table 1).

| Horizon index, depth (cm) | Fraction (mm* %) | | | | Cs-137 in fractions (%) | | | |
|---|---|---|---|---|---|---|---|---|
| | Coarse organic debris | | Mineral fraction | | Coarse organic debris | | Mineral fraction | |
| | 1* | 2 | 2 | 3 | 1 | 2 | 2 | 3 |
| 0i | 35 | 0,0 | 9,4 | 5,6 | 33 | 0,0 | 0,0 | 67 |
| OeA1(0-2) | 12 | 7,9 | 0,0 | 80 | 19 | 15 | 0,0 | 66 |
| A (2-4) | 10 | 0,0 | 5,2 | 8,5 | 13 | 0,0 | 9,3 | 77 |
| A (4-6) | 6,7 | 0,0 | 12 | 81 | 19 | 0,0 | 29 | 52 |
| A/Eol(6-8) | 3,7 | 0,0 | 9,2 | 87 | 24 | 0,0 | 19 | 57 |
| Eol(8-10) | 2,9 | 1,5 | 13 | 82 | 39 | 7,7 | 26 | 28 |
| Ab(12-14) | 3,7 | 13 | 0,0 | 84 | 27 | 73 | 0,0 | 0,0 |
| A/Eb(14-16) | 2,1 | 0,0 | 14 | 84 | 48 | 0,0 | 16 | 36 |
| Eb (16-18) | 37 | 0,0 | 7,1 | 56 | 57 | 0,0 | 21 | 23 |
| B1s(18-20) | 0,5 | 0,0 | 16 | 83 | 0,0 | 0,0 | 100 | 0,0 |
| B2hs(24-26) | 0,4 | 0,0 | 27 | 72 | 0,0 | 0,0 | 100 | 0,0 |
| BChs(26-28) | 0,8 | 0,0 | 35 | 65 | 100 | 0,0 | 0,0 | 0,0 |
| BCs(28-30) | 1,2 | 0,0 | 29 | 70 | 24 | 0,0 | 0,0 | 77 |
| BC(30-33,5) | 3,6 | 0,0 | 30 | 66 | 0,0 | 0,0 | 100 | 0,0 |
| C(40-50) | 0,1 | 11 | 0,0 | 89 | 0,0 | 28 | 0,0 | 72 |
| C(50-60) | 0,0 | 0,0 | 7,9 | 92 | 0,0 | 0,0 | 100 | 0,0 |

*1- <1mm; 2 - 1–.25 mm; 3 - >0.25 mm.

layers sampled on Kermundej Island

Concentration peaks in the terrace undisturbed tundra peaty and humus-peaty gley soils corresponded to the top 2-cm layer, to the boundary of the organic and gley mineral horizons (from 20 to 45 cm), and to the bottom of the active layer (40–60 cm) with the maximum radiocesium specific activity in the top organic horizon.

In the southern part of the study area, where the terrace soils are subjected to strong wind erosion and sand deposition, the soil profile (NM3) consisted of a sequence of organic layers or lenses interlacing with pure sands. Easy leaching of these horizons cause formation of podzolized, illuvial organic and ferric layers forming beneath the humic one. The most pronounced $^{137}$Cs peak corresponded to the top organic layer (13–29 Bq/kg). Below the $^{137}$Cs curve acquires a saw-tooth character with double increase in the buried humus horizon (5.5 Bq/kg). Contamination density of each layer reduced to its thickness allowed compare the horizons of the terrace and floodplain soils by $^{137}$Cs fixation ability within the volume unit and demonstrated that maximum $^{137}$Cs fixation in floodplain and terrace soil layers are of similar order (Fig. 3).

To study $^{137}$Cs fixation in particles bound to organic matter, we undertook dry sieving of samples from profile NM3 and measured $^{137}$Cs in fractions >1, 1, 1–0.25 and <0.25 mm. The coarse fraction consisted mainly of organic debris (litter, bark, roots) in various stages of decomposition. Fraction 1–0.25 mm, referred to as coarse and medium sand fraction according to U.S.D.A (Shaetzl & Anderson 2006), was a mixture of humified organic debris and organo-mineral aggregates which were separated visually into two parts: one enriched in organic debris and one not enriched. The smallest sandy fraction was

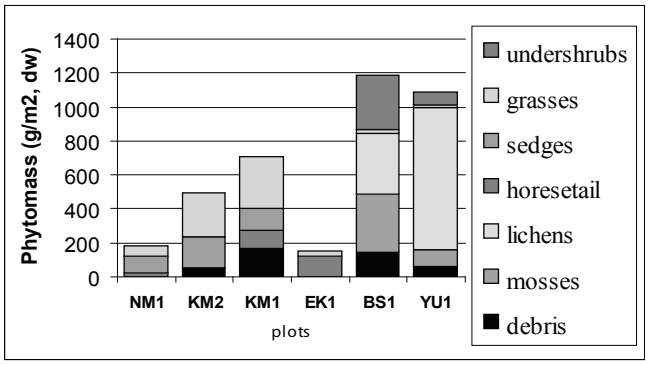


Figure 4. Phytomass of the selected plots and its composition. Plots indices – see Table 1.

mainly mineral. However, organic and ferric coating and charcoal particles were also present.

Fraction <0.25mm dominated by weight throughout the whole pedon (Table 3). Fine fraction played the main role in $^{137}$Cs fixation in the top, newly formed organic horizon. In the buried organic lenses the major radionuclide portion (73%) was associated with slightly decomposed and humified organic debris. Mineral grains and aggregates 1–0.25 mm in diameter, enriched in $^{137}$Cs, were found in textured illuvial horizons with humus and ferric iron accumulation. In transition to parent alluvium and sandy alluvium, all cesium supply was retained in this mineral fraction. Such distribution clearly showed that the organic matter is able to conserve $^{137}$Cs for a long time. The form of the curve below the buried horizon and the low value of $^{137}$Cs concentration give reason to suggest periodic deposition of slightly contaminated sediments by wind or water. However, a simple downward radionuclide migration in highly permeable sandy soils cannot be excluded.

Floodplain soils had several peaks of $^{137}$Cs at definite depths (KM6, Fig. 3). On Kermundej Island, most profiles had three peaks, that is, 1, 15, and 30 cm in the silty gley soil on low-level floodplain (KM1) and 8–13, 25–30 and 52–57 cm on the medium level (KM4, KM5, KM6). The primitive sandy soil of the riverside high ridge (KM3) had the first pronounced peak at the depth of 50–60 cm. Similarity in radiocesium curves suggests synchronic sedimentation of the layers with the corresponding depth peak concentration. Higher $^{137}$Cs deposition during flooding is usually explained by river erosion of the contaminated sediments and soil layer over vast areas. Using hydrological data helps to reconstruct maximum local flooding periods and to evaluate erasing and depositing capacity of the river.

The low contribution of the Chernobyl accident cannot be separated out from the total contamination using our data. However, this does not contradict the suggestion that the upper peak in soil profiles includes the Chernobyl contribution.

Three cuts were investigated on the left bank of Ekushansky Island severely eroded by the Pechora opened (1) old peaty deposits 1.5–3 m thick, (2) the young soddy sandy soil of the medium level floodplain, and (3) a fresh sandy alluvium. In old peat deposits $^{137}$Cs was detected fragmentally (3 to 9 Bq/kg) to the depth of 23 cm. In the young soddy soil the layer with 13–14 Bq/kg of $^{137}$Cs was buried at the depth of 62–75 cm under the less contaminated ones. In sandy alluvium only a minor amount (2–2.5 Bq/kg) was determined in horizon 70–100 cm deep.

Table 4. $^{137}$Cs in plant groups.

| Plant groups | n | m | s | min | max | V,% |
|---|---|---|---|---|---|---|
| Mosses | 19,0 | 88,9 | 20,4 | 14,0 | 364,9 | 89 |
| Lichens | 11,0 | 36,9 | 11,1 | 7,1 | 79,4 | 72 |
| Willow* | 4,0 | 74,9 | 37,5 | 35,3 | 141,7 | 62 |
| Horsetail | 11,0 | 49,0 | 14,8 | 6,2 | 118,7 | 84 |

*leaves, Cape Bolvansky

Performed analysis revealed roughly two to three contamination levels of the alluvial soil layers: (1) small (2–5 Bq/kg) or close to small (7–10 Bq/kg) and (2) medium (16–18 Bq/kg). The depths of the layers with similar sequence of contamination levels were believed to correspond to similar contamination events either due to direct aerial deposition or secondary deposition during flooding. An additional analysis of the appropriate hydrological data would help to reconstruct the flooding and to estimate sedimentation rates at the study plots.

## $^{137}$Cs Accumulation in Vegetation Cover and Plant Species

Vegetation cover of the studied plots, described in Table 1, varied in total biomass from 0.15 to 5.77 kg/m$^2$ dw (excluding the tree layer at plots NM2 and NM3). The largest phytomass (mostly presented by willow shrubs - 81%–95%) developed on the medium and high level floodplains. Willow biomass sequentially increased from locations of the young rare willow growth pioneering high ridges (1, 2 kg/m$^2$, KM3) to mature willow thickets at the head of Gluboky Island (maximum value, GL1). In woodless areas the main mass contribution in floodplain landscapes belonged to mosses (30%) and lichens (up to 75%) on high terraces and to grasses and sedges (20%–53%) (Fig. 4).

Mean concentration of radiocesium in plant groups formed the row: mosses>horsetail>lichens (Table 4). High variation of the mean value within a group (62%–89%) was caused by considerable diversity in contamination level, landscape conditions, and species composition.

*Site-specific $^{137}$Cs accumulation by plant species*

Radiocesium values exceeding 100 Bq/kg were found in plant species collected on the high terrace landscapes on Cape Bolvansky (mosses, horsetail, willow, grasses) near Yushino (Yu2, peaty soil, mosses) and Naryan Mar under old spruce forest (NM2, moss).

The moss species growing on terraces formed a row: *Hylocomium splendens>Pleurozium schreberi≥Sphagnum sp.* The highest $^{137}$Cs accumulation was found in *Hylocomium* growing on Cape Shaitansky (365 Bq/kg). Sphagnum sampled in 5-cm layers in marshy depression near Yushino contained maximum $^{137}$Cs amount in the top layer (95 Bq/kg against 45–49 Bq/kg down to 20 cm) that moss and lichen growing on Cape Bolvansky and near Yushino, as well as horsetail species collected on the floodplain were at least twice richer

in $^{137}$Cs as compared to Naryan Mar and Bolshaya Sopka sites. At Naryan Mar and Bolshaya Sopka sites, radiocesium content in the upper litter layer did not exceed 45%, while on Plot Yu2 it reached 80%. This can be caused by a difference in precipitation between the forest-tundra and tundra zones, leading to better leaching of the upper layers. The age of the ecosystem was also significant for $^{137}$Cs fixation by plant species. Both *Hylocomium* and *Cladonia* species were 3 and 5 times richer when collected on plot NM2-03 located in old spruce forest with highly developed overgrown cover as compared to young coniferous forest near Naryan Mar (NM3). Correlation between $^{137}$Cs-specific activity in the plant and the top 10 cm layer was significant for horsetail ($r$=0.710; $n$=11). Unlike the Lower Yenisey, $^{137}$Cs content in horsetail increased seaward. This supported our earlier conclusion that horsetail is a suitable species for monitoring purposes (Korobova et al. 2007).

## Conclusion

Low $^{137}$Cs specific activity of soils and plants in the Pechora delta terrace and floodplain landscapes proved the global character of contamination. $^{137}$Cs maximum content in terrace landscapes and their topsoil layer indicated aerial pollution that was higher in the soils and moss cover of the northern plots. Despite different water migration conditions and a pronounced marine influence increasing seaward that can be followed in chlorine content both in river and groundwater samples, $^{137}$Cs fallout was strongly fixed by organo-mineral soil particles, reflected in maximum concentration of radiocesium in the undisturbed terrace organic horizons and particles enriched in organic debris, $^{137}$Cs depth peaks in floodplain soils. Floodplain accumulation of ed $^{137}$Cs was comparable and exceeded the inventories on the adjacent terraces that could occur due to both the direct fixation by dried surfaces and secondary accumulation of contaminated sediments. The most pronounced $^{137}$Cs peaks in the lower layers covered by clean sandy alluvial or wind deposits are likely to correspond to the period of maximum $^{137}$Cs global fallout (the year of 1963; Walling & He 1999). In case of constant flux, this allows a rough comparison of the deposition rates. Similar to the Yenisey, the Pechora terrace soils had pronounced minor $^{137}$Cs peaks at the bottom of the active layer water, presumably due to $^{137}$Cs sorption by suspension during concentration of water solution above the permafrost table due to freezing.

## Acknowledgments

Authors are much obliged to Dr. I. Studenov and his colleagues who made field investigations possible. Thanks are due to E. Sedykh, N. Starchinova, N. Korsakova (Vernadsky Institute), and S. Kirov (Institute of Global Ecology, Russian Ac. of Sci.) for chemical analysis.

## References

Anisimova, N.P. 1981. *Cryohydrogeochemical Peculiarities of the Frozen Zone.* Novosibirsk: Nauka, 89 pp.

*Atlas of Radioactive Contamination of the European Part of Russia, Belarus and Ukraine*. 1998. Moscow: FSGK, IGKE, 80 pp.

Bostick, B.C., Vairavamurthy, M.A., Karthikeyan, K.G. & Chorover, J. 2002. Cesium Adsorption on Clay Minerals: An EXAFS Spectroscopic Investigation. *Journal of Environment and Science Technology* 36(12): 2670 -2676.

Cornell, R.M. 1993. Adsorption of cesium on minerals: a review. *Journal of Radioanalytical and Nuclear Chemistry* 171(2): 483-500.

Dubikov, G.I. & Ivanova, N.V. 1990. Salty frozen deposits and their distribution in the USSR. In: *Salty Frozen Sediments as the Basement for Constructions*. Moscow: Nauka, 3-9.

Evans, D.W., Alberts, J. & Clark III R.A. 1983. Reversible ion-exchange fixation of cesium-137 leading to mobilization from reservoir sediments. *Geochimica et Cosmochimica Acta* 47: 1041-1049.

Ivanov, A.V. & Vlasov, N.A. 1974. Influence of cryogene processes on formation of hydro-carbonate-sodium waters. *Hydrochemical Materials* 60: 55-61.

Korobova, E.M., Ukraintseva, N.G., Surkov, V.V. & Linnik, V.G. 2004. Radionuclides in soils of the Yenisey river Gulf and delta coast. In: Engineering Geology and Environmental Protection. Sergeev Readings. Moscow: *GEOS* 6: 259-263.

Korobova, E.M., Brown, J.B. Ukraintseva, N.G. & Surkov V.V. 2007. $^{137}$Cs and $^{40}$K in the terrestrial vegetation of the Yenisey Estuary: landscape, soil and plant relationships. *Journal of Environmental Radioactivity* 96: 144-156.

Korobova, E.M., Ukraintseva, N.G., Surkov, V.V. & Brown, J.B. 2003. Geochemical study of the tundra landscapes in the Yenisey delta and gulf area Permafrost. *Proceedings of the Eight International Conference on Permafrost, Zurich, July 21–25*: 601-606.

Nifontova, M.G. 1998. Content of long-lived artificial radionuclides in moss-lichen cover of the terrestrial ecosystems in the Urals-Siberia region. *Ekologia* 3: 196-200.

Sanchini, P.H. 1988. Factors controlling the biogeochemical cycles of trace elements in fresh and coastal marine waters as revealed by artificial isotopes. Limnol. *Oceanogr* 33: 848-866.

Shaetzl, R. & Anderson, S. 2006. *Soils: Genesis and Geomorphology*. New York: Cambridge University Press, 817 pp.

Strand, P., Balonov, M., Aarkrog, A., et al. 1998. *AMAP Assessment Report: Arctic Pollution Issues*. Radioactivity. Oslo.

Walling, D.E. & He, Q. 1999. Investigating spatial patterns of overbank sedimentation on river flood plains. *Water, Air and Soil Pollution* 99: 9-20.

Wright, S.M., Howard B.J., Strand, P., et al. 1997. Prediction of $^{137}$Cs deposition from atmospheric nuclear weapons tests within the Arctic. *Environmental Pollution* 4: 131-143.

# Thermal State of Permafrost in the Eastern Arctic

G. Kraev, A. Abramov, S. Bykhovets, D. Fyodorov-Davydov, A. Kholodov, A. Lupachev, V. Mamykin, V. Ostroumov, V. Sorokovikov, D. Gilichinsky
*Soil Cryology Laboratory, Institute of Physicochemical & Biological Problems in Soil Sciences, Russian Academy of Sciences, Pushchino, Russia*
G. Zimova, N. Zimov
*Northeast Scientific Station, Pacific Institute of Geography, Russian Academy of Sciences, Far Eastern Branch, Cherskii, Sakha Republic, Russia*

## Abstract

The thermal state of the permafrost of the Eastern Arctic lowlands lying between the Lena Delta and the mouth of the Kolyma River is described in this paper. Three datasets were considered: (a) soil temperature from 12 federal weather stations at 0.2 to 3.2 m depths, (b) the thawing depth dynamics from 20 various environmental Circumpolar Active Layer Monitoring (CALM) sites, and (c) the permafrost temperature of the upper 25 m measured in about 100 boreholes. The stability of the permafrost's thermal state during the last 25–30 years was revealed. In spite of the slow increase in the mean annual air temperature (0.01°C/yr to 0.02°C/yr), only cyclic fluctuations in soil temperature and depth of thawing rather than notable trends were observed.

**Keywords:** active layer; boreholes; climate change; soil temperature; thermal state of permafrost.

## Introduction

Monitoring of the thermal state of ground outside the permafrost zone is performed occasionally according to special needs only. The necessity of such activities in the area of permafrost expansion (at 20% of the land) increases due to the projected permafrost response to climate change. Since the thermal capacities of the upper permafrost are controlled by climate, the climatic change tendencies are believed to be spatiotemporally reflected in the thermal state of permafrost. This study concerns the permafrost response to these changes during the last quarter of the 20th century, which was the period of global warming.

## Object of Study

The thermal state of permafrost is known to respond to climate fluctuations by changes in the upper layers, as follows (Fig.1):

I. The active (seasonally thawing) layer, matching with the profile of modern cryosol, and is characterized by above-zero temperatures during summer and below-zero temperatures during winter. It ranges from ground surface to maximal depth reached by the thawing front in a given year by the end of the warming period. The maximal depth referred to as the active layer thickness (ALT) is usually implemented to models.

II. The layer of annual temperature oscillations. The temperature oscillations penetrate into the layer allowing the temperature to redistribute along the vertical axis in accordance with the basic Fourier conduction law. The bottom of the layer is referred to as the depth of zero annual amplitudes of temperature (*H*), which usually varies from 15 to 20 m depending on the thermal capacities of the ground and soil covers. The temperature fluctuations gradually lower to the bottom, and the temperature at the *H* depth is thought to represent the mean annual temperature of the permafrost ($T_0$).

III. Deeper layer of constant annual temperatures, where upper boundary condition changes are reflected with attenuation. It changes non-linearly and is believed to reflect the decadal to centennial fluctuations of soil temperature (Lachenbruch & Marshall 1986). The lower boundary is the permafrost bottom. The thermal pattern in this layer is usually characterized by the geothermal gradient (*g*) taken from the slope of the temperature curve.

## Study Area

Investigations were carried out at Seaside Lowlands in the eastern Arctic in tundra, forest-tundra, and north taiga between the Lena Delta and the mouth of the Kolyma River (125–162°E, 65–72°N) at elevations up to 100 m above sea level. They spread up to 400 km latitudinally from the coasts of the Laptev and East-Siberian Seas to the mountainous areas of the Verkhoyansk and Cherskogo Ranges and the Yukagir Plateau (Fig. 2).

The topography of the study area is as follows: (a) drained watersheds composed of the late Pleistocene Ice Complex, (b) alas depressions, the result of subsidence of watersheds in the Holocene, (c) river flood plains, and (d) sand plains (like Khallerchinskaya Tundra) in the lower streams of the Indigirka, and Kolyma Rivers and the Lena Delta. The climate at the lowlands is arctic continental. According to Cherskii, Chokurdakh, and Tiksi weather stations the mean annual air temperature varies from -10°C to -16°C; the mean temperature of the warmest month (July) varies 8°C to 12°C, and that of the coldest month (January) varies -32°C to -34°C. The transition to above zero mean daily temperatures usually occurs in the second half of May, and the thermal

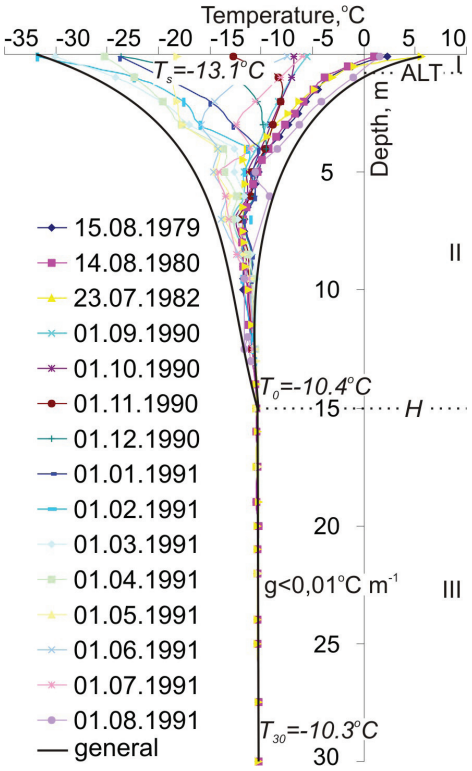


Figure 1. Temperature regime of the drained tundra watershed (Chukchee River, 69.48°N, 147.04°E). I-active layer; II-layer of annual temperature oscillations; III-layer of constant annual temperature. Data on every measurement are provided to assure the "general" envelopes are lined adequately; *g* was counted by dividing the difference in permafrost temperature, $T_0$, and the deepest temperature measured by the difference in depths of both measurements.

regime reverts to dominantly subzero temperatures at the end of September. The duration of the period with positive mean daily air temperatures is about 115–140 days. The mean annual atmospheric precipitation is 200–300 mm, with 80–130 mm of the total occurring during the warm season.

Snow cover is present from the end of September to mid-June having a maximal thickness of 30–70 cm, increasing eastwards, with more snow accumulating in depressions.

Continuous permafrost occurs to 290–420 m depths along the Kolyma River valley as found by Russian Geological Survey drilling in taiga at the southern margin of the study area and goes to 600–800 m along the Arctic coast in tundra, as calculated from the mean annual temperature and the geothermal gradient.

## Materials and Methods

To estimate the thermal state of permafrost in the last 2–3 decades, three independent datasets were used:

1. ALT measured in variously located Circumpolar Active Layer Monitoring (CALM) sites, where observations have been held during the last 10–15 years since 1989.

2. The long-term soil temperature records at 0.2–3.2 m depth from the federal weather stations network, which

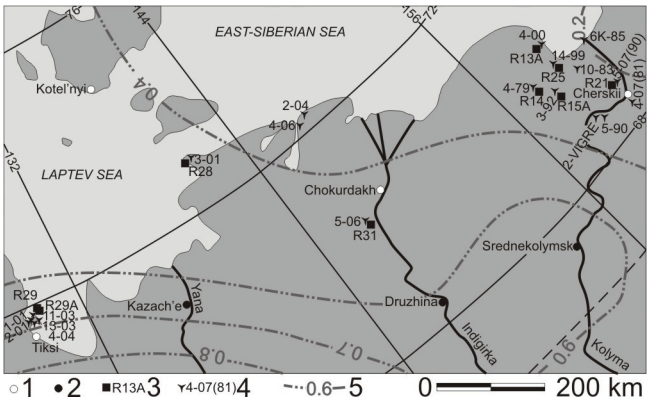


Figure 2. Locations of federal weather stations, boreholes and active layer monitoring sites considered in this paper. Key: 1–air temperature monitoring sites; 2–soil temperature monitoring sites; 3–active layer monitoring sites according to the CALM program numeration, with A designating the alas depression sites; 4–permafrost temperature monitoring in boreholes; the number after the dash is the year of drilling, which would be the starting year of the measurements if the other is not shown in brackets; 5–the current air temperature increase trends (Pavlov & Malkova 2005).

represent long-term soil temperature observations since the 1960s. They characterize both the active layer and the upper part of the layer of annual temperature oscillations in permafrost.

3. Permafrost temperature measured in boreholes since the 1970s. It characterizes both the layer of annual oscillations and the layer of constant annual temperature down to 25–50 m.

Soil temperature data are available for 12 weather stations located in taiga north of the Polar Circle, surrounding the area of study. They can be obtained from the Frozen Ground Data Center (http://nsidc.org/fgdc/). Srednekolymsk, Druzhina, and Kazaché are located at Seaside Lowlands (Fig. 2). Kazaché operated in the 1930s–1950s and further data are absent, though it was excluded from our consideration. The Druzhina and Srednekolymsk stations, located in taiga, have records continuous enough to consider. Soil temperature measurements were made with outtake mercury thermometers (for detailed description of the measurement technique see Gilichinsky et al. 1998, 2000; Zhang et al. 2001, 2005; Frauenfeld et al. 2004; Bykhovets et al. 2007). In spite of being out of date, the monitoring system has distinctive preference of long-term continuous observations. The Srednekolymsk and Druzhina sites measure soil temperature since 1960 more or less constantly. The longest datasets of mean annual soil temperature have been chosen at 0.4 and 1.6 m depths. Gaps in the datasets were interpolated from neighboring depths, when the temperature correlation exceeded 0.7 (n>10; n – number of years). Ten-year averaging gave poorly representable results, and thus to acquire reflection of the 11-year sun cycle we used the 5-year running averages to compile the dataset for each depth.

ALT was measured at the CALM sites. All sites consist of the square net of regular observation points occupying 1

ha. Sampling points are arrayed with 10 m spacing in rows aligned with the cardinal directions and probed according to the CALM protocol (Nelson et al. 1996). The resulting datasets consist of 121 values for each site. Data are available at http://www.udel/geog/CALM. There are 20 sites located at the study area (for detailed site description see Brown et al. 2000, Fyodorov-Davydov et al. 2004). The detailed analysis of spatial and temporal patterns of seasonal thawing at the area under study could be found in the paper of Fyodorov-Davydov et al. in these proceedings. Only the sites having permafrost temperature boreholes in the vicinity were taken into account in this paper, as follows: R14 - tundra watershed on Chukochya River, R15A - alas depression on Kon'kovaya River, R21 - shrub tundra growing at sandy plain near Akhmelo Lake were measured since 1996, and R25 at the watershed residual hill slope near Yakutskoe Lake did from 1999. Site R13A - alas at Chukochii Cape was established in 2000. Several sites were established after 2000, as follows: R28 – polar tundra watershed at Svyatoi. Nos Cape measured only once in 2001; R29 and R29A at Bykovskii Peninsula in the Lena delta at watershed and alas, respectively, introduced in 2003, and R31 site at the left bank of the Indigirka River valley measured since 2004.

Single temperature measurements in boreholes started in 1979 according to the Techniques of Permafrost Survey (1979), as a rule to the depth of 25 m, using copper resistance thermometer strings and DC bridge (Russia) at each 0.5 m to 5 m depth, 1 m - from 5 m to 15 m depth, and 2.5 m down to borehole bottom. Boreholes diameter varied from 78 mm in the top to 63 mm in the bottom. Liners were installed to three meters only to prevent water leaking from the permafrost table. Later the resistance thermometers were replaced by thermoresistors with the same accuracy of ±0.1°C, but the measurements still were carried out once per year during 4–5 years. To determine the depth of constant annual temperatures with these means is possible in deep holes. Thus the necessary depth of the boreholes was not less than 25 m, and the period of observation has to be several years at least. The shallower of several measurements at neighboring measuring depths showing similar temperature were considered the depth of zero annual amplitudes. Since the mid-90s the boreholes have been step-by-step equipped by dataloggers for continuous year-round observations. At the moment two and four channel HOBO Pro series dataloggers with 0.25°C accuracy and ten-channel loggers with 0.01°C accuracy (LPC, Geomonitoring, Russia) are used. One sensor is usually installed at the surface, the others at various depths inside the borehole. Temperatures were measured four times per day.

The study area had more than 100 monitoring boreholes in 1979–92. Unfortunately most of them are lost nowadays. The new boreholes were drilled since 2000 at the same places and equipped with modern instruments for temperature measurements to re-involve the old data and quantitatively estimate the changes in the thermal state of permafrost. The changes were estimated using the 25-year old temperature records and the recent data.

Geothermal gradient measurements were measured to the depth 250 m in Geological Survey parametric borehole 2-VIGRE in 1979.

## Results and Discussion

*Soil temperature*

Soil temperature measured at Srednekolymsk and Druzhina stations are shown in Figure 3. Two synchronous for both measuring depth and station periods of warming roughly at 1970–1975 and 1980–85, and those of cooling during 1975–80 and 1985–87 were revealed. The 1990s warming started earlier at more continental and cold Druzhina. The mean annual soil temperature in Srednekolymsk is -1.5±0.3°C ($n$=25, 1969–94) at 0.4 m (within the active layer), and 2.4±0.3°C ($n$=25) at 1.6 m (within permafrost). The mean annual soil temperature in Druzhina is -5.2±0.5°C at 0.4 m (active layer), and -4.6± 0.6°C ($n$=25) at 1.6 m (permafrost). The maximal difference in soil temperature during cold and warm periods reached 1°C in Srednekolymsk and up to 2°C in Druzhina. The soil temperature seems to be stable in Srednekolymsk, experiencing cyclic fluctuations during the study period of 1969–94. So does soil temperature in Druzhina at 0.4 m, while at 1.6 m it was warming with the rate of 0.03°C/yr.

Analysis of soil temperature trends at 0.4, 0.8, 1.6, and 3.2 m depths at 10 surrounding-the-lowlands weather stations located in Larix taiga north of the Polar Circle showed the maximal trend being 0.027°C /yr at 1.6 m in Druzhina, with most of thee stations having negligible (less than 0.01°C/yr) trends, while 3 stations showed even slightly negative trend. Chudinova et al. (2006) analyzing trends in soil temperature to the east of Lena River found a variety of tendencies for soil temperatures at 0.2–3.2 m depths have concluded the least soil temperature increase during 1960s–1990s beneath all the Federal weather stations. It could only be explained by the active layer having successful amounts of summer moisture and winter cold to discharge supplementary heat through the phase transitions. We let alone the discussion on reasons of trend variability in the study area. Above mentioned results confirm the fact that no significant changes occurred in soil temperature during the last 30 years.

Monthly time series of soil temperature at 0.4 and 1.6

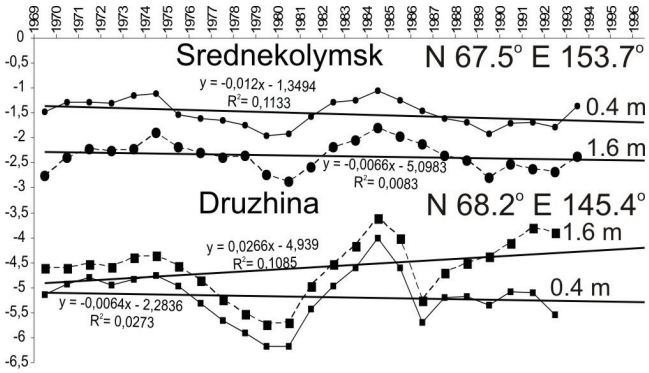


Figure 3. Five-year running average soil temperature measured at Federal weather stations during 1969–96.

Table 1. Mean annual soil temperature at the drilling sites according to monthly monitoring data.

| | 1981 | | Sep 1990-Aug 1991 | |
|---|---|---|---|---|
| | active layer 0.4 m | perma-frost 1.6 m | active layer 0.4 m | perma-frost 1.6 m |
| Flood plain (4-07) | -4.7 | -4.5 | | |
| Sand plain (5-07) | | | -0.9 | -1.1 |
| Watershed (4-79) | | | -11.9 | -11.6 |
| Srednekolymsk | -1.6 | -1.3 | -0.7 | -2.0 |
| Druzhina | -7.2 | -6.7 | -4.5 | -3.7 |

m depths in our boreholes in tundra conducted in 1981, 1990–1991 correlate well (r2>0.9, 5<n<12) with those made at the weather stations in taiga. Mean annual soil temperatures on tundra watersheds are much (more than 5°C) lower than in taiga (Table 1). Thermal regime of soils in taiga flood plain is colder than Srednekolymsk, while warmer than the Druzhina, lying south and characterized as more continental, having severe winters and less precipitation (data not shown). Borehole 5-07 showed abnormal, high soil temperature which is a subject of discussion below. However, the data are insufficient to reproduce the temperature, in our boreholes from the years of measurements at the weather stations only.

*Active layer observations*

Mean values of active layer thickness in the northern part of the Kolyma lowland vary significantly (see Fig. 4).

The largest discrepancies within tundra are associated with texture of parent materials. Sand plain tundra thaws two to three times deeper than wetter loams of watersheds. Besides the influence of lithology, the effect of locally higher permafrost temperatures, which promote deeper thawing, can be observed (Fyodorov-Davydov et al. 2004). Significant latitudinal differences within single topographic levels occurred only in 2005, when the deepest thawing occurred at all watersheds but the westernmost R29 site at Bykovskii Peninsula and R31 at the left bank of the Indigirka valley. The least ALT occurred in 1998 when only three of the sites were in operation. The longest dataset available is for the sand plain R21 site (see Fig. 3 in Fyodorov-Davydov et al., these proceedings). It shows the cyclic fluctuations of ALT. Decreasing of the ALT occurred through the 1990s, when the soil temperature remained relatively stable or even slightly decreased at both weather stations (Fig. 3). However, passing the highest value in 2004-05, the curve in 2007 returns to 1990s 101 cm ALT.

The influence of latitudinal irradiance on the spatial pattern of ALT is rather obvious in watersheds having relatively homogeneous texture (Table 2). Active layer thickness increases from north to south. At the R28 and R29 sites in grass-dominated tundra the ALT was 32±5 cm. Shrub tundra of R31, R14, and R25 had the mean ALT of 42±7

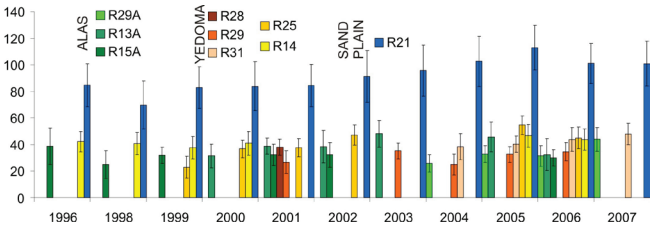


Figure 4. Mean annual ALT data (cm) monitored at the CALM sites. Green, red-yellow and blue colors represent different topographic levels. Sites are listed according to latitude southwards. Bars indicate ±1 standard deviation of 121 to 600 measuring points annually.

Table 2. Active layer thickness (cm) at the drilling sites according to monitoring data.

| | 72.87° R28 | 71.78° R29 | 70.55° R31 | 69.85° R25 | 69.48° R14 |
|---|---|---|---|---|---|
| 1996 | | | | | 42±8 |
| 1998 | | | | | 41±8 |
| 1999 | | | | 23±8 | 38±8 |
| 2000 | | | | 37±7 | 41±9 |
| 2001 | 38±6 | 27±9 | | 38±7 | |
| 2002 | | | | 47±8 | |
| 2003 | | 35±6 | | | |
| 2004 | | 25±8 | 38±10 | | |
| 2005 | | 33±6 | 40±6 | 55±7 | 47±8 |
| 2006 | | 35±7 | 44±9 | 45±8 | 44±8 |
| 2007 | | | 48±8 | | |

cm. Thaw depressions formed by thermokarst are usually waterlogged and accumulate peat, leading to a decrease of ALT. Thaw depths in alas are similar or slightly lower than on watershed.

In the area of study the close correlation between active layer thickness and thermal characteristics was observed at Site R25 (r2>0.7 for air temperature) and all other sites for the sum of summer above-zero temperature, but for R13A (Fyodorov-Davydov et al. 2004; see also Fyodorov-Davydov et al., these proceedings).

*Permafrost temperature*

The data on permafrost temperature at the depth of zero annual amplitudes are presented in Table 3. The depth of zero annual amplitude (*H*) was found at various depths: 8–10 m in alas depressions, 12–15 m at loamy watersheds, and 18–20 m within ice wedges and at the sand plain.

Temperature measurements conducted show the mean temperature on tundra watersheds of -10.5±0.9°C (*n*=8). The temperature rises up to -6.2°C in taiga watershed (5_90). Watershed permafrost temperature has significant negative correlation with latitude (r2=-0.79, *n*=8) designating the falling of permafrost temperature with latitude.

Alas depressions show the mean of -9.2±1.0°C (*n*=6), with the lowest temperature found at the highest alas at Chukochii Cape. The correlation with latitude is -0.55 (*n*=6),

Table 3. Temperature monitoring of permafrost in boreholes.

| | Hole | Lat. | Long. | Temperature, ºC | |
|---|---|---|---|---|---|
| | | | | 1980s | 2000s |
| | 4_04 | 71.7 | 129.4 | | -9.3 |
| | 13_03 | 71.7 | 129.4 | | -9.8 |
| alases | 2_01 | 71.8 | 129.4 | | -9.5 |
| | 3_92 | 69.4 | 158.6 | -7.9 | -7.4 |
| | 4_00 | 70.1 | 159.8 | | -10.2 |
| | 14_99 | 69.9 | 159.5 | | -9 |
| | 11_03 | 71.7 | 129.4 | | -11.3 |
| | 2_04 | 72.3 | 141.1 | | -11.2 |
| | 5_90 | 68.7 | 158.9 | -6.2 | |
| water- | 4_06 | 72.3 | 141.1 | | -10.3 |
| sheds | 3_01 | 72.9 | 141 | | -11.7 |
| | 1_01 | 71.8 | 129.4 | | -10.9 |
| | 5_06 | 70.6 | 147.4 | | -9.5 |
| | 4_79 | 69.5 | 157.0 | -10.5 | -10.4 |
| flood | 6K_85 | | | -6.1 | |
| plains | 4_07 | 68.6 | 161.4 | -5.6 | -5.7 |
| sand | 5_07 | 68.8 | 161 | -7.9 | -3.9 |
| plain | 10_83 | 69.4 | 159.5 | -9.4 | |

Notes: 1980s involve temperature measurements made before 1990, while the 2000s include measurements made after 1995.

which suggests other controls on permafrost temperature like wetness, relative depth of alas depression within the watershed, and peat thickness.

Permafrost temperature at levels experiencing present day sedimentation and syncryogenic formation of permafrost at flood plains and in Kamenka Island in the Kolyma delta is -5.9±0.2°C ($n$=2).

Measurements of permafrost temperature performed in the 1980s and 2000s differ by 0.1°C at watersheds and flood plains (Fig. 5), about 0.5°C in alas depressions.

From the bottom of the layer of zero temperature amplitudes ($H$) to 100 m depth $g$ = 0, followed with the stepwise temperature rise, giving the mean g of 0.015°C /m.

Sand plain temperature is -9.4°C at the northernmost site, while it was suggested to be out of order at the 5_07 borehole representing the thermal anomaly site (see Tables 1, 3). Having the data on surface thermal capacities change through the years, we suppose the location of the borehole above the geological fault where the heat flux from the earth crust warms permafrost up to about -4°C. 3_92 borehole drilled in the very deep alas depression to 55 m depth shows positive gradient g down from the depth of zero annual amplitudes, which allows us to suggest the alas continuing to thaw having the long period heat wave penetrating to permafrost. Hence the temperature increase of 0.5 in alas depression is thought to be measured in atypical environment.

Permafrost warming was reported for many surrounding regions. For example Osterkamp (2005) reported on recent warming of Alaskan permafrost. The mean annual temperature of Eastern Arctic permafrost is in equilibrium

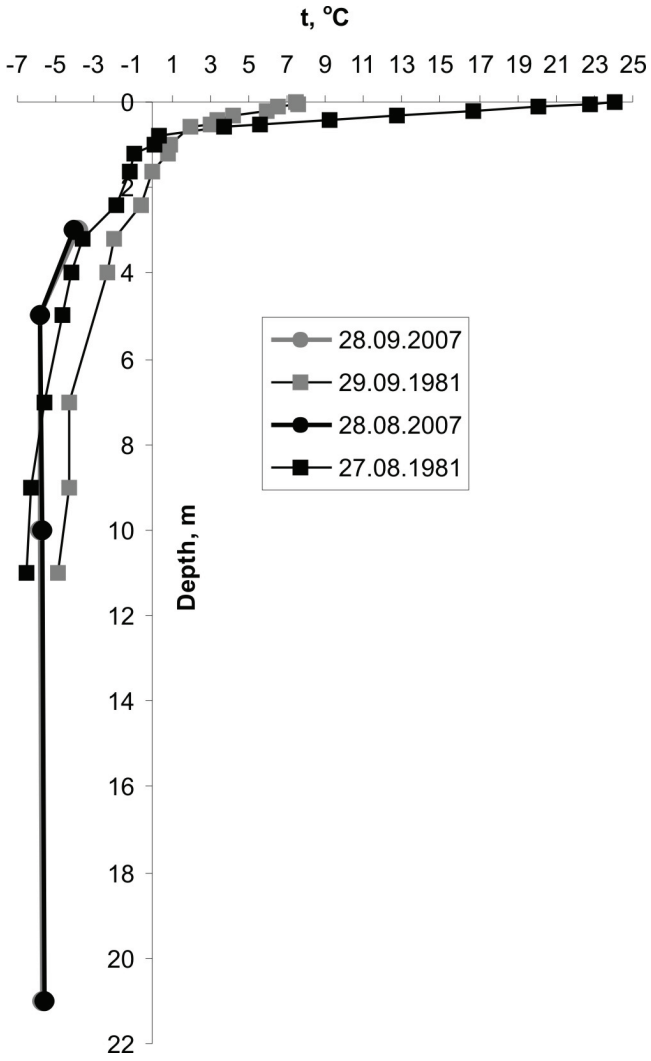


Figure 5. Temperature regime in 4_07 borehole at the Kolyma River flood plain.

with present-day climate. Long-term measurements do not reveal significant changes in permafrost temperature or even the timing of thermal wave penetration through the soils. We should not forget the stability of permafrost in the study area during Pleistocene. Even when regional permafrost degradation has occurred during climatic optimums, it was stable in the study area. However, as temperatures rise faster in the high-latitude continental regions, permafrost could be greatly impacted.

## Conclusion

Today depths of seasonally thawing, soil and permafrost temperatures on wide eastern Arctic lowlands indicate the stable thermal state of permafrost during the last 30 yrs. The periods of warming of nearly 1970–75, 1980–85, 1989–93, and since 1999 till present, are reflected in the increase of less than 20% in ALT and 1°C–2°C in soil temperature.

This stability allows us to use data of single measurements in characteristics of permafrost thermal state in the Eastern Arctic. It is as follows.

Upper soils, permafrost temperature, and ALT are subject to change latitudinally, with the highest change occurring at sandy drained plains and between tundra and taiga. Watersheds usually have around -11°C temperature of permafrost and less than 0.6 m ALT. Widespread alas depressions have -9°C cold permafrost and nearly the same depth of seasonal thawing as watersheds. Flood plains characterize with -6°C cold permafrost.

The study area had more than 100 monitoring boreholes in 1980s with the network being recreated currently. Extensive temperature monitoring of permafrost allows the exclusion of temperature anomalies from modeling of thermal response of permafrost to climate changes. Reconstruction of old borehole networks gives the most precise evidence of permafrost thermal state change.

## Acknowledgments

This study was supported by the Russian Academy of Sciences and also funded by the Polar Earth Science Program, Office of Polar Programs, National Science Foundation (ARC-0632400, ARC-0520578) and CALM (Circumpolar Active Layer Monitoring) Program (RUG2-1468-MO-04).

## References

Brown, J., Hinkel, K.M. & Nelson, F.E. 2000. The Circumpolar Active Layer Monitoring (CALM) program: Research designs and initial results. Polar Geogr. 24(3): 165-258.

Bykhovets, S.S., Sorokovikov, V.A., Martuganov, R.A., Mamykin, V.G. & Gilichinsky, D.A. 2007. The history of soil temperature studies by the Russian weather station network. *Earth's Cryosphere* 11(1).

Chudinova, S.M., Frauenfeld, O.W., Barry, R.G., Zhang, T. & Sorokovikov, V.A. 2006. Relationship between trends and periodical components in air and soil temperature time-series over the permafrost-occupied regions of the Asian Territory of Russia. *J. Geophys. Res.*

Frauenfeld, O.W., Zhang, T., Barry, R.G. & Gilichinsky, D. 2004. Interdecadal changes in seasonal freeze and thaw depths in Russia. *J. Geophys. Res.* 109.

Fyodorov-Davydov, D.G., Sorokovikov, V.A., Ostroumov, V.E., Kholodov, A.L., Mitroshin, I.A., Mergelov, N.S., Davydov, S.P., Zimov, S.A. & Davydova, A.I. 2004. Spatial and temporal observations of seasonal thaw in the northern Kolyma Lowland. *Polar Geogr.* 28(4): 308-325.

Fyodorov-Davydov, D.G., Kholodov, A.L., Ostroumov, V.E., Kraev, G.N., Sorokovikov, V.A., Davydov, S.P. & Merekalova, A.A. 2007. Seasonal thaw of soils in North Yakutian Ecosystems. *Proceedings of the Ninth International Conference on Permafrost, Fairbanks, Alaska, June 29-–July 3, 2008* (these proceedings).

Gilichinsky, D.A., Barry, R.G., Bykhovets, S.S., Sorokovikov, V.A., Zhang, T., Zudin, S.L. & Fyodorov-Davydov, D.G. 1998. A century of temperature observations of soil climate: methods of analysis and long-term trends. In: A.G. Lewkowicz & M. Allard (eds.), *Proceedings of the Seventh International Conference on Permafrost:* 313-317.

Gilichinsky, D.A., Bykhovets, S.S., Sorokovikov, V.A., Fyodorov-Davydov, D.G., Barry, R.G., Zhang, T., Gavrilova, M.K. & Alekseeva, O.I. 2000. Weather station data: estimation of perennial changes in soil temperature in seasonally frozen grounds and permafrost zone of Russia. *Earth's Cryosphere* 4(3): 59-65.

Lachenbruch, A.H. & Marshall, B.V. 1986. Changing climate: geothermal evidence from permafrost in the Alaskan Arctic. *Science* 234: 689-696.

Nelson, F.E., Brown, J., Lewkowicz, T. & Taylor, A. 1996. Active layer protocol. In: U. Molau & P. Molgaard (eds.), *ITEX Manual, second edition*. Copenhagen: International Tundra Experiment: 14-16.

Osterkamp, T.E. 2005. The recent warming of permafrost in Alaska. *Global Planet. Change* 49: 187-202.

Pavlov, A.V. & Malkova, G.A. 2005. Current climate change in Northern Russia. The collection of maps. Novosibirsk, Russia: Geo, 54 pp.

*Techniques of Permafrost Survey.* 1979. Moscow State University Publishers, 328 pp.

Zhang, T, Barry, R., Gilichinsky, D., Bykhovets, S., Sorokovikov, V. & Ye, J. 2001. An amplified signal of climatic change in ground temperatures during the last century at Irkutsk, Russia. *Climate Change* 49: 41-76.

Zhang, T, Barry, R., Frauenfeld, O., Gilichinsky et al. 2005. Spatial and temporal variability in active layer thickness over the Russian Arctic drainage basin. *J. Geophys. Res.* 110.

# Rock Permafrost Geophysics and Its Explanatory Power for Permafrost-Induced Rockfalls and Rock Creep: A Perspective

M. Krautblatter
*Institute of Geography, University of Bonn, Germany*

## Abstract

Rockfalls and rock creep in permafrost-affected bedrock are an increasing hazard in high mountain areas. Besides temperature measurements and physically-based temperature modeling, geophysics in permafrost rocks provides a new methodology for investigating spatial and temporal patterns of permafrost rocks. First examples of 2D electrical resistivity tomographies and refraction seismic tomographies in permafrost rocks are displayed as well as 3D electrical tomographies. ERT time-lapse inversion routines allow for a direct comparison of subsequent time-sections and provide insight into temporal phenomena of heat propagation and permafrost aggradation and degradation. This article aims to show that in the case of ice-filled discontinuities and hydrological pressures geophysical results can potentially be linked to parameters that control rock stability.

**Keywords:** ERT; ice-mechanics; permafrost; refraction seismics; resistivity; rock creep; rockfalls.

## Introduction

Degrading permafrost in rock walls is hazardous, partly due to the amount of potential energy that is released in case of instabilities (Harris et al. 2001). In 2002, the Dzhimarai-khokh rock/ice avalanche (Russian Caucasus) detached approximately 4 million m³ from a 1 km wide starting zone and caused more than 140 casualties (Haeberli, 2005, Kääb et al. 2003). Even smaller permafrost rockfalls, such as the 2003 Matterhorn rockfall, are considered major hazards in densely populated high mountain areas (Gruber et al. 2004). Inventories show that the frequency of these rockfalls has considerably increased in the warm 1990s and was boosted by the hot summer of 2003 (Schoeneich et al. 2004). Moreover, slow rock creep in permafrost rocks causes significant damage especially to tourist infrastructure in high mountain areas.

Besides temperature logger data, borehole information, and rock temperature modeling approaches, the geophysical applications described here provide a new tool for the spatial and temporal analysis of rock permafrost. In some cases, information on the thermal state of permafrost reveals sizeable information for stability consideration (Davies et al. 2001), but changing hydrological properties of ice, such as water content, may also play a vital part in decreasing resistive forces of ice-contained rock masses (Gruber & Haeberli 2007). This paper combines a review of existing geophysical techniques that are applicable in permafrost rocks and a perspective on how these can contribute to understanding mass movements in permafrost-affected bedrock in future. It will address three questions:

(1) What geophysical methods can be applied in permafrost rocks? (2) What properties do they detect? (3) What is their explanatory power for permafrost-induced mass movements?

## Investigation Sites

Methods described in this article were tested at three investigation sites: the "Steintälli," a N-S exposed crestline (Matter/Turtmann Valleys, Switzerland) at about 3070–3150 m a.s.l. with slaty paragneiss (see Fig. 1); the North Face of the Zugspitze limestone summit (Wetterstein Mountains, Germany/Austria) at about 2800 m a.s.l., and the gneissic Gemsstock crestline (Switzerland) at 2900 m a.s.l. in collaboration with Marcia Phillips. Figure 1 shows a typical arrangement of a 2D-ERT in steep, permafrost-affected bedrock. More detailed site characteristics can be sourced from Krautblatter and Hauck (2007) and Gude and Barsch (2005). Problems associated with the comparison of different field sites and extrapolation of results are discussed in Krautblatter & Dikau (2007).

Figure 1. Electrical resistivity measurement at the Matter/Turtmann Valleys crestline, 3150 m a.s.l., Switzerland. 41 large steel screws serve as electodes along each transect.

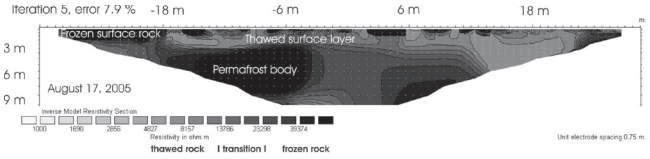


Figure 2. ERT in an east-facing rock wall recorded at August 17, 2005, at the Matter/Turtmann Valleys crestline, 3130 m a.s.l. Switzerland).

## Geophysical Methods for Rock Permafrost and Detectable Properties

Surface-based geophysical methods represent a cost-effective approach to permafrost mapping and characterisation (Harris et al. 2001). Hauck (2001) provided a systematic comparison of different geophysical methods for monitoring permafrost in high-mountain environments. However, the application of geophysical methods to permafrost rock walls just began in 2005 (Krautblatter & Hauck 2007). This section will give a quick overview of methods that have successfully been applied to permafrost rocks in the last three years. Data used for Figures 2, 6, and 8 were previously published in Krautblatter & Hauck (2007) and are described there in detail.

*Electrical resistivity tomography (ERT)*

ERT is a key method in permafrost research, as freezing and thawing of most materials are associated with a resistivity change that spans one order of magnitude, which is, in turn, easily detectable. The first approach to derive spatial information from rock faces by ERT was applied by Sass (2003). In subsequent studies he provided further evidence that ERT measurements are capable of measuring the degree of rock moisture (Sass 2005) and temporal and spatial variations of freeze and thaw limits (Sass 2004) in rock faces. These ERT measurements were confined to the monitoring of the upper weathering crust (centimeter- to decimeter-scale) of non-permafrost rock faces. Krautblatter and Hauck (2007) extended this method to a decameter-scale and applied it to the investigation of active layer processes in permafrost-affected rock walls.

Arrays with centimeter-long steel screws as electrodes were drilled into solid rock (see Fig. 1) and were measured repeatedly with high voltages (mostly $10^2$–$10^3$ V) to improve the signal to noise ratio. A detailed survey of hardware and software adaptations and a systematic discussion of error sources is provided by Krautblatter and Hauck (2007). Errors associated with different ERT-arrays were assessed along with the impact of topography and other geometric error sources (Krautblatter & Verleysdonk 2008a). The Res2DInv software was chosen, as it is capable of topographic correction and "real" time-lapse inversion of subsequent measurements. To cope with high resistivity gradients, inversions models with mesh size smaller than the electrode distance and robust inversion routines provide better results. Resistivity values that correspond to the transition between frozen and thawed rock were measured repeatedly at the rock

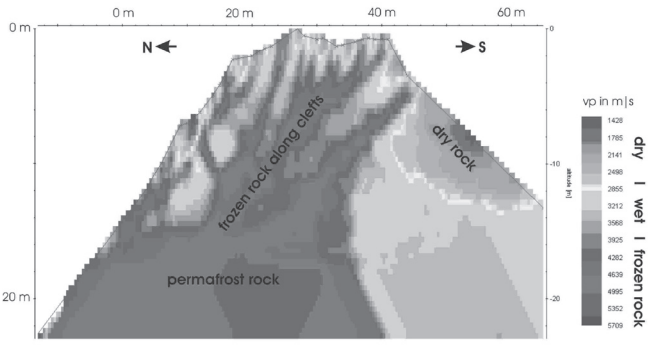


Figure 3. RST – north-south transect 9 (September 20, 2006), measured at the Matter/Turtmann Valleys crestline, 3150 m a.s.l.

surface along different arrays and yielded evidence that the transition occurs between 13 and 20 kΩm for the gneissic rocks at the Steintälli (Krautblatter & Hauck 2007) and are in the same range as those established for carbonate rocks at the Zugspitze by Sass (2004) and our own measurements (Krautblatter & Verleysdonk 2008b). Figure 2 shows an ERT that was measured close to Figure 1 at an east-facing part of the rock crestline between Matter and Turtmann Valleys. It shows a 3 m thick thawed surface layer of rock above a constantly frozen permafrost layer; a plunge in temperature following August 14th is evident due to frozen rock close to the surface in all parts of the transect. Resistivity–temperature patterns of rock samples of all field sites are currently tested in a freezing chamber in the laboratory.

The relation between measured resistivity and rock temperature is straightforward. For temperatures below the freezing point, resistivity ($p$) depends mainly on unfrozen water content until most of the pore water is frozen. In Alpine environments resistivity can be calculated based on a reference value $p_o$ as an exponential response to the temperature below the freezing point ($T_f$) according to McGinnis et al. (1973):

$$\rho = \rho_0 e^{b(T_f - T)} \quad (1)$$

The factor $b$ in Equation (1) determines the rate of resistivity increase and can be derived empirically (Hauck 2001, Hauck 2002). Short-term changes in resistivity can be attributed to changes in pore water content and temperature, while changes in porosity and water chemistry can be neglected over daily to monthly measurement intervals in low-porosity rocks. Due to the exponential response of resistivity to temperatures below 0°C, freeze-thaw transitions correspond to an increase in resistivity by one order of magnitude and are thus a very sensitive method for detecting the state of rock permafrost close to 0°C. On the other hand, deeply frozen bedrock (below -5°C) along the measured transects causes problems for the electrode contact.

*Refraction seismic tomography (RST)*

The application of refraction seismics in permafrost studies is based on the interpretation of refracted headwaves that indicate the transition of a slower, unfrozen top layer

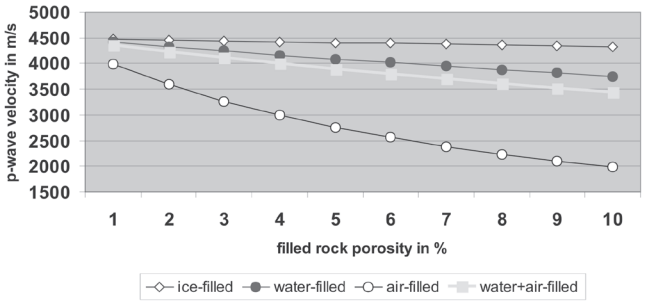


Figure 4. Estimation of P-wave velocities of rock with different porosity and pore content.

to a frozen layer with faster P-wave propagation below. Recent approaches apply tomographic inversion schemes (Otto & Sass 2006) often based on high-resolution datasets (Maurer & Hauck 2007, Musil et al. 2002). Seismics are also applied to determine 2D and 3D rock mass properties and potential instabilities (Heincke et al. 2006). Preliminary results from Krautblatter et al. (2007) indicate that refraction seismics are applicable for permafrost detection in solid rock walls, even if they provide less depth information than ERT measurements. On the other hand, it appears that they resolve small-scale features such as ice-filled clefts in more detail. For instance, Figure 3 shows a cross-cut through the E-W trending Steintälli crestline at Transect 9. Thoroughly frozen rock aligns along ice-filled discontinuities indicating the good thermal conduction (k = 2.2 W/(m*K)) without latent buffers in the readily frozen ice in clefts.

In practice P-Waves were stimulated with a 5 kg sledgehammer. Per transect, 24 drilled geophone positions in bedrock and 40 marked and fixed shot positions were arranged in line with the ERT transects so that RST and ERT were measured simultaneously (Krautblatter et al. 2007). A direct comparison of ERT and RST showed that frozen high-resistivity rocks in the ERT typically have P-wave velocities significantly above 4000 m/s (see section below) while wet and dry rock masses indicate a significantly slower propagation. As P-wave velocities of frozen and thawed rock differ only by a few hundred m/s in velocity, it is important to define the geometry of shot and recording position exactly, which was done using a high-resolution tachymeter. High P-wave velocities in rock necessitate high temporal resolution of geophone signals. Surface waves are not decelerated by a soft surface layer, such as soil, and thus often disturb signals recorded by geophones close to the shot position. We applied REFLEXW, Version 4.5 by Sandmeier Scientific Software, with model settings, such as initial P-wave velocity assumption, adjusted to bedrock conditions.

Air-, water-, and ice-filled pores in rock lead to significantly different attenuation of P-wave velocities. This is especially true for air-filled porosity. Figure 4 shows theoretical P-wave velocity for different pore-fillings and rock porosities derived from mixing laws. However, it appeared in simultaneous ERT and RST measurements that carefully conducted RST can resolve the difference between water and ice-filled rock even in low-porosity (2%–3%) bedrock, and that velocity

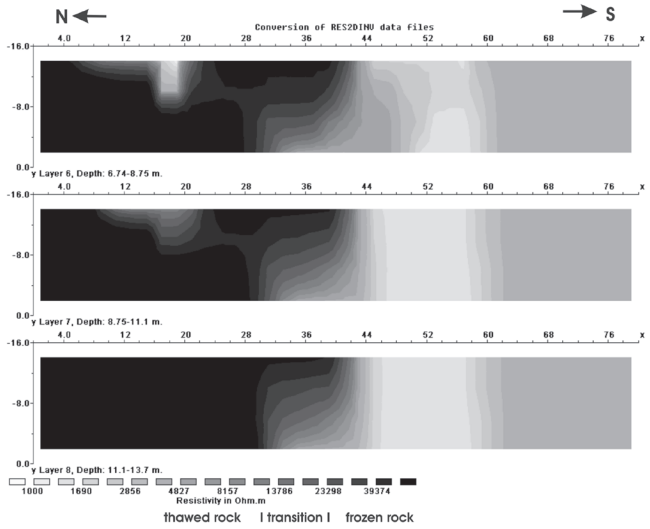


Figure 5. 3D-ERT cross sections at three different depths cutting the Turtmann/Matter Valley crestline N-S. Measured with ca. 1000 datum points from ca. 200 electrodes at September 5–9, 2006.

differences are larger than expected from mixing laws for certain rock porosities. This could be due to the fact that melting in low-permeability rocks leads to a small gas content in pores to compensate the ice-water volume reduction or that the seismic velocities provide a more integral signal that includes ice in discontinuities in the rock mass.

*The third dimension: 3D ERT and RST*

ERT and RST can be conducted in 3D. Figure 5 shows three horizontal sections cut at depths of 7–9 m, 9–11 m and 11–14 m with N-S orientation that indicate a sharp divide between frozen rock to the north and thawed rock to the south at meter 44. Problems that arise when conducting three-dimensional geophysics in permafrost rocks are time-consuming measurements (ca. one week of uninterrupted measurements), the necessity of highly precise topographic information, and the required high resolution due to the enormous resistivity/seismic velocity gradients present in permafrost rock systems. Moreover, traditional 3D arrays (e.g., Pole-Pole or Dipol-Dipol ERT) result in bad signal to noise ratios (Krautblatter & Verleysdonk 2008a) and electrode/geophone spacing and arrays must be adjusted to local conditions. Therefore, the first 3D ERT and 3D RST array in permafrost rocks, which was conducted in 2006, relied on a very close (2 m) arrangement of geophones (120), electrodes (205), and shot positions (200) (Fig. 6) (Krautblatter et al. 2007) and is based on Wenner-arrays that yield much better signal to noise ratios than Pole or Dipole-type arrays.

*The fourth dimension: Time-lapse ERT*

The installation of permanent electrodes and modeling of subsequent resistivity datasets within the same inversion routine (so-called time-lapse inversion) allows for a direct assessment of spatial and temporal permafrost variability (Hauck 2002, Hauck & Vonder Mühll 2003). Figure 6 shows the freezing of the previously thawed surface rock up to 3 m

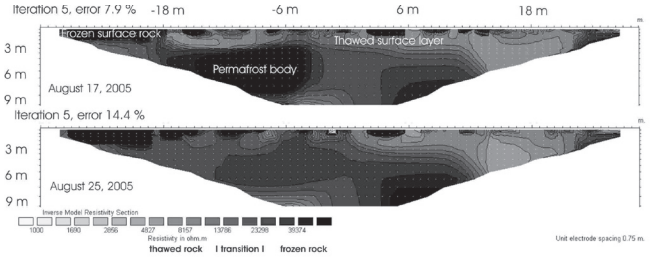


Figure 6. Freezing of surface rock from August 17 (top) to August 25, 2005 (bottom) due to a severe drop in air temperature recorded at the Steintälli E-transect (3130 m a.s.l., Matter/Turtmann Valleys, Switzerland).

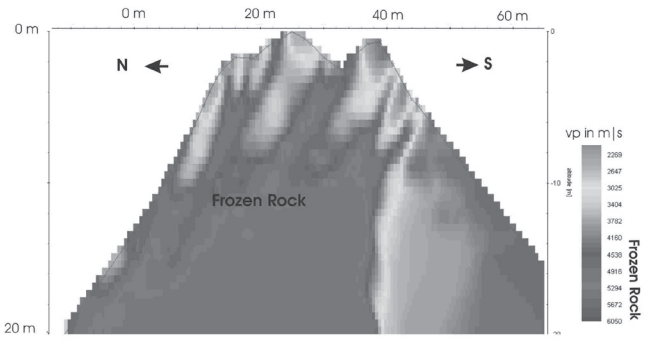


Figure 7. RST – north-south transect 7 (August 31, 2006) of the Matter/Turtmann Valleys crestline, 3150 m a.s.l. Mention the disposition of the frozen discontinuity zones as possible detachment zones with daylighted bedding.

depth following a plunge in temperature after August 14, 2005. While time-lapse routines for ERT are already in place, time-lapse routines for RST are still more difficult to perform.

Time-lapse inversion of subsequent measurements provides insights into short-term and long-term freeze-thaw thermal regimes (Krautblatter & Hauck 2007), response times (Krautblatter & Verleysdonk 2008b), changes in hydrological rock conductivity, and permafrost aggradation and degradation (Krautblatter 2008). Moreover, changes in subsequent time sections can definitely be attributed to changes in rock moisture or the state of freezing, while changes in geological properties can be ruled out for short-timescales.

## Explanatory Power for Permafrost-Induced Mass Movements

We define permafrost-induced mass movements as those whose kinematical behavior is at least partly influenced by ice mechanics and permafrost hydrology. The most common types are rockfalls and rock block creep. These are usually explained (1) by a reduction of the resisting force, e.g., shear-strength in ice-filled clefts (Davies et al. 2001, Davies et al. 2000) or (2) an increase in the driving force, e.g., hydrological pressure (Fischer et al. 2007).

*Ice-filled discontinuities*

Figure 7 shows a cross-cut through the E-W trending Steintälli crestline. Geometrical position, orientation, and

Table 1. Geophysically detectable properties of permafrost rocks

| | |
|---|---|
| ERT | Space-referenced integral tomography of frozen and thawed rock and hydrological conductivity at all measured depths. |
| | Temperature estimation (0° to -5°C) in combination with laboratory measurements (McGinnis). |
| RST | Space-referenced integral tomography of air-, water-, and ice-filled rock porosity. |
| | Exact positions of the uppermost freezing/thawing front and dominant air-, water-, and ice-filled rock discontinuities. |
| 3D-measurements | 3D spatial information on the freezing/ melting front, hydraulic conductivity, and the persistence/ importance of discontinuity zones. |
| Time-lapse inversions | Development of heat fluxes, the permafrost system (aggradation/ degradation), and the hydraulic system over time. |

persistence of ice-filled clefts in the upper 10 m can be well detected in RST surveys. It is assumed that ice-filled discontinuities react according to stress-strain behavior of weight-loaded polycrystalline ice. The deformation of ice at constant stress is characterized by four phases: (1) elastic deformation that is followed by permanent deformation, first at a decreasing rate (2) primary creep, then at a constant rate (3) secondary creep, and finally at an increasing rate (4) tertiary creep (Budd & Jacka 1989). Mostly secondary creep and tertiary creep occur at speeds relevant for mass movements. The flow relation for secondary creep relates the shear strain rate $\varepsilon_{xy}$ to the shear stress $\tau_{xy}$,

$$\varepsilon_{xy} = A \tau_{xy}^{n} \quad (2)$$

where $A$ depends mainly on ice temperature, anisotropic crystal orientation, impurity content, and water content, and $n$ increases at shear stresses greater than 500 kPa (Barnes et al. 1971). Crystal orientation, impurity content, and shear stresses remain more or less constant over short timescales. In contrary, ice temperature and water content in mass movement systems are subject to major annual and interannual changes. Thus, for temperatures above -10°C, $A$ can be approached by

$$A = A_0 \exp(-\frac{Q}{RT}) \approx A_0 \exp(-\frac{16700}{T}) \quad (3)$$

where $A_0$ is independent of temperature, $R$ is the universal gas constant, and $Q$ is the activation energy (Weertman

1973) and $A_{0t}$ for tertiary creep

$$A_{0t} = (3.2 + 5.8W) * 10^{-15} (kPa)^{-3} s^{-1} \quad (4)$$

can be related to the percentage water content $W$. It must be stressed that the water content strongly decreases with temperature. Paterson (2001) states -2°C as the lowest temperature at which the effect of water in the ice is relevant for the stress-strain behavior.

Equations (3) and (4) show that both ice temperature and water content play a dominant role in the mechanical behavior of ice-filled clefts at temperatures close to -0°C. Assuming moderate water content of 0.6%, the creep rate at 0°C is three times the rate at -2°C (Paterson 2001), which has serious effects on displacement rates and factors of safety considerations of mass movements.

As has been shown above, ERT and refraction seismics are highly susceptible to water/ice content inside the rock system just below the freezing point. Thus, the susceptibility range of seismic velocity and resistivity (ca. -0°C to -5°C) corresponds to the most important changes in ice-mechanical properties. This means the values temperature and water content, which are relevant for stability considerations in well-jointed permafrost rocks, are targeted by ERT and refraction seismics and combined interpretation strategies.

*Hydrological pressure*

Figure 8 shows light-colored, low-resistivity cleft water zones percolated by glacial meltwater that were observed to persist over several years and to limit the spatial extension of permafrost bodies (Krautblatter 2008). While pressure effects only have a small effect on the stress-strain behavior of ice itself (resisting force) (Weertman 1973), the reduction of applied normal stress and the increase in shear stress (driving force) may play a key role in preparing and triggering mass movements (Fischer et al. 2007, Terzaghi 1962). According to Wegmann (1998), permafrost degradation and aggradation in rocks in response to altered hydraulic conductivity occurs at all depths and quickly responds to annual melting patterns. He could also show that rock deformation quickly responds to spatial changes in permafrost rock conductivity.

Unfrozen cleft zones can easily be detected at the surface with RST and with ERT measurements possibly up to the maximum depth of the applied array (e.g., 80 m at the Zugspitze, 400 m Schlumberger-array). As shown in Figure 8, resistivity in water-filled cleft zones and frozen rock typically differs by 1–2 orders of magnitude and is, thus, easily detectable even at greater depths (Krautblatter & Hauck 2007). This opens up a whole range of new possibilities e.g., for the investigation of rock permafrost hydrology (Wegmann 1998), glacier-permafrost inter-connectivity (Moorman 2005), and rock deformation processes that are closely linked to freeze-thaw processes by latent heat transfer in clefts (Murton et al. 2006, Wegmann 1998).

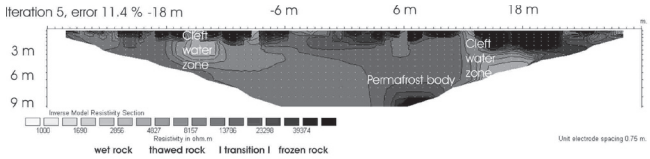


Figure 8. ERT of Transect NE (September 13, 2005). Mention the persistently thawed deep- reaching cleft water zones.

## Conclusion

Resistivity monitoring may provide indications on temperature changes and water saturation, while refraction seismics help to gain insight into discontinuity zones and exact geometric properties of instable bodies. Repeated time-sections reveal interannual, annual, and multiannual time-patterns as well as response times, the fourth dimension of rock permafrost systems.

For permafrost-induced mass movements, with secondary and tertiary creep of ice close to -0°C, three highly-variable forces play a key role in unbalancing resisting and driving forces. The resisting force of ice-creep in clefts is mainly controlled by (1) temperature and (2) water content in the ice. Due to the laws of electrolytic conductivity, resistivity values assessed by ERT react sensitively to both parameters, and water content is a key control for P-wave velocity. The highly variable driving force, (3) hydrological pressure, is well detectable in ERT time-sections as pore and cleft space supersaturation lead to a plunge in electrolytic resistivity. However, many other anisotropic factors distort ERT and seismic measurements, and further field and laboratory experience is needed for the allocation of their influence and for the "suppression" of such noise.

## Acknowledgments

This work has been funded by the German Research Foundation as part of the graduate school 437 "Relief." Special thanks to C. Hauck, J.-C. Otto, R. Dikau, M. Moser, S. Wolf, S. Verleysdonk, and all who participated in the fieldwork.

## References

Barnes, P., Tabor, D. & Walker, J.C.F. 1971. Friction and creep of polycrystalline ice. *Proceedings of the Royal Society of London, Series A*, 324(1557): 127-155.

Budd, W.F. & Jacka, T.H. 1989. A review of ice rheology for ice-sheet modeling. *Cold Regions Science and Technology* 16: 107-144.

Davies, M.C.R., Hamza, O. & Harris, C. 2001. The effect of rise in mean annual temperature on the stability of rock slopes containing ice-filled discontinuities. *Permafrost and Periglacial Processes* 12(1): 137-144.

Davies, M.C.R., Hamza, O., Lumsden, B.W. & Harris, C. 2000. Laboratory measurements of the shear strength of ice-filled rock joints. *Annals of Glaciology* 31: 463-467.

Fischer, L., Huggel, C. & Lemy, F. 2007. Investigation and modeling of periglacial rock fall events in the European Alps. *Geophysical Research Abstracts* 9(08160).

Gruber, S. & Haeberli, W. 2007. Permafrost in steep bedrock slopes and its temperature-related destabilization following climate change. *Journal of Geophysical Research - Earth Surface* 112(F2): F02S13.

Gruber, S., Hoelzle, M. & Haeberli, W. 2004. Permafrost thaw and destabilization of Alpine rock walls in the hot summer of 2003. *Geophys. Res. Lett.* 31(13): L15054.

Gude, M. & Barsch, D. 2005. Assessment of geomorphic hazards in connection with permafrost occurrence in the Zugspitze area (Bavarian Alps). *Geomorphology* 66: 85-94.

Haeberli, W. 2005. Investigating glacier-permafrost relationships in high-mountain area: historical background, selected examples and research needs. In: C. Harris & J.B. Murton (eds.), *Cryospheric Systems: Glaciers and Permafrost.* London: Geological Society Special Publication, 29-37.

Harris, C., Davies, M.C.R. & Etzelmüller, B. 2001. The assessment of potential geotechnical hazards associated with mountain permafrost in a warming global climate. *Permafrost and Periglacial Processes* 12(1): 145-156.

Hauck, C. 2001. Geophysical methods for detecting permafrost in high mountains. *Mitt. Versuchsanst. Wasserbau, Hydrologie und Glaziologie, PhD-thesis ETH Zürich* 171: 1-204.

Hauck, C. 2002. Frozen ground monitoring using DC resistivity tomography. *Geophys. Res. Lett.* 29, 2016, doi: 10.1029/2002GL014995: 12-1.

Hauck, C. & Vonder Mühll, D. 2003. Inversion and interpretation of two-dimensional geoelectrical measurements for detecting permafrost in mountainous regions. *Permafrost Periglac. Process.* 14(4): 305-318.

Heincke, B., Maurer, H., Green, A.G., Willenberg, H., Spillmann, T. & Burlini, L. 2006. Characterizing the fracture distribution on an unstable mountain slope using shallow seismic tomography: 2-D versus 3-D approaches. *Geophysics* 71(6): B241-256.

Kääb, A., Wessels, R., Haeberli, W., Huggel, C., Kargel, J.S. & Khalsa, S.J. 2003. Rapid aster imaging facilitates timely assessments of glacier hazards and disasters. *EOS* 13(84): 117, 121.

Krautblatter, M. 2008. Permafrost aggradation in the rock crest "Steintälli" (Valais, Switzerland) as a multiannual response to cool summers recorded by a three-year monitoring of rock permafrost by 2D/3D ERT and refraction seismics. *Geophysical Research Abstracts* 10: A-10496.

Krautblatter, M. & Dikau, R. 2007. Towards a uniform concept for the comparison and extrapolation of rock wall retreat and rockfall supply. *Geografiska Annaler* 89A(1): 21-40.

Krautblatter, M. & Hauck, C. 2007. Electrical resistivity tomography monitoring of permafrost in solid rock walls. *Journal of Geophysical Research-Earth Surface* 112. doi:10.1029/2006JF000546.

Krautblatter, M., Hauck, C. & Wolf, S. 2007. Geophysical 2D and 3D-monitoring of permafrost in rock walls. *Geophysical Research Abstracts* 9: A-09884.

Krautblatter, M. & Verleysdonk, S. 2008a. Rock wall permafrost monitoring with high-resolution 2D-ERT: lessons learnt from error estimates and a comparison of Wenner, Schlumberger, Gradient and Dipole-type arrays. *Geophysical Research Abstracts* 10: A-10383.

Krautblatter, M. & Verleysdonk, S. 2008b. Thawing regime and response time of present-day and relict permafrost revealed by monthly geophysical monitoring (Zugspitze, German/Austrian Alps). *Geophysical Research Abstracts* 10: A-10455.

Maurer, H. & Hauck, C. 2007. Instruments and methods: geophysical imaging of alpine rock glaciers. *Journal of Glaciology* 53(180): 110-120.

McGinnis, L.D., Nakao, K. & Clark, C.C. 1973. Geophysical identification of frozen and unfrozen ground, Antarctica. *2nd Int. Conf. on Permafrost, Yakutsk, Russia*, 136-146.

Moorman, B.J. 2005. Glacier-permafrost hydrological interconnectivity: Stagnation Glacier, Bylot Island, Canada. In: C. Harris & J.B. Murton (eds.), *Cryospheric Systems: Glaciers and Permafrost*, London: Geological Society Special Publication, 63-74.

Murton, J.B., Peterson, R. & Ozouf, J.-C. 2006. Bedrock fracture by ice segregation in cold regions. *Science* 314: 1127-1129.

Musil, M., Maurer, H., Green, A.G., Horstmeyer, H., Nitsche, F., Vonder Mühll, D. & Springman, S. 2002. Shallow seismic surveying of an alpine rock glacier. *Geophysics* 67(6): 1701-1710.

Otto, J.C. & Sass, O. 2006. Comparing geophysical methods for talus slope investigations in the Turtmann valley (Swiss Alps). *Geomorphology* 76(3-4): 257-272.

Paterson, W.S.B. 2001. *The Physics of Glaciers.* Oxford: Butterworth & Heinemann.

Sass, O. 2003. Moisture distribution in rock walls derived from 2D-resistivity measurements. *Z. Geomorph. N.F.*, Suppl.-Bd. 132(51-69).

Sass, O. 2004. Rock moisture fluctuations during freeze-thaw cycles: preliminary results from electrical resistivity measurements. *Polar Geography* 28(1): 13-31.

Sass, O. 2005. Rock moisture measurements: techniques, results, and implications for weathering. *Earth Surf. Process. Landforms* 30(3): 359-374.

Schoeneich, P., Hantz, D., Vengon, M., Frayssines, M., Deline, P., Amelot, F. & Savary, J. 2004. *A New Rlpine Rockfall Inventory.* Swiss Geoscience Meeting, Lausanne.

Terzaghi, K. 1962. Stability of steep slopes in hard unweathered rock. *Geotechnique* 12: 251-270.

Weertman, J. 1973. Creep of ice. In: E. Whalley, S.J. Jones & L.W. Gold (eds.), *Physics and Chemistry of Ice*. Ottawa: Royal Soc. of Canada, 320-337.

Wegmann, M. 1998. *Frostdynamik in hochalpinen Felswänden am Beispiel der Region Jungfraujoch - Aletsch.* Ph.D. Thesis. Mitt. Versuchsanst. Wasserbau, Hydrologie und Glaziologie, ETH Zürich 161: 1-144.

# Temperatures in Coastal Permafrost in the Svea Area, Svalbard

Lene Kristensen
*The University Centre in Svalbard, UNIS, Longyearbyen, Norway*
Hanne H. Christiansen
*The University Centre in Svalbard, UNIS, Longyearbyen, Norway*
Fabrice Caline
*The University Centre in Svalbard, UNIS, Longyearbyen, Norway*

## Abstract

Temperature data from three boreholes located on an ice-cored moraine near sea level are analyzed. One of these boreholes was drilled 6 m from the shore and shows significantly higher temperatures than the holes about 150 m from the shore. Using meteorological data and measurements of water temperatures, we model the permafrost distribution into the fjord as well as the influence of the sea on permafrost temperatures near the shore. The model results suggest that permafrost, as defined solely on temperature, is present beneath Van Mijenfjorden.

**Keywords:** borehole temperatures; coastal; geothermal modeling; permafrost; subsea permafrost; Svalbard.

## Introduction

Permafrost on Svalbard is classified as continuous. It is more than 500 m thick in the highlands and less than 100 m near the coasts (Humlum et al. 2003). While considerable knowledge of permafrost conditions in the mountains exists from the extensive coal mining, little has been published on the permafrost in the shore areas of Svalbard. Exceptions are Gregersen & Eidsmoen (1988) that compares deep borehole temperatures at the shore with inland boreholes in Longyearbyen and Svea, and Harada & Yoshikawa (1996) that uses DC resistivity soundings to estimate the permafrost thickness of marine terraces at the shore of Adventfjorden near Longyearbyen.

The aim of this paper is to describe the permafrost conditions in the ice-cored moraine, Crednermorenen,a peninsula in Van Mijenfjorden in central Spitsbergen (Fig. 1). Since April 2005 temperatures have been logged every two hrs in three boreholes on the moraine each with 16 thermistors down to eight m. One of the boreholes is located only six m from the shoreline. Permafrost conditions in the shore area are important since the permafrost here is "warm" and thin. When constructing in such areas, particular attention must therefore be given to the permafrost conditions. In most other parts of Svalbard, permafrost is thicker, colder and more stable.

Due to the few previous studies of near-shore permafrost on Svalbard, an attempt was made to model both the effect of the sea on the onshore permafrost as well as the possibility of subsea permafrost. We use a transient 2D finite element geothermal model (TEMP/W from Geoslope International, Calgary, Canada; Krahn 2004) that is forced with meteorological data and measured water temperatures as boundary conditions.

## Field Site

Crednermorenen is a lateral moraine deposited by a surge of the tidewater glacier Paulabreen (Fig. 1) around 1300 A.D. (Hald et al. 2001). The moraine forms a peninsula (1x3 km),

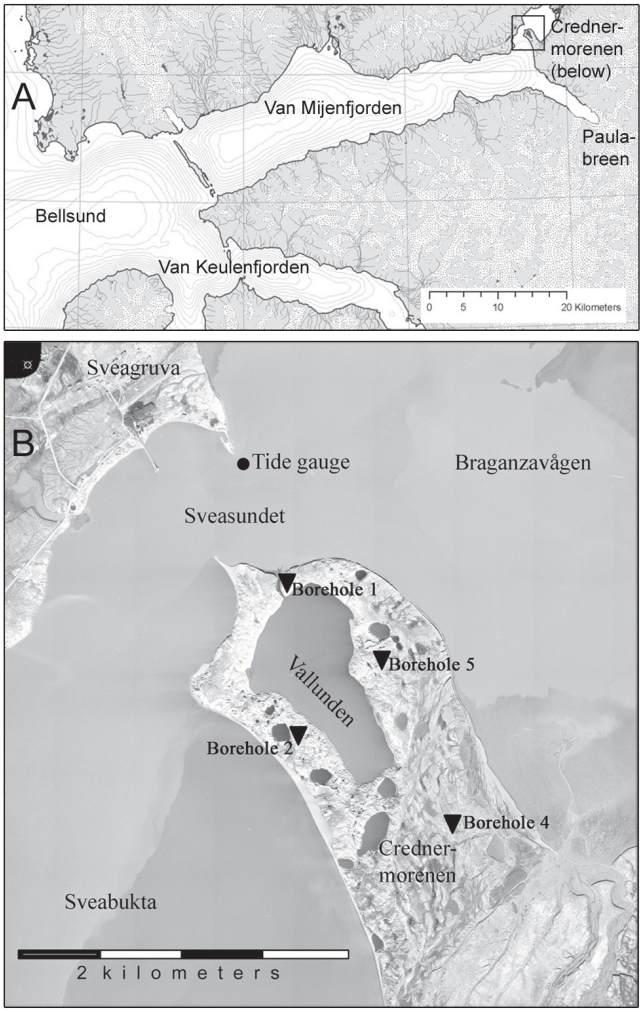


Figure 1. Field site. A) Van Mijenfjorden with Crednermorenen (in upper right corner). Map from: http://www.iopan.gda.pl. B) Crednermorenen with the location of the boreholes and the tide gauge. Air photo: Norsk Polarinstitutt, 1977.

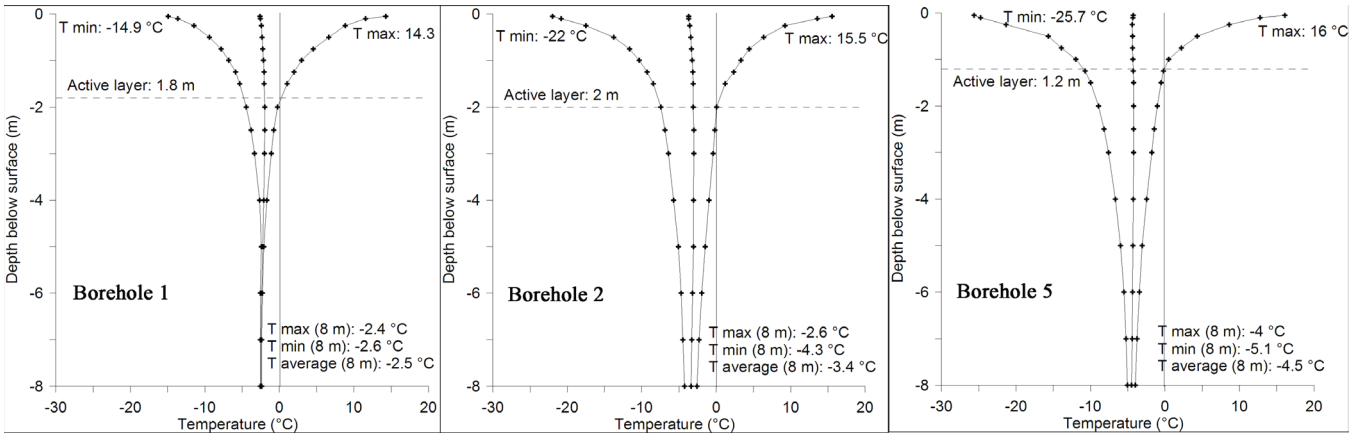


Figure 2. Maximum, minimum, and average temperatures in all depths from 10 September 2006 to 9 September 2007 for Boreholes 1, 2, and 5.

Table 1. Average annual temperature at the ground surface, at the top of the permafrost (TTOP).

| | (Air) | Hole 1 | Hole2 | Hole 5 |
|---|---|---|---|---|
| T surface (°C) | -4.6 | -2.6 | -3.7 | -4.2 |
| TTOP (°C) | | -2.0 | -3.1 | -4.3 |

partly ice-cored and partly consisting of proglacially pushed marine clays (Kristensen et al., in press). It is surrounded by water on three sides and in its northern part lies a 1 km long lagoon, —Vallunden—that, is connected to the sea by a 15m-wide channel near Borehole 1. The water in Vallunden is salty as the tide flows in and out through the channel.

The oceanography in Van Mijenfjorden is strongly affected by an island at the fjord mouth, Akseløya (Fig. 1A), which nearly blocks the water exchange between the fjord and the warmer Atlantic water outside (Nilsen 2002). The water column is thus dominated by cold local water. Shore-fast ice is usually present from December to June. Bottom water salinity is around 34‰ (Hald et al. 2001), and July temperatures of -1.53°C and and -1.27°C have been measured in two basins in Van Mijenfjorden at 112 m and 74 m depth (Gulliksen et al. 1985). The climate in Sveagruva is slightly colder and more humid than in Longyearbyen 45 km to the NNE, but the meteorological record is shorter and more irregular. Mean annual air temperature close to sea level was -5.4°C in the period 1997–2006, and precipitation in the period 1995–2002 was on average 244 mm/y (www.met.no).

## Temperature Measurements in Boreholes

Four 10 m deep boreholes (Fig. 1B) were drilled on Crednermorenen in March 2005 using an air pressure driven drilling rig. Coring was not possible, but the pulverized blown up sediment was collected from three of the holes, described and analyzed for water content and salinity. Borehole 1 was located two m above sea level and six m from the channel that connects Vallunden with Sveasundet. Borehole 2 was drilled into the ice-cored part of the moraine 17 m a.s.l. and 150 m from Sveabukta. Borehole 5 was established on top of the moraine ridge 145 m from Vallunden and 20 m a.s.l. Hole four was located on the marine clay part of Crednermorenen, but was destroyed by a bear in October 2006, and therefore no data are presented from that hole. In each borehole an eight m thermistor string (EBA Engineering, Edmonton, Canada) with 16 thermistors at decreasing spacing towards the surface was inserted. The uppermost sensor in each hole was placed at roughly three cm depth, and was measuring the surface temperature in this paper. Temperatures have been logged every two hour using Lakewood dataloggers; the accuracy of the thermistors is around 0.1°C. The annual temperature envelopes recorded in the three boreholes are shown in Figure 2. The maximum surface temperature for holes one and five occurred on 16 July 2007, and for hole two on 18 June 2007. The maximum temperature was very similar for the three holes, probably indicating that the barren surface provided similar summer conditions. The minimum surface temperature for all three holes occurred on 23 January 2007, which was contemporary with the minimum air temperature (-32.9°C) being recorded. The minimum surface temperature was much lower in hole two and five than in hole one. The latter had usually a snow cover of around 20 cm whereas both holes two and five were usually snow-free in winter due to wind redistribution in these more exposed sites. In Borehole 1 the seasonal temperature fluctuation became insignificant (0.25°C) below six meters depth, whereas the difference between annual maximum and minimum temperature at eight m in Boreholes 2 and 5 were 1.7°C and 1.1°C respectively.

Table 1 shows that all ground surface temperatures in the investigated period were higher than the mean air temperature. Hole one was warmest, reflecting the thickest snow cover during winter. The snow insulated the surface against cold winter temperatures creating a positive surface offset as demonstrated by, for example, Smith & Riseborough (1996). Hole 5 had the smallest surface offset as this site is usually never snow covered.

Smith & Riseborough (1996) also demonstrated that, due to higher thermal conductivity in frozen ground than in unfrozen, temperatures will tend to decrease from the ground surface to the top of the permafrost table (TTOP). Table 1 shows

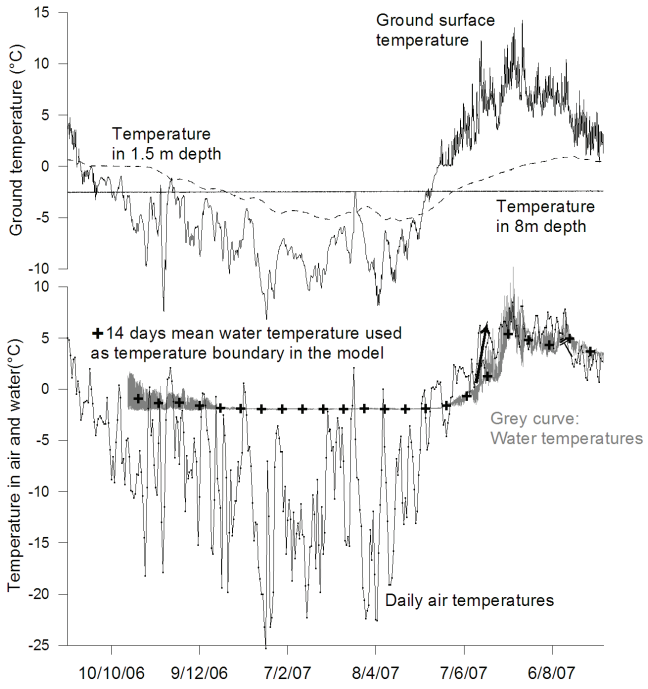


Figure 3. Upper part: Temperatures in Borehole 1 at the surface, in 1.5 m depth (dotted line) and in 8 m depth (no variation). Lower part: Air temperatures and water temperatures.

that in Boreholes 1 and 2 TTOP was higher than the surface temperature whereas in hole five it was practically the same. The active layer offset therefore seemed not to be important for the ground temperatures on the moraine, whereas snow depth in winter certainly was.

## Tide and Water Temperature Measurements

Water temperatures in the narrow and shallow strait Sveasundet were measured and recorded every 20 min from 10 October 2006 to 9 September 2007 by a tidal gauge placed at two m water depth. The data can be seen in Figure 3 together with temperature measurements from Borehole 1 from three selected depths and air temperature measurements over the same time interval.

The freshwater from Kjellstrømsdalen passes the Sveasundet strait, and strong tidal currents flowing in and out of Braganzavågen ensure mixing of salt and fresh water here. For this reason the summer water temperatures were high compared to what has been measured in the deep basins in the fjord during summer. Winter temperatures however appeared to be constant around -1.93°C in most of the fjord.

The measured water temperatures can be divided in three distinct periods:

1) An autumn period when the temperature fluctuated in relation to the tide between -1.9 and +1.7°C lasting from 21 October to 26 December. Temperatures rose when the tide was moving through Sveasundet into the tidal flat Braganzavågen and fell when the tide flowed out again. This is consistent with observations that sea ice started forming in Braganzavågen before other places in the fjord. An example

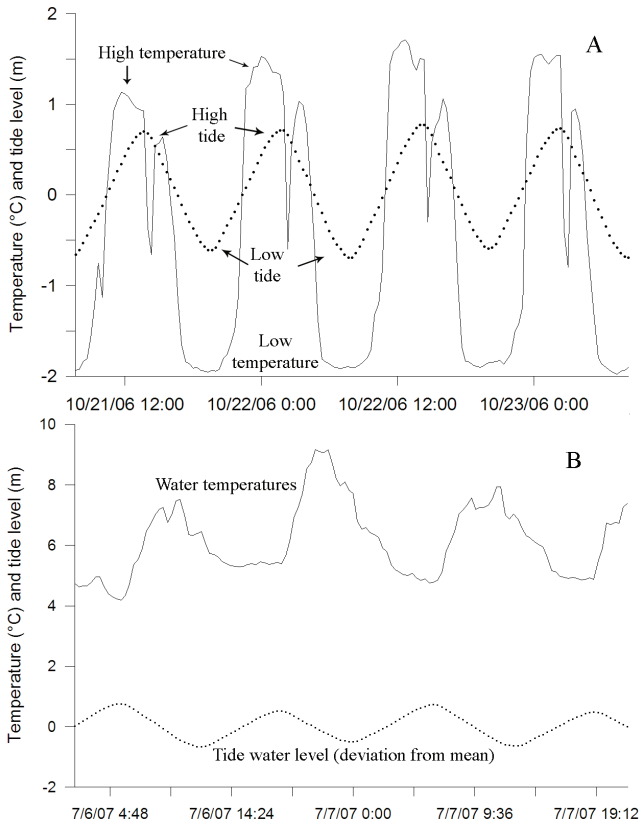


Figure 4. Examples of the relationship between water temperatures and the tide. A: Autumn conditions when the first sea ice forms, B: summer conditions.

of the coupling between tide and temperatures in the autumn can be seen in Figure 4A**.** November 28 was the last time the temperature rose above zero.

2) A winter period from 26 December to 22 May 2007. The temperature was nearly constant around -1.93, and no temperature fluctuations with tide were observed. The temperature corresponded to the freezing point of sea water and the fjord was covered by ice throughout this time. This winter period with constant water temperatures is easily identifiable in Figure 3.

3) A summer period from 22 May 2007 to the end of the measurements. Here the water temperatures increased and gradually approached the air temperature. The water temperature rose above zero for the first time on 13 June 2007. The temperature fluctuations were again controlled by tidal currents and were opposite in phase to those of the autumn. Now rising tide was associated with lower temperatures and falling tide with increasing temperatures (Fig. 4B). The reason is that water was now heated in the tidal flat Braganzavågen, where it was cooled during the autumn.

## Modeling the Effect of the Sea on the Permafrost Temperatures

Studying the measured borehole temperatures, one can see that Borehole 1 deviated significantly from Boreholes

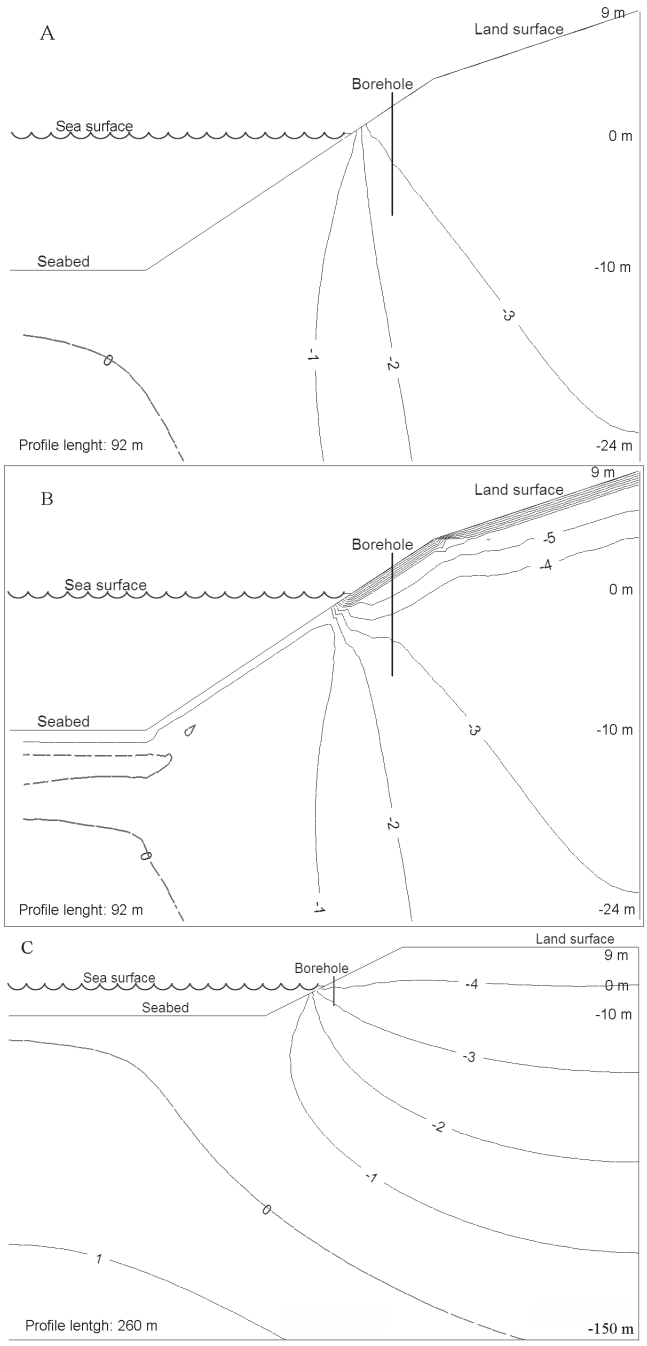


Figure 5. Three model output results. A: Steady state simulation of the ground temperatures in the immediate shore area. B: The same section but run in a transient mode forced with measured climatic data and sea water temperatures. Snapshot from 7 April 2007. C: Steady state simulation of a wider and deeper section with the boundary conditions the same as in A.

2 and 5 in respect both to the thermal regime and the depth of zero annual amplitude. While some of this deviation can be explained by a thicker snow cover during winter, most likely the proximity (6 m) to the sea affected the permafrost temperatures here. Located two m a.s.l. and being eight m deep, most of the borehole also lay below sea level. At eight m depth in Borehole 1, the temperature was -2.5°C. This indicates that permafrost probably extends into the seabed

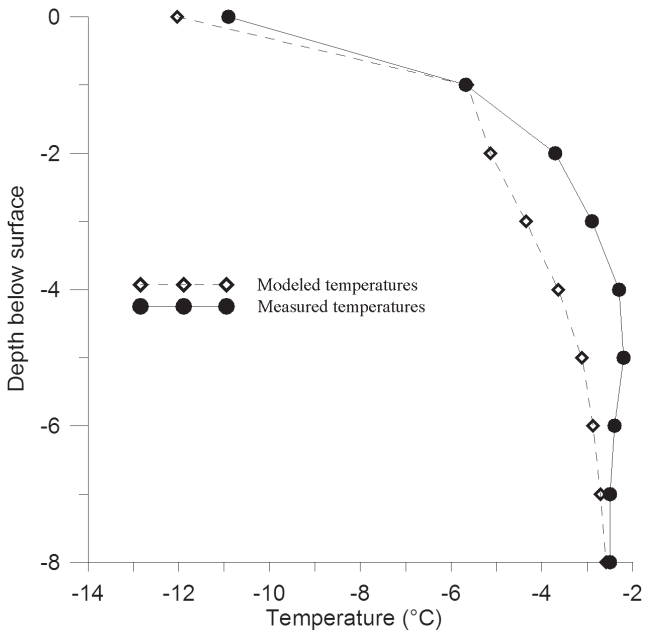


Figure 6. Comparison of the temperatures measured in Borehole 1 on 7 April 2007 and the modeled temperatures on the same day.

from the shore. An attempt was made to model both the effect of the sea on the onshore permafrost temperatures as well as the possibility of subsea permafrost existence. Gregersen & Eidsmoen (1988) previously tried to model the possible subsea permafrost in the area, but they had no information on the water temperatures in the fjord.

*Model description and input*

A 2D finite element program (TEMP/W) was used to model the permafrost thickness in Crednermorenen and the extent below the fjord bottom. The model is described in detail by Krahn (2004). Two temperature-dependent input functions (unfrozen water content and thermal conductivity) and overall water content are laboratory data from a nearby moraine, Damesmorenen, four km from hole 1, published by Gregersen et al. (1983). Volumetric heat capacity was set to 2000 and 3000 kJ/(m$^3$ x K) for frozen and unfrozen states respectively. Only one set of thermal properties was supplied to the model. It is obviously incorrect to assume homogeneous subsurface conditions, but we have no other thermal properties data available nor information on the subsea stratigraphy. A geothermal gradient of 35 mW/m$^2$ was set as a flux boundary condition at the bottom of the profiles. The vertical profile sides were set as zero flux boundaries.

To obtain a first estimate of the subsurface temperatures, the model was initially run in a steady state mode (Figs. 5A, 5C) using an estimated annual surface temperature and the average water temperatures as upper boundary conditions. A ground surface temperature of -4°C was used; this is slightly warmer than the mean annual air temperature due to the surface offset demonstrated in Table 1. A temperature of -0.1°C was used as the seabed boundary condition; this is the mean annual measured water temperature with interpolated

temperatures for the missing 1.5 months of data.

The model was also run in a transient mode (snapshot in Fig. 5B) to compare the model results with the temperatures measured in Borehole 1. In the transient mode, eight simulations were run per day, and each node result was input to the next model run. Here the model was forced with meteorological data from 1 Jan 2006 to 10 September 2007. The meteorological inputs were maximum and minimum daily temperature, maximum and minimum daily humidity, and average wind speed. Latitude and longitude were supplied and the TEMP/W program used an energy balance approach to model the surface energy balance. To simulate the seabed temperature, a time dependent te mperature function was supplied as boundary condition, consisting of the average measured water temperature on 14 day basis. These are seen as crosses in the lower part of Figure 3.

No attempts were made to simulate the tidal fluctuation and its affect on the ground temperatures.

The model was run on two profile sections of different lengths and depths to both obtain detailed information on the near surface conditions, and impressions of the larger-scale ground temperatures in the coastal zone. The profiles were 92 m and 260 m long respectively and simplify a profile across the moraine and into Vallunden crossing Borehole 1.

*Model results*

Figure 5A shows a steady-state simulation for the immediate shore area. A high horizontal thermal gradient is seen in a narrow zone just below the shoreline. Since the mean annual water temperature is slightly below zero (-0.1°C), permafrost is modeled to be present in a thin layer below the seabed.

Figure 5B shows a snapshot plot from the transient model run from 7 April 2007. The sharp decrease of near surface temperatures reflects the winter freezing on land. A -1 °C isotherm has formed close below the seabed reflecting that the water temperatures approach -2°C during winter.

Figure 5C is a model run of the larger and deeper section but with the boundary conditions as those of Figure 5A. The pattern is similar as the one in Figure 5A but suggests that at depth, the presence of the sea will affect the ground thermal conditions more than 100 m from the shore, and similarly, that the cold temperatures from land will affect the sub-seabed temperatures at a similar distance offshore.

Figure 6 compares the measured and modeled temperatures in Borehole 1 for 7 April 2007. The discrepancy of model temperatures near the surface and towards the bottom is quite small, whereas the modeled temperature is up to 1.4°C wrong in the middle of the borehole. This and other snapshots throughout the year show that, while the general pattern is simulated reasonably well, there are discrepancies. These are often larger than those shown in Figure 6. However, the reasonable agreement of the modeled to the measured temperatures gives us some confidence in the general modeling results.

## Discussion

The pronounced sill, Akseløya, restricts warm coastal water from entering Van Mijenfjorden and probably makes this fjord colder than other western Spitsbergen fjords. Sea ice cover is longer-lasting and more stable here. Therefore, this fjord is a primary candidate for possible subsea permafrost in western Spitsbergen fjords.

The modeling results of the subsea permafrost extend presented here should be seen as a minimum scenario. This is because the water temperatures were measured in a shallow, high-current strait, where the fjord water is strongly mixed with warmer fresh water during the summer. July temperature measurements from two deep basins in Van Mijenfjorden (Gulliksen et al. 1985) of -1.53°C and -1.27°C, respectively, indicate that water temperature in the deeper parts of the fjord remains below 0°C all year.

Permafrost, as defined solely on the basis of temperature, may not necessarily indicate cryotic subsea conditions. Sea water freezes at temperatures slightly above -2°C but capillarity and adsorption—in particular in fine-grained sediments—can further reduce the freezing point (Williams & Smith 1989). Thus, depending on the sediment properties, the seabed may well have permafrost by definition but still remain unfrozen. If the seabed consists of saline marine deposits, they will not be cryotic, even if thermally defined permafrost exists.

The 1300 A.D. surge of Paulabreen deposited lateral moraines in a rim around the inner parts of the fjord. A new detailed bathymetric survey indicates that glacial deposits also occupy the seabed here (Ottesen et al., in prep.). A seabed consisting of terrestrial sediments of glacial origin and with fresh rather than saline porewater could actually be frozen, but this hypothesis has not yet been tested.

The Crednermorenen moraine contains large amounts of buried glacier ice. It is possible that the unusual cold water conditions in Van Mijenfjorden are influencing the preservation potential of the ice-core in this moraine.

## Conclusions

The permafrost temperatures measured in three boreholes in the ice-cored Crednermorenen moraine were studied for a period of a year. The surface temperatures in all holes were higher than the corresponding air temperature. The highest surface temperature was measured in Borehole 1 that normally has a snow cover of 20 cm while the two other boreholes are nearly snow free during winter. Most likely the warmer surface temperature in Borehole 1 is due to a surface offset (Smith & Riseborough 1996) caused by the insulating effect of snow.

Increasing temperatures were observed from the surface down through the active layer to the top of the permafrost in two of the boreholes. This is opposite to what would be expected if higher thermal conductivity of frozen ground compared to unfrozen ground causes an active layer (or thermal) offset. So this offset appears not to be important here; probably the ground is too dry.

Borehole 1 is located six m from the shore and is significantly warmer than two other boreholes both about 150 m away from the shoreline. To investigate the effect of the proximity to the sea, the finite element program TEMP/W was used to model the ground temperatures at the shore and below the seabed in both a steady-state and transient mode. Meteorological data and water temperature measurements were used to force the model.

The program manages reasonably well to simulate the ground temperatures in the near-shore borehole. The simulations indicate that permafrost, as defined solely on temperature, is present in a thin layer beneath the seabed of Van Mijenfjorden. Whether it is frozen or unfrozen will depend on the material properties.

At depth, the warming effect of the sea on the ground temperatures is modeled to penetrate more than 100 m inland and the cooling effect of land is affecting the seabed at an equal distance. The temperatures closer to the surface, however, are primarily locally controlled.

## Acknowledgments

Many thanks to Store Norske Spitsbergen Kulkompani for funding the drilling and instrumentation of the boreholes and for providing logistical support when collecting data. LNSS, local contractor, preformed the drilling. Jomar Finseth, NTNU, supervised the drilling, sediment sampling, and laboratory work. John Inge Karlsen, logistics at UNIS, dived twice in muddy waters to emplace and recover the tide gauge that also recorded the water temperatures. The manuscript was improved by comments of an anonymous reviewer.

## References

Gregersen, O. & Eidsmoen, T. 1988. Permafrost conditions in the shore area at Svalbard. *Proceedings of the Fifth International Conference on Permafrost, Trondheim, Norway, August 2-5,1988*: 933-936.

Gregersen, O., Phukan, A. & Johansen, T. 1983. Engineering properties and foundation design alternatives in the marine Svea clay, Svalbard. *Proceedings of the Fourth International Conference on Permafrost, Fairbanks, Alaska, July,17-22, 1983*: 384-388.

Gulliksen, B., Holte, B. & Jakola, K.J. 1985. The soft bottom fauna in Van Mijenfjorden and Raudfjorden, Svalbard. In: J.S. Grey & M.E. Christiansen (eds.), *Marine Biology of Polar Regions and Effects ofStress on Marine Organisms*. Oslo: John Wiley & Sons, 199-215

Hald, M., Dahlgren, T., Olsen, T.E. & Lebesbye, E. 2001. Late Holocene palaeoceanography in Van Mijenfjorden, Svalbard. *Polar Research* 20(1): 23-35

Harada, K. & Yoshikawa, K. 1996. Permafrost age and thickness near Adventfjorden, Spitsbergen. *Polar Geography* 20(4): 267-281

Humlum, O., Instanes, A. & Sollid, J.L. 2003. Permafrost in Svalbard: a review of research history, climatic background and engineering challenges. *Polar Research* 22(2): 191-215. ‘

Krahn, J. 2004. *Thermal modeling with TEMP/W–An engineering methodology*. Calgary, Alberta, Canada: Geo-slope International Ltd., 282 pp.

Kristensen, L., Juliussen, H., Christiansen, H.H. & Humlum, O. 2008. The structure and composition of a tidewater push moraine, Svalbard, revealed by DC resistivity profiling. *Boreas* (in press).

Nilsen, F. 2002. Measured and Modeled Tidal Circulation Under Ice Cover Van Mijenfjorden. Abstract: www.cosis.net/abstracts/EGS02/06395/EGS02-A-06395-2.pdf

Ottesen, D., Dowdeswell, J.A., Benn, D.A., Kristensen, L., Christiansen, H.H., Christensen, O., Hansen, L. & Lebesbye, E. Submarine landforms characteristic of glacier surges in two Spitsbergen fjords (in prep.).

Smith, M.W. & Riseborough, D.W. 1996. Permafrost monitoring and detection of climate change. *Permafrost and Periglacial Processes* 7(4): 301-309.

Williams. P. J. & Smith, M.W. 1989. *The Frozen Earth: Fundamentals of Geocryology.* Cambrigde: Cambridge University Press, 306 pp.

# Thermal Deformation of Frozen Soils

G.P. Kuzmin
*Melnikov Permafrost Institute, SB RAS, Yakutsk, Russia*
V.N. Panin
*Melnikov Permafrost Institute, SB RAS, Yakutsk, Russia*

## Abstract

A relationship between temperature deformations of frozen soil and physical characteristics that change with increasing or decreasing temperature has been derived. This relationship is based on the assumption that the volumetric expansion of the soil is equal to the sum of the volume changes of its components. The gaseous component is assumed to change in volume due to both thermal deformation of the gas and elastic deformation caused by a change in thermal stresses in the soil. This assumption is confirmed by the results of experiments.

**Keywords:** gaseous constituent; phase change; soil components, temperature deformation.

## Introduction

Frost cracking of frozen soils subject to sub-freezing temperature fluctuations is a common phenomenon in permafrost regions. It is responsible for the formation of widely occurring polygonal features and affects various types of engineering structures (Ershov 2002).

Prediction of frost cracking in frozen ground requires knowledge of the thermal expansion coefficients, along with temperature data, and the soil thermal and mechanical properties (Grechishchev 1972).

The purpose of this paper is to derive an equation for obtaining the thermal deformation coefficients for frozen soils instead of time-consuming experimental determinations.

Thermal deformation of frozen soils, which generally consist of solid mineral particles, ice, water, and gases, determine the processes of the cryogenic rebound and formation and development of frost cracks.

Temperature change causes all frozen soil components to change volume in conditions of free or finite deformation. The most significant soil volumetric changes happen as a result of the water phase change, accompanied with the volume change accounting some 9% (Votyakov 1975). However frost penetration is accompanied with frost heave only if there is sufficient water-saturation (Votyakov 1975). When the water content is less than the plastic limit, freezing clay soils compress. When the water content is more than this limit, expansion develops during the freezing, and compression develops after freezing. Thus, the final deformation can be either positive or negative depending on initial in-situ water content.

No data is available on the influence of the soil gaseous constituent that reaches more than 10% in volume (Brodskaya 1962) on temperature deformations of frozen soils. Internal structural transformations of soil at freezing can not but influence the elastic deformations of gaseous constituent.

## The Dependence of Temperature Deformations on Physical Characteristics of Frozen Soils

The resulting volumetric change of the frozen soil with temperature is not the direct sum of thermal deformations of its components (Ershov 2002). However, the internal structural transformations in the soil caused by changes in its temperature should have an effect on elastic deformations of the gaseous component. Therefore, the increment of volume change of the frozen soil at a change of temperature from $t_1$ to $t_2$ can be written as the sum of its components volume increments

$$\Delta V = \Delta V_d + \Delta V_W + \Delta V_i + \Delta Va \tag{1}$$

where $\Delta V_d$, $\Delta V_W$, $\Delta V_i$, and $\Delta V_a$ are the increment of volume of soil skeleton, water, ice, and gaseous constituent, respectively.

Volumes of frozen soil components can be expressed through the physical characteristics and the whole soil volume.

$$V_d = \frac{\rho_d}{\rho_S} V \tag{2}$$

$$V_W = \frac{w_W \rho_d}{\rho_W} V \tag{3}$$

$$V_i = \frac{(w - w_W)\rho_d}{\rho_i} V \tag{4}$$

where $\rho_d$, $\rho_S$, $\rho_W$, and $\rho_i$ are densities of the soil, mineral particles, water, and ice accordingly; $w$ and $w_W$ are the total water content and unfrozen water content.

Equation (1) in view of Equations (2)–(4) can be given as:

$$V_2 - V_1 = \left(\frac{\rho_{d,2}}{\rho_{S,2}}V_2 - \frac{\rho_{d,1}}{\rho_{S,1}}V_1\right) + \left(\frac{w_{W,2}\rho_{d,2}}{\rho_{W,2}}V_2 - \frac{w_{W,1}\rho_{d,1}}{\rho_{W,1}}V_1\right) + \left(\frac{w - w_{W,2}}{\rho_{i,2}}\rho_{d,2}V_2 - \frac{w - w_{W,1}}{\rho_{i,1}}\rho_{d,1}V_1\right) + (V_{a,2} - V_{a,1}) \quad (5)$$

Characteristics for $t_2$ can be expressed through the corresponding parameters for $t_1$ in Equation (5).

The soil volume at $t_2$ can be presented as:

$$V_2 = (1 + \beta\Delta t)V_1 \quad (6)$$

where β=coefficient of volumetric temperature deformation; $\Delta t = t_2 - t_1$.

At temperature change the soil skeleton weight remains unchanged, hence:

$$\rho_{d,1}V_1 = \rho_{d,2}V_2. \quad (7)$$

The volume change of the closed-form gaseous constituent of frozen soils is the result of both its temperature deformations and action of temperature induced stress. Hence

$$\rho_{a,2}V_{a,2} = \rho_{a,1}V_{a,1}k \quad (8)$$

where $\rho_a$ is soil gaseous constituent density; $k$ is the coefficient considering the gases elastic deformations under the action of soil temperature stress.

The frozen soil components density for $t_2$ can be expressed through corresponding components for $t_1$

$$\rho_{S,2} = \frac{\rho_{S,1}}{1 + \beta_S\Delta t} \quad (9)$$

$$\rho_{W,2} = \frac{\rho_{W,1}}{1 + \beta_W\Delta t} \quad (10)$$

$$\rho_{a,2} = \frac{\rho_{a,1}}{1 + \beta_a\Delta t} \quad (11)$$

$$\rho_{i,2} = \frac{\rho_{i,1}}{1 + \beta_i\Delta t} \quad (12)$$

The coefficient of volumetric temperature deformation for frozen soils is related to the linear coefficient of deformation as

$$\beta = 3\alpha \quad (13)$$

In view of Equations (6)–(13) we find formula of coefficient of linear soil temperature deformation from Equation (5).

$$\alpha = -\frac{1}{3\Delta t}\left\{\begin{array}{l}\rho_{d,1}\left[\begin{array}{l}\frac{3\alpha_S\Delta t}{\rho_{S,1}} + \frac{w_{W,2}(1+3\alpha_W\Delta t) - w_{W,1}}{\rho_{W,1}} + \\ \frac{(w - w_{W,2})(1+3\alpha_i\Delta t) - (w - w_{W,1})}{\rho_{i,1}}\end{array}\right] + \\ \frac{V_{a,1}}{V_1}\left[(1+3\alpha_a\Delta t)k - 1\right]\end{array}\right\} \quad (14)$$

In Equation (14) gaseous constituent abundance in the soil $V_{a,1}/V_1$ can be evaluated as follows. We present the total soil volume as the sum of volumes of its components.

$$V = V_d + V_W + V_i + V_a \quad (15)$$

Having substituted in Equation (15) formulas of volumes of components Equations (2)–(4), we get

$$\frac{V_{a,1}}{V} = 1 - \rho_{d,1}\left(\frac{1}{\rho_{S,1}} + \frac{w_{W,1}}{\rho_{W,1}} + \frac{w - w_{W,1}}{\rho_{i,1}}\right). \quad (16)$$

Then the temperature deformation coefficient Equation (14) in view of Equation (16) is:

$$\alpha = \frac{1}{3\Delta t}\left\{\begin{array}{l}\rho_{d,1}\left[\begin{array}{l}\frac{3\alpha_S\Delta t}{\rho_{S,1}} + \frac{w_{W,2}(1+3\alpha_W\Delta t) - w_{W,1}}{\rho_{W,1}} + \\ \frac{(w - w_{W,2})(1+3\alpha_i\Delta t) - (w - w_{W,1})}{\rho_{i,1}}\end{array}\right] + \\ \left[1 - \rho_{d,1}\left(\frac{1}{\rho_{S,1}} + \frac{w_{W,1}}{\rho_{W,1}} + \frac{w - w_{W,1}}{\rho_{i,1}}\right)\right] * \\ \left[(1+3\alpha_a\Delta t)k - 1\right]\end{array}\right\} \quad (17)$$

## Results, Analysis, and Summary

The coefficient $k$ is unknown in Equation (17) and can be determined from experimental data. To this end, the thermal deformation coefficients were determined experimentally for artificially prepared frozen samples of loam and sandy loam, at two moisture contents, and sand, at one moisture content (Table 1). To prevent water drainage, the samples were insulated with a polyethylene film. After rapid freezing at low temperatures (20 C–30 C below zero), they were placed in a chamber with temperature $t_1$= -17°C, and maintained until

Table 1. The soil characteristics and results of definitions of coefficients and *k*.

| Type of soil | $\rho_d$, g/cm$^3$ | $\rho_S$, g/cm$^3$ | w, fraction | $\alpha \cdot 10^6$, gr$^{-1}$ | $w_{W1}$ fraction | $w_{W2}$ fraction | k |
|---|---|---|---|---|---|---|---|
| Loam | 1.524 | 2.7 | 0.25 | 417 | 0.083 | 0.068 | 0.834 |
| Loam | 1.301 | 2.7 | 0.35 | 465 | 0.083 | 0.068 | 0.832 |
| Sand loam | 1.918 | 2.65 | 0.13 | 113 | 0.048 | 0.031 | 0.707 |
| Sand loam | 1.320 | 2.65 | 0.34 | 143 | 0.048 | 0.031 | 0.830 |
| Sand | 1.698 | 2.65 | 0.19 | 71 | 0.016 | 0.009 | 0.836 |

stabilization. Then, the samples were moved to a chamber with temperature $t_2$= -4.1 C, and the changes in length were observed until the cessation of deformation. The changes in length of the samples were measured using a dial gage with an accuracy of 0.01 mm.

The temperature deformation coefficient was calculated by the formula

$$\alpha = \frac{\Delta l}{l_1 \Delta t} \tag{18}$$

where $\Delta l = l_2 - l_1$; $l_1$ and $l_2$ are initial and final lengths of the sample; $\Delta t = t_2 - t_1$.

The *k* values were calculated by Equation (17) using the experimentally determined α values. Herewith the following values were introduced: $\alpha_S$=10•x 10$^{-6}$gr.$^{-1}$; $\alpha_W$=17.4•x 10$^{-6}$ gr.$^{-1}$; $\alpha_i$=50•x 10$^{-6}$ gr.$^{-1}$; $\alpha_a$=1217•x 10$^{-6}$ gr.$^{-1}$. The unfrozen water content at $t_1$ and $t_2$ for all types of tested soils were taken from Votyakov (1975).

Experimental values of the coefficient of the temperature deformation, the deformations of samples received after stabilization, rather exceed the one-daily values, given in the paper by Votyakov (1975). The changes in the internal structure of the frozen soils with increasing thermal stresses caused elastic compression of the gaseous component, as is indicated by the values *k*<1.

## Conclusion

1. The dependence of the frozen soils temperature deformation coefficient on its physical characteristics, where the gaseous constituent elastic deformations come into account, has been received.
2. The elastic compression of the jammed gaseous constituent occurs when the cooling of frozen soils in the range of water change phase.
3. The *k* values, obviously, depend on conditions of the frozen soil cooling.

## References

Brodskaya, A.G. 1962. *The Compressibility of the Frozen Soils.* Moscow: Academy of Science Press: 83 pp.

Crechishchev, S.E. 1972. *Methodological Recommendations for Predicting Frost Cracking in Soils.* Moscow: VSEGINGEO: 38 pp.

Ershov, E.D. 2002. *General Geocrylogy: Manual for High School.* Moscow: Moscow Universiti Press: 682 pp.

Votyakov, I.N. 1975. *Physiomechanical Properties of the Frozen and Thawing Soils in Yakutia.* Novosibirsk: Nauka: 177 pp.

# Channel Realignment Using Natural Channel Design Principles

Alexandre Lai
*Alyeska Pipeline Service Company, Fairbanks, Alaska, USA*
Marc N. Gaboury
*LGL Limited environmental research associates, Nanaimo, British Columbia, Canada*

## Abstract

The Trans-Alaska Pipeline crosses Hess Creek on a 180 foot steel plate girder bridge. Thermal and hydraulic erosion altered the stream pattern with formation of a meander bend upstream of the bridge, leading to misalignment of the stream with the bridge abutments. To meet diverse stakeholder needs, an innovative approach to river engineering was implemented. Instead of a traditional riprap revetment, redirectional flow vanes were installed along an 800 foot meander bend. The vanes manipulate flow direction upstream of the bend, nudging the stream to a shallower curvature prior to entering the bridge opening. This new alignment improved conveyance through the bridge, created an active floodplain between eroding bank and the active channel, and over time will reestablish a functional riparian zone. Besides ecological benefits of a functioning floodplain, the riparian zone creates a buffer that insulates the ice-rich stream bank from further thermal and hydraulic erosion.

**Keywords:** erosion; floodplain; meander; realignment; stream; vanes.

## Introduction

Hess Creek is located 85 miles north of Fairbanks, Alaska at Dalton Highway milepost 24 and is approximately 32 miles south of the Yukon River. The Trans-Alaska Pipeline crosses Hess Creek at pipeline milepost 375 on its 800 mile journey from the Beaufort Sea at Deadhorse, Alaska, to the port of Valdez. At the pipeline crossing, the creek corridor is 130 ft wide, and the pipeline is supported by a 180 ft single span steel plate girder bridge. The drainage basin is 508 $mi^2$ and the bankfull discharge is 3375 $ft^3/s$ (cfs), based on a flood frequency analysis for gauged station USGS 15457800 on Hess Creek near Livengood, Alaska (1970–86; 662 $mi^2$). The area has discontinuous permafrost, and a typical floodplain soil profile consists of an organic layer, followed by silts, and alluvial gravels and sands down to bedrock.

At the time of construction in 1976, the pipeline crossing was in a stable reach of the creek with well-vegetated banks and no signs of bank erosion. A decade later, bank erosion upstream of the pipeline bridge was observed, and remedial action was taken to protect the north bridge abutment. But thermal and hydraulic erosion continued upstream of the bridge abutment and accelerated in the early years of 2000, most likely due to wildfires in the area. Continued erosion resulted in formation of a meander bend upstream of the bridge that previously was a relatively straight reach at the time of construction. This resulted in a misalignment of the bridge with the upstream and downstream reaches of the creek that could outflank the bridge abutment in a major flood event (Fig. 1). To meet the various stakeholder needs, such as protection of critical infrastructure, habitat preservation, and protection of an ecologically delicate region, an innovative approach to river engineering was used.

Figure 1. Hess Creek looking downstream, spring 2005 breakup. Hydraulic and thermal erosion of right bank resulting in misalignment with pipeline bridge.

## Design Concept

A riprap revetment is typically used to halt streambank erosion (Alyeska Pipeline Service Company 1973). However, unless a new bank and floodplain are built, rip-rapping the existing bank will lock in a radius of curvature for the meander bend that will continue to be misaligned with the pipeline bridge opening. Instead of a traditional riprap treatment of the streambank, a series of flow deflector vanes were installed in Hess Creek to readjust the existing stream alignment into a smooth curvature with the bridge orientation. The vane design was based on an approach applied by the Rural Water Commission of Victoria in Australia (Standing Committee on Rivers and Catchments 1991). The design relied on a visual estimation of the critical line of attack (i.e., notional straight lines of maximum stream velocity that align the riverward tip of the upstream vane to the base of the next consecutive vane downstream to ensure the eroding bank is not attacked directly during floods) on

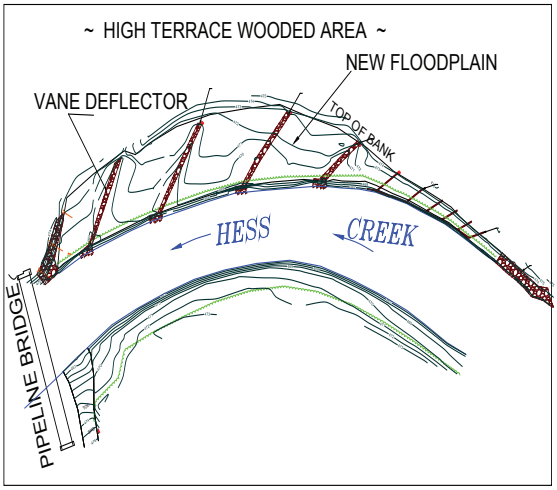


Figure 2. Plan view of 10 deflector vanes, new floodplain, and alignment of meander bend.

the outside streambank of the meander during flood stage. Detailed planimetric drawings, based on topographic surveys, and aerial photographs were used to estimate the critical line of attack and to position, through an iterative process, the location of the deflector vanes (Fig. 2). The guidelines followed during the design stage were that: (1) the radius of curvature for the eroding meander bend would be realigned with the bridge orientation, (2) the new channel design width and meander radius would mimic stable channel and meander radii upstream and downstream of the project site, (3) each deflector vane would be spaced so the flow passing around and downstream from the riverward end of the vane intersected the next vane and not the eroding bank, and (4) vanes would be angled approximately 10° downstream of the perpendicular to the estimated critical line of attack.

Prior to construction of the deflector vanes, the channel was realigned laterally towards the south (left bank looking downstream), gradually from 0 ft at the upstream end to 40 ft at the downstream end, just before the bridge abutments (Fig. 3).

Based on reference reach surveys upstream and downstream of the work site, the bankfull channel width of the new channel was set at 82 ft. The channel realignment was about 800 ft long and gravel excavated from the point bar was used to build a floodplain terrace along the right bank in space created by the channel realignment. To provide a stable transition from the new floodplain to the existing terrace on the north banks, a 3H:1V slope was shaped.

After the new floodplain footprint was established, 10 riprap directional flow vanes, 10–98 ft long and up to 6 ft wide and 6 ft deep, were installed orienting downstream along the 800 ft meander bend. The vanes manipulated flow direction, nudging the stream into a shallower curvature prior to entering the pipeline bridge opening. The vanes were constructed of riprap, ranging in diameter from 1–4 ft. Spacing and length of the vanes increased from upstream to downstream in the meander bend. Vane spacing and length were dependent on the estimated critical line of attack and the existing and proposed radius of curvatures for the

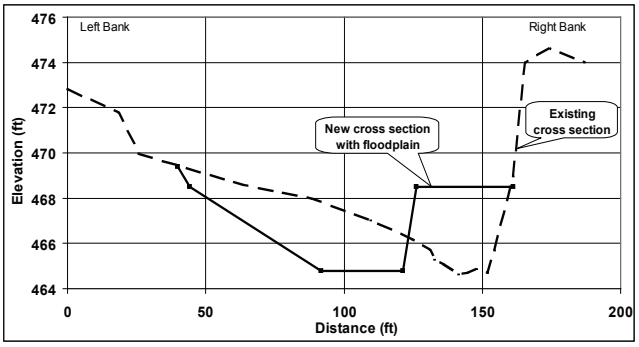


Figure 3. New cross section superimposed over existing eroding bank. A floodplain on the right bank was created from realignment of the meander bend.

Figure 4. Hess Creek upstream of pipeline bridge. Willows were planted along the bank and on the newly created floodplain.

meander bend. A riprap-armored guidebank was constructed along a 50 ft section at the upstream end of the meander to prevent flood flows from outflanking the vanes located downstream. The tops of the vanes were generally level with bankfull elevation along much of their length, with a gradual slope at the landward end to the top of the shallow streambank. Height of the vanes was approximately 4 ft above the new channel thalweg (defined as the deepest point in a given cross-section). The vane was keyed into the streambed and bank about 3 ft with riprap. About 650 $yd^3$ of riprap were used to build the vanes, and an additional 100 $yd^3$ were used to reinforce the existing guidebank on the north bank. To enhance instream cover for fish, logs were buried into the floodplain between the downstream vanes. The logs extended instream about 12 ft and were submerged at low-water level.

Once the vanes were completed, willow cuttings were installed along the riverward edge of the new right bank. In addition, the floodplain was vegetated with live stakes and willow transplants the following summer (2006) (Fig. 4).

## Post-Construction Monitoring

Although additional time is needed to properly assess the success of the design concept, initial results based on

two full years of monitoring, since their installation in the fall of 2005, are encouraging. No additional bank erosion has occurred, and the active floodplain is slowly becoming vegetated with natural riparian species. Deflector vanes have effectively nudged the thalweg away from the eroding terrace. Cross section surveys confirm that the thalweg is along the tip of the vanes as can be seen from Figure 5, where the main current is away from the right bank and flowing in the middle of the flooded channel during breakup.

Continuous riprap treatments typically halt bank erosion entirely, while discontinuous measures like deflector vanes or bank barbs deflect flows with discreet instead of continuous hardpoints. Therefore, some limited adjustments between structures after construction are expected until a stable "scalloped" bank line is formed (McCullah & Gray 2005).

A scalloped bank line developed in between the constructed deflector vanes on the newly constructed floodplain in Hess Creek (Fig. 6). This occurred after the first snowmelt flood following construction, but has remained stable since 2006. These scallops are a result of flow separation due to expansion of flow lines downstream of the rock deflector vanes. The expansion zones are beneficial to the aquatic ecosystem because they provide back eddies, hydraulic complexity, refuge and resting areas for fish.

The low profile deflector vanes provide flood capacity during peak flows when the floodplain is overtopped relieving stresses along the bank and the vane structures. These floodplain overflows result in deposition of seeds and woody material, which over time will hopefully result in a healthy riparian zone.

## Conclusion

The deflector vanes provided bank protection by realigning the channel thalweg away from the eroding streambank and by providing a riprap key tie-in of the vane to the streambank. The former measure provided stability along the toe of the bank, and the latter safeguarded against outflanking of the vane structures during extreme floods. The new alignment improved conveyance through the bridge, created an active floodplain between the eroding bank and the active channel, and will reestablish over the long term a stable streambank and functional riparian zone. By adopting a channel width and meander radius based on channel morphology in undisturbed natural reaches in Hess Creek, it is expected that the stability of the channel and constructed works will be maintained under the range of existing hydrological conditions. Incorporating these natural channel characteristics in the meander realignment will also help to create and maintain some of the key physical components of a healthy aquatic ecosystem. These key components could include, for example, deep residual pool depth along the bend to provide high-quality holding pools for fish, sorting and distribution of substrates to obtain suitable sizes and quantities of spawning gravels, and over-stream deciduous vegetation and recruitment of woody debris from the new floodplain to provide cover for rearing fish. In addition to the ecological benefits of a functioning floodplain, the constructed works also created a buffer to insulate the exposed ice-rich streambank from further thermal and hydraulic erosion. There is also a direct economic benefit to this design approach, because only one third of the rock quantity typically used in a traditional riprap revetment was needed to build the structures.

Figure 5. Post-construction spring breakup 2006, as compared with Figure 1. Overbank flow completely submerged floodplain and deflector vanes. No bank erosion, and main flow current is along the tip of deflection vanes, away from the right bank (note location of white "bubble line").

Figure 6. Looking upstream from the bridge, September 2007, showing scallops between deflector vanes and woody material that accumulated along the bank and floodplain.

## Acknowledgments

Many individuals provided invaluable input to the design of this project, among them are, Wim Veldman, P.E., Philip Hoffman, P.E., and Habitat Biologist Kenneth Wilson. Their diligent review and suggestions contributed to improvement of the overall design and satisfying stakeholder needs.

## References

Alyeska Pipeline Service Company. 1973. *Summary Report River and Floodplain Design Criteria for the Trans Alaska Pipeline System*.

McCullah, J. & Gray, D. 2005. *Environmentally Sensitive Channel and Bank-Protection Measures*. Washington, D.C.: National Cooperative Highway Research Program, NCHRP, Rep. 544.

Standing Committee on Rivers and Catchments. 1991. *Guidelines for Stabilizing Waterways*. Rural Water Commission of Victoria, Australia: 32 pp.

# ERS InSAR for Assessing Rock Glacier Activity

Christophe Lambiel
*Institute of Geography, University of Lausanne, Switzerland*
Reynald Delaloye
*Dept. of Geosciences, Geography, University of Fribourg, Switzerland*
Tazio Strozzi
*Gamma Remote Sensing, Switzerland*
Ralph Lugon
*Kurt Bösch University Institute, Sion, Switzerland*
Hugo Raetzo
*Federal Office for the Environment, Bern, Switzerland*

## Abstract

The potential of space-borne synthetic aperture radar interferometry (InSAR) to estimate both magnitude and spatial pattern of slope motion in a periglacial environment has been evaluated over a large area of the western Swiss Alps, using data from the ERS-1 and ERS-2 satellites. About 280 active rock glaciers with different classes of velocities have been identified on the analyzed interferograms. The velocities range from a few centimeters per year to several meters per year. These data were validated by some differential GPS measurements and compared to numerous field observations. The resulting classification permits a better description of the full range of rock glaciers velocities and dynamics. Therefore, ERS InSAR reveals itself to be an efficient remote sensing technique, not only for inventorying active rock glaciers over a wide area, but also for estimating and categorizing rock glacier displacement velocities.

**Keywords:** InSAR; permafrost creep; rock glacier activity; Swiss Alps.

## Introduction

The study of rock glacier dynamics constitutes one of the major topics in alpine periglacial research (e.g., Haeberli et al. 2006). The abundant literature related to the creeping of ice-rich permafrost attests the great diversity of rock glacier velocities, from a few centimeters per year for the slowest ones to more than 5 m per year for the fastest ones (e.g.. Roer 2005). Recent studies in the European Alps have evidenced (1) the great inter-annual variation of rock glacier velocities (Delaloye et al. 2008a), (2) an acceleration since the 1980s (Kääb et al. 2007), and (3) the partial or complete destabilization of some rock glaciers (e.g., Delaloye et al. 2008b, Roer et al. 2008). For these reasons, it appears that the usual classification—active, inactive, relict—does not permit the whole range of rock glacier velocities and dynamics to be described accurately. Therefore, a more precise classification of rock glacier velocities would be desirable.

Space-borne Synthetic Aperture Radar Interferometry (InSAR) is a well-established technique for mapping centimeter temporal changes in surface topography (Bamler & Hartl 1998, Rosen et al. 2000, Strozzi et al. 2001). In mountain areas above the tree line, it is possible to detect mass movements mostly during the snow-free period (Rott et al. 1999, Delaloye et al. 2007a). In particular, several studies have demonstrated the efficiency of InSAR for estimating rock glacier displacements (e.g., Kenyi & Kaufmann 2003, Strozzi et al. 2004, Kääb et al. 2005, Kaufmann et al. 2007). In the framework of the ESA (European Space Agency) SLAM (Service for Landslide Monitoring) project and with the support of the Swiss Federal Office for the Environment, the potential of InSAR to inventory mass wasting in the alpine periglacial belt has been tested. Both magnitude and spatial pattern of slope instabilities have been evaluated over a large area of the western Swiss Alps (50 x 30 km) (Fig. 1), using data of the European Remote Sensing satellites ERS-1 and ERS-2 dating from 1995 to 2000.

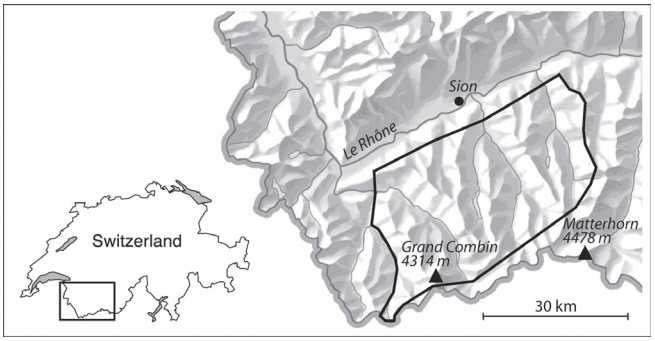

Figure 1. Area investigated.

This paper focuses on the various rates of rock glacier activity, which can be evaluated by ERS InSAR. After presenting the method and the dataset, the paper proposes a classification of rock glaciers, according to their typical ERS InSAR signals and morphological characteristics. Special attention was put on destabilization signs, which indicate a change in rock glacier dynamics.

## Methods and Datasets

For this study, a total of 34 interferograms computed from ERS SAR images acquired at C-band (wavelength: 5.6 cm)

between 1995 and 2000, with baselines shorter than 100-150 m, were used. Time lapse ranges between 1 day and 1085 days (in fact multiples of 35 days ± 1 day). The topographic reference was determined from an external digital elevation model with a spatial resolution of 25 m and an estimated vertical accuracy of 3 m (DHM25 © 2003 swisstopo). The InSAR products were also computed at 25 m spatial resolution. A change of the InSAR phase of one cycle is related to a movement of half the wavelength (2.8 cm) in the satellite line-of-sight direction, which is inclined at ~23° from the nadir and, in the western Swiss Alps, oriented toward the east +~12° for ascending orbits and toward the west -~12° for descending orbits. Thus, phase signals (i.e., change in the InSAR phase) detected on 1-day lag, 35-day lag, and 1-year lag interferograms can be interpreted as three orders of velocities, that is, respectively, centimeters per day, per month, and per year.

Important limiting factors of InSAR in mountainous terrain arise from temporal decorrelation, the satellite viewing geometry, and inhomogeneities in the tropospheric path delay. Atmospheric perturbations may cause phase changes related to the altitude. Among the other disruptive parameters, the wet snow, typically, can strongly reduce the reliability of an interferogram. This problem is especially present when working in alpine periglacial areas. In the Alps, above 2500 m a.s.l., the snow-free period is reduced to a few months, between July and early October. In addition, summer snowfalls are not uncommon at these altitudes, which can make many acquisitions unusable. On the other hand, cold snow is almost transparent to a radar wave. Thus, if the snow cover does not evolve, which may be possible only for few days, rapid movements can be identified in winter (Strozzi et al. 2004). Another limitation is the vegetation, which disturbs the radar backscatter and prevents any analysis in forest areas. Rock walls appear also strongly decorrelated, because of topographic effects. Finally, it is not possible to identify creeping landforms smaller than at least 2 x 2 grid cells (i.e., 50 x 50 m).

In order to identify the various rates of activity of active rock glaciers, different steps were followed:

- Evaluation of the reliability of the different interferograms. In particular, it was necessary to select the images for which the signal was not perturbed by the snow cover (both from the previous winter and from recent snowfalls). As a result, several interferograms could not be used in this study. The eight most reliable interferograms are listed in Table 1.
- Identification and delimitation of areas showing signals of potential slope motion by analysing the selected interferograms with various time scales and with different zoom levels.
- Determination of the corresponding geomorphological process (or landform) by orthophoto analysis or field observations.
- When available, comparing the InSAR estimated velocities to differential GPS data or airborne photogrammetric analysis.

Table 1. Dates of the best suited ERS SAR interferograms.

| Dates | Direction | Days |
|---|---|---|
| 11-12 March 1997 | asc./desc. | 1 |
| 29-30 July 1997 | asc./desc. | 1 |
| 3 Sept. - 8 Oct. 1997 | descending | 35 |
| 29 July - 3 Sept. 1997 | ascending | 35 |
| 18 Sept. 1996 - 30 July 1997 | descending | 315 |
| 8 Oct. 1997 - 23 Sept. 1998 | descending | 350 |
| 15 July 1998 - 8 Sept. 1999 | descending | 420 |
| 7 Oct. 1997 - 14 July 1998 | ascending | 279 |

## InSAR-Detected Velocities

About 600 polygons corresponding to spatially limited slope movements were identified throughout the whole investigated area. Among these polygons, about 280 were attributed to "active" rock glaciers. The other ones correspond to landslides, solifluction, push moraines, or debris-covered glaciers.

For four rock glaciers of the inventory, an obvious phase signal is detected on 1-day lag interferograms. Figure 2 illustrates the data for the Tsaté-Moiry rock glacier. The summer interferogram displays a very clear signal all along the rock glacier (Fig. 2a). On the winter interferogram (Fig. 2b), the signal is a little less marked, which may indicate slower winter velocities. These data mean that the motion is in the cm range per day, which corresponds to more than 3 m $a^{-1}$. Terrestrial measurements with differential GPS carried out on the rock glacier revealed velocities even up to 7 m $a^{-1}$ between 2006 and 2007. Similar InSAR signals were observed on the Petit Vélan rock glacier, where seasonal velocities up to 2 cm per day were measured in summer 2005 and 2007 (Delaloye et al. 2008b).

Some rock glaciers display a low 1-day phase signal, whereas the 1-month signal is decorrelated, that is larger than 1-phase cycle (2.8 cm). This is, for example, the case for the Tsarmine rock glacier (Fig. 3). In Figure 3a, a low signal can be detected on the 1-day summer interferogram (arrow), even if it is close to the noise level. The corresponding velocity can be estimated to a few millimeters per day, that is 1-2 m $a^{-1}$, which is confirmed by differential GPS measurements carried out since 2004 (see also Lambiel 2006). On the 1-month interferogram, the decorrelation is widespread over the landform (Fig. 3b).

Rock glaciers with velocities corresponding to the two previous categories constitute 5% maximum of the sample. On most of the InSAR-identified rock glaciers, a signal can only be detected with a 1-month interval. These rock glaciers can appear widely decorrelated, as it is the case for the Becs-de-Bosson rock glacier (Fig. 4) (Perruchoud & Delaloye 2007). This corresponds to minimum velocities of 20-30 cm $a^{-1}$. Another example is the Milon east rock glacier (Fig. 5a).

On numerous rock glaciers, the signal is hardly detectable at a 35-day lag, but is evident at a 1-year interval. The Milon west rock glacier is a nice example of this type (Fig. 5). Whereas only a very low signal occurs on the

1-month interferogram, the signal is evident on the 1-year interferogram. However, it remains rather correlated on the major part of the landform, which indicates a surface velocity of 2-3 cm $a^{-1}$.

Finally, rock glaciers showing only a low 1-year ERS InSAR signal or no signal at all creep with velocities slower than the phase cycle, i.e., 2.8 cm $a^{-1}$.

## Interpretation

The presented examples show the strength of InSAR for distinguishing the large range of active rock glaciers velocities. Table 2 summarizes the ERS InSAR-detected velocities and the corresponding classification which can be proposed. The frequency of destabilization indices for each category, which attests a change in the rock glacier dynamics, is also reported in the table.

*Very high velocity*

Phase signals observed on 1-day lag interferograms allowed movements in the order of a centimeter per day, which means several meters per year, to be identified. This magnitude of velocities, which can be qualified of *very high*, has rarely been mentioned hitherto. However, recent studies have reported the existence of other unusually rapid rock glaciers (e.g., Roer et al. 2008). Landslide-like features, like well-developed scars and crevasses, are often observed on these landforms (Fig. 2c), which indicates a strong destabilization and a complete change in the rock glacier dynamics.

*High velocity*

Rock glaciers showing a low 1-day and a decorrelated 1-month ERS InSAR signal move with a speed of 1-2 m $a^{-1}$. Such velocities are in the upper range of the typical rock glacier velocities. These landforms may creep with such velocities because of a large amount of ice, relatively warm temperature, or steep slope, but some of them display indices of a recent acceleration. Among these indices, the thinning of the upper part and associated thickening of the lower part is frequently observed, as it is the case for the Tsarmine rock glacier (Fig. 3c). On such landforms, destabilization signs, like scars and crevasses, are frequent, but are often not as pronounced and obvious as for rock glaciers of the previous category.

*Medium velocity*

Rock glaciers only detected with a 1-month interval and for which the signal is decorrelated correspond to the classical active rock glaciers. Velocities are comprised between 20 cm $a^{-1}$ and about 1 m $a^{-1}$. Indices of destabilization are occasionally observed. They may result from strong activity periods, as for the Mont Gelé B rock glacier, which moved with velocities of 120 cm $a^{-1}$ between 2003 and 2004, whereas the velocities measured since 2000 are normally comprised between 20 to 60 cm $a^{-1}$ (Lambiel 2006, Delaloye et al. 2008a).

*Low velocity*

Rock glaciers showing a correlated or a low signal on 35-day interferograms and a decorrelated signal on 1-year interferograms are active, but the deformation rate is only a few cm $a^{-1}$ (max. 0.2 m $a^{-1}$). A cold permafrost temperature, low ice content or low inclined slope generally explain these moderate velocities. Even if they are rare, destabilization indices occur in some cases, as for example on Les Lués Rares rock glacier (Fig. 6). On this landform, which is located below the regional lower limit of permafrost (front at 2320 m a.s.l), numerous indices, such as subsidence features, blocks densely covered with lichens and bushes on the front should indicate a very low activity. However, fresh scars in the front underline the current instability of the rock glacier (Fig. 6c), which is confirmed by the obvious and coherent signal visible on the 35-day lag interferogram, indicating velocities of about 10-20 cm $a^{-1}$ (Fig. 6a). Both these velocities and the limit of the moving area are confirmed by GPS measurements. About ten rock glaciers of the inventory display such characteristics. They all show evidences of a former inactivity or at least a very low activity (like vegetation growth and abundance of lichens), but display some recent destabilization indices.

*Very low velocity*

The rock glaciers which are only detected on 1-year lag interferograms correspond to the classical *inactive* landforms. Their velocity is in the cm range per year.

## Discussion

The inventory of creeping frozen debris bodies over a wide area is rarely exhaustive and the delimitation of the landforms can be highly subjective, whatever the method used. This is particularly the case with InSAR, as a potential signal may be due to other causes than a change in topography (atmospheric perturbations, vegetation, snow cover, etc.). Thus, the successfulness of such a study depends mainly on the availability of reliable interferograms. In this project, the discovery of a few very rapid rock glaciers was possible thanks the availability of very good quality summer and winter 1-day lag interferograms. Likewise, two excellent 35-day interval images, both in the ascending and descending mode, permitted us to delimitate classical active rock glaciers with a good accuracy. On the other hand, 1-year interferograms were not as reliable, but the identification of several low active rock glaciers was nonetheless possible.

In some cases, the signal is very low, such as, for example, the Tsarmine rock glacier on the 1-day interferogram (Fig. 3a) and the Milon west rock on the 35-day interferogram (Fig. 5a). For the Tsarmine rock glacier, the reliability of the signal was confirmed by GPS measurements. In the absence of terrestrial data, only the analysis of several interferograms and a good knowledge of the corresponding geomorphology allow the signal to be interpreted as a movement and not attributed to noise or atmospheric artefacts. However, the presence of a clear signal on a wider time interval,

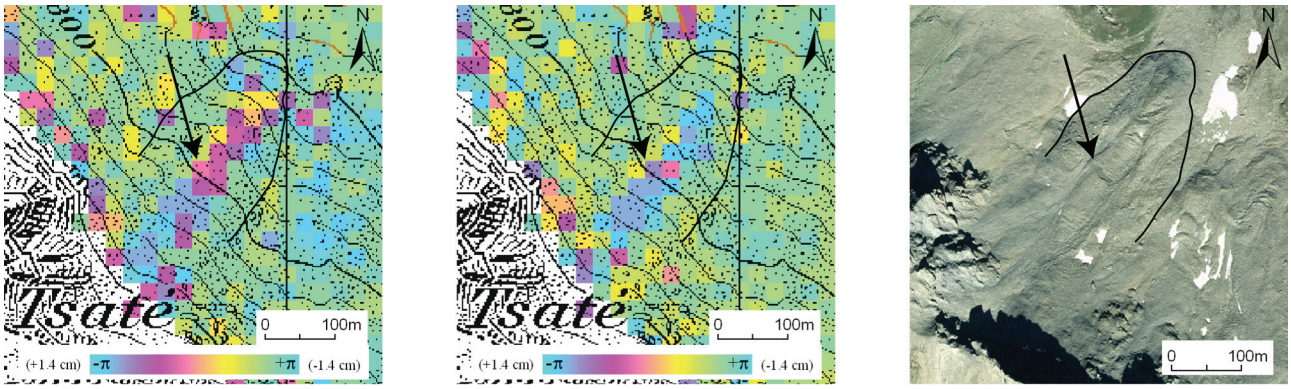


(a) (b) (c)

Figure 2. The active Tsaté-Moiry rock glacier. (a) 29-30 July 1997 (1d), ascending orbit; (b) 11-12 March 1997 (1d), ascending orbit; (c) orthoimage (Sept. 1999); scars are clearly visible on the centre of the rock glacier (arrow). Reproduced by permission of swisstopo (BA081058).

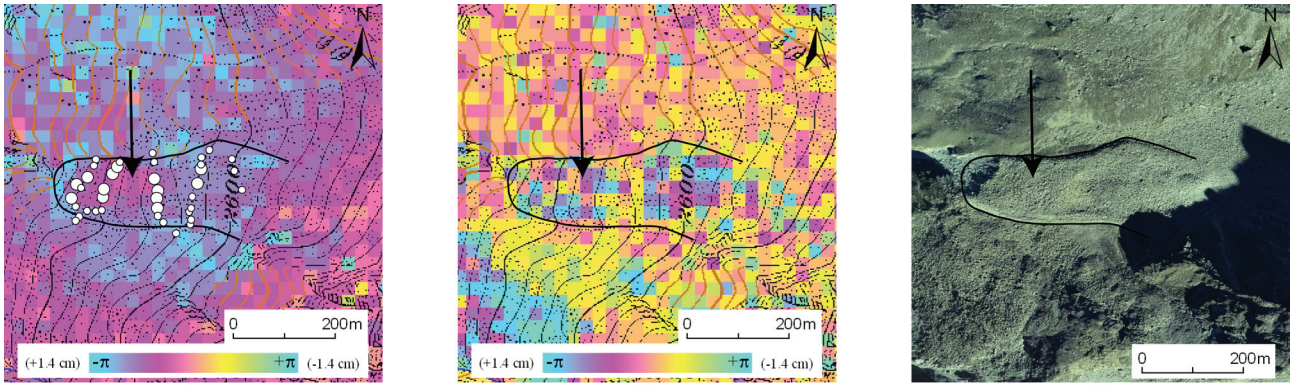


(a) (b) (c)

Figure 3. The active Tsarmine rock glacier. (a) 29-30 July 1997 (1d), descending orbit; white dots indicate horizontal surface velocities measured with differential GPS between 2004 and 2005; big dots = velocities > 4 mm/day; small dots = velocities < 4 mm/day; (b) 3 Sept..-8 Oct. 1997 (35d), descending orbit; (c) orthoimage (Sept. 1999). Reproduced by permission of swisstopo (BA081058).

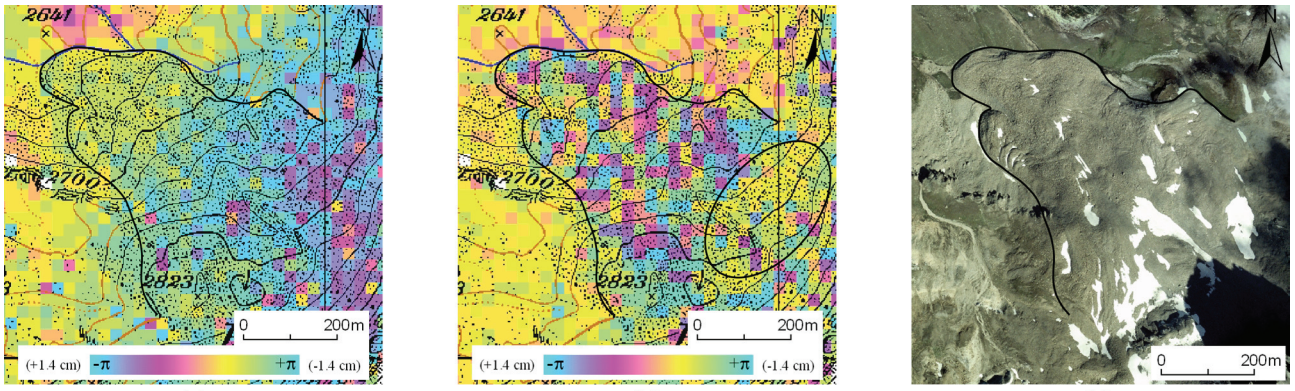


(a) (b) (c)

Figure 4. The active Becs-de-Bosson rock glacier. (a) 29-30 July 1997 (1d), descending orbit; (b) 3 Sept..-8 Oct. 1997 (35d), descending orbit; the circled area indicates an absence of movement, which is confirmed by GPS data (Perruchoud & Delaloye 2007); (c) orthoimage (Sept. 1999). Reproduced by permission of swisstopo (BA081058).

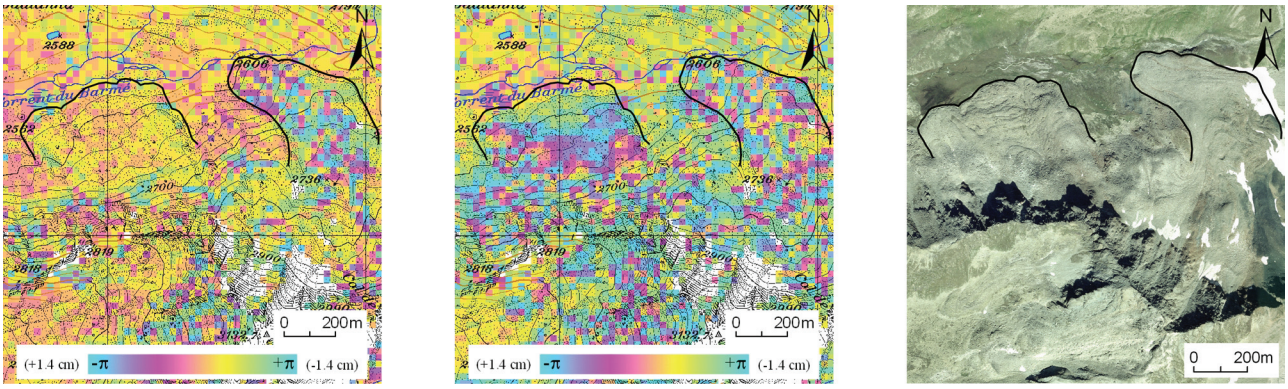


Figure 5. The active Milon east (right) and low active Milon west (left) rock glaciers. (a) 3 Sept..-8 Oct. 1997 (35d), descending orbit; (b) 18 Sept. 1996-30 July 1997 (315d), descending orbit; (c) orthoimage (Sept. 1999). Reproduced by permission of swisstopo (BA081058).

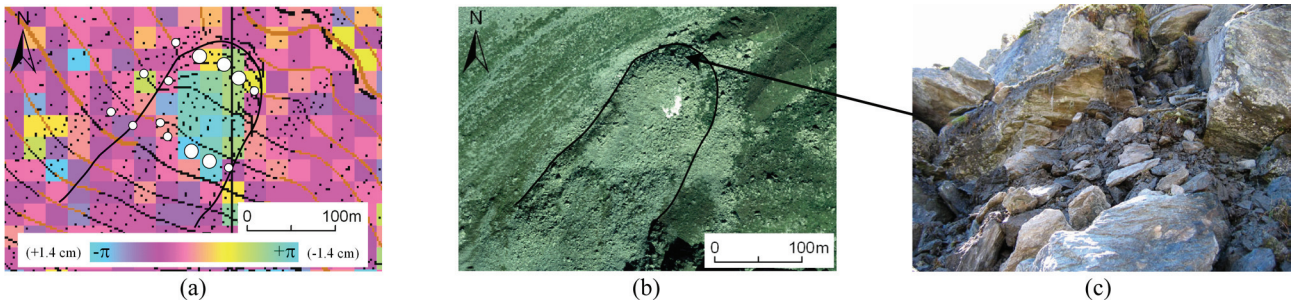


Figure 6. Les Lués Rares rock glacier. (a) 29 July-3 Sept. 1997 (35d), ascending orbit; white dots indicate horizontal surface velocities measured with differential GPS between 2006 and 2007; big dots = velocities of 1-2 cm/35 days; small dots = velocities < 0.5 cm/35 days or no movement; (b) orthoimage (Sept. 1999); (c) view on the destabilised front. Reproduced by permission of swisstopo (BA081058).

Table 2. Classification of the rock glaciers according to their surface velocities.

| Classical classification | ERS InSAR signal | Estimated surface velocity | Velocity classification | Destabilization |
|---|---|---|---|---|
| Active | 1 day | > 2 m $a^{-1}$ | very high | very frequent |
| | (1 day)/ 35 days decorrelated | 1-2 m $a^{-1}$ | high | Frequent |
| | 35 days | 0.2-1 m $a^{-1}$ | medium | Possible |
| | (35 days correlated) / 1 year | 0.03-0.2 m $a^{-1}$ | low | Rare |
| Inactive | (1 year) | up to a few cm $a^{-1}$ | very low | No |
| Relict | No | - | - | No |

which confirms the activity of the landform, is an absolute prerequisite for attributing the signal to a change in the topography rather to noise.

One limiting factor for using InSAR in the study of rock glacier velocities is the fact that this technique gives an estimation of the movement for a time-delimited period. For this study, most of the interferograms used correspond to the period 1996–1997. Thus, the observed velocities should be valid only for this period. In addition, numerous active rock glaciers are in an acceleration phase since the 1980s (Kääb et al. 2007), and some of them are suffering strong changes in the process regime (Roer et al. 2008). Thus, the phase signal detected on the available interferograms may no longer reflect the current state of activity of the corresponding rock glaciers. However, the comparison of the ERS InSAR-detected signals to velocities measured with differential GPS on 15 landforms since 2004, that is nearly 10 years later, permitted us to validate the InSAR data. Moreover, additional field observations on several tens of rock glaciers allowed us to understand the cause of such and such range of velocities, like, for instance, the observation of destabilization processes, which are clearly connected to the very high velocities observed on some rock glaciers (Roer et al. 2008). Thus, even if the velocities may have changed since the end of the 1990s, it is very probable that most of the rock glaciers are still in the same range of velocities as ten years before.

## Conclusion and Perspectives

ERS InSAR has revealed itself to be an efficient remote sensing technique, not only for inventorying active rock glaciers over wide areas, and more generally the creeping landforms of the alpine periglacial belt, but also for

estimating and categorizing their displacement velocities. Thus, InSAR constitutes an interesting tool for the study of rock glacier dynamics in the context of a general acceleration of these landforms. However, the detected signal can be sometimes close to the noise level. Thus, reliable interferograms, orthophotos, and a good knowledge of the local geomorphology are necessary to interpret the detected signal correctly.

Further InSAR studies are feasible with the SAR sensors on board of the European Environmental Satellite ENVISAT (C-band, 5.6 cm wavelength, 35 days repeat cycle), the Japanese Advanced Land Observing Satellite ALOS (L-band, 23.6 cm wavelength, 46 days repeat cycle) and the German TerraSAR-X mission (X-band, 3.1 cm wavelength, 11 days repeat cycle), in orbit since 2002, 2006, and 2007, respectively. They should permit recent data on rock glacier velocities throughout wide areas to be obtained. However, no one is able to provide reliable data on rock glaciers with very high velocities anymore (Delaloye et al. 2008b), as did the ERS-1/2 tandem between 1995 and 1999.

## Acknowledgments

We would like to thank the Associate Editor and the two anonymous reviewers for their useful feedback, and Meredith Blake for proofreading the English.

## References

Bamler, R. & Hartl, P. 1998. Synthetic aperture radar interferometry. *Inverse Problems* 14: 1-54.

Delaloye, R., Lambiel, C., Lugon, R., Raetzo, H. & Strozzi, T. 2007a. Typical ERS InSAR signature of slope movements in a periglacial mountain environment (Swiss Alps). *Proceedings Envisat Symposium 2007, Montreux, Switzerland 23–27 April 2007* (ESA SP-636, July 2007), 3P7.

Delaloye, R., Lambiel, C., Lugon, R., Raetzo, H. & Strozzi, T. 2007b. ERS InSAR for detecting slope movement in a periglacial mountain environment (western Valais Alps, Switzerland). *Proceedings HMRSC-IX, Grazer Schriften der Geographie und Raumforschung*. 43: 113-120.

Delaloye, R., Perruchoud, E., Avian, M., Kaufmann, V., Bodin, X., Hausmann, H., Ikeda, A., Kääb, A., Kellerer-Pirklbauer, A., Krainer, K., Lambiel, C., Mihajlovic, D., Staub, B., Roer, I. & Thibert, E. 2008a. Recent interannual variations of rockglaciers creep in the European Alps. *Proceedings of the Ninth International Conference on Permafrost, Fairbanks, Alaska, June 29-July 3, 2008* (this proceedings).

Delaloye, R., Strozzi, T., Lambiel, C. & Perruchoud, E. 2008b. Landslide-like development of rockglaciers detected with ERS-1/2 SAR interferometry. *Proceedings ESA FRINGE Symposium 2007* (in press).

Haeberli, W., Hallet, B., Arenson, L., Elconin, R., Humlum, O., Kääb, A., Kaufmann, V., Ladanyi, B., Matsuoka, N., Springman, S. & Vonder Mühll, D. 2006. Permafrost creep and rock glacier dynamics. *Permafrost and Periglacial Processes* 17: 189-214.

Kääb, A., Huggel, C., Fischer, L., Guex, S., Paul, F., Roer, I., Salzmann, N., Schlaefli, S., Schmutz, K., Schneider, D., Strozzi, T. & Weidmann, Y. 2005. Remote sensing of glacier- and permafrost-related hazards in high mountains: an overview. *Natural Hazards and Earth System Science* 5: 527-554.

Kääb, A., Frauenfelder, R. & Roer, I. 2007. On the response of rockglacier creep to surface temperature increase. *Global and Planetary Change* 56(1-2): 172-187.

Kaufmann, V., Ladstädter, R. & Kienast, G. 2007. 10 years of monitoring of the Doesen rock glacier (Ankogel group, Austria) - A review of the research activities for the time period 1995-2005. In: D. Petrovič, (ed.), *Proceedings of 5th Mountain Cartography Workshop, 29 March-1 April 2006, Bohinj, Slovenia*: 129-144.

Kenyi, L. & Kaufmann, V. 2003. Measuring rock glacier surface deformation using SAR Interferometry. *Proceedings of the Eighth International Conference on Permafrost, Zürich, Switzerland, June 2003*. Balkema 1: 537-541.

Lambiel, C. 2006. *Le Pergélisol Dans les Terrains Sédimentaires à Forte Déclivité: Distribution, Régime Thermique et Instabilités*. Thèse, Université de Lausanne, Institut de Géographie, coll. "Travaux et Recherches" 33: 260 p.

Perruchoud, E. & Delaloye, R. 2007. Short-term changes in surface velocities on the Becs-de-Bosson rock glacier (western Swiss Alps). *Proceedings HMRSC-IX, Grazer Schriften der Geographie und Raumforschung* 43: 131-136.

Roer, I. 2005. *Rockglacier Kinematics in a High Mountain Geosystem*. PhD Thesis. Rheinischen Friedrich-Wilhelms Universität Bonn, 217 pp.

Roer, I., Avian, M., Delaloye, R., Lambiel, C., Haeberli, W., Kääb, A. & Kaufmann, V. 2008. Observations and considerations on collapsing active rockglaciers in the Alps. *Proceedings of the Ninth International Conference on Permafrost, Fairbanks, Alaska, June 29-July 3, 2008* (this proceedings).

Rosen P., Hensley, S., Joughin, I., Li, F., Madsen, S., Rodriguez, E. & Goldstein, R. 2000. Synthetic aperture radar interferometry. *Proceedings of the IEEE*, 88(3): 333-382.

Rott, H., Scheuchl, B., Siegel, A. & Grasemann, B. 1999. Monitoring very slow slope movements by means of SAR interferometry: A case study from a mass waste above a reservoir in the Ötztal Alps, Austria. *Geophysical Research Letters* 26(11): 1629-1632.

Strozzi, T., Wegmüller, U., Tosi, L., Bitelli, G. & Spreckels, V. 2001. Land Subsidence Monitoring with Differential SAR Interferometry. *Photogrammetric Engineering & Remote Sensing (PE&RS)* 67(11): 1261-1270.

Strozzi, T., Kääb, A. & Frauenfelder, R. 2004. Detecting and quantifying mountain permafrost creep from in situ inventory, space-borne radar interferometry and airborne digital photogrammetry. *International Journal of Remote Sensing* 25(15): 2919-2931.

# Sensitivity of Coastal Erosion to Ground Ice Contents: An Arctic-Wide Study Based on the ACD Classification of Arctic Coasts

Hugues Lantuit
*Alfred Wegener Institute for Polar and Marine Research, Potsdam, Germany*
Pier Paul Overduin
*Alfred Wegener Institute for Polar and Marine Research, Potsdam, Germany*
Nicole Couture
*Dept. of Geography, McGill University, Montréal, Canada*
Rune Strand Ødegård
*Gjøvik University College, Gjøvik, Norway*

## Abstract

Changing sea ice conditions and thawing permafrost in the Arctic could lead to dramatic changes in coastal erosion dynamics. To address this issue, the Arctic Coastal Dynamics (ACD) project brought together experts from all circum-Arctic countries around a common project: the ACD classification of Arctic coasts. This paper uses 545 segments from the beta version of the ACD classification to investigate statistical relations between coastal erosion rates on Arctic coasts and ground ice content. Ground ice content and retreat rates are only weakly correlated statistically ($r = 0.48$, relationship statistically significant at $\alpha = 0.01$), but the multifactor nature of coastal erosion in the Arctic shows us that ground ice is a major factor affecting erosion processes. The current study integrates several geographical settings and time scales and is therefore integrative enough to be used as a benchmark for future empirically based models

**Keywords:** Arctic; coastal erosion; GIS; ground ice.

## Introduction

Arctic coasts are among the most vulnerable environments to climate change. Changing sea ice conditions and thawing permafrost could lead to dramatic changes in coastal erosion dynamics. To address this issue, ACD was initiated to provide a comprehensive review of coastal erosion processes at the Arctic scale. This paper uses data from the beta version of the ACD classification to investigate statistical relations between coastal erosion rates on Arctic coasts and ground ice content. Close to 600 segments were used to systematically compare and plot ground ice content and coastal erosion rates. The specific aims of this paper are to document the statistical relation between ground ice and coastal erosion rates and to compare those relations with previously published studies. The statistical relationship extracted from this study will be used as a benchmark for empirical models of coastal erosion.

## Background

*Arctic coastal erosion*

Coastal erosion in the Arctic is different from its counterpart in temperate regions due to the short open-water season (3-4 months) and to the presence of permafrost, and thus of ground ice, in coastal sediment.

Coastal retreat rates are also highly variable both spatially and temporally (Lantuit & Pollard 2008, Rachold et al. 2000, Solomon 2005). Spatial variability is mainly due to changes in the lithology, cryology, and geomorphology of coastal cliffs, including ground ice content.

Ground ice is a unique feature of polar coastal systems. It is present in the subaerial part of the shore profile, but also underneath the water column, as submarine ground ice (Mackay 1972, Rachold et al. 2007). Its presence affects both the response of the shore to thermal-hydrodynamical forcing and the sediment budget of the coast (Are 1988, Dallimore et al. 1996). The presence of ground ice leads to a process termed "thermal abrasion" (Are 1988) which encompasses the combined action of waves and thawing of the permafrost. It has been shown to facilitate erosion (Héquette & Barnes 1990, Kobayashi et al. 1999), through the presence of ice in coastal cliffs, or through the occurrence of large thermokarst features in the coastal zone (Lantuit and Pollard 2005, Lantuit & Pollard 2008, Wolfe et al. 2001). Dallimore et al. (1996) suggested that thaw settlement of ice-rich sediments in the nearshore zone could induce a change in the shoreface profile, hence enhancing wave efficiency during storms.

However, not all Arctic coastlines are characterized by subsea ice-rich permafrost and other explanations must be sought. Héquette and Barnes (1990) attributed those to the occurrence of ice scours and sediment entrainment by sea ice in the offshore zone, which as shown by Forbes and Taylor (1994) can alter significantly the coastal sediment budget. They based their hypothesis on the weak correlation between retreat rates and several factors including ground ice, wave height, and grain size (Fig. 1). This paper attempts at providing an expanded characterization (Arctic-wide) of the statistical relation between ground ice contents and re-evaluating the relation proposed by Héquette and Barnes (1990) for the southern Beaufort Sea by using the ACD classification of Arctic coasts.

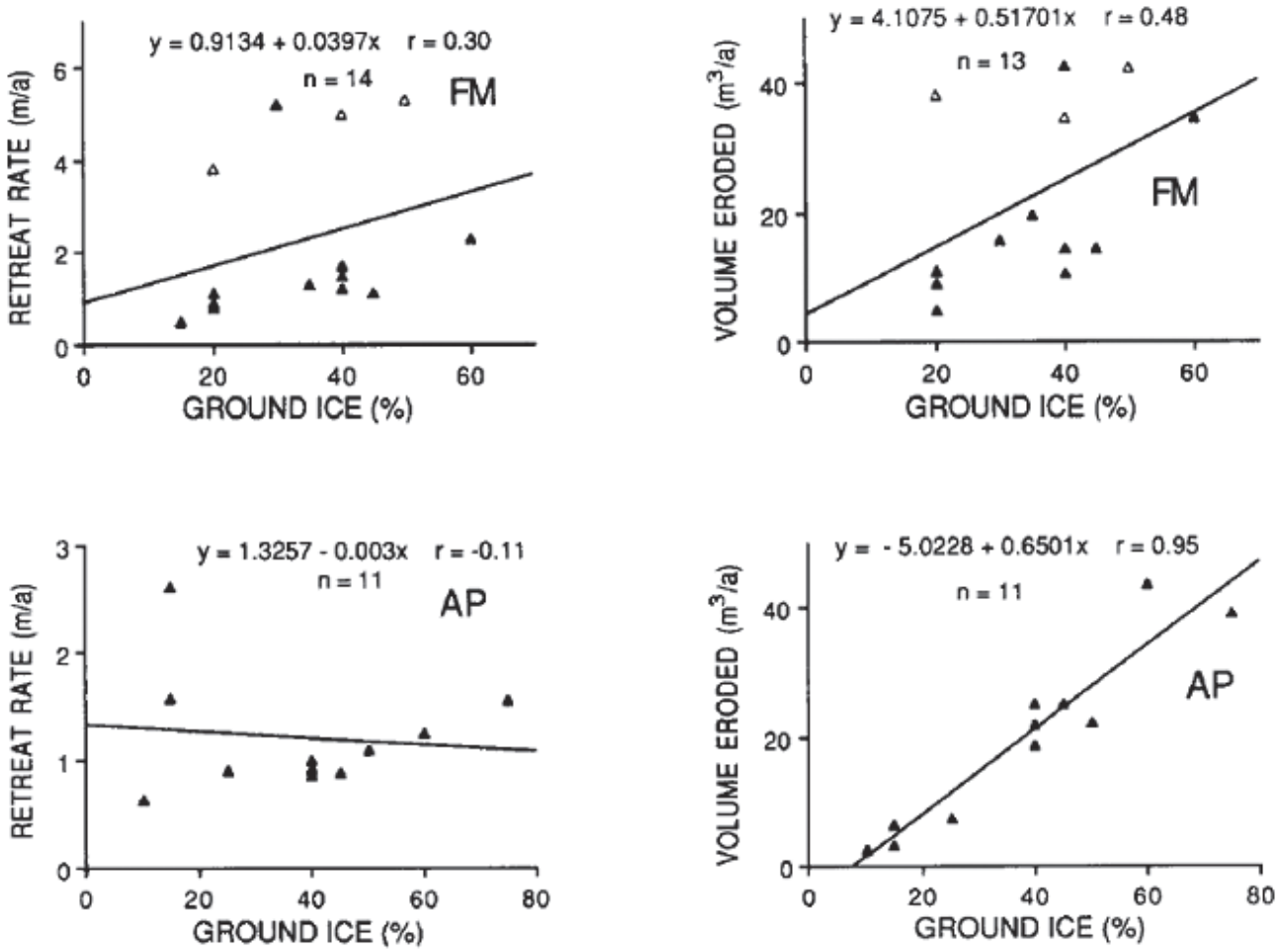


Figure 1. Coastal retreat and erosion as a function of visible ground ice in the bluffs. FM - field measurement sites; AP - aerial photograph sites; open triangles indicate minimum values of retreat rate (after Héquette & Barnes, 1990).

*The ACD classification of Arctic coasts*

The ACD classification was conceived as a broad enough framework to encompass existing classification schemes while capturing fundamental information for the assessment of climate change impacts and coastal processes. The implementation of the classification was done by so-called "regional experts", who, based on digital and paper products and personal knowledge provided information which was subsequently gathered into a circum-Arctic coastal database. The classification was primarily geomorphological in nature and considered: (1) the shape or form of the subaerial part of the coastal tract, (2) the marine processes acting upon the coast, (3) the shape or the form of the subaqueous part of the coastal tract and (4) the lithofacies of the materials constituting the coastal zone

The beta version of the classification is made of 1331 segments each characterized by a series of geomorphological quantitative and qualitative variables. The classification is stored as an ISO 19115-compliant personal geodatabase and is therefore mappable in off-the-shelf Geographical Information Systems (GIS) (e.g., Fig. 2).

## Methods

The first step of the processing consisted in reducing the dataset to a set of usable segments: Of the 1331 segments available in the beta version of the ACD classification of Arctic coasts, only segments for which ground ice content, coastal erosion rate, and backshore elevation (i.e. cliff height) were conjointly available were retained. The resulting dataset was reduced to 561 segments.

Subsequently, we consolidated the dataset by removing segments for which the presence of permanent sea ice cover in the summer hampered the development of erosion. The objective was to remove segments for which ground ice contents can be medium to high, yet unaffected by erosion due to sea ice presence in the summer. We used the NSIDC 1979-2000 median sea ice edge position and simply excluded segments located within the permanent sea ice zone in the dataset. We chose not to take into account the marked decreases observed in recent years in order to remain consistent with the times at which coastal erosion rates were mostly determined in the ACD classification.

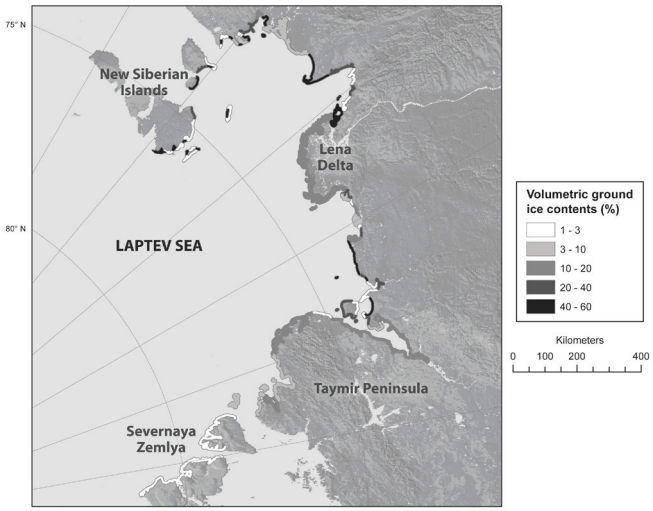


Figure 2. An example of the ACD classification capabilities: Volumetric ground ice contents of shore sediments in the Laptev Sea region (after Lantuit et al. 2008).

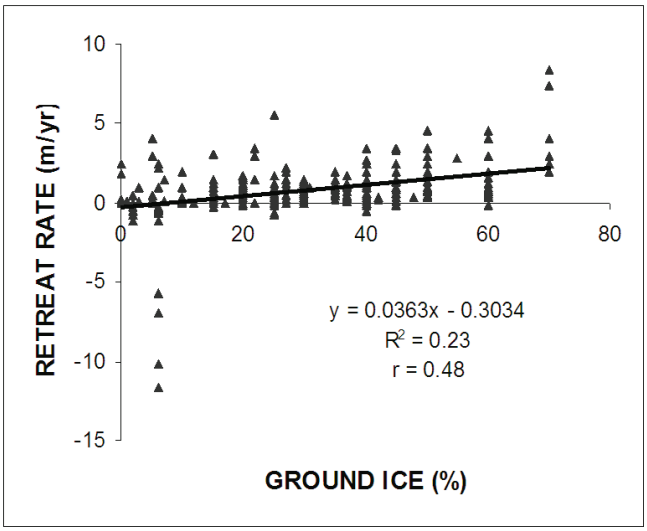


Figure 3. Retreat rate as a function of volumetric ground ice contents.

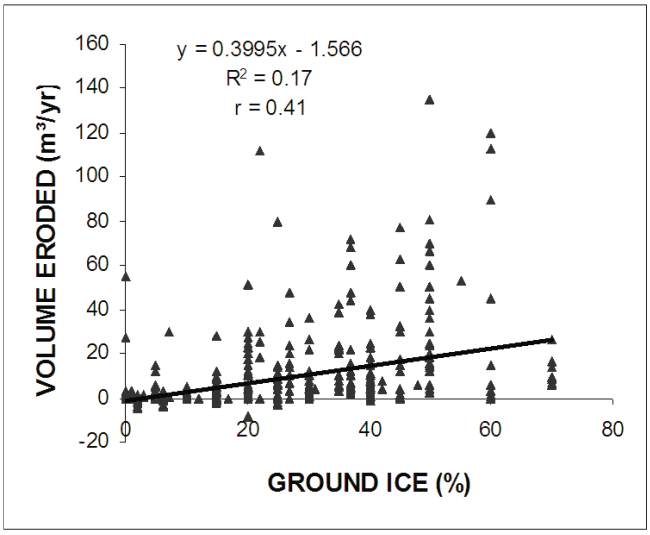


Figure 4. Volume eroded as a function of volumetric ground ice contents.

Using this criterion to consolidate the datasets we brought down the number of segments for analysis to 545. The resulting segments were remarkably ubiquitously distributed along coastal regions of the Arctic and can therefore be considered to be spatially unbiased. The Coast of the Canadian Archipelago was the only section, for which the entire coastline was not retained, due to the presence of sea ice throughout the summer season. At least 50 segments were used for each of the seven other sectors considered in the Analysis (Barents Sea, Kara Sea, Laptev Sea, East Siberian Sea, Chukchi Sea, Beaufort Sea)

We then ran two sets of analysis using retreat rates in m/yr and eroded volumes in $m^3$/yr (for a 1 m stretch of coastline). Eroded volumes were calculated by combining backshore elevations and retreat rates and constraining artificially the calculation to a 1 km stretch of coastline:

$$V = l \cdot h \cdot CRR \quad (1)$$

where $V$ is the yearly eroded volume, $h$ the backshore elevation, and $CRR$ the annual coastal retreat rate. In our calculation, we normalized all l values to 1 km to facilitate comparison of segments

## Results and Discussion

*Simple regression analyses*

The analysis of the retreat rates versus the percentages of visible ground-ice revealed a relatively weak relationship with a correlation coefficient r = 0.48 ($R^2$ = 0.23) (Fig. 3). The correlation between volumes eroded and ground ice was weaker (r = 0.41, $R^2$ = 0.17) (Fig. 4).

Both relations were statistically significant at $\alpha$=0.01. Though weak, the correlation coefficient relating ground ice contents to retreat rates is considerably greater than the coefficients published by Héquette and Barnes (1990) (Fig. 1). In contrast, the correlation coefficient relating ground ice contents to eroded volumes is lower than the one observed by Héquette and Barnes (1990).

One can logically conclude that coastal erosion in the Arctic is not uniquely related to the presence of ground ice, but that the presence of ground ice significantly influences the process. The data available in the classification doesn't include hydrodynamic forcing and a multi-regression analysis is not currently possible. It should nevertheless be conducted in the future to better assess the statistical weight of ground ice in the thermal abrasion process.

*Discussion*

The lack of a correct indicator for ground ice in the nearshore zone is a strong deterrent in attempting to establish such relationships. The complex nature of ground ice, including its temperature and cryostructure, makes it difficult to correctly statistically relate ground ice to other

variables using volumetric ice contents. One would gain from incorporating heat transfer and temperature properties for instance. For the lack of a better dataset, the relationship established using the ACD classification of Arctic coasts is probably the most detailed attempt at establishing such a relation.

These contradictory results between this paper and Héquette and Barnes (1990) can be explained by the multifaceted interaction of ground ice with coastal processes. Ground ice presence in the nearshore zone influences the course of erosion by modifying the shoreface profile (see above) when it thaws. It also provides the sediments at sea level with a transient strength which lasts until beach sediments are removed during storms and ice-rich sediments are exposed. Most importantly it induces the presence of large thermokarst processes in the subaerial part of the nearshore zone.

Thermokarst processes in the nearshore zone, such as retrogressive thaw slumps, are cyclic and their activity is intimately linked to the removal of sediment by storms. Following periods of large activity, the amount of sediment released by direct melting of ground ice by short-wave radiation influx above water accumulates at the foot of these landforms and progressively impedes the development of new slumps. This lasts until large storms occur and remove the sediment lobes, providing room for a new cycle of activity (Wolfe et al. 2001, Lantuit & Pollard 2008). The timescales at which these processes occur are comprised between $10^1$ and $10^2$ years (Lantuit & Pollard 2008) and are necessarily larger than the time spans used to calculate erosion rates or eroded volumes. Furthermore, because the cycle is strongly associated with storm activity, it is necessarily local.

This paper hypothesizes that the statistical relations extracted from the ACD classification of Arctic coasts, by their wide geographic distribution integrate this cyclic dimension better than the data from the Beaufort Sea only and should therefore be used in future applications. The two correlation coefficients obtained in this study are much closer to one another than the ones obtained by Héquette and Barnes (1990).

## Conclusion

Ground ice content and retreat rates are only weakly correlated statistically, even though the relationship is statistically significant at $\alpha = 0.01$. However, due to the presence of multiple factors acting upon the coast in the Arctic realm, one cannot exclude that ground ice is a major, if not the most important, factor affecting erosion processes. Further studies will be needed to assess the role of each factor in a single integrated framework.

The relation presented in this paper should contribute to parameterization of future empirical models of coastal erosion as the most extensive effort to relate ground ice to retreat rates.

## Acknowledgments

The authors wish to thank F. Steenhuisen, from the Arctic Centre, Groningen, The Netherlands and the members of the ACD group for their contribution to the beta version of the ACD classification of Arctic coasts. This paper is a contribution to the Fourth International Polar Year (IPY), 2007-2008.

## References

Aré, F.E. 1988. Thermal abrasion of sea coast. *Polar Geography and Geology* 12. VH. Winston & Sons, 157 pp.

Dallimore, S.R., Wolfe, S.A. & Solomon, S.M. 1996. Influence of ground ice and permafrost on coastal evolution, Richards Island, Beaufort Sea coast, N.W.T. *Canadian Journal of Earth Sciences* 33: 664-675.

Forbes, D.L. & Taylor, R.B. 1994. Ice in the shore zone and the geomorphology of cold coasts. *Progress in Physical Geography* 18: 59-89.

Héquette, A. & Barnes, P.W. 1990. Coastal retreat and shoreface profile variations in the Canadian Beaufort Sea. *Marine Geology* 91: 113-132.

Kobayashi, N., Vidrine, J.C., Nairn, R.B. & Solomon, S.M. 1999. Erosion of frozen cliffs due to storm surge on Beaufort sea coast. *Journal of coastal research* 15: 332-344.

Lantuit, H. & Pollard, W.H. 2005. Temporal stereophotogrammetric analysis of retrogressive thaw slumps on Herschel Island, Yukon Territory. *Natural. Hazards and Earth System. Sciences* 5: 413-423.

Lantuit, H. & Pollard, W.H. 2008. Fifty years of coastal erosion and retrogressive thaw slump activity on Herschel Island, southern Beaufort Sea, Yukon Territory, Canada. *Geomorphology* doi:10.1016/j.geomorph.2006.07.040.

Lantuit, H., Steenhuisen, F., Graves-Gaylord, A., Ødegård, R. & Atkinson, D. accepted. 2008. The Arctic Coastal Dynamics geospatial framework. In: W.H. Pollard, N. Couture, H. Lantuit & V. Rachold (eds.), *Arctic Coasts - Circum-Polar Processes and Dynamics*. Montréal, Canada: McGill-Queens University Press.

Mackay, J.R., 1972. Offshore permafrost and ground ice, southern Beaufort Sea, Canada. *Canadian Journal of Earth Sciences* 9: 1550-1561.

Rachold, V., Grigoriev, M.N., Are, F.E., Solomon, S., Reimnitz, E., Kassens, H. & Antonow, M. 2000. Coastal erosion vs. riverine sediment discharge in the Arctic shelf seas. *International Journal of Earth Sciences* 89: 450-460.

Rachold, V., Bolshiyanov, D.Y., Grigoriev, M.N., Hubberten, H.-W., Junker, R., Kunitsky, V.V., Merker, F., Overduin, P.P. & Schneider, W. 2007. Near-shore Arctic subsea permafrost in transition, *EOS Transaction of the American Geophysical Union* 88(13): 149-156.

Solomon, S.M. 2005. Spatial and temporal variability of shoreline change in the Beaufort-Mackenzie region, northwest territories, Canada. *Geo-Marine Letters* 25(2-3): 127-137.

Wolfe, S.A., Kotler, E. & Dallimore, S.R. 2001. *Surficial Characteristics and the Distribution of Thaw Landforms (1970 to 1999), Shingle Point to Kay Point, Yukon Territory.* Open File 4115, Geological Survey of Canada.

# The Kind and Distribution of Mid-Latitude Periglacial Features and Alpine Permafrost in Eurasia

Frank Lehmkuhl
*Department of Geography, RWTH Aachen University, Templergraben 55, D-52056 Aachen, Germany*

## Abstract

The distribution of different periglacial landforms in various mid-latitude mountains of Eurasia is described. Alpine discontinuous and continuous permafrost is present in all these mountains, but in the humid mountains, this zone is very small due to the lower elevation of the glacier snowline (or ELA). In the more continental regions of Asia, this zone is much broader due to high elevation of the ELA. In these areas cryoplanation terraces, patterned ground, and rock glaciers occur in relative low elevations and are also widespread within the forest ecotone. On the other hand, solifluction features occur in higher regions due to arid conditions and especially the lack of soil humidity during the freeze-thaw cycles. In the Verkhoyansk Mountains further north in latitude, even in the mountain foreland and in the boreal forest of the Lean-Aldan Basin, periglacial features are widespread on continuous permafrost.

**Keywords:** Central Asia; European Alps; mid-latitude; periglacial features; permafrost.

## Introduction

This paper presents a comprehensive review study concerning the kind and distribution of periglacial phenomena of mid-latitude mountains of Eurasia. New results are from continental Asia, in particular the mountain areas of Western Mongolia, the Russian Altai, and the Verkhoyansk Mountains (Fig. 1). The distribution of different periglacial landforms in these mountains is compared to the European and Japanese Alps. A first overview concerning mid-latitude periglacial landforms is given by Höllermann (1985); an overview for the high Asian mountains is given by Matsuoka (2003).

## Periglacial Landforms in Mountain Areas

Concerning periglacial phenomena in mountain environments, especially small-scale periglacial or cryogenic landforms, are studied in the literature (e.g., Washburn 1979). Active solifluction (or gelifluction) generally occurs above the timberline as the forests stabilise and protect the ground. In general, the periglacial zone can divide into two sub-belts: First, the lower periglacial sub-belt, which includes mainly bound or turf-banked solifluction (steps, benches, terraces, lobes), and second, the upper sub-belt. The latter is characterized by unbound (or free) solifluction, blockfields, debris, stone pavements, and patterned ground (Troll 1973, Höllermann 1985). This periglacial zonation is obvious in most mid-latitude mountains above the timberline and provides information on the geoecology of high mountain environments, as the distribution of these landforms depends on several different factors (e.g., topography, geology and substrate, climate, vegetation, and soil water; see Fig. 2). Periglacial phenomena are generally controlled by cold climatic conditions, where the mean annual air temperature (MAAT) as well as the duration and depth of snow cover are low. The modern altitudinal belts of the vegetation, the soils, and the geomorphological processes are controlled by these general climatic conditions, but also by the different radiation on the northern and southern slopes (Höllermann 1985). However, new results from the European Alps show that active soil movements only occur in the upper sub-belt (Veit 2002).

Besides the different small-sized landforms of solifluction rock glaciers are typical landforms of high mountain environments. Two types are distinguished: (1) ice-cemented rock glaciers built up by unconsolidated rock or talus, and (2) morainic deposits. They are generated by the creep of mountain permafrost saturated or supersaturated with ice. Ice-cored rock glaciers consist of glacier ice mantled with a debris cover and originate from dead ice (Ishikawa et al. 2001). Rock glaciers affect unconsolidated but frozen rock fragments, creating characteristic landforms with a tongue or lobate shape and a surficial pattern of furrows and ridges that indicate the internal flow process (Barsch 1996, Fort 2002, Haeberli 2000). In addition, protalus ramparts, and talus slope or talus cone rock glaciers are described in the literature (e.g., Barsch 1996).

It is generally accepted that the distribution of rock glaciers is a good marker of discontinuous mountain permafrost (e.g., Barsch 1996). However, Fort (2002) mentioned that the identification of rock glaciers in the Himalayas is similar to other features such as rockslides and/or debris covered glaciers and, therefore, it is sometimes difficult to distinguish these landforms. Rock glaciers are described in detail especially in the European Alps and in mountain regions of North America (see reference in Barsch 1996). The knowledge of the distribution of rock glaciers in the different mountain systems on Earth is still very incomplete (Barsch 1996). Nevertheless, mountains with a continental climate, and thus the greatest differences between timberline and snowline (up to 1500 m) are more favourable for rock glaciers than those with a difference of less than 500 m (Höllermann 1985, Barsch 1996).

The upper limit of the periglacial belt results from steep high mountain topography or from the extent of perennial snow and ice in the higher altitudes (glacial belt).

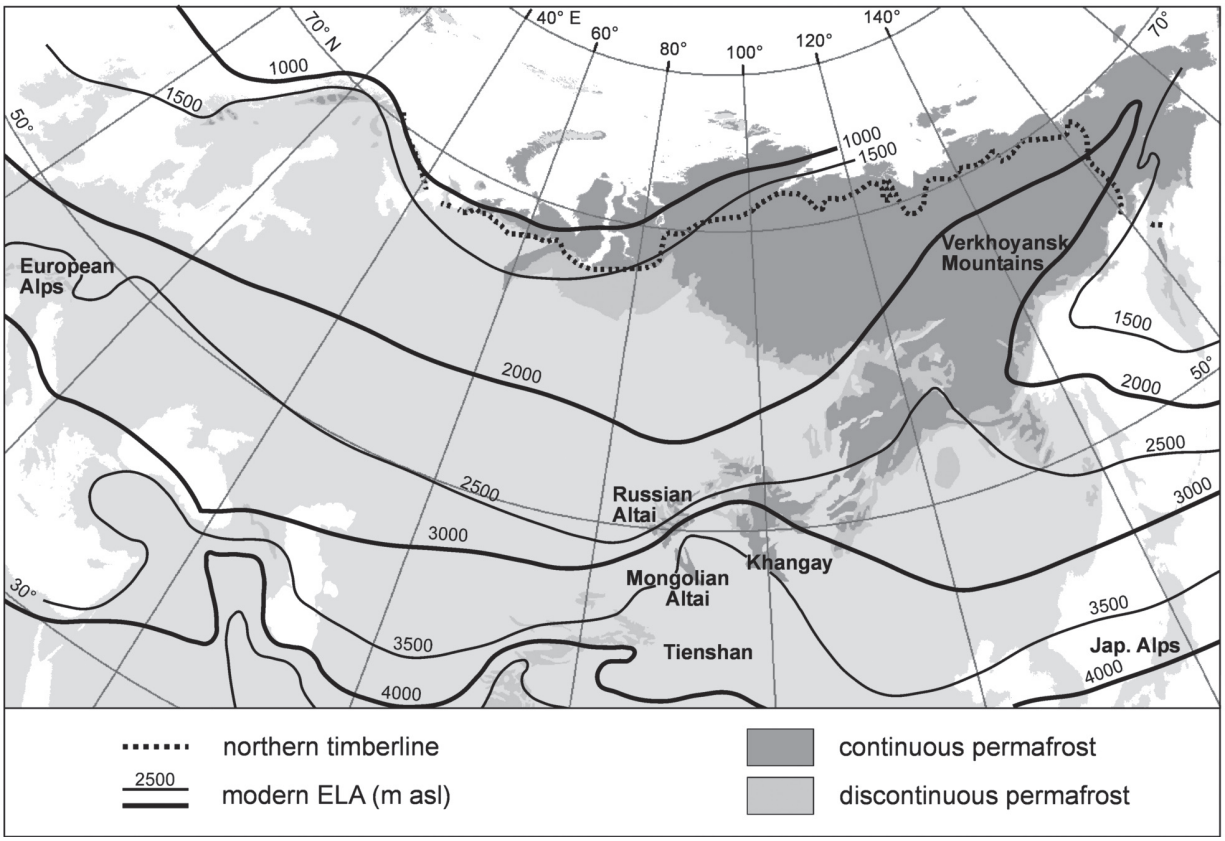


Figure 1. Map of study areas including the distribution of permafrost (modified according to Brown et al. 2001) and the modern ELA (m a.s.l., modified according to Wilhelm 1995).

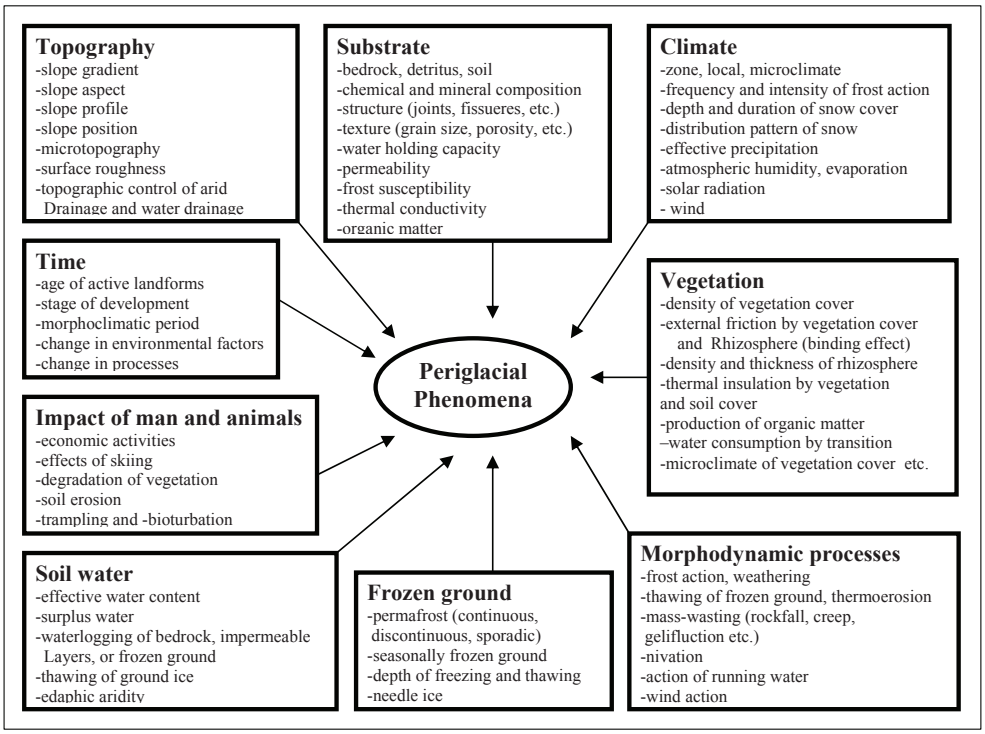


Figure 2. Main factors for the development and distribution of periglacial phenomena. Modified according to Höllermann (1985).

## Results

In the following, the distribution of periglacial phenomena, such as lower limit of solifluction and rock glaciers, are described for the different mountain areas. The details for the lower limit of different periglacial and glacial features are given in Fig. 5 and Table 1.

*European Alps*

In the European Alps there are several studies regarding the periglacial phenomena. Veit (2002) summarized the current state of research for the European Alps. The periglacial phenomena can be divided in the humid European Alps into two sub belts: the lower limit of bound or turf-banked solifluction (occurs roughly above the timberline, Fig. 3) and the zone of unbound solifluction, dominated by blockfields, patterned ground, and bare bedrock. Active rock glaciers and other indicators of discontinuous permafrost are assumed to be generally in the upper periglacial sub-belt of the European Alps and of similar mountains. Active solifluction (or gelifluction) generally occurs above the timberline (see above). However, studies concerning the processes show that active movements occurs only in the upper part of the periglacial sub-belt (unbound solifluction); the turf-banked solifluction are fossil landforms (Jaesche 1999, Veit 2002).

Figure 3. Solifluction lobe (bound or turf-banked solifluction) in the Grossglockner region, European Alps, Elevation: 2200 m a.s.l.

Figure 4. Rock glacier in the Khangay Mountains, Mongolia. Granite bedrock on the eastern slope of the Otgon Tenger. Elevation: about 3000 m a.s.l.

In this paper the results from own field work from two mountain areas with the central part of the European Alps are described (Lehmkuhl 1989). These are the southernmost glaciated areas in the western part of the Alps (Pelvoux Mountains, France, 45°N/6°30′E) and the easternmost glaciated part of the Alps (Hohe Tauern, Austria, 47°N/13°E). Both regions are situated in the central part of the Alps, having more continental climatic conditions much more suitable for rock glaciers than the more humid margin ranges of the Alps (Barsch 1986, Höllermann 1985). The mean monthly air temperature in 2000 m a.s.l. varies between -4°C in January and +12°C in July (MAAT around 0°C). Annual precipitation ranges between 900 mm in valleys and >2000 mm in the mountains.

Rock glaciers occur in 2400 to 2500 m a.s.l., turf-banked solifluction in 2350 and 2200 m a.s.l. and unbound solifluction in 2750 and 2500 m a.s.l. (see Table 1 and Fig. 5).

*Tianshan and Russian Altai*

There are only a few studies regarding periglacial features in the Russian Altai. Schröder et al. (1996) and Fickert (1998) summarized in a north-south transect the distribution of periglacial phenomena. Their results concerning Tienshan (Sailijskij-Alatau, 42°N/77°E) and the results from own observations from the central part Russian Altai (Katun Ridge, 50°N/86°E) are given in Figure 5 and Table 1. The latter region is characterized by continental conditions with mainly summer precipitation and low winter temperatures resulting in the distribution of rock glaciers down to elevations of about 1600 m a.s.l. These low elevation rock glaciers occur in the forest belt indicating the high amplitude of temperatures with winter temperatures below -20°C and relative high summer precipitation. The precipitation values above 1000 mm/a are similar to those of the central European Alps. Further references see Marchenko et al. (2007).

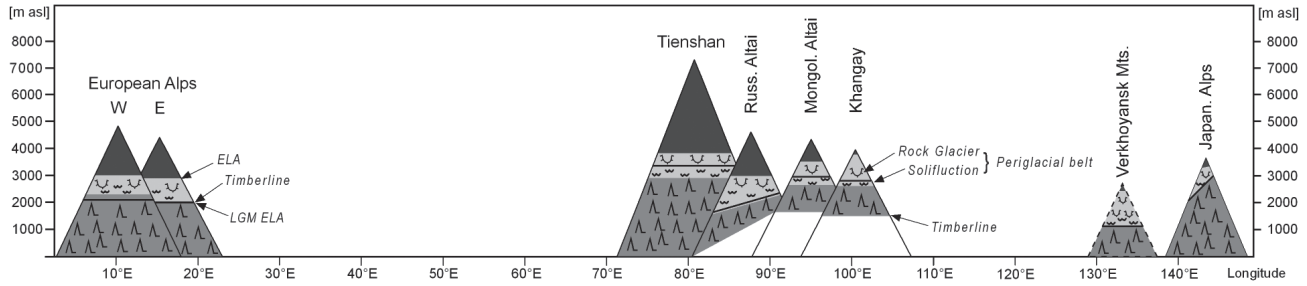


Figure 5. Periglacial belt (rock glacier and solifluction), timberline and snowline (modern ELA and Last Glacial Maximum ELA) of mid-latitude mountains from the European Alps to the Japanese Alps.

Table 1. Elevations (m a.s.l.) of snowline (ELA), timberline and selected lower limits of rock glaciers and solifluction (for the Alps: unbound solifluction in parentheses) from selected mid-latitude mountains between 40 and 50°N.

| | Western European Alps | Eastern European Alps | Tienshan | Russian Altai | Mongolian Altai | Khangay | Verkhoyansk |
|---|---|---|---|---|---|---|---|
| Modern snowline (ELA) | 3000 | 2900 | 3700-3900 | 2900-3000 | 3500 | >3800 | 2500 |
| Timberline | 2300 | 2050 | 2900 (N) | 2200-2400 | 2600–2700 (N) | 2600 (N) | 1100 |
| Late Pleistocene ELA | ca. 2100 | ca. 2000 | 2700? | 1800-2200 | 2900–3000 | 2700-2900 | 1200 |
| Pleistocene ELA-depression | ca. 1200 | ca. 1100 | 1000? | 800–1200 | 600 | 1000-1200 | 1300 |
| Diff. Timberline-ELA | 700 | 750 | 800 | 700 | 800–900 | >1200 | 1400 |
| Rock glaciers | 2400 | 2500 | 2900 | 1600 | 2600 | 3200 | -- |
| Solifluction | 2350 (2750) | 2200 (2500) | 2600 | 2200 | 2700 | 2900 | 800 |

*Mongolian Altai and Khangay*

Due to the low winter temperatures and the small amount of snow, frost weathering occurs in the mountains of Mongolia down to the basins below 900 m a.s.l. Other periglacial phenomena, such as solifluction, palsas, and earth hummocks are related to soil moisture, and therefore occur in higher elevations or exceptional geoecological sites with a higher water supply; for example, on north-facing slopes below larch forest spots. However, the distribution of rock glaciers in the continental climate conditions of western Mongolia is determinate on low temperatures, and mainly on the occurrence of granite and metamorphic rocks (Fig. 4). The detailed observations concerning the distribution of periglacial landforms and processes are based on several joint field expeditions and studies of the processes (Lehmkuhl 1999). Detailed investigations from the Mongolian Altai and Khangay are presented, for example, by Klimek & Starkel (1980), Pekala & Repelewska-Pekalowa (1993), Lombroinchen (1998), Lehmkuhl & Klinge (2000), Klinge (2001), Lehmkuhl et al. (2003) and Sharkhuu (2003). Further references can be found therein.

Hourly measurements of the soil temperatures of different depths at distinct geoecological sites in elevations between 1775 and 2760 m a.s.l. were carried out in two measuring cycles (Lehmkuhl & Klinge 2000). The main difference in the intensity of periglacial processes in the basins and mountains areas, respectively, can be seen in the freeze-thaw cycles in springtime. In this time the precipitation in the mountains is still snowfall, and moisture can infiltrate into the soils. Due to higher temperatures the precipitation (mainly rain) in the basins evaporates and rapid drying out of the soils occurs. Therefore, the main controlling factor for the cryogenic and especially solifluction processes in the mountains is the amount of precipitation during springtime. The freeze-thaw cycles during the relatively dry autumn season are a subordinated factor for the periglacial activity. At sites with low radiation, as caused for example, through shading effects in relief, the freeze-thaw cycles displace towards the summer with more precipitation. Therefore, periglacial processes on low-radiation sites are laced to the strength of the summer precipitation. On the other hand, the frequent freeze-thaw cycles at sites with high radiation drop towards the dry winter season, and therefore, the periglacial activity is low at such sites. Accumulation of snow (e.g., in nivation hollows) and/or the occurrence of frozen ground could guarantee sufficient soil humidity apart from the distribution of precipitation during the highest freeze-thaw cycles in the spring and autumn seasons and determines cryogenic processes and periglacial forms (e.g., earth hummocks, patterned grounds). This local influence can be reinforced by effects of radiation. In the larch forests at northern slopes, a cooler local climate with reduced transpiration in the summer allows the preservation of frozen ground and/or permafrost.

The details presented for this paper (Table 1) are based on two mountains ranges: (1) the Turgen-Kharkhiraa Mountains (49°30′N/91°E) as the northernmost part of the Mongolian Altai and (2) the Angarkhoy Mountains (47°N/101°E) as the central part of the Khangay. Mean monthly air temperature varies between -20°C in January and +20°C in July. The MAAT is, for example, about -4°C in the basin of the Uvs Nuur. Annual precipitation ranges between 200 mm in the basins and up to >400 mm in the mountain ranges. Solifluction and rock glaciers occur in elevations above 2600 m. Initial observations from other parts of the Mongolian Altai and the western Russian Altai show that such landforms can be found in almost every mountain system which comprise granite or other metamorphic rocks.

*Verkhoyansk Mountains*

The Verkhoyansk Mountains are much further north in latitude, and the climate is extremely continental. Mean monthly air temperature varies between -40°C in January and +20°C in July. Annual precipitation ranges between 220 mm in the lowlands around Yakutsk and up to 700 mm on the western flank of the Verkhoyansk Mountains. The observations presented in this paper focused on the central part of the Verkhoyansk Mountain range (64–65°N, 126–130°E) and based on fieldwork and remote sensing analysis (Stauch 2006, Stauch et al. 2007). Permafrost features such

as pingos and thermokarst depressions and lakes (alases) are widespread on continuous permafrost even in the mountain foreland and in the boreal forest of the Lean-Aldan Basin. However, solifluction, nivation, and cryoplanation terraces can be found in elevations above 800 m a.s.l. only. No rock glaciers can be found in this study area.

*Japanese Alps*

Studies concerning mountain permafrost in Japan are summarised in Ishikawa et al. (2003). Mountain permafrost seems to be restricted mainly to north-facing slopes above 3000 m a.s.l. and in some rock glaciers. Matsuoka (2003) presents some more details concerning other periglacial features.

The details presented for this paper (Table 1) based also on own observations and discussions during an excursion led by Y. Ono in 2001 in the central Japanese Alps. MAAT in 2600 m a.s.l. is about 0°C, mean temperature in January and July were estimated to be -11.3 and +12.6°C, respectively. Annual precipitation is rather high (no data published) and northwestly wind across the Japan Sea provides a large amount of snow on the northern and eastern ranges in winter, the Pacific part of the mountains is much drier (Ishikawa et al. 2003).

Solifluction and rock glaciers occur in elevations above 2600 m a.s.l.; there are no modern glaciers in this part of the Japanese Alps.

## Conclusion

As stated above, the distribution of various periglacial landforms depends on several different factors (e.g., climate, topography, geology and substrate, vegetation, and soil water; see Fig. 2). Periglacial phenomena are generally controlled by cold climatic conditions, where the mean annual air temperature is below 0°C and the duration and depth of snow cover are low.

The distribution of the periglacial belt in Eurasia at 40 to 50°N is given in the schematic profile in Fig. 6. All altitudinal lines are drawn relatively to the timberline as base level. Alpine discontinuous and continuous permafrost is present in all these mountains, but in the humid this zone is very small due to the lower elevation of the snowline (or recent equilibrium line of glaciers = ELA). In the more continental regions of Asia, like the Altai Mountains, this zone is much broader due to high elevation of the ELA. In addition, cryoplanation terraces, patterned ground, and rock glaciers occur in relative low elevations and are also widespread within the forest ecotone (Table 1).

The Verkhoyansk Mountains are further north in latitude and much drier. In this region, even the mountain foreland and in the boreal forest, permafrost activity and pingos are widespread. However, periglacial features, especially solifluction, occur only in mountain ranges above 800 m a.s.l. There are no active rock glaciers, as the humidity is not sufficient. These results fit recent observations in 2007 in the Gobi Altai, a mountain range within the driest part

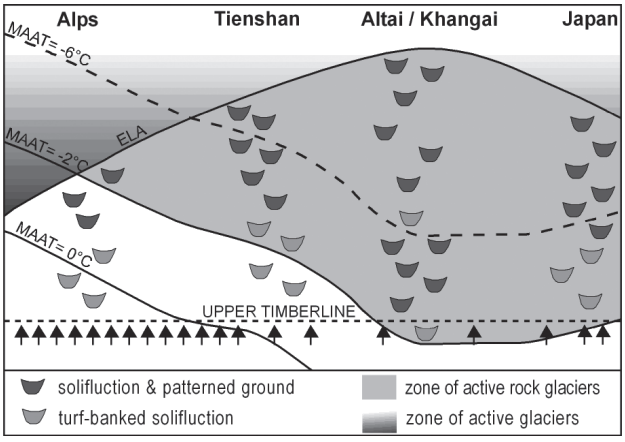


Figure 6. Schematic profile of the periglacial belt in Eurasia at 40 –50°N. All altitudinal lines are drawn relatively to the timberline as base level. Modified according to Höllermann (1985).

of Mongolia, where a few rock glaciers occur only in the highest and more humid parts of the Ikh Bogd Mountain above 3500 m a.s.l. (44°57′N, 100°18′E).

The Japanese Alps are more humid, and especially the thick winter snow cover reduced periglacial activity and permafrost distribution, including rock glaciers, toward a small zone in the highest mountain areas.

These results show that periglacial phenomena occur in the continental part of Asia even in the forest zone. Especially solifluction, but also rock glaciers, are determined through existence of soil humidity during the freeze-thaw cycles. Therefore the distribution of these features in the continental areas of Asia is smaller than in the humid European and Japanese Alps and, for example, restricted to northern slopes or higher elevations. Observations and soil temperature measurements in the Altai Mountains show that active rock glaciers and discontinuous permafrost occur in lower elevations than solifluction features. Thus, solifluction landforms in continental Asia depend more on moisture supply than rock glaciers. However, towards the arid regions of Central Asia, the lower limit of solifluction landforms, glaciers, and the lower timberline are rising in general; whereas the distribution of rock glaciers is even lower than in the humid parts of Europe and Pacific parts of Asia including Japan.

The modern ELA has the lowest position in the humid European Alps. The most significant difference between the timberline and the modern ELA occurs in the Khangay and Verkhoyansk Mountains. (Fig. 5, Table 1). The smallest amount of Pleistocene ELA-depression is in the arid regions of the Altai. However, the distribution of glaciers is related to temperature and moisture supply. The generalised contour lines of the modern ELA in Figure 1 show the influence of the humid mountains of the Altai and the dry part of eastern Siberia on the elevation of the snowline. As the northern timberline is related to summer temperatures and the humidity is even sufficient in the continual parts of Asia, this line shows a west–east latitudinal trend.

## Acknowledgments

The fieldwork in Asia was funded by the Deutsche Forschungsgemeinschaft (DFG, LE 730/2-1,2; 7-1; 10-1,2). For help during fieldwork and several discussions, the author would like to thank especially Dr. O. Batkhishig, Mongolian Academy of Sciences, and Dr. N. Lachinski from the Siberian Botanical Garden, Russian Academy of Sciences, and the other Mongolian and Russian colleagues and co-workers. In addition, I would like to thank G. Stauch (Aachen) for discussions.

## References

Barsch, D. 1996. *Rock Glaciers: Indicators for the Present and Former Geoecology in High Mountain Environments*. Berlin: Springer, 331 pp.

Brown, J., Ferrians, O.J., Heginbottom, J.A. & Melnikov, E.S. 2001. *Circum-arctic map of permafrost and ground ice conditions*. National Snow and Ice Data Center/World Data Center for Glaciology, Boulder, Colorado.

Fickert, T. 1998. Vergleichende Beobachtungen zu Solifluktions- und Frostmustererscheinungen im Westteil Hochasiens. *Erlanger Geogr. Arb.* 60: 1-150.

Fort, M. 2002. Are high altitude, lava stream-like, debris mixtures all rock glaciers? A perspective from the western Himalaya. *Z. f. Geomorph. N.F.,* Suppl. 130: 11-29.

Haeberli, W. 2000. Modern research perspectives relating to permafrost creep and rock glaciers: a discussion. *Permafrost and Periglacial Processes* 11: 290-293.

Höllermann, P. 1985. The periglacial belt of mid-latitude mountains from a geoecological point of view. *Erdkunde* 39: 259-270.

Ishikawa, M., Fukai, K., Aoyama, M., Ikeda, A., Sawada, Y. & Matsuoka, N. 2003. Mountain permafrost in Japan: distribution, landforms and thermal regime. *Z. f. Geomorph. N.F.,* Suppl. 130: 99-116.

Ishikawa, M., Watanabe, T. & Nakamura, N. 2001. Genetic differences of rock glaciers and the discontinuous mountain permafrost zone in Kanchanjunga Himal, Eastern Nepal. *Permafrost and Periglacial Processes* 12: 243-253.

Jaesche, P. 1999. Bodenfrost und Solifluktionsdynamik in einem alpinen Periglazialgebiet (Hohe Tauern, Osttirol). *Bayreuther Geowis. Arb.* 20: 1-136.

Klimek, K. & Starkel, L. (eds.) 1980. Vertical zonality in the Southern Khangai Mountains (Mongolia). Results of the Polish-Mongolian physico-geographical expedition, Vol. I. *Geographical Studies* 136: 1-107.

Klinge, M. 2001. Glazialgeomorphologische Untersuchungen im Mongolischen Altai als Beitrag zur jungquartären Landschafts- und Klimageschichte der Westmongolei. *Aachener Geogr. Arb.* 35: 1-125.

Lehmkuhl, F. 1989. Geomorphologische Höhenstufen in den Alpen unter besonderer Berücksichtigung des nivalen Formenschatzes. *Göttinger Geogr. Abh.* 88: 1-113.

Lehmkuhl, F. 1999. Rezente und jungpleistozäne Formungs- und Prozeßregionen im Turgen-Charchira, Mongolischer Altai. *Die Erde* 130: 151-172.

Lehmkuhl, F. & Klinge, M. 2000. Bodentemperaturmessungen aus dem Mongolischen Altai als Indikatoren für periglaziale Geomorphodynamik in hochkontinentalen Gebirgsräumen. *Z. f. Geomorph. N.F.,* Suppl. 44: 75-102.

Lehmkuhl, F., Stauch, G. & Batkhishig, O. 2003. Rock glacier and periglacial processes in the Mongolian Altai. *Proceeding of the Eighth International Conference on Permafrost, Zurich, Switzerland, July 21–25, 2003*: 639-644.

Lombroinchen, R. 1998. Short communication: periglacial processes and physical (frost) weathering in Northern Mongolia. *Permafrost and Periglacial Processes* 9: 185-189.

Marchenko, S.S., Gorbunov, A.P. & Romanovsky, V.E. 2007. Permafrost warming in the Tien Shan Mountains, Central Asia. *Proceeding of the Eighth International Conference on Permafrost, Zurich, Switzerland, July 21–25, 2003*: 311-327.

Matsuoka, N. 2003. Contemporary permafrost and periglaciation in Asian high mountains: an overview. *Z. f. Geomorph. N.F.,* Suppl. 130: 145-166.

Pekala, K. & Repelewska-Pekalowa, J. 1993. Solifluction and related slope processes in the mountains of Central Asia (Mongolia). *Paläoklimaforschung/ Palaeoclimate Research* 11: 87-101.

Schröder, H., Gunia, A. & Fickert, T. 1996. Vergleichende Periglazialmorphologie im zentralen Teil des nördlichen Tien-Shan. *Mitt. der Fränkischen Geogr. Ges.* 43: 275-300.

Serebryanny, L.R. & Gravis, G.F. 1993. Solifluction in northern Eurasia: a review. *Paläoklimaforschung/ Palaeoclimate Research* 11: 103-382.

Sharkhuu, N. 2003. Recent changes in the permafrost of Mongolia. *Proceeding of the Eighth International Conference on Permafrost, Zurich, Switzerland, July 21–25, 2003*: 1029-1034.

Stauch, G. 2006. Jungquartäre Landschaftsentwicklung im Werchojansker Gebirge, Nordost Sibirien. *Aachener Geogr. Arb.* 45: 1-176.

Stauch, G., Lehmkuhl, F. & Frechen, M. 2007. Luminescence chronology from the Verkhoyansk Mountians (North-Eastern Siberia). *Quaternary Geochronology* 2: 255-259.

Troll, C. 1973. High mountain belts between the polar caps and their definition and lower limit. *Arctic and Alpine Research* 3: A19-A27.

Veit, H. 2002. *Die Alpen – Geoökologie und Landschaftsentwicklung.* Stuttgart: Eugen Ulmer, 352 pp.

Washburn, A.L. 1979. *Geocryology.* London: Edward Arnold, 406 pp.

Wilhelm, F. 1995. *Schnee- und Gletscherkunde.* Berlin, New York: Walter de Gruyter, 434 pp.

# Coastal Processes at the Tabular-Ground-Ice-Bearing Area, Yugorsky Peninsula, Russia

Marina Leibman
*Earth Cryosphere Institute SB RAS, Tyumen, Russia*
Anatoly Gubarkov
*Tyumen State Oil and GAS University, Tyumen, Russia*
Artem Khomutov
*Earth Cryosphere Institute SB RAS, Tyumen, Russia*
Alexandr Kizyakov
*Institute VNIIIST, Moscow, Russia*
Boris Vanshtein
*FGUP Vniiokeangeologia, St-Petersburg, Russia*

## Abstract

Observations on Yugorsky Peninsula since 1998 cover periods with changing climatic controls of coastal processes. Coastal dynamics are connected to the activation of thermal denudation, the most widespread process in the area with tabular ground ice enclosed in geological sequences. Thermodenudation comprises cryogenic landslides, slumps, and earth flows resulting from tabular ground ice thaw. Thermoabrasion is a less common mechanism of coastal retreat in the study area. The dominating mechanism allows subdivision of coasts into thermodenudation, thermoabrasion, and mixed types. Coast types are time-dependent, and alternation of types depends on climate fluctuations. For the bluffs with tabular ground ice exposures, the increase of sediment yield onto the beach is determined on the one hand, by a relative amount of tabular ice in a section, and on the other, by increase in the thaw index. Activation of thermoabrasion depends on sea ice coverage along with wind speed and direction. Activation of thermoerosion results from heavy winter precipitation followed by a bursting spring.

**Keywords:** climatic controls; coastal dynamics; earth flows; thermoabrasion; thermodenudation; thermoerosion.

## Introduction

Observations on Yugorsky Peninsula since 1998 cover the basic climatic controls of various coastal processes in the study area (Kizyakov et al. 2006): periods with changing summer temperature, ice coverage of the Kara Sea, amount of summer and winter precipitation, wind speed and direction, and wave action.

Coastal dynamics result from the activation of thermal denudation, the most widespread process in the area with tabular ground ice enclosed in geological sequences. The importance of the massive (tabular) ground ice occurrence as a major factor in coastal retreat is recognized in the literature (Lantuit & Pollard 2003, Solomon 2003, Lantuit et al. 2005, Kizyakov et al. 2006). Thermal denudation comprises cryogenic landslide/slump/earth flow processes, resulting from tabular ground ice thaw and removal of meltwater and waste material onto the beach and into the sea by gravitation (Leibman & Kizyakov 2007). Depending on climate fluctuations, coastal dynamics result from alternating or coinciding cryogenic landslide/slump/earth flow, thermoabrasion, and thermoerosion mechanisms. According to the dominating mechanism, coasts are subdivided into thermodenudation, thermoabrasion and mixed types (Sovershaev 1992, Kizyakov et al. 2003). Coasts are affected by nivation, earth falls, and aeolian processes as well, though they play subordinate roles.

Thermodenudation assumes special features in the tabular ground ice areas. These features are the formation of specific thermodenudation landforms such as thermocirques and thermoterraces, resulting from the tabular ground ice thaw and slope mass waste. The rate of coastal retreat at the backwalls of these forms is much higher than the coastal retreat rate at the adjacent portions of the coastal bluffs (Kizyakov et al. 2006).

This paper deals with coastal dynamics at the Yugorsky Peninsula coast. Field observations and monitoring reveal the main mechanisms which determine coastal types and destruction rates.

## Study Area, Terms, and Methods

The study area, Yugorsky Peninsula at the southern coast of the Kara Sea (Fig. 1), is located on the Pai-Khoi Mountain range piedmont, a relief of rolling hills being affected by thermokarst and various slope and coastal processes. According to the records of the Amderma weather station, mean annual (summer) temperature for the period of observation ranged from -5.8 to -7.7°C (5.0–6.7°C); summer wind speed may exceed 20 m/sec, mainly in a southwestern direction; and the perennial average of annual/summer precipitation is rather low: 314/148 mm.

The area is characterized by continuous permafrost

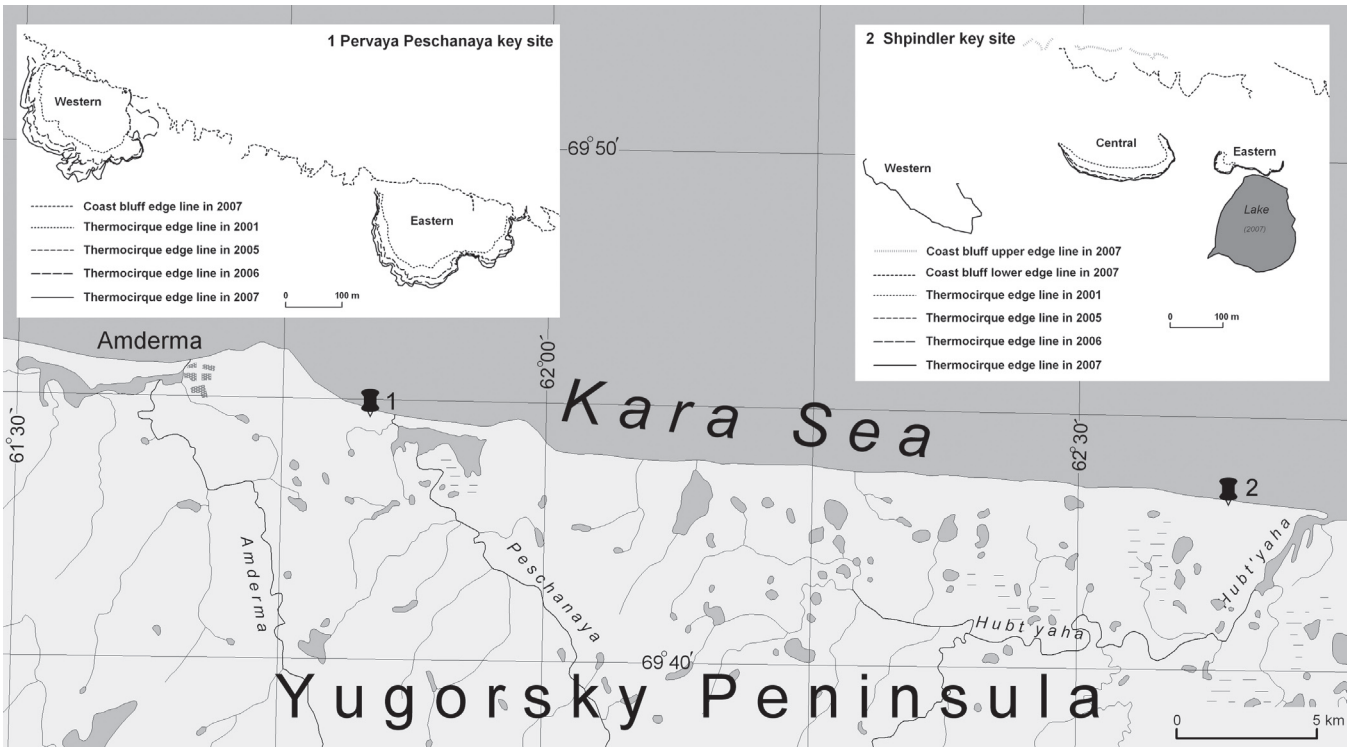


Figure 1. Yugorsky Peninsula. Pervaya Peschanaya (1, left inset map), and Shpindler (2, right inset map) key sites. Thermocirque configuration as well as annual coastlines are shown on inset maps.

distribution with ground temperature as low as -5°C, up to 400 m thickness, with an active-layer depth maximum exceeding 1.5 m, with average around 1 m, and widespread tabular ground ice in layers of 3–12 m thick enclosed in sandy-clayey deposits of glacial (?), marine, fluvial, Aeolian, and slope-wash genesis (Manley et al. 2001, Leibman et al. 2003). Two key sites are under study: Shpindler site is located west of the Hubt'Yakha River at the easternmost end of the coastal zone under study. The westernmost end is Pervaya Peschanaya site, west of the Pervaya Peschanaya River. At both key sites several thermocirques are mapped, four of which are monitored: the western and eastern thermocirques of Pervaya Peschanaya site, and the eastern and central thermocirques of Shpindler site (Fig. 1, inset maps). The coastal zone between these two key sites was described and the thermocirque/bluff edge position measured during a foot and boat trip along the coast.

The methods applied were as follows: A network of transects perpendicular to the edge of most actively retreating thermocirques and flat coastal bluffs was established. Repeated accurate tacheometric surveys were used to create a digital model of thermocirque relief at several time slices so that coastal dynamics were characterized not only in one dimension as a shoreline retreat, but also in two and three dimensions, as area and volume losses. The area loss allows better determination of the average retreat for an edge of complicated configuration, while volumetric loss allows calculation of the volume of material transported onto the beach during the period between two survey dates (Kizyakov et al. 2006).

Retreat measurements were performed in July and August. To better understand climate controls, retreat rates and thaw index were calculated for the entire period between measurements and thus include the warm period of the preceding and following year, not of a calendar warm period.

A tacheometric survey was implemented in 2001, 2003, 2005, and 2006. In the intermediate years, a GPS survey was used to measure the shoreline position and to extend transects farther inland after stakes closer to the edge were lost through the retreat. GPS is of less accuracy compared to tacheometry, but it is still within 1 m, due to repeated measurements in a closed loop.

In Russian literature, different terms are used for coastal and lateral thermoerosion, which make coastal mechanisms easier to understand; in this paper we will use the term *thermoabrasion* for coastal thermoerosion which is the formation of wave-cut niches followed by earth falls resulting in coastal bluff retreat. The term *thermoerosion* will be used to indicate only lateral thermoerosion (linear or ravine thermoerosion produced by running water/mud flows).

A substantial portion of the coast is represented by thermocirques and thermoterraces. Mechanisms of their formation are revealed by A. Kizyakov as depending on the localization of the initial thaw. Thermocirques are formed when the tabular ground ice body gets exposed by thermodenudation inland, and waste material is transported to the shore by local streams. While thermoterraces are formed by ice exposures directly on the bluff planes facing the sea; retrogressive thaw slumps and earth flows deliver waste material directly onto the beach (Fig. 2).

Thermodenudation landforms at the coasts are step-

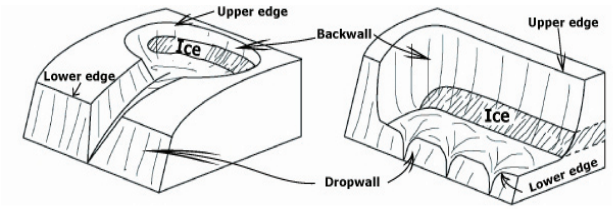


Figure 2. Thermocirque (left) and thermoterrace (right) landforms.

shaped with two retreating planes and respective edges: a thermocirque/thermoterrace backwall (retreating "upper" edge) and a dropwall to the beach (retreating "lower" edge) (Fig. 2).

## Results

Table 1 shows the retreat rate in relation to air temperature fluctuations. As instrumental measurements of coastal retreat were performed in mid-summer, long before the coastal processes "winter sleep," we applied a special procedure to make interannual data comparable: thaw index is calculated as a sum of positive temperatures of the preceding year, starting immediately after the date of measurement, plus a sum of positive temperatures of the next year up to the date of measurement. If a period between measurements was more than a year, both total sum and annual average are calculated. The length of the period with positive temperatures is highly variable and depends, along with climate fluctuations, on field logistics. For this reason, we are using a diurnal "thaw index" as a measure of air temperature impact on retreat rate.

Calculations indicate that maximum retreat rate depends directly on degree-days. Each period of measurements is characterized by about 0.8–0.9 cm of retreat per one degree-day of summer temperature.

According to our observations, in 1998–2005, the lower edge retreat was minimal. A boat trip along the coastline did not show any niches or failures, except for several thermocirques. This was most likely related to rather high sea ice coverage till late summer in 1998–1999, and moderate wind speed in 1998–2005. A summer 2003 trip indicated an increase in the number and size of thermocirques and thermoterraces, mainly due to a warm summer (Kizyakov et al. 2003, 2004). But climatic events of spring–summer 2006 changed the rate of the process, especially in the dropwall along the entire 43 km of shoreline observed. That year was marked by extreme wind speed with direction toward the coast, with northern winds prevailing in frequency and speed (Leibman et al. 2006).

In 2007, winter was snowier and spring was cooler than usual. Snow patches covered a significant portion of coastal bluffs preventing wave action. At the same time, snow patches provided active thermoerosion by meltwater. This was made possible by a bursting spring with June–July diurnal temperature some days as high as 24°C. That high temperature stayed only for a few days; the rest of the days the air temperature was below 10°C, thus most snow patches were preserved, but meltwater was abundant. Thermoerosion activated retrogressive thaw slumps and earth flows with mud streams running over snow patches directly onto the beach. Thus processes of coastal destruction proceeded by the alternation of thermodenudation in 2000–2005, thermoabrasion in 2006, and joint thermoerosion and thermodenudation in 2007.

Table 1. Shpindler monitoring key site, Yugorsky Peninsula, Russia. Central thermocirque backwall retreat in relation to thaw index.

| Period | Average* backwall retreat, m | Days between measurement | Warm period** | Thaw index total/ diurnal degree-days |
|---|---|---|---|---|
| 16.09.2001 10.08.2002 | 1.6 | 328 | 77 | 398.4/5.2 |
| 11.08.2002 22.08.2003 | 4.2 | 377 | 122 | 755.2/6.2 |
| 23.08.2003 05.08.2005 | 7.65 (3.83) | 714 | 252 | 1401.9/5.6 |
| 06.08.2005 28.07.2006 | 3.74 | 358 | 120 | 839.3/7 |
| 29.07.2006 15.07.2007 | 1.25 | 353 | 93 | 502.4/5.4 |

*Calculated as average from retreat measured along the fixed transects, in parentheses annual value if period exceeds 1 year.
**Calculated for the period between measurements including preceding and following year's warm period.

Table 2. Retreat rate of the thermocirque's upper edge at key sites "Shpindler" and "Pervaya Peschanaya," Yugorsky Peninsula in 2001–2007.

| Thermocirque | Average linear retreat, m* | | |
|---|---|---|---|
| | 2001–2005/annual | | 2006–2007 |
| Shpindler, Central | 14/3.5 | 4 | 1.25 |
| Shpindler, Eastern | 4/1 | 1 | 0.48 |
| Pervaya Peschanaya, Eastern | 14/3.5 | 5 | 3.00 |
| Pervaya Peschanaya, Western | 18/4.5 | 10 | 3.83 |

*Calculated as retreat area divided by a bluff edge length in 2001

Table 2 presents the average annual retreat at all 4 key thermocirques for various periods of measurement.

Analysis of Table 2 indicates that the maximum annual retreat rate of the backwall was observed in 2005–2006 when the thaw index was maximum. Thermocirques at Pervaya Peschanaya site show a higher retreat rate compared to Shpindler site. Though the thaw index reduces in 2006–2007, retreat at Pervaya Peschanaya site is rather essential (almost 4 m average). Extremes of 2005–2006 were not only due to the high summer temperature (see Table 1, thaw index per day), but also because of strong wave uprush (Leibman et al. 2006). The lower edge started retreating fast, niches were formed, earth falls occurred, and ice exposures appeared at formerly stable slopes (Fig. 3).

Figure 3. The wave uprush in 2006 caused thermoabrasion and exposed tabular ground ice at the base of the coastal bluff, Yugorsky Peninsula, Kara Sea coast.

Figure 4. Snow patches in 2007 protect coastal bluffs from thermoabrasion at Yugorsky Peninsula, Kara Sea coast.

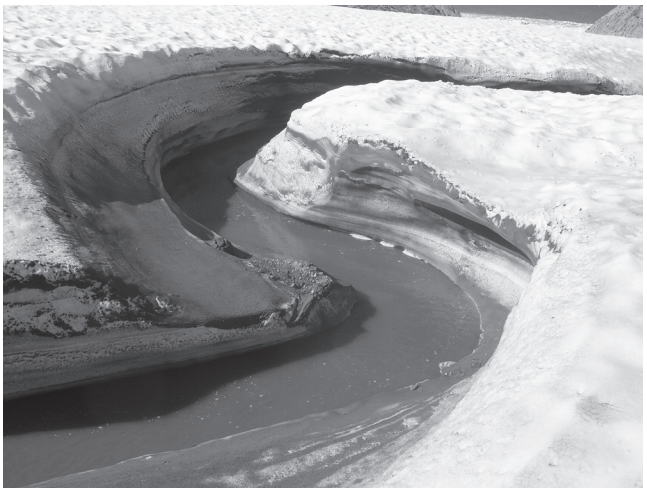

Figure 5. Snow patches filling coastal thermocirque bottoms in 2007 cut through by the meltwater streams bearing and transporting sediment load towards the beach at Yugorsky Peninsula, Kara Sea coast.

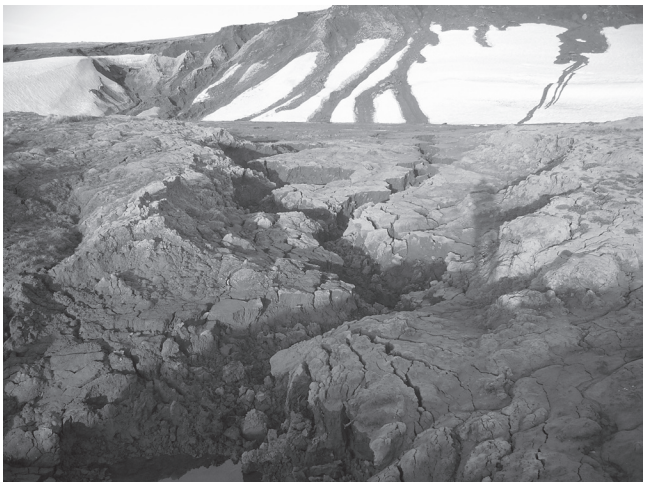

Figure 6. Snow patches in 2007 provide domination of mudflows and thermoerosion in destruction of coastal bluffs at Yugorsky Peninsula, Kara Sea coast.

Summer of 2007 was very different compared to 2001–2006. Snow patches covered most of the coastal bluffs (about 50% of the shoreline) protecting them from thermoabrasion (Fig. 4).

The high retreat rate at Pervaya Peschanaya in summer 2006–2007 is explained by both extreme wave action of fall 2006 and the increased effect of thermoerosion through the meltwater from snow patches in spring 2007 (Fig. 5). Also, nivation promotes retrogressive thaw slump/earth flow activity. Earth flows cut the surface of snow patches (Fig. 6) or run over the snow surface onto the beach. Thus, in 2007 landslides/slumps/earth flows and thermoerosion canals, promoted by snowmelt and nivation, dominate in coastal destruction mechanisms. Calculations show that a 2-week snowmelt period due to thermoerosion, transports as much sediment downslope as earth flow/slump activity during the entire warm period of any previous year.

While thermoerosion provides more intensive sediment transport compared to earth flows and retrogressive thaw slumps, thermoabrasion is quite a sparse and sporadic process at Yugorsky coast, though with an extensive mass waste due to earth falls (Fig. 7).

The rates of coastal retreat for thermocirque edges may be 2–5 times higher than thermoabrasion retreat rates. Sediment transport through a narrow (10–30 m) exit from thermocirque onto a beach is equal to the sediment yield from 500–1000 m portion of a flat-bluff coast (Kizyakov et al. 2006).

## Discussion

Observations in the key area with tabular ground ice occurrence show results close to those obtained in the Canadian Arctic by Lantuit & Pollard (2003), Lantuit et al. (2005), and Solomon (2003): tabular ground ice through thermodenudation (retrogressive thaw slumps) essentially increases the rate of coastal retreat, not only in the area of their direct occurrence, as in our study, but in the nearest vicinity (Lantuit & Pollard 2003).

The long-term retreat rate calculated from analysis of remote-sensing data at the Yugorsky coast (Kizyakov et al.

2006) was close to that obtained for various arctic areas and is around 1 m/yr for the period 1948–2001. Rather similar areas of the Canadian Arctic, as mentioned above, show a retreat rate of 1.03 m/yr in 1970–2000 (Lantuit et al. 2005). Though records averaged for a long period (53 years for Yugorsky Peninsula after Kizyakov et al. 2006, and 30 years after Lantuit et al. 2005) show a relatively low retreat rate, annual data at the coasts with tabular ground ice and respective retrogressive thaw slumps (thermal denudation in Russian terminology) display much higher rates. The highest rates are not directly connected to immediate climate warming. Lewkowizc (1987) reported retreat rates for slumpy slopes on Banks Island at 8.6–11.4 m/yr in average with a maximum 15.5 m/yr in 1983–1984. Lantuit & Pollard (2003) noted that the retreat rate was much higher in 2000–2001 (average 7.6 m) and even higher in 2001–2004 (9.6 m/yr).

These data correlate with our observations of increased retreat rates in the 2000s (up to 10 m/yr average, Table 2), exceeding a 55-year average by an order of magnitude. An order of magnitude difference between perennial average retreat rate and seasonal rates at the years of process activation shows that coastal retreat is of a cyclic character, and after several years of thermodenudation activity (12–15 years as in Lewkowicz 1987), a period of recession follows, compensating high rates of coastal destruction on the long-term scale.

High retreat rates result from tabular ground ice representing an essential part of the geological section. At Yugorsky Peninsula this part may be as high as 30–35% of the section as at the Central thermocirque of Shpindler site (Leibman et al. 2003).

As retreat rates appear to depend essentially on the tabular ground ice amount, it is critical to subdivide coastal types based on the existing exposures. At the coast under study, there are one or two ice layers depending on the marine terrace origin, age, and height. At the high terraces (35 to 45 m above sea level) two ice layers are exposed, the upper being 8–12 m thick at depths 15–25 m from the hilltop surface.

The lower ice layer dips westward, with the lower limit from 5–10 m above sea level at the Shpindler key site, and to below sea level at the Pervaya Peschanaya key site. The lower ice layer is found at practically all the terraces, both low and high ones. Flat coastal bluffs separating areas with tabular ground ice exposures may contain ground ice as well, only well insulated by thick scree deposits separating the ice surface from seasonal thaw even in warm years. But of course it should be taken into consideration that these areas are potential resources for activation of coastal destruction in a case of considerable climate warming. One more way to trigger the ice thaw is active thermoabrasion at the now stable flat bluffs.

A two-layer ice distribution pattern produces a specific shape of the coastal profile. The sea-facing macro-slope may consist of several steps with hanging thermocirque/thermoterrace bottoms formed by the thawed upper ice layer, and lower steps based on the toe of the lower ice layer. Only in the case of ice occurrence below sea level, as at Pervaya Peschanaya key site no steps are formed, but rather a thermokarst depression (Leibman et al. 2003, Leibman & Kizyakov 2007).

Figure 7. Intensive mass waste due to thermoabrasion (frozen-block falls) at Yugorsky Peninsula, Kara Sea coast.

Upper thermocirque/thermoterrace edges are located at a distance (several dozen to several hundred meters away) from the shoreline, they are not interacting with the sea. Even low terraces with thermocirques formed due to lower ice layer thaw are not affected by wave action and develop only due to air temperature and precipitation.

An overview of the flat coastal bluffs, thermocirques/thermoterraces, and thermoabrasion coasts during 7 years at the key sites, as well as observations during a long-shore trip showed the following: There were 2 periods of active coastal destruction. The summers of 2000 and 2001 were noted for re-activation of thermodenudation and exposure of tabular ground ice at the eastern (2000) and western (2001) thermocirques of Pervaya Peschanaya key site.

The summer of 2006 changed the whole coastal type structure. Most of the stable dry slopes, as well as dropwalls of thermodenudation slopes, turned into thermoabrasion coastal types with niches, frozen block falls, and cracks at the bluff edges, which prepared continuous failures for the remaining summer months of 2006. In 2007 about 50% of the coasts turned into the thermodenudation-thermoerosion type, thermoabrasion being almost entirely suppressed because wave action was prevented by abundant sea ice and snow patches armoring the dropwalls.

Thus, a combination of coasts of various types at any given time slice constitute the Yugorsky coasts. Coasts are represented by flat to convex bluffs, retreating parallel to themselves due to slow gravitation processes (scree and slopewash) or thermoabrasion (formation of niches followed by earth falls), combined with stepped, concave coasts with thermocirques/thermoterraces and ravines developing due to thermodenudation and thermoerosion. Material transported to the beach is evacuated, depending on the wave activity, in a few days under a strong wind and open sea conditions, to a few weeks if none of the above occur.

After a year of active thermoabrasion in 2006, the lower tabular ice layer was exposed, and this started thermodenudation at the dropwall, which continued in 2007 beneath the snow patches when the melt season started.

The basic conditions for proceeding activation are: (1) presence of rather thick ice layers; and (2) removal of the material delivered from the bluff onto the beach. For the bluffs with tabular ground exposures, the increase of material yield to the beach is determined on the one hand, by a relative amount of tabular ice in a section, and on the other hand, by an increase in summer air temperature, surface-thaw rate, summer atmospheric precipitation, speed and sediment load of eroding flows, and accordingly, amount of sediment and distance of its transportation.

The dual role belongs to winter precipitation. Plentiful snow preserves slopes from thaw. However, the snow contributes to thermodenudation through the nivation process, and provides excessive meltwater flow, increasing sediment yield to the bluff toe, at the same time speeding up the sediment removal from the beach.

Air temperature acts dually as well. High summer temperature prolongs the ice-free period, and along with the intensive wind enhances wave action, promoting both thermoabrasion and removal of sediment. If the summer temperature rise is not accompanied by significant atmospheric precipitation, then sediment yield and removal are slowed down by landslide bodies in the transition zone.

The activity of cryogenic processes unequivocally amplifies only at increase of the thickness and proportion of tabular ground ice.

## Conclusions

A coastal dynamics study at the Yugorsky Peninsula coast (Kara Sea) was performed in 2001–2007. Tabular ground ice in the geological sections is responsible for the essential role of thermodenudation in the coastal destruction. Two commonly subdivided types of coasts: thermoerosion and thermodenudation cannot be applied in a study devoted to time-related patterns. Any portion of the coastline in a short-term dynamic under the climate fluctuations cannot only be transformed from stable into actively retreating, but also into a different type or into a mixed type existing within one time slice. Years with a wave uprush increase the proportion of coastal bluffs with the thermoabrasion mechanism dominating. Mixed type occurs when the "upper" edge is retreating according to thermodenudation pattern, while the "lower" edge is destructed by thermoabrasion.

From climatic controls, the main forcing factor for the rate of coastal retreat is summer air temperature (thaw index). The dominating mechanism for the time-dependent coastal destruction (dynamic type of coasts) is determined by different climatic parameters such as wave uprush caused by low sea ice coverage and strong landward winds, intensive winter precipitation resulting in numerous snow patches, which in the conditions of a bursting spring cause domination of thermoerosion and earth flows.

## Acknowledgments

Research was supported by Russian Federal Agency of Science and Innovations, Federal Program "World Ocean."

## References

Kizyakov, A.I., Perednya, D.D., Firsov, Yu.G., Leibman, M.O. & Cherkashov, G.A. 2003. Character of the costal destruction and dynamics of the Yugorsky Peninsula coast. In: *Reports on Polar and Marine Research* 443: 47-49.

Kizyakov, A.I., Leibman, M.O. & Perednya, D.D. 2006. Destructive relief-forming processes at the coasts of the Arctic plains with tabular ground ice. *Kriosfera Zemli* X(2): 79-89 (in Russian).

Kizyakov, A.I., Zimin, M.T., Leibman, M.O. & Cherkashov, G.A. 2004. Mapping of the coasts of Yugorsky peninsula, Kara Sea. In: *Reports on Polar and Marine Research* 482: 80-83.

Lantuit, H. & Pollard, W. 2003. Remotely sensed evidence of enhanced erosion during the twentieth century on Herschel Island, Yukon Territory. *Reports on Polar and Marine Research* 443: 54-59.

Lantuit, H., Couture, N., Pollard, W.H., Haltigin, T., De Pascale, G. & Budkewitsch, P. 2005. Short-term evolution of coastal polycyclic retrogressive thaw slumps on Herschel Island, Yukon Territory. *Reports on Polar and Marine Research* 506: 72-75.

Leibman, M.O. & Kizyakov, A.I. 2007. *Cryogenic landslides of the Yamal and Yugorsky Peninsular*. Moscow-Tyumen: IKZ SO RAN, 206 pp. (in Russian).

Leibman, M.O., Hubberten, H.-W., Lein, A.Yu., Streletskaya, I.D. & Vanshtein, B.G. 2003. Tabular ground ice origin in the Arctic coastal zone: cryolythological and isotope-geochemical reconstruction of conditions for its formation. *Permafrost. Proceedings of the 8th International Conference, Zurich, July 21–25 2003*. Lisse, *Netherlands*: A.A. Balkema Publishers, I: 645-650.

Leibman, M.O., Khomutov, A.V., Cherkashev, G.A. & Vanshtein, B.G. 2006. Advantages of various land-based methods to study dynamics of the ice-bearing coasts. *Program and Abstracts of the 6th ACD Workshop, 22-26 October 2006, Groningen, Netherlands*: 29.

Lewkowicz, A.G. 1987. Nature and Importance of Thermokarst Processes, Sand Hills Moraine, Banks Island, Canada. *Geografiska Annaler. Series A, Physical Geography* 69(2): 321-327.

Manley, W.F., Lokrantz, H., Gataullin, V.N., Ingolfsson, O., Forman, S.L. & Andersson, T. 2001. Quaternary stratigraphy, radiocarbon chronology, and glacial history at Cape Shpindler, southern Kara Sea, Arctic Russia. *Global and Planetary Change* 31: 239-254.

Solomon, S.M. 2003. A new shoreline change database for the Mackenzie-Beaufort region, NWT, Canada. *Reports on Polar and Marine Research* 443: 108-109.

Sovershaev, V.A. 1992. Coastal zone of the Arctic seas. In: *Geoecologia Severa*. Moscow: Moscow State University Press, 55-60 (in Russian).

# Gully-Polygon Interactions and Stratigraphy on Earth and Mars: Comparison of Cold-Desert, Near-Surface, Fluvial, and Periglacial Processes

Joseph Levy
*Brown University Department of Geological Sciences, Providence, RI, USA*
James W. Head
*Brown University Department of Geological Sciences, Providence, RI, USA*
David R. Marchant
*Boston University Department of Earth Sciences, Boston, MA, USA*

## Abstract

We examine the distribution and structure of composite-wedge polygons in the South Fork region of Wright Valley, Antarctica, in order to document the manner in which patterned ground contributes to the flow of water in cold desert gully systems. These gully-polygon systems are comparable to terrains observed in high-resolution images of the martian surface. We find that thermal contraction crack polygons contribute to the generation, transport, and storage of water in the Wright Valley gully systems. Further, we evaluate the formation sequence of gully-polygon systems. Similar relationships between gully alcoves, channels, and fans, and patterned ground on Mars suggest that many martian gullies formed on patterned surfaces, cross-cutting a continuous permafrost layer. Therefore, these gullies may result from the melting of atmospherically derived ice under appropriate microclimate conditions.

**Keywords:** Antarctica; Dry Valleys; gullies; Mars; microclimates; polygons.

## Introduction

Gullies on Mars are a class of young features, initially interpreted to have formed by the surficial flow of rapidly released groundwater (Malin & Edgett 2000, 2001), and which may still be active (Malin et al. 2006). Although numerous alternative formation mechanisms have been proposed, however, many workers conclude that an aqueous phase is involved in gully erosion, making gullies features of great astrobiological interest (Malin et al. 2001, SR-SAG 2006). Recent terrestrial analog fieldwork in the Antarctic Dry Valleys (ADV) of Southern Victoria Land, Antarctica, has reported on the primacy of top-down melting of snow as a source for water flowing through the active layer and hyporheic zone of terrestrial gullies (Dickson et al. 2007, Head et al. 2007a, Levy et al. 2007, Morgan et al. 2007).

Although the role of ice wedge polygons in the development of Arctic fluvial systems has been addressed (e.g., Lachenbruch 1962, Fortier et al. 2007), the effects of patterned ground on cold desert fluvial systems have not been broadly discussed, despite the observation of gullies in periglacial terrains on Earth and Mars (e.g., Bridges & Lackner 2006, Levy et al. 2008). Physical models constraining the deposition and behavior of ice-rich soils under present Mars surface conditions suggest that ice deposition and melting can occur on pole-facing slopes at high latitudes under suitable microclimate conditions (Hecht 2002) and that ice-rich soils can undergo thermal contraction cracking, generating patterned ground (Mellon 1997). We present the results of ADV gully-polygon interaction studies, outlining the use of polygons as for determining the stratigraphic sequence of gullied landscape evolution. This analysis provides a baseline for interpreting relationships between gullies and polygons observed in 70 HiRISE images of the martian surface. Analysis indicates that thermal contraction crack polygons play a similar role in the accumulation and transport of gully materials on both Earth and Mars, and that some gullies form or evolve in the continuous presence of actively expanding thermal contraction crack polygons.

## ADV Analog Studies

The South Fork of Wright Valley, Antarctica is located at 77°33′36″S, 161°17′24″E in the Intermediate Mixed Zone of the ADV (Marchant & Head 2007) (Figure 1). Gullies, composed of a broad alcove, a sinuous channel, and a distal fan (e.g., Malin & Edgett 2000) are common on the southern wall of the valley (elevation spanning: ~300–1000 m) (Levy et al. 2007). Continuous permafrost is present in the South Fork region beneath a dry active layer 20–45 cm deep (McGinnis & Jensen 1971). Composite-wedge polygons are common on the unconsolidated colluvium surfaces of Wright Valley and show a wide variety of sub-forms. Climatically, the South Fork study area is a cold, hyper-arid desert, with mean annual temperatures of -20°C (Ragotzkie & Likens 1964).

*Gully-polygon processes*

Monitoring of polygonally patterned ground covering all components of the South Fork gully systems (alcoves, channels, and fans), suggests that polygons modulate the accumulation, transport, and storage of meltwater in the Antarctic gully systems.

Previous work has shown that windblown snow accumulated in gully channels and alcoves is the primary source of meltwater for ADV gullies (Dickson et al. 2007,

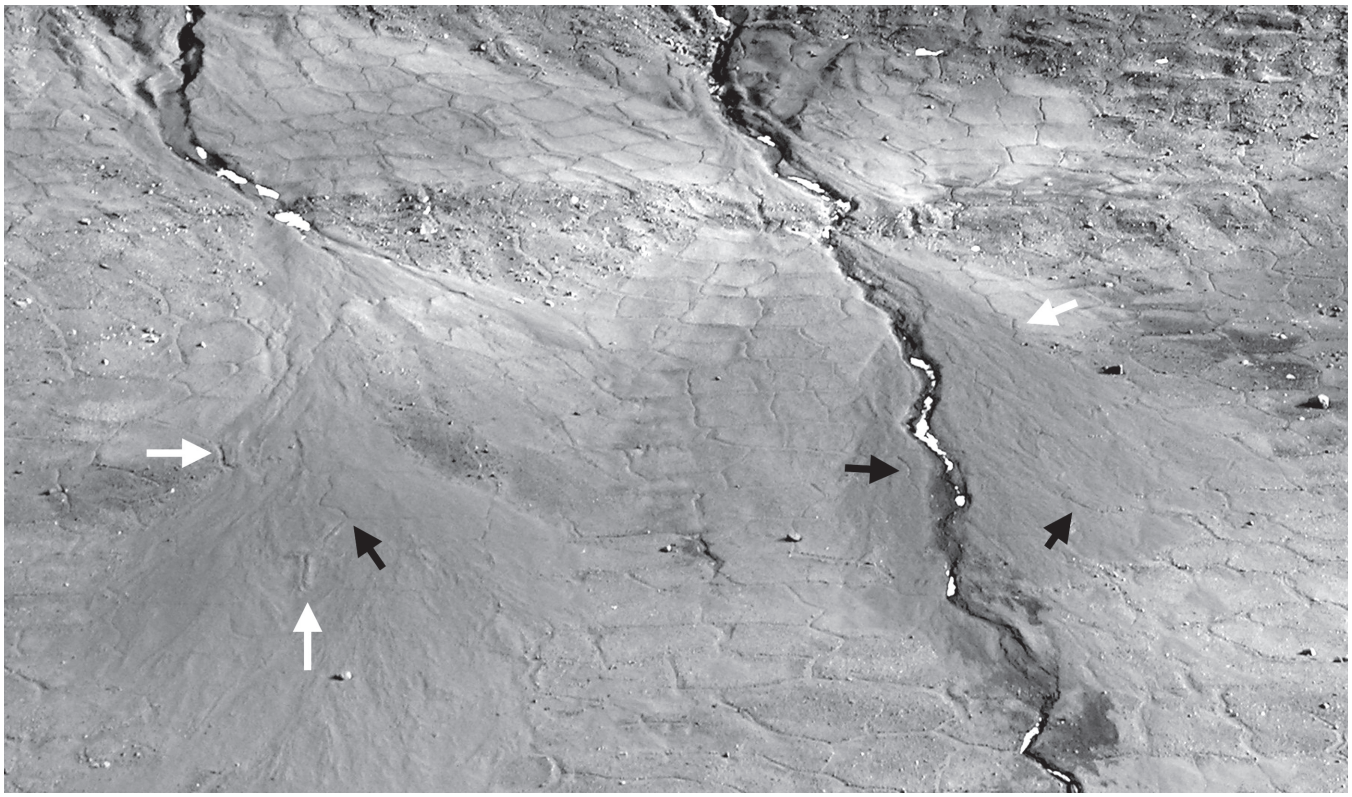

Figure 1. Gullies in the South Fork region of Wright Valley, ADV. Polygons are ~16 m wide. White arrows indicate embayment of patterned surfaces by fan deposits; black arrows indicate dissection of fans by thermal contraction crack polygons.

Levy et al. 2007, Morgan et al 2007, Head et al. 2007a). Windblown snow also accumulates in polygon troughs (~5–30 cm deep) in the South Fork study site, and ablates by melting and sublimation over the course of the austral summer (Levy et al. 2008). Polygon troughs intersecting a gully channel were measured, and the maximum volume of trapped snow was calculated to be comparable to or exceed the volume of windblown snowbanks calculated to be stored in the gully channel (~135 $m^3$). Where polygon trough snowbank melt-water can be transported into the channel, it becomes available to augment gully flow.

Water transport within South Fork gullies is enhanced by changes to ice-cement-table topography produced by polygon trough evolution. In some sediment excavations, liquid water is observed to flow along the base of the ice-cement table, through the active layer overlying depressed polygon troughs (the surficially depressed region above the polygon wedge). The ice-cement table depth and gradient are locally steepened by the development of polygon troughs, resulting in the concentration of meltwater derived from the melting and infiltration of overlying snow banks (Levy et al. 2008). Where water sources are large enough to initiate overland, channelized flow (i.e., gully channels), polygons directly contribute to gully water transport. At locations where gully channels intersect down-slope-oriented polygon troughs, the troughs are "annexed," as surface flow is transferred into the polygon troughs (Fig. 1). Annexed polygon troughs are generally wider, and more sinuous than adjacent non-annexed polygon troughs.

Water storage in the South Fork gullies is influenced by the presence of polygons in the distal hyporheic zone (Levy et al. 2007, 2008). Colluvium darkening in the distal hyporheic zone results from darkening of clay and silt-rich polygon interiors due to enhanced water content (~5% water by mass) (Levy et al. 2008). In contrast, pebble-rich polygon-wedge materials are bright and considerably drier (0.3–0.5% water by mass) than average colluvium surfaces in the South Fork study area (1.1–1.3% water by mass) (Levy et al. 2008). The concentration of wet, fine-grained colluvium in distal hyporheic zone polygon interiors and coarse, dry colluvium in distal hyporheic zone polygon troughs suggests that localized freeze-thaw processing is sorting grains within gully-terminal composite-wedge polygons, modulating spatial water distribution within the distal hyporheic zone.

*Gully-polygon stratigraphic relationships*

Relationships between polygon troughs and gully channels in Wright Valley indicate cross-cutting of pre-existing polygons by the gully channel. Polygon troughs intersect gully channels at oblique and near-orthogonal angles, and polygon wedge material is exposed on both sides of the gully channel. Some polygons are cut twice by the same gully channel (on up-slope and down-slope margins). Further, annexed polygon troughs could only develop if polygons preceded the presence of the gully channel. Taken together, these observations suggest that South Fork region gully channels were incised into previously extant polygons.

Contacts between gully fan surfaces and inter-gully,

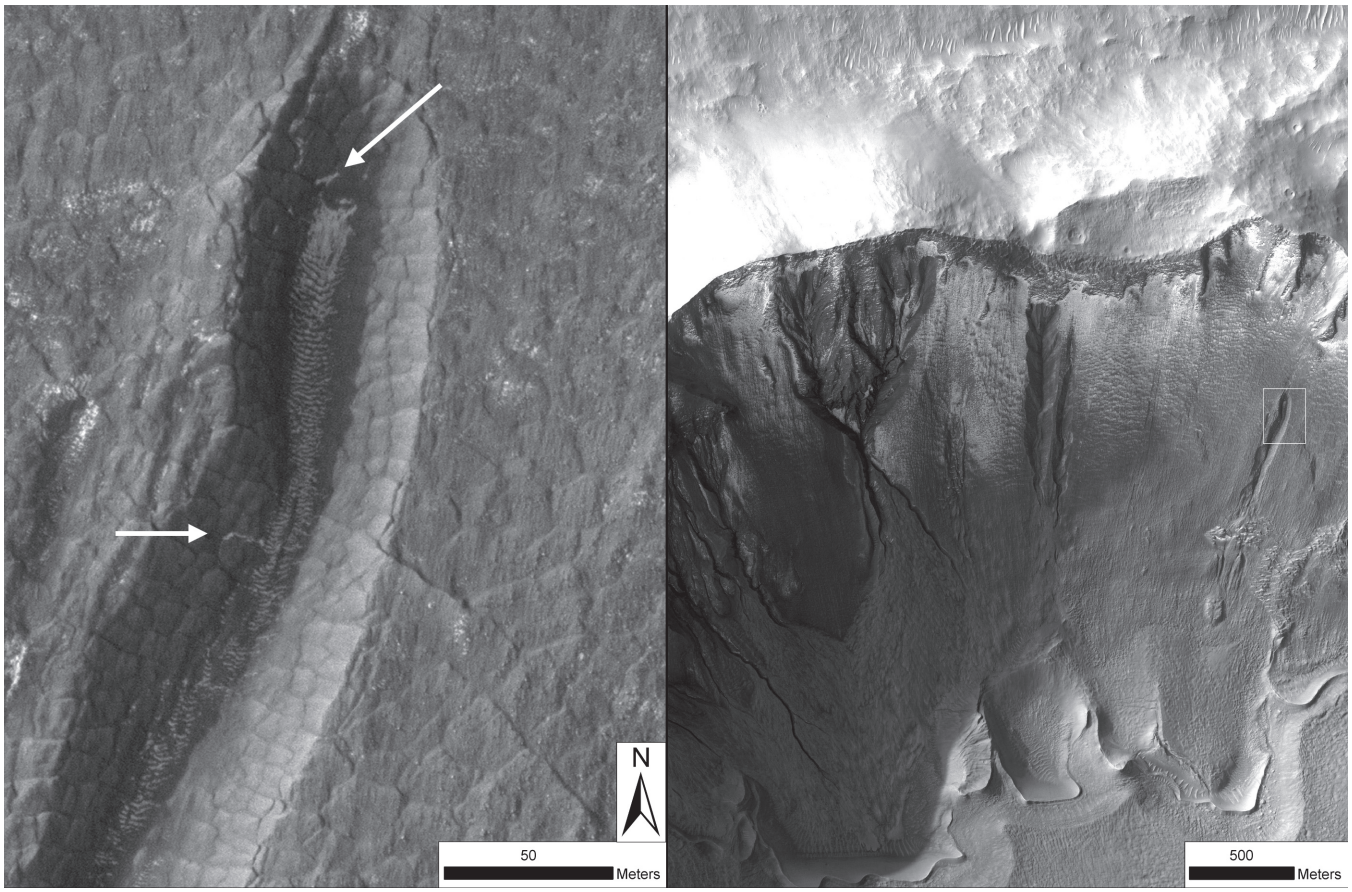


Figure 2. Left: Gully alcove surface with patterned ground. Arrows indicate frost preferentially present in polygon troughs during southern hemisphere winter. Right: Crater interior with gully-polygon suite. Area shown at left is boxed. Both images are from PSP_001882_1410. Illumination from left.

polygonally-patterned colluvium deposits can be used to trace the formation sequence of gully fans (Fig. 1). Local topographic high areas of patterned colluvium, including raised polygon shoulders, are embayed by gully fan deposits. Fan deposition is also blocked in places by the presence of a deep polygon trough (Fig. 1). Fan deposits are dissected by fine thermal contraction cracks which form a polygonal network continuous with the polygon network on the inter-fan surfaces. Taken together, these observations suggest that South Fork region gully fans formed in the presence of polygonally patterned ground, and that the expansion of thermal contraction cracks has kept pace with the aggradation of the gully fans, implying the continued presence of near-surface ice-cemented sediment during the entire process of gully channel and fan formation and evolution.

## Gully-Polygon Interactions on Mars

Polygonally patterned ground is a ubiquitous surface feature of high-latitude terrains on Mars (Mangold 2005). Thermal contraction cracking is expected in ice-cemented regolith polewards of ~30° (Mellon 1997), and features interpreted as thermal contraction crack polygons are mapped to within ~10° of the martian poles (Mangold 2005); higher latitudes are dominated by polar cap processes.

A survey of high-resolution (30 cm per pixel) images of the martian surface between 30°–80° latitude was conducted, comprising 537 HiRISE camera images from the primary science phase of the HiRISE mission. Gullies are present in 118 of the images, and occur in conjunction with polygons in 70 of the images: primarily in the southern hemisphere (on account of higher topographic roughness). In both hemispheres, gully-polygon suites commonly occur within multi-kilometer impact craters. Northern hemisphere gullies have little aspect preference at the scale of MOLA gridded altimetry data (~460 m per pixel), while southern hemisphere gullies have a strong pole-facing preference, consistent with the extensive survey results of Dickson et al. (2007). Gullies forming in association with polygonally patterned ground show an equally strong pole-facing preference in the southern hemisphere (58%), and little aspect bias in the northern hemisphere.

Three gully-polygon suites were selected for initial stratigraphic and process analysis. Physical characteristics for the three sites are summarized in Table 1.

*Mars gully-polygon process*

Morphological analysis of HiRISE images shows relationships between martian polygonally patterned ground and gullies analogous to those observed in Antarctica.

Polygons in and around the alcoves of two gullies (Figs. 2, 3) are outlined by bright deposits which have accumulated preferentially in polygon troughs (either through direct deposition of frost, after Hecht 2002, or wind-capture of ice or particulates, after Morgan et al., 2007): a process analogous to the accumulation of windblown snow in Antarctic polygon troughs. Polygon-modified transport of gully materials on Mars is evidenced by the presence of sinuous, sub-linear, bright features interpreted to be analogous to annexed polygon troughs (Fig. 4). High-albedo material with a similar texture and brightness to the primary gully fan deposits is present in polygon troughs which extend down-slope of the gully fans. The polygon troughs filled by the material are wider than adjacent troughs, have less angular intersections between polygon trough segments, and are more sinuous along the lengths of the trough segments than neighboring troughs. Taken together, we interpret these features as evidence of preferential transport of gully-fan-forming material through these polygon troughs, and erosion of pre-existing polygon troughs during gully fan formation. Preferential storage of gully-related fluids within polygons is not directly observed in HiRISE images. Sorting of polygon-forming sediments by freeze-thaw/sublimation processes may be occurring below martian gullies, however, this process is not visible at 30 cm pixel scales. Alternatively, little grain-size dependent partitioning of water within polygons in martian gully distal hyporheic zones may be occurring on account of the precarious metastability of water at the martian surface (e.g., Hecht 2002).

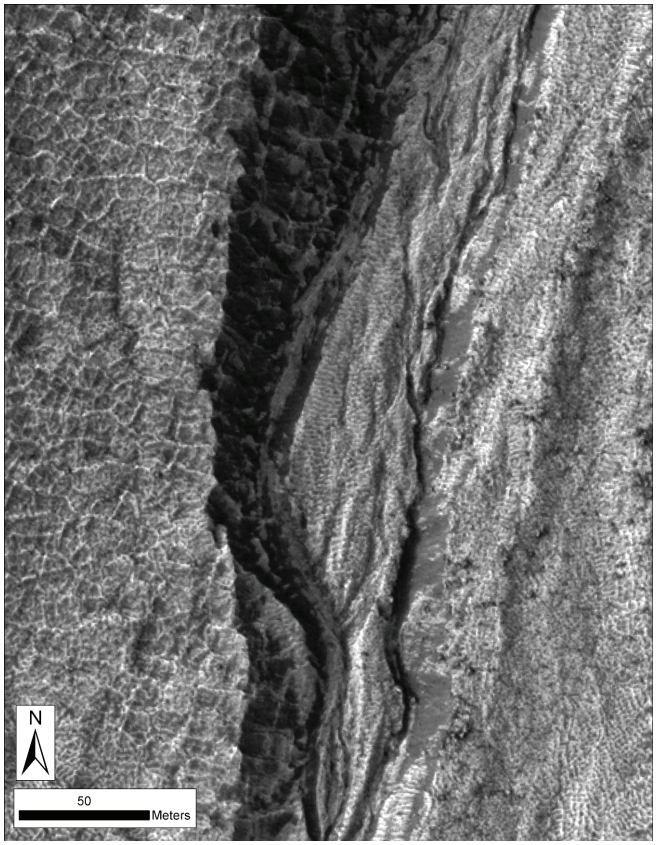


Figure 3. Portion of PSP_002368_1410 showing frost preferentially present in gully-alcove polygon troughs.

No evidence of any gully-polygon interaction is observable within gullies on equator-facing slopes, even those present within the same craters as gully-polygon suites on pole-facing slopes (Fig. 5). When present, equator-facing gullies appear to be extensively softened by sublimation and deflated by aeolian modification.

*Mars gully-polygons stratigraphic relationships*

As on Earth, polygons present in gullied terrains can be used to determine the formation sequence of landscape elements. A continuous network of polygonally patterned ground is commonly present across gully alcoves and inter-gully surfaces (Fig. 2). This relationship suggests that formation of polygonally patterned ground has continued through the period of gully alcove incision, making these polygons the youngest elements within the gully polygon system (in contrast to previous observations by Malin & Edgett, 2000, suggesting gullies exclusively overlie polygons). Contacts between gully fans and polygons (Fig. 4) show blocking of fan expansion by polygon troughs, annexation of polygon troughs (and filling with fan-like sediments), and incision of gully fans by polygons. Polygons present within gully fans 1) have narrower trough widths than polygons on inter-gully walls, 2) have subdued topographic relief, and 3) have interiors surfaced by gully fan material. Taken together, these observations suggest that these gully fans formed in the presence of polygonally patterned ground, overprinted the previously extant polygons, and were incised by continuously expanding thermal contraction crack polygons during fan emplacement.

## Conclusions

Polygonally patterned ground in the South Fork of Wright Valley was analyzed as a component of a near-surface hydrological system in which channelized, subaerial water flow occurs under cold desert conditions. Patterned ground

Table 1. Summary of gully-polygon suite characteristics.

| Image Number | PSP_001846_2390 | PSP_002368_1275 | PSP_001882_1410 |
|---|---|---|---|
| Image Location | South of Copias Palus | South of Porter Crater | East of Gorgonum Chaos |
| Latitude, Longitude | 58.7° N, 82.4°E | 52.1°S, 246.8°E | 38.7°S, 194.0°E |
| Altitude | -3800 m | 2000 m | 1000 m |
| Aspect | Pole-Facing and Equator-Facing | Pole-Facing | Pole-Facing |
| Gully Slope | 9.3° | 10.0° | 17.5° |
| Image $L_s$ | 152 (Northern Summer) | 174 (Southern Winter) | 154 (Southern Winter) |

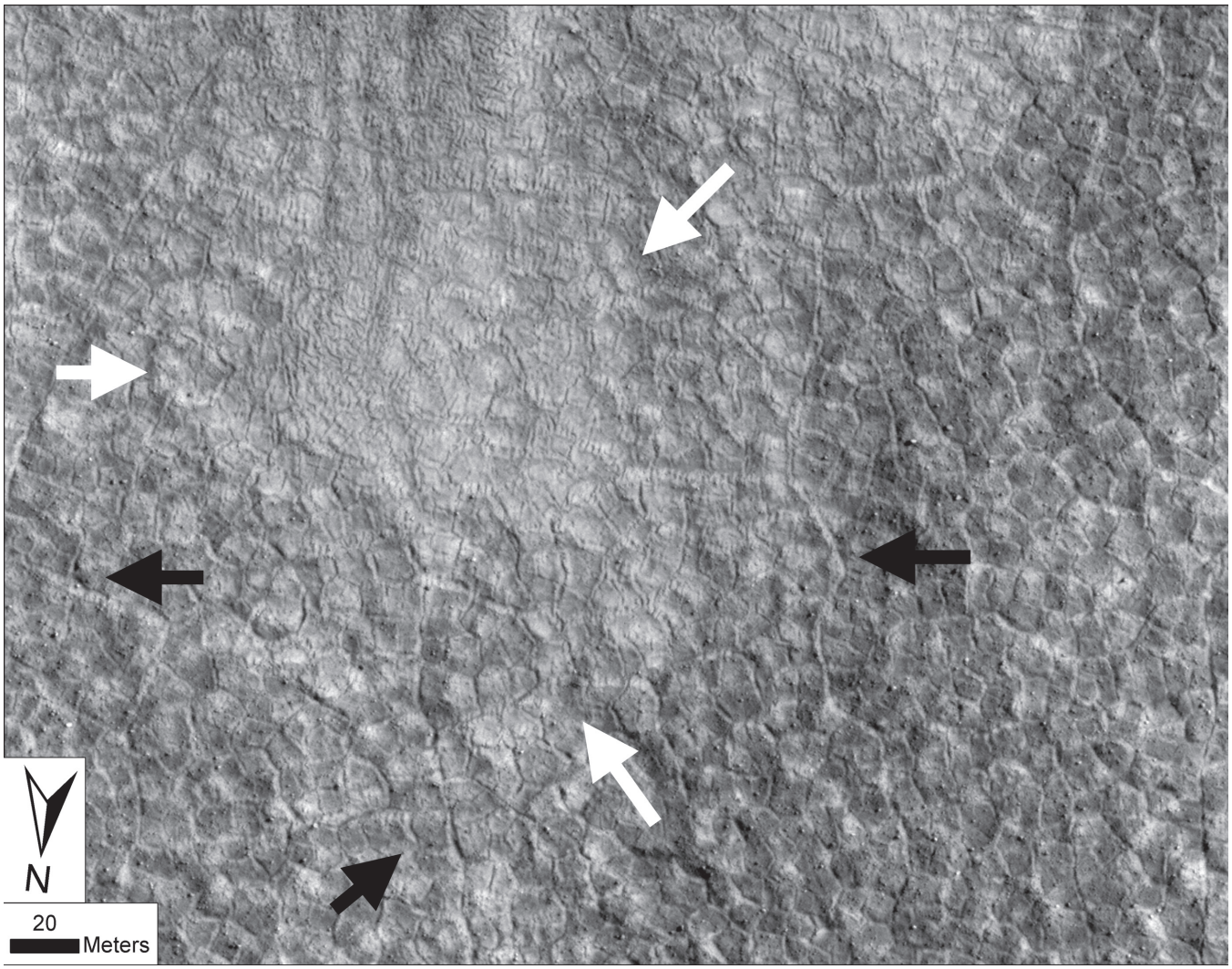


Figure 4. Gully fan from PSP_001846_1410. White arrows indicate extent of bright continuous fan deposit. Black arrows indicate annexed polygon troughs. Illumination from right.

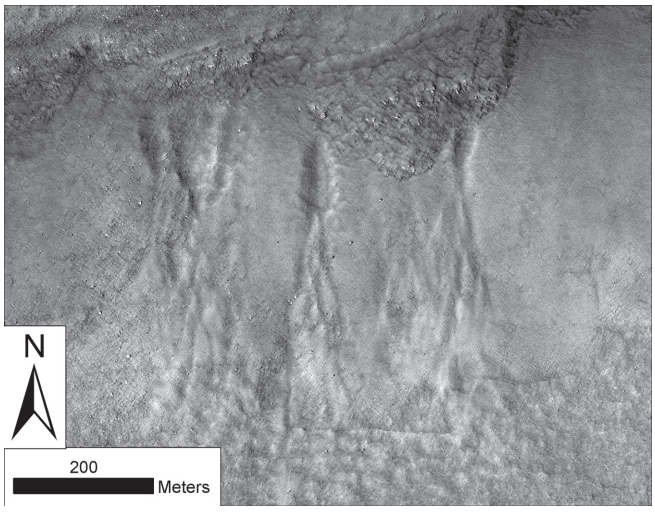


Figure 5. Gullies on equator facing slope, opposite gullies in Figure 4 (PSP_001882_1410). Illumination from left.

was found to play a significant role in the accumulation, transport, and storage of atmospherically-derived gully meltwater. Gully-polygon stratigraphic relationships indicate that patterned ground formation preceded gully formation and continued throughout gully evolution. This suggests the continuing presence of climate conditions permitting the expansion of composite-wedge polygons. Further, these results suggest the continuous presence of an impermeable ice-cemented sediment permafrost layer during the entire course of gully evolution.

Analysis of 537 HiRISE images in the 30°–80° latitude range revealed 70 gullies on the martian surface interacting with polygonally patterned ground. Our analysis indicates that patterned ground on Mars plays an analogous role in the accumulation and transport of martian gully materials to those observed on Earth. Further, stratigraphic relationships between gullies and polygons on Mars indicate that some gullies have formed in the presence of continuously expanding thermal contraction crack polygons. In some gullies, thermal contraction cracks are the youngest stratigraphic element in

the gully system. The processes of frost-trapping by polygon troughs, polygon trough annexation, polygon overprinting by gully fans, and dissection of gully fans by thermal contraction crack polygons, have all been observed in martian gullies, suggesting that some martian gullies have formed and evolved on surface units underlain by a continuous layer of shallow permafrost during the most recent period of gully activity. No evidence of catastrophic water release was observed. Polygon-gully interactions and fresh-looking gully structures were found to form preferentially on pole-facing slopes in the presence of shaded alcoves. Taken together these lines of evidence suggest an atmospheric origin for some gully volatiles, consistent with the model of gully activity observed in the Antarctic Dry Valleys.

## Acknowledgments

This work was made possible with support of JSL by the Rhode Island Space Grant Consortium, by NSF Grant ANT-0338291 to David Marchant and James Head, and by NASA MFRP Grant NNX06AE32G. Thanks to J. Dickson, D. Kowalewski, G. Morgan, D. Shean, and K. Swanger for field and data support. Thanks to A. McEwen and the HiRISE team for Mars image data. Also, thanks to PHI, the staff of RPSC, and the personnel of McMurdo Station.

## References

Bridges, N.T. & Lackner, C.N. 2006. Northern hemisphere martian gullies and mantled terrain: implications for near-surface water migration in Mars' recent past. *Journal of Geophysical Research* 111: doi: 10.1029/2006/JE002702.

Dickson, J.L., Head, J.W., Marchant, D.R., Morgan, G.A., & Levy, J.S. 2007. Recent gully activity on Mars: Clues from late-stage water flow in gully systems and channels in the Antarctic Dry Valleys. *LPSC 38*, Houston, TX, March 12-16, 2007: 1678.

Fortier, D., Allard, M., & Shur, Y. 2007. Observation of rapid drainage system development by thermal erosion of ice wedges on Boyt Island, Canadian Arctic Archipelago. *Permafrost and Periglacial Processes* 18: 229-243.

Head, J.W., Marchant, D.R., Dickson, J.L., Morgan, G.A., & Levy, J.L. 2007a. Mars gully analogs in the Antarctic Dry Valleys: Geological setting and processes. *LPSC 38*, Houston, TX, March 12-16, 2007: 1617.

Hecht, M.H. 2002. Metastability of water on Mars. *Icarus* 156: 373-386.

Lachenbruch, A.H. 1962. Mechanics of thermal contraction cracks and ice-wedge polygons in permafrost. *GSA Special Papers* 70: 1-69.

Levy, J.S., Head, J.W., Marchant, D.R., Morgan, G.A., & Dickson, J.L. 2007. Gully surface and subsurface structure in the south fork of Wright Valley, Antarctic Dry Valleys: Implications for gully activity on Mars. *LPSC 38*, Houston, TX, March 12-16, 2007: 1728.

Levy, J.S., Head, J.W., Marchant, D.R., Morgan, G.A., & Dickson, J.L. 2008. The Role of Thermal Contraction Cracks in Cold-Desert Fluvial Systems. *Antarctic Science*, In Press.

Malin, M.C. & Edgett, K.S. 2000. Evidence for recent groundwater seepage and surface runoff on Mars. *Science* 288 (5475): 2330-2335.

Malin, M.C. & Edgett, K.S. 2001. Mars Global Surveyor Mars Orbiter Camera: Interplanetary cruise through primary mission. *Journal of Geophysical Research* 106 (E10): 23,429-23,540.

Malin, M.C., Edgett, K.S., Pasiolova, L.V., McColley, S.M., & Dobrea, E.Z.N. 2006. Present-day impact cratering rate and contemporary gully activity on Mars. *Science* 314 (5804): 1573-1577.

Mangold, N. 2005. High latitude patterned grounds on Mars: Classification, distribution, and climatic control. *Icarus* 174: 336-359.

Marchant, D.R. & Head, J.W. 2007. Antarctic Dry Valleys: Microclimate zonation, variable geomorphic processes, and implications for assessing climate change on Mars. *Icarus* 192: 187-222.

McGinnis, L.D. & Jensen, T.E. 1971. Permafrost-hydrogeologic regimen in two ice-free valleys, Antarctica, from electrical depth sounding. *Quaternary Research* 1: 31-38.

Mellon, M.T. 1997. Small-scale polygonal features on Mars: Seasonal thermal contraction cracks in permafrost. *Journal of Geophysical Research* 102 (E11): 25,617-25,628.

Morgan, G.A., Head, J.W., Marchant, D.R., Dickson, J.L., & Levy, J.S. 2007. Gully formation on Mars: Testing the snowpack hypothesis from analysis of analogs in the Antarctic Dry Valleys. *LPSC 38*, Houston, TX, March 12-16, 2007: 1656.

SR-SAG. 2006. Findings of the Mars special regions science analysis group. *Astrobiology* 6(5): 677-732.

Ragotzkie, R.A. & Likens, G.E. 1964. The heat balance of two Antarctic lakes. *Limnology and Oceanography* 9(3): 412-425.

# Computation of Critical Heights of Embankments on High-Temperature Permafrost Regions in the Eastern Tibetan Plateau

Dongqing Li
*SKLFSE, Cold and Arid Regions Environmental and Engineering Research Institute, CAS, Lanzhou 730000, China*
Jin Chen
*SKLFSE, Cold and Arid Regions Environmental and Engineering Research Institute, CAS, Lanzhou 730000, China*
Qingzhou Meng
*SKLFSE, Cold and Arid Regions Environmental and Engineering Research Institute, CAS, Lanzhou 730000, China*
Jiankun Liu
*School of Civil Engineering and Architecture, Beijing Jiaotong University, Beijing 100044, China*
Jianhong Fang
*Highway Research and Survey Design Institute of Qinghai Province, Xining, 810008, China*

## Abstract

Ccritical embankment heights were computed for warm permafrost regions in the eastern Tibetan Plateau using geographical and geological conditions. The resulting modeled results agree well with the data collected on the Qinghai-Xizang Highway over the past 30 years. At first, for concrete and gravel road surfaces, the thermally-stable critical heights of embankments were estimated to be 2.50 m for concrete surfaces and 2.00 m for gravel surfaces, using regression analysis. When the heights of embankments are higher than the critical heights, the degrading permafrost table will gradually stabilize after construction. However there is no critical height of embankments for the asphalt pavement road in warm permafrost regions according to our models.

**Keywords:** degrading permafrost table; embankment stability; highway engineering; mathematical models; pavements; permafrost; thermal analysis.

## Introduction

When the natural ground surface is changed by roadway embankment construction, the thermal balance of the permafrost is also altered. Thermal equilibrium will not be reached for many years. As a result, the permafrost table under the roadbed is also degraded. As thermal balance is achieved, the permafrost table may rise or lower depending on roadway thickness and surface. For example, after construction of the Qinghai-Xizang Highway, the permafrost temperature under the roadbed increased, and the permafrost table was lowered. The roadway was paved with asphalt, which absorbs heat resulting in higher surface temperatures. Thaw settlement of the embankment occurred, destroying the road (Li & Wu 1997). Consequently, it is very important to understand the thermal stability of embankments after construction in permafrost regions, especially warm permafrost regions where the mean annual ground temperature is higher than or equal to -1.0°C. This corresponds to a mean annual air temperature of -3.5°C or higher.

The Qinghai-Sichuang Highway crosses the eastern part of the Qinghai-Xizang Plateau, China. The highway crosses about 300 km of mostly warm permafrost. The thickness of the permafrost has been degrading in this region since the 1960s (Zhu 1995, Li 1996).

We analyzed the thermal stability of embankments on permafrost in an effort to predict the temperature of the permafrost with different road surfaces and estimate critical heights.

## Methods and Conditions

*Mathematical model*

Since Harlan (1973) presented the first model for coupled heat and mass transfer in freezing soils, his strategy has been referred to and further developed by many other researchers (Guyman & Luthin 1974, Outcalt 1977, Taylor & Luthin 1978, Jame & Norum 1976, Nixon 1975, Li & Wu 1996). These authors applied two partial differential equations, using temperature and water (ice) content or water pressure to describe the transient heat and water flows in freezing soils. The two equations are coupled through the relationship between unfrozen water content and temperature. If vapor transfer and heat convection are omitted, the application of the laws of heat balance to saturated or unsaturated soil and the mass conservation of water in soil pores result in the following two equations:

$$\frac{\partial}{\partial x}(\lambda_x \frac{\partial T}{\partial x}) + \frac{\partial}{\partial y}(\lambda_y \frac{\partial T}{\partial y}) = C\rho \frac{\partial T}{\partial t} - L\rho_i \frac{\partial \theta_i}{\partial t} \quad (1)$$

$$\frac{\partial}{\partial x}(\mathrm{K}_x \frac{\partial \psi}{\partial x}) + \frac{\partial}{\partial y}(\mathrm{K}_y \frac{\partial \psi}{\partial y}) = \frac{\partial \theta_u}{\partial t} + \frac{\rho_i}{\rho_w} \frac{\partial \theta_i}{\partial t} \quad (2)$$

where $\rho_w$, $\rho$, and $\rho_i$ are the densities of water, soil, and ice, respectively; *t, x,* and *y* denote the time and two space coordinates; $\theta_i$ and $\theta_u$ are the volumetric fractions of the ice content and the unfrozen water content; $\lambda x(\lambda y)$ and $\mathrm{K}x(\mathrm{K}y)$ are the thermal and the hydraulic conductivities in the *x* and *y* directions; *T* is the temperature; *C* is the specific heat; *L* is

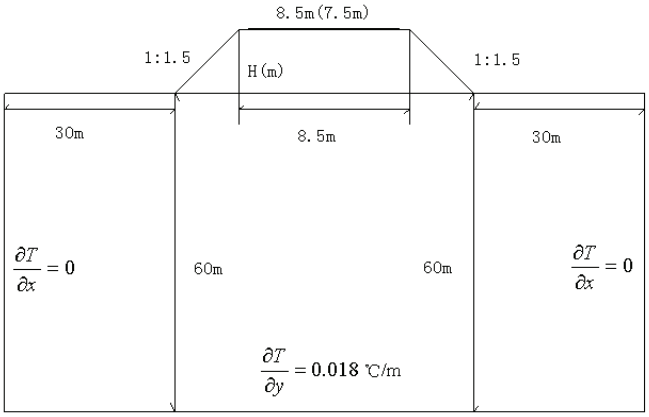


Figure 1. The profile of embankment for calculations.

the latent heat; $\psi$ is the total potential of water in soil; $\psi=\varphi+Z$, where $\varphi$ and $Z$ denote the volumetric potential of water in the soil and the gravitational potential, respectively. In general, $Z$ can be omitted and therefore $\psi=\phi$.

According to the characteristic relationship, $\theta_u=f(T)$ between the unfrozen water content $\theta_u$ and the temperature $T$, we obtain the following differential relationship:

$$\frac{\partial \theta_u}{\partial t}=\frac{\partial \theta_u}{\partial T}\frac{\partial T}{\partial t} \tag{2a}$$

Substituting this differential relationship into Equation (2) and reducing Equation (1), we can derive:

$$(C\rho+L\rho_w\frac{\partial \theta_u}{\partial T})\frac{\partial T}{\partial t}= \frac{\partial}{\partial x}(\lambda_x\frac{\partial T}{\partial x})+\frac{\partial}{\partial y}(\lambda_y\frac{\partial T}{\partial y})+L\rho_w\left[\frac{\partial}{\partial x}(\mathrm{K}_x\frac{\partial \psi}{\partial x})+\frac{\partial}{\partial y}(\mathrm{K}_y\frac{\partial \psi}{\partial y})\right] \tag{3}$$

Equations (2) and (3) can be solved when given the function $\psi$ and the characteristic relationship between the unfrozen water content and temperature. The temperature is determined empirically. From these equations, we can develop several models.

Taylor (1976, 1978) investigated the volumetric potential of unfrozen water in frozen soil. He showed the volumetric potential could be determined using the characteristic relationship between the unfrozen water content and temperature, similar to the volumetric potential of unfrozen soil, when the action of ice in the frozen soil is omitted. The characteristic relationship of moisture for unfrozen soil is suitable for frozen soil.

By introducing the new differential relationship:

$$\frac{\partial \psi}{\partial T}=\frac{\partial \psi}{\partial \theta_u}\frac{\partial \theta_u}{\partial T} \tag{3a}$$

and using the terms of the differential water capacity $c=\partial\theta/\partial\psi$ and the soil-water diffusivity $D=\mathrm{K}/c$, we reduce Equation (3) to:

$$C(T)\frac{\partial T}{\partial t}=\frac{\partial}{\partial x}(\beta_x(T)\frac{\partial T}{\partial x})+\frac{\partial}{\partial y}(\beta_y(T)\frac{\partial T}{\partial y}) \tag{4}$$

where:

$$C(T)=C\rho+L\rho_w\frac{\partial \theta_u}{\partial T}$$

$$\beta_x(T)=\lambda_x+L\rho_w D_x\frac{\partial \theta_u}{\partial T}$$

$$\beta_y(T)=\lambda_y+L\rho_w D_y\frac{\partial \theta_u}{\partial T}$$

$$D_x=\frac{\mathrm{K}_x}{\frac{\partial \theta_u}{\partial \psi}},\ D_y=\frac{\mathrm{K}_y}{\frac{\partial \theta_u}{\partial \psi}}$$

Since the characteristic relationship between the unfrozen water content and the temperature can be determined by testing, the set nonlinear Equations (2) and (4) can be solved. The implicit finite difference method was used to derive the results reported in this paper.

*Boundary and initial condition*

The input for the derived equations is established in part by Chinese standards and in part based on experience. According to the Chinese standards for designing and building national highways, road surface width is 8.5 m, and shoulder width is 0.5 m. The height of embankment varies. The side-slope is 1:1.5. Finally, the bottom boundary is located at 60 m depth. Based on drilling records, the temperature and the heat flux at the bottom of the permafrost were found to be constant on the Eastern Tibetan Plateau (Li et al. 1998). The ground temperature gradient at the lower boundary was estimated to be 0.018°C per meter. The lateral boundary (30 m from the slope corner) is situated so far from the road that the temperature gradient is regarded as 0.0°C/m horizontally (see Fig. 1).

The initial ground temperature field under the road was obtained from a borehole. The ground temperature without embankment was simulated using the boundary conditions noted until stable temperature field under the natural ground surface was established. This initial temperature profile was used to estimate the transient temperature field after road construction. The initial temperature in the embankment was assumed to be -1.0°C. The mean annual temperature of the embankment slope is 0.5°C lower than the upper boundary temperature of road surface, because that is often influenced by traffic.

Using meteorological information from Hua Shixia Valley and Ma Duo County in the Eastern Tibetan Plateau (Yu 1993), and by regression analysis of the sine function, we can reduce the upper boundary temperature of road surface to the following sine function:

$$T=T_s+G(t)+12.2\sin\left(\frac{2\pi}{8640}t+\frac{4\pi}{3}\right)$$

Here, $T_s$ is the mean annual temperature at the ground surface; $t$ is the time in hours of the annual cycle after the construction of embankment, respectively ranging from 0 to 8640 hours; $G(t)$ is the mean annual climate warming rate; here $G(t)=0$.

The mean annual air temperature in the warm permafrost regions was taken as -3.5°C. Ground temperature in the eastern part of the Qinghai-Xizang Plateau, $T_s$ is -1.0°C for natural ground, +3.0°C for an asphalt surface, +1.5 for a concrete surface and +1.0°C for a gravel road surface (Wu 1988). The natural permafrost table is about 2.00–2.20 m in the Hua Shixia Valley, a continuous permafrost region.

The hydrogeological conditions and heat parameters are as follows:

1. 0.00–2.00 m, organic clayey soil, water content 40.0%, dry density 0.9 g/cm3, heat capacities of unfrozen and frozen soils 1.17 J/cm³·°C and 1.34 J/cm³·°C and thermal conductivities of that 13.97 J/cm·h·°C and 16.72 J/cm·h·°C, respectively.
2. 2.00–3.30 m, clayey soil, water content 178.5%, dry density 0.36 g/cm³, heat capacities of unfrozen and frozen soils 1.03 J/cm³·°C and 0.89 J/cm³·°C, and thermal conductivities of that 26.36 J/cm·h·°C and 77.40 J/cm·h·°C, respectively.
3. 3.30–7.60 m, gravel, water content 24.5%, dry density 1.52 g/cm³, heat capacities of unfrozen and frozen soils 2.82 J/cm³·°C and 2.23 J/cm³·°C, and the thermal conductivities of that 40.59 J/cm·h·°C and 56.90 J/cm·h·°C, respectively.
4. Below 7.60 m, mantle rock, water content 4.0%, heat capacity of soil 2.29 J/cm³·°C, thermal conductivity of soil 97.20 J/cm·h·°C.
5. Fill materials of embankment contain clayey soil with coarse-grained gravel; water content 8.0%–10.0%, dry density 2.0 g/cm³. The capacities and conductivities of unfrozen and frozen soils were taken as those in 3.30–7.60 m deep gravel soil.

The relationships between unfrozen water content, temperature, total moisture, and thermal properties are taken from experimental research on moisture transfer in frozen soil (Xu & Deng 1991).

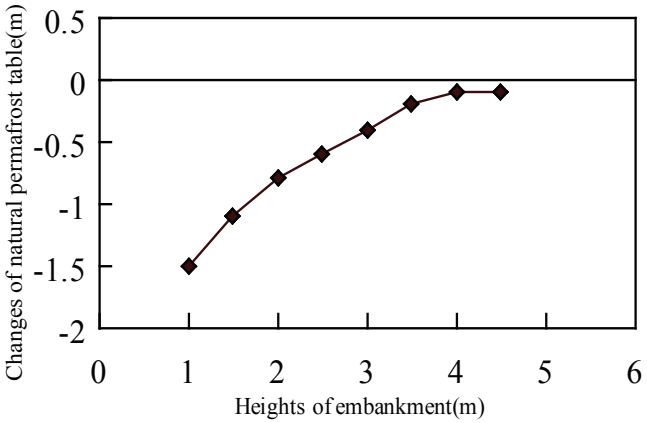


Figure 2a. Relation between height of embankment and the changes of natural permafrost tables under roadbed (asphalt).

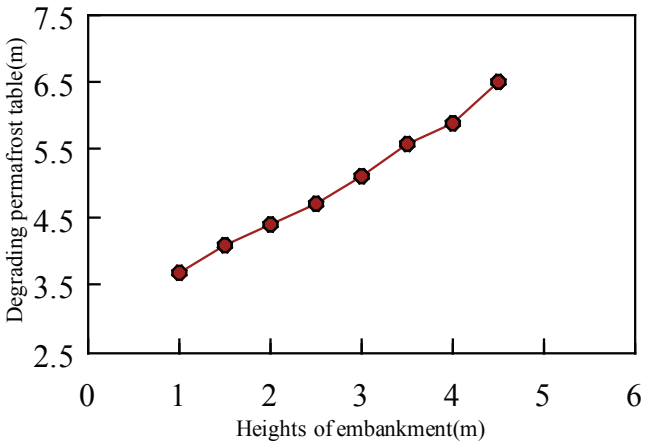


Figure 2b. Relation between height of embankment and the degrading permafrost table of embankment (asphalt).

## Results and Discussion

Because traffic is increasing, replacing the existing gravel surface with pavement is necessary. To keep the road surface smooth, the fill stability must be maintained. In order to prevent thaw settlement, the permafrost table under the roadbed must be maintained and not lowered. Frost heaving of the active layer above the permafrost must be controlled to less than 1%. The calculations in this paper use the two principles as guidelines. Using the different types of road surface and embankment heights, changes in the level of the permafrost table as a function of time are analyzed. Using the results, the critical design heights of the embankment for a 30-year period after construction are determined using linear regression analysis between heights of embankment and changes of the natural permafrost table.

The analysis is summarized in Figures 2–6. Figures 2a–4a show for asphalt, concrete, and gravel road surface the relation between the height of embankment and the changes of the level of the natural permafrost table under the middle sections of road in the 30 years after construction on the high-temperature permafrost sections. On the other hand, Figures 2b–4b show the relation between the height of embankment and the degrading permafrost table (changed permafrost table under the roadbed) under the middle sections of the road; that is, the critical design heights have a relationship with the age of the road after construction. Figures 5 and 6 show the zero degree isothermal curves under the roadbed with asphalt pavement at the embankment height of 4.0 m and 3.5 m in 30 years.

From Figure 3 to Figure 4, for concrete and gravel surface embankments, when the embankment height is lower than 3.0 m, it can be seen that there is an almost linear relation between the height of embankment and change in the natural permafrost table and degrading permafrost table under the road in the thirtieth year after construction. This is in agreement with that for low-temperature permafrost regions (Li et al. 1998); therefore, from a linear regression analysis, the heat-stable critical heights of embankment for concrete and gravel roads are figured out as 2.50 m and 2.00 m in the thirtieth year after construction.

From Figure 2, however, for the asphalt pavement road, the above-mentioned relation is nonlinear. After 10 years the permafrost table under the roadbed is always lower than the natural permafrost table. As shown in Figures 5 and 6, when the height of embankment is higher than 3.5 m for an asphalt

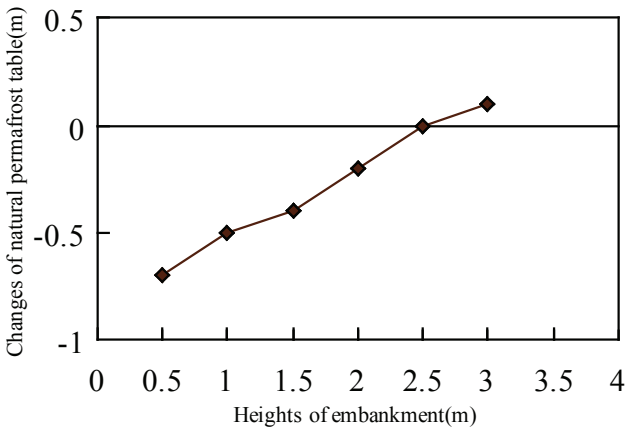


Figure 3a. Relation between height of embankment and the change of natural permafrost tables under roadbed (concrete).

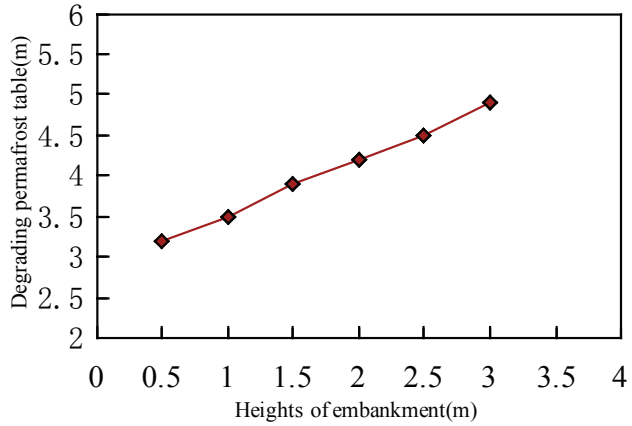


Figure 3b. Relation between height of embankment and the degrading permafrost table of embankment (concrete).

road, there will be a residual thaw zone (an upper thawed course) (Huang 1983) above the degrading permafrost table in the embankment more than 10 years after construction. Again, the predicted permafrost table is lower than the natural permafrost table under the road from that point forward. Consequently, the degrading permafrost table under the roadbed was always lower than the natural permafrost table under the roadbed after 10 years following construction or in the thirtieth year; we cannot get any critical height for asphalt pavement, as we did for concrete-surface and gravel-surface roads. Because of the existence of the upper thawed course (an unfrozen area in the embankment above the degrading permafrost table), the frost deformation of the embankment, therefore, would be largely increased making it impossible to maintain smoothness specifications. In other words, it is not desirable to build an asphalt-pavement road in the warm permafrost regions of the Tibetan Plateau.

For concrete and gravel surface roads, there is no upper thawed course (an unfrozen area in the embankment above the degrading permafrost table) in the embankment for embankment heights less than 3.0 m; that is, there are critical heights of embankment. These are in correspondence with the observed results on high-temperature permafrost regions in the Qinghai-Xizang Highway during the 30 years or more of the last century (Wu et al. 1988).

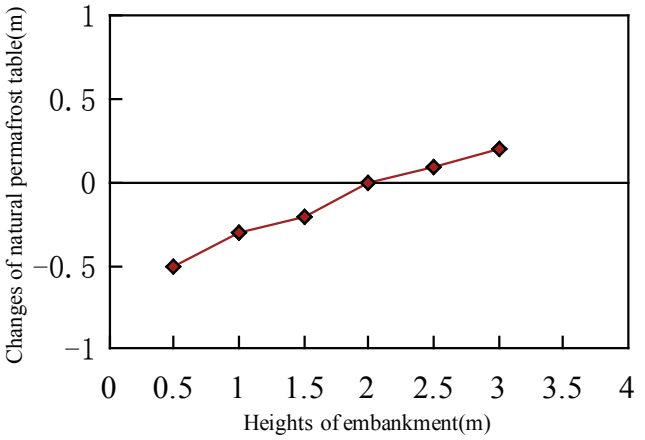


Figure 4a. Relation between height of embankment and the changes of natural permafrost tables under roadbed (gravel).

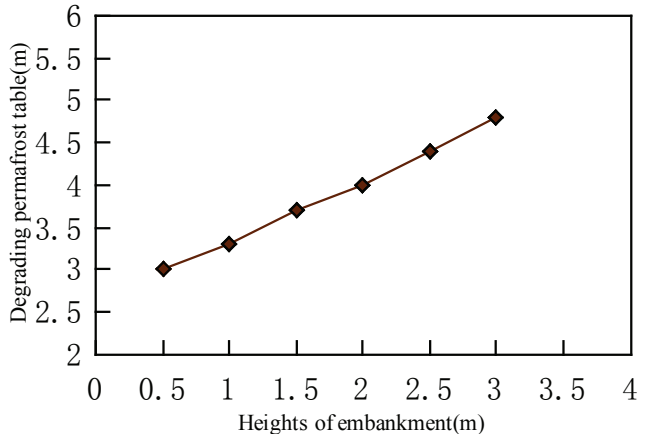


Figure 4b. Relation between height of embankment and the degrading permafrost table of embankment (gravel).

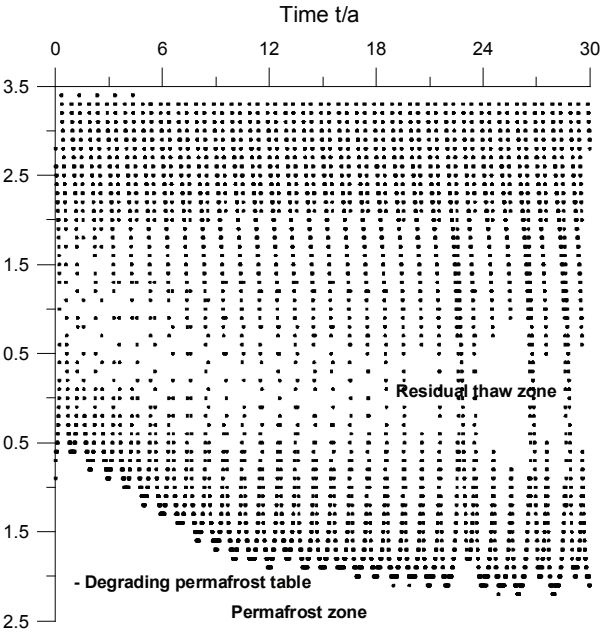


Figure 5. The zero degree isothermal curves under the roadbed at the embankment height of 3.5 m in 30 years (asphalt).

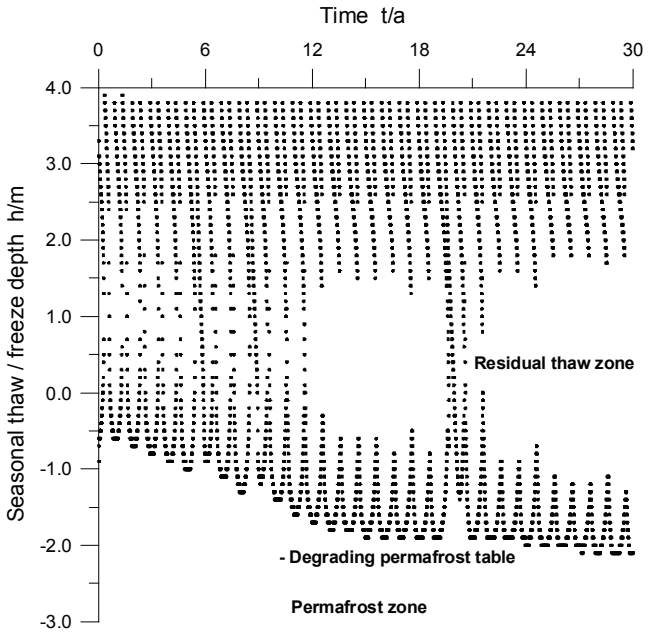


Figure 6. The zero degree isothermal curves under the roadbed at the embankment height of 4.0 m in 30 years (asphalt).

## Conclusions

1. It is important to predict permafrost change under the road with running time after construction. The applied numerical model provides the ability to predict and estimate critical heights of embankment in cold regions.

2. The heat-stable critical heights of embankment on the high-temperature permafrost regions in the Eastern Tibetan Plateau are 2.50 m and 2.00 m for a 30-year analysis period after construction for concrete and gravel road surfaces, respectively.

3. According to the principle of protecting the permafrost, it is not desirable to build an asphalt pavement road in the area; that is, there is no critical height of embankments for the asphalt pavement road in high-temperature permafrost regions in this area.

## Acknowledgments

The research was supported by the National Natural Science Foundation of China (No. 40671039), the Talent Project of Cold and Arid Regions Environmental and Engineering Research Institute (No. 2004122), the program for New Century Excellent Talents, NCET-05-0092, the grant of the Knowledge Innovation Program of the Chinese Academy of Sciences (No. KZCX3-SW-351), the grant of the Western Project Program of the Chinese Academy of Sciences (No. KZCX2-XB2-10), and the National Science Supporting Project of the Ministry of Science and Technology of China (2006BAC07B02).

## References

Guyman, G.L. & Luthin, J.N. 1974. A coupled heat and moisture transport model for arctic soils. *Water Resources Research* 10: 1314-1323.

Harlan, R.L. 1973. An analysis of coupled heat-fluid transport in partially frozen soil. *Water Resources Research* 9: 1314-1323.

Huang, X.M. 1983. Determination of the critical height of embankment for highway in permafrost regions of Tibetan Plateau. *Proceedings of the second national conference on permafrost (selection)*. China: Gansu People's Publishing House, 391-397.

Jame, Y.W. & Norum, D.I. 1976. Heat and mass transfer in freezing unsaturated soil in a closed system. *Proceedings of the 2nd Conference on Soil Water Problem in Cold Region, Edmonton, Alba*: 1-18.

Li, D., Wu, Z., Fang, J. et al. 1998. Heat stability analysis of embankment on the degrading permafrost district in the East of Tibetan Plateau, China. *Cold Regions Science and Technology* 28: 183-188.

Li, D.Q. & Wu, Z.W. 1996. Numerical calculation on permafrost degradation. *Proceedings of the fifth chinese conference on Glaciology and Geocryology*, Vol.2, China: Gansu Culture Press, 1082-1086.

Li, S. & Wu, Z. 1997. The forming and changing property of thawed course under roadbed on the permafrost regions of Tibetan Plateau. *Journal of Glaciology and Geocryology* 19(2): 133-140.

Ma, Y. 1993. The reconfirmation on climatic change of Qinghai Province. *Meteorology of Qinghai* 3: 13-19.

Nixon, J.F. 1975. The role of convective heat transport in the thawing of frozen soils. *Canadian Geotechnical Journal* 12(4): 425-429.

Outcalt, S. 1977. Numerical modelling of the ice lensing processes. *Proc., Int. Symp. On Frost Action in Soils*, *Lulea, Sweden, Feb 1977.* Lulea University of Technology, Vol. 2: 75-91.

Taylor, G.S. & Luthin, J.N. 1976. Numeric results of coupled heat mass flow during freezing and thawing. *IProc. 2nd. Conf. on Soil Water Problems in Cold Regions*, Edmonton Alta: 1-2.

Taylor, G.S. & Luthin, J.N. 1978. A model for coupled heat and moisture transfer during soil freezing. *Canadian Geotechnical Journal* 15(3): 548-555.

Wu, Z.W., Cheng, G.D., Zhu, L.N. & Liu, Y.Z. 1988. Adhere layer and engineering signification. *Road Engineering of Frozen Soil*. Lanzhou, China: Lanzhou University Press, 48-60.

Xu, X.Z. & Deng, Y.S. 1991. Driving force of water migration in freezing and frozen soils. *Experimental Study on Water Migration in Freezing and Frozen Soil.* Pecking, China: Science Press, 9-29.

Zhu, L.N., Wu, Z.W. & Liu, Y.Z. 1995. Permafrost degeneration in the east of Tibetan Plateau. *Journal of Glaciology and Geocryology*, Pecking, China: Science Press, 17(2):120-124.

# Author Index


Aalto, R., 613
Abliazina, D., 1131
Abnizova, A., 2003
Abramenko, O., 971
Abramov, A., 993, 1251
Aðalgeirsdóttir, G., 1705
Adam, J.C., 177
Adams, P.C., 1845
Addison, J., 95
Affleck, R.T., 1
Aguirre, A., 7
Akagawa, S., 13, 327, 895, 1573
Akerman, H.J., 19, 851
Aksenov, V.I., 25
Alexeev, S.V., 31
Alexeeva L.P. 31
Allard, M., 591
Allen, S., 37
Amils, R., 523
Andersen, D.T., 43
Anderson, S.L., 49
Andreev, A., 1191
Anisimov, O., 779
Anisimova, N.P., 55
Arena, L., 1781
Arenson, L.U., 59, 89, 1261, 1411, 1685
Argunov, R.N., 983
Arnold, F., 1131
Atkinson, D.E., 65
Aubé-Maurice, B., 457
Aus der Beek, T., 71
Avian, M., 77, 343, 1505
Azelton, M.T., 83
Azmatch, T.F., 59, 89

Bach, M., 675
Bakulina, N.T., 1681
Barbour, E.M., 1893
Barnet, C., 1981
Barrett, J.E., 529
Battogtokh, D., 821
Bauer, A., 77
Bayasan, R.M., 1787
Beget, J.E., 95
Bellefleur, G., 101
Belova, N.G., 107, 1671
Bennett, P.C., 1327
Benowitz, J., 95
Beutel, J., 669
Biggar, K.W., 89, 815
Bing, H., 113
Bjella, K.L., 119
Blaks M.R., 1369
Blanco, J.J., 1463, 1839
Blanco-Chao, R., 1799
Blikra, L.H., 789
Bo, H., 839
Bockheim, J.G., 125
Bode, J.A., 131
Bodin, X., 137, 343
Böhlert, R., 143
Boike, J., 149, 155, 1549, 1589
Bolton, W.R., 155
Bommer, C., 159
Boschi, D., 569
Boudreau, L. D., 1405
Bowden, W.B., 165
Bowen, R.G., 171
Bowling, L.C., 177
Bradford, J., 165
Brandová, D., 143
Bray, M.T., 183, 889
Brent, T., 101
Brewer, M.C., 189
Broll, G., 195, 1717, 1751
Brosten, T., 165
Brown, J., 7, 199, 1267, 1273, 1369, 1647,
Brunstein, D., 493
Bubier, J., 649
Bubnov, N.G., 25
Buhanov, B.A., 205
Buldovich, S., 211
Burgess, M.M., 1665
Burn, C.R., 901, 907, 1363
Busey, R.C., 215
Butzbach, R., 773
Bykhovets, S., 993

Caline, F., 1005
Callaghan, T.V., 851
Campbell, I.B., 125, 221
Cannone, N., 227
Cao, W., 1921
Caplan-Auerbach, J., 747
Caranti, G., 1781
Carey, S.K., 233
Carpenter,G.W., 1481
Carreau, R., 285
Carrera-Gómez, P., 1799
Casais, M.C., 1381
Cassano, E., 215
Cassano, J.J., 215
Cassie, J.W., 285
Chan, E., 469
Chang, X., 1921
Chehina, I.V., 1493
Chen, J., 1049, 1179
Chen, W., 2055
Chen, Y., 845
Cheng, G., 239
Cherkauer, K.A., 177
Chernyadyev, V., 1775
Chestnykh, O., 1155
Christensen, J.H., 247, 1705
Christensen, T.R., 251, 851
Christiansen, H.H., 257, 877, 1005, 1149, 1369, 1933
Christl, M., 143
Chuvilin, E.M., 205, 263
Clague, J.J., 269
Claridge, G.G.G., 221
Clark, E., 1
Clark, M.H., 275
Clarke, J., 279
Claypool, G., 285
Cleall, P., 919
Collett, T.S., 291
Collins, C.M., 1
Coronato, A., 1381
Costard, F., 297, 391, 493
Côté, M.M., 171
Couture, N.J., 303, 1025, 1433
Cremonese, E., 1427
Croll, J.G.A., 309
Crossen, K.J., 1993
Cuchí, J.A., 1621
Cuomo, C.J., 415
Cysewski, M., 315

D'Agata, C., 569
Daanen, R., 321, 1519, 1705
Dallimore, S.R., 101, 171, 1757
Darrow, M.M., 327
Dashtseren, A., 821
Davies, M., 663
Davydov, S.P., 333, 481
Davydova, A.I. 333
De Pascale, G.P., 337
DeBeer, C.M., 233
Dech, S., 947
Delaloye, R., 343, 699, 1019, 1233, 1505
Deline, P., 143, 349
Demitroff, M., 355

Derevyagin, A.Y., 1595
Diekmann, B., 1601
Dietrich, R., 1589
DiFurio, S., 469
Dillon, M., 361
Ding, Y., 1061, 1975, 2071
Dobinski, W., 367
Doolittle, J.A., 355
Dorjgotov, B., 795
Dorthe, J., 1233
Dou, F., 1197
Douglas, T.A., 373, 1887
Drozdov, D.S., 379, 1511
Duchesne, C., 385, 403
Duguay, C., 591
Dupeyrat, L., 391
Durán, J.J., 1621
Dutilleul, P., 639
Dutta, U., 1227

Easton, N.A., 1993
Ebohon, B., 397
Ednie, M., 385, 403
Efremov, V.N., 409
Egli, M., 143
Eiken, T., 789, 1311
Eisner, W.R., 415
Ellis-Evans, C., 569
Etzelmüller, B., 421, 427, 1627
Everts, J.R., 1339

Fang, J., 1049
Farbrot, H., 421, 427, 789
Fedorov, A.N., 433, 493, 1077
Fedorov, G., 1601
Feklistov, V.N., 1173
Feng, W., 113
Fenton, C., 279
Fernández-Remolar, D.C., 523, 1445
Fernández-Sampedro, M., 523, 1445
Ferris, G.F. 1327
Fiencke, C., 1567
Fischer, L., 439
Foged, N., 445, 773
Font, M., 297, 663
Förster, A., 1601
Fortier, D., 361, 451, 889
Fortier, R., 457
Frape, S., 469
Frauenfelder, R., 463
Freifeld, B.M., 469
French, H.M. 199, 475
Friborg, T., 251
Fukuda, M., 645
Fuller, C.C., 649
Fyodorov-Davydov, D.G., 333, 481, 993

Gaboury, M.N., 1015
Gailhardis, E. C., 391
Gasselt, S., 487, 1531
Gattinger, A., 1875
Gautier, E., 493
Gavriliev, P.P., 499
Gavriliev, R., 505
Gaylord, A., 7
Gens, A., 279
Georgiadi, A.G., 511
Gerasimov, E.Y., 983, 1077
Germogenova, A., 2095
Gevorkyan, S.G., 25
Gex, P., 1583
Giardino, J.R., 1857
Giardino, M., 1427
Giebels, M., 1549
Gieck, R.E., 711, 883
Gilichinsky, D.A., 517, 993
Goldberg, M., 1981
Gómez Ortiz, A., 1321
Gómez, F., 523, 1445
Gómez-Elvira, J., 523, 1445
Gómez-Ortiz, D., 1445
Gooseff, M.N., 165, 529
Gorelik, J.B., 535
Gorshkov, S., 1769
Goryachkin, S.V., 1093
Goulden, C.E., 1627
Grebenets, V.I., 541, 2037
Grechishchev, S.E., 1105
Greenwald, M.J., 165
Grigoriev, M.N., 1345
Groisman, P.Y., 1643
Grom, J.D., 545
Grosse, G., 551, 1239, 1595
Gruber, S., 143, 557, 597, 669, 723, 747, 1293, 1427, 1463, 1839
Guan, X.J., 1951
Gubarkov, A.A., 563, 1037
Gubin, S.V., 1083, 1827
Guðmundsson, Á., 421
Guenther, K.P., 947
Günzel, F.K., 581
Guggenberger, G., 1077
Guglielmin, M., 125, 227, 569
Gugolj, D., 575
Guo, Y., 1921
Guodong, C., 199
Guryanov, I.E., 587
Guryeva, O.M., 205, 263

Hachem, S., 591
Haeberli, W., 143, 597, 607, 1505
Hagedorn, B., 149, 613
Hallégouët, B., 619
Hallet, B., 613, 625, 631
Haltigin, T.W., 639
Hamilton, T.D., 1255
Hammadi, J., 493
Hao, J., 845, 1639
Harada, K., 645, 809
Harden, J.W., 649
Harris, C., 655, 663, 919
Hartikainen, J., 1833
Hasler, A., 669
Hatano, R., 1077
Hauber, E., 487, 1531
Hauck, C., 463, 675, 699, 1293, 1463, 1839
Hausmann, H., 343
Hayley, D.W., 681
Haywood, H., 1143
He, J., 687
He, P., 113
He, R., 693, 845, 1939
Head, J.W., 1043
Hegdal, L.A., 857
Heggem, E.S.F., 1627
Hiasa, S., 13
Hibsch, C., 619
Hidalgo, M.A., 1463
Hilbich, C., 463, 675, 699, 1293
Hinkel, K.M., 415, 705, 1267, 1273, 1647
Hinzman, L.D., 65, 215, 711, 883, 1613
Hjort, J., 717, 1137
Hoelzle, M., 463, 557, 699, 723, 1293
Hoeve, E., 2089
Hohmann, R., 607
Holden, B., 469
Hollister, R.D., 729
Holubec, I., 735
Hoque, M.A., 303, 741
Horne, B., 681
Huang, S.L., 13, 327, 941, 1179
Huggel, C., 37, 439, 747
Humbolt, D., 1857
Humlum, O., 257, 753, 877

Iijima, Y., 761, 795, 821
Ikard, S., 529
Ikeda, A., 343, 767, 1733, 1933
Ingeman-Nielsen, T., 445, 773, 865
Instanes, A., 779, 785
Instanes, B., 785
Iospa, A.V., 25
Isaev, V., 971
Isaksen, K., 427, 655, 789, 1311
Ishii, T., 1733
Ishikawa, M., 795, 809, 821
Istratov, V., 1221

Ivanova, L.D., 801
Ivanova, R.N., 805
Ivy-Ochs, S., 143
Iwahana, G., 327, 809
Iwakun, O., 815

Jaillet, S., 137, 349
Jambaljav, Y., 821
Janowicz, J.R., 827
Jardine, J., 735
Jardine, R., 279
Jenkins, R.E.L., 833, 965
Ji, C., 839
Ji, Y., 845, 1939
Jin, H., 189, 845, 1055, 1921, 1939, 2009
Johansen, B., 789
Johansson, M., 251, 851
Johnson, A., 469
Johnson, E.R., 857
Jonasson, C., 851
Jones, A., 1717
Jones, B.M., 415
Jørgensen, A S., 773, 865
Jorgenson, M.T., 373, 869, 1087, 1197, 1423
Jorgenson, T., 889
Juliussen, H., 877

Kääb, A., 343, 1505
Kadota, T., 795, 821
Kalling, K., 1745
Kane, D.L., 711, 883, 1067
Kanevskiy, M., 361, 373, 451, 889, 1423, 1721
Kanie, S., 13, 895, 1573
Kanigan, J.C.N., 833, 901
Karelin, D., 2021
Karunaratne, K.C., 907
Kashutina, E.A., 511
Katamura, F., 809
Kaufmann, V., 343, 1505
Kellerer-Pirklbauer, A., 77, 343, 913
Kern-Luetschg, M., 663, 919
Kershaw, G.P., 925
Keusen, H.R., 159
Kholodov, A.L., 481, 993, 1511
Khomutov, A., 1037
Kidd, J.G., 931
Kienast, F., 937
Kienholz, H., 1209
Kim, K., 941
Kirschke, S., 947
Kizyakov, A., 1037
Klene, A.E., 705, 953, 1727
Klinova, G.I., 25
Kneisel, C., 463, 959
Koch, K., 1875
Koemle, N.I., 113
Kokelj, S.V., 833, 901, 907, 965, 1763
Kolisoja, P., 1299
Komarov, I., 971
Kondratiev, V.G., 977
Kononov, A.M., 31
Konstantinov, P.Y., 433, 983
Korobova, E.M., 987
Kotov, A., 2021
Kotov, P.I., 205
Kraev, G.N., 481, 993, 1499
Krainer, K., 343
Krautblatter, M., 999
Kristensen, L., 877, 1005
Krummenacher, B., 1209
Krzewinski, T.G., 49
Kubik, P.W., 143
Kuhry, P., 247, 1493
Kunitsky, V.V., 1595
Kurchatova, A.N., 1659
Kutvitskaya, N.B., 1105
Kutzbach, L., 1549
Kuzmin, G.P., 1011
Kuznetsova, T.V., 1595

LaDouceur, M., 321
Lagarde, J.L., 297
Lai, A., 1015
Lambiel, C., 343, 1019, 1505, 1583
Lantuit, H., 551, 1025
Layer, P., 95
Lehmkuhl, F., 1031, 1701
Leibman, M.O., 563, 1037, 1815
Levy, J., 1043
Li, D., 1049, 1179
Li, G., 845, 1055, 1639
Li, R., 1061
Li, S., 1969
Li, Y., 919
Lilly, M.R., 1067
Lin, Z., 1287
Lipski, A., 1875
Liu, J., 1049
Liu, X., 1981
Liu, Y., 1921, 1963
Long, E.L., 1073
Lopez, L., 1077
López-Martínez, J., 125, 1621, 1839
Lorenson, T.D., 171
Lü, L., 845, 1055
Lugon, R., 1019
Luo, T., 687
Luoto, M., 717, 1137
Lupachev, A.V., 993, 1083
Lynn, L.A., 1087, 1197, 1423
Lyuri, D.I., 1093

Ma, W., 239, 1099, 1917, 2077
Ma, X., 2043
Maddy, E., 1981
Magomedgadzhieva, M.A., 1105
Maier, H.A., 1255, 1893
Maisch, M., 143
Majhi, I., 1109
Majorowicz, J.A., 1113
Malkova, G.V., 379, 1119, 1155, 1375, 1511
Mamykin, V., 993
Marchant, D.R., 1043
Marchenko, Sergei, 1125
Marchenko, Sergey, 1131, 1705
Marchenko, S.S., 1511, 1519, 2061
Margreth, S., 1417
Marmion, M., 1137
Marsh, P., 1143
Martín Redondo, M.P., 1445
Martin, C., 279
Matsuoka, N., 1149, 1733, 1933
Maximov, T.C., 761
Mazhitova, G., 1155, 1493
McGraw, M., 1161
McHattie, R.L., 1167
McKay, C.P., 43
McNamara, J.P., 165
Melnikov, V.P., 379, 1173
Meng, Q., 1049, 1179
Meng, X., 1921
Merekalova, A.A., 481
Mesquita, P.S., 1185
Meyer, H., 1191, 1595, 1945
Michaelson, G.J., 1087, 1197, 1423
Michel, F.A., 1203
Mihajlovic, D., 343, 1209
Mikami, T., 1573
Mikhailov, V.M., 1215
Milanovskiy, S., 1221
Milyukova, I.P., 511
Mink, S., 1621
Miranda, R., 1227
Mölders, N., 1351
Molnia, B.F., 747
Montanarella, L., 1717
Moorman, B.J., 131, 575, 1711, 1881
Morard, S., 1233
Morgenstern, A., 551, 1239
Morra Di Cella, U., 1427
Moskalenko, N.G., 1245, 1511, 1815
Motenko, R.G., 1251
Munger, C.A., 1255
Murton, J., 663, 1905
Muslimov, A.V., 1607
Myers-Smith, I., 649

Narita, K., 645

Näslund, J.O., 1833
Nater, P., 1261
Navas, A., 1621
Neff, J.C. 333
Neill, I., 469
Nelson, F.E., 355, 475, 705, 729, 953, 1267, 1273, 1633, 1647, 1727
Nesterov, A.N., 1173
Nethercot, D., 279
Neukum, G., 487, 1531
Nicolsky, D.J., 1281
Nikitina, N.M., 801
Nishimura, S., 279
Niu, F., 1287, 2049
Noetzli, J., 1293, 1869
Northcott, M., 529
Nurmikolu, A., 1299
Nussbaum, A., 1209

Oberman, N.G., 1305, 1511
Ødegård, R.S., 1025, 1311
Ogorodov, S.A., 1317
Ohata, T., 761, 795
Okamoto, H., 895
Okoemova, A.P., 1787
Oliva, M., 1321
Olivella, S., 279
Omelon, C.R., 1327
Onclin, C., 1143
Onstott, T.C., 469
Osadetz, K., 1113
Osinski, G.R., 639
Osterkamp, T.E., 869, 1333
Ostroumov, V.E., 481, 993
Oswell, J.M., 1339
Overduin, P.P., 155, 1025, 1345, 1369
Owens, I., 37

Paetzold, R.F., 1067
PaiMazumder, D., 1351
Panda, S.K., 1357
Pang, Q., 1969
Panin, V.N., 1011
Parameswaran, V.R., 1363
Park, H., 761
Parmuzin, I.S., 1493
Parsons M.A., 1369
Parviainen, M., 1137
Pavlov, A.V., 1375
Pavlova, N.A., 55
Perez-Alberti, A., 1381, 1799
Perlshtein, G.Z., 1387, 1391
Perruchoud, E., 343
Peterson, R.A., 1399
Petrone, R.M. 1405
Pfeiffer, E.M., 1567, 2095
Pfiffner, S.M., 469
Pham, H.N., 1411
Phillips, M., 159, 1417
Ping, C.L., 1087, 1197, 1423
Pogliotti, P., 1427
Pollard, W.H., 43, 303, 337, 545, 639, 741, 1327, 1433
Pondrelli, M., 1531
Ponomareva, O., 1439
Popova, A.P., 1493
Postigo Cacho, M., 523
Prakash, A., 1357
Pratt, L.M., 469
Prieto-Ballesteros, O., 523, 1445
Prowse,T.D., 1185, 1763
Pu, Y., 2077
Pustovoit, G.P., 1787
Putkonen, J., 631, 1451

Qi, J., 1055, 1457

Rabassa, J., 1381
Rabatel, A., 349
Rachold, V., 1345
Raetzo, H., 1019
Ramachandran, K., 101
Ramos, M., 1463, 1839
Randriamazaoro, R., 391
Ravanel, L., 349
Raynolds, M.K., 1469
Razzhivin, V., 2021
Regmi, D., 1475
Regmi, N.R., 1857
Reifen, C., 279
Reshetnikov, A.M., 1173
Reynard, E., 1583
Riddle, C.H., 1481, 1525
Riedel, M., 101
Riseborough, D.W., 1487, 1665, 2055
Rivkin, F.M., 1493
Rivkina, E., 1499
Rodríguez-Manfredi, J.A., 523, 1445
Roer, I., 343, 1505, 1869
Romanenko, F.A., 107
Romanovskiy, N., 211
Romanovsky, V.E., 211, 247, 321, 373, 551, 1125, 1267, 1281, 1369, 1511, 1519, 1633, 1705
Rooney, J.W., 1481, 1525
Rossi, A.P., 487, 1531
Roth, K., 149, 2009
Roujanski, V.E., 1537
Rouse, W.R., 1405
Ruskeeniemi, T., 469
Russell, M., 1143
Rutter, P., 279

Saarelainen, S.M.I., 1543
Sachs, T., 947, 1549
Safanda, J., 1113
Saito, K., 1555
Saito, T., 1561
Sanders, T., 1567
Saruulzaya, A., 821
Sato, M., 895, 1573
Sawada, Y., 645, 809, 1577
Scapozza, C., 1583
Scheller, S., 1589
Scheritz, M., 1589
Schirrmeister, L., 937, 1191, 1239, 1595, 1601, 1945, 2095
Schneider, W., 1589
Schoeneich, P., 137
Schrott, L., 397
Schuler, T.V., 421
Schulte, L., 1321
Schwamborn, G., 1601
Schwindt, D., 959
Seaquist, J.W., 639
Sedov, B.M., 1607
Seelen, S.J., 1613
Sego, D.C., 59, 89, 815, 1411
Sekulich, I.R., 1617
Sergeev, D.O., 211, 1511, 1519, 1695
Serrano, E., 1621, 1839
Shangin, M., 2027
Sharkhuu, A., 1627, 1633
Sharkhuu, N., 795, 1627, 1633, 2061
Sheng, Y., 845, 1055, 1639
Sherstyukov, A.B., 1643
Sherstyukov, B.G., 1643
Shiklomanov, N.I., 333, 953, 1267, 1273, 1369, 1633, 1647, 1727, 2037
Shimazaki, K., 1573
Shoop, S.A., 1
Shur, Y., 315, 361, 373, 451, 869, 889, 1423, 1439
Siegert, C., 1595, 1945
Skachkov, Y.B., 1653
Skryabin, P.N., 1653
Slagoda, E.A., 1659
Sletten, R.S., 613, 631
Slider, R.T., 729
Smith, F., 663
Smith, S.L., 1369, 1665
Solie, D.N., 1357
Sollid, J.L., 789, 1311
Solomatin, V.I., 107, 1671
Solomon, S.M., 131, 1675, 1711
Solongo, D., 821
Sone, T., 809
Sorensen, S., 2027

Sorokovikov, V.A., 481, 993
Spektor, V.B., 1681
Spektor, V.V., 1681
Spieck, E., 1567
Springman, S.M., 1261, 1685
Stanilovskaya, J., 1695
Staub, B., 343, 1209
Stauch, G., 1701
Stendel, M., 247, 1705
Stevens, C.W., 131, 1675, 1711
Stolbovoy, V., 1717
Stone, D., 95
Stotler, R., 469
Strasser, F., 279
Streletskaya, I.D., 1721
Streletskiy, D.A., 953, 1267, 1647, 1727, 1957, 2037
Strozzi, T., 1019
Sueyoshi, T., 809, 1733
Surkov, V.V., 987
Swendseid, J., 49

Tahirkheli, S.N., 1739
Tait, M.P., 575
Talzi, I., 669
Tammiksaar, E., 1745
Tarnocai, C., 195, 1717, 1751
Taylor, A.E., 1675, 1757
Teichert, E., 71
Thibert, E., 343
Thomas, H., 919
Thompson, D.K., 1951
Thompson, M.S., 965, 1763
Tikhmenev, P.E., 1607
Tikhonova, E.P., 1251
Tipenko, G., 211, 1125, 1281, 1387
Tishkova, M., 1769
Titkov, S., 1775
Tomé, D., 1463
Torres Redondo, J., 523, 1445
Toumi, R., 279
Trainor, T., 1613
Trombotto Liaudat, D., 1781
Trumbore, S.E., 649
Tschudin, C., 669
Tseeva, A.N., 1787
Tsvetkova, M., 1775
Tweedie, C.E., 7, 729

Ugarov, I.S., 983
Ukhova, J., 1695
Ukraintseva, N.G., 987, 1793
Utkina, I., 1695

Valcarcel-Diaz, M., 1381, 1799
Vanshtein, B., 1037
Varlamov, S.P., 1653
Vasil'chuk, A.C., 1803, 1809
Vasil'chuk, Y.K., 1803, 1809
Vasiliev, A.A., 1511, 1721, 1815
Vasiliev, I.S., 1821
Védie, E., 297
Velikin, S., 1221
Veremeeva, A., 1827
Vesbach, C., 529
Vidstrand, P., 1833
Vieira, G., 1463, 1839
Viereck, L.A., 1845
Vinson, T.S., 1167, 1851
Vitek, J.D., 1857
Vlasova, J.V., 1493
Vliet-Lanoë, B. Van 619
Volokhov, S.S., 1863
Vonder Mühll, D.S., 1869

Wagner, D., 1875
Wainstein, P.A., 1881
Wake, T., 1927
Waldrop, M.P., 1887
Walker, D.A. 321, 1255, 1281, 1469, 1519, 1893
Walker, H.J., 1899
Waller, R., 1905
Walsh, J., 247, 1911
Walter, K., 551
Wang, D., 1917
Wang, G., 1921
Wang, L., 1987
Wang, P., 1287
Wang, S., 2049
Watanabe, K., 1927
Watanabe, T., 1933
Watt, B., 735
Webber, P.J., 729
Wei, Z., 845, 1939
Wen, Z., 1639, 1917
Werdin-Pfisterer, N.R., 1845
Wessels, R.L., 747
Wetterich, S., 937, 1595, 1945, 2095
White III, R., 1887
Whitehead, K., 1881
Whiteman, C., 1905
Wille, C., 1549
Wilmking, M., 649
Wisskirchen, K., 947
Woo, M., 1951
Wood, K.R., 1957
Worland, M.R., 569
Wright, J.F., 171, 385, 403, 1757
Wrona, F.J., 1185, 1763
Wu, Q., 239, 1099, 1963
Wu, T., 1969, 1975, 2061, 2071, 2083
Wu, W., 845, 1639
Xie, C., 1969, 1975, 2071
Xiong, X., 1981
Xu, A., 839, 1179
Xu, J., 1287
Xu, X., 1987

Yabuki, H., 761, 795, 821
Yamazaki, T., 761
Yang, C., 1921
Yang, D., 493, 1109
Yang, S., 1939
Yang, Z., 1227
Yarmak, E. Jr., 1073
Yesner, D.R., 1993
Yoshikawa, K., 373, 767, 1191, 1267, 1561, 1613, 1633, 1845, 1997
Young, K.L., 1951, 2003
Yu, F., 1921
Yu, H., 1963
Yu, L., 1987
Yu, Q., 839, 845, 1921, 2009
Yu, S., 839, 1939
Yu, W., 1055

Zabolotnik, S.I., 2015
Zajdlik, B., 965
Zamolodchikov, D., 1155, 2021
Zarling, J.P., 2027
Zarnetske, J.P., 165
Zegers, T., 1531
Zeglin, L., 529
Zemskova, A.M., 2033
Zepalov, F.N., 2037
Zhang T., 1369
Zhang, A., 2089
Zhang, Jianming, 845, 1457, 1921, 1939, 2043
Zhang, Jinzhao, 2049
Zhang, L., 1099
Zhang, W., 1969
Zhang, Y., 795, 821, 2055
Zhao, L., 1061, 1969, 1975, 2061, 2071, 2083
Zhao, S., 2077
Zhao, Y., 845, 2049, 2083
Zheleznyak, M.N., 1511
Zheng, B., 2043
Zheng, J., 2077
Zhou, F., 2089
Zhou, W., 941
Zhuang, Q., 687
Zimov, N., 993
Zimov, S., 551
Zimova, G., 993
Zubrzycki, S., 2095
Zufelt, J.E., 83

# Subject Index


Active layer, 155, 221, 257, 321, 385, 409, 481, 529, 625, 645, 711, 729, 761, 795, 809, 821, 865, 877, 919, 931, 983, 993, 1061, 1077, 1083, 1125, 1155, 1203, 1267, 1273, 1451, 1463, 1487, 1519, 1627, 1647, 1665, 1727, 1815, 1839, 1845, 1869, 1975, 2037, 2083
  thickness (ALT), 333, 481, 529, 729, 931, 983, 1647, 2021, 2037
Agricultural landscape, 499, 805, 1093, 1627, 2021
Alas depression, 937
Alaska, 7, 65, 83, 95, 189, 291, 415, 705, 711, 747, 767, 857, 869, 883, 889, 931, 953, 1015, 1067, 1073, 1087, 1161, 1191, 1197, 1255, 1267, 1281, 1333, 1357, 1423, 1445, 1525, 1613, 1727, 1845, 1887, 1899, 1993, 2027
Anabar shield, 31
Anchor, 159
Antarctica, 125, 149, 221, 227, 529, 569, 631, 1043, 1463, 1621, 1839
Anthropogenic impact, 221, 587, 693, 705, 805, 987, 1245, 1439, 1617, 1627
Arctic, 149, 177, 251, 291, 613, 947, 1025, 1087, 1423, 1469, 1911
  ecology, 19, 805
  storms, 65, 83
Argentina, 1381, 1781, 1799
Astrobiology, 43, 517, 523, 523, 1445
Aufeis (naleds), 1543, 1881
Austrian Alps, 77, 397

Bearing capacity, 159, 1787
Beaufort Sea, 7, 303, 741
Bibliography, 1739
Biogeochemistry, 165
Biological activity, 1185, 1327, 1567, 1945
Boreal, 649, 1845
Borehole, 469, 655, 723, 993, 1005, 1267, 1333, 1463, 1561, 1577, 1633, 1695
Brine, 31, 1345

CALM, 257, 1155, 1273, 1647, 1727, 1815, 2021, 2037
Canada, 291, 681
  High Arctic, 43, 639, 1327, 1433, 1881, 1951, 2003
  Manitoba, 925, 1405
  northwestern, 101, 337, 815, 827, 907, 1143, 1339, 1363, 1665
  Nunavut, 285, 1537
Carbon
  budget, 1493
  content, 1751
  dioxide, 251, 2083
  dissolved organic (DOC), 333
  processes, 687
  sequestration, 687
  stocks, 195, 649, 1751
Cations, 327
Chemical thaw, 25, 31
China, northeast, 693, 839, 1639, 1939
Climate, 753, 1405, 1439, 1653, 2015
  change, 95, 171, 189, 211, 215, 269, 279, 337, 403, 433, 439, 469, 493, 597, 607, 655, 681, 711, 779, 947, 965, 993, 1113, 1119, 1203, 1209, 1245, 1255, 1273, 1317, 1531, 1685, 1705, 1717, 1751, 1763, 1769, 1793, 1815, 1939, 1957, 2003, 2055, 2061, 2089, 2095
  controls, 1037
  global, 247, 511, 1093, 1555
  reconstruction, 1191
  scenarios, 65, 71, 1351, 1705, 1833
  warming, 239, 385, 457, 499, 901, 1073, 1077, 1155, 1305, 1333, 1375, 1525, 1733, 1781, 1827, 2071
Coastal, 1037, 1317, 1345
  erosion, 7, 83, 303, 1025, 1087, 1197, 1317, 1423
Colorado, 1857
Confining pressure, 1917
Contaminants, 815, 833, 987
Continental Shelf, 1345
Convective
  cooling, 83
  natural, 113, 557, 1215, 1233, 1411
Cost assessment, 2089
Cracks, 59, 309, 631, 925, 1131, 1149, 1863

Creep, 119, 227, 343, 463, 999, 1019, 1417, 1531, 1863, 1869
Crude oil, 857
Cryogenic
  processes, 379, 433, 535, 541, 563, 1375, 1391, 1601
  structure, 183, 355, 361, 451, 889, 1659
Cryolithology, 1595, 1681, 2009
Cryopegs, 25, 31, 517
Cut-off wall, 49

Dam, 1221, 1607
  design, 49
  seepage, 1601, 1757
Dansgaard-Oeschger events, 1809
Data management (archiving), 1369, 1647
Debris flow, 297, 1839
DEM, 77, 131, 137, 1589
Diffusion, 505

Earthquakes, 619, 1227
Ecological survey, 275, 587
Effective pressure, 13
Electrical freezing potential, 1363
Embankment, 239, 445, 839, 977, 1049, 1055, 1099, 1543, 1963, 2043, 2049
  orientation, 247, 1099
Energy balance, 1405
Engineering, 279, 285, 475, 693, 735, 779, 785, 857, 1015, 1049, 1167, 1227, 1287, 1573, 1787, 1921, 2049
  geology, 845, 1227, 1391, 1685, 1851
Eurasia, 795, 1643
Europe, 655
European Alps, 343, 439, 1031, 1505

Finland, 717, 1137, 1543
Foundation, 159, 315, 735, 779, 785, 1417, 1481, 1787, 1921, 1987, 2089
  pile, 1787, 1851
Freeze-back, 285
Freezing, 1917
  axial, 2077
  one-sided, 663
  point depression, 445
  radial, 2077
  two-sided, 663, 919

Freezing index, 591, 1463, 1821, 1969, 2015
French Alps, 137
Frost
  action, 1537
  blister, 1997
  boils, 613
  bulb, 895
  heave, 13, 59, 89, 535, 541, 575, 625, 845, 941, 1055, 1105, 1281, 1299, 1399, 1439, 1481, 1519, 1543
  number, 71
  seasonal, 1711
  susceptibility, 59, 89, 845, 1299
Frozen fringe, 13, 59
Fungi, 1887

Gas
  flux, 251, 1499, 1549
  hydrates, 101, 171, 205, 263, 291, 1113, 1173
  seep, 171
  trace, 1197
GCM, 71, 681
Geoarchaeology, 1993
Geochemistry, 987, 1613
Geocryological, 821, 1493
Geomorphology, 625, 753, 1893
Geophysics, 675, 959, 1221, 1583
  model, 675
Geotechnical investigation, 49, 779, 785, 1685
Geothermal, 469, 1005, 1757
GIS, 379, 415, 493, 767, 1025, 1239, 1255, 1893
Glacial maximum, 107
Glacial tectonics, 1905
Glacier, 607, 1701, 1881
  mass wasting, 269
Grassland, 2083
Greenland, 613, 773, 865, 1705
Ground
  frozen, 199, 409, 625, 1179, 1227, 1261, 1369, 1381, 1387, 1391, 1555, 1561
  ice, 7, 337, 451, 1025, 1191, 1203, 1451, 1681, 1775, 2033
  patterned, 227, 309, 569, 613, 625, 631, 639, 925, 1043, 1087, 1131, 1137, 1255, 1281, 1399, 1519, 1537, 1589, 1775, 1857, 1933, 1997, 2009
  subsidence (settlement), 131, 575, 833, 845, 977, 1155, 1273, 1639, 1665, 1727, 1963
  thermal regime, 65, 421, 433, 711, 729, 773, 789, 821, 851, 901, 925, 983, 1067, 1125, 1215, 1221, 1233, 1267, 1487, 1511, 1665, 1775, 1799, 1815, 1957, 2055
Groundwater, 211, 801, 1387, 1613, 1833
  chemistry, 55, 1613
  infiltration, 1613
  mineralized, 25
  springs, 43
  subpermafrost, 801
Gullies, 297, 1043

Hazards, 597, 1287, 1375, 1921
Heat
  balance, 391, 795, 1215
  latent, 1113
  pipes, 2027
  storage, 983
  transfer, 149, 557, 877, 971, 1411, 1481, 1927
Heinrich events, 1803
History, 199, 475, 1525, 1739, 1745, 1957
Holocene, 1945
Hydraulic conductivity, 155, 1105, 1927
Hydrochemistry, 1951
Hydrograph recession, 233
Hydrology, 19, 177, 233, 711, 1109, 1881, 1951, 1975, 2003
  effects, 1975
  evapotranspiration, 761, 883
  modeling, 155, 177
  processes, 563
  rainfall, 761, 883
  runoff, 233, 827, 883, 1143
  surface storage, 883
Hyporheic zone, 165

Ice, 1173
  age, 1745
  avalanche, 747
  basal, 361
  blister, 1997
  bottom-fast, 1675, 1711
  classification, 1671
  genesis, 1671
  glacial, 361, 1781
  ground, 177, 303, 1037
  lens, 59, 89, 1399
  massive, 107, 119, 337, 545, 1433, 1721, 1775
  mechanics, 999
  nearshore, 1675, 1711
  segregation, 451, 575, 1863
  sheet, 107, 1905
  strength, 581
  types, 1671
  wedge, 119, 131, 741, 1131, 1149, 1161, 1721, 1803, 1809, 1887, 1899, 1933
  wedge casts, 95, 619
Iceland, 421
Indigenous knowledge, 415
Infiltration, 211
Infrastructure, 1921, 1987, 2027
Instrumentation (methods)
  aerial balloon, 1589
  atmospheric infrared sounder, 1981
  centrifuge, 919
  closed chamber, 1549
  ground penetrating radar, 131, 337, 355, 865, 1711, 1881
  nuclear magnetic resonance (NMR), 327
  particle image velocimetry, 89
  radiocarbon dating, 1577
  radiowave impedance, 409
  reflectance spectroscopy, 143
  refraction seismic, 675, 747, 959, 999
  resistivity, 337, 367, 373, 463, 645, 675, 699, 767, 773, 959, 999, 1293
  Schmidt-hammer, 913
  Self-potential, 1583
  TDR, 1927
  terrestrial laser scanning, 349
  thermostabilizer, 1787
  tomography, 101, 361, 367, 463, 699, 1293, 1445
  ultrasonic velocity, 1179
  wireless sensor, 669
  x-ray, 361
Insulation, 1481
International Permafrost Association, 199, 1369
International Polar Year, 199, 1369, 1511, 1957, 2033
IPCC, 1911
  projections, 215, 1911
ITEX, 729

Japan, 809, 1577

Kara Sea, 107, 1317

Lake (pond), 551, 901, 965, 1143, 1161, 1185, 1239, 1363, 1405, 1445, 1757, 1763, 1899, 1945, 1951, 2003

Landscapes, 1245, 1493, 1653, 1695, 1827, 2033
Landslides, 269, 563, 1793
Laptev Sea, 1345, 1875
Last Glacial Maximum, 1701
Lena
  Delta, 1239, 1567, 2095
  River, 55, 493
LIDAR, 77, 137, 349
Little Ice Age, 269

Mackenzie
  Delta, 131, 171, 833, 901, 965, 1113, 1675, 1763
  River, 385, 901
  Valley, 403
Mars, 43, 297, 487, 517, 631, 639, 971, 1043, 1531
Methane, 251, 263, 947, 1173, 1197, 1499, 1549, 1875, 1981
  methanogenesis, 1875
Microbiology, 469, 517, 523, 1567
Mining, 815
Modeling, 753, 947, 971, 1487, 1511, 1757
  erosion, 303
  forecast, 1939
  GCM, 71, 279, 1555
  hydroclimate, 1555
  limitations, 247
  numerical, 211, 215, 385, 403, 1049, 1125, 1281, 1387, 1399, 1411, 1685, 1733, 1833, 1987
  permafrost, 247, 215, 397, 421, 569, 1939, 2055
  physical, 297, 663, 895, 1555
  regional climate, 1705, 1911
  thermal, 279, 575, 747, 901, 1049, 1293, 1451
Mongolia, 1627, 2061
Monitoring, 257, 333, 373, 379, 655, 699, 753, 789, 809, 821, 977, 1119, 1149, 1209, 1221, 1267, 1305, 1311, 1339, 1391, 1487, 1601, 1633, 1647, 1653, 1695, 1727, 1815, 1857, 1869, 1963, 1969, 2071
Mountains, 597, 607

NDVI, 1469, 1893
Nepal, 1475
New Zealand, 37
N-Factor, 315, 705, 907, 953, 2027
Nitrogen cycle, 1567
Non-sorted circles, 321
Norway, 427, 789, 1311
Nutrients, 165

Off-road (trails), 415, 1067

Paleoenvironment, 1595, 1601, 1701
Paleogeography, 107
Peat (peatland), 649, 907, 1665, 1751
Periglacial, 199, 227, 391, 487, 569, 619, 625, 631, 717, 753, 1031, 1149, 1381, 1475, 1531, 1621
  morphology, 309, 619 717, 1031, 1137, 1621
Permafrost
  affected soils, 195, 805, 1093, 2061, 2071
  aggrading, 1363
  alpine, 137, 143, 397, 723, 1261, 1293, 1311, 1417, 1427, 1775, 1799, 1869
  bluffs, 7, 1423
  cold, 189, 1433, 2015
  dating, 1191, 1577
  degradation, 1499, 1643, 1733, 1769, 1839, 1845, 1851, 2071, 2089
  discontinuous, 211, 233
  distribution, 37, 71, 1621
  dry-frozen, 125
  fossil, 367
  ground surface temperature, 591, 953, 1209
  ice content, 183, 535
  ice-cemented, 125
  ice-rich, 1167, 2043
  mapping, 125, 427, 457, 889, 1137, 1273, 1357, 1469, 1827, 1851
  mountain, 37, 159, 557, 669, 699, 809
  paleo, 427
  planetary, 487
  process, 499, 1511
  publications, 1739
  retrogressive thaw slumps, 545, 741, 965, 1185, 1433, 1763
  science, 475
  sensitivity, 1769
  strength, 183, 1167, 1261, 1639
  subsea (submarine), 1005, 1345, 1875
  temperature, 257, 529, 541, 655, 669, 699, 729, 851, 971, 993, 1119, 1305, 1463, 1633, 1643, 1653, 1727, 1821, 1869, 1911
  thawing, 269, 373, 457, 541, 869, 1125, 1161, 1167, 1511, 1981
  thermal state, 993, 1633, 1695, 2061
  tunnel, 119, 451, 1887
  type, 1659
  warm, 239, 779, 785, 795, 833, 1209, 1457, 1733, 2043
Phase change, 391, 941, 1011
Pipeline, 845, 857, 895, 941, 1015, 1105, 1391, 1573, 1639, 2027
  pipe-in-pipe, 1573
Pleistocene, 1659, 1905, 1993
Pollen, 1803
Pore-water pressure, 13

Qinghai-Tibet, 113, 239, 687, 1061, 1099, 1287, 1963, 1969, 1975, 2009, 2043, 2049, 2061, 2071, 2083
Quaternary, 95, 1191, 1721, 2033

Radiation
  global, 1061
  reflective surface, 865
  solar, 865, 1061
Railroad, 113, 239, 977, 1299, 1963, 2043
Reclamation, 681
Remote sensing, 355, 551, 591, 1019, 1239, 1357, 1893
Road, 977, 1049, 1055, 1543, 2049
Rock
  falls (avalanches), 349, 747, 999
  glaciers, 77, 137, 343, 463, 487, 557, 767, 877, 913, 1019, 1031, 1209, 1475, 1505, 1583, 1781, 1799, 1869
  joints, 581
  motion, 343
  slopes, 581
  stability, 37, 143, 349, 439, 581
  surface age, 143, 913
  wall, 439, 767, 1427
  weathering, 1327, 1601
Runoff, 511
Russia, northeast, 2021
Rutting, 1

Sea ice, 19
Sea water, 25
Seasonal terrain, 1
Sediments
  frozen, 205
  hydrate-bearing, 205, 263

Seismic data, 101
Shear, 1863
Siberia, 511, 761, 937, 983, 1109, 1131, 1245, 1351, 1439, 1549, 1589, 1659, 1695, 1701, 1745, 1769, 1793, 1809, 1815, 2033, 2037, 2095
Slope
  scree (talus), 959, 1233, 1583
  stability, 597, 607, 1505
Snow, 321, 505, 557, 705, 789, 851, 925, 953, 1073, 1109, 1519, 1543, 1643, 1821, 2055
  ablation, 391
Socio-economic changes, 1093
Soil, 221, 481, 2095
  biocoenoses, 195
  carbon, 649, 1197, 1751
  classification, 1423, 1717
  clay, 13
  components, 1005
  crushed rock, 1099, 1299
  cryoturbation, 1087
  development, 2095
  gravel, 113, 119
  loess, 119
  marine, 1721, 1793
  moisture, 1067
  organics, 1083
  properties, 1179, 1457, 1917
  saline, 25, 445, 773, 1055, 1077
  sand, 83, 107
  saturated, 2077
  seasonally frozen, 195, 1055, 1321
  sensitivity, 275
  silt, 89
  surveys, 275, 321, 1717
  unsaturated, 1927, 2077
  volcanic, 1251
  wedge, 1381, 1933
Solifluction, 663, 919, 1321
Spain, 1321
Spatial analysis, 639
Stable isotope, 1809, 1997
Streams/rivers, 165, 1215
  erosion, 1015, 1899
Stress/strain, 895, 1105, 1457
Structural bending, 1573
Svalbard, 19, 257, 785, 877, 1005, 1149, 1933
Sweden, 367, 851
Swiss Alps, 463, 669, 959, 1019, 1233, 1293, 1417, 1583
Switzerland, 723, 1209

Talik, 101, 285, 385, 801, 1215, 1221, 1305, 1487, 1833
  open, 55
  suprapermafrost, 55
  thaw bulb, 165, 1757
Thaw settlement, 25
Thaw weakening, 1055
Thawing condition, 1, 189
Thawing index, 591, 1155, 1969
Thermal
  analysis, 681, 1351, 1647
  conductivity, 113, 205, 315, 839, 971
  diffusivity, 1427
  erosion, 391, 493, 563, 889, 1037
  mitigation, 1339
  offset, 557, 723, 907, 1519
  processes, 149
  properties, 1251
Thermokarst, 355, 415, 433, 457, 499, 545, 551, 649, 869, 925, 931, 937, 1239, 1333, 1433, 1439, 1617, 1775, 1827, 1839, 1945
Thermosyphon, 681, 735, 1073, 1987
  flat-looped, 735
Transitional layer, 333, 1083

Unfrozen water, 327, 675, 1451
Upfreezing, 625

Vapor flux, 505
Vegetation, 227, 373, 937, 1245, 1255, 1469, 1617, 1627, 1793, 1893, 1951, 2009
  mapping, 1469
  recovery (and disturbance), 1, 373, 1617
Vehicle disturbance, 1
Volcanoes, 517, 1251

Water
  balance, 511, 883
  migration, 2077
  quality, 1763
  soil-water, 149, 1927
Water supply, 1525
WaterGap, 71
Water-heat coupling, 1975
Wetland, 177, 931, 1951, 1981, 2003
Wildfire, 645, 1077, 1845
Wooly mammoths, 1745

Yakutsk (Yakutia), 481, 587, 1681, 1803, 1821, 1945, 2015
Yedoma, 333, 551, 937, 1595

Zero Curtain, 1451